Please type a plus sign (+) inside this box ⊓   [+] 4·26-06

TRANSMITTAL FORM

(to be used for all correspondence after initial filing)

Application Number	10/006,856
Filing Date	DECEMBER 6, 2001
First Named Inventor	KEVIN P. BAKER
Group/Art Unit	1636
Examiner Name	NANCY S. VOGEL

Total Number of Pages in This Submission	226	**Attorney Docket Number**	39780-2830P1C14

ENCLOSURES *(check all that apply)*

☒ **FEE TRANSMITTAL FORM**
   ☐ Fee Attached
☐ Response/Amendment
   ☐ After Final
   ☐ Version With Markings Showing Changes
   ☐ Affidavits/declaration(s)
☐ Extension of Time Request
☐ Information Disclosure Statement
☐ Certified Copy of Priority Document(s)
☐ Response to Missing Parts/ Incomplete Application
   ☐ Response to Missing Parts under 37 CFR 1.52 or 1.53
   ☐ Copy of Notice

☐ Copy of an Assignment
☐ Drawing(s)
☐ Licensing-related Papers
☐ Petition Routing Slip (PTO/SB/69) and Accompanying Petition
☐ Petition to Convert to a Provisional Application
☐ Power of Attorney, by Assignee to Exclusion of Inventor Under 37 C.F.R. §3.71 With Revocation of Prior Powers
☐ Terminal Disclaimer
☐ Small Entity Statement
☐ Request for Refund

☐ After Allowance Communication to Group
☐ Appeal Communication to Board of Appeals and Interferences
☒ **Appeal Communication to Group** *(Appeal Notice, Brief, Reply Brief)*
☐ Proprietary Information
☐ Status Letter
☒ **ADDITIONAL ENCLOSURE(S)** *(PLEASE IDENTIFY BELOW):*
☒ EVIDENCE APPENDIX ITEMS 1-18; AND STAMPED RETURN POSTCARD

Remarks

AUTHORIZATION TO CHARGE DEPOSIT ACCOUNT <u>08-1641</u> FOR ANY FEES DUE IN CONNECTION WITH THIS PAPER, REFERENCING ATTORNEY'S DOCKET NO. <u>39780-2830 P1C14</u>.

SIGNATURE OF APPLICANT, ATTORNEY OR AGENT

Firm *or* Individual name	HELLER EHRMAN LLP	BARRIE D. GREENE (REG. NO. 46,740)	
	275 Middlefield Road, Menlo Park, California 94025	Telephone: (650) 324-7000	Facsimile: (650) 324-0638
Signature			
Date	APRIL 24, 2006	Customer Number:	35489

CERTIFICATE OF EXPRESS MAILING

I hereby certify that this correspondence is being deposited with the United States Postal Service "Express Mail Post Office to Addressee" service under 37 C.F.R. §1.10 on the date indicated below and addressed to: **MAIL STOP APPEAL BRIEF - PATENTS**, Commissioner for Patents, PO Box 1450, Alexandria, Virginia 22313-1450, on this date: **APRIL 24, 2006**

Express Mail Label **EV 765 974 098 US**

Typed or printed name	**L. ACOSTA**		
Signature		Date	APRIL 24, 2006

OIPE
APR 24 2006
PATENT & TRADEMARK OFFICE
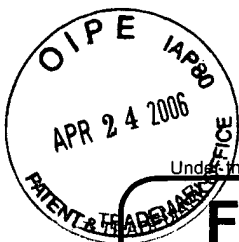
PTO/SB/17 (12-04)
Approved for use through 07/31/2006. OMB 0651-0032
U.S. Patent and Trademark Office; U.S. DEPARTMENT OF COMMERCE
Under the Paperwork Reduction Act of 1995, no persons are required to respond to a collection of information unless it displays a valid OMB control number.

FEE TRANSMITTAL
for FY 2005
Effective 10/01/2003. Patent fees are subject to annual revision.

☐ Applicant claims small entity status. See 37 CFR 1.27

TOTAL AMOUNT OF PAYMENT	($) 500.00

Complete if Known	
Application Number	10/006,856
Filing Date	December 6, 2001
First Named Inventor	Kevin P. Baker
Examiner Name	Nancy S. Vogel
Art Unit	1636
Attorney Docket No.	39780-2830 P1C14

METHOD OF PAYMENT (check all that apply)

☐ Check ☐ Credit card ☐ Money Order ☐ Other ☐ None

☑ Deposit Account:

Deposit Account Number: 08-1641(39780-2830 P1C14)

Deposit Account Name: HELLER EHRMAN, LLP

The Director is authorized to: (check all that apply)
☑ Charge fee(s) indicated below   ☑ Credit any overpayments
☑ Charge any additional fee(s) or any underpayment of fee(s)
☐ Charge fee(s) indicated below, **except for the filing fee**
to the above-identified deposit account.

FEE CALCULATION

1. BASIC FILING FEE

Large Entity Fee Code	Fee ($)	Small Entity Fee Code	Fee ($)	Fee Description	Fee Paid
1001	300	2001	150	Utility filing fee	
1002	200	2002	100	Design filing fee	
1003	200	2003	100	Plant filing fee	
1004	300	2004	150	Reissue filing fee	
1005	200	2005	100	Provisional filing fee	

SUBTOTAL (1) ($)

2. EXTRA CLAIM FEES FOR UTILITY AND REISSUE

	Extra Claims		Fee from below	Fee Paid
Total Claims	-20** =	X		
Independent Claims	- 3** =	X		
Multiple Dependent				

Large Entity Fee Code	Fee ($)	Small Entity Fee Code	Fee ($)	Fee Description
1202	50	2202	25	Claims in excess of 20
1201	200	2201	100	Independent claims in excess of 3
1203	360	2203	180	Multiple dependent claim, if not paid
1204	200	2204	100	** Reissue independent claims over original patent
1205	50	2205	25	** Reissue claims in excess of 20 and over original patent

SUBTOTAL (2) ($)

**or number previously paid, if greater; For Reissues, see above

FEE CALCULATION (continued)

3. ADDITIONAL FEES

Large Entity Fee Code	Fee ($)	Small Entity Fee Code	Fee ($)	Fee Description	Fee Paid
1051	130	2051	65	Surcharge - late filing fee or oath	
1052	50	2052	25	Surcharge - late provisional filing fee or cover sheet	
1053	130	1053	130	Non-English specification	
1812	2,520	1812	2,520	For filing a request for *ex parte* reexamination	
1804	920*	1804	920*	Requesting publication of SIR prior to Examiner action	
1805	1,840*	1805	1,840*	Requesting publication of SIR after Examiner action	
1251	120	2251	60	Extension for reply within first month	
1252	450	2252	225	Extension for reply within second month	
1253	1,020	2253	510	Extension for reply within third month	
1254	1,590	2254	795	Extension for reply within fourth month	
1255	2,160	2255	1,080	Extension for reply within fifth month	
1401	500	2401	250	Notice of Appeal	
1402	500	2402	250	Filing a brief in support of an appeal	500.00
1403	1,000	2403	500	Request for oral hearing	
1451	1,510	1451	1,510	Petition to institute a public use proceeding	
1452	500	2452	250	Petition to revive - unavoidable	
1453	1,500	2453	750	Petition to revive - unintentional	
1501	1,400	2501	700	Utility issue fee (or reissue)	
1502	800	2502	400	Design issue fee	
1503	1,100	2503	550	Plant issue fee	
1460	130	1460	130	Petitions to the Commissioner	
1807	50	1807	50	Processing fee under 37 CFR 1.17(q)	
1806	180	1806	180	Submission of Information Disclosure Stmt	
8021	40	8021	40	Recording each patent assignment per property (times number of properties)	
1809	790	2809	395	Filing a submission after final rejection (37 CFR 1.129(a))	
1810	790	2810	395	For each additional invention to be examined (37 CFR 1.129(b))	
1801	790	2801	395	Request for Continued Examination (RCE)	
1802	900	1802	900	Request for expedited examination of a design application	

Other fee (specify) _____
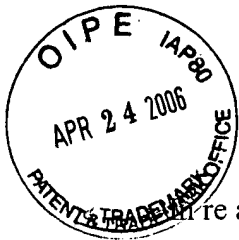
*Reduced by Basic Filing Fee Paid

SUBTOTAL (3) ($) 500.00

SUBMITTED BY (Complete (if applicable))

Name (Print/Type)	Barrie D. Greene	Registration No. (Attorney/Agent)	46,740	Telephone	(650) 324-7000
Signature				Date	April 24, 2006

IN THE UNITED STATES PATENT AND TRADEMARK OFFICE

In re application of:)	Examiner: Vogel, Nancy S.
)	
Kevin P. BAKER, et al.)	Art Unit: 1636
)	
Application Serial No. 10/006,856)	Confirmation No: 8365
)	
Filed: December 6, 2001)	Attorney's Docket No. 39780-2830 P1C14
)	
For: **SECRETED AND**)	**Customer No. 35489**
TRANSMEMBRANE)	
POLYPEPTIDES AND NUCLEIC)	
ACIDS ENCODING THE SAME)	

EXPRESS MAIL LABEL NO. : <u>EV 765 974 098 US</u>
DATE MAILED: APRIL 24, 2006

ON APPEAL TO THE BOARD OF PATENT APPEALS AND INTERFERENCES

APPELLANTS' BRIEF

MAIL STOP APPEAL BRIEF - PATENTS
Commissioner for Patents
P.O. Box 1450
Alexandria, Virginia 22313-1450

Dear Sir:

On September 22, 2005, the Examiner made a Final Rejection to pending Claims 28-35 and 38-40. A Notice of Appeal was filed on February 22, 2006.

Appellants hereby appeal to the Board of Patent Appeals and Interferences from the last decision of the Examiner.

The following constitutes Appellants' Brief on Appeal.

-1-

1.   **REAL PARTY IN INTEREST**

The real party in interest is Genentech, Inc., South San Francisco, California, by an assignment of the patent application U.S. Serial No. 09/946,374 recorded January 8, 2002, at Reel 012288 and Frame 0504.

2.   **RELATED APPEALS AND INTERFERENCES**

The claims pending in the current application are directed to a polypeptide referred to herein as "PRO1303." A related patent application, U.S. Serial No. 10/006,116, filed December 6, 2001 (containing claims directed to antibodies that bind the PRO1303 polypeptide), is also under final rejection from the same Examiner and based upon the same outstanding rejection, and appeal of this final rejection is being pursued independently and concurrently herewith.

3.   **STATUS OF CLAIMS**

Claims 28-35 and 38-40 are in this application.

Claims 1-27 and 36-37 are canceled.

Claims 28-35 and 38-40 stand rejected and Appellants appeal the rejection of these claims.

A copy of the rejected claims involved in the present Appeal is provided in the Claims Appendix.

4.   **STATUS OF AMENDMENTS**

The claims involved in the appeal were amended in the Response filed December 14, 2005. In the Advisory Action mailed January 25, 2006, the Examiner stated that this amendment would not be entered. Accordingly, the claims listed in the Claims Appendix do not incorporate the changes made by the amendment of December 14, 2005.

5.   **SUMMARY OF CLAIMED SUBJECT MATTER**

The invention claimed in the present application is related to an isolated polypeptide comprising the amino acid sequence of the polypeptide of SEQ ID NO:194; the amino acid

-2-

sequence of the polypeptide of SEQ ID NO:194, lacking its associated signal peptide; or the amino acid sequence of the polypeptide encoded by the full-length coding sequence of the cDNA deposited under ATCC accession number 203232 (Claims 33-35 and 38). The invention is further directed to polypeptides having at least 80%, 85%, 90%, 95%, or 99% amino acid sequence identity to the amino acid sequence of the polypeptide of SEQ ID NO:194; the amino acid sequence of the polypeptide of SEQ ID NO:194, lacking its associated signal peptide; or the amino acid sequence of the polypeptide encoded by the full-length coding sequence of the cDNA deposited under ATCC accession number 203232, wherein the polypeptide inhibits the uptake of glucose or FFA (free fatty acid) by adipocyte cells (Claims 28-32). The invention is further directed to a chimeric polypeptide comprising one of the above polypeptides fused to a heterologous polypeptide (Claim 39), and to a chimeric polypeptide wherein the heterologous polypeptide is an epitope tag or an Fc region of an immunoglobulin (Claim 40).

The full-length PRO1303 polypeptide having the amino acid sequence of SEQ ID NO:194 is described in the specification at, for example, page 15, lines 9-25, page 343, lines 6-10, Example 57, in Figure 108 and in SEQ ID NO:194. The cDNA nucleic acid encoding PRO1760 is described in the specification at, for example, Example 57, in Figure 107 and in SEQ ID NO:193. Page 291, lines 18-22 of the specification provides the description for Figures 107 and 108. PRO polypeptide variants having at least about 80% amino acid sequence identity with a full length PRO polypeptide sequence, a PRO polypeptide sequence lacking the signal peptide are described in the specification at, for example, page 302, lines 4-26. The preparation of chimeric PRO polypeptides, including those wherein the heterologous polypeptide is an epitope tag or an Fc region of an immunoglobulin, is set forth in the specification at page 358, lines 11-34. Examples 128-131 describe the expression of PRO polypeptides in various host cells, including *E. coli*, mammalian cells, yeast and Baculovirus-infected insect cells. Example 149, in the specification at page 511, line 34, to page 512, line 10, sets forth an Adipocyte Glucose/FFA Uptake assay which shows that PRO1303 is a stimulator of glucose/FFA uptake in adipocyte cells (see page 512, lines 7-8). Finally, Example 143, in the specification at page 494, line 20, to page 508, line 28, sets forth a Gene Amplification assay which shows that the

-3-

PRO1303 gene is amplified in the genome of certain human lung and colon cancers (Table 8; page 507, lines 14-21).

6.   GROUNDS OF REJECTION TO BE REVIEWED ON APPEAL

I.   Whether Claims 28-35 and 38-40 satisfy the utility requirement of 35 U.S.C. §101.

II.   Whether Claims 28-35 and 38-40 satisfy the enablement requirement of 35 U.S.C. §112, first paragraph.

7.   ARGUMENT

Summary of the Arguments

Issue I: Utility

Patentable utility of the PRO1303 polypeptide is based upon the results of the adipocyte glucose/FFA uptake assay for the PRO1303 polypeptide. The specification discloses that the adipocyte glucose/FFA uptake assay is designed to determine whether a polypeptide is capable of modulating, either positively or negatively, the uptake of glucose or free fatty acids in adipocyte cells. By making such determinations, the assay identifies polypeptides that are expected to be useful for treating disorders wherein stimulation or inhibition of glucose uptake by adipocytes is expected to be therapeutically effective, for example, diabetes, and hyper- or hypo-insulinemia.

The glucose/FFA uptake assay as described in Example 149 of the instant application was well known in the art at the time of the effective filing date of the instant application. As demonstrated by the references of record, similar assays were commonly used to identify potential anti-diabetic agents.

The Examiner has asserted that stimulation of glucose and/or FFA uptake is actually "three very different activities" and that "it is unclear how increasing uptake of FFA into adipocytes would treat obesity (or thus diabetes)." (Pages 7-8 of the Office Action mailed March 31, 2005). In fact, the references cited by the Examiner support Appellants' position that decreasing circulating FFA levels is beneficial in the treatment of disorders such as diabetes and obesity.

-4-

The Examiner has also questioned the statistical significance of the observed results. Appellants note that the evidentiary standard to be used throughout *ex parte* examination in setting forth a rejection is a preponderance of the totality of the evidence under consideration. Thus, to overcome the presumption of truth that an assertion of utility by the applicant enjoys, the Examiner must establish that it is more likely than not that one of ordinary skill in the art would doubt the truth of the statement of utility. Only after the Examiner has made a proper *prima facie* showing of lack of utility, does the burden of rebuttal shift to the applicant. Therefore, the legal standard for patentable utility is not absolute certainty. Clear evidence supports the glucose/FFA uptake inhibition activity of PRO1303. The Examiner has provided no evidence to demonstrate that it more likely than not that one of skill in the art would doubt the truth of this asserted utility of PRO1303 as an inhibitor of glucose/FFA uptake.

The Examiner has further asserted that "the specification does not actually describe whether PRO1303 actually increases glucose uptake because the assay results were set forth as being positive for glucose and/or FFA uptake" and that "the applicant fails to show that uptake of FFA is a hallmark of therapeutically effective agents to treat the indicated diseases." (Pages 15-16 of the Office Action mailed September 22, 2005).

It is known in the art that FFA levels regulate glucose uptake by adipocytes. Thus, even if the actual mechanistic effect of PRO1303 is only to directly increase FFA uptake by adipocyte cells, this will necessarily result in indirectly increasing glucose uptake by adipocytes. Furthermore, agents which are well known in the art as useful in the treatment of diabetes, such as the thiazolidenediones, have been shown to exert their effects, at least in part, through the increase of FFA uptake by adipocytes. Accordingly, an agent which increases FFA uptake by adipocytes has the same utility in the treatment of disease as those recognized by the Examiner for agents which increase glucose uptake.

While Appellants are required to demonstrate only a single patentable utility for their claimed invention, Appellants submit that patentable utility of the PRO1303 polypeptide is also based upon the gene amplification data for the gene encoding the PRO1303 polypeptide. The specification discloses that the gene encoding PRO1303 showed significant amplification, ranging from 2.19 to 2.68, in five different lung and colon tumors. Appellants have submitted,

-5-

with their Response filed June 29, 2005, the Declaration of Dr. Audrey Goddard, which explains that a gene identified as being amplified at least 2-fold by the disclosed gene amplification assay in a tumor sample relative to a normal sample is <u>useful as a marker for the diagnosis of cancer</u>, for monitoring cancer development and/or for measuring the efficacy of cancer therapy.

The Examiner has asserted that that the gene amplification data discussed above does not provide utility for PRO1303 because "[i]ncreased copy number of DNA in a cancer or transformed cell does not necessarily result in an increased level of expression of the polypeptide." (Page 5 of the Office Action mailed March 31, 2005). In support of this assertion the Examiner has cited references by Pennica *et al.* and Konopka *et al.* The references cited by the Examiner do not suffice to make a *prima facie* case that more likely than not no generalized correlation exists between gene (DNA) amplification and increased polypeptide levels.

In contrast, Appellants have submitted ample evidence to show that, in general, if a gene is amplified in cancer, it is more likely than not that the encoded protein will be expressed at an elevated level. First, the articles by Orntoft *et al.*, Hyman *et al.*, and Pollack *et al.* (made of record in Appellants' Response filed June 29, 2005) collectively teach that <u>in general, gene amplification increases mRNA expression</u>. Second, the Declaration of Dr. Paul Polakis, principal investigator of the Tumor Antigen Project of Genentech, Inc., the assignee of the present application, shows that, <u>in general, there is a correlation between mRNA levels and polypeptide levels</u>. Therefore, one of skill in the art would reasonably expect in this instance, based on the amplification data for the PRO1303 gene, that the PRO1303 polypeptide is concomitantly overexpressed. Thus, the claimed PRO1303 polypeptides have utility in the diagnosis of cancer.

Accordingly, Appellants submit that when the proper legal standard is applied, one should reach the conclusion that the present application discloses at least one patentable utility for the claimed PRO1303 polypeptides.

Issue II: Enablement

Claims 28-35 and 38-40 stand rejected under 35 U.S.C. §112, first paragraph, allegedly "since the claimed invention is not supported by either a specific and substantial asserted utility or a

well established utility for the reasons set forth above, one skilled in the art clearly would not know how to use the claimed invention." (Page 10 of the Office Action mailed March 31, 2005).

As described above, the PRO1303 polypeptides have utility both in the treatment of disorders for which modulation of glucose uptake by adipocytes would be beneficial, such as obesity, diabetes, and hyper- or hypo-insulinemia, and in the diagnosis of cancer. Based on such utilities, one of skill in the art would know exactly how to use the claimed polypeptides without any undue experimentation.

These arguments are all discussed in further detail below under the appropriate headings.

ISSUE I: Claims 28-35 and 38-40 satisfy the utility requirement of 35 U.S.C. §101

Claims 28-35 and 38-40 stand rejected under 35 U.S.C. §101 because allegedly "the claimed invention is not supported by either a specific and substantial asserted utility or a well-established utility." (Page 3 of the Office Action mailed September 22, 2005).

Appellants submit, for the reasons set forth below, that the specification discloses at least one credible, substantial and specific asserted utility for the claimed PRO1303 polypeptides.

A.   The Legal Standard for Utility

According to 35 U.S.C. §101:

Whoever invents or discovers any new and *useful* process, machine, manufacture, or composition of matter, or any new and *useful* improvement thereof, may obtain a patent therefor, subject to the conditions and requirements of this title. (Emphasis added).

In interpreting the utility requirement, in *Brenner v. Manson,*[1] the Supreme Court held that the *quid pro quo* contemplated by the U.S. Constitution between the public interest and the interest of the inventors required that a patent applicant disclose a "substantial utility" for his or her invention, i.e. a utility "where specific benefit exists in currently available form."[2] The Court concluded that "a patent is not a hunting license. It is not a reward for the search, but

---

[1] *Brenner v. Manson,* 383 U.S. 519, 148 U.S.P.Q. (BNA) 689 (1966).

[2] *Id.* at 534, 148 U.S.P.Q. (BNA) at 695.

compensation for its successful conclusion. A patent system must be related to the world of commerce rather than the realm of philosophy."[3]

Later, in *Nelson v. Bowler,*[4] the C.C.P.A. acknowledged that tests evidencing pharmacological activity of a compound may establish practical utility, even though they may not establish a specific therapeutic use. The court held that "since it is crucial to provide researchers with an incentive to disclose pharmaceutical activities in as many compounds as possible, we conclude adequate proof of any such activity constitutes a showing of practical utility."[5]

In *Cross v. Iizuka,*[6] the C.A.F.C. reaffirmed *Nelson*, and added that *in vitro* results might be sufficient to support practical utility, explaining that "*in vitro* testing, in general, is relatively less complex, less time consuming, and less expensive than *in vivo* testing. Moreover, *in vitro* results with the particular pharmacological activity are generally predictive of *in vivo* test results, i.e. there is a reasonable correlation there between."[7] The court perceived "No insurmountable difficulty" in finding that, under appropriate circumstances, "in vitro testing, may establish a practical utility."[8]

The case law has also clearly established that applicants' statements of utility are usually sufficient, unless such statement of utility is unbelievable on its face.[9] The PTO has the initial burden to prove that applicants' claims of usefulness are not believable on their face.[10] In general, an Applicant's assertion of utility creates a presumption of utility that will be sufficient

---

[3] *Id.* at 536, 148 U.S.P.Q. (BNA) at 696.

[4] *Nelson v. Bowler*, 626 F.2d 853, 206 U.S.P.Q. (BNA) 881 (C.C.P.A. 1980).

[5] *Id.* at 856, 206 U.S.P.Q. (BNA) at 883.

[6] *Cross v. Iizuka*, 753 F.2d 1047, 224 U.S.P.Q. (BNA) 739 (Fed. Cir. 1985).

[7] *Id.* at 1050, 224 U.S.P.Q. (BNA) at 747.

[8] *Id.*

[9] *In re Gazave*, 379 F.2d 973, 154 U.S.P.Q. (BNA) 92 (C.C.P.A. 1967).

[10] *Ibid.*

to satisfy the utility requirement of 35 U.S.C. §101, "unless there is a reason for one skilled in the art to question the objective truth of the statement of utility or its scope."[11,12]

Compliance with 35 U.S.C. §101 is a question of fact.[13] The evidentiary standard to be used throughout *ex parte* examination in setting forth a rejection is a preponderance of the totality of the evidence under consideration.[14] Thus, to overcome the presumption of truth that an assertion of utility by the applicant enjoys, the Examiner must establish that it is more likely than not that one of ordinary skill in the art would doubt the truth of the statement of utility. Only after the Examiner made a proper *prima facie* showing of lack of utility, does the burden of rebuttal shift to the applicant. The issue will then be decided on the totality of evidence.

The well established case law is clearly reflected in the Utility Examination Guidelines ("Utility Guidelines")[15], which acknowledge that an invention complies with the utility requirement of 35 U.S.C. §101, if it has at least one asserted "specific, substantial, and credible utility" or a "well-established utility." Under the Utility Guidelines, a utility is "specific" when it is particular to the subject matter claimed. For example, it is generally not enough to state that a nucleic acid is useful as a diagnostic without also identifying the conditions that are to be diagnosed.

In explaining the "substantial utility" standard, M.P.E.P. §2107.01 cautions, however, that Office personnel must be careful not to interpret the phrase "immediate benefit to the public" or similar formulations used in certain court decisions to mean that products or services based on the claimed invention must be "currently available" to the public in order to satisfy the utility requirement. "Rather, any reasonable use that an applicant has identified for the invention that can be viewed as providing a public benefit should be accepted as sufficient, at least with regard

---

[11] *In re Langer*, 503 F.2d 1380,1391, 183 U.S.P.Q. (BNA) 288, 297 (C.C.P.A. 1974).

[12] *See also In re Jolles*, 628 F.2d 1322, 206 U.S.P.Q. 885 (C.C.P.A. 1980); *In re Irons*, 340 F.2d 974, 144 U.S.P.Q. 351 (1965); *In re Sichert*, 566 F.2d 1154, 1159, 196 U.S.P.Q. 209, 212-13 (C.C.P.A. 1977).

[13] *Raytheon v. Roper*, 724 F.2d 951, 956, 220 U.S.P.Q. (BNA) 592, 596 (Fed. Cir. 1983) *cert. denied*, 469 US 835 (1984).

[14] *In re Oetiker*, 977 F.2d 1443, 1445, 24 U.S.P.Q.2d (BNA) 1443, 1444 (Fed. Cir. 1992).

[15] 66 Fed. Reg. 1092 (2001).

to defining a 'substantial' utility."[16] Indeed, the Guidelines for Examination of Applications for Compliance With the Utility Requirement,[17] gives the following instruction to patent examiners: "If the applicant has asserted that the claimed invention is useful for any particular practical purpose . . . and the assertion would be considered credible by a person of ordinary skill in the art, do not impose a rejection based on lack of utility."

B.   **The results of the adipocyte glucose/FFA uptake assay provide utility for the PRO1303 polypeptide**

Appellants respectfully submit that they rely in part on the adipocyte glucose/FFA uptake assay) for patentable utility of the PRO1303 polypeptides, and that the adipocyte glucose/FFA uptake assay data for the PRO1303 polypeptide is clearly disclosed in the instant specification under Example 149.

The adipocyte glucose/FFA uptake assay is designed to determine whether a polypeptide is capable of modulating, either positively or negatively, the uptake of glucose or free fatty acids in adipocyte cells. By making such determinations, the assay identifies polypeptides that are expected to be useful for treating disorders wherein stimulation or inhibition of glucose uptake by adipocytes is expected to be therapeutically effective. Examples of these types of disorders include obesity, diabetes, and hyper- or hypo-insulinemia.

The adipocyte glucose/FFA assay is performed as follows: primary rat adipocyte cells are plated on a 96 well plate and incubated overnight with media supplemented with PRO1303 polypeptide. After the initial overnight incubation, samples of the media are taken at hour 4 and hour 16 and residual glycerol, glucose and FFA are measured. After the hour 16 sample is taken, insulin is added to the media and the adipocytes are allowed to incubate for an additional 4 hours. After this final 4 hour incubation, another sample is taken and residual glycerol, glucose and FFA is measured again. As a control, identical incubations and samplings are performed on cells that have been incubated overnight in media initially supplemented with insulin rather than PRO1303 polypeptide. Results are scored as positive in the assay if the uptake is greater than 1.5 times

---

[16.] M.P.E.P. §2107.01.

[17] M.P.E.P. §2107 II(B)(1).

-10-

(stimulatory) or less than 0.5 times (inhibitory) the uptake of the insulin control. As PRO1303 resulted in more than 1.5 times the uptake of the insulin control, <u>PRO1303 tested positive as a stimulator of glucose/FFA uptake in adipocyte cells</u>.

The glucose/FFA uptake assay as described in Example 149 of the instant application was also well known in the art at the time of the effective filing date of the instant application. Similar assays were commonly used to identify potential anti-diabetic agents and to study the regulatory mechanisms of important molecules involved in fat cell metabolism.

For example, at the time of the effective filing date of the instant application, it was well known in the art that increasing glucose uptake by adipocyte cells is a hallmark of a number of therapeutically effective agents, such as troglitazone and pioglitazone. (Tafuri, *Endocrinology*, 137(11): 4706-4712 (1996); Sandouk, *et al., Endocrinology*, 133(1):352-359 (1993) - copies enclosed). Both troglitazone and pioglitazone are members of the thiazolidinedione class of compounds and have been used to effectively treat noninusulin-dependent diabetes mellitus (NIDDM), the most common form of diabetes. Both compounds function, at least in part, by increasing the number of cellular glucose transporters in order to facilitate increased glucose uptake.

Further, at the time of the effective filing date of the instant application, vanadium salts were considered as a possible treatment for diabetes, and several clinical trials had already been performed. (Page 26617, right column, Goldwaser *et al., J. Biol Chem.*, 274(37):26617-26624 (1999) - copy enclosed). Using a rat adipocyte culture system similar to the system disclosed in the instant application, Goldwaser *et al.*, showed that vanadium ligand l-Glu (γ)HXM potentiates the capacity of free vanadium ions to activate glucose uptake and glucose metabolism in rat adipocytes *in vitro* by 4-5 folds and to lower blood glucose levels in hyperglycemic rats *in vivo* by 5-7 fold. This is further evidence that at the effective filing date of the present application one skilled in the art would have reasonably expected that molecules activating glucose uptake would find utility in the treatment of diabetes and related diseases.

In addition, the investigators in Mueller *et al.*, who were interested in determining the influence of glucose uptake on leptin secretion, employed essentially the same assay to measure changes in glucose uptake after insulin exposure. (Mueller *et al., Endocrinology*, 139(2): 551-

-11-

558 (1998) - copy enclosed). Figure 1A shows the glucose concentrations in medium from 0-96 hours from isolated rat adipocytes in primary culture with various insulin concentrations. As indicated by the decrease in glucose in the medium in the Figure, Mueller *et al.* suggest that insulin produced a concentration-dependent increase in glucose uptake by the cultured adipocytes. Based on these experimental results, the authors stated that insulin increased leptin secretion over 96 hours, and that the increase in leptin was closely related to the amount of glucose taken up by the adipocytes than to the insulin concentration, suggesting a role for glucose transport and/or metabolism in regulating leptin secretion. (See Abstract).

Using the same assay system, Mueller *et al.* further studied the effect on leptin secretion of two well-known anti-diabetic agents, metformin and vanadium, which were known to enhance glucose uptake. (Muller *et al.*, *Obesity Research,* 8(7): 530-539 (2000) - copy enclosed). The experimental data indicated that both metformin and vanadium increased glucose uptake and inhibit leptin secretion from cultured adipocytes.

Accordingly, Appellants respectfully submit that at the effective filing date of the instant application, one of skill in the art would have reasonably accepted that various compounds, such as PRO1303, that are capable of modulating glucose uptake have a substantial, practical, real life utility. The above-mentioned studies have clearly established that the glucose/FFA uptake assay as described in the instant application is a reliable assay system to identify therapeutic agents for treating diseases and conditions such as obesity, diabetes, and hyperinsulinemia. Therefore, Appellants respectfully submit that a variety of real-life utilities, such as treatments for glucose uptake related diseases, including obesity and diabetes, are envisioned for PRO1303 based on the glucose/FFA uptake assay results disclosed herein.

1.   *A prima facie case of lack of utility has not been established*

The Examiner has asserted that "the specification does not indicate which asserted utilities correspond specifically to glucose uptake stimulation as opposed to glucose uptake inhibition." (Page 7 of the Office Action mailed March 31, 2005). As discussed above, it was known in the art at the time of filing that agents which increased glucose uptake, such as troglitazone and pioglitazone, were useful in the treatment of diabetes. Treatment with vanadium salts, another agent which increased glucose uptake, was shown to lower glucose levels in

-12-

hyperglycemic rats. Diabetes, hyperglycemia, and obesity were know at the time of filing to be closely linked conditions (see, for example, Sandouk, page 352). Thus one of skill in the art would have understood that stimulators of glucose uptake would be useful in the treatment of diabetes, obesity, and hyperglycemia.

The Examiner has asserted that "the specification does not indicate what, if any, of the utilities set forth correspond to stimulation of FFA uptake." (Page 7 of the Office Action mailed March 31, 2005). The Examiner has further asserted that stimulation of glucose and/or FFA uptake is actually "three very different activities (stimulation of glucose uptake only, stimulation of FFA uptake only, and stimulation of uptake of both)." (Pages 7-8 of the Office Action mailed March 31, 2005). Appellants respectfully point out that it was well known in the art at the time of filing that both glucose and FFA levels were associated with diabetes/hyperinsulinemia. See, for example, the discussion below of Fabris et al., cited by the Examiner. Stimulation of uptake of either or both of glucose and FFA are not "very different activities" but closely related activities. Accordingly, it is not necessary to specify which utilities correspond to FFA uptake versus glucose uptake, as the utilities are the same.

The Examiner has asserted that "it is unclear how increasing uptake of FFA into adipocytes would treat obesity (or thus diabetes)." (Page 8 of the Office Action mailed March 31, 2005). The Examiner cites Fabris et al. as teaching that "FFA-induced insulin resistance saves scarce glucose for central nervous system requirements, but this becomes counterproductive in obesity because it inhibits glucose utilization when there is no need to save it." ((Page 7 of the Office Action mailed March 31, 2005). Appellants respectfully direct the Board's attention to the later discussion in Fabris et al., where the authors make clear that FFA-induced insulin resistance is a result of high circulating FFA levels (page 604, col. 2). As the portion of Fabris et al. cited by the Examiner explains, this resistance leads to less utilization of glucose, which contributes to the development of obesity or diabetes. Thus Fabris et al. supports Appellants' assertion that decreasing circulating FFA levels, by increasing FFA uptake into adipocytes, will run counter to this trend and help in the treatment of obesity or diabetes. In addition, the reference by Santomauro et al., cited by the Examiner, confirms that "lowering of elevated plasma FFA levels can reduce insulin resistance/hyperinsulinemia and improve oral

-13-

glucose tolerance in lean and obese nondiabetic subjects and in obese patients with type 2 diabetes" (Abstract).

The Examiner has further asserted that "the observed differences do not appear to be statistically significant, and the cutoff points appear to be arbitrary and there is no scientific basis for them." (Page 8 of the Office Action mailed March 31, 2005). In support of this assertion, the Examiner cites Santomauro *et al.* Santomauro *et al.* teach that 56.5% decreases in FFA levels are statistically significant and correlated with physiological improvement. The Examiner has stated that "it is not clear whether 50% decreases are useful." (Page 9 of the Office Action mailed March 31, 2005). Appellants respectfully submit that the difference between 56.5% and 50% is not large. Appellants further respectfully point out that the treatments in Santamauro *et al.* resulted in lowering FFA levels to below normal. One of skill in the art would expect that lowering FFA levels to only normal levels (requiring a decrease of only 41-44%) would also be useful.

The Examiner has further stated that "the observation that 56.5% decreases in circulating FFAs is significant and correlated with physiological improvements does not mean that a doubling of uptake of FFAs by adipocytes will lead to the same decreases in FFAs." (Page 9 of the Office Action mailed March 31, 2005). Appellants respectfully note that no evidence is provided for this assertion. To the contrary, the art indicates that *in vitro* uptake experiments with rat adipocytes actually underpredict the effects of treatment *in vivo*. For example, Goldwaser *et al.* demonstrated that vanadium ions increased glucose uptake in rat adipocytes *in vitro* by 4-5 fold, but lowered blood glucose levels in hyperglycemic rats *in vivo* by 5-7 fold (see Abstract).

Finally, Appellants respectfully point out that the standard for utility is not absolute certainty, but more likely than not. As discussed above, at the time of the effective filing date of the instant application, it was well known in the art that increasing glucose uptake by adipocyte cells is a hallmark of a number of therapeutically effective agents, such as troglitazone and pioglitazone. The art has also shown that agents which decrease circulating FFA levels are also useful in the treatment of disorders such as diabetes, hyperglycemia, and obesity. One of ordinary skill in the art would therefore find it more likely than not that an agent which increases

-14-

uptake of glucose and/or FFA by adipocytes would also be useful in the treatment of disorders such as diabetes, hyperglycemia, and obesity. Accordingly, since the standard is not absolute certainty, a *prima facie* showing of lack of utility has not been made in this instance and the burden to provide further evidence of utility has not shifted to Appellants.

2. *The asserted utilities apply to both glucose and FFA uptake*

The Examiner has asserted that "the specification does not actually describe whether PRO1303 actually increases glucose uptake because the assay results were set forth as being positive for glucose and/or FFA uptake. If PRO1303 was positive for only FFA uptake, then the arguments concerning utility based on glucose uptake are not persuasive." (Pages 15-16 of the Office Action mailed September 22, 2005).

Appellants respectfully point out that it was well known in the art at the time of filing that both glucose and FFA levels were associated with diabetes, obesity, and hyperinsulinemia. In fact, FFA levels are one of the factors which regulate glucose uptake. As discussed above, Fabris *et al.* (made of record by the Examiner in the Office Action mailed March 31, 2005) explains that high circulating FFA levels lead to FFA-induced insulin resistance (page 604, col. 2). This resistance leads to less utilization of glucose, which contributes to the development of obesity or diabetes. Santomauro *et al.* (made of record by the Examiner in the Office Action mailed March 31, 2005) demonstrated that lowering plasma FFA levels increases insulin sensitivity, and thus increases glucose uptake in response to insulin.

The Examiner has asserted that "the applicant fails to show that uptake of FFA is a hallmark of therapeutically effective agents to treat the indicated diseases." (Page 16 of the Office Action mailed September 22, 2005). In fact, the reference by Santomauro *et al.*, cited by the Examiner in the previous Office Action, confirms that "lowering of elevated plasma FFA levels can reduce insulin resistance/hyperinsulinemia and improve oral glucose tolerance in lean and obese nondiabetic subjects and in obese patients with type 2 diabetes" (Abstract). Thus it is clear that agents which decrease circulating FFA levels are effective in the treatment of diseases such as obesity and diabetes.

It was further known in the art at the time of filing that antidiabetic agents such as the thiazolidinediones (including troglitazone and pioglitazone) discussed above as agents which

-15-

increase glucose uptake, <u>also increase FFA uptake by adipocytes</u>. For example, Frohnert *et al.* (J. Biol. Chem. 272:3970-3977 (1999); submitted with Appellants' Response filed December 14, 2005) found that troglitazone stimulates increased expression of fatty acid transport protein (FATP) in adipocytes by 3-fold (page 3974, col. 1; Fig. 5). Troglitazone was also found to significantly increase uptake of fatty acids by adipocytes (page 3974, col. 2 and Fig. 8). The authors conclude that the antidiabetic effects of troglitazone may be due to improved fatty acid uptake by adipocytes (page 3976, col. 2). Similarly, Martin *et al.* (J. Biol. Chem. 272:28210-28217 (1997); submitted with Appellants' Response filed December 14, 2005) found that the antidiabetic thiazolidinedione BRL 49653 "resulted in a significant induction of adipose tissue FATP (7-fold) ... mRNA levels" (page 28213, col. 2). The induction of FATP mRNA also resulted in increased FFA uptake into adipocytes (page 28214, col. 2). The authors conclude that "thiazolidinedione antidiabetic agents seem to favor adipocyte-specific FA uptake relative to muscle, perhaps underlying in part the beneficial effects of these agents on insulin-mediated glucose dispersal" (Abstract). Thus the art at the time of filing demonstrated that <u>agents which increased FFA uptake by adipocytes were useful in the treatment of diabetes</u>.

The Examiner has asserted that "there is still no indication that compounds in the art which increase uptake of FFA alone (not increasing glucose uptake) are effective for the treatment of any particular disease." (Page 16 of the Office Action mailed September 22, 2005).

As discussed above, circulating FFA levels <u>regulate</u> glucose uptake by adipocytes. Thus, even if the actual mechanistic effect of PRO1303 is only to directly increase FFA uptake by adipocyte cells, this will <u>necessarily result</u> in indirectly increasing glucose uptake by adipocytes. The effect of FFA levels on glucose uptake has been clearly demonstrated in the references previously cited by the Examiner. Furthermore, agents which are well known in the art as useful in the treatment of diabetes, such as the thiazolidenediones, have been shown to exert their effects, at least in part, through the increase of FFA uptake by adipocytes. Accordingly, an agent which increases FFA uptake by adipocytes has the <u>same utility</u> in the treatment of disease as those recognized by the Examiner for agents which increase glucose uptake.

Based on the above arguments, Appellants have clearly demonstrated a credible, specific and substantial asserted utility for the PRO1303 polypeptide, for example in the treatment of

-16-

disorders such as obesity, diabetes, and hyper- or hypo-insulinemia. Further, based on this utility and the disclosure in the specification, one skilled in the art at the time the application was filed would know how to use the claimed polypeptides.

C. **The results of the gene amplification assay also provide utility for the PRO1303 polypeptide**

Appellants respectfully note that they are required to disclose only a single patentable utility for their claimed invention. Nonetheless, in addition to the utilities discussed above in the treatment of disorders such as obesity, diabetes, and hyper- or hypo-insulinemia, Appellants further respectfully submit that the gene amplification data also demonstrates patentable utility for the PRO1303 polypeptide. The gene amplification data for the gene encoding the PRO1303 polypeptide is clearly disclosed in the instant specification under Example 143.

It was well known in the art at the time the invention was made that gene amplification is an essential mechanism for oncogene activation. The gene amplification assay is well-described in Example 143 of the present application. Example 143 discloses that the inventors isolated genomic DNA from a variety of primary cancers and cancer cell lines that are listed in Table 8, including primary lung and colon tumors of the type and stage indicated in Table 7. As a negative control, DNA was isolated from the cells of ten normal healthy individuals, which was pooled and used as a control. Gene amplification was monitored using real-time quantitative TaqMan™ PCR. Table 8 shows the resulting gene amplification data. Further, Example 143 explains that the results of TaqMan™ PCR are reported in ΔCt units, wherein one unit corresponds to one PCR cycle or approximately a 2-fold amplification relative to control, two units correspond to 4-fold amplification, 3 units to 8-fold amplification etc.

The specification discloses that the nucleic acids encoding PRO1303 had ΔCt value of > 1.0, which is a **more than 2-fold increase**, for primary lung tumors LT13, LT15, LT16; for lung cell line A549; and for the primary colon tumor CT16. PRO1303 showed approximately 1.13 to 1.42 ΔCt units which corresponds to $2^{1.13}$ to $2^{1.42}$- fold amplification or 2.19 to 2.68 fold amplification in primary lung tumors LT13, LT15, LT16; for lung cell line A549; and for the primary colon tumor CT16. (See Table 8 of the specification). Accordingly, the present

-17-

specification clearly discloses strong evidence that the gene encoding the PRO1303 polypeptide is <u>significantly</u> amplified in a number of lung and colon tumors.

In further support, Appellants have submitted, in their Response filed June 29, 2005, a Declaration by Dr. Audrey Goddard. Appellants particularly draw the Board's attention to page 3 of the Goddard Declaration which clearly states that:

> It is further my considered scientific opinion that an at least **2-fold increase** in gene copy number in a tumor tissue sample relative to a normal (*i.e.,* non-tumor) sample <u>is significant</u> and useful in that the detected increase in gene copy number in the tumor sample relative to the normal sample serves as a basis for using relative gene copy number as quantitated by the TaqMan PCR technique as a diagnostic marker for the presence or absence of tumor in a tissue sample of unknown pathology. Accordingly, a gene identified as being amplified at least 2-fold by the quantitative TaqMan PCR assay in a tumor sample relative to a normal sample is **useful as a marker for the diagnosis of cancer,** for monitoring cancer development and/or for measuring the efficacy of cancer therapy. (Emphasis added).

As indicated above, the gene encoding the PRO1303 polypeptide shows <u>at least</u> a two fold amplification in <u>five</u> different lung and colon tumors and tumor cell lines. In addition, the Goddard Declaration clearly establishes that the TaqMan real-time PCR method described in Example 143 has gained wide recognition for its versatility, sensitivity and accuracy, and is in extensive use for the study of gene amplification. The facts disclosed in the Declaration also confirm that based upon the gene amplification results, one of ordinary skill would find it credible that the PRO1303 polypeptides have utility in the diagnosis of cancer.

1.   *A* **prima facie** *case of lack of utility has not been established*

The Examiner has asserted that although "the DNA encoding PRO1303 has diagnostic utility based upon these results, the PRO1303 polypeptide does not." In particular, the Examiner has asserted that "[i]ncreased copy number of DNA in a cancer or transformed cell does not necessarily result in an increased level of expression of the polypeptide." (Page 5 of the Office Action mailed September 22, 2005). In support of this assertion the Examiner has cited references by Pennica *et al.* and Konopka *et al.*

Appellants submit that Pennica *et al.* does <u>not</u> show a lack of correlation between gene (DNA) amplification and mRNA levels. According to Pennica *et al.,* "WISP-1 gene

-18-

amplification in human colon tumors showed a correlation between DNA amplification and over-expression, whereas overexpression of WISP-3 RNA was seen in the absence of DNA amplification. In contrast, WISP-2 DNA was amplified in colon tumors, but its mRNA expression was significantly reduced in the majority of tumors compared with expression in normal colonic mucosa from the same patient" (Abstract). From this, the Examiner correctly concludes that increased copy number does not *necessarily* result in increased polypeptide expression. The standard, however, is not absolute certainty.

In fact, as noted even in Pennica *et al.*, "[a]n analysis of *WISP*-1 gene amplification and expression in human colon tumors *showed a correlation between DNA amplification and over-expression...*" (Pennica *et al.*, page14722, left column, first full paragraph, emphasis added). Thus the findings of Pennica *et al.* with respect to WISP-1 support Appellants' arguments. In the case of WISP-3, the authors report that there was no change in the DNA copy number, but there was a change in mRNA levels. This apparent lack of correlation between DNA and mRNA levels is not contrary to Appellants' assertion that a change in DNA copy number generally leads to a change in mRNA level. Appellants are not attempting to predict the DNA copy number based on changes in mRNA level, and Appellants have not asserted that the only means for changing the level of mRNA is to change the DNA copy number. Therefore a change in mRNA without a change in DNA copy number is not contrary to Appellants' assertions.

The fact that the single WISP-2 gene did not show the expected correlation of gene amplification with the level of mRNA/protein expression does not establish that it is more likely than not, in general, that such correlation does not exist. The Examiner has not shown whether the lack or correlation observed for the WISP-2 gene is typical, or is merely a discrepancy, an exception to the rule of correlation. More importantly, the teaching of Pennica *et al.* is specific to *WISP* genes. Pennica *et al.* has no teaching whatsoever about the correlation of gene amplification and protein expression in general.

Appellants next respectfully submit that, contrary to the PTO's assertions, Konopka *et al.* supports Appellants' position that mRNA levels correlate with protein levels. Konopka *et al.* states that "the 8-kb mRNA that encodes $P210^{c\text{-abl}}$ was detected at a 10-fold higher level in SK-CML7bt-333 (Fig. 3A, +) than in SK-CML16Bt-1 (B, +), which **correlated** with the relative

-19-

On Appeal to the Board of Patent Appeals and Interferences
Appeal Brief
Application Serial No. 10/006,856
Attorney's Docket No. 39780-2830 P1C14

level of P210$^{c\text{-}abl}$ detected in each cell line. Analysis of additional cell lines demonstrated that the level of 8-kb mRNA **directly correlated** with the level of P210$^{c\text{-}abl}$ (Table 1)" (page 4050, col. 2, emphasis added).

Nor does Konopka *et al.* support the PTO's position that DNA amplification is not correlated with mRNA or protein overexpression. Konopka *et al.* show only that, of the cell lines known to have increased abl protein expression, only one had amplification of the abl gene (page 4051, col. 1). This result proves only that increased mRNA and protein expression levels can result from causes <u>other</u> than gene amplification. Konopka *et al.* do <u>not</u> demonstrate that when gene amplification <u>does</u> occur, it does not result in increased mRNA and protein expression levels, particularly given that the cell line with amplification of the abl gene <u>did</u> show increased abl mRNA and protein expression levels.

In summary, Appellants respectfully submit that the Examiner has <u>not</u> shown that a change in gene expression level in tumor as compared to normal tissue is not correlated with a change in protein expression. Since, as discussed above, the standard is <u>not</u> absolute certainty, a *prima facie* showing of lack of utility has not been made in this instance. The Patent Office has failed to meet its initial burden of proof that Appellants' claims of utility are not substantial or credible. The arguments presented by the Examiner in combination with the Pennica *et al.* and Konopka *et al.* articles do not provide sufficient reasons to doubt the statements by Appellants that PRO1303 has utility. The law does not require that gene amplification "necessarily" results in increased expression at the mRNA and polypeptide levels. Therefore, Appellants submit that the Examiner's reasoning is based on a misrepresentation of the scientific data presented in the above cited references and application of an improper, heightened legal standard. In fact, contrary to what the Examiner contends, the art indicates that, if a gene is amplified in cancer, it is more likely than not that the encoded protein will be expressed at an elevated level.

2. *It is "more likely than not" for amplified genes to have increased mRNA and protein levels*

Appellants respectfully submit that there are numerous articles which show that generally, if a gene is amplified in cancer, it is more likely than not that the encoded protein will be expressed at an elevated level. For example, Orntoft *et al.* (*Mol. and Cell. Proteomics*, 2002,

vol. 1, pages 37-45 - made of record in Appellants' Response filed June 29, 2005) studied transcript levels of 5600 genes in malignant bladder cancers, many of which were linked to the gain or loss of chromosomal material using an array-based method. Orntoft *et al.* showed that there was a gene dosage effect and taught that "in general (18 of 23 cases) chromosomal areas with more than 2-fold gain of DNA showed a corresponding increase in mRNA transcripts" (see column 1, abstract). In addition, Hyman *et al.* (*Cancer Res.*, 2002, vol. 62, pages 6240-45 - made of record in Appellants' Response filed June 29, 2005) showed, using CGH analysis and cDNA microarrays which compared DNA copy numbers and mRNA expression of over 12,000 genes in breast cancer tumors and cell lines, that there was "evidence of a prominent global influence of copy number changes on gene expression levels." (See page 6244, column 1, last paragraph). Additional supportive teachings were also provided by Pollack *et al.*, (*PNAS*, 2002, vol. 99, pages 12963-12968 - made of record in Appellants' Response filed June 29, 2005) who studied a series of primary human breast tumors and showed that "...62% of highly amplified genes show moderately or highly elevated expression, and DNA copy number influences gene expression across a wide range of DNA copy number alterations (deletion, low-, mid- and high-level amplification), and that on average, a 2-fold change in DNA copy number is associated with a corresponding 1.5-fold change in mRNA levels." Thus, these articles collectively teach that in general, gene amplification increases mRNA expression.

In addition, in their Response filed June 29, 2005, Appellants submitted a Declaration by Dr. Polakis, principal investigator of the Tumor Antigen Project of Genentech, Inc., the assignee of the present application, to show that mRNA expression correlates well with protein levels, in general. As Dr. Polakis explains, the primary focus of the microarray project was to identify tumor cell markers useful as targets for both the diagnosis and treatment of cancer in humans. The scientists working on the project extensively rely on results of microarray experiments in their effort to identify such markers. As Dr. Polakis explains, using microarray analysis, Genentech scientists have identified approximately 200 gene transcripts (mRNAs) that are present in human tumor cells at significantly higher levels than in corresponding normal human cells. To the date of the Declaration, they have generated antibodies that bind to about 30 of the tumor antigen proteins expressed from these differentially expressed gene transcripts and have

used these antibodies to quantitatively determine the level of production of these tumor antigen proteins in both human cancer cells and corresponding normal cells. Having compared the levels of mRNA and protein in both the tumor and normal cells analyzed, they found a very good correlation between mRNA and corresponding protein levels. Specifically, in approximately 80% of their observations they have found that increases in the level of a particular mRNA correlates with changes in the level of protein expressed from that mRNA. While the proper legal standard is to show that the existence of correlation between mRNA and polypeptide levels is more likely than not, the showing of approximately 80% correlation for the molecules tested according to the Polakis Declaration greatly exceeds this legal standard. Based on these experimental data and his vast scientific experience of more than 20 years, Dr. Polakis states that, for human genes, increased mRNA levels typically correlate with an increase in abundance of the encoded protein. He further confirms that "it remains a central dogma in molecular biology that increased mRNA levels are predictive of corresponding increased levels of the encoded protein."

The Examiner has asserted that "[f]rom the uncertainty in the cited art concerning the correlation between gene amplification and gene product overexpression, one of ordinary skill in the art would doubt the alleged utility because in the absence of information showing the correlation, one would doubt that the correlation exists." (Pages 13-14 of the Office Action mailed September 22, 2005). In particular, the Examiner has asserted that the cited art (specifically, the Pollack *et al.* paper) showing that 62% of highly amplified genes show moderately or highly elevated expression "very much shows the uncertainty in the art concerning the correlation of DNA copy number and RNA expression." (Page 14 of the Office Action mailed September 22, 2005). The Examiner has further asserted that the data cited in the Polakis Declaration showing that 80% of the time there was a correlation between mRNA and corresponding protein levels "shows the uncertainty in the art whether there is any correlation between overexpressed RNA and overexpressed protein." (Page 15 of the Office Action mailed September 22, 2005). The Examiner concluded that the actual level of correlation is 62% multiplied by 80%, or about 50%.

Appellants respectfully submit that Pollack *et al.* state that "we are likely underestimating the contribution of DNA copy number changes to altered gene expression" (page 12967, col. 2),

-22-

indicating that the 62% number cited by the Examiner is <u>most probably an underestimate</u>. This conclusion is consistent with the results presented by Orntoft *et al.*, who found that the level of correlation between DNA copy number and increased mRNA levels was from **77-80%** (page 40, col. 2). Orntoft *et al.* also found a "highly significant" correlation between mRNA and protein levels, with the two data sets studied having correlations of 39/40 (98%) and 19/26 (73%). This data is consistent with the 80% correlation noted in the Polakis Declaration.

Appellants note that the Hyman reference "found 44% of highly amplified genes showing overexpression at the mRNA level." However, in the more detailed discussion of their results, Hyman *et al.* teach that "[u]p to 44% of the highly amplified transcripts (CGH ratio, >2.5) were overexpressed (*i.e.,* **belonged to the global upper 7% of expression ratios**) compared with only 6% for genes with normal copy number." (See page 6242, col. 1; emphasis added). These details make it clear that Hyman *et al.* set <u>a highly restrictive standard</u> for considering a gene to be overexpressed; yet <u>almost half of all highly amplified genes met even this highly restrictive standard</u>. Therefore, the analysis performed by Hyman *et al.* clearly shows that "it is more likely than not" that a gene which is amplified in tumor cells will have increased gene expression.

Appellants also respectfully point out that the Examiner's calculation of DNA/protein correlation by taking the product of the (underestimated) DNA/mRNA correlation and the mRNA/protein correlation is not valid because <u>not all mRNA amplification is the result of gene copy number increases</u>. Transcripts that are elevated due to other mechanisms may be less likely to result in increased protein levels, and thus would bring down the average correlation. Even if this calculation is accurate, Appellants respectfully note that taking a more accurate correlation for DNA/mRNA of 79%, as observed by Orntoft *et al.*, leads to an overall correlation for DNA with protein levels of 63%, which is certainly <u>more likely than not</u>.

Accordingly, since the standard is <u>not</u> absolute certainty, a *prima facie* showing of lack of utility has not been made in this instance and the burden to provide further evidence of utility has not shifted to Appellants. Taken together, although there are some examples in the scientific art that do not fit within the central dogma of molecular biology that there is a correlation between polypeptide and mRNA levels, these instances are exceptions rather than the rule. <u>In the vast majority of amplified genes</u>, the teachings in the art, as exemplified by Orntoft *et al.,* Hyman *et*

-23-

al., Pollack *et al.,* and the Polakis declaration, overwhelmingly show that gene amplification influences gene expression at the mRNA and protein levels.

Thus, one of skill in the art would reasonably expect in this instance, based on the amplification data for the PRO1303 gene, that the PRO1303 protein is concomitantly overexpressed. Accordingly, one skilled in the art at the time the application was filed would have understood that the claimed PRO1303 polypeptide had utility in, for example, the diagnosis of cancer, and would have known exactly how to use the claimed polypeptides without any undue experimentation.

3. *Even if a prima facie case of lack of utility had been established, it should be withdrawn on consideration of the totality of evidence*

Even if one assumes *arguendo* that it is more likely than not that there is no correlation between gene amplification and increased mRNA/protein expression, a polypeptide encoded by a gene that is amplified in cancer would still have a specific and substantial utility. In support, Appellants particularly draw the Board's attention to page 2 of the Declaration by Dr. Ashkenazi (submitted with Appellants' Response filed June 29, 2005) which explains that:

> even when amplification of a cancer marker gene does not result in significant over-expression of the corresponding gene product, this very absence of gene product over-expression still provides significant information for cancer diagnosis and treatment. Thus, if over-expression of the gene product does not parallel gene amplification in certain tumor types but does so in others, then parallel monitoring of gene amplification and gene product over-expression enables more accurate tumor classification and hence better determination of suitable therapy. In addition, absence of over-expression is crucial information for the practicing clinician. If a gene is amplified but the corresponding gene product is not over-expressed, the clinician accordingly will decide not to treat a patient with agents that target that gene product.

Appellants thus submit that simultaneous testing of gene amplification and gene product over-expression enables more accurate tumor classification, even if the gene-product, the protein, is not over-expressed. This leads to better determination of a suitable therapy. Further, as explained in Dr. Ashkenazi's Declaration, absence of over-expression of the protein itself is crucial information for the practicing clinician. If a gene is amplified in a tumor, but the corresponding gene product is not over-expressed, the clinician will decide not to treat a patient

-24-

with agents that target that gene product. This not only saves money, but also the patient need not be exposed to the side effects associated with such agents.

This is further supported by the teachings of the article by Hanna and Mornin (submitted with Appellants' Response filed June 29, 2005). The article teaches that the HER-2/neu gene has been shown to be amplified and/or over-expressed in 10%-30% of invasive breast cancers and in 40%-60% of intraductal breast carcinoma. Further, the article teaches that diagnosis of breast cancer includes testing both the amplification of the HER-2/neu gene (by FISH) as well as the over-expression of the HER-2/neu gene product (by IHC). Even when the protein is not over-expressed, the assay relying on both tests leads to a more accurate classification of the cancer and a more effective treatment of it.

Therefore, Appellants respectfully submit that the gene amplification data provided in the present application, as discussed above, are sufficient to establish a specific, substantial and credible utility for the PRO1303 polypeptide, for example, to be used as a diagnostic marker of human lung or colon cancer.

Accordingly, given that the specification discloses <u>at least one patentable utility</u> for the claimed PRO1303 polypeptides, Appellants respectfully request reconsideration and reversal of the rejection of Claims 28-35 and 38-40 under 35 U.S.C. §101.

<u>ISSUE II: Claims 28-35 and 38-40 satisfy the enablement requirement of 35 U.S.C. §112, first paragraph.</u>

Claims 28-35 and 38-40 stand rejected under 35 U.S.C. §112, first paragraph, allegedly "since the claimed invention is not supported by either a specific and substantial asserted utility or a well established utility for the reasons set forth above, one skilled in the art clearly would not know how to use the claimed invention." (Page 10 of the Office Action mailed March 31, 2005).

In this regard, Appellants refer to the arguments and information presented above in response to the outstanding rejection under 35 U.S.C. §101, wherein those arguments are incorporated by reference herein. Appellants respectfully submit that as described above, the PRO1303 polypeptides have utility in the treatment of disorders for which modulation of glucose uptake by adipocytes would be beneficial, such as obesity, diabetes, and hyper- or hypo-

-25-

insulinemia, and based on such a utility, one of skill in the art would know exactly how to use the claimed polypeptides without undue experimentation.

In addition, Appellants respectfully submit that as described above, the PRO1303 polypeptides also have utility in the diagnosis of cancer and based on such a utility, one of skill in the art would know exactly how to use the claimed polypeptides for diagnosis of cancer, without undue experimentation.

Accordingly, Appellants respectfully request reconsideration and reversal of the enablement rejection of Claims 28-35 and 38-40 under 35 U.S.C. §112, first paragraph.

CONCLUSION

For the reasons given above, Appellants submit that the adipocyte glucose/FFA uptake assay disclosed in Example 149 of the specification provides at least one asserted specific and substantial patentable utility for the claimed PRO1303 polypeptides, and that one of ordinary skill in the art would accept this asserted utility as credible and would understand how to make and use the claimed polypeptides. In addition, the gene amplification results disclosed in Example 143 <u>also</u> provide a specific and substantial patentable utility for the claimed PRO1303 polypeptides and based upon these results one of ordinary skill in the art would understand how to used the claimed polypeptides in the diagnosis of lung and colon tumors.
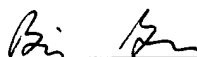
Therefore, Claims 28-35 and 38-40 meet the requirements of 35 U.S.C. §101 and 35 U.S.C. §112, first paragraph.

Accordingly, reversal of all the rejections of Claims 28-35 and 38-40 is respectfully requested.

Please charge any additional fees, including fees for additional extension of time, or credit overpayment to Deposit Account No. **08-1641** (referencing Attorney's Docket No. **39780-2830 P1C14**).

Respectfully submitted,

Date: April 24, 2006

By: _____
Barrie D. Greene (Reg. No. 46,740)

HELLER EHRMAN LLP
275 Middlefield Road
Menlo Park, California 94025-3506
Telephone: (650) 324-7000
Facsimile: (650) 324-0638

-27-

8. CLAIMS APPENDIX

Claims on Appeal

28. An isolated polypeptide having at least 80% amino acid sequence identity to:

(a)   the amino acid sequence of the polypeptide of SEQ ID NO:194;

(b)   the amino acid sequence of the polypeptide of SEQ ID NO:194, lacking its associated signal peptide;

(c)   the amino acid sequence of the polypeptide encoded by the full-length coding sequence of the cDNA deposited under ATCC accession number 203232;

wherein the polypeptide stimulates the uptake of glucose or FFA (free fatty acid) by adipocyte cells.

29. The isolated polypeptide of Claim 28 having at least 85% amino acid sequence identity to:

(a)   the amino acid sequence of the polypeptide of SEQ ID NO:194;

(b)   the amino acid sequence of the polypeptide of SEQ ID NO:194, lacking its associated signal peptide;

(c)   the amino acid sequence of the polypeptide encoded by the full-length coding sequence of the cDNA deposited under ATCC accession number 203232;

wherein the polypeptide stimulates the uptake of glucose or FFA (free fatty acid) by adipocyte cells.

30. The isolated polypeptide of Claim 28 having at least 90% amino acid sequence identity to:

(a)   the amino acid sequence of the polypeptide of SEQ ID NO:194;

(b)   the amino acid sequence of the polypeptide of SEQ ID NO:194, lacking its associated signal peptide;

(c)   the amino acid sequence of the polypeptide encoded by the full-length coding sequence of the cDNA deposited under ATCC accession number 203232;

wherein the polypeptide stimulates the uptake of glucose or FFA (free fatty acid) by adipocyte cells.

31.   The isolated polypeptide of Claim 28 having at least 95% amino acid sequence identity to:

(a)   the amino acid sequence of the polypeptide of SEQ ID NO:194;

(b)   the amino acid sequence of the polypeptide of SEQ ID NO:194, lacking its associated signal peptide;

(c)   the amino acid sequence of the polypeptide encoded by the full-length coding sequence of the cDNA deposited under ATCC accession number 203232;

wherein the polypeptide stimulates the uptake of glucose or FFA (free fatty acid) by adipocyte cells.

32.   The isolated polypeptide of Claim 28 having at least 99% amino acid sequence identity to:

(a)   the amino acid sequence of the polypeptide of SEQ ID NO:194;

(b)   the amino acid sequence of the polypeptide of SEQ ID NO:194, lacking its associated signal peptide;

(c)   the amino acid sequence of the polypeptide encoded by the full-length coding sequence of the cDNA deposited under ATCC accession number 203232;

wherein the polypeptide stimulates the uptake of glucose or FFA (free fatty acid) by adipocyte cells.

33.   An isolated polypeptide comprising:

(a)   the amino acid sequence of the polypeptide of SEQ ID NO:194;

(b)   the amino acid sequence of the polypeptide of SEQ ID NO:194, lacking its associated signal peptide;

(c)   the amino acid sequence of the polypeptide encoded by the full-length coding sequence of the cDNA deposited under ATCC accession number 203232.

34.   The isolated polypeptide of Claim 33 comprising the amino acid sequence of the polypeptide of SEQ ID NO:194.

35.   (The isolated polypeptide of Claim 33 comprising the amino acid sequence of the polypeptide of SEQ ID NO:194, lacking its associated signal peptide.

38.   The isolated polypeptide of Claim 33 comprising the amino acid sequence of the polypeptide encoded by the full-length coding sequence of the cDNA deposited under ATCC accession number 203232.

39.   A chimeric polypeptide comprising a polypeptide according to Claim 28 fused to a heterologous polypeptide.

40.   The chimeric polypeptide of Claim 39, wherein said heterologous polypeptide is an epitope tag or an Fc region of an immunoglobulin.

9. EVIDENCE APPENDIX

1. Tafuri, S.R., "Troglitazone Enhances Differentiation, Basal Glucose Uptake, and Glut 1 Protein Levels in 3T3-L1 Adipocytes," Endocrinology, 137:4706-4712 (1996).

2. Sandouk, T., et al., "The Antidiabetic Agent Pioglitazone Increases Expression of Glucose Transporters in 3T3-F442A Cells by Increasing Messenger Ribonucleic Acid Transcript Stability", Endocrinology 133:352-359 (1993).

3. Goldwaser, I., et al., "L-Glutamic Acid γ-Monohydroxamate: A potentiator of vanadium-evoked glucose metabolism *in vitro* and *in vivo*", J. Biol. Chem. 274:26617-26624 (1999).

4. Mueller, W. M., et al., "Evidence That Glucose Metabolism Regulates Leptin Secretion from Cultured Rat Adipocytes", Endocrinology 139:551-558 (1998).

5. Mueller, W. M., et al., "Effects of Metformin and Vanadium on Leptin Secretion from Cultured Rat Adipocytes", Obesity Research 8:530-539 (2000).

6. Orntoft, T.F., et al., "Genome-wide Study of Gene Copy Numbers, Transcripts, and Protein Levels in Pairs of Non-Invasive and Invasive Human Transitional Cell Carcinomas," *Molecular & Cellular Proteomics* 1:37-45 (2002).

7. Hyman, E., et al., "Impact of DNA Amplification on Gene Expression Patterns in Breast Cancer," *Cancer Research* **62**:6240-6245 (2002).

8. Pollack, J.R., et al., "Microarray Analysis Reveals a Major Direct Role of DNA Copy Number Alteration in the Transcriptional Program of Human Breast Tumors," *Proc. Natl. Acad. Sci. USA* **99**:12963-12968 (2002).

9. Hanna, J.S., et al., "HER-2/neu Breast Cancer Predictive Testing," Pathology Associates Medical Laboratories (1999).

10. Declaration of Audrey D. Goddard, Ph.D. under 37 C.F.R. §1.132, with attached Exhibits A-G:

A. Curriculum Vitae of Audrey D. Goddard, Ph.D.

B. Higuchi, R. et al., "Simultaneous amplification and detection of specific DNA sequences," *Biotechnology* **10**:413-417 (1992).

C. Livak, K.J., et al., "Oligonucleotides with fluorescent dyes at opposite ends provide a quenched probe system useful for detecting PCR product and nucleic acid hybridization," *PCR Methods Appl.* **4**:357-362 (1995).

D. Heid, C.A. et al., "Real time quantitative PCR," *Genome Res.* **6**:986-994 (1996).

E. Pennica, D. et al., "WISP genes are members of the connective tissue growth factor family that are up-regulated in Wnt-1-transformed cells and aberrantly expressed in human colon tumors," *Proc. Natl. Acad. Sci. USA* **95**:14717-14722 (1998).

F. Pitti, R.M. et al., "Genomic amplification of a decoy receptor for Fas ligand in lung and colon cancer," *Nature* **396**:699-703 (1998).

G. Bieche, I. et al., "Novel approach to quantitative polymerase chain reaction using real-time detection: Application to the detection of gene amplification in breast cancer," *Int. J. Cancer* **78**:661-666 (1998).

11. Declaration of Paul Polakis, Ph.D. under 37 C.F.R. §1.132.

12. Declaration of Avi Ashkenazi, Ph.D. under 37 C.F.R. §1.132; with attached Exhibit A (Curriculum Vitae).

13. Konopka, J.B. et al., "Variable expression of the translocated c-abl oncogene in Philadelphia-chromosome-positive B-lymphoid cell lines from chronic myelogenous leukemia patients," *Proc. Natl. Acad. Sci. USA* **83**:4049-4052 (1986).

14. Pennica, D. et al., "WISP genes are members of the connective tissue growth factor family that are up-regulated in Wnt-1-transformed cells and aberrantly expressed in human colon tumors," *Proc. Natl. Acad. Sci. USA* **95**:14717-14722 (1998).

15. Fabris, R. et al., "Preferential channeling of energy fuels toward fat rather than muscle during high free fatty acid availability in rats," *Diabetes*, **50**:601-608 (2001).

-32-

16. Santomauro, A. T. M. G. et al., "Overnight lowering of free fatty acids with Acipimox improves insulin resistance and glucose tolerance in obese diabetic and nondiabetic subjects," *Diabetes* **48**:1836-1841 (1999).

17. Frohnert, B. I. et al., "Identification of a functional peroxisome proliferator-responsive element in the murine fatty acid transport protein gene," *J. Biol. Chem.* **274**:3970-3977 (1999).

18. Martin, G. et al., "Coordinate regulation of the expression of the fatty acid transport protein and acyl-CoA syntetase genes by $PPAR\alpha$ and $PPAR\gamma$ activators," *J. Biol. Chem.* **272**:28210-28217 (1997).

Items 1-9 were made of record by Appellants in their IDS filed June 29, 2005, and were initialed as considered by the Examiner on September 19, 2005.

Items 10-12 were submitted with Appellants' Response filed June 29, 2005, and made of record by the Examiner in the Office Action mailed September 22, 2005.

Items 13-16 were made of record by the Examiner in the Office Action mailed March 31, 2005.

Items 17-18 were submitted with Appellants' Response filed December 14, 2005, and considered in the Advisory Action mailed January 25, 2006.

10. RELATED PROCEEDINGS APPENDIX

None.

Troglitazone Enhances Differentiation, Basal Glucose Uptake, and Glut1 Protein Levels in 3T3-L1 Adipocytes

SHERRIE R. TAFURI

Department of Cell Biology, Parke-Davis Pharmaceutical Research Division, Warner-Lambert Co.,
Ann Arbor, Michigan 48105

ABSTRACT

Troglitazone is a member of the thiazolidinedione class of compounds, which act as insulin-sensitizing agents when administered to human patients and animal models displaying noninsulin-dependent diabetes mellitus. In Zucker rats, the antidiabetic activity is associated with increased glucose uptake in adipose tissue. To understand the direct effects troglitazone has on adipocyte metabolism, 3T3-L1 preadipocytes and adipocytes were treated with the compound. The addition of troglitazone enhanced the rate and percent differentiation of fibroblasts to adipocytes. Northern analysis indicated that during differentiation, expression of the adipocyte-specific transcription factor, CCAAT enhancer binding protein-α, increased more rapidly in troglitazone-treated cells, but did not change in fully differentiated adipocytes. To assess the metabolic consequences of troglitazone treatment, both basal and insulin-stimulated glucose uptake were monitored in treated cells. Troglitazone treatment increased basal glucose transport 1.5- to 2.0-fold, whereas insulin-stimulated uptake was unaffected. Enhanced basal transport was caused by an increased synthesis of both Glut1 glucose transporter messenger RNA and protein. These results suggest the possibility that in vivo, the troglitazone-dependent increase in glucose disposal may be attributable in part to modifications in the expression of Glut1 in insulin-responsive tissues. (Endocrinology 137: 4706–4712, 1996)

N ONINSULIN-DEPENDENT diabetes mellitus (NIDDM), the most common form of diabetes, is estimated to affect more than 4 million people in the United States (1). This disease commonly develops during middle age and is characterized by hyperglycemia, hyperinsulinemia, and insulin resistance. At present, treatment consists of behavioral modifications in conjunction with the administration of insulin and oral hypoglycemic agents (sulfonylureas and biguanide compounds). However, these treatments often fail to ameliorate one of the main underlying causes of the disease, insulin resistance. The thiazolidinediones, a new class of compounds, differ markedly from other antidiabetic agents in that they decrease hyperglycemia and hyperinsulinemia by increasing insulin sensitivity in target tissues. These compounds increase peripheral glucose uptake while decreasing insulin secretion and gluconeogenesis in a wide variety of type II animal models (2–4). Troglitazone, a member of this compound class, improves glucose tolerance and insulin sensitivity in both diabetic (5, 6) and glucose-intolerant (7) patients. Little is known about the biochemical mechanism of action of these compounds.

Adipose tissue is highly responsive to insulin. Its primary role is to store energy when nutrients are plentiful and to release energy during fasting and starvation. Adipose tissue also plays a pivotal role in metabolic homeostasis. Adipose tissue is responsible for 50–70% of lactate production in the adult and consequently contributes to the regulation of glycogen synthesis and gluconeogenesis (8). Moreover, the recent discovery of the ob gene product indicates that adipose tissue secretes hormones capable of regulating feeding patterns, satiety, and adiposity (9). Because of the importance of adipose tissue in metabolic regulation and insulin resistance, it may play an important role in the mechanism of action of thiazolidinediones.

To understand if and how the thiazolidinediones affect adipose cell metabolism, a study was designed to determine how troglitazone affects glucose utilization in 3T3-L1 adipocytes. This system was chosen because it is easily manipulated and is not complicated by the problems associated with the metabolic feedback loops present in vivo. Additionally, previous experiments with pioglitazone, another member of the thiazolidinedione family, in 3T3-F442A adipose cells suggested that these compounds increase differentiation (10, 11) and glucose uptake (12) in adipocytes. In the studies discussed here, troglitazone increased differentiation in 3T3-L1 cells when administered at the initiation of the differentiation protocol. Furthermore, troglitazone enhanced glucose uptake in these cells by altering the total number of basal glucose transporters within the cell.

Materials and Methods

Materials

3T3-L1 cells were obtained from the American Type Tissue Culture Collection (Rockville, MD). High glucose DMEM culture medium and bovine serum were purchased from Life Technologies (Gaithersburg, MD). Insulin, dexamethasone, and isomethylbutylxanthine were purchased from Sigma Chemical Co. (St. Louis, MO). Troglitazone and pioglitazone were synthesized by Parke-Davis (Ann Arbor, MI) and Sankyo (Tokyo, Japan), respectively.

Cell culture

3T3-L1 fibroblasts were grown and passaged in DMEM containing 10% FBS. For adipocyte differentiation, 2 day postconfluent cells were placed in 10% FBS-DMEM, 1 μg/ml insulin, 0.25 μM dexamethasone,

and 0.5 mM isomethylbutylxanthine. Forty-eight hours later, the medium was changed to 10% FBS-DMEM containing 1 μg/ml insulin, and after an additional 48 h, the medium was replaced with 10% FBS-DMEM. Thereafter, the medium was changed every 2 days. Troglitazone was dissolved in dimethylsulfoxide as a 1000-fold stock solution and administered at the initiation of differentiation and with every medium change unless otherwise indicated.

Glucose uptake

Basal glucose uptake was measured using a modified version of the hexose transport procedure described by de Herreros and Birnbaum (13). Briefly, cells were washed with PBS and placed in glucose-free DMEM containing 1% BSA for 30 min at 37 C. At this time, 1 μCi/ml [^{14}C]2-deoxyglucose and 1 mM glucose were added, and the cells were incubated for 30 min at 22 C. Subsequently, the cells were washed with PBS and 10 mM glucose at 4 C and lysed with 0.5 N NaOH. The lysates were neutralized with acetic acid and counted. To measure insulin-stimulated glucose uptake, cells were serum starved for 3 h before initiation of the assay. Stimulation with insulin (1 × 10^{-6} M) was initiated 15 min before the addition of labeled glucose.

RNA preparation, Northern blot analysis, and ribonuclease (RNase) protection assays

The guanidinium lysis method (Ultraspec RNA isolation system, Biotecx, Houston, TX) was used to prepare RNA samples. For Northern analysis, 15–30 μg RNA/sample were resolved on an 0.8–1% agarose formaldehyde gel and transferred to nitrocellulose. The blots were hybridized in 1 M NaCl, 1% SDS, and 10% dextran sulfate for 16–20 h at 42 C. Washes were conducted in 0.1 × SSC (standard saline citrate)–0.1% SDS at 50 C. The indicated complementary DNAs were labeled with [α-^{32}P]deoxy-CTP using the random prime method and used as probes. RNase protection assays were performed using the RNase A nuclease assay according to manufacturer's instructions (Ambion, Houston, TX). [α-^{32}P]UTP-labeled singled stranded RNA probes were generated using T3/T7 in vitro transcription procedures. All results were quantitated using a Molecular Dynamics PhosphorImager (Sunnyvale, CA).

Western blot analysis

Cell lysates were prepared in HNTG buffer (50 mM HEPES, 150 mM NaCl, 1% Triton X-100, 10% glycerol, and 1 mM EDTA). The Bio-Rad protein analysis system (Bio-Rad Laboratories, Richmond, CA) was used to determine protein content. Western blots were performed using standard protocols. Antibody interactions were detected using the chemiluminescent assay (ECL, Amersham, Arlington Heights, IL). The Glut1 antibody was produced using a glutathione S-transferase fusion protein encoding the last 39 amino acids of the Glut1 glucose transporter. The antibody was immunoaffinity purified and shown not to cross-react with purified Glut4 glucose transporter protein. The Glut4-specific antibody was kindly provided by Dr. Michael Mueckler.

Results

Troglitazone enhances adipocyte differentiation in 3T3-L1 cells

The differentiation of 3T3-L1 preadipocytes into adipocytes is a complex process that is affected by cell passage number and a variety of environmental conditions. Under ideal conditions, 95–100% of confluent preadipocytes can be converted into fat droplet-containing adipocytes in 5–7 days, with fat droplets first appearing on day 4. However, as the preadipocytes are passaged, the efficiency of differentiation diminishes in a clonal manner, such that a confluent plate will contain islands of adipocytes within undifferentiated fibroblasts. This loss of phenotype is also associated with a decrease in the rate of differentiation, causing the initial appearance of fat droplets to occur around day 5 or 6. Initial experiments were conducted using cells with an adipocyte

conversion frequency of approximately 50%. To study the effects of troglitazone on differentiation, 0.5–5 μM compound was added with 167 nM insulin, 0.25 μM dexamethasone, and 0.5 mM isomethylbutylxanthine (hormone cocktail) at the initiation of differentiation and reapplied with each medium change. Eight-day troglitazone treatment without hormone cocktail showed minimal differentiation (Fig. 1, A and B). Less than 1% of the cells became adipocytes; however, the number of adipocytes in the drug-treated sample was greater than that in the untreated sample. In the presence of hormone cocktail, troglitazone significantly enhanced the percentage of adipocyte differentiation (Fig. 1, C and D). Nearly 100% of treated cells contained fat droplets compared to 50% of the untreated group. Additionally, the rate of differentiation was enhanced as fat droplets began to accumulate in the treated group 1 day before the control group.

Adipocyte differentiation has been shown to be dependent upon the activation of several transcription factors, which, in turn, initiate the expression of a repertoire of adipocyte genes. One such factor, CCAAT enhancer binding protein-α (C/EBPα), has been shown to be necessary and sufficient for adipocyte conversion in both preadipocyte and fibroblast cell lines (14–17). Moreover, mice lacking C/EBPα expression fail to accumulate both white and brown fat, suggesting that C/EBPα is required for terminal adipoctye differentiation (18). C/EBPα mRNA is not expressed in preadipocytes, is induced 2–3 days after the initiation of differentiation, and is maintained at a high level in the adipocyte (19). As troglitazone increases adipocyte differentiation, total RNA was isolated from differentiating cells treated with hormone cocktail containing 0 or 5 μM troglitazone and probed with labeled C/EBPα complementary DNA to determine whether troglitazone enhances C/EBPα expression. The control cells used in this experiment differentiated 95–100% without the
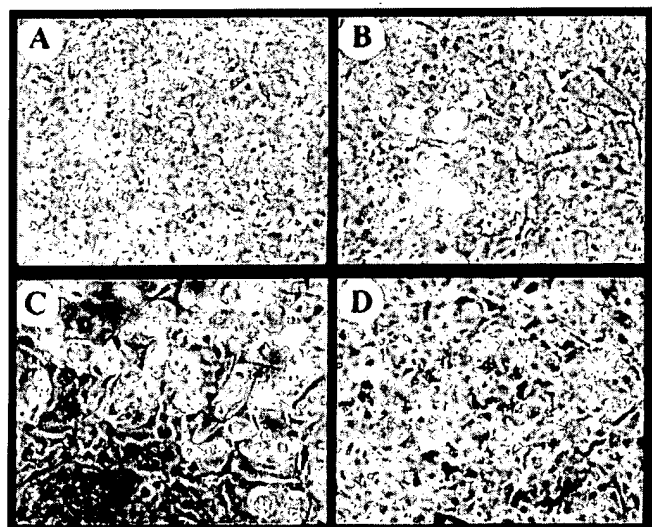

FIG. 1. Troglitazone enhances the differentiation of 3T3-L1 preadipocytes to adipocytes. Confluent preadipocytes were maintained in culture for 8 days without compound (A) or with 5 μM troglitazone (B), as described in Materials and Methods. Identical cells were treated with differentiation cocktail (167 nM insulin, 0.25 μM dexamethasone, and 0.5 mM isomethylbutylxanthine) with (D) or without (C) 5 μM troglitazone.

addition of drug; therefore, the ratio of adipocytes/preadipocytes in the drug-treated and untreated samples was identical. As shown in Fig. 2, troglitazone increased the rate of C/EBPα mRNA accumulation during differentiation, but did not affect the levels of C/EBPα message after differentiation was complete. At 48 h, treated cells contained 2.5 times the level of C/EBPα mRNA found in control cells. Conversely, the levels on day 6 were nearly identical in both samples. Multiple experiments demonstrated that the onset of C/EBPα expression varied with the passage number of the cells; however, in all cases troglitazone enhanced the rate of C/EBPα expression. This suggests that troglitazone influences factors that regulate when C/EBPα mRNA production is induced, but not those that modulate the total amount of C/EBPα mRNA expressed.

Troglitazone increases basal glucose uptake in differentiated adipocytes

To determine whether troglitazone has a direct effect on glucose metabolism in the adipocytes, the 3T3-L1 tissue culture system was used to mimic adipocyte function in a controlled environment. Initial experiments were performed using 3T3-L1 cells, which showed a 35% conversion frequency without troglitazone. Cells were differentiated under standard conditions with or without troglitazone for 8 days, as described in Materials and Methods. On day 9, basal glucose uptake was assessed by monitoring the accumulation of [¹⁴C]deoxyglucose within the adipocytes. As shown in Fig. 3, 0.5 μM troglitazone treatment enhanced basal glucose uptake 9.6-fold in these cells. No effect was observed if cells were
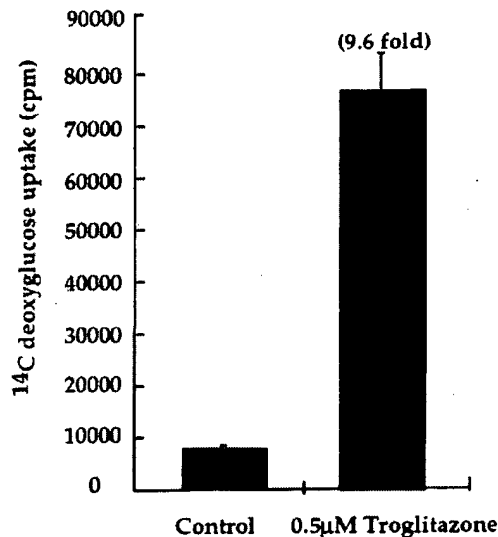
FIG. 3. Troglitazone treatment in combination with insulin increases basal glucose uptake in adipocytes. Adipocytes were differentiated using 100 nM insulin in combination with 0.25 μM dexamethasone and 0.5 mM isomethylbutylxanthine. After 8 days, the cell [¹⁴C]deoxyglucose uptake was monitored, as described in Materials and Methods. The values were obtained from duplicate samples. When assayed, the control cells exhibited 10% differentiation, whereas the troglitazone-treated cells showed 80% differentiation.

treated without the addition of the hormone cocktail (data not shown). This suggests that troglitazone increases the activity or number of functional glucose transporters per cell, or both.

Noninsulin-dependent (basal) glucose uptake is a result of transport through the membrane-associated Glut1 glucose transporter, whereas insulin-stimulated glucose uptake results from the combined activities of Glut1 and the hormone-sensitive glucose transporter, Glut4, which are associated with both the plasma membrane and microsomal compartments. Comparison studies have shown that the levels of these two glucose transporter proteins differ between preadipocytes and adipocytes (13, 20, 21) (see Fig. 7). Total cellular levels of Glut1 decline slightly with differentiation. Conversely, the amount of Glut4 transporter in the adipocyte increases from undetectable in the preadipocyte to a value 2-fold greater than that of Glut1. Comparison of the adipocyte morphology between the cultures in the glucose uptake experiment in the previous experiment indicated that the troglitazone-treated samples had a higher adipocyte/preadipocyte ratio than the control samples (data not shown). Therefore, because the number and type of glucose transporters change during adipocyte differentiation, the adipocyte/preadipocyte ratio must be equivalent between samples to accurately determine how troglitazone affects glucose transport. To do this, we repeated the previous experiment using 3T3-L1 cells that differentiated more than 95% under standard differentiation conditions without troglitazone and whose morphology and final C/EBPα mRNA levels (Fig. 2) were not significantly enhanced by troglitazone treatment. In addition, we compared the basal glucose uptake to insulin-stimulated glucose uptake, which distinguishes between Glut1 and Glut4 transporter activities. As shown in Fig. 4,
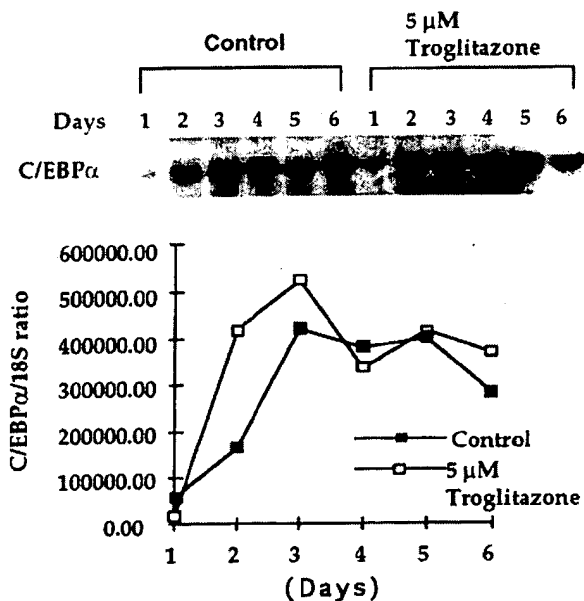

FIG. 2. Troglitazone affects the rate of C/EBPα message accumulation during differentiation, but not the overall level of message in the adipocyte. Northern analysis of total RNA collected every 24 h during adipocyte differentiation with and without 5 μM troglitazone using a 32P-labeled, random primed, C/EBPα probe. RNA loading was evaluated by quantitation of 18S RNA. Multiple experiments demonstrated that the onset of C/EBPα expression varied with the passage number of the cells; however, in all cases, troglitazone enhanced the rate of C/EBPα expression.
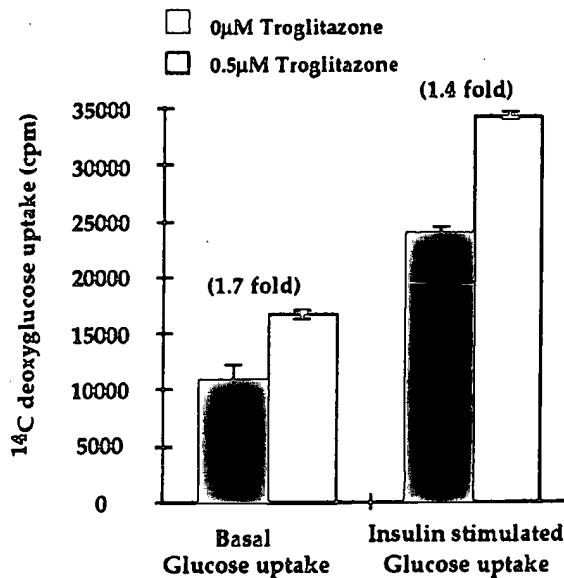
FIG. 4. Troglitazone increases basal glucose uptake in adipocytes. Adipocytes were differentiated under standard conditions in the presence or absence of 0.5 μM troglitazone. The percentage of adipocyte differentiation in all samples was more than 95%. [^{14}C]Deoxyglucose uptake was monitored 8 days after differentiation. For insulin-stimulated uptake, the cells were incubated for 30 min in 1×10^{-6} M insulin after a 3-h preincubation in serum-free DMEM. All values were obtained from duplicate samples.

basal glucose uptake increased 1.7-fold in response to 0.5 μM troglitazone. Similar results (1.4-fold) were found for Glut4-dependent insulin-stimulated glucose uptake. As basal glucose uptake is a function of Glut1 transporters, and insulin-stimulated uptake results from the combination of Glut1 and Glut4 transporter activities, the fact that troglitazone enhances both basal and insulin-stimulated glucose uptake equivalently suggests that the compound only alters Glut1 transporter activity.

To further separate the effects of troglitazone on glucose uptake from those on adipocyte differentiation, adipocytes differentiated in the absence of troglitazone were treated with 0.5 or 5 μM troglitazone for 48 h before the glucose uptake assay. As shown in Fig. 5, 0.5 and 5 μM troglitazone treatment produced 2- and 2.7-fold increases in basal glucose transport activity. As there was no change in morphology in the cells during treatment, these data show that troglitazone can enhance basal glucose uptake activity without affecting cell differentiation.

To determine whether the enhancement of glucose transporter activity is due to an increase in transporter number or an increase in transporter function, Western analysis was performed on whole cell lysates (from cells differentiated in the presence or absence of troglitazone) using either Glut1- or Glut4-specific antibodies (Fig. 6). Again, the adipocyte/ preadipocyte ratio required to eliminate the effects of differentiation on transporter levels was identical in treated and untreated samples. As previously described (13, 20, 21), Glut1 transporter levels decreased slightly with adipocyte differentiation, whereas Glut4 levels increased dramatically. Troglitazone caused a 2.3-fold increase in Glut1 protein without altering Glut4 levels. Thus, troglitazone enhances glu-
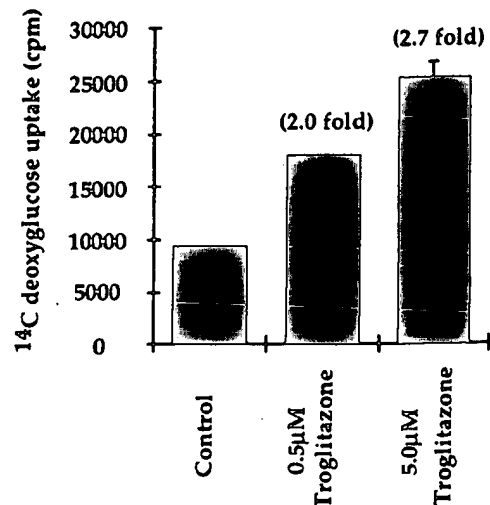
FIG. 5. Troglitazone enhances basal glucose uptake in fully differentiated adipocytes. Fully differentiated adipocytes were treated with 0, 0.5, or 5 μM troglitazone. Basal glucose uptake was assessed 48 h after treatment. All values were obtained from duplicate samples. The percentage of adipocyte differentiation in all samples was more than 95%.

cose uptake by increasing the number of basal glucose transporters per cell. Additionally, a Glut1 RNase protection assay was performed on RNA isolated from cells differentiated in the presence or absence of 5 μM troglitazone (Fig. 7). The Glut1/actin ratio was approximately 1.5–2 fold higher in the RNA samples isolated from troglitazone-treated cells. This directly correlates with the 2-fold increase in glucose transport and shows that troglitazone increases the number of Glut1 transporters in adipocytes.

As differentiation also affects Glut1 mRNA stability, and a previous report (12) indicated that thiazolidinediones increased mRNA stability, a Glut1 RNase protection assay was performed on RNAs isolated from adipocytes treated with 5 μg/ml actinomycin D. Figure 8 shows that when the control cells and troglitazone cells displayed the same adipocyte/ preadipocyte ratio, the rate of Glut1 mRNA decay was the same for both treated and untreated cells. Identical results were obtained from cells treated with pioglitazone, another antidiabetic thiazolidinedione (data not shown). Albeit indirectly, these data also suggest that the increase in Glut1 mRNA is due to an increase in Glut1 transcription.

Discussion

Troglitazone treatment of 3T3-L1 cells increases both the rate and percentage of adipocyte differentiation. This phenomenon is linked to the increased rate of C/EBPα accumulation in differentiating cells. Because this accumulation of C/EBPα message occurs within 24 h of drug treatment, it implies that troglitazone interacts with proteins that are present in the preadipocyte or are rapidly induced by the differentiating hormone cocktail. Recent work on adipocyte differentiation suggests that the proteins involved are members of the peroxisome proliferator-activated receptor (PPAR) family (22, 23). These nuclear receptors are activated by endogenous fatty acid or PG ligands (24–26) and in combination with C/EBP family members are believed to induce
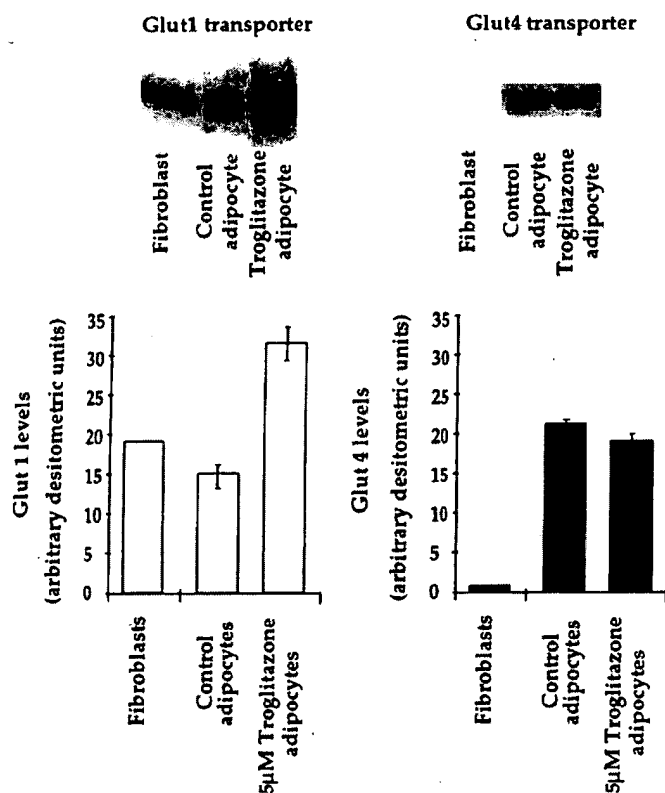
FIG. 6. Troglitazone increases the synthesis of the Glut1 transporter protein in adipocytes. Western analysis was performed using a Glut1- or Glut4-specific antibody of protein samples collected from adipocytes treated with or without 5 μM troglitazone. The percentage of adipocyte differentiation in all samples was more than 95%. Thirty micrograms of protein were loaded per lane, as determined using Bio-Rad analysis. Histograms represent data acquired from two independent experiments.

FIG. 7. The levels of Glut1 mRNA were increased in response to 5 μM troglitazone. A RNase protection assay was performed on RNAs collected at the indicated times from cells treated with or without 5 μM troglitazone. Ten micrograms of RNA per sample were hybridized to mouse Glut1 and β-actin probes and processed as described in *Materials and Methods*. Message levels were quantitated using a Molecular Dynamics PhosphorImager, and the values are represented as the Glut1/actin ratio.

adipocyte differentiation (27–29). Lehmann and colleagues (30) have shown that another thiazolidinedione, BRL 49653, is a ligand for PPARγ, the adipocyte-specific PPAR family member. This suggests that by interacting with the PPARs, troglitazone initiates the cascade of transcriptional events that enhances the rate of adipogenesis.

To determine whether the increased glucose uptake in adipocytes *in vivo* is a direct effect of troglitazone or a consequence of secondary effects brought about by insulin sensitization, the effects of troglitazone were assessed in the isolated 3T3-L1 tissue culture system. Apart from the enhanced glucose uptake associated with adipocyte differentiation, troglitazone directly increased glucose uptake 2-fold in these cells. This effect was shown to be a direct result of an increased synthesis of Glut1 transporter mRNA and protein. This disagrees with previously reported results (12), which have shown that pioglitazone, another thiazolidinedione with antidiabetic activity, enhances glucose uptake in 3T3-442A adipocytes by increasing both Glut1 and Glut4 transporter mRNA and protein via mRNA stabilization. However, this study failed to distinguish between the increases in glucose uptake associated with the enhancement of adipocyte differentiation and those resulting from the direct effects of the thiazolidinedione on the adipocyte. By

controlling for the ratio of adipocytes/preadipocytes in the experiments presented here, the indirect effects of differentiation by the compound on Glut4 were eliminated, demonstrating that troglitazone enhances glucose uptake by increasing Glut1 mRNA and protein levels. Additionally, identical experiments with pioglitazone yielded similar results (data not shown).

These results provoke at least two questions. First, can a 2-fold increase in adipocyte glucose uptake account for the decreased hyperglycemia *in vivo* or must other tissues also be affected? Secondly, are the transcriptional responses involved in differentiation the same as those used in the expression of Glut1; do both require the activation of PPARs by the thiazolidinediones?

Glucose transporter number has been shown to directly affect glucose transport and blood glucose levels in animal models. Several transgenic mice have been engineered that overexpress the glucose transporters in a tissue-specific fashion (30–34). In general, overexpression of either Glut1 or Glut4 enhanced glucose transport in the targeted tissue. Enhanced transport directly correlated with decreased plasma glucose levels in both fasted and fed animals, demonstrating that enhanced transporter expression has profound effects on glucose disposal *in vivo*. Surprisingly, however, increased Glut1 expression in skeletal muscle, and hence increased muscle basal transport, resulted in resistance of Glut4 to insulin stimulation and various other stimuli, including contraction and hypoxia (32). Additionally, Glut 4 overproduction in fat cells did not protect animals from the impaired glucose tolerance induced by a high fat diet (34). Thus, although enhanced transporter synthesis can ameliorate hy-
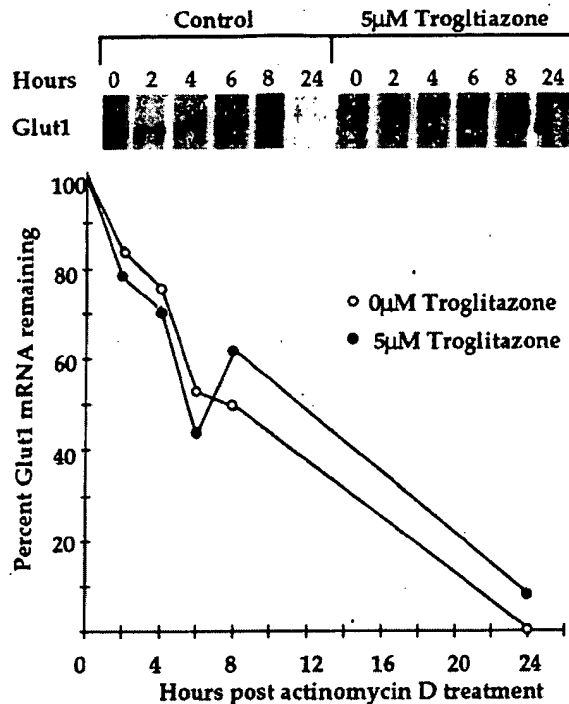
FIG. 8. Troglitazone does not alter the stability of Glut1 mRNA. RNase protection assay of Glut1 message was performed on RNA collected after actinomycin D (5 μg/ml) treatment of adipocytes differentiated in the presence or absence of 5 μM troglitazone. Ten micrograms of RNA were used per sample, and message levels were quantitated using a Molecular Dynamics PhosphorImager.

perglycemia, it does not appear to directly influence insulin resistance. This would imply that enhanced Glut1 synthesis in adipocytes would only represent a portion of troglitazone's antidiabetic activity. This is supported by data indicating that troglitazone influences the metabolic activities of skeletal muscle, liver, and pancreas (35–38).

The precise role of PPARs in the antidiabetic activities of the thiazolidinediones has yet to be fully explored. Clearly, the PPARs are intimately involved in lipid metabolism in a number of tissues, including adipose and liver, and are responsible for the lipid-lowering effects of the fibric acids (39). Interestingly, the lipid-lowering effects associated with thiazolidinedione treatment are similar to those of other PPAR-activating, lipid-lowering compounds (40). Moreover, as elevated lipid levels have been linked to peripheral insulin resistance, the alteration of lipid metabolism may ameliorate insulin resistance (41). However, *in vitro*, thiazolidinediones bind specifically to the PPARγ isoform, which is mainly present in adipose tissue (22, 23). Thiazolidinediones have been shown to influence metabolism in liver, pancreas, and skeletal muscle. If all of these antidiabetic responses are to be attributed to PPAR activation, all insulin-responsive tissues must contain sufficient levels of this isoform. Alternatively, it is possible that the ligand binding specificity *in vivo* differs from that *in vitro*, and/or that the compounds stimulate the formation of ligands that activate the PPAR isoforms present in these other tissues. Future studies addressing these issues will undoubtedly reveal the role of the PPARs in the antidiabetic activity of the thiazolidinediones. However, it is clear

that the regulation of Glut1 transporter synthesis could contribute to the antidiabetic activity of troglitazone.

References

1. Harris MI 1995 Summary. In: Harris MI, Cowie CC, Stern MP, Boyko EJ, Reiber GE, Bennett PH (eds) Diabetes in America, ed 2. NIDDK, NIH publication 95–1468. NIH, Bethesda, p 13
2. Fujiwara T, Yoshioka A, Yoshioka T 1980 Characterization of a new oral anti-diabetic agent, CS-045: studies in KK and ob/ob mice and Zucker fatty rats. Diabetes 37:1549–1558
3. Stevenson R, Hutson N, Krupp MN, Volkman R, Holland G, Eggler JF, Clark D, McPherson RK, Hall KL, Danbury BH, Gibbs M, Kreutter D 1990 Actions of novel antidiabetic agent englitazone in hyperglycemic hyperinsulinemic Ob/Ob mice. Diabetes 39:1218–1226
4. Oakes ND, Kennedy CJ, Jenkins AB, Laybutt DR, Chisholm DJ, Kraegen EW 1994 A new antidiabetic agent, BRL 49653, reduces lipid availability and improves insulin action and glucoregulation in the rat. Diabetes 43:1203–1210
5. Akanuma Y, Kosaka K, Kuzuya T, Shigeta Y, Kaneko T 1993 Clinical evaluation of a new oral hypoglycemic agent CS-045 in NIDDM. Diabetologia [Suppl 1] 36:A182
6. Mimura K, Umeda F, Hiramatsu S, Taniguchi S, Ono Y, Nakashima N, Kobayashi N, Masakado M, Sako Y, Nawata H 1994 Effects of a new oral hypoglycemic agent (CS-045) on metabolic abnormalities and insulin resistance in type 2 diabetes. Diabetic Med 11:685–691
7. Nolan JJ, Ludvik B, Beerdsen P, Joyce M, Olefsky J 1994 Improvement in glucose tolerance and insulin resistance in obese subjects treated with troglitazone. N Engl J Med 331:1188–93
8. Digirolamo M, Newby FD, Lovejoy J 1992 Lactate production in adipose tissue: a regulated function with extra-adipose implications. FASEB J 6:2405–2412
9. Zhang Y, Proenca R, Maffei M, Barone M, Leopold L, Friedman J 1994 Positional cloning of the mouse obese gene and its human homologue. Nature 372:425–432
10. Kletzien RF, Clarke SD, Ulrich RG 1991 Enhancement of adipocyte differentiation by an insulin sensitizing agent. Mol Pharmacol 41:393–398
11. Sandouk T, Reda D, Hofmann C 1993 Antidiabetic agent pioglitazone enhances adipocyte differentiation of 3T3-F442A cells. Am J Physiol 264:C1600–C1608
12. Sandouk T, Reda D, Hofmann C 1993 The antidiabetic agent pioglitazone increases the expression of glucose transporters in 3T3-F442A cells by increasing messenger ribonucleic acid transcript stability. Endocrinology 133:352–359
13. de Herreros AG, Birnbaum MJ 1989 The acquisition of increased insulin-responsive hexose transport in 3T3-L1 adipocytes correlates with expression of a novel transporter gene. J Biol Chem 264:19994–19999
14. Umek RM, Friedman AD, McKnight SL 1991 CCAAT-enhancer binding protein: a component of a differentiation switch. Science 251:288–292
15. Lin FT, Lane MD 1992 Antisense CCAAT/enhancer-binding protein RNA suppresses coordinate gene expression and triglyceride accumulation during differentiation of 3T3-L1 preadipocytes. Genes Dev 6:533–544
16. Lin FT, Lane MD 1994 CCAAT/enhancer binding protein α is sufficient to initiate the 3T3-L1 adipocyte differentiation program. Proc Natl Acad Sci 91:8787–8761
17. Freytag S, Geddes T 1992 Reciprocal regulation of adipogenesis by Myc and C/EBPα. Science 256:379–382
18. Wang N-D, Finegold MJ, Bradley A, Ou CN, Abdelsayed SV, Wilde MD, Taylor LR, Wilson DR, Darlington GJ 1995 Impaired homeostasis in C/EBPα knockout mice. Science 269:1108–1112
19. Cao Z, Umek RM, McKnight SL 1991 Regulated expression of three C/EBP isoforms during adipose conversion of 3T3-L1 cells. Genes Dev 5:1538–1552
20. Weiland M, Schurmann A, Schimidt WE, Joost HG 1990 Development of the hormone-sensitive glucose transport activity in differentiating 3T3-L1 murine fibroblasts. Biochem J 270:331–336
21. Ziehm D, Schurmann A, Weiland M, Joost HG 1992 Biphasic alteration of glucose transport in 3T3-L1 cells during differentiation to the adipocyte-like phenotype. Horm Metab Res 25:71–76
22. Tontonoz P, Hu E, Graves RA, Budavari AI, Spiegelman BM 1994 mPPARγ: tissue-specific regulator of an adipocyte enhancer. Genes Dev 8:1224–1234
23. Chawla A, Schwarz EJ, Dimaculanga DD, Lazar MA 1994 Peroxisome proliferator-activated receptor (PPAR) γ: adipose-predominant expression and induction early in adipocyte differentiation. Endocrinology 135:798–800
24. Forman BM, Tontonoz P, Chen J, Brun R, Spiegelman BM 1995 15-

Deoxy-^{12,14}-prostaglandin J$_2$ is a ligand for the adipocyte determination factor PPARγ. Cell 83:803–812

25. Kliewer SA, Lenhard JM, Wilson TM, Patel I, Morris DC, Lehmann JM 1995 A prostaglandin J$_2$ metabolite binds peroxisome proliferator-activated receptor γ and promoter adipocyte differentiation. Cell 83:813–819

26. Yu K, Bayona W, Kallen CB, Harding HP, Ravera CP, McMahon G, Brown M, Lazar MA 1995 Differential activation of peroxisome proliferator-activated receptors by eicosanoids. J Biol Chem 270:23975–23983

27. Tontonoz P, Hu E, Spiegelman BM 1994 Stimulation of adipogenesis in fibroblasts by PPARγ, a lipid-activated transcription factor. Cell 79:1147–1156

28. Brun RP, Tontonoz P, Forman BM, Ellis R, Chen J, Evans R, Spiegelman BM 1996 Differential activation of adipogenesis by multiple PPAR isoforms Genes Dev 10:974–984

29. Wu Z, Xie Y, Bucher NLR, Farmer SR 1995 Conditional ectopic expression of C/EBPβ in NIH-3T3 cells induces PPARγ and stimulates adipogenesis. Genes Dev 9:2350–2363

30. Lehmann JM, Moore LB, Smith-Oliver TA, Wilkinson WO, Wilson TM, Kliewer SA 1995 An antidiabetic thiazolidinedione is a high affinity ligand for peroxisome proliferator-activated receptor γ (PPARγ). J Biol Chem 270:12953–12956

31. Shepherd PR, Gnudi L, Tozzo E, Yang H, Leach F, Kahn BB 1993 Adipose cell hyperplasia and enhanced glucose disposal in transgenic mice overexpressing Glut4 selectively in adipose tissue. J Biol Chem 268:22243–22246

32. Gulve EA, Ren J-M, Marshell BA, Gao J, Hansen PA, Holloszy JO, Mueckler M 1994 Glucose transport activity in skeletal muscles from transgenic mice overexpressing Glut1. J Biol Chem 269:18366–18370

33. Hansen PA, Gulve EA, Marshell BA, Gao J, Pessin JE, Holloszy JO, Mueckler M 1995 Skeletal muscle glucose transport and metabolism are enhanced in transgenic mice overexpressing the Glut4 glucose transporter. J Biol Chem 270:1679–1684

34. Gnudi L, Tozzo E, Shepherd PR, Bliss JL, Kahn BB 1995 High level overexpression of glucose transporter-4 driven by an adipose-specific promoter is maintained in transgenic mice on a high fat diet, but does not prevent impaired glucose tolerance. Endocrinology 136:995–1002

35. Furuta H, Sowa R, Tabata H, Hirayama J, Negoro T, Sanke T, Nanjo K 1994 Effect of new antidiabetic drug CS-045 on peripheral insulin resistance. J Jpn Diabetes Soc 37:343–348

36. Horikoshi H, Okuno A, Fujiwara T, Shiota M, Sugano T 1993 Peripheral effects of a new antidiabetic agent, CS-045: acute stimulation of insulin-induced glucose uptake in perfused rat hindlimb. Diabetes 42:59A

37. Inoue Y, Tanigawa K, Nakamura S, Tamura K, Kato Y, Nakase A 1993 Effect of CS-045, a new oral antidiabetic agent, on B-cell function in rats after 90% pancreatectomy. Diabetologia 36:A182

38. Lee MK, Miles PDG, Khoursheed M, Gao KM, Moosa AR, Olefsky JM 1994 Metabolic effects of troglitazone on fructose-induced insulin resistance in the rat. Diabetes 43:1435–1439

39. Auwerx J 1992 Regulation of gene expression fatty acids and fibric acid derivatives: an integrative role for peroxisome proliferator activated receptors. Horm Res 38:269–177.

40. Mimura K, Umeda F, Hiramatsu S, Taniguchi S, Ono Y, Nakashima N, Kobayashi K, Masakado M, Sako Y, Nawata H 1994 Effects of a new oral hypoglycemic agent (CS-045) on metabolic abnormalities and insulin resistance in type 2 diabetes. Diabetic Med 11:685–691

41. McGarry JD 1992 What if Minkowski had been ageusic? An alternative angle on diabetes. Science 258:776–770

The Antidiabetic Agent Pioglitazone Increases Expression of Glucose Transporters in 3T3-F442A Cells by Increasing Messenger Ribonucleic Acid Transcript Stability*

TAGRID SANDOUK, DOMENIC REDA‡, AND CECILIA HOFMANN

Department of Molecular and Cellular Biochemistry (T.S., C.H.) and Department of Surgery, Loyola University Stritch School of Medicine, Maywood, Illinois 60153; and Research Service (C.H.) Hines VA Hospital (D.R., C.H.), Hines, Illinois 60141

ABSTRACT

Whereas adipocytes normally play an important role as a major site for systemic energy homeostasis, adipocyte function is markedly altered in disorders such as diabetes. In this study, we investigated the effect of pioglitazone, a novel antidiabetic agent known to lower plasma glucose in animal models of diabetes mellitus, on expression of glucose transporters GLUT1 and GLUT4 in 3T3-F442A cells. Treatment of confluent 3T3-F442A preadipocyte cultures for 7 days with pioglitazone (1 μM) and insulin (1 μg/ml) resulted in nearly 100% differentiation of cells to lipid-accumulating adipocytes, and such adipocytes showed a markedly increased capacity for glucose uptake. Analysis of messenger RNA transcripts encoding GLUT1 and GLUT4 glucose transporters over the 7-day differentiation period indicated time-dependent in-

creases in abundance of each type that were maximal at more than 5-fold with the combined presence of insulin and pioglitazone. In accord, GLUT1 and GLUT4 protein levels also increased to maximal levels of 10-fold and 7-fold, respectively, over those in undifferentiated preadipocytes. Increased messenger RNA half-lives from 2.2 to greater than 24 h for GLUT1 and from 1.2 to greater than 24 h for GLUT4 correlated with this induced adipocyte differentiation. Taken together, these findings indicated that pioglitazone markedly enhanced expression of cellular glucose transporters, and the mechanism for this action was mainly stabilization of transporter messenger RNA transcripts. Such increased expression of glucose transporters in adipocytes establishes the cells in a state active for glucose uptake, thus ultimately facilitating storage and metabolism as well. (*Endocrinology* **133**: 352–359, 1993)

ADIPOSE tissues play a key role in systemic energy homeostasis. Adipocytes possess hormonally regulated transport and metabolic systems allowing energy storage as triglycerides when nutrients abound or energy release during nutritional dearth. In accord with this role, a recent report indicated that adipose may be responsible for up to 30% of whole body glucose metabolism (1). Altered adipocyte function has been associated with abnormal physiological states including obesities and obesity-linked diabetes (2–4). In non-insulin-dependent diabetes mellitus, elevated blood glucose levels result from insufficient glucose uptake in adipose and muscle, a consequence of insulin resistance (5, 6).

The hyperglycemia of noninsulin-dependent diabetes mellitus can be corrected clinically by treatment of patients with oral hypoglycemic agents. Whereas presently used sulfonyl-urea agents appear to act principally as secretagogues to increase the availability of insulin to enhance glucose disposal (7, 8), an alternate treatment strategy could employ agents acting as insulin sensitizers, thus overcoming target tissue insulin resistance. New antidiabetic compounds belonging to the thiazolidinedione class of drugs appear to lower blood glucose in animal models of diabetes by improv-

ing insulin sensitivity in peripheral tissues (9). Treatment of insulin-resistant fatty rats or mice with the thiazolidinedione pioglitazone resulted in lowered blood glucose, triglyceride, and insulin levels (10, 11).

We and others have previously reported that thiazolidinedione agents enhanced insulin sensitivity for glucose uptake and metabolism in adipose tissues of diabetic animals (10–13). It has also been found that such agents have potent adipogenic effects on preadipocyte cell cultures (14–16). We therefore sought to more fully investigate the mechanism underlying the effect of pioglitazone to promote adipocyte differentiation with the aim of gaining insight into how such an effect could contribute to regulation of cellular glucose uptake. Findings in our present report indicate that pioglitazone treatment of 3T3-F442A preadipocytes markedly enhances expression of glucose transporters GLUT1 and GLUT4, and the mechanism for this action is a stabilization of transporter messenger RNA (mRNA) transcripts.

Materials and Methods

Cells and tissue culture

3T3-F442A fibroblasts were grown as monolayer cultures at 37 C in an atmosphere of 10% CO_2-90% air essentially as described previously (17). Subcultured cells were grown to confluence (usually 7 days) in Dulbecco's Modified Eagle's Medium (DMEM) containing glucose (4.5 g/L), bovine serum (10%), streptomycin (50 μg/ml), penicillin (50 U/ml), Fungizone (0.25 μg/ml), and glutamine (2 mM). Confluent cell cultures were then converted to adipocytes by culture for 7 days in

DMEM in the presence of 10% fetal calf serum and insulin (1 μg/ml) and/or pioglitazone (1 μM). Cell differentiation was assessed by evaluating cell morphology under phase contrast microscopy; cells were considered to be adipocytes if numerous lipid droplets were observed in the cytoplasm. The cell line was used during the 10th to 20th passage after clone isolation.

Measurement of 2-deoxy-D[¹⁴C]glucose uptake

For assay, 3T3-F442A cell monolayers (~10⁶ cells/17 mm well) were rinsed with PBS and incubated with 0.5 ml assay medium (DMEM, no glucose, 5 mM NaHCO₃, 20 mM N-[2-hydroxyethyl]-N'piperazine-[2-ethanesulfonic acid], 0.1% BSA, pH 7.4) for 15 min at 22 C. Then 0.5 μCi D-[U-¹⁴C]glucose (stock = 57 mCi/mmol, Amersham Corp., Arlington Heights, IL) was added for an additional 15 min. After this incubation, medium was aspirated, and cells were rinsed with ice-cold PBS containing 10 mM glucose. Cells were then solubilized with 0.5 ml 0.5 N NaOH, transferred to vials, neutralized with 52 μl glacial acetic acid, and counted for radioactivity using 5 ml Ready Value scintillation fluid (Beckman, Inc., Palo Alto, CA).

Northern blot analysis of RNA for determination of GLUT1 and GLUT4 mRNA transcript abundance

Total RNA was extracted from 3T3-F442A cell monolayers essentially according to the method of Chomczynski and Sacchi (18). RNA was then size-fractionated on 1% agarose gels and transferred to nylon membranes according to the method of Fourney et al. (19). RNA transcripts were cross-linked to the membrane with a UV Stratalinker (Stratagene, La Jolla, CA).

Hybridization was performed using anti-sense RNA Riboprobes prepared according to the protocol of the reagent supplier (Promega Corp., Madison, WI). For GLUT1, pSPGT-1 (20) was kindly provided by Dr. Graeme Bell (Chicago, IL), and the entire 1591 base pair coding region of rat brain glucose transporter was excised using BglII and subcloned into the BamHI site of pGEM-4Z. EcoRI was used for linearization, and T7 RNA polymerase was used for GLUT1 Riboprobe transcription. A GLUT4 construct pSM1D2 in the pBluescript KS⁺ (21) was generously provided by Dr. Morris Birnbaum (Boston, MA). For GLUT4 Riboprobe preparation, this construct was linearized with Hind III, and T7 RNA polymerase was used for Riboprobe preparation.

High stringency hybridizations with Riboprobes were performed by 65 C overnight incubation of membranes in glass tubes in a Hybaid Oven (National Labnet Co., Woodbridge, NJ) using procedures we have detailed previously (11). After rinses, labeled membranes were exposed at −70 C to Hyperfilm-MP (Amersham Corp., Arlington Heights, IL) with an intensifying screen. Autoradiographic bands on film were quantitated by two-dimensional densitometry using an AMBIS Optical Imaging System (San Diego, CA). RNA samples were quantitated for correction of minor loading differences by densitometry of ethidium bromide-stained 28S ribosomal bands (22) on photographic negatives (type 55 P/N film, Polaroid, Cambridge, MA).

Measurement of GLUT1 and GLUT4 mRNA stability

Confluent 3T3-F442A cells were induced to differentiate with insulin, pioglitazone, or both as described above. On day 7 of treatment, the transcription inhibiting agent Actinomycin D (Act D) was added (5 μg/ml) to treated cell cultures as well as undifferentiated control cultures, essentially as reported earlier (23–26). Total RNA was extracted from these cells at selected time points after Act D addition (0, 1, 2, 4, 6, and 24 h), and abundance of remaining GLUT1 and GLUT4 mRNA transcripts was assessed by Northern blot analyses as described above. Glucose transporter mRNA abundance data were fitted to a single exponential decay curve by nonlinear least square regression analysis. The estimated first-order rate constant was used to calculate the mRNA half-life. Since it was suggested that Act D may have nonspecific effects with long-term (24 h) treatments (24), glucose transporter mRNA half-life calculations were based on changes in mRNA abundance over only the first 6 h of Act D treatment.

Western blot analysis of glucose transporter proteins

Total particulate membrane proteins were prepared as previously described (27). Briefly, cells were washed with PBS and scraped into homogenization buffer [20 mM Tris-HCl, 255 mM sucrose, 1 mM EDTA, 1 mM phenylmethyl sulfonylfluoride, 10 U/ml Trasylol] and were homogenized with 10 pulses by a Tekmar Tissuemizer (Tekmar Inc., Cincinnati, OH). A total membrane fraction was prepared by centrifugation of the homogenate at 200,000 × g at 4 C. Protein concentrations were determined by the Bradford assay (28) using BSA as a standard. Initial Western blot analyses revealed diffuse bands of GLUT1 and GLUT4 proteins, possibly due to heterogenous glycosylation of the transport proteins. Therefore, samples were routinely treated with peptide N-glycosidase F (1 U/100 μg protein) in a buffer containing 20 mM sodium phosphate, pH 7.5, 10 mM EDTA, 1.7% Triton X-100, and 1 mM phenylmethyl sulfonylfluoride for 48–72 h at 37 C to remove sugar residues (23). Treated protein samples were then mixed with one fourth volume of 4× electrophoretic sample buffer [200 mM Tris-HCl at pH 6.8, 400 mM dithiothreitol, 8% sodium dodecyl sulfate, 40% glycerol, 0.4% bromophenol blue] and stored at −20 C. Samples were thawed and loaded in parallel onto two discontinuous 12% polyacrylamide gels, and size-fractionated according to the method of Laemmli (29) using a Mini-Protean II Dual Slab Cell (Bio-Rad, Richmond, CA). The amount of protein loaded (10 μg/lane for GLUT1 and 60 μg/lane for GLUT4) was determined empirically to be within the linear response range for the system used. Proteins separated on each gel were electrophoretically transferred to Immobilon PVDF membranes (Millipore Corp., Bedford, MA) using a Mini-Transblot electrophoretic transfer cell (Bio-Rad). One membrane was stained for total protein (0.1% Coomassie R-250, 40% methanol, 10% acetic acid). The second membrane was immunostained for GLUT1 or GLUT4 using a double antibody system and the Immuno-Blot Assay Kit (Bio-Rad). The supplier's instructions were followed except 5% BSA was used for membrane blocking. The primary antibodies (RaGLUTRANS for GLUT1 and RaIRGT for GLUT4, East Acres Biologicals, Southbridge, MA) were diluted 1:3000 and 1:2000, respectively, and the alkaline phosphatase-conjugated second antibody (GAR-AP, Bio-Rad) was diluted 1:3000 for use. Resulting signals were quantitated with the reflective mode of a Model 620 Video Densitometer (Bio-Rad). Sample loading corrections were made based on densitometry data from the Coomassie-stained membrane.

Data analysis

Statistical analysis was performed using SAS version 6 (SAS Institute, Inc., Cary, NC). All hypothesis tests were two-sided and were considered significant if the P value was less than or equal to 0.05.

Results

Induction of preadipocyte differentiation and glucose transport by insulin and pioglitazone

Treatment of confluent 3T3-F442A cells for 7 days with insulin (1 μg/ml), pioglitzone (1 μM), or both agents in the presence of 10% fetal calf serum resulted in conversion of cells into lipid-accumulating adipocytes. Whereas some cells differentiated into adipocytes by either treatment alone (insulin, 60%; pioglitazone, 80%), nearly complete differentiation (95%) was achieved with both agents together. Such cellular differentiation was associated with markedly increased capacity for glucose transport. Treatment of 3T3-F442A cells for 7 days with insulin or pioglitazone resulted in basal glucose transport levels that were 22- and 30-fold increased compared to untreated fibroblasts (Table 1). Together, both agents appeared to act additively for a maximal enhancement of 61-fold at day 7. Age-matched, undifferentiated cells maintained in growth medium showed no

TABLE 1. P and I-induced increases in glucose transport activity in differentiating 3T3-F442a Cells

| Cell treatment	Glucose uptake (dpm/cell ± SEM)
Control, day 0	0.0030 ± 0.00007
Control, day 7	0.0013 ± 0.00031
Insulin	0.0670 ± 0.0076
Pioglitazone	0.0887 ± 0.015
Insulin + pioglitazone	0.1830 ± 0.037

Confluent monolayer cultures of preadipocytes in DMEM (day 0) were induced to differentiate by treatment with insulin and/or pioglitazone. Preadipocyte cells maintained for 7 days in DMEM without added insulin and/or pioglitazone also served as controls. After treatment for 7 days, glucose transport actvity was measured by uptake of 2-deoxy-D[^{14}C]glucose as described in *Materials and Methods*. Since the radiolabeled glucose has a specific activity of 300 mCi/mmol, there are 1.5 f/dpm. Thus, maximal basal transport was approximately 0.3 fmol/cell for cells differentiated in medium containing insulin and pioglitazone.

increase in glucose transport over the 7-day interval, and actually declined about 60%, likely an indication of quiescence.

Insulin- and pioglitazone-enhanced expression of glucose transporters in 3T3-F442A cells

To assess whether such increased glucose transport activity could be explained by amplified expression of glucose transporters in adipocytes, we analyzed the levels of GLUT1 and GLUT4 mRNA abundance. When assessed by Northern blotting, the abundance of mRNA transcripts encoding GLUT1 and GLUT4 glucose transporters increased in a time-dependent manner (Figs. 1, 2). Whereas 7-day treatment with either insulin (1 μg/ml) or pioglitazone (1 μM) increased GLUT1 mRNA abundance by 2.3- and 1.5-fold, respectively, above the level in undifferentiated cells (day 0), insulin and pioglitazone together acted synergistically to increase this message by almost 6-fold (Fig. 1). GLUT1 mRNA levels did not change in age-matched undifferentiated cells maintained in growth medium over the same interval. In contrast to the observed synergistic treatment effects on GLUT1 mRNA levels, GLUT4 mRNA abundance was increased to similar levels above undifferentiated cells (day 0) reaching 3.8-, 4.6-, and 5.2-fold elevation by respective treatments for 7 days with insulin, pioglitazone, or both (Fig. 2). Whereas these values for GLUT4 mRNA abundance reflected an overall increase at day 7, a small decline was observed at this time point in some experiments with combined treatment by insulin and pioglitazone (Fig. 2, lower). Such results indicate that some down-regulation may occur in the final differentiated state.

These changes in GLUT1 and GLUT4 glucose transporter mRNA levels were accompanied by changes in levels of the encoded transporter proteins as determined by Western blotting. Whereas either insulin or pioglitazone treatment appeared to increase GLUT1 protein levels on day 7 of differentiation by 2.3- and 3.5-fold respectively, the agents together seemed to act synergistically to increase protein levels by almost 10-fold above those of age-matched undifferentiated cells (Fig. 3). In contrast to the observed synergistic

GLUT1 mRNA

-3.0 kb

CS   INS   PIO   I+P
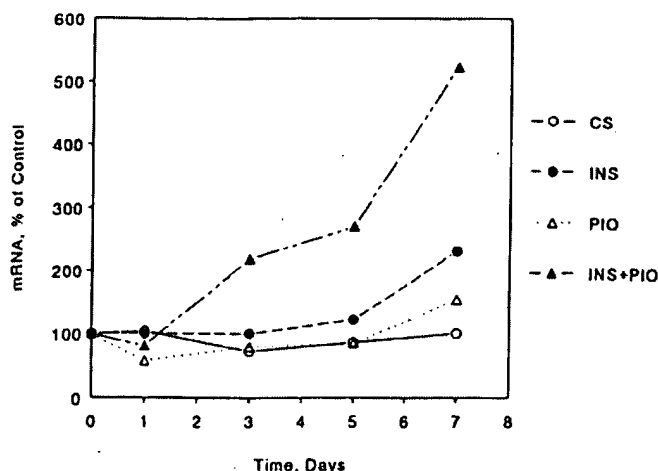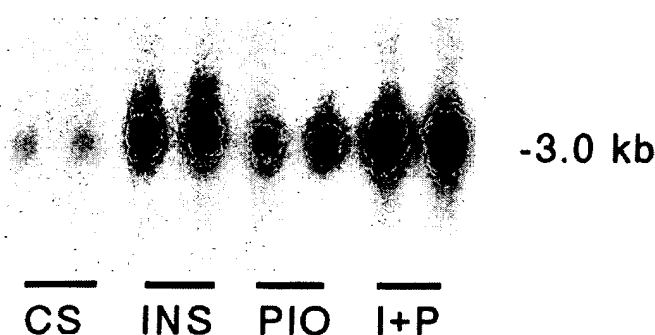
FIG. 1. Effect of insulin and pioglitazone treatment on GLUT1 mRNA abundance. *Upper,* Time-dependent increases in abundance of GLUT1 mRNA during differentiation of 3T3-F442A cells induced by insulin (INS), pioglitazone (PIO), or both. Cells were seeded, grown to confluence, and differentiated as described in *Materials and Methods*. Untreated age-matched fibroblasts maintained in DMEM containing only 10% calf serum were used as control (CS). Total RNA was isolated at indicated time points, and samples (10 μg/lane) were electrophoretically size-fractionated on agarose gels. Northern blots were hybridized to Riboprobes specific for rat GLUT1 mRNA. Autoradiographic bands were quantitated by densitometry and normalized for minor loading differences as described in *Materials and Methods*. Data represent mean values for n = 5-6 determinations. A three factor analysis of variance (ANOVA; insulin, pioglitazone, time) with interactions showed a significant effect on GLUT1 mRNA abundance from combined treatment with I and P ($P < 0.001$). *Lower,* Representative Northern blot showing GLUT1 mRNA abundance in control (CS) and treated (INS, PIO, I + P) cells on day 7 of differentiation.

effect on GLUT1 protein, GLUT4 protein levels increased by about 2.2-, 6.6-, and 4-fold by insulin, pioglitazone, or both, respectively (Fig. 4).

Increased stability of glucose transporter messages

We next investigated possible effects of insulin and pioglitazone on the stability of GLUT1 and GLUT4 mRNAs. Fibroblast 3T3-F442A cells were induced to differentiate by treatment with insulin (1 μg/ml), pioglitazone (1 μM), or both for 7 days. The transcription inhibiting agent, Act D (5 μg/ml), was added to differentiated cells on day 7 or to undifferentiated control cells just before such cells reached conflu-
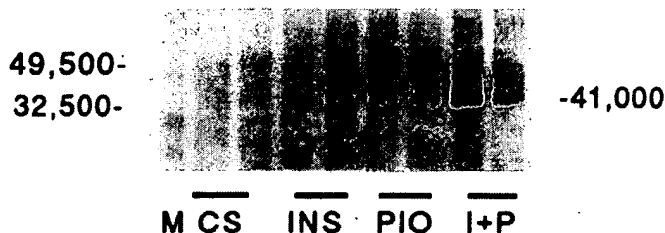
GLUT4 mRNA

-3.0 kb

___CS___ ___INS___ ___PIO___ ___I+P___

FIG. 2. Effect of insulin and pioglitazone treatment on GLUT4 mRNA abundance. *Upper*, Time-dependent increases in GLUT4 mRNA abundance in 3T3-F442A cells during differentiation. Cells were grown to confluence, and differentiated in the presence of insulin (INS), pioglitazone (PIO), or both (INS + PIO) as described in *Materials and Methods*. Untreated, age-matched fibroblasts maintained in DMEM containing only 10% calf serum were used as control (CS). Total RNA was isolated, Northern blots were prepared as described for Fig. 1, and membranes were hybridized with Riboprobe transcripts specific for rat GLUT4. Quantitation of resultant autoradiographs was done as described in *Materials and Methods*. Data represent mean values for n = 5–6 determinations. A three factor ANOVA (insulin, pioglitazone, time) with interactions showed significant effects on GLUT4 mRNA abundance by INS ($P = 0.001$) or PIO ($P < 0.0001$). *Lower*, Northern blot showing GLUT4 mRNA abundance in control (CS) and treated (INS, PIO, I + P) cells on day 7 of differentiation.

ence, and total RNA was extracted from cells at indicated times after addition of the transcription inhibitor (0, 1, 2, 4, 6, and 24 h). Even after 24-h treatment with Act D, cell membranes remained intact and appeared refractile, and there was no visible sloughing of cells from the plates. The abundance of remaining mRNA transcripts for each of the glucose transporter genes was assessed on Northern blots. Differentiation of 3T3-F442A cells increased the GLUT1 mRNA half-life from about 2.2 h in control undifferentiated cells to about 5.7, 3.6, and greater than 24 h in adipocytes differentiated by treatment with insulin, pioglitazone, or both, respectively (Fig. 5, Table 2). The stabilization of GLUT1 mRNA appeared to account for corresponding increases in GLUT1 mRNA abundance. Similarly, GLUT4

GLUT1 Protein

FIG. 3. Effect of insulin and pioglitazone treatments on GLUT1 protein abundance. *Upper*, Increased GLUT1 protein abundance on differentiation of 3T3-F442A cells. Confluent 3T3-F442A cells were differentiated with I (INS), P (PIO), or both (INS + PIO) as described in *Materials and Methods*. On day 7, cellular membranes were isolated from undifferentiated (CS) or differentiated (INS-, PIO-, or INS + PIO-treated) cells, and protein (10 μg/lane) was electrophoresed and immunoblotted for GLUT1 detection using the rabbit anti-GLUT1 primary antibody (see *Materials and Methods*). Resulting colorimetrically stained bands were quantitated by densitometry and normalized for minor loading differences. Data are expressed as percent of control and represent mean values ± SEM for n = 8 determinations. With background subtraction, the mean basal value was 0.20 ± 0.06 arbitrary density units. Two factor ANOVA showed significant effects on GLUT1 protein by INS ($P = 0.014$), PIO ($P = 0.015$), and INS + PIO ($P < 0.0001$). *Lower*, Representative immunoblot showing expression of GLUT1 protein in selected samples from control (CS) and treated (INS, PIO, I + P) cells on day 7 of differentiation. Molecular weight markers are indicated in lane M; the GLUT1 band ran as $M_r = 41,000$.

mRNA half-life increased from about 1.2 h in undifferentiated control cells to about 14.2, 10.3, and greater than 24 h in cells differentiated with insulin, pioglitazone, or both, respectively (Fig. 5, Table 2). Again, GLUT4 mRNA stabilization appeared to account for observed increases in mRNA abundance.

As shown in Fig. 6, we were able to quantitate differential expression of transporter messages in cells undergoing different treatments by differentially exposing the Northern blots to film. This allowed calculation of message half-lives even when transcripts were present only at relatively low levels.

Discussion

Pioglitazone, 5-[4-(2-(5-ethyl-pyridyl)ethoxy]-2,4-thiazolidinedione, is an antidiabetic agent that has been shown to

GLUT4 Protein

49,500-
32,500-   -46,000

M CS   INS   PIO   I+P
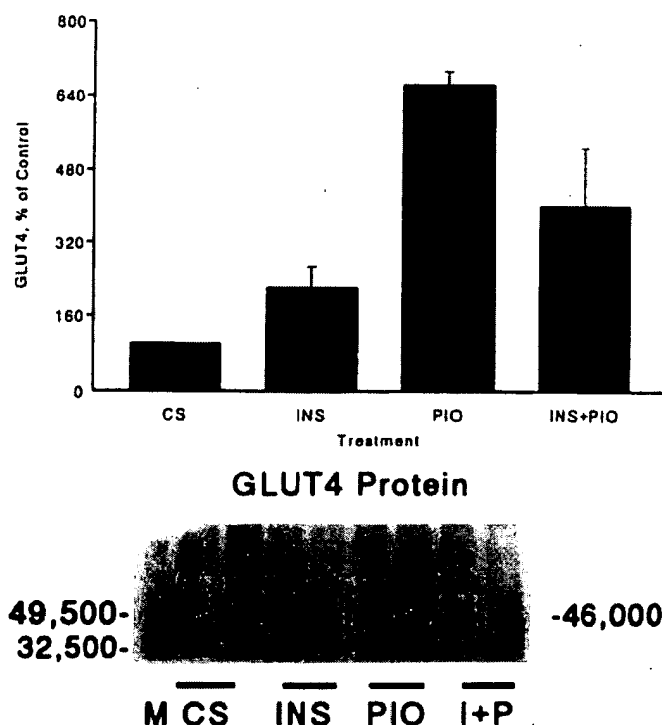
FIG. 4. Effect of insulin and pioglitazone treatments on GLUT4 protein abundance. *Upper*, Increased GLUT4 protein levels on differentiation of 3T3-F442A cells. Cell culture, treatment conditions, protein extraction, and Western blot analyses were performed as described in Fig. 3 legend, except that 60 μg/lane total protein were loaded for detection using the rabbit anti-GLUT4 primary antibody. Data are expressed as percent of control and represent mean ± SEM for n = 10 determinations. After background subtraction, the mean basal value was 0.57 ± 0.11 arbitrary density units. Two factor ANOVA showed significant effects on GLUT4 by INS ($P = 0.015$), PIO ($P = 0.007$), and INS + PIO ($P = 0.0003$). *Lower*, Representative immunoblot showing increased levels of GLUT4 protein in 7 day-treated (INS, PIO, I + P) compared to untreated control (CS) cells. GLUT4 protein appears as a stained band with apparent M, of 46,000. In control cells (CS), a nonspecific band of apparent M, 60,000 cross-reacted with the secondary antibody.

ameliorate hyperglycemia in animal models of noninsulin-dependent diabetes mellitus (10, 11, 30). The purpose of our study was to further probe cellular action mechanisms underlying the antidiabetic effects of pioglitazone. Our prior findings indicated that the antidiabetic agent pioglitazone acted as a potent accelerator of adipocyte differentiation of 3T3-F442A cells (14). This was evidenced by our demonstration that treatment of fibroblast-like preadipocytes with pioglitazone led to expression of fat-specific genes along with acquisition of the morphological appearance of lipid-accumulating adipocytes with concomitant increases in triglyceride accumulation (14). In the present study, we showed that such pioglitazone-treated cells showed an increased capacity for glucose uptake, with associated increases in GLUT1 and GLUT4 proteins. We further measured increased levels of mRNA transcripts encoding these glucose transporters, and found that these increases corresponded with markedly enhanced stability of both GLUT1 and GLUT4 mRNA messages. Such increased expression of glucose transporters in adipocytes established the cells in a state active for glucose

GLUT1 mRNA stability

GLUT4 mRNA Stability
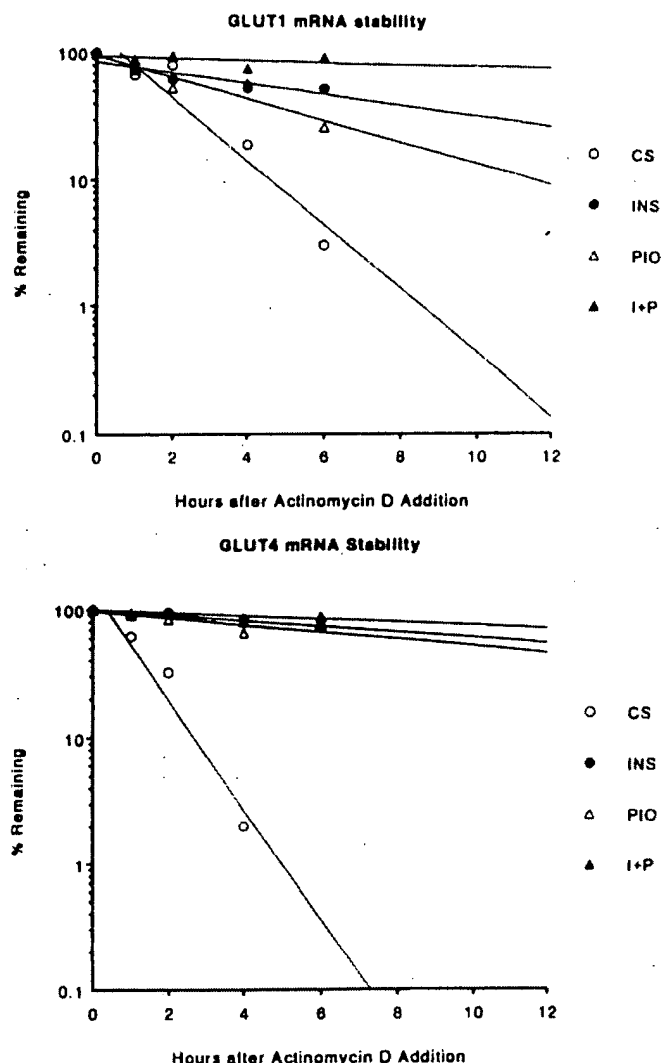
FIG. 5. *Upper*, Enhanced GLUT1 mRNA stability associated with treatment of 3T3-F442A cells with insulin (INS), pioglitazone (PIO), or both (I + P). *Lower*, Enhanced GLUT4 mRNA stability associated with treatment of 3T3-F442A cells with I, P, or both. Confluent 3T3-F442A cells were differentiated with INS, PIO, or I + P for 7 days as described in *Materials and Methods*. On day 7 of treatment, Act D (5 μg/ml) was added to differentiated (INS, PIO, I + P) and undifferentiated (CS) control cells, and total RNA was extracted from cells at indicated time points (0, 1, 2, 4, 6, and 24 h). Abundance of mRNA was assessed by Northern blotting analysis as described earlier. Data are expressed as percent of mRNA remaining after Act D treatment relative to the levels before the treatment time 0. Each data point represents a mean value for n = 2 determinations. Calculated mRNA half-lives are shown in Table 2.

uptake, thus ultimately facilitating glucose storage and metabolism as well.

Results of our present study showed that the differentiation of 3T3-F442A cells by treatment with insulin and pioglitazone was accompanied by strikingly increased capacity for basal glucose transport (60-fold) compared to that for fibroblast-like preadipocytes. Facilitated diffusion of glucose across the plasma membrane of adipocytes is known to be mediated by two glucose transporter proteins. *i.e.* GLUT1

TABLE 2. Calculated mRNA half-lives in undifferentiated and differentiated 3T3-F442A cells

Treatment	mRNA half-life (h)			
	CS	INS	PIO	INS + PIO
Transporter				
GLUT1	2.2	5.7	3.6	>24
GLUT4	1.2	14.3	10.3	>24

Data from the experiment involving Act D treatment (Fig. 5) were fitted to a single exponential decay curve by nonlinear least square regression analysis. The estimated first-order rate constant was used to calculate the mRNA half-life.

GLUT1 mRNA Stability

Hours after Actinomycin D Addition
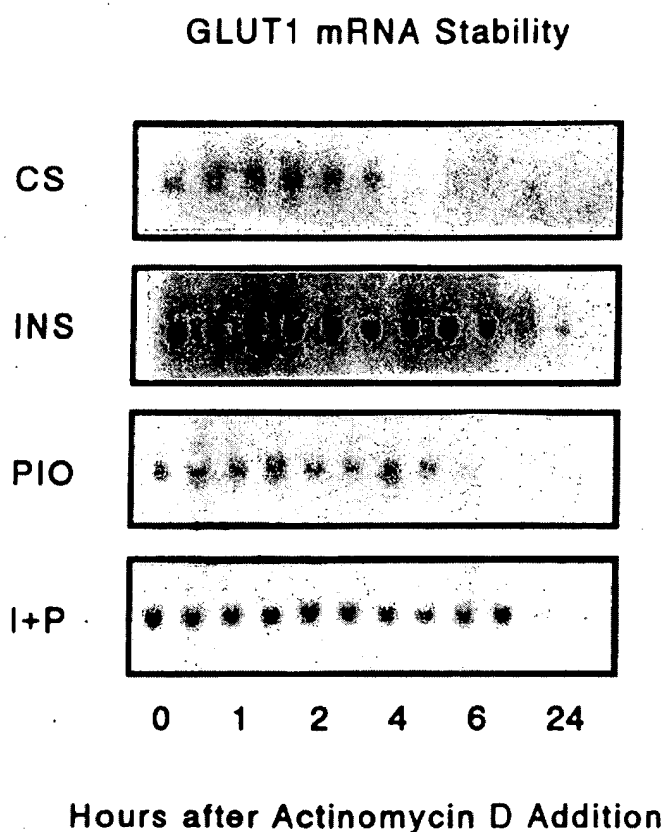
FIG. 6. Autoradiographs of Northern blots probed for GLUT1 mRNA transcript abundance after D treatment. Experimental samples were prepared as described in Fig. 5. Data shown represent duplicate experimental points, except for the time 0 INS, where only a single sample is shown. Hours of film exposure to the radiolabeled blot were 40, 18, 24, and 8 for CS, INS, PIO, and INS + PIO, respectively. Some films required longer exposure intervals for detection of low level transcripts.

and GLUT4 (31). Multiple mechanisms exist by which hormones and other factors control the rate of cellular glucose uptake via these transporters. These include the rapid translocation of preexisting transporters from an intracellular pool to the plasma membrane, modulation of the intrinsic activity of preexisting plasma membrane glucose transporters, and stimulation of the synthesis of new transporters (32). We clearly observed increased transporter synthesis, since our results demonstrated increases in the expression of both GLUT1 and GLUT4 transporters on mRNA and protein

levels (5- to 10-fold maximal enhancement for each). These results are in agreement with previous studies in which GLUT1 and GLUT4 mRNA and protein levels were shown to increase during differentiation of 3T3 preadipose cells (27, 33). Our observed increase in glucose transporter activity appeared to be somewhat greater in proportion than the combined increases in the synthesis of the two transporter proteins. This observation indicated that another mechanism, such as increased intrinsic activity of transporters, may also contribute to the effect. Such regulation of intrinsic transporter activity has previously been reported (34, 35). Inhibition of 3T3-L1 adipocyte protein synthesis by anisomycin, for instance, appeared to stimulate glucose transport primarily by enhancing the intrinsic catalytic activity of cell surface GLUT1, and to a lesser extent GLUT4 proteins (34). Further, treatment of 3T3-L1 preadipocytes with tumor necrosis factor-α reportedly increased glucose transport and GLUT1 transporter intrinsic activity (35). Alternatively, it is possible that the apparent difference in glucose transport activity and glucose transporter protein levels may be a consequence of our presentation of data as fold-enhancement relative to low level controls. As such, we may have some differences in detection sensitivity rather than absolute differences in the magnitude of changes.

Increased mRNA abundance can be attributed to enhanced RNA transcription and/or increased message stability. It was previously established that increases in the steady state level of several mRNAs during differentiation were accompanied by activation of specific gene transcription (36–39). This was particularly shown for mRNAs whose abundance was increased markedly (20- to 100-fold) during differentiation, including the aP2 and glycerolphosphate dehydrogenase genes (36). The same report showed no significant changes in the rates of transcription of mRNAs for which abundance was more moderately altered (2- to 4-fold) during differentiation, such as those encoding fructose-1,6-biphosphate, β-actin, and β-tubulin (36). In any case, most adipocyte mRNAs were far more abundant than would be predicted by their increased nuclear transcription rates. When increases in steady state mRNA levels cannot be attributed to changes in transcription, other levels of control such as mRNA stability likely contribute to the relative abundance of mRNAs during adipocyte differentiation. Since we observed moderate increases in GLUT1 and GLUT4 mRNA abundance (about 5-fold) with adipocyte differentiation, we compared mRNA half-lives in undifferentiated and differentiated cells using Act D (a transcription inhibitor) chase experiments. Differentiation of 3T3-F442A cells by insulin and/or pioglitazone dramatically increased the mRNA half-lives for GLUT1 and GLUT4 above their values in undifferentiated cells, i.e. from 1–2 h up to greater than 24 h. Such stabilization of these mRNAs with adipocyte differentiation correlated well with increases in the mRNA steady state levels. It is interesting to note that Actinomycin D itself has been reported in a few instances to have mRNA stabilizing effects (40–42). It would therefore be possible to extend our observations by conducting experiments using different transcription inhibitors such as 5,6-dichloro-1-β-D-ribofuranosylbenzimidazole or thiolutin, or using a different method such as [^{3}H]uridine pulse to

verify message stability. However, our observed dramatic increase in the stability of transcripts encoding glucose transporters in adipocytes versus fibroblasts seems likely to remain, though there may be some differences in the absolute calculated half-lives.

Our findings represent the first study that directly associates increased steady state mRNA levels during adipocyte differentiation with increased mRNA stability. This process was, however, predicted earlier based on observed increases in mRNA transcript levels that could not be explained by increased gene transcription (36–38). Regulation of mRNA stability in such cells has, in fact, been reported for other conditions. Treatment of 3T3-F442A mature adipocytes with retinoic acid, for instance, specifically decreased the adipsin mRNA level (43). For such studies, the rate of adipsin gene transcription remained unchanged, whereas the half-life of adipsin mRNA was greatly shortened in retinoic acid-treated adipocytes as compared with untreated cells (37.6–7.3 h). Another example is the induction of GLUT1, as well as other immediate-early growth-related protooncogenes, in 3T3-L1 fibroblasts by treatment with tumor necrosis factor-α (26, 35) and 8-bromo-cAMP (44). Whereas transcriptional activation of immediate-early genes correlated well with subsequent accumulation of their respective mRNAs, increased GLUT1 mRNA was due to an apparent increase in the stability of this message (45 min to several hours) without changes in its transcription. Another study showed that increased GLUT1 mRNA abundance by chronic exposure of L6 myocytes to insulin was due to increased transcription as well as prolonged half-life (2–5 h) (45).

In general, the stabilization/destabilization of mRNAs in response to biological and pharmacological stimuli has been recognized as an important posttranscriptional step for regulation of gene expression (46–49). Despite that, the mechanisms underlying such processes, including the signals that trigger mRNA degradation or stabilization, the structural elements of the RNA that are recognized by degradative enzymes or stabilization factors, as well as the enzymes or other *trans*-acting factors themselves, are largely unknown (46, 49–52). Interestingly, a recent report indicated that the 3'-untranslated region of GLUT1 mRNA contains a single copy of the destabilizing AUUUA motif in the context of an AU-rich region (26). The stability of GLUT1 mRNA was found to be partially controlled by its interaction with a sequence-specific mRNA binding protein, the adenosine-uridine binding factor which was speculated to mediate mRNA stabilization by blocking the AU-destabilizing motifs (26). We therefore propose that increasing mRNA abundance during differentiation by increasing message stability presents an interesting phenomenon awaiting further examination. Future efforts should be particularly directed toward identifying common mRNA sequences that may function as stabilizing elements in the differentiation-induced mRNAs as well as identifying their regulatory binding proteins.

Acknowledgments

References

1. DiGirolamo M, Newby FD, Lovejoy J 1992 Lactate production in adipose tissue: a regulated function with extra-adipose implications. FASEB J 6:2405–2412
2. Lonnroth P 1991 Regulation of insulin action at the cellular level. J Int Med 229:23–29
3. Spiegelman BM 1988 Regulation of gene expression in the adipocyte: implications for obesity and proto-oncogene function. Trends Genet 4:203–207
4. Olefsky JM, Garvey WT, Henry RR, Brillon D, Matthei S, Freidenberg GR 1988 Cellular mechanisms of insulin resistance in non-insulin dependent (type II) diabetes. Am J Med 85:86–104
5. Moller DE, Flier JS 1991 Insulin resistance–mechanisms, syndromes, and implications. N Engl J Med 325:938–948
6. DeFronzo RA, Bonadonna RC, Ferrannini E 1992 Pathogenesis of NIDDM: a balanced overview. Diabetes Care 15:318–353
7. Gerich JE 1989 Oral hypoglycemic agents. N Engl J Med 321:1231–1245
8. Melander A, Bitzen P, Faber O, Groop L 1989 Sulfonylurea antidiabetic drugs. An update of their clinical pharmacology and rational therapeutic use. Drugs 37:58–72
9. Hofmann CA, Colca JR 1992 New oral thiazolidinedione antidiabetic agents act as insulin-sensitizers. Diabetes Care 15:1075–1078
10. Ikeda H, Taketomi S, Sugiyama Y, Sodha T, Meguro K, Fujita T 1990 Effects of pioglitazone on glucose and lipid metabolism in normal and insulin resistant animals. Arzneim-Forsch/Drug Res 40:156–160
11. Hofmann C, Lorenz K, Colca JR 1991 Glucose transport deficiency in diabetic animals is corrected by treatment with the oral antihyperglycemic agent pioglitazone. Endocrinology 129:1915–1925
12. Kraegen EW, James DE, Jenkins AB, Chisholm DJ, Storlien LH 1989 A potent *in vivo* effect of ciglitazone on muscle insulin resistance induced by high fat feeding of rats. Metabolism 38:1089–1093
13. Chang AY, Wyse BM, Gilchrist BJ 1983 Ciglitazone, a new hypoglycemic agent. II. Effect on glucose and lipid metabolisms and insulin binding in the adipose tissue of C57BL/6J-ob/ob and -+/? mice. Diabetes 32:839–845
14. Sandouk T, Reda D, Hofmann C, The antidiabetic agent pioglitazone enhances adipocyte differentiation of 3T3-F442A cells. Am J Physiol, in press
15. Kletzien RF, Clarke SD, Ulrich RG 1992 Enhancement of adipocyte differentiation by an insulin-sensitizing agent. Mol Pharmacol 41:393–398
16. Hiragun A, Sato M, Mitsui H 1988 Preadipocyte differentiation in vitro: identification of a highly active adipogenic agent. J Cell Physiol 134:124–130
17. Schwartz J, Carter-Su C 1988 Effects of growth hormone on glucose metabolism and glucose transport in 3T3-F442A cells: dependence on cell differentiation. Endocrinology 122:2247–2256
18. Chomczynski P, Sacchi N 1987 Single-step method of RNA isolation by acid guanidinium thiocyanate-phenol-chloroform extraction. Anal Biochem 162:156–159
19. Fourney RM, Miyashi J, Day RS, Paterson MC 1988 Northern blotting: efficient RNA staining and transfer. FOCUS 10:5–7
20. Gould GW, Lienhard GE 1989 Expression of a functional glucose transporter in Xenopus oocytes. Biochem 28:9447–9452
21. Birnbaum MJ 1989 Identification of a novel gene encoding an insulin-responsive glucose transporter protein. Cell 57:305–315
22. Bonini J, Hofmann C 1991 A rapid, accurate, nonradioactive method for quantitating RNA on agarose gels. Biotechnology 11:708–709
23. Kaestner KL, Flores-Riveros JR, McLenithan JC, Janicot M, Lane MD 1991 Transcriptional repression of the mouse insulin-responsive glucose transporter (GLUT4) gene by cAMP. Proc Natl Acad

Sci USA 88:1933–1937

24. Dani C, Bertrand B, Bardon S, Doglio A, Amri EZ, Grimaldi P 1989 Regulation of gene expression by insulin in adipose cells: opposite effects on adipsin and glycerolphosphate dehydrogenase genes. Mol Cell Endocrinol 63:199–208

25. Cornelius P, Marlowe M, Lee MD, Pekala PH 1990 The growth factor-like effects of tumor necrosis factor-alpha. Stimulation of glucose transport activity and induction of glucose transporter and immediate early gene expression in 3T3-L1 preadipocytes. J Biol Chem 265:20506–20516

26. Stephens JM, Carter BZ, Pekala PH, Malter JS 1992 Tumor necrosis factor-alpha induced glucose transporter (GLUT1) mRNA stabilization in 3T3-L1 preadipocytes. J Biol Chem 267:8336–8341

27. Weiland M, Schurmann A, Schmidt WE, Joost H 1990 Development of the hormone-sensitive glucose transport activity in differentiating 3T3-L1 murine fibroblasts. Biochem J 270:331–336

28. Bradford MM 1976 A rapid and sensitive method for the quantitation of microgram quantities of protein using the principle of protein-dye binding. Anal Biochem 72:248–254

29. Laemmli UK 1970 Cleavage of structural proteins during the assembly of the head of bacteriophage T4. Nature 227:680–685

30. Sugiyama Y, Shimura Y, Ikeda H 1990 Effects of pioglitazone on hepatic and peripheral insulin resistance in Wistar fatty rats. Arzneim-Forsch/Drug Res 40:436–440

31. Kayano T, Burant CF, Fukumoto H, Gould GW, Fan Y, Eddy R, Byers MG, Shows TB, Seino S, Bell GI 1990 Human facilitative glucose transporters. J Biol Chem 265:13276–13282

32. Pessin JE, Bell GI 1992 Mammalian facilitative glucose transporter family: structure and molecular regulation. Annu Rev Physiol 54:911–930

33. Hainque B, Guerre-Millo M, Hainault I, Moustaid N, Wardzala LJ, Lavau M 1990 Long term regulation of glucose transporters by insulin in mature 3T3-F442A adipose cells. J Biol Chem 265:7982–7988

34. Harrison SA, Clancy BM, Pessino A, Czech MP 1992 Activation of cell surface glucose transporters measured by photoaffinity labeling of insulin-sensitive 3T3-L1 adipocytes. J Biol Chem 267:3783–3788

35. Cornelius P, Marlowe M, Douglas LM, Pekela PH 1990 The growth factor-like effects of tumor necrosis factor-alpha. J Biol Chem 265:20506–20516

36. Bernlohr DA, Bolanowski MA, Kelly TJ, Lane MD 1985 Evidence for an increase in transcription of specific mRNAs during differentiation of 3T3-L1 preadipocytes. J Biol Chem 260:5563–5567

37. Djian P, Phillips M, Green H 1985 The activation of specific gene transcription in the adipose conversion of 3T3 cells. J Cell Physiol 124:554–556

38. Cook KS, Hunt CR, Spiegelman BM 1985 Developmentally regulated mRNAs in 3T3-adipocytes: analysis of transcriptional control. J Cell Biol 100:514–520

39. Chapman AB, Knight DM, Ringold GM 1985 Glucocorticoid regulation of adipocyte differentiation: hormonal triggering of the developmental program and induction of a differentiation-dependent gene. J Cell Biol 101:1227–1235

40. Knutsen HK, Tasken KA, Eskild W, Jahnsen T, Hansson V 1991 Adenosine 3',5'-monophosphate-dependent stabilization of messenger ribonucleic acids (mRNAs) for protein kinase-A (PKA) subunits in rat sertoli cells: rapid degradation of mRNAs for PKA subunits is dependent on ongoing RNA and protein synthesis. Endocrinology 129:2496–2502

41. Pontecorvi A, Jamshed JR, Phyillaier M, Robbins J 1988 Selective degradation of mRNA: the role of short-lived proteins in differential destabilization of insulin-induced creatine phosphokinase and myosin heavy chain mRNAs during rat skeletal muscle L6 cell differentiation. EMBO J 7:1489–1495

42. Iynedijan PB, Jotterand D, Nouspikel T, Asfari M, Pitot PR 1989 Transcriptional induction of glucokinase gene by insulin in cultured liver cells and its repression by the glucagon-cAMP system. J Biol Chem 264:21824–21829

43. Antras J, Lasnier F, Pairault J 1991 Adipsin gene expression in 3T3-F442A adipocytes is posttranscriptionally down-regulated by retinoic acid. J Biol Chem 266:1157–1161

44. Cornelius P, Marlowe M, Call K, Pekala PH 1991 Regulation of glucose transport as well as glucose transporter and immediate early gene expression in 3T3-L1 preadipocytes by 8-bromo-cAMP. J Cell Physiol 146:298–308

45. Maher F, Harrison LC 1990 Stabilization of glucose transporter mRNA by insulin/IGF-1 and glucose deprivation. Biochem Biophys Res Commun 171:210–215

46. Raghow R 1987 Regulation of messenger RNA turnover in eukaryotes. Trends Biochem Sci 12:358–360

47. Ross J 1988 Messenger RNA turnover in eukaryotic cells. Mol Biol Med 5:1–4

48. Stephens JM, Pekala PH 1991 Transcriptional repression of the GLUT4 and C/EBP genes in 3T3-L1 adipocytes by tumor necrosis factor-alpha. J Biol Chem 266:21839–21845

49. Stephens JM, Pekala PH 1992 Transcriptional repression of the C/EBP-alpha and GLUT4 genes in 3T3-L1 adipocytes by tumor necrosis factor. J Biol Chem 267:13580–13584

50. Jackson RJ, Standart N 1993 Do the poly(A) tail and 3' untranslated region control mRNA translation? Cell 62:15–24

51. Klausner RD, Horford JB 1989 Cis-trans models for post-transcriptional gene regulation. Science 246:870–872

52. Brawerman G 1989 mRNA decay: finding the right targets. Cell 57:9–10

L-Glutamic Acid γ-Monohydroxamate

A POTENTIATOR OF VANADIUM-EVOKED GLUCOSE METABOLISM *IN VITRO* AND *IN VIVO**

Itzhak Goldwaser‡§¶, Jinping Li‡, Eytan Gershonov‡§, Michal Armoni‖, Eddy Karnieli‖, Mati Fridkin§, and Yoram Shechter‡ ‡‡**

From the ‡Departments of Biological Chemistry and §Organic Chemistry, The Weizmann Institute of Science, Rehovot 76100, Israel and the ‖Institute of Endocrinology, Rambam Medical Center and the B. Rappaport Faculty of Medicine, Technion, Haifa 31096, Israel

We report that the vanadium ligand L-Glu(γ)HXM potentiates the capacity of free vanadium ions to activate glucose uptake and glucose metabolism in rat adipocytes *in vitro* (by 4–5-fold) and to lower blood glucose levels in hyperglycemic rats *in vivo* (by 5–7-fold). A molar ratio of two L-Glu(γ)HXM molecules to one vanadium ion was most effective. Unlike other vanadium ligands that potentiate the insulinomimetic actions of vanadium, L-Glu(γ)HXM partially activated lipogenesis in rat adipocytes in the absence of exogenous vanadium. This effect was not manifested by D-Glu(γ)HXM. At 10–20 μM L-Glu(γ)HXM, lipogenesis was activated 9–21%. This effect was approximately 9-fold higher (140 ± 15% of maximal insulin response) in adipocytes derived from rats that had been treated with vanadium for several days. Titration of vanadium(IV) with L-Glu(γ)HXM led to a rapid decrease in the absorbance of vanadium(IV) at 765 nm, and ^{51}V NMR spectroscopy revealed that the chemical shift of vanadium(IV) at −490 ppm disappeared with the appearance of a signal characteristic to vanadium(V) (−530 ppm) upon adding one equivalent of L-Glu(γ)HXM. In summary, L-Glu(γ)HXM is highly active in potentiating vanadium-activated glucose metabolism *in vitro* and *in vivo* and facilitating glucose metabolism in rat adipocytes in the absence of exogenous vanadium probably through conversion of trace intracellular vanadium into an active insulinomimetic compound. We propose that the active species is either a 1:1 or 2:1 L-Glu(γ)HXM vanadium complex in which the endogenous vanadium(IV) has been altered to vanadium(V). Finally we demonstrate that L-Glu(γ)HXM- and L-Glu(γ)HXM·vanadium-evoked lipogenesis is arrested by wortmannin and that activation of glucose uptake in rat adipocytes is because of enhanced translocation of GLUT4 from low density microsomes to the plasma membrane.

Intensive studies have been carried out during the last two decades on the insulinomimetic effects of vanadium (1–4). Vanadium salts mimic most of the effects of insulin on the main target tissues of the hormone *in vitro* and also induce normoglycemia and improve glucose homeostasis in insulin-deficient (5–7) and insulin-resistant diabetic rodents *in vivo* (5–8). On the basic research frontier, data continue to accumulate showing that vanadium salts manifest their insulin-like metabolic effects through alternative pathways not involving insulin receptor tyrosine kinase activation or phosphorylation of insulin receptor substrate 1 (9–19). The key events of this backup system appear to involve inhibition of protein-phosphotyrosine phosphatases and activation of nonreceptor protein-tyrosine kinases (20–23).

Vanadium salts are seriously considered as a possible treatment for diabetes, and several clinical studies have already been performed. In those studies, because of its toxicity, only low doses of vanadium (2 mg/kg/day) were used. Although ∼20-fold lower than doses used in most animal studies, several beneficial effects were observed and documented (24–26). Any manipulation to elevate the insulinomimetic efficacy of vanadium without increasing its toxicity is of major clinical interest for the future care of diabetes (reviewed in Ref. 27).

Organically chelated vanadium compounds, such as vanadium·acetylacetonate and vanadium·RL-252,[1] are more potent than free vanadium in facilitating insulin-like effects in rat adipocytes (28, 29). Similarly, chelated vanadium compounds such as bis(maltolato)oxovanadium and bis(picolinato)oxovanadium are more effective than free vanadium in reducing circulating glucose levels in hyperglycemic streptozocin-treated rats (30–33).

In the wake of these findings, we have continued our search for more effective vanadium binding agents. Of special interest to us were vanadium chelators that synergize with vanadium both *in vivo* (*i.e.* in streptozocin rats) and *in vitro* (*i.e.* in isolated rat adipocytes) and therefore enable us to gain insight into the basic mechanism(s) by which such compounds potentiate the insulinomimetic activity of vanadium. Specifically, we have studied hydroxamic acid derivatives. These compounds are involved in the microbial transport of iron and are therefore applied therapeutically in conditions of iron deficiency (34). They are also inhibitors of urease activity and have been used in the treatment of hepatic coma. Monoamino acid hydroxamates are simple, nontoxic derivatives of amino acids. D-Aspartic acid β-hydroxamate was shown to have antitumoral activity on murine leukemia L5178Y, both *in vitro* and *in vivo*, and is

[1] The abbreviations used are: RL-252, [(CH$_2$)$_2$-C-[CH$_2$O-(CH$_2$)$_2$-CO-NHCH(iBu)CONOHCH$_2$]$_2$]; L-Glu(γ)HXM, L-glutamic acid γ-monohydroxamate; GLUT4, glucose transporter 4; PM, plasma membranes; LDM, low density microsomes; BSA, bovine serum albumin; VOCl$_2$, vanadyl dichloride; NaVO$_3$, sodium metavanadate.
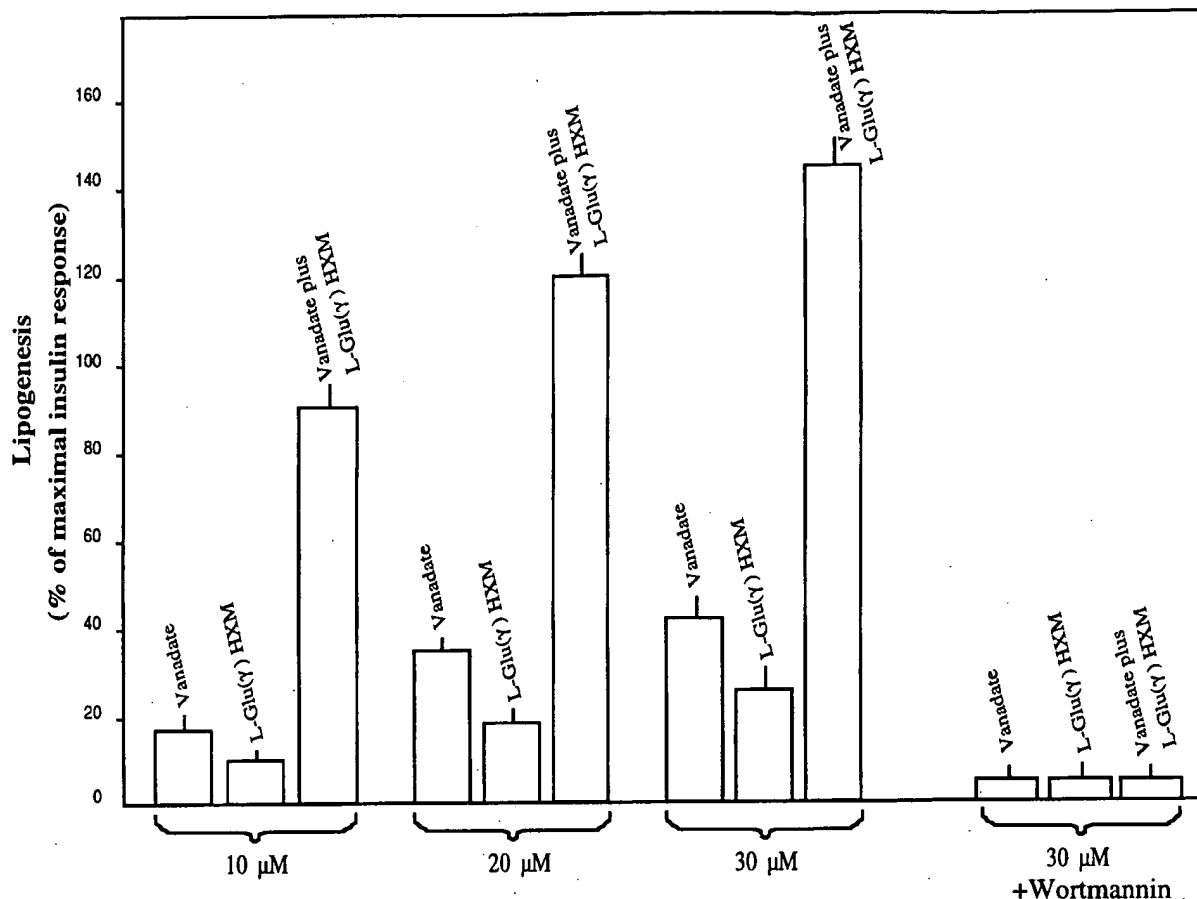
FIG. 1. **Increase in the lipogenic capacity of vanadium(V) following the addition of L-glutamic acid(γ)monohydroxamate.** Freshly prepared rat adipocytes (3 × 10^5 cells/ml) suspended in KRB buffer, pH 7.4, containing 0.7% BSA were preincubated for 10 min with the indicated concentrations of NaVO$_3$, free Glu(γ)HXM, and a 1:1 complex of L-Glu(γ)HXM·NaVO$_3$. The cells were then supplemented with [U-^{14}C]glucose, and lipogenesis was performed for 2 h at 37 °C. Radioactivity incorporated into extracted lipids was then determined. Maximal response (100%) is that obtained in the presence of 17 nM insulin.

active against Friend leukemia cells *in vitro* as well (35). L-Glu(γ)HXM is cytotoxic against L1210 cells in culture and remarkably antitumoral against L1210 leukemia and B16 melanoma *in vivo* (35, 36).

EXPERIMENTAL PROCEDURES

Materials—D-[U-^{14}C]glucose and 2-deoxy-D-[G-^{3}H]glucose were purchased from NEN Life Science Products. Collagenase type I (134 units/mg) was obtained from Worthington. Porcine insulin was purchased from Eli Lilly Co. (Indianapolis, IN). Phloretin, 2-deoxyglucose, L-glutamic acid(γ)-monohydroxamate, L-aspartic acid(β)monohydroxamate, glycine hydroxamate, L-isoleucine(α)hydroxamate, and L-tyrosine(α)hydroxamate were purchased from Sigma. RL-252 was prepared and characterized as described earlier (28).

Krebs-Ringer bicarbonate (KRB) buffer (pH 7.4) contained 110 mM NaCl, 25 mM NaHCO$_3$, 5 mM KCl, 1.2 mM KH$_2$PO$_4$, 1.3 mM CaCl$_2$, 1.3 mM MgSO$_4$. Krebs-Ringer bicarbonate HEPES (KRBH) buffer (pH 7.4) consisted of 117 mM NaCl, 10 mM NaHCO$_3$, 1 mM CaCl$_2$, 1 mM MgSO$_4$, 4 mM KH$_2$PO$_4$, 30 mM HEPES. All other chemicals and reagents used in this study were of analytical grade.

Streptozocin-treated Rats—Diabetes was induced by a single intravenous injection of a freshly prepared solution of streptozocin (55 mg/kg body weight) in 0.1 M citrate buffer, pH 4.5 (9). The effect of the L-Glu(γ)HXM·vanadium complex on blood glucose level was determined 8 days after induction of diabetes by streptozocin.

Cell Preparation and Bioassays—Rat adipocytes were prepared from the fat pads of male Wistar rats (130–150 g) by collagenase digestion according to the method of Rodbell (37). Cell preparations showed more than 95% viability by Trypan blue exclusion at least 3 h after digestion. All bioassays were performed as described in figure legends. Glucose transport was carried out using 2-deoxy-D-[G-^{3}H]glucose uptake (38),

and lipogenesis (the incorporation of U-^{14}C-labeled glucose into lipids) was performed according to Moody *et al.* (39). Briefly, freshly prepared rat adipocytes were suspended in KRBH, 0.7% BSA buffer and divided into about 50 plastic vials. Each vial contained 0.5 ml of adipocyte suspension (about 1.5 × 10^5 cells). These were incubated for 2 h at 37 °C under an atmosphere of 95% O$_2$, 5% CO$_2$ with 0.16 mM [U-^{14}C]glucose. Each assay contained vials with and without 17 nM insulin and the various test compounds. Lipogenesis was terminated by adding toluene-based scintillation fluid, and the extracted lipids were counted (39). Results are expressed as a percent of maximal insulin response. Only assays in which insulin activated lipogenesis 5–6-fold above basal (basal ~4000 cpm/1.5 × 10^5 cells/2 h, $V_{insulin}$ = 20,000–24,000 cpm/1.5 × 10^5 cells/2 h) were taken into consideration. Insulin activated lipogenesis in this assay at an ED$_{50}$ value of 33 ± 3 pM. A concentration of 0.3 nM insulin and above already facilitated maximal (100%) response (*i.e.* Ref. 16). All assays were performed in duplicate or triplicate.

Western Immunoblot Analysis of GLUT4 in Subcellular Membranes Following Stimulation of Rat Adipocytes—Adipocytes prepared from 6-week-old rats were incubated with and without insulin and with L-Glu(γ)HXM alone and complexed with vanadate as specified in the figure. Cells were then homogenized and fractionated to low density microsomal membrane (LDM) and plasma membrane (PM) fractions by differential ultracentrifugation according to Ref. 40. Membrane proteins were then solubilized in sample buffer for 30 min at 25 °C, resolved on 10% SDS-polyacrylamide gel electrophoresis, transferred to nitrocellulose paper, and immunoblotted with anti-GLUT4 antisera (41). Visualization was performed by phosphoimaging. The relative intensity of bands corresponding to GLUT4 was quantitated using MacBas 1000.

^{51}*V NMR Spectroscopy*—The ^{51}V NMR spectra were recorded on a 200-MHz Bruker WPS4 (4.7T) spectrometer. Spectrum width of 16,000
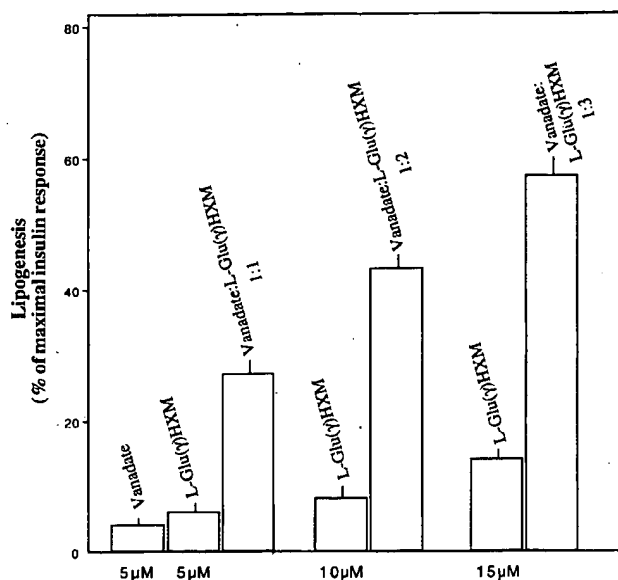
FIG. 2. **Stimulation of lipogenesis at varying molar ratios of** L-Glu(γ)HXM **to vanadium(V).** Freshly prepared rat adipocytes (3 × 10^5 cells/ml) suspended in KRB buffer, pH 7.4, containing 0.7% BSA were preincubated for 10 min with the indicated concentrations of 1:1 to 3:1 molar stoichiometry of L-Glu(γ)HXM to NaVO₃ or with free NaVO₃(V) and free L-Glu(γ)HXM. The cells were then supplemented with [U-^{14}C]glucose, and lipogenesis was performed for 2 h at 37 °C. Radioactivity incorporated into extracted lipids was then determined. Maximal response (100%) is that obtained in the presence of 17 nM insulin.

H_3, a 90° pulse angle, and an accumulation time of 0.28 were used. The chemical shifts are reported relative to the external reference standard $VOCl_2$ (−490 ppm).

RESULTS

L-Glutamic Acid(γ)Monohydroxamate Potentiates Vanadium-evoked Lipogenesis in Rat Adipocytes—In this set of experiments, rat adipocytes were incubated for 10–20 min with submaximal concentrations of vanadate (10–30 μM), L-Glu(γ)HXM (10–30 μM), or an equimolar combination of them. The capacity to activate lipogenesis relative to insulin was then determined. As shown in Fig. 1, the combination was highly synergistic. For example, at 10 μM vanadate or L-Glu(γ)HXM, lipogenesis was 17 ± 3 and 9 ± 2%, respectively, whereas the combination produced a marked incredible 93 ± 4% activation of maximal insulin response. At 20 μM, the extent of lipogenesis was 37 ± 3, 20 ± 3, and 121 ± 7%, and at 30 μM, it was 42 ± 4, 23 ± 4, and 143 ± 7% of maximal. Wortmannin (100 nM), an inhibitor of phosphatidylinositol 3-kinase, fully blocked the activating effects of vanadate, L-Glu(γ)HXM, and its combination with vanadate (Fig. 1, *right columns*). Thus L-Glu(γ)HXM potentiated vanadate-evoked lipogenesis about 3.5–5-fold; the higher concentrations reached a level that is about 140% of that achieved by saturating concentrations of insulin or vanadate. A finding of significant interest to us was the ability of L-Glu(γ)HXM to partially activate lipogenesis even in the absence of exogenous vanadium (Fig. 1). This finding is examined in great detail in connection with Fig. 6.

In Fig. 2, lipogenesis in rat adipocytes was evaluated at a fixed, low concentration of vanadate (5 μM) with increasing concentrations of L-Glu(γ)HXM. Lipogenesis was negligible at 5 μM vanadate or L-Glu(γ)HXM alone (4–6% of maximal insulin effect) but is augmented to 27.0 ± 3% when they were given in combination (at a molar stoichiometry of 1:1). At 2:1 and 3:1 Glu(γ)HXM-vanadium molar stoichiometry, lipogenesis expanded to 43 and 57%, respectively, of maximal response. Thus
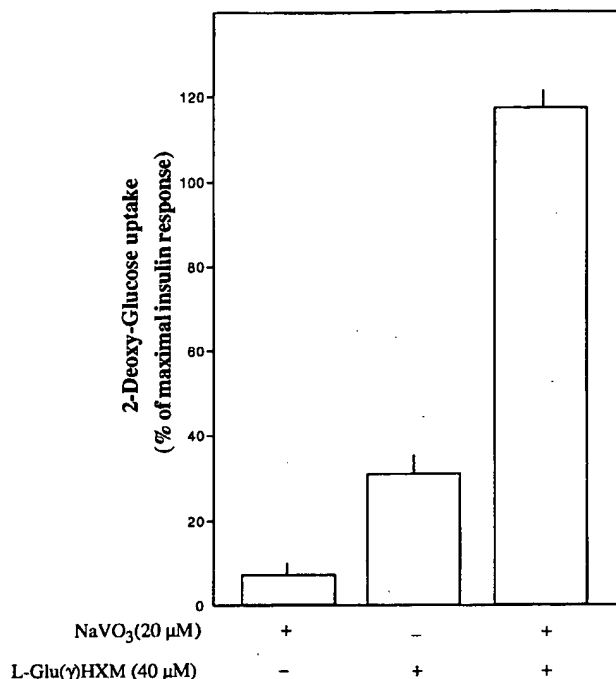
FIG. 3. **Potentiation of hexose uptake by** L-Glu(γ)HXM·**vanadium** (2:1). Adipocytes (2 × 10^6 cells/ml) suspended in KRBH buffer containing 1% BSA were preincubated in the presence and absence of insulin (17 nM), sodium metavanadate (20 μM), L-Glu(γ)HXM (40 μM), and their combination (at 1:2 molar stoichiometry). Aliquots (70 μl) were transferred into tubes containing 2-deoxy-D-[6-^{3}H]glucose (0.1 mM final concentration). Phloretin (0.1 mM) was added after 3 min for transport termination. This was followed by centrifugation of aliquots through a silicone layer.

a substantial synergistic effect is obtained at a 1:1 molar ratio and is increased further at a 2:1 molar stoichiometry and even higher, though much less pronounced, at a 3:1 molar ratio (Fig. 2).

L-Glu(γ)HXM Potentiates Vanadate-evoked Glucose Uptake—Fig. 3 shows activation of 2-deoxyglucose uptake by low concentrations of vanadate (20 μM), L-Glu(γ)HXM (40 μM), and by the 2:1 molar combination, of them. 2-Deoxyglucose undergoes insulin- or vanadate-evoked influx into the cell via the same transporters as glucose and is phosphorylated *in situ* to 2-deoxyglucose 6-phosphate with no further metabolism (42, 43). Therefore, this measurement reflects an effect on glucose entry into the cell in a manner largely independent of the metabolism of the endogenous saccharide. Vanadate (20 μM) and L-Glu(γ)HXM (40 μM) affected 2-deoxyglucose uptake of 7 ± 0.7 and 31 ± 4% of maximal insulin effect, respectively. Together they caused 2-deoxyglucose uptake 117 ± 9% of maximal insulin response (Fig. 3).

L-Glu(γ)HXM Alone and L-Glu(γ)HXM·*Vanadate Lead to Translocation of GLUT4 from LDM to PM Fractions in Rat Adipocytes*—Incubation of rat adipocytes with L-Glu(γ)HXM and L-Glu(γ)HXM·vanadate led to a decrease in the content of GLUT4 in the LDM fraction and an increase in the PM fraction (Fig. 4). The decrease in GLUT4 content in the low density lipoprotein fraction amounted to 32 ± 3, 3 ± 1, and 68 ± 5% of maximal insulin response upon incubating the cells with L-Glu(γ)HXM (40 μM), vanadate (20 μM, not shown), and the combination, respectively (calculated from Fig. 4). Under similar experimental conditions, L-Glu(γ)HXM, vanadate, and the combination activated 2-deoxyglucose uptake to an extent of 31 ± 4, 7 ± 0.7, and 117 ± 9% of maximal insulin response (Fig. 3), suggesting a contributing effect of the complex to glucose influx in addition to its effect in recruiting GLUT4 transporters
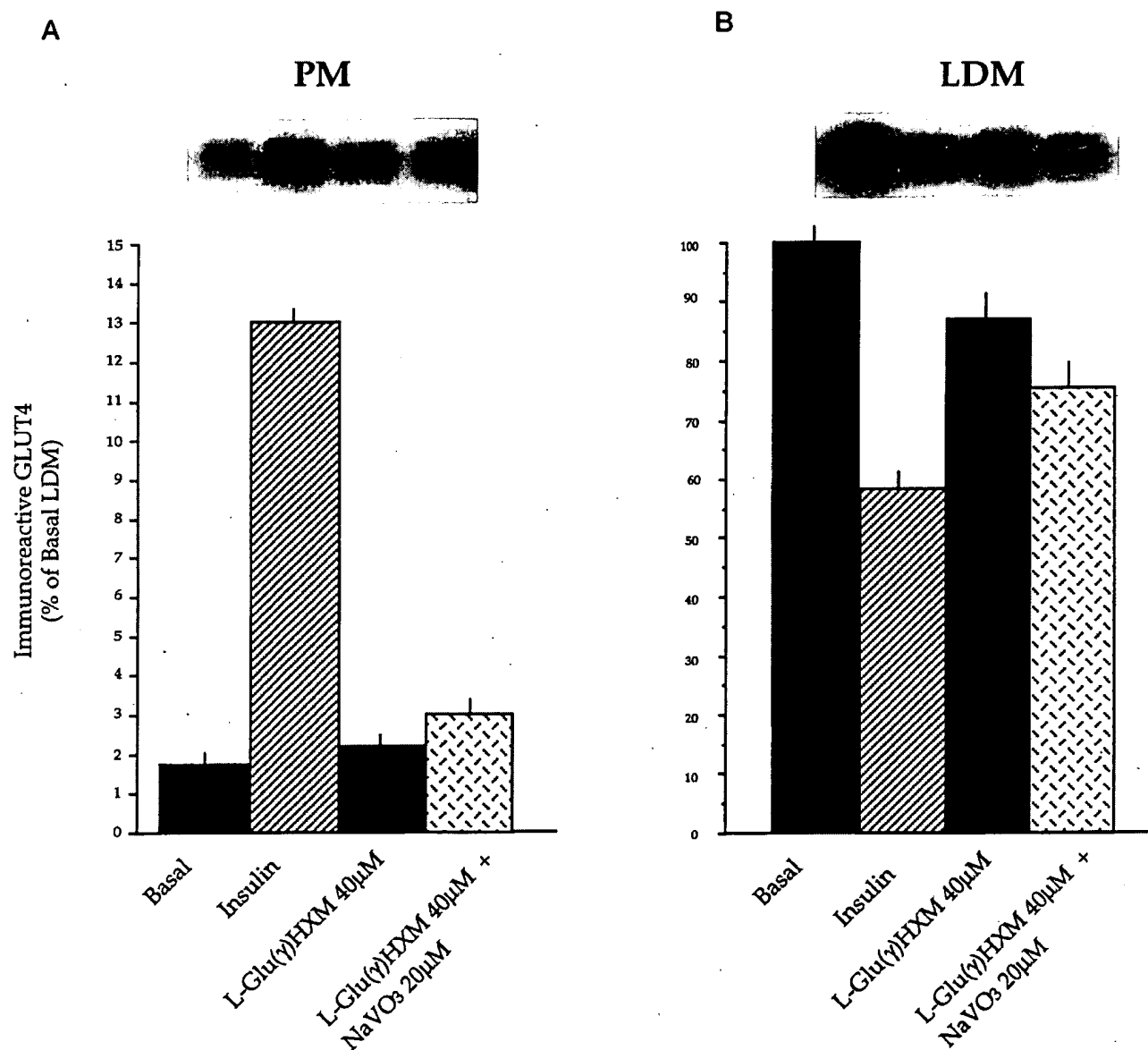
A

PM

B

LDM

FIG. 4. L-Glu(γ)HXM alone or complexed with vanadate induces translocation of GLUT4 from LDM to PM fraction in rat adipocytes. Rat adipocytes were incubated for 30 min at 37 °C in the presence and the absence of insulin (17 nM) and the indicated concentrations of L-Glu(γ)HXM or L-Glu(γ)HXM·vanadate. Cells were then homogenized and fractionated to PM and LDM by differential ultracentrifugation, and GLUT4 protein was identified by Western immunoblot analysis ("Experimental Procedures"). Immunoreactive GLUT4 proteins were visualized by phosphoimaging (*top panels*) and were quantitated using MacBas 1000 software (histograms, *bottom panels*).

from the low density lipoprotein to the PM fraction.[2]

L-Glu(γ)HXM·Vanadate Normalizes Blood Glucose Levels in Streptozocin-treated Diabetic Rats—In the experiments summarized in Fig. 5, streptozocin-treated rats received intraperitoneally sodium metavanadate (0.05 mmol/kg body weight), L-Glu(γ)HXM (0.1 mmol/kg body weight), or a combination of the two compounds 8 days after the induction of diabetes. As shown in the figure, vanadate and L-Glu(γ)HXM, at these concentrations, had a rather minor effect in reducing the high circulating glucose levels characterizing these hyperglycemic rats. The combination, however, was highly efficient at normalizing blood glucose levels. Normoglycemia was evident 1 day after the first administration and remained so following two more administrations. The glucose levels then remained close

to normal for the next 3 days (Fig. 5).

Activation of Lipogenesis in Rat Adipocytes by L-Glu(γ)HXM in the Absence of Exogeneous Vanadium—L-glutamic acid(γ)HXM also activated lipogenesis in the absence of added vanadium, and this effect was studied in detail (Fig. 6). The dose-response curve (Fig. 6A) indicates that activation is already evident at 5 μM L-Glu(γ)HXM and that higher concentrations reach a level of 40 ± 7% of maximal insulin response (median effective dose = 35 ± 4 μM). Other amino acid hydroxamates such as L-Tyr(α)HXM, Gly(α)HXM, and L-Ile(α)HXM also activated lipogenesis, but they were considerably less potent (ED$_{50}$ = 250 ± 30 μM, 40 ± 5% of maximal insulin effect). L-Aspartic acid β-monohydroxamate showed higher lipogenic activity compared with the α-amino acid hydroxamates and was slightly less potent than L-Glu(γ)HXM (ED$_{50}$ = 45 ± 7 μM, Fig. 6B). N-acetyl-L-Glu(γ)HXM and L-Glu(γ)HXM-α-methyl ester were virtually ineffective, indicating the need for a free α-amino and, to a somewhat lesser extent, a free

---

[2] I. Goldwaser, J. Li, E. Gershonov, M. Armoni, E. Karnieli, M. Fridkin, and Y. Shechter, manuscript in preparation.

α-carboxyl moiety for the activation of lipogenesis by L-Glu(γ)HXM in the rat adipose cell (Fig. 6C). Stereospecificity appears crucial as well, because the D-isomer of Glu(γ)HXM was ineffective. All these
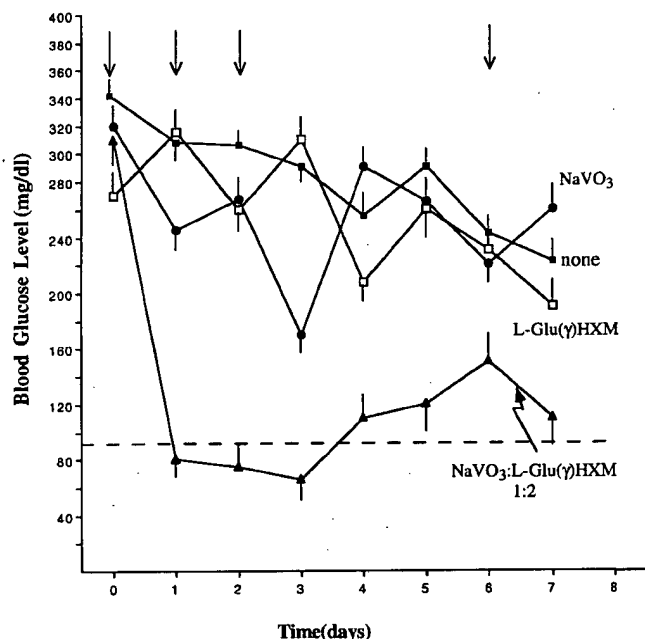

FIG. 5. Effect of L-Glu(γ)HXM·vanadate administration on blood glucose levels of streptozocin-treated rats. Male Wistar rats, 8 days after induction of diabetes (circulating glucose levels 310–340 mg/dalton), were divided into several groups. At the time points indicated by the *arrows* (intraperitoneal, at 11:00 a.m.), groups of diabetic rats received either vanadate (0.05 mmol/kg body weight ●), L-Glu(γ)HXM (0.1 mmol/kg body weight □), L-Glu(γ)HXM (0.1 mmol/kg) and vanadate (0.05 mmol/kg, ▲), or none (■). Circulating glucose levels were determined daily (at 8.00 a.m.). Each point in the figure represents the arithmetic mean of plasma glucose for 5 rats. The *dashed line* indicates the arithmetic mean of plasma glucose of control healthy male Wistar rats.

findings indicate that activation of lipogenesis by L-Glu(γ)HXM depends on a specific entry of this L-amino acid analog into the adipose cell. Further investigation has led us to suggest that L-Glu(γ)HXM enters the adipose cell primarily through the non-Na^+-dependent glutamine transport system.[2]

Several organic chelators, which potentiate the insulinomimetic activity of vanadium either *in vitro* or *in vivo*, have been documented. These include acetylacetonate (29), maltol (30, 31), picolinate (32, 33), and RL-252 (28). In Fig. 6D, we have examined whether they are capable of activating lipogenesis in the absence of exogenous vanadium. Unlike L-Glu(γ)HXM, none of these agents were able to activate lipogenesis in the rat adipose cell at concentrations of 100 μM (Fig. 6D) or lower (not shown).

Extensive Potentiation of L-Glu(γ)HXM-evoked Lipogenesis in Rat Adipocytes in Vitro Following Enrichment with Vanadium in Vivo—The findings presented in Figs. 1–4 have taught us that L-Glu(γ)HXM potentiates the insulinomimetic potency of vanadium and that activation of lipogenesis by L-Glu(γ)HXM alone never exceeds 40 ± 7% of maximal insulin effect (Fig. 6). To examine whether L-Glu(γ)HXM-evoked lipogenesis can be affected by the level of intracellular vanadium, a group of male Wistar rats received daily subcutaneous administrations of vanadate (0.1 mmol/kg/day) over a period of 5 days to raise the level of endogenous vanadium. Rats were then sacrificed 7 h after the last administration. Adipocytes were prepared, and the effect of L-Glu(γ)HXM on lipogenesis was compared with that in nontreated freshly prepared adipocytes. As shown in Fig. 7, vanadium-enriched adipocytes became dramatically sensitive to L-Glu(γ)HXM-evoked lipogenesis. This was valid both in terms of a leftward shift in the dose-response curve to L-Glu(γ)HXM ($ED_{50} = 6.4 ± 0.3$ μM *versus* $ED_{50} = 35 ± 4$ μM in control adipocytes) and in terms of the degree of lipogenesis (145 ± 15 *versus* 40 ± 7% of maximal insulin response, *i.e.* Fig. 6). At 10 μM, L-Glu(γ)HXM already stimulated lipogenesis and amounted to 120% of maximal insulin effect in the vanadium-enriched adipose cells (as opposed to only 8.0 ± 1.5% in control adipocytes) (Fig. 7).

FIG. 6. Activation of lipogenesis by L-Glu(γ)HXM in the absence of exogenous vanadium. Comparison to other amino acid(α)hydroxamates and ineffectiveness of the D-isomer and of chemically modified L-Glu(γ)HXM derivatives. Freshly prepared adipocytes (3 × 10^5 cells/ml) suspended in KRB buffer, pH 7.4, containing 0.7% BSA were preincubated for 10 min with the indicated concentrations of the various test compounds. The cells were then supplemented with [U-^{14}C]glucose (final concentration 0.16 mM), and lipogenesis was performed for 2 h at 37 °C. Radioactivity incorporated into extracted lipids was then determined. Maximal response (100%) is that obtained in the presence of 17 nM insulin.

FIG. 7. **Activation of lipogenesis by L-Glu(γ)HXM.** Comparison between normal adipocytes and vanadium-enriched adipocytes. Male Wistar rats received daily subcutaneously injected $NaVO_3$ (0.1mmol/kg/day) for 5 days (called enriched vanadium rats). The rats were then sacrificed (7 h after the last administration). Lipogenesis was performed comparing the freshly prepared rat adipocytes (3×10^5 cells/ml) from nonenriched vanadium rats with the enriched ones suspended in KRB buffer, pH 7.4, containing 0.7% BSA. The cells were preincubated for 10 min with the indicated concentrations of L-Glu(γ)HXM. The cells were then supplemented with $[U-^{14}C]$glucose, and lipogenesis was performed for 2 h at 37 °C. Radioactivity incorporated into extracted lipids was then determined. Maximal response (100%) is that obtained in the presence of 17 nM insulin.
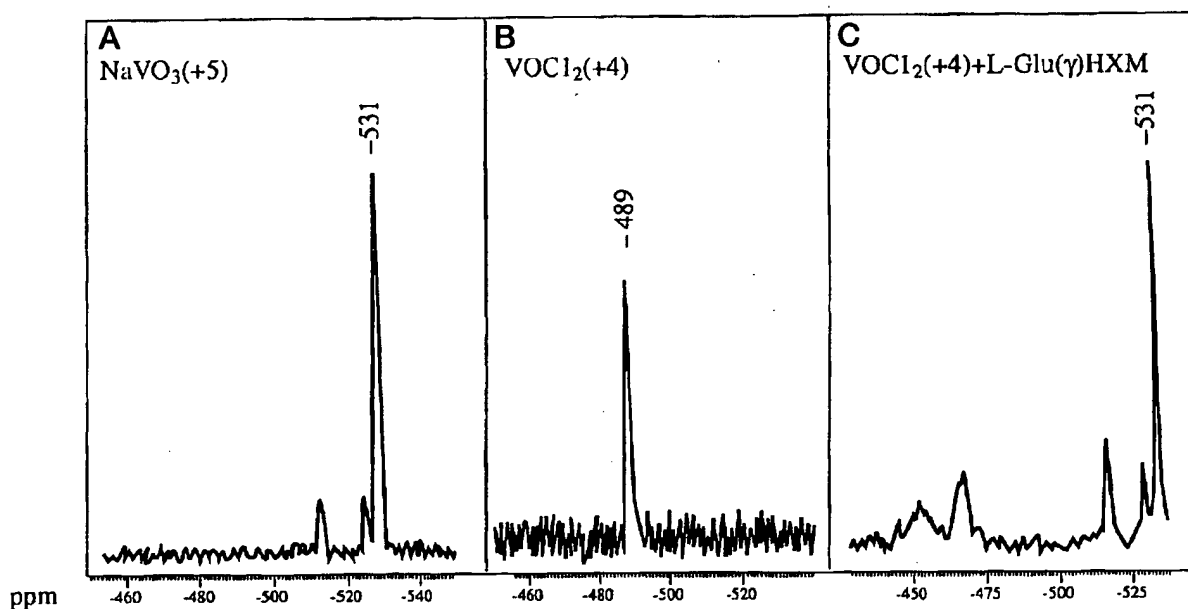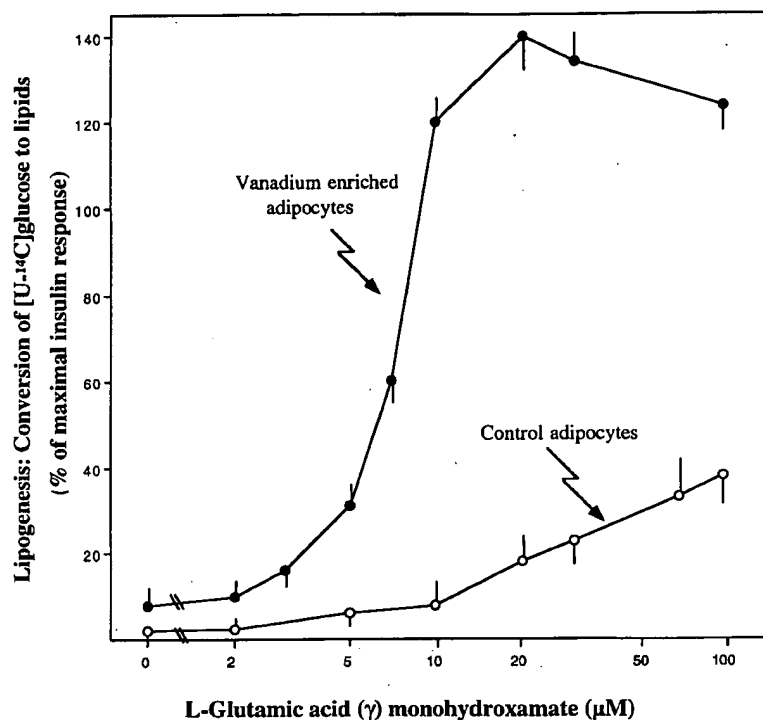
FIG. 8. ^{51}V NMR spectra of vanadium(V), vanadium(IV), and a mixture of vanadium(IV) with L-Glu(γ)monohydroxamate. *A*, ^{51}V NMR spectrum of sodium metavanadate (20 mM, pH 7.1); *B*, ^{51}V NMR spectrum of vanadium dichloride(IV) (20 mM, pH 6.8); *C*, ^{51}V NMR spectrum of a mixture (1:1 molar ratio) of $VOCl_2$(IV) and L-Glu(γ)HXM (20 mM, pH 7.0). Spectra were monitored with fresh solutions. In *C*, the spectrum was monitored 5 min after the addition of L-Glu(γ)HXM to $VOCl_2$.

Spectroscopic Studies—Previously we found in cell-free experiments that vanadium(IV), at neutral pH values, undergoes slow spontaneous oxidation to vanadium(V). This occurs similarly in the presence of 10 mM reduced glutathione, an ineffectual reductant of vanadium(V), at neutral pH values with a t_{ν_2} value of 1 ± 0.1 h at 25 °C (29). The results summarized in Fig. 8 show the V^{51} NMR spectra of vanadium dichloride(IV) at pH 7.0 prior to and after the addition of L-Glu(γ)HXM. Vanadium dichloride(IV) appeared as a single peak with a chemical shift of −490 ppm in its ^{51}V spectrum, indicating one main species present at >95% purity. Upon the addition of L-Glu(γ)HXM (1

equivalent), the chemical shift of vanadium(IV) at −490 ppm disappeared within minutes and the principal chemical shift characterizing vanadium(V) at −530 ppm appeared (Fig. 8).

Vanadium(IV) (*i.e.* vanadyl sulphate or $VOCl_2$) has a characteristic "blue" absorbance with $\epsilon_{765\ nm} = 14 \pm 0.3$, whereas vanadium(V) does not absorb at all at this wavelength (29). The addition of 2–3 equivalents of L-Glu(γ)HXM to $VOCl_2$(IV) (50 mM at pH 7.5) led rapidly to a near total decrease in vanadium(IV) absorbance at 765 nm (Fig. 9). Fig. 8*B* depicts complex formation as a function of the pH in the range of pH 2–9. Decrease is minimal at pH 4.0, quite significant at pH 5.0,

FIG. 9. **Decrease in absorbance of vanadium(IV) at 765 nm upon addition of L-Glu(γ)HXM.** Effect of pH: *A, left column,* absorbance of $VOCl_2$ alone (50 mM in H_2O); *right column,* absorbance of $VOCl_2$ (50 mM) and L-Glu(γ)HXM (150 mM) titrated with $NaHCO_3$ to pH 7.4. *B,* samples of $VOCl_2$ (50 mM) and L-Glu(γ)HXM (100 mM) in H_2O were titrated either with HCl or with $NaHCO_3$ before absorbance at 765 nm and were monitored to obtain the pH values indicated in the figure. L-Glu(γ)HXM alone does not absorb at 765 nm. Vanadium dichloride alone, which tends to precipitate at neutral pH values, remains completely soluble at all pH values in the presence of two or more equivalents of L-Glu(γ)HXM.
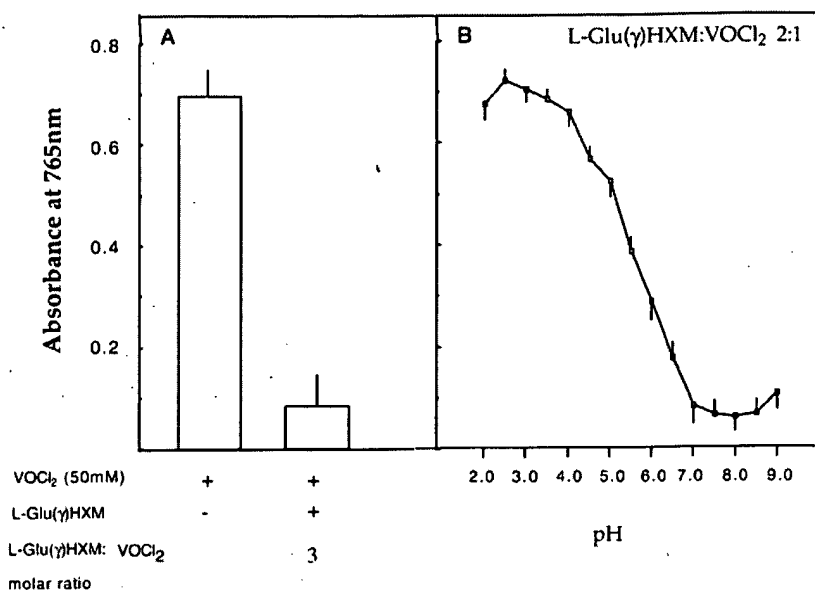
half-maximal at pH 5.7, and reaches a stable plateau at pH range 7–9 (Fig. 9*B*).

DISCUSSION

It has been consistently observed that chelated vanadium compounds are more potent than the free metaloxide in facilitating the metabolic actions of insulin. This was demonstrated *in vitro* with systems like rat adipocytes, as well as in diabetic rodents such as streptozocin-treated hyperglycemic rats (28–33, 44). Because of the variations in the experimental models used, the oxidation state of vanadium applied, and the different administration modes, the basis for the higher insulinomimetic potencies of complexed vanadium remained rather speculative. Because this topic has immediate therapeutic relevance, we looked for new vanadium chelators characterized by: (*a*) higher synergistic potencies than previously documented for vanadium chelators with respect to vanadium-evoked glucose uptake and glucose metabolism both *in vitro* and in diabetic rats *in vivo,* (*b*) low indices of toxicity, and (*c*) reasonable solubility in aqueous, neutral media after complexation with vanadium.

In this study, we have introduced the L-isomer of glutamic acid(γ)monohydroxamate as it satisfactorily fulfilled the above criteria. It potentiated vanadium-activated hexose uptake, glucose metabolism, and recruitment of GLUT4 transporters from LDM to PM fractions (Figs. 1–4). *In vivo* it potentiated the efficacy of vanadium to lower blood glucose levels in streptozocin rats (Fig. 5). This amino acid analog has negligible toxicity in mammals.[2] Both L-Glu(γ)HXM alone and its complexes with vanadium are fairly soluble in aqueous media at neutral pH values. An important finding was that L-Glu(γ)HXM alone, in the absence of exogenous vanadium, showed a reasonable amount of insulinomimetic activity in that it activated glucose uptake and glucose metabolism in the rat adipose cell (Figs. 1–3). Further investigation revealed that this activating effect is unique to the L-isomer of Glu(γ)HXM but is not facilitated by the D-isomer. Nonmodified α-amino and α-carboxyl moieties appear essential. This intrinsic activity is exclusive to L-Glu(γ)HXM not being shared by any of the other vanadium chelators that potentiate the actions of vanadium *in vivo* or *in vitro* (Fig. 6, *A–D,* and Refs. 28–33). Our assumption that L-Glu(γ)HXM permeates into the cell interior and transforms the "dormant" intracellular vanadium pool into an insulinomimetic-activated species gains credence from the dramatic sen-

sitization of vanadium-enriched adipocytes to L-Glu(γ)HXM-evoked lipogenesis (Fig. 7).

It should be mentioned at this point that because of the extreme complexity of aqueous vanadium chemistry (reviewed in Refs. 46–49), the intracellular milieu of the mammalian cell is still "a black box" with respect to the state and the form of entered vanadium. With the endogenously present vanadium pool, experiments have shown that it exists mostly as vanadium(IV), though some researchers may wonder even about this experimental finding because vanadium in its IV oxidation state is only stable at acidic pH values (pH < 3.0) and readily oxidizes to vanadium(V) at neutral pH even in the presence of high glutathione concentrations (28, 46). The intracellular vanadium pool, however, can be preserved in its IV oxidation form at neutral pH values if it is chelated by ascorbic acid (not shown) or to endogenous proteins (50, 51). At the low physiological level of intracellular vanadium, the cell should have the capacity to chelate all the endogenous vanadium.

Our experimental findings that L-Glu(γ)HXM alone enhances glucose uptake and glucose metabolism (Figs. 1 and 2) together with the apparent rapid conversion of vanadium(IV) to vanadium(V) upon complexation (Figs. 8 and 9) strongly support the contention that vanadium(V) rather than vanadium(IV), and in a chelated form, is the active insulinomimetic species that facilitates the activation of glucose uptake and its metabolism in rat adipocytes. Although most of our previous cell-free experiments support this conclusion, we were not fully convinced prior to the completion of this study. This is because protein phosphotyrosine phosphatases (with *p*-nitrophenylphosphate as a substrate) are inhibited by both vanadium(IV) and vanadium(V), free or chelated, at nearly the same concentrations (see Ref. 52). On the other hand, adipose non-receptor protein-tyrosine kinases, whether cytosolic or membranal, are with one exception activated by vanadium(V) but not at all by vanadium(IV) (22, 23). We have only observed vanadium(IV)-evoked activation of nonreceptor protein-tyrosine kinases when membranal protein phosphotyrosine phosphatases were extracted with Triton X-100 and added to the cytosolic protein-tyrosine kinase fraction (29). These experimental conditions, however, are not likely to occur in the intact cell system. For example, broken plasma membrane fragments (or deoxycholate-treated membranal fragments) did not sup-

port activation of cytosolic protein-tyrosine kinases in the presence of vanadium(IV) (29).

In summary, L-Glu(γ)HXM appears superior to previously documented organic chelators of vanadium in potentiating its activation of glucose uptake and glucose metabolism *in vitro* and *in vivo*. Taken together with earlier studies, this may be attributed to one or more of the following: (*a*) increased efficiency of this specific combination to permeate into cells or tissues; (*b*) a favorable 5-coordinated, rather than octahedral topography of this complex in an aqueous, neutral environment (Ref. 50);[2] and/or (*c*) higher intracellular stability of the L-Glu(γ)HXM-vanadium complex. Finally, we have recently observed that vanadate does not inhibit alkaline phosphatase in the presence of L-Glu(γ)HXM.[2] This inhibitory effect of vanadate (53) is undesirable from our point of view as it may contribute to vanadium toxicity in mammals, but not to the efficacy of vanadium to manifest the metabolic actions of insulin (reviewed in Ref. 54). This and other basic and diabetological aspects raised here are being further investigated.

REFERENCES

1. Shechter, Y., and Karlish, S. J. (1980) *Nature* **284**, 556–558
2. Shechter, Y. (1990) *Diabetes* **39**, 1–5
3. Shechter, Y., Li, J., Meyerovitch, J., Gefel, D., Bruck, R., Elberg, G., Miller, D. S., and Shisheva, A. (1995) *Mol. Cell. Biochem.* **153**, 39–47
4. Brichard, S. M., and Henquin, J. C. (1995) *Trends Pharmacol. Sci.* **16**, 265–270
5. Heyliger, C. E., Tahiliani, A. G., and McNeill, J. H. (1985) *Science* **227**, 1471–1476
6. Meyerovitch, J., Farfel, Z., Sack, J., and Shechter, Y. (1987) *J. Biol. Chem.* **262**, 6658–6662
7. Brichard, S. M., Okitolonda, W., and Henquin, J. C. (1988) *Endocrinology* **123**, 2048–2053
8. Brichard, S. M., Bailey, C. J., and Henquin, J. C. (1990) *Diabetes* **39**, 1326–1332
9. Meyerovitch, J., Rothenberg, P., Shechter, Y., Bonner-Weir, S., and Kahn, C. R. (1991) *J. Clin. Invest.* **87**, 1286–1294
10. Brichard, S. M., Pottier, A. M., and Henquin, J. C. (1989) *Endocrinology* **125**, 2510–2516
11. Brichard, S. M., Assimacopoulos-Jeannet, F., and Jeanrenaud, B. (1992) *Endocrinology* **131**, 311–317
12. Mooney, R. A., Bordwell, K. L., Luhowsky, J. S., and Casnellie, J. E. (1989) *Endocrinology* **124**, 422–429
13. Strout, H. V., Vicario, D. D., Superstein, R., and Slater, E. E. (1989) *Endocrinology* **124**, 1918–1924
14. Venkatesan, N., Avidin, A., and Davidson, M. B. (1991) *Diabetes* **40**, 492–498
15. Fantus, I. G., Kadota, S., Deragon, G., Foster, B., and Posner, B. I. (1989) *Biochemistry* **28**, 8864–8871
16. Shisheva, A., and Shechter, Y. (1992) *Biochemistry* **31**, 8059–8063
17. Green, A. (1986) *Biochem. J.* **238**, 663–669
18. D'Onofrio, F., Le, M. Q. U., Chiasson, J.-L., and Srivastava, A. K. (1994) *FEBS Lett.* **340**, 269–275
19. Dadney, S. K., Chiasson, J.-L., and Srivastava, A. K. (1995) *Mol. Cell. Biochem.* **153**, 69–78
20. Shisheva, A., and Shechter, Y. (1991) *FEBS Lett.* **300**, 93–96
21. Shisheva, A., and Shechter, Y. (1993) *J. Biol. Chem.* **268**, 6463–6469
22. Elberg, G., Li, J., and Shechter, Y. (1994) *J. Biol. Chem.* **269**, 9521–9527
23. Elberg, G., He, Z., Li, J., Sekar, N., and Shechter, Y. (1997) *Diabetes* **46**, 1684–1690
24. Goldfine, A. B., Simonson, D. C., Folli, F., Patti, M. E., and Kahn, C. R. (1995) *J. Clin. Endocrinol. Metab.* **80**, 3311–3320
25. Cohen, N., Halberstam, M., Shlimovich, P., Chang, C. J., Shamoon, H., and Rossetti, L. (1995) *J. Clin. Invest.* **95**, 2501–2509
26. Halberstam, M., Cohen, N., Shlimovich, P., Rossetti, L., and Shamoon, H. (1996) *Diabetes* **45**, 659–666
27. Sekar, N., Li, J., and Shechter, Y. (1996) *Crit. Rev. Biochem. Mol. Biol.* **31**, 339–359
28. Shechter, Y., Shisheva, A., Lazar, R., Libman, J., and Shanzer, A. (1992) *Biochemistry* **31**, 2063–2068
29. Li, J., Elberg, G., Crans, D. C., and Shechter, Y. (1996) *Biochemistry* **35**, 8314–8318
30. McNeill, J. H., Yuen, V. G., Hoveyda, H. R., and Orvig, C. (1992) *J. Med. Chem.* **35**, 1489–1491
31. McNeill, J. H., Yuen, V. G., Dai, S., and Orvig, C. (1995) *Mol. Cell. Biochem.* **153**, 175–180
32. Sakurai, H. (1994) *Environ. Health Perspect.* **3**, 35–36
33. Sakurai, H., Fujii, K., Watanabe, H., and Tamura, H. (1995) *Biochem. Biophys. Res. Commun.* **214**, 1095–1101
34. Fishbein, W. N., Strecter, C. L., and Daly, J. E. (1973) *J. Pharmacol. Exp. Ther.* **186**, 173–178
35. Vila, J., Thomasset, N., Navarro, C., and Dore, J. F. (1990) *Int. J. Cancer* **45**, 737–743
36. Boehlein, S. K., Schuster, S. M., and Richards, N. G. (1996) *Biochemistry* **35**, 3031–3037
37. Rodbell, M. (1964) *J. Biol. Chem.* **239**, 375–380
38. Whitesell, R. R., and Gliemann, J. (1979) *J. Biol. Chem.* **254**, 5276–5283
39. Moody, A. J., Stan, M. A., Stan, M., and Glieman, J. (1974) *Horm. Metab. Res.* **6**, 12–16
40. Hissin, P. J., Foley, J., Wardzala, L. J., Karnieli, E., Simpson, I. A., and Salans, L., B. (1982) *J. Clin. Invest.* **70**, 780–790
41. Armoni, M., Harel, C., Burvin, R., and Karnieli, E. (1995) *Endocrinology* **136**, 3292–3298
42. Olson, A. L., and Pessin, J. E. (1996) *Annu. Rev. Nutr.* **16**, 235–256
43. McLean, P., Brown, J., and Greenbaum, A. L. (1968) *Handbook of Biochemistry* (Dickens, F., Whelan, W. J., and Randle, P. J., eds) Academic Press, New York
44. Watanabe, H., Nakai, M., Komazawa, K., and Sakurai, H. (1994) *J. Med. Chem.* **37**, 876–877
45. Deleted in proof
46. Macara, J. G. (1980) *Trends Biochem. Sci.* **5**, 92–94
47. Crans, D. C. (1994) *Comm. Inorg. Chem.* **16**, 1–33
48. Crans, D. C., Mahroof Tahir, M., and Keramidas, A. D. (1995) *Mol. Cell. Biochem.* **153**, 17–24
49. Dekoch, R. J., West, D. J., Cannon, J. C., and Chasteen, N. D. (1974) *Biochemistry* **13**, 4347–4354
50. Casteen, N. D. (1981) in *Biological Magnetic Resonance* (Berliner, L., and Reuben, J., eds) Vol. II, pp. 53–119, Plenum Press, New York
51. Crans, D. C., Bunch, R. L., and Theisen, L. A. (1989) *J. Am. Chem. Soc.* **111**, 7597–7607
52. Li, J., Elberg, G., Sekar, N., bin He, Z., and Shechter, Y. (1997) *Endocrinology* **138**, 2274–2279
53. Lopez, V., Stevens, T., and Lindquist, R. N. (1976) *Arch. Biochem. Biophys.* **175**, 31–38
54. Elberg, E., Li, J., and Shechter, Y. (1997) in *Vanadium in the Environment* (Nriagu, J. O., ed) pp. 277–296, John Wiley & Sons, Inc., New York

Evidence That Glucose Metabolism Regulates Leptin Secretion from Cultured Rat Adipocytes*

WENDY M. MUELLER, FRANCINE M. GREGOIRE, KIMBER L. STANHOPE, CHARLES V. MOBBS, TOORU M. MIZUNO, CRAIG H. WARDEN, JUDITH S. STERN, AND PETER J. HAVEL

Department of Nutrition (W.M.M., K.L.S., J.S.S., P.J.H.), and Department of Pediatrics (F.M.G., C.H.W.), School of Medicine, University of California, Davis, California 95616; and Neurobiology of Aging Laboratories, Mount Sinai School of Medicine (C.V.M., T.M.M.), New York, New York 10021

ABSTRACT

Circulating leptin secreted from adipocytes is correlated with fat mass and plasma insulin concentrations in humans and rodents. Plasma leptin, insulin, and glucose decrease during fasting and increase after refeeding; however, the underlying mechanisms regulating the changes of leptin secretion are not known. To investigate the role of insulin-stimulated glucose metabolism in the regulation of leptin secretion, we examined the effects of insulin and inhibitors of glucose transport and metabolism on leptin secretion from rat adipocytes in primary culture. Insulin (0.16–16 nM) increased leptin secretion over 96 h; however, the increase in leptin was more closely related to the amount of glucose taken up by the adipocytes (r = 0.64; P < 0.0001) than to the insulin concentration *per se* (r = 0.20; P < 0.28), suggesting a role for glucose transport and/or metabolism in regulating leptin secretion.

2-Deoxy-D-glucose (2-DG), a competitive inhibitor of glucose transport and phosphorylation, caused a concentration-dependent (2–50 mg/dl) inhibition of leptin release in the presence of 1.6 nM insulin. The inhibitory effect of 2-DG was reversed by high concentrations of glucose. Two other inhibitors of glucose transport, phloretin (0.05–0.25 mM) and cytochalasin-B (0.5–50 µM), also inhibited leptin secretion. Inhibition of leptin secretion by these agents was proportional to the inhibition of glucose uptake (r = 0.60 to 0.86; all P < 0.01). Two inhibitors of glycolysis, iodoacetate (0.005–1.0 mM) and sodium fluoride (0.1–5 mM), produced concentration-dependent inhibition of leptin secretion in the presence of 1.6 nM insulin. In addition, both 2-DG and sodium fluoride markedly decreased the leptin (*ob*) messenger RNA content of cultured adipocytes, but did not affect 18S ribosomal RNA content.

We conclude that glucose transport and metabolism are important factors in the regulation of leptin expression and secretion and that the effect of insulin to increase adipocyte glucose utilization is likely to contribute to insulin-stimulated leptin secretion. Thus, *in vivo*, decreased adipose glucose metabolism may be one mechanism by which fasting decreases circulating leptin, whereas increased adipose glucose metabolism would increase leptin after refeeding. (*Endocrinology* **139:** 551–558, 1998)

T HE ADIPOCYTE hormone, leptin is implicated in the regulation of food intake, energy expenditure, and body fat stores (1). Circulating leptin decreases after fasting or caloric restriction in both humans (2–4) and rodents (5–7), and increases a number of hours after refeeding (3, 6). In humans, there is a nocturnal rise of plasma leptin (8), which has been hypothesized to be due to a delayed effect of insulin released during earlier meals. Consistent with this hypothesis, insulin increases expression of the *ob* gene in rodents (9–11) and in adipocytes *in vitro* (12, 13) after a number of hours. In humans, plasma insulin and leptin concentrations decrease in parallel after weight loss, independently of changes of adiposity (14). Furthermore, plasma leptin is negatively correlated with insulin sensitivity independently of adiposity in subjects with impaired glucose tolerance (15).

Short term insulin administration does not affect plasma leptin concentrations in human subjects (16, 17), but increases in circulating leptin have been reported after 4–6 h of high dose insulin administration (18, 19). These studies by

necessity require the infusion of large amounts of glucose to prevent hypoglycemia. Similarly, prolonged hyperglycemia in response to extended glucose infusions increases plasma leptin after several hours in nonhuman primates (20) and human subjects (21); however, glucose administration also markedly increases endogenous insulin levels. Therefore, the role of insulin *per se* on the adipocyte *vs.* the effect of insulin to increase glucose flux into adipocytes was not addressed by these experiments.

Several lines of evidence have led us to hypothesize that glucose is an important regulator of leptin expression and secretion. First, increases in *ob* messenger RNA (mRNA) after glucose administration in mice are more closely related to plasma glucose concentrations than to plasma insulin concentrations (22). Second, infusion of small amounts of glucose to prevent the decline of glycemia during fasting in humans also prevents the decrease in plasma leptin (2). Third, the decrease in plasma leptin during marked caloric restriction in humans is better correlated with the decrease in plasma glucose than with changes in insulinemia (4). Fourth, we have found that low plasma leptin levels in streptozotocin diabetic rats are acutely increased by insulin administration in proportion to the degree of glucose lowering (23). Lastly, lowering plasma glucose concentrations in hyperglycemic insulin-dependent diabetic human subjects by

infusing insulin at rates that produced physiological insulinemia increases circulating leptin (24).

To investigate the mechanisms by which glucose influences leptin secretion, we adapted and modified an *in vitro* system for culturing rat adipocytes in which the adipocytes are anchored in a defined mixture of extracellular matrix components (25) This matrix, Matrigel, appears to simulate normal basement membrane attachment of cells and may allow cell to cell interactions between adipocytes. Cells cultured in this system are, therefore, in an environment closer to their normal physiological milieu than in systems where adipocytes are free floating in the culture medium. Adipocytes cultured on Matrigel have been shown to maintain many of their differentiated characteristics and, in contrast with free-floating adipocytes, show no sign of dedifferentiation after 6 days of culture (25, 26). With this system we have investigated the regulation of leptin secretion by glucose and insulin and the effects of inhibitors of adipocyte glucose transport and metabolism on leptin secretion. The leptin (*ob*) mRNA content of the adipocytes after culture with insulin and inhibitors was also examined.

Materials and Methods

Materials

DMEM and FBS were purchased from Life Technologies (Grand Island, NY). The media were supplemented with 6 ml each of MEM nonessential amino acids, penicillin/streptomycin (5000 U/ml/5000 μg/ml), and nystatin (10,000 U/ml; all from Life Technologies) per 500 ml DMEM. BSA fraction V, HEPES, collagenase (*Clostridium histolyticum*; type II, Sigma Chemical Co., St. Lousi, MO; SA, 456 U/mg), insulin, D-glucose, sodium fluoride (NaFl), phloretin, iodoacetate, and fructose were purchased from Sigma Chemical Co. Matrigel matrix was purchased from Becton Dickinson (Franklin Lakes, NJ). 2-Deoxy-D-glucose (2-DG) was obtained from U.S. Biochemical Corp. (Cleveland, OH). Six-well Falcon tissue culture plates were purchased from Fisher Scientific (Pittsburgh, PA). Nylon filters were purchased from Tetko (Kansas City, MO).

Animals

Male Sprague-Dawley rats were obtained from Charles River (Wilmington, MA). Animals were housed in hanging wire cages in temperature controlled rooms (22–24 C) with a 12-h light-dark cycle and fed Purina chow diet (Ralston-Purina, St. Louis, MO) and given deionized water *ad libitum*. The study protocol was approved by the University of California-Davis animal care and use committee.

Cell isolation / preparation

Adipocytes were prepared from epididymal fat pads of male Sprague-Dawley rats (300–600 g) anesthetized with halothane. Epididymal fat depots were resected under aseptic conditions, and adipocytes were isolated by collagenase digestion according to the Rodbell procedure (27) with minor modifications as described below. The fat pads were minced into pieces in Krebs-Ringer HEPES buffer (pH 7.4; containing 5 mM D-glucose, 2% BSA, 135 mM NaCl, 2.2 mM CaCl$_2$.2H$_2$O, 1.25 mM MgSO$_4$·7H$_2$O, 0.45 mM KH$_2$PO$_4$, 2.17 mM Na$_2$HPO$_4$, and 10 mM HEPES). Adipose tissue fragments were digested in the same buffer in the presence of type II collagenase (2.5 mg/2 ml buffer·g tissue) at 37 C with gentle shaking at 60 cycles/min for 45 min. The resulting cell suspension was diluted in 24 ml cold HEPES-phosphate buffer. Isolated adipocytes were separated from undigested tissue by filtration through a 400-μm nylon mesh and washed three times. For washing, cells were centrifuged at 500 rpm for 5 min. Each time the infranatant was discarded, and the adipocytes were resuspended in Krebs-Ringer HEPES buffer, with the final wash being in 0, 5, or 10 mM glucose culture medium supplemented with 1% or 5% FBS. The isolated adipocytes were then incubated for 30 min at 37 C before being plated in Matrigel-coated culture plates.

Adipocyte culture

Matrigel was thawed on ice to a liquid and uniformly applied to the surface of the culture dish (300 μl Matrigel/35-mm well). After the incubation, 150 μl of the adipocyte suspension (2:1 ratio of packed cells to medium) were plated on the liquid matrix. The warmth of the cells and buffer caused the Matrigel to gel around the adipocytes, effectively anchoring them to the culture dish. After a 30-min incubation at 37 C, 2 ml warm culture medium supplemented with FBS were added. The cells were maintained in an incubator at 37 C in 6% CO$_2$ for 96 h.

The initial medium concentration of glucose for the cultures conducted in the insulin dose-response experiment was 10.0–10.5 mM (180–190 mg/dl) to ensure that the cells would not deplete the glucose supply during the 96-h incubation when higher concentrations of insulin were used. Only 1% FBS was used in the insulin dose-response study to minimize the small amount of insulin present in the serum, which at 1% was less than 0.1 μU/ml. In the fructose study, medium made with glucose-free DMEM and 1% fetal serum was used to minimize the amount of glucose available to the adipocytes (<0.1 mmol/liter). However, it was not possible to eliminate all glucose from culture preparation because the Matrigel matrix itself contains ~4.2 mmol/liter glucose. For the fructose experiment, the Matrigel was diluted 1:2 with glucose-free medium to approximately 1.5 mmol/liter glucose.

In the other experiments with inhibitors of glucose transport, 2-DG (28), phloretin (29), and cytochalasin B (30), or with inhibitors of glycolysis, iodoacetate (31), and NaFl (32), the initial medium glucose concentration was (5.0–5.5 mM; 90–100 mg/dl) with 5% fetal serum. These agents were used at concentrations at or below those typically employed to inhibit glucose transport or glycolysis in adipocytes (28–32). Cytochalasin B was initially dissolved in ethanol and diluted to 0.5% ethanol in the well with the highest dose. Therefore, the medium in all wells in the cytochalasin B experiment was equalized to 0.5% ethanol. Aliquots of adipocytes from each animal were divided into wells with the responses to insulin, the various inhibitors, or fructose being compared with those of an appropriate control well containing adipocytes from the same animal. In a preliminary insulin dose-response study, we found that medium leptin concentrations in the presence of insulin were not increased over those in control medium (no insulin) until after 24 h of incubation. Therefore, for the remainder of the studies, 300-μl samples (15% of the medium volume) were collected at 24, 48, 72, and 96 h and replaced with 300 μl fresh medium containing the appropriate concentrations of glucose, insulin, and/or inhibitors. Cultures were observed daily with a phase contrast microscope. After 96 h, a subset of the culture plates was frozen until analyzed for leptin (*ob*) mRNA content by Northern blot.

Assays

Leptin concentrations in the medium were determined with a sensitive and specific RIA for mouse leptin as previously described (7) (Linco Research, St. Charles, MO). Leptin concentrations in medium from cultured rat adipocytes measured with this assay are very similar to those obtained with a newly developed assay specific for rat leptin. With the rat-specific assay, measured leptin concentrations in culture medium were 86 ± 3% of the mouse values and were highly correlated between the two assays (r = 0.97; P < 0.0001; unpublished data). Therefore, measurements of rat leptin made with the mouse assay provide a reliable measurement of leptin concentrations. The intra- and interassay coefficients of variation for this assay are 4.0% and 11.2%, respectively (7). The antibody used in the assay does not cross-react with insulin, proinsulin, glucagon, pancreatic polypeptide or somatostatin. Glucose and lactate were measured with a YSI glucose analyzer (model 2300, Yellow Springs Instruments, Yellow Springs, OH).

Northern blot procedure

The following procedures were performed on culture plates incubated with 5 mM glucose and 5% fetal serum alone (control), 1.6 nM insulin, and 1.6 nM insulin with 10 mg/dl 2-DG or 1 mM NaFl for 48 and 96 h. Northern blot analysis was performed as previously described (33).

In brief, 1 ml RNAzol B (Tel-Test, Friendswood, TX) was added directly to the wells containing the adipocytes and matrix. The solution was repetitively taken in and expelled from the pipette to maximize dissolution of the adipose tissue. UV absorbance and integrity gels were used to estimate RNA. To allow loading of equal mass of RNA in each well, after analysis of leptin mRNA using a single-stranded complementary DNA probe followed by quantification of bands on a phosphoimager as well as from film, the blots were reanalyzed using a probe complementary to mouse 18S ribosomal RNA. Leptin mRNA was then normalized with respect to the 18S ribosomal signal, according to the absolute signal. The 18S RNA results were virtually identical in all cases. In particular, experimental conditions did not influence the 18S ribosomal signal.

Calculations and data analysis

The uptake of glucose was assessed by measuring the concentration of glucose in the medium in each well before and after 96 h of incubation and calculating the decrease over 96 h. To examine the relationship between adipocyte carbon flux and leptin secretion in response to increased insulin-mediated glucose uptake, the amount of carbon released as lactate per amount of carbon taken up as glucose over 96 h was calculated as Δ[lactate]/Δ[glucose], where Δ is the change, and expressed as a percentage. The area under the curve for leptin concentrations in the medium between 0–96 h was calculated by the trapezoidal method. The means of two groups were compared by paired t test. The means of more than two groups were compared by ANOVA. To examine the relationships between the medium concentrations of insulin or inhibitors employed, the amount of glucose taken up by the adipocytes, and leptin secretion, simple and multiple linear regression analyses were performed with a statistics software package (StatView for Macintosh, Abacus Concepts, Inc., Berkeley, CA). Data are expressed as the mean $\pm$ SEM.

Results

Responses to insulin (0.16–16.0 nM)

The effects of insulin on leptin secretion, and the relationship between glucose uptake by adipocytes cultured with different concentrations of insulin and leptin secretion were examined. Insulin produced a concentration-dependent increase in glucose uptake by the cultured adipocytes ($r = 0.61$; $P < 0.0002$ vs. insulin concentration), as assessed by the decrease in glucose in the medium (Fig. 1A). With no added insulin, the medium glucose concentration decreased from 10.1 ± 0.1 to 8.2 ± 0.3 mmol/liter (Δ, -1.9 ± 0.3 mmol/liter; $P < 0.0001$). The addition of 0.16, 1.6, and 16.0 nM insulin increased glucose uptake (Δglucose, -2.7 ± 0.4, -3.3 ± 0.3, and -3.9 ± 0.4 mmol/liter, respectively; all $P < 0.01$ vs. no insulin). Insulin also produced a concentration-dependent increase in lactate production ($r = 0.70$; $P < 0.0001$), which was well correlated with the decrease in glucose in the medium over 96 h ($r = 0.61$; $P < 0.0002$), suggesting that a significant portion of the glucose entering the adipocytes was metabolized only as far as lactate and released from the cells into the medium (34, 35).

Leptin secretion was increased over the control value by all three concentrations of insulin (Fig. 1B). The production of lactate was not related to the leptin response ($r = 0.10$; $P = 0.59$). The area under the leptin concentration curve (AUC) from 0–96 h was independently related to the decrease in glucose in the medium during the incubation (Fig. 1C), but not to the insulin concentration (Table 1). Similarly, with a multiple regression model, the AUC for leptin was related to the decrease in glucose, but not to the insulin concentration. In addition, the percentage of carbon released as lactate per amount of carbon taken up as glucose was calculated. Over-
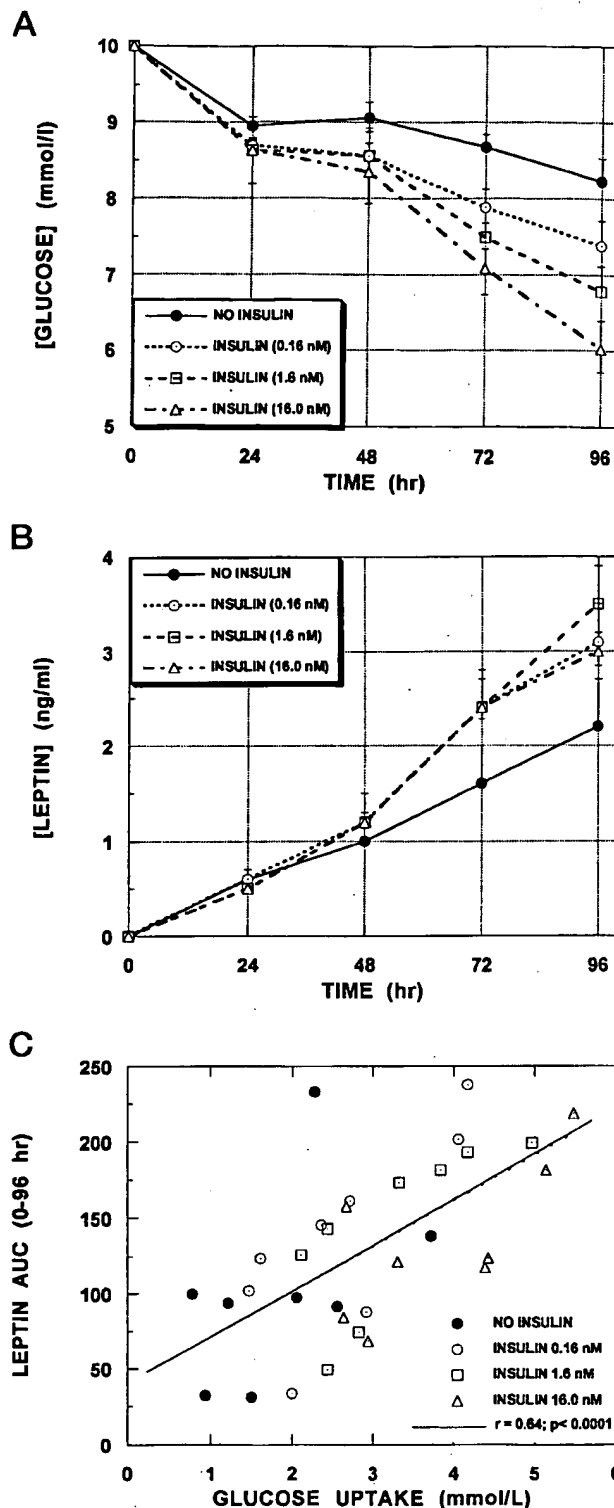
FIG. 1. A, Glucose concentrations in medium from 0–96 h from isolated rat adipocytes in primary culture with insulin concentrations from 0–16 nM (n = 8/treatment). B, Leptin concentrations from 0–96 h from isolated rat adipocytes in primary culture with insulin concentrations from 0–16 nM (n = 8/treatment). C, Relationship between glucose uptake, as assessed by the decrease in glucose in the culture medium, and leptin secretion, expressed as the AUC from 0–96 h, during incubation of adipocytes with 0–16 nM insulin (n = 32).

TABLE 1. Relationship between glucose uptake (ΔGluc), leptin secretion (ΔLept) and the concentration of insulin or inhibitors of glucose uptake and metabolism after 96-h incubation of adipocytes with insulin and insulin plus inhibitors (2-DG, phloretin, cytochalasin-B, iodocetate, or sodium fluoride at varying concentrations; see *Materials and Methods*)

| Insulin or inhibitor (n) | Simple Regression | | | | Multiple regression | |
| | ΔLept vs. ΔGluc | | ΔLept vs. [inhibitor] | | ΔLept vs. ΔGluc (P) | ΔLept vs. [inhibitor] (P) |
	r	P	r	P		
Insulin (32)	0.64	0.0001	0.20	0.28	0.0001	0.09
2-DG (38)	0.67	0.0001	0.51	0.001	0.001	0.29
Phloretin (38)	0.86	0.0001	0.78	0.0001	0.0012	0.75
Cytochalasin-B (19)	0.60	0.01	0.58	0.02	0.22	0.25
Iodoacetate (34)	0.83	0.0001	0.74	0.0001	0.0001	0.17
Sodium fluoride (28)	0.85	0.0001	0.60	0.001	0.0001	0.73
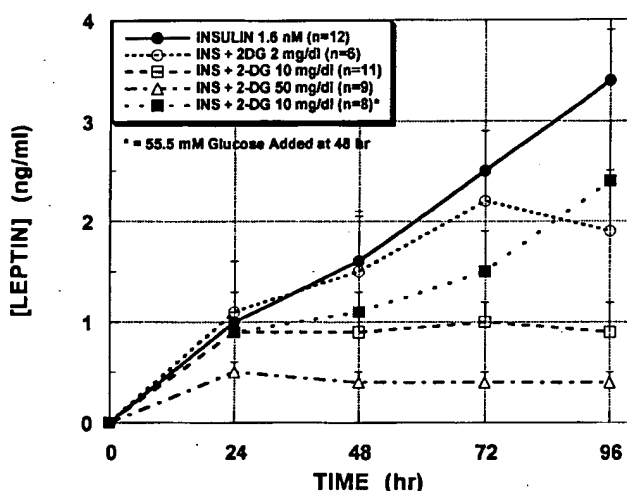
FIG. 2. Effects of inhibiting glucose transport and metabolism with 2-DG on leptin concentrations from 0–96 h in medium from isolated rat adipocytes in primary culture for 96 h with 1.6 nM insulin and the effect of adding glucose (55 mM) at 48 h on the inhibition of leptin secretion produced by 10 mg/dl 2-DG.
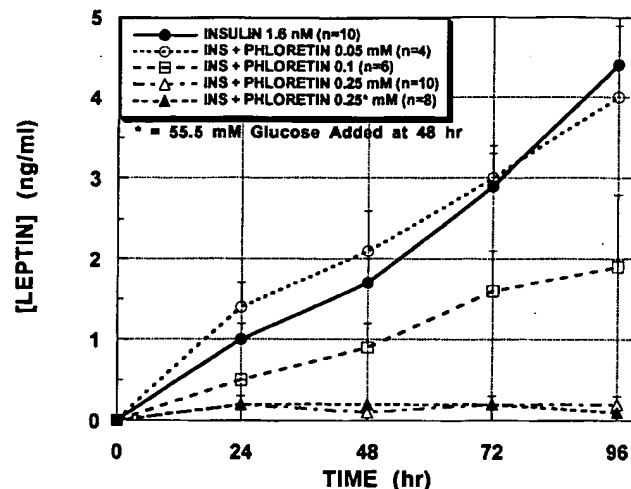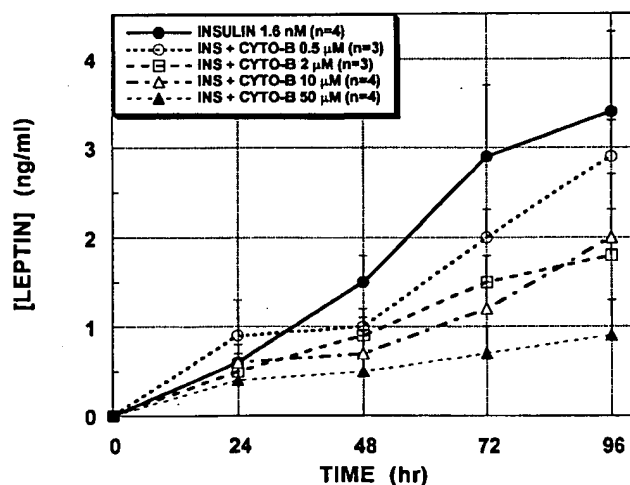

FIG. 3. Effects of inhibiting glucose transport with phloretin on leptin concentrations from 0–96 h in medium from isolated ra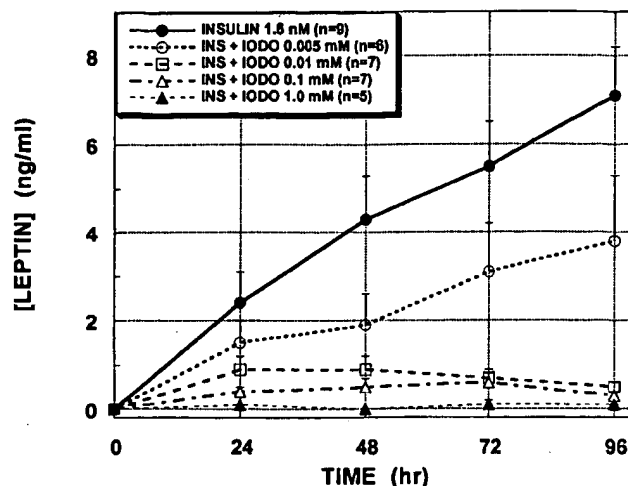t adipocytes in primary culture for 96 h with 1.6 nM insulin and the effect of adding glucose (55 mM) at 48 h on the inhibition of leptin secretion produced by 0.25 mM phloretin.

all, in the insulin experiment between 10–68% of the amount of carbon taken up as glucose was released as lactate (mean, 34 ± 2%). There was no direct relationship between this parameter and the insulin concentration; however, it was inversely proportional to the amount of leptin secreted, as expressed by the 0–96 h leptin AUC (r = 0.64; P < 0.0001). By multiple regression analysis, the relationship between glucose conversion to lactate and leptin secretion was not significantly related to lactate production (P = 0.06), but leptin secretion was equally related to both the change in glucose and the amount of glucose carbon released as lactate (both P < 0.001).

Effects of 2-DG (2–50 mg/dl)

The effect of inhibiting glucose uptake and metabolism with 2-DG on leptin secretion and its relationship to adipocyte glucose uptake were examined. 2-DG at a concentration of 50 mg/dl completely inhibited glucose uptake (Δ, 0.1 ± 0.3 mmol/liter) in the presence of 1.6 nM insulin (Δglucose, −4.0 ± 0.6 mmol/liter) and inhibited the leptin response (AUC 0–96 h) by 69 ± 4% (P < 0.0001) compared with insulin alone (Fig. 2A). At a lower concentration of 2-DG (10 mg/dl), glucose uptake was still markedly inhibited (Δ, −0.1 ± 0.4

mmol/liter) and leptin secretion was inhibited by 47 ± 5% (P < 0.0001). The lowest concentration of 2-DG (2 mg/dl) produced less of an inhibition of glucose uptake (Δ, −1.5 ± 0.9 mmol/liter; P < 0.01 vs. insulin alone). At this concentration, the leptin response was not significantly inhibited until the 96 h point (P < 0.02 vs. insulin alone; Fig. 2A).

Overall, the change in leptin at 96 h was related to the concentration of 2-DG and was well correlated with the decrease in medium glucose (Table 1). By multiple regression, the leptin concentration in the medium at 96 h was significantly correlated with the change in glucose, but not to the 2-DG concentration (Table 1). The addition of glucose (55.5 mM) at 48 h reversed the inhibition of leptin secretion produced by 2-DG at 10 mg/dl by 96 h (P < 0.01 vs. 2-DG; NS vs. insulin alone; Fig. 2).

Effects of phloretin (0.05–0.25 mM)

The effect of inhibiting glucose uptake with phloretin on leptin secretion was examined. Phloretin at a concentration of 0.25 mM completely inhibited leptin secretion (Fig. 3). The 0–96 h AUC for leptin was inhibited by 91 ± 2% of insulin alone (P < 0.0001). This higher concentration of phloretin (0.25 mM) also completely blocked glucose uptake in the

presence of 1.6 nM insulin (Δglucose, 0.7 ± 0.1 mmol/liter). Overall, the leptin response was inversely related to the concentration of phloretin and was highly correlated with the decrease in glucose in the medium (Table 1). However, by multiple regression, the leptin response was correlated with the decrease in glucose, but not with the concentration of phloretin (Table 1). The addition of 55.5 mM glucose at 48 h did not reverse the inhibition of leptin secretion by phloretin (Fig. 3).

Effects of cytochalasin B

The effect of inhibiting glucose uptake with cytochalasin B on leptin secretion was examined. Cytochalasin B produced a concentration-dependent inhibition of glucose uptake and leptin secretion (Fig. 4). The leptin response was significantly correlated with glucose uptake by simple regression (Table 1), but was not significantly correlated with glucose uptake (as observed with the other inhibitors; Table 1) by multiple regression, perhaps due to the smaller number of replicates (n = 19) in this experiment.

Effects of iodoacetate (0.005–1.0 mM)

The effect of inhibiting glycolysis with iodoacetate on leptin secretion was examined. Iodoacetate at 1.0, 0.1, and 0.01 mM markedly inhibited glucose uptake (Δglucose, −0.1 ± 1.1, 0.5 ± 0.2, and 0.3 ± 0.2 mmol/liter, respectively) and leptin secretion. The 0–96 h AUC for leptin was inhibited by −95 ± 2%, −91 ± 2%, and −87 ± 3%, respectively, compared with insulin alone; (all P < 0.0001). The lowest concentration of iodoacetate (0.005 mM) produced less of an inhibition of glucose uptake (Δglucose, −1.8 ± 0.8 mmol/liter) and less of an inhibition of leptin secretion (−51.0 ± 16%) than insulin alone (P < 0.02; Fig. 5). By simple regression, the release of leptin was related to the concentration of iodoacetate and was highly correlated with the change in glucose in the medium (Table 1). However, by multiple regression, the leptin secreted at 96 h was related to the change in glucose, but not to the concentration of iodoacetate (Table 1).

FIG. 4. Effects of inhibiting glucose transport with cytochalasin B on leptin concentrations from 0–96 h in medium from isolated rat adipocytes in primary culture for 96 h with 1.6 nM insulin.

FIG. 5. Effects of inhibiting glycolysis with iodoacetate on leptin concentrations from 0–96 h in medium from isolated rat adipocytes in primary culture for 96 h with 1.6 nM insulin.
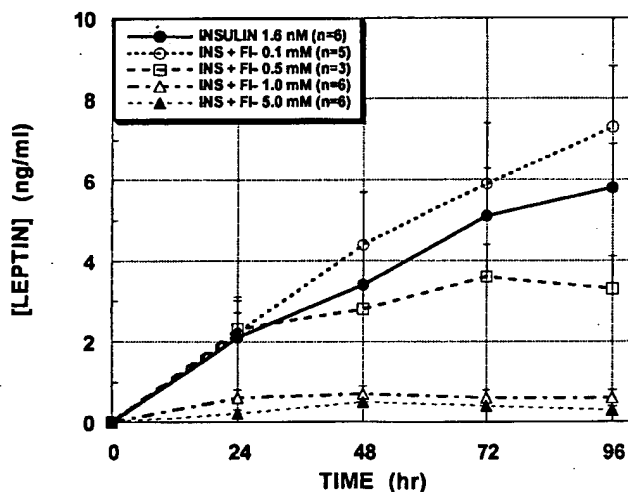
FIG. 6. Effects of inhibiting glycolysis with NaFl on leptin concentrations from 0–96 h in medium from isolated rat adipocytes in primary culture for 96 h with 1.6 nM insulin.

Effects of NaFl (0.1–5.0 mM)

The effect of inhibiting glycolysis with NaFl was examined. The two highest concentrations of NaFl (5.0 and 1.0 mM) completely inhibited glucose uptake (Δglucose, 0.2 ± 0.1 and 0.0 ± 0.3 mmol/liter, respectively). The 0.5 mM concentration of NaFl produced less of an inhibition of glucose uptake (Δ, −2.1 ± 0.6 mmol/liter), and the lowest concentration (0.1 mM) of NaFl did not inhibit glucose uptake (Δglucose, −3.9 ± 0.5 mmol/liter) compared with the effect of insulin alone. The two highest concentrations of NaFl (5.0 and 1.0 mM) markedly inhibited leptin secretion (−81 ± 6% vs. insulin alone; P < 0.0001). The next concentration of NaFl (0.5 mM) produced an intermediate inhibition of leptin secretion (−47 ± 15% of insulin alone; P < 0.05). The 0.1-mM concentration of NaFl did not inhibit leptin secretion (−4 ± 15% vs. insulin alone; P = NS; Fig. 6).

Overall, the decline in medium glucose was significantly

correlated with the concentration of NaFl and highly correlated with the 96 h leptin concentration (Table 1). By multiple regression, the amount of leptin secreted at 96 h was strongly correlated with the change in glucose in the medium ($P <$ 0.0001), but not to the NaFl concentration (Table 1).

Effects of insulin, 2-DG, and NaFl on leptin (ob) mRNA and 18S ribosomal RNA

The effects of inhibiting glucose uptake and metabolism with 2-DG or NaFl on leptin gene expression and ribosomal 18S RNA were examined. As shown in Fig. 7A, leptin (ob)

mRNA was detectable in adipocytes incubated for 48 h either with 1.6 nM insulin or without insulin (control). However, the leptin mRNA signal was reduced to near undetectable levels when adipocytes were incubated with 1.6 nM insulin and either 2-DG (10 mg/ml) or 1.0 mM NaFl (Fig. 7A). The effect of 2-DG and NaFl was specific, because in the same samples there was no effect of these concentrations of 2-DG or NaFl on 18S ribosomal RNA (Fig. 7B) or on nonspecific RNA bands (with a different mol wt than leptin mRNA) that could be detected on the Northern blots after long exposures (data not shown). Leptin mRNA was significantly reduced by 2-DG or NaFl regardless of whether the signal was normalized for 18S ribosomal signal ($P = 0.0174$). Qualitatively similar effects of 2-DG or NaFl were observed in cultures incubated for 96 h ($P = 0.0228$; data not shown).

Effects of fructose (5 mM)

The addition of 5 mM fructose to medium of cultures in which the glucose concentration was minimized by diluting the Matrigel 1:2 and using glucose-free DMEM with 1% serum augmented leptin secretion after 48 h. The initial response in the control wells was probably due to the residual glucose (~1.5 mmol/L) in the diluted Matrigel. However, both the integrated AUC from 0–96 h ($P < 0.02$) and the leptin concentration at 96 h ($P < 0.01$) were increased by fructose (Fig. 8).

Discussion

In the present study we found that addition of physiological concentrations of insulin stimulates leptin secretion from isolated rat adipocytes in primary culture. In this *in vitro* system we did not see an acute effect of insulin on leptin secretion. This is in agreement with previous reports that have demonstrated that the expression of *ob* gene and leptin protein release are not acutely regulated by insulin *in vivo* and *in vitro* (17, 36). The strong correlation between adipocyte glucose uptake measured by the decrease in glucose in the media during incubation with insulin and the amount of

FIG. 7. A, Effects of no insulin (control), 1.6 nM insulin, and 1.6 nM insulin plus 10 mg/dl 2-DG or 1.0 mM NaFl on leptin (*ob*) mRNA after 48 h of incubation, as assessed by Northern blots. The *inset above each bar* is representative of the signal obtained for each condition. B, Effects of control (no insulin), 1.6 nM insulin, and 1.6 nM insulin plus 10 mg/dl 2-DG or 1.0 mM NaFl on 18S ribosomal RNA after 48 h of incubation, as assessed by Northern blots. The *inset above each bar* is representative of the signal obtained for each condition.

FIG. 8. Effect of fructose (5 mM) on leptin concentrations from 0–96 h in medium from isolated rat adipocytes in primary culture with a low (~1.5 mmol/liter) initial glucose concentration (n = 6/treatment).

leptin secreted from isolated adipocytes is consistent with the hypothesis that the rate of glucose metabolism is a determinant of leptin secretion. In addition, the absolute insulin concentration was not related to the leptin response, independently of the effect of insulin to increase glucose uptake.

Blockade of glucose transport with 2-DG, phloretin, or cytochalasin B at concentrations at or below those typically used in adipocytes (29, 30) produced a dose-dependent decrease in leptin secretion in the presence of high physiological concentrations of insulin. The competitive inhibition produced by 2-DG could be reversed by the addition of a high concentration of glucose, suggesting that 2-DG did not inhibit leptin secretion via a nonspecific toxic effect on the adipocytes. As expected, the inhibition by phloretin was not reversed by glucose, as phloretin is not a competitive inhibitor and, therefore, produces an irreversible inhibition of glucose transport that is not readily overcome by high glucose concentrations. These experiments provide evidence that glucose uptake is required to increase leptin secretion from isolated adipocytes despite the presence of high physiological insulin concentrations.

Inhibition of glycolysis with either iodoacetate or NaFl at low concentrations (31, 32) also produced concentration-dependent inhibition of leptin secretion in the presence of insulin. When glycolysis is inhibited, glycolytic intermediates accumulate, resulting in a secondary impairment of glucose uptake. As with primary blockade of glucose uptake, during inhibition of glucose metabolism by either glycolytic inhibitor, the amount of glucose taken up over 96 h of incubation was highly correlated with the amount of leptin secreted despite the presence of insulin. These results suggest that the stimulation of leptin secretion by insulin is unlikely to be due to a direct effect of insulin *per se*, but is secondary to the effect of insulin to stimulate glucose uptake and metabolism in adipocytes.

We also found that inhibition of glucose transport and metabolism with 2-DG or glycolysis with NaFl markedly inhibited leptin (*ob*) gene expression, as assessed by Northern blot analysis of leptin mRNA. In the same cultures, 18S ribosomal RNA levels were unaffected by either 2-DG or NaFl, suggesting that the decrease in leptin gene expression was not due to a nonspecific overall effect of these inhibitors to impair adipocyte RNA synthesis. In addition, we examined the amount of heparin-released lipoprotein lipase (LPL) from adipocytes cultured with the various inhibitors (data not presented). Although LPL was modestly decreased by the inhibitors (~25–50% of insulin-stimulated levels), the suppression of leptin secretion was significantly greater (80–90%), suggesting a relative specificity of blocking glucose uptake and metabolism on leptin secretion *vs.* that on another protein (LPL) produced by adipose tissue. Lastly, the effects of the blockers to inhibit leptin expression and secretion are unlikely to be due to a depletion of adipocyte energy stores, as it is known that adipocytes can generate energy (ATP) by oxidizing fatty acids via mitochondrial β-oxidation (37, 38).

Taken together, these data suggest a physiological role for glucose in the regulation of leptin expression and secretion by adipocytes. Accordingly, we hypothesize that during fasting, when circulating insulin and glucose concentrations are low and glucocorticoids are elevated, leptin secretion declines secondary to decreased glucose transport into adipose tissue. Upon refeeding, increases in circulating insulin and glucose and the resulting increases in adipose glucose uptake and metabolism stimulate leptin secretion and restores circulating leptin concentrations to prefasting levels. This model, therefore, can explain the effects of fasting and refeeding on circulating leptin in humans (2–4) and rodents (5–7). In addition, the nocturnal increase in plasma leptin observed in humans could potentially arise as a delayed consequence of increased insulin-stimulated glucose metabolism following meals (8). The effect of glucose infusions to prevent the fall of plasma leptin during fasting in human subjects may be similarly mediated (2).

Thus, leptin secretion appears to reflect the amount of glucose transported and metabolized by adipose tissue. There is convincing evidence that suggests that a significant portion of glucose entering adipose tissue is metabolized to lactate and released (34, 35). This lactate may contribute to the pool of gluconeogenic precursors during fasting. Our results show that when a smaller proportion of glucose carbon taken up by adipocytes is released as lactate, more leptin is secreted. These data are consistent with the changes in leptin secretion observed during fasting and refeeding. In addition, fructose, in the presence of low glucose concentrations, stimulates leptin secretion, demonstrating that a nonglucose substrate can induce the adipocyte to secrete leptin and suggesting that stimulation of leptin secretion by glucose metabolism occurs downstream of phosphofructokinase.

In summary, blockade of glucose transport or inhibition of glycolysis inhibits leptin secretion from and gene expression in isolated cultured adipocytes. The secretion of leptin is directly proportional to the amount of glucose taken up by the adipocytes. These results suggest that leptin secretion is linked to glucose transport and metabolism and help to explain the known effects of feeding/fasting and long term glucose and insulin administration on circulating leptin concentrations.

References

1. Caro JR, Sinha MK, Kolaczynski JW, Zhang PL, Considine RV 1996 Leptin: the tale of an obesity gene. Diabetes 45:1455–1461
2. Boden G, Chen X, Mozzoli M, Ryan I 1996 Effect of fasting on serum leptin in normal human subjects. J Clin Endocrinol Metab 81:3419–3423
3. Weigle DS, Duell PB, Connor WE, Steiner RA, Soules MR, Kuijper JL 1997 Effect of fasting, refeeding, and dietary fat restriction on plasma leptin levels. J Clin Endocrinol Metab 82:561–565
4. Dubuc GR, Phinney SD, Stern JS, Havel PJ, Changes of serum leptin and endocrine and metabolic parameters after 7 days energy restriction in men and women. Metabolism, in press
5. Ahima SR, Prabakaran D, Mantzoros C, Qu D, Lowell B, Maratos-Flier E, Flier JS 1996 Role of leptin in the neuroendocrine response to fasting. Nature 382:250–252
6. Hardie LJ, Rayner DV, Holmes S, Trayhurn P 1996 Circulating leptin levels are modulated by fasting, cold exposure and insulin administration in lean but not Zucker (*fa/fa*) rats as measured by ELISA. Biochem Biophys Res Commun 223:660–665
7. Ahren B, Mansson S, Gingerich RL, Havel PJ 1997 Regulation of plasma leptin in mice: influence of age, high-fat diet and fasting. Am J Physiol 273:R113–R120
8. Sinha MK, Ohannesian JP, Heiman ML, Kriauciunas A, Stephens TW,

Magosin S, Marco C, Caro JF 1996 Nocturnal rise of leptin in lean, obese, and non-insulin-dependent diabetes mellitus subjects. J Clin Invest 97:1344–1347

9. Becker DJ, Ongemba LN, Brichard V, Henquin J-C, Brichard SM 1995 Diet- and diabetes-induced changes of *ob* gene expression in rat adipose tissue. FEBS Lett 371:324–328

10. Cusin R, Sainsbury A, Doyle P, Rohner-Jeanrenaud F, Jeanrenaud B 1995 The *ob* gene and insulin: a relationship leading to clues to the understanding of obesity. Diabetes 44:1467–1470

11. Saladin R, De Vos P, Guerre-Millo M, Leturque A, Girard J, Staels B, Auwerx J 1995 Transient increase in obese gene expression after food intake or insulin administration. Nature 377:527–529

12. Leroy P, Dessolin S, Villageois P, Moon BC, Friedman JM, Ailhaud G, Dani C 1996 Expression of *ob* gene in adipose cells. J Biol Chem 271:2365–2368

13. Yoshida T, Hayashi M, Monkawa T, Saruta T 1996 Regulation of obese gene expression by hormonal factors in primary cultures of rat adipocytes. Eur J Endocrinol 135:619–625

14. Havel PJ, Kasim-Karakas S, Mueller W, Johnson PR, Gingerich RL, Stern JS 1996 Relationship of plasma leptin to plasma insulin and adiposity in normal weight and overweight women: effects of dietary fat content and sustained weight loss. J Clin Endocrinol Metab 81:4406–4413

15. Larrson H, Elmstahl S, Ahren B 1996 Plasma leptin levels correlate to islet function independently of body fat in postmenopausal women. Diabetes 45:1580–1584

16. Dagogo-Jack S, Fanelli C, Paramore D, Brothers J, Landt M 1996 Plasma leptin and insulin relationships in obese and nonobese human. Diabetes 45:695–698

17. Kolaczynski JW, Nyce MR, Considine RV, Boden G, Nolan JJ, Henry R, Mudaliar SR, Olefsky J, Caro JF 1996 Acute and chronic effect of insulin on leptin production in humans: studies *in vivo* and *in vitro*. Diabetes 45:699–701

18. Havel PJ, Aoki TT, Grecu EO, Stern JS, Kasim-Karakas S 1996 Leptin/adiposity relationships in intensively treated IDDM and NIDDM and increased plasma leptin after 6 hours of high dose insulin infusion. Obesity Res 4:15S (Abstract)

19. Utriainen R, Malmstrom R, Makimattila S, Yki-Jarvinen H. 1996 Supraphysiological hyperinsulinemia increases plasma leptin concentrations after 4 h in normal subjects. Diabetes 45:1364–1366

20. Havel PJ 1997 Glucose infusion increases circulating leptin in proportion to adipose stores in rhesus monkeys. J Endocrinol Diabetes [Suppl 3] 105:37–38

21. Sonnenberg GE, Krakower GR, Hoffmann RG, Maas DL, Hennes MMI, Kissebah AH 1996 Plasma leptin concentrations: effects of extended fasting and stepwise increases in glucose infusions. Obesity Res 4:13S (Abstract)

22. Mizuno T, Bergen H, Kleopoulos S, Bauman WA, Mobbs CV 1996 Effects of nutritional status and aging on leptin gene expression in mice: importance of glucose. Horm Metab. Res 28:679–684

23. Havel PJ, Uriu-Hare JY, Stanhope KL, Stern JS, Keen CL 1997 Marked and rapid decrease of plasma leptin in insulin deficient diabetes: reversal by insulin. Diabetologia [Suppl 1] 40:A270 (Abstract)

24. Havel PJ, Connors MH, Acerini CL, Crowne ED, Dunger DB 1997 Plasma leptin is increased proportionally to adiposity by physiologic insulinemia in insulin-dependent diabetes. Diabetologia [Suppl 1] 40:A268 (Abstract)

25. Hazen SA, Rowe WA, Lynch CJ 1995 Monolayer cell culture of freshly isolated adipocytes using extracellular basement membrane components. J Lipid Res 36:868–878

26. Hajduck EJ, Guerre-Millo M, Hainault IA, Guichard CM, Lavau MM 1992 Expression of glucose transporters (GLUT1 and GLUT4) in primary cultured rat adipocytes: differential evolution with time and chronic insulin effect. J Cell Biochem 49:251–258

27. Rodbell M 1964 Metabolism of isolated fat cells. I. Effects of hormones on glucose metabolism and lipolysis. J Biol Chem 239:375–380

28. Brown J 1962 Effects of 2-deoxyglucose on carbohydrate metabolism: review of the literature and studies in the rat. Metabolism 11:1098–1112

29. Wierlinga T, Van Putten JP, Krans HM 1981 Rapid phloretin-induced dephosphorylation of 2-deoxyglucose-6-phosphate in rat adipocytes. Biochem Biophys Res Commun 103:841–847

30. Marette A, Bukowiecki LJ 1991 Noradrenaline stimulates glucose transport in rat brown adipocytes by activating thermogenesis. Evidence that fatty acid activation of mitochondrial respiration enhances glucose transport. Biochem J 277:119–124

31. Nimmo GA, Nimmo HG 1984 Studies of rat adipose tissue glycerol phosphate acyltransferase. Biochem J 224:101–108

32. Holland RI 1977 Effect of fluoride on glycerol production in rat adipocytes *in vitro*. Acta Pharmacol Toxicol 41:97–102.29

33. Mizuno TM, Bergen H, Funabashi T, Kleopoulos SP, Zhong YG, Bauman WA, Mobbs CB 1996 Obese gene expression: reduction by fasting and stimulation by insulin and glucose in lean mice, and persistent elevation in acquired (diet-induced) and genetic (yellow agouti) obesity. Proc Natl Acad Sci USA 93:3434–3438

34. Digirolamo M, Newby FD, Lovejoy J 1992 Lactate production in adipose tissue: a regulated function with extra-adipose implications. FASEB J 6:2405–2412

35. Heckler BK, Carey GB 1997 Lactate production by swine adipocytes: effects of age, nutritional status, glucose concentration, and insulin. Am J Physiol 272:E957–E966

36. Vidal H, Auboeuf D, De Vos P, Staels B, Riou JP, Auwerx J, Laville M 1996 The expression of *ob* gene is not acutely regulated by insulin and fasting in human abdominal subcutaneous adipose tissue. J Clin Invest 98:251–255

37. Mayers PA 1993 Lipid transport and storage. In: Murray RK, Granner DK, Mayes PA, Rodwell VW (eds) Harper's Biochemistry. Appleton and Lange, Norwalk, pp 250–265

38. Moore KH, Tsatsos P, Staudacher DM, Kiechle FL 1996 Counter modulation of adipocyte mitochondrial processes by insulin and S-oxalylglutathione. Int J Biochem Cell Biol 28:183–191

Effects of Metformin and Vanadium on Leptin Secretion from Cultured Rat Adipocytes

Wendy M. Mueller,* Kimber L. Stanhope,* Francine Gregoire,† Joseph L. Evans,‡ and Peter J. Havel*

Abstract

MUELLER, WENDY M., KIMBER L. STANHOPE, FRANCINE GREGOIRE, JOSEPH L. EVANS, AND PETER J. HAVEL. Effects of metformin and vanadium on leptin secretion from cultured rat adipocytes. *Obes Res.* 2000;8:530–539.

Objective: We have reported that glucose utilization regulates leptin expression and secretion from isolated rat adipocytes. In this study, we employed two antidiabetic agents that act to increase glucose uptake by peripheral tissues, metformin and vanadium, as pharmacological tools to examine the effects of altering glucose utilization on leptin secretion in primary cultures of rat adipocytes.

Research Methods and Procedures: Isolated adipocytes (100 μL of packed cells per well) were anchored in a defined matrix of basement membrane components (Matrigel) with media containing 5.5 mM glucose and incubated for 96 hours with metformin or vanadium. Leptin secretion, glucose utilization, and lactate production were assessed.

Results: Metformin (0.5 and 1.0 mM) increased glucose uptake in the presence of 0.16 nM insulin by 37 ± 10% ($p < 0.005$) and 62 ± 8% ($p < 0.0001$) over insulin alone, respectively. Metformin from 0.5 to 5.0 mM increased lactate production by 105 ± 43% ($p < 0.025$) to 202 ± 52% ($p < 0.0025$) and at 1.0 and 5.0 mM increased the proportional rate of glucose conversion to lactate by 78 ± 18% ($p < 0.005$) and 166 ± 41% ($p < 0.0025$), respectively. At concentrations less than 0.5 mM, metformin did not affect leptin secretion, but at 0.5 mM, the only concentration that significantly increased glucose utilization without increasing glucose conversion to lactate, leptin secretion was modestly stimulated (by 20 ± 9%; $p < 0.05$). Concentrations from 1.0 to 25 mM inhibited leptin secretion by 25 ± 8% ($p < 0.005$) to 89 ± 4% ($p < 0.0001$). Across metformin doses, leptin secretion was inversely related to the percentage of glucose taken up and released as lactate ($r = -0.74$; $p < 0.0001$). Vanadium (5 to 20 μM) increased glucose uptake from 20 ± 7% ($p < 0.01$) to 34 ± 13% ($p < 0.02$) and increased lactate production at 5 μM by 17 ± 8% ($p < 0.025$) and 10 μM by 61 ± 20% ($p < 0.02$) but did not alter the conversion of glucose to lactate. Vanadium (5 to 50 μM) inhibited leptin secretion by 33 ± 6% ($p < 0.0025$) to 61 ± 8% ($p < 0.0001$).

Discussion: Both metformin and vanadium increase glucose uptake and inhibit leptin secretion from cultured adipocytes. The inhibition of leptin secretion by metformin is related to an increase in the metabolism of glucose to lactate. The inhibition by vanadium most likely involves direct effects on cellular phosphatases. We hypothesize that the effect of glucose utilization to stimulate leptin production involves the metabolism of glucose to a fate other than anaerobic lactate production, possibly oxidation or lipogenesis.

Key words: glucose uptake, lactate production, anaerobic metabolism

Introduction

The adipocyte hormone, leptin, has a central role in the regulation of food intake, energy expenditure, and body fat stores (1,2). Circulating leptin concentrations are well correlated with adipose stores in humans (3–5) and animals (5–7). However, leptin production is also acutely regulated by nutritional status. For example, circulating leptin decreases after fasting (6,8–10) or energy restriction (11,12) and increases after refeeding or overfeeding (9,13). These changes of circulating leptin are disproportionate to the relatively small changes of body fat. Although the regulation of leptin expression and secretion is incompletely understood, changes of insulin secretion during fasting and refeeding precede changes of circulating leptin concentrations. There is a growing body of evidence that suggests a role for insulin and glucose in mediating changes of circulating leptin levels in vivo. For example, infusion of small amounts of glucose to prevent the reductions of insulin and

glucose during fasting in humans also prevents the decrease in plasma leptin (8). Although insulin administration does not acutely increase plasma leptin concentrations in human subjects (14,15) increases have been reported after 4 to 6 hours during insulin infusions producing supraphysiological (16,17) or physiological (18) increments of plasma insulin levels. Similarly, prolonged hyperglycemia and hyperinsulinemia in response to extended glucose infusions increases plasma leptin after several hours in nonhuman primates (7) and human subjects (19). Lastly, leptin concentrations increase 4 to 6 hours after high carbohydrate meals, which induce large plasma insulin and glucose responses in humans (20).

In vitro studies have shown that insulin increases leptin expression and secretion in isolated rodent (21–23) and human (15,24) adipocytes. It has not, however, been clear whether the effect of insulin to increase leptin production is a direct consequence of increased insulin signaling or might be indirectly mediated by insulin's actions on glucose metabolism. Several in vivo studies have provided support for the latter explanation. First, glucose administration induces increases of *ob* mRNA expression, which are more closely related to changes of plasma glucose than to plasma insulin concentrations (25,26).

In addition, the decrease in plasma leptin during marked caloric restriction in humans is better correlated with the decrease in plasma glucose than with changes in insulinemia (11,12). Furthermore, we have found that low plasma leptin levels in insulin-deficient streptozotocin diabetic rats are acutely increased by insulin administration in proportion to the degree of glucose lowering (27). Further support from in vitro experiments for a role for adipose glucose utilization in the regulation of leptin production is provided by our recent report that increased glucose metabolism is an important mediator of insulin-stimulated leptin expression and secretion. Blockade of glucose uptake or inhibition of glycolysis decreases *ob* gene expression and leptin secretion in isolated rat adipocytes (28). However, glucose uptake, by itself, only seems to be important in that glucose must first be taken up by the adipocytes before it can be metabolized. Rather than glucose uptake per se, the inverse relationship observed, between the proportional conversion of glucose to lactate and leptin secretion by isolated adipocytes (28), suggests that a regulatory step for glucose metabolism to mediate changes of leptin production involved the metabolism of glucose to a point beyond the anaerobic metabolism of glucose-derived pyruvate to lactate.

Metformin and vanadium are two antidiabetic agents, which are able to enhance glucose uptake and utilization by peripheral tissues (29,30). In the present study, we employed metformin and vanadium as pharmacological tools to examine the effects of altering adipocyte glucose utilization on leptin production in primary cultures of isolated adipocytes. Glucose utilization, lactate production, and lep-

tin secretion were measured over 96 hours in isolated rat adipocytes cultured in a basement membrane matrix that maintains adipocyte differentiation.

Research Methods and Procedures

Materials
Media (Dulbecco's modified Eagle's medium [DMEM]) and fetal bovine serum (FBS) were purchased from Life Technologies (Grand Island, NY). The media was supplemented with 6 mL each of minimal essential medium amino acids, penicillin/streptomycin (5000 U/mL/5000 μg/mL), and nystatin (10,000 U/mL; all from Life Technologies) per 500 mL of DMEM. Bovine serum albumin fraction V, 4-(2-hydroxyethyl)-1-piperazineethansulfonic acid (HEPES), collagenase (*Clostridium histolyticum*, type II; specific activity, 456 U/mg), insulin, and metformin were purchased from Sigma Chemical Co. (St. Louis, MO). Matrigel matrix was purchased form Becton Dickinson (Franklin Lakes, NJ). Bis(maltolato) oxovanadium(IV) (BMOV), an organified form of vanadium (31), was a gift from Drs. John McNeill and Violet Yuen, Department of Pharmaceutical Sciences, University of British Columbia, Vancouver, BC, Canada. Six-well Falcon plates were purchased from Fisher Scientific (Pittsburgh, PA). Nylon filters were purchased from Tetko (Kansas City, MO).

Animals
Male Sprague-Dawley rats (3 to 6 months of age) were obtained from Charles River (Wilmington, MA). Animals were housed in hanging wire cages in temperature-controlled rooms (22 °C) with a 12-hour light-dark cycle and fed Purina chow diet (Ralston-Purina, St. Louise, MO) and given deionized water ad libitum. Animal use and care was in accordance with the National Institutes of Health Guide for the Use and Care of Laboratory Animals and conducted in facilities accredited by the American Association for Accreditation of Laboratory Animal Care. The study protocol was approved by the Administrative Animal Use and Care Committee at University of California, Davis.

Methods
Cell Isolation/Preparation. Adipocytes were prepared from epididymal fat pads from male Sprague-Dawley rats weighing 300 to 600 g. Epididymal fat depots were resected from halothane-anesthetized rats under aseptic conditions, and adipocytes were isolated by collagenase digestion by the Rodbell method (32) with minor modifications as previously described (28). The isolated adipocytes were then incubated for 30 minutes at 37 °C before being plated and cultured on Matrigel-coated plates.

Adipocyte Culture. Adipocytes were maintained in culture anchored to a basement membrane matrix (Matrigel, Becton Dickinson). Although all in vitro systems have

inherent advantages and disadvantages, advantages of this system compared with cultures containing free-floating adipocytes are that the matrix simulates their normal basement membrane attachment and that the cells are maintained in close proximity to each other, allowing direct cell-to-cell contact. Together the cell contact and basement membrane attachment help to maintain differentiation, because adipocytes have a strong tendency to dedifferentiate in long term (>24-hour) culture. In addition, the matrix and the small amount of serum in the media both contain growth factors, which are also likely to help maintain cell differentiation. Furthermore, the adipocytes in this system are not exposed to toxic levels of oxygen at the interface of the media and the incubator atmosphere, as opposed to free-floating adipocytes which aggregate at the surface of the media. An advantage of the system over those containing minced adipose tissue is that all of the cells in the culture are equally exposed to the nutrients and the oxygen dissolved in the media. Thus, although clearly different from the in vivo situation, we believe that this system provides a more physiological environment than most systems for maintaining adipocytes in long term culture. In the case of the present studies, the goal was to examine the direct actions of metformin and vanadium on leptin production and adipocyte metabolism. Therefore, the advantage of employing in vitro experimentation for this purpose over in vivo models was that it was possible to control confounding variables, such as effects of these agents on food intake, which would indirectly influence leptin production via changes of insulin secretion (18,20). Unlike an in vivo system, in this study the environment surrounding the adipocytes within the individual wells of each culture plate was identical with the exception of the presence or absence and the concentration of metformin or vanadium, allowing assessment of the direct effects of the treatments.

In culturing each suspension, Matrigel was first thawed on ice to a liquid and uniformly applied to the surface of culture dishes (300 μL of Matrigel/35-mm well). After the incubation period, 150 μL of the adipocyte suspension (2:1 ratio of packed cells to media) were plated on the liquid Matrigel matrix. Adipocytes from each suspension were thoroughly mixed with a transfer pipette before plating to insure that a similar number of adipocytes with a similar size distribution were added to the control and experimental wells for each suspension. The warmth of the added cells and media caused the Matrigel to gel around the adipocytes, effectively anchoring them to the culture dish. After a 30-minute incubation at 37 °C, 2 mL of warm culture medium was added. The cells were maintained in an incubator at 37 °C for 96 hours with 6% CO_2. Aliquots of adipocytes from each animal were divided into wells, with the

different concentrations of either metformin or vanadium (as detailed below). In each plate an appropriate control well contained adipocytes from the same animal. Adipocytes were incubated with media (DMEM) containing 5.5 mM (100 mg/dL) glucose plus 5% FBS at five concentrations of Metformin (0.1, 0.25, 0.5, 1.0, 5.0, and 25.0 mM). A low basal concentration of insulin (0.16 nM) was added to the incubations performed with metformin, because metformin is thought to act in part by increasing insulin signaling (33,34). Vanadium was added at four concentrations (5.0, 10.0, 20.0, and 50.0 μM) in DMEM with 5.0 to 5.5 mM glucose and 1% FBS. Adipocytes were cultured with vanadium without added insulin, because vanadium action is considered to be largely independent of insulin (35,36). To examine the responses to insulin in the adipocytes obtained from each adipocyte suspension in the vanadium experiments, a separate well containing 1.6 nM insulin was included for each suspension. In all experiments, aliquots of media (300 μL, 15% of the media volume) were collected from culture wells and replaced with fresh media containing the appropriate concentrations of metformin or vanadium at 24, 48, 72, and 96 hours.

Assays. Leptin concentrations in the medium were determined with a sensitive and specific radioimmunoassay for rat leptin (37) with reagents obtained from Linco Research, St. Charles, MO. Glucose and lactate were measured with a glucose analyzer (model 2300, YSI, Yellow Springs, OH).

Data Analysis. The uptake of glucose was assessed by measuring the concentration of glucose in the media in each well before and at 24, 48, 72, and 96 hours of incubation and calculating the decrease over 96 hours after correcting for the amount of glucose that was removed during each 24-hour media sampling and the amount added by the replacement of fresh media (15% of total volume). Lactate production was calculated as the increase of media lactate at 24, 48, 72, and 96 hours by correcting for the amount of lactate removed by sampling and added with media replacement. To examine the relationship between adipocyte carbon flux and leptin secretion in adipocytes cultured with metformin or vanadium, the amount of carbon released as lactate per amount of carbon taken up as glucose over 96 hours was calculated as lactate production/glucose utilization and expressed as a percentage (28). Cumulative leptin production was calculated as the change of media leptin concentrations at 24, 28, 72, and 96 hours with correction for the amount of leptin removed during sampling. The area under the curve for leptin production between 0 and 96 hours was calculated by the trapezoidal method. The experimental results from each adipocyte suspension prepared from a single animal were analyzed in relation to a control well from the same suspension. Given the

individual variation in leptin responses between animals and/or suspensions, it was not appropriate to compare means from control and treated adipocytes from different animals and/or suspensions. Therefore, the means for all the controls in the metformin ($n = 18$) and vanadium ($n = 14$) experiments contain a larger sample size (n) of animals and/or suspensions than all except the 1.0 mM metformin dose, which was studied in every experiment. Thus, when the number of wells with a particular concentration of metformin or vanadium differed from the total number of control wells (e.g., 0.5 mM metformin; $n = 9$), each result was compared only to that obtained in a corresponding control well from the same suspension in a pair-wise comparison. To examine the relationships between the medium concentrations of metformin or vanadium, glucose uptake, lactate production, and glucose conversion to lactate, and leptin secretion, simple and multiple linear regression analyses were performed with a statistics software package (StatView for Macintosh, Abacus Concepts, Inc., Berkeley, CA).

Because metformin exhibited toxic effects on adipocyte metabolism at concentrations greater than 5.0 mM, results from cultures incubated with metformin at concentrations greater than 5.0 mM were not included in these analyses. The relationship between lactate production from glucose and leptin secretion was also examined within the control groups alone. Data are expressed as means + SEM.

Results

Effects of Metformin

The effects of metformin on glucose uptake, lactate production, and leptin secretion were examined. Metformin at a concentration of 0.1 mM did not affect glucose uptake compared with the corresponding control suspensions containing insulin (0.16 nM) alone. At 0.25 mM, glucose uptake was increased (%$\Delta = +9 \pm 8$%), but the effect was not statistically significant perhaps due to the smaller number of trials ($n = 5$) performed at this concentration. Metformin stimulated glucose uptake at concentrations of 0.5 mM ($+37 \pm 10$%, $p < 0.005$) and 1.0 mM ($+62 \pm 8$%, $p < 0.0001$) compared with that in the corresponding control suspensions (Table 1, Figure 1). At 5.0 mM, glucose uptake was not significantly different from control. Higher concentrations of metformin (≥ 25.0 mM) markedly inhibited glucose uptake most likely reflecting a toxic effect of metformin at these very high concentrations. Metformin had no significant effect on lactate production at concentrations lower than 0.5 mM but increased lactate production at concentrations of 0.5 mM ($+105 \pm 43$%, $p < 0.025$), 1.0 mM ($+186 \pm 31$%, $p < 0.0001$), and 5.0 mM ($+202 \pm 52$%, $p < 0.0025$) vs. insulin alone (Table 1, Figure 1). At concentrations of 25.0 mM, lactate production was markedly inhibited ($p < 0.0001$), because glucose utilization was

almost completely suppressed. Concentrations of metformin of 0.5 mM and below did not affect the proportional conversion of glucose to lactate (Table 1). However, glucose conversion to lactate was increased at a concentration of 1.0 mM, and this effect was marked at 5.0 mM with more than twice the amount of glucose released as lactate (Table 1). Although 1.0 mM metformin did increase mean glucose uptake over control rates, a significantly larger proportion of the glucose that was taken up was released as lactate. The concentration of 0.5 mM was the only level of metformin that induced a significant increase of glucose utilization without increasing the proportion of glucose carbon released as lactate (Table 1).

At concentrations of metformin lower than 0.5 mM, leptin secretion was unaffected. With metformin at 0.5 mM, the area under the curve (AUC) for leptin secretion over 96 hours was significantly greater ($+20.5 \pm 9$%, $p < 0.05$) than control (Figure 2). Metformin inhibited leptin secretion at concentrations of 1.0 mM (-25 ± 8%, $p < 0.005$), 5.0 mM (-89 ± 4%, $p < 0.0001$), and by 90% at toxic concentrations of 25.0 mM ($p < 0.0001$) (Figure 2).

Within the 18 control wells, leptin secretion was inversely related to the conversion of glucose to lactate ($r = -0.61$; $p < 0.01$). At metformin concentrations from 0 to 5.0 mM, leptin secretion was inversely proportional to the log of the metformin concentration ($r = -0.53$; $p < 0.0001$), to lactate production ($r = -0.53$; $p < 0.0001$), and to the proportional conversion of glucose to lactate across metformin doses ($r = -0.74$; $p < 0.0001$)(Figure 3) but was not related to glucose uptake ($r = 0.13$; $p = 0.27$) by simple regression. By multiple regression analysis, leptin secretion was inversely related to the conversion of glucose to lactate ($p < 0.0001$) but not to the log of the metformin concentration ($p = 0.91$), lactate production ($p = 0.39$), or glucose uptake ($p = 0.62$). Leptin secretion was only increased over control by metformin at 0.5 mM, which was also the only concentration that significantly increased glucose uptake without shunting a greater proportion of the glucose into lactate production (Table 1). A similar inverse relationship ($r = -0.73$; $p < 0.0025$) between leptin production and anaerobic glucose metabolism to lactate was observed in 32 control wells containing either no insulin or a low insulin concentration of 0.16 nM (~20 μU/mL) (Figure 4).

Effects of Vanadium

The effects of vanadium on glucose uptake, lactate production, and leptin secretion were examined in adipocytes cultured with concentrations of vanadium of 0 to 50 μM. Vanadium at 5.0 μM ($+20 \pm 7$%, $p < 0.01$), 10.0 μM ($+38 \pm 12$%, $p < 0.02$), and 20.0 μM ($+34 \pm 13$%, $p < 0.02$) increased glucose uptake, compared with rates of glucose uptake in the corresponding control suspensions (Table 2, Figure 5). The effect of vanadium at these con-

Table 1. Effects of metformin in the presence of 0.16 nM insulin on glucose uptake, lactate production, and the percentage of glucose carbon taken up that was released as lactate by isolated rat adipocytes over 96 hours in culture (mean ± SEM)

[Metformin] (mM) + Insulin (0.16 nM)	Glucose uptake (μmol) over 96 hours	Lactate production (μmol) over 96 hours	Glucose to lactate (%)
Control (n = 18)	7.5 ± 0.7	5.7 ± 0.5	40.9 ± 3.6
0.1 (n = 4)	6.5 ± 0.9	5.9 ± 0.6	47.2 ± 6.3
0.25 (n = 5)	11.0 ± 1.4	8.6 ± 1.3	40.2 ± 5.9
0.5 (n = 9)	11.0 ± 1.2†	9.5 ± 1.2†	44.9 ± 5.1
1.0 (n = 18)	11.6 ± 0.7‡	14.4 ± 0.9‡	63.8 ± 3.4*
5.0 (n = 15)	8.3 ± 0.6	14.4 ± 1.0‡	85.6 ± 4.1‡

$* p = 0.01$; $† p = 0.005$; $‡ p = 0.0005$; vs. corresponding controls from the same adipocyte suspensions.

centrations was comparable to that of insulin at 1.6 nM, which increased glucose uptake by 38 ± 8% ($p <$ 0.0001)(Table 2, Figure 5). Vanadium at 50.0 μM did not significantly affect glucose uptake (%Δ = −4 ± 14%). Vanadium at 5.0 μM increased lactate production by + 17 ± 8% ($p <$ 0.025). Mean lactate production in the six wells that served as controls for the 10.0 μM concentration of vanadium was lower than average; however, lactate production was increased in five of six corresponding experimental wells. Thus, vanadium at 10 μM increased lactate production by 61 ± 20% ($p <$ 0.02) despite absolute lactate production being similar to the mean of the total 14 control wells. At 20.0 and 50.0 μM, lactate production was not significantly different from that of the control (Table 2).

Insulin at 1.6 nM increased leptin secretion over 96 hours by 59 ± 15% ($p <$ 0.005) and the 0- to 96-hour AUC by 38 ± 8% ($p <$ 0.0001)(Figure 5). Leptin secretion was unaffected by vanadium at a concentration of 5 μM. Higher concentrations of 10, 20, and 50 μM consistently inhibited leptin secretion over 96 hours by −33 ± 6% ($p <$ 0.0025), −53 ± 7% ($p <$ 0.0001), and −61 ± 8% ($p <$ 0.001), respectively (Figure 6). Across vanadium concentrations, leptin secretion at 96 hours was positively correlated with glucose uptake ($r = 0.35$; $p <$ 0.02) and inversely related to the log of the vanadium concentration ($r = −0.44$; $p <$ 0.0001), to lactate production ($r = −0.30$; $p <$ 0.025), and to the conversion of glucose to lactate ($r = −0.58$; $p <$
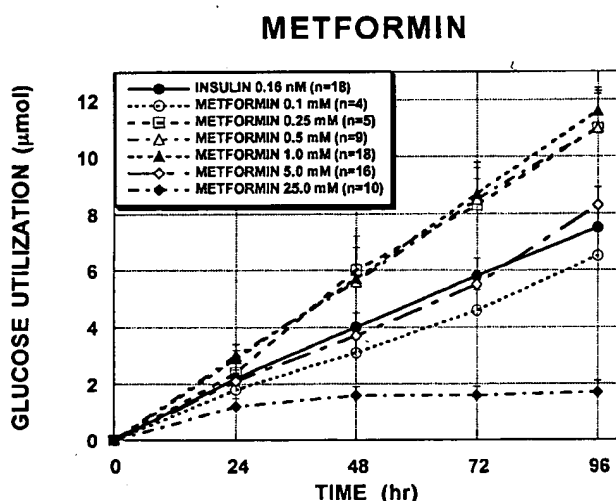
Figure 1. Glucose utilization (corrected for media sampling and replacement) over 96 hours by isolated rat adipocytes in primary culture with insulin at 0.16 nM and metformin at concentrations from 0 to 25.0 mM.
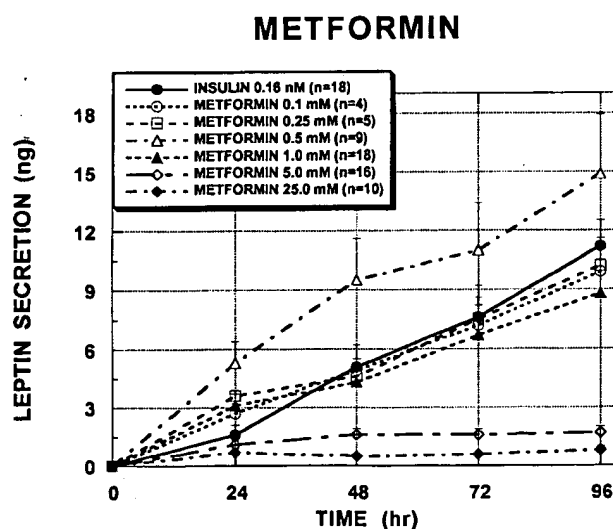
Figure 2. Leptin secretion (corrected for media sampling and replacement) over 96 hours by isolated rat adipocytes in primary culture with insulin at 0.16 nM and metformin at concentrations from 0 to 25.0 mM.
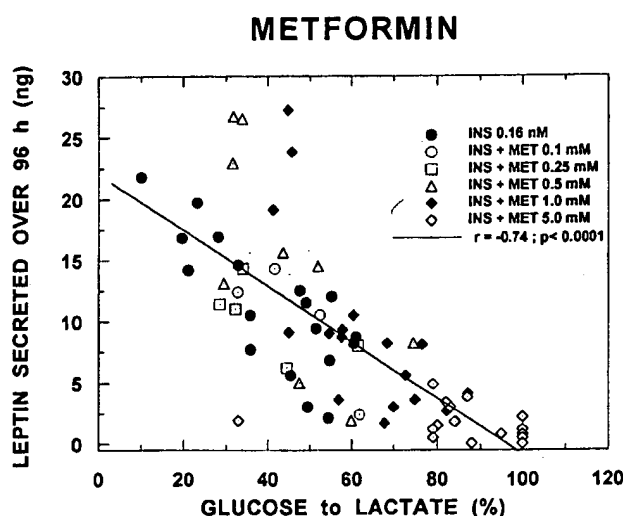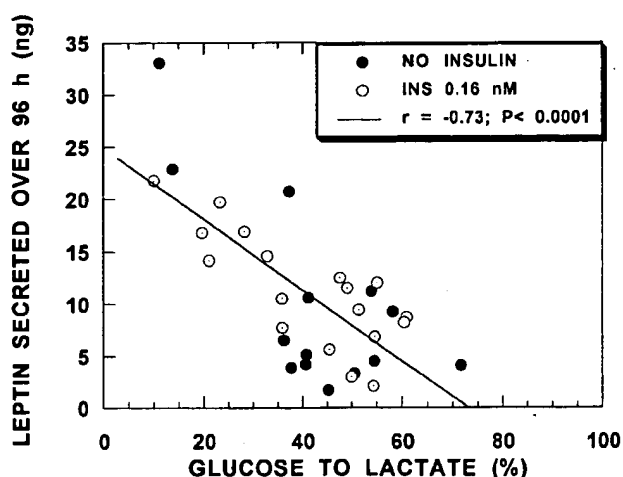
METFORMIN

Figure 3. Relationship between the percentage of glucose taken up and released as lactate and leptin secretion over 96 hours by adipocytes in primary culture with insulin (INS) at 0.16 nM and metformin (MET) at concentrations from 0 to 5.0 mM. Leptin secretion, glucose utilization, and lactate production are corrected for media sampling and replacement.

0.0001) (data not shown). By multiple regression analysis, leptin secretion at 96 hours was more closely related to glucose conversion to lactate ($p < 0.0001$) than to absolute lactate production ($p < 0.02$) or the log of the vanadium concentration ($p < 0.005$) and was not related to absolute

Figure 4. Relationship between the percentage of glucose taken up and released as lactate and leptin secretion over 96 hours by adipocytes in primary culture in 32 control wells containing no added insulin or insulin at a low concentration of 0.16 nM. Leptin secretion, glucose utilization, and lactate production are corrected for media sampling and replacement.

glucose uptake ($p = 0.22$). Despite the relationship between leptin secretion and the conversion of glucose to lactate across vanadium concentrations, unlike with metformin, the percentage of glucose released as lactate was not altered by any concentration of vanadium (Table 2). In contrast, insulin at 1.6 nM, which significantly decreased the proportional conversion of glucose to lactate (i.e., anaerobic glucose metabolism) (Table 2), stimulated leptin secretion (Figure 6).

Discussion

We have recently reported that insulin-mediated glucose metabolism is an important factor regulating leptin expression and secretion in isolated rat adipocytes (28). Some previous studies have shown that drugs in the thiazolidinedione class, which are used in the treatment of type 2 diabetes, can inhibit leptin production in vitro and in vivo (38,39). In the present study, we examined the effects of metformin and vanadium, two other antidiabetic drugs known to increase cellular glucose utilization, on leptin secretion, glucose uptake, and lactate production in isolated cultured rat adipocytes. Our goal was to use these compounds as tools to examine their effects for altering adipocyte glucose utilization on leptin secretion. Therefore, we used concentrations within a range that were found to produce significant increases of adipocyte glucose uptake. Particularly in the case of metformin, these concentrations (0.25 to 5.0 mM) were far above the range of plasma concentrations (0.005 to 0.02 mM) observed in patients treated with therapeutic doses of metformin (40). In fact, at therapeutic concentrations, metformin seems to act primarily to inhibit hepatic glucose production with limited, if any, effects on peripheral glucose uptake (41–43). At therapeutic concentrations, metformin generally has little direct effect on glucose utilization in vitro (44,45). At concentrations higher than those achieved in serum with therapeutic metformin administration, metformin stimulates glucose transport by rat (46,47) and human adipocytes (48), and in rat and human skeletal muscle (see reviews in 29,34,48,49). At the cellular level, high concentrations of metformin increase insulin receptor binding, along with tyrosine kinase activity, glucose transport, and glycogen synthesis (33,34).

In the present study, metformin concentrations ranging from 0.5 to 5.0 mM increased both glucose uptake and lactate production. In addition to increasing absolute lactate production, metformin at 1.0 and 5.0 mM increased the percentage of glucose carbon that was metabolized to lactate and released into the culture media by 80% to 170%. At high concentrations of metformin (= 25.0 mM), both glucose uptake and lactate production were markedly inhibited, most likely due to a toxic effect of very high levels of metformin on cellular metabolism. Metformin at 0.5 mM modestly increased leptin secretion by ~20%.

Table 2. Effects of insulin (1.6 nM) or vanadium on glucose uptake, lactate production, and the percentage of glucose carbon taken up that was released as lactate by isolated rat adipocytes over 96 hours in culture (mean ± SEM)

[Vanadium] (μM); no insulin added	Glucose uptake (μmol) over 96 hours	Lactate production (μmol) over 96 hours	Glucose to lactate (%)
Control ($n = 14$)	6.8 ± 0.5	5.6 ± 0.6	42.4 ± 4.3
1.6 nM Ins ($n = 14$)	9.4 ± 0.9§	5.7 ± 0.7	33.0 ± 3.5‡
5.0 ($n = 12$)	7.8 ± 1.1§	5.7 ± 0.6*	40.5 ± 4.7
10.0 ($n = 6$)	8.2 ± 1.3‡	5.2 ± 0.8†	36.0 ± 6.5
20.0 ($n = 12$)	8.7 ± 1.2‡	6.3 ± 0.6	41.6 ± 5.0
50.0 ($n = 13$)	6.9 ± 1.02	4.9 ± 0.5	53.3 ± 9.4

* $p = 0.05$; † $p = 0.02$; ‡ $p = 0.0025$; § $p = 0.0005$; vs. corresponding control wells from the same adipocyte suspensions.

Importantly, this was the only concentration of metformin tested that increased glucose uptake without shunting a greater proportion of glucose into lactate production. In contrast, at concentrations of 1.0 mM and higher, leptin secretion was modestly to markedly suppressed.

A significant proportion of glucose taken up by adipose tissue is metabolized to lactate and released (50). At metformin concentrations ≤ 5.0 mM, leptin secretion was inversely related to the amount of glucose taken up by the adipocytes, converted to lactate, and released into the media. We have previously observed that the stimulation of leptin secretion by insulin is associated not only with increased glucose utilization, but with a decrease in the pro-

portional conversion of glucose to lactate (28), a finding that was also observed within the control groups in the present study (Figure 4). Thus, when lactate production is increased, less carbon derived from glucose is available to enter the tricarboxylic acid cycle either for oxidation or use in de novo lipogenesis. Together, these data suggest that it is not glucose uptake, per se, but its metabolism beyond pyruvate and lactate in the adipocyte that is involved in the action of glucose to stimulate leptin secretion. Thus, the anaerobic metabolism of glucose does not stimulate leptin production. The entry of glucose into the hexosamine biosynthetic pathway and the production of UDP-glucosamine have been suggested as a mechanism by which glucose utilization can
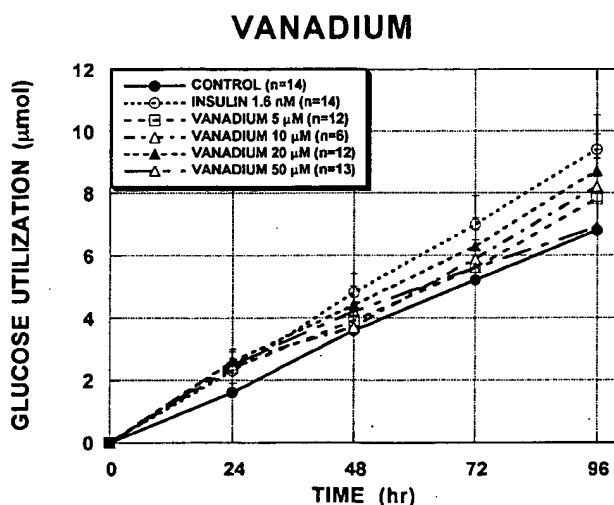
Figure 5. Glucose utilization (corrected for media sampling and replacement) over 96 hours in by isolated rat adipocytes in primary culture with vanadium at concentrations from 0 to 50.0 μM or with insulin at 1.6 nM.
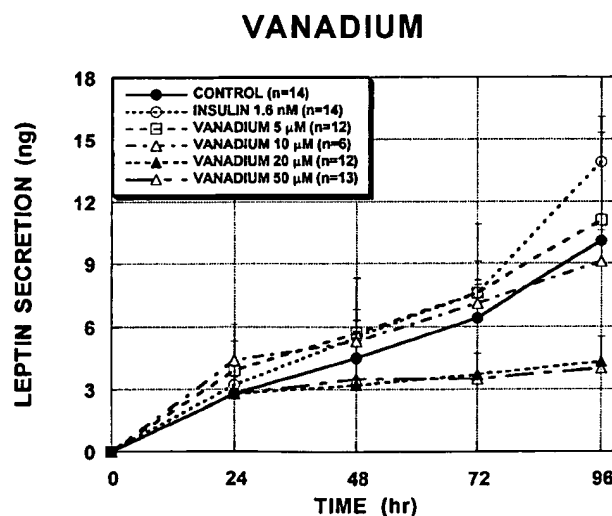
Figure 6. Leptin secretion (corrected for media sampling and replacement) over 96 hours by isolated rat adipocytes in primary culture with vanadium at concentrations from 0 to 50.0 μM or with insulin at 1.6 nM.

stimulate leptin production in adipose tissue (51). However, our results indicate that glucose can be metabolized to lactate, a point well beyond where glucose enters the hexosamine pathway, without stimulating leptin production. Therefore, if the hexosamine pathway were to be the sole mechanism by which glucose regulates leptin production, one would need to postulate that either anaerobic glucose metabolism and/or metformin itself, have an inhibitory effect on glucose entry into this pathway. The results of the present study suggest that it is more likely that the effect of glucose metabolism to stimulate leptin production involves glucose oxidation and/or the production of lipogenic precursors.

Metformin at 0.1 and 0.25 mM did not effect glucose metabolism or leptin secretion. Thus, metformin at therapeutic levels is unlikely to affect leptin production in vivo. Of the concentrations of metformin tested in this study, only 0.5 mM increased glucose uptake without shunting a larger proportion of the glucose into lactate. As previously discussed, this was the only concentration of metformin that had effects on glucose metabolism that did not inhibit leptin secretion, and, in fact, leptin secretion was modestly increased at 0.5 mM. Thus, only when glucose uptake *and* its metabolism beyond lactate were simultaneously increased, did we observe an increase, and not an inhibition, of leptin secretion. Therefore, it seems that only within a very narrow concentration range is metformin able to have a net effect to increase glucose uptake as well as its metabolism beyond lactate in isolated adipocytes. Accordingly, the effects of metformin to inhibit leptin secretion at most concentrations examined is likely to be a result of its effects to direct pyruvate metabolism into lactate and away from other potential pathways for pyruvate metabolism such as oxidation or lipogenesis.

The use of vanadium-containing compounds in the treatment of diabetes has been widely investigated in animals (52,53), and a few clinical trials have been conducted in human patients (54,55). A compound structurally similar to the form of organified vanadium used in this study (BMOV) has recently entered Phase 1 clinical trials. To our knowledge, the present study is the first report examining the effects of a vanadium compound on leptin production in vivo or in vitro.

Vanadium stimulated glucose uptake at concentrations up to 20 μM, whereas glucose uptake was not affected by a concentration of 50 μM. Lactate production was modestly increased at the lower concentrations of vanadium. We found that vanadium at a low concentration of 5.0 μM did not affect leptin production, however, concentrations of 10.0 μM and higher inhibited leptin secretion from isolated adipocytes by 30% to 60%. Although the amount of leptin secreted was inversely proportional to the percentage conversion of glucose to lactate across the concentrations of

vanadium tested, this relationship was significantly weaker than that observed across metformin concentrations.

Furthermore, the proportion of glucose taken up and released as lactate was unaffected by vanadium at any concentration. Thus, in contrast to what was observed with metformin, the ability of vanadium to inhibit leptin secretion seems to be independent of any effects on glucose metabolism or lactate production, most likely because it does not increase the proportion of glucose fluxing into anaerobic metabolism.

The observed effects of vanadium result from one or more of the multiple known biological actions of vanadium in cells. These include the inhibition of protein tyrosine phosphatases and the activation of cytosolic protein-tyrosine kinases, resulting in the alteration of cellular tyrosine phosphorylation content (30,56). Vanadium has also been shown to exert direct inhibitory effects on a number of other cellular enzymes, including acid, alkaline, and dual-function phosphatases, ATPases, glucose-6-phosphatase, and fructose-2,6-bisphosphatase (30,55). At high concentrations, vanadium might exert some toxic effects on the cells, an effect which could underlie the lack of effect of the highest concentration of vanadium to stimulate glucose uptake, as well as the inhibition of leptin production at the two highest concentrations examined. In particular, the effects of vanadium to inhibit the activity of one or more enzymes involved in cellular energy metabolism could both inhibit leptin production and, at high concentrations, impair the ability of the cell to utilize energy derived from glucose metabolism.

In vanadium-treated animals, plasma vanadium concentrations have been estimated to be in the 10 to 20 μM range and in human clinical trials in the 1 to 5 μM range (53). Although it is unlikely based on the present results that the concentration of vanadium achieved in humans would be sufficient to affect leptin production, previous human studies employed low doses of vanadyl sulfate or sodium meta-vanadate, which are molecular forms that exhibit poor bioavailability. The potential effects on leptin secretion of the more readily absorbed forms of vanadium, such as the organified vanadium compound (BMOV) used in the present study (31), should therefore be considered.

In summary, both metformin and vanadium inhibit leptin secretion from primary cultures of rat adipocyte at concentrations that significantly increase glucose utilization. The inhibition of leptin production by metformin, but not by vanadium, is related to an increased conversion of glucose to lactate (i.e., anaerobic metabolism). This effect of metformin, coupled with our previous findings (28), suggests that the effect of glucose utilization to stimulate leptin production is not mediated by glucose uptake per se but involves the metabolism of glucose beyond pyruvate to a fate other than lactate, possibly oxidation or lipogenesis. Thus, metformin is a useful tool for examining the effects of

increasing anaerobic glucose metabolism. Further research, including examination of the potential roles of glucose oxidation and lipogenesis, needs to be conducted to determine the precise biochemical and molecular mechanisms by which glucose metabolism regulates leptin production.

Acknowledgments

References

1. Friedman JM, Halaas JL. Leptin and the regulation of body weight in mammals. *Nature.* 1998;395:763–770.
2. Havel PJ. Mechanisms regulating leptin production: implications for control of to energy balance. *Am J Clin Nutr.* 1999; 70:305–306.
3. Considine RV, Sinha MK, Heiman ML, et al. Serum immunoreactive-leptin concentrations in normal-weight and obese humans. *N Engl J Med.* 1996;334:292–295.
4. Havel PJ, Kasim-Karakas S, Mueller WM, Johnson PR, Gingerich RL, Stern JS. Relationship of plasma leptin to plasma insulin and adiposity in normal weight and overweight women: effects of dietary fat content and sustained weight loss. *J Clin Endocrinol Metab.* 1996;8:4406–13.
5. Maffei M, Halaas J, Ravussin E, et al. Leptin levels in human and rodents measurement of plasma leptin and *ob* RNA in obese and weight-reduced subjects. *Nat Med.* 1995;1: 1155–61.
6. Ahren B, Mansson S, Gingerich RL, Havel PJ. Regulation of plasma leptin in mice: influence of age, high-fat diet and fasting. *Am J Physiol.* 1997;273:R113–R20.
7. Havel PJ. Glucose infusion increases circulating leptin in proportion to adipose stores in rhesus monkeys. *J Exp Endocrinol Diabetes.* 1997;105(Suppl 3):37–8.
8. Boden G, Chen X, Mozzoli M, Ryan I. Effect of fasting on serum leptin in normal human subjects. *J Clin Endocrinol Metab.* 1996;81:3419–23.
9. Kolaczynski JW, Considine RV, Ohannesian J, et al. Responses of leptin to short-term fasting and refeeding in humans: a link with ketogenesis but not ketones themselves. *Diabetes.* 1996;45:1511–15.
10. Weigle DS, Duell PB, Conner WE, et al. Effect of fasting, refeeding, and dietary fat restriction on plasma leptin levels. *J Clin Endocrinol Metab.* 1997;82:561–5.
11. Dubuc GR, Phinney SD, Stern JS, Havel PJ. Changes of serum leptin and endocrine and metabolic parameters after 7 days energy restriction in men and women. *Metab Clin Exp.* 1998;47:429–34.
12. Keim NL, Stern JS, Havel PJ. Relationship between circulating leptin concentrations and appetite during a prolonged, moderate energy deficit in women. *Am J Clin Nutr.* 1998;68: 794–801.
13. Kolaczynski JW, Ohannesian JP, Considine RV, Marco CC, Caro JF. Response of leptin to short-term and prolonged overfeeding in humans. *J Clin Endocrinol Metab.* 1996;81: 4162–5.
14. Dagogo-Jack SC, Fanelli D, Paramore J, Brothers, Landt M. Plasma leptin and insulin relationships in obese and nonobese human. *Diabetes.* 1996;45:695–8.
15. Kolaczynski JW, Nyce MR, Considine RV, et al. Acute and chronic effect of insulin on leptin production in humans: studies *in vivo* and *in vitro. Diabetes.* 1996;45:699–701.
16. Havel PJ, Aoki TT, Grecu EO, Stern JS, Kasim-Karakas S. Leptin/adiposity relationships in intensively treated IDDM and NIDDM and increased plasma leptin after 6 hours of high dose insulin infusion. *Obes Res.* 1996;4:15S.
17. Utriainen R, Malmstrom R, Makimattila S, Yki-Jarvinen H. Supraphysiological hyperinsulinemia increases plasma leptin concentrations after 4 h in normal subjects. *Diabetes.* 1996;45:1364–6.
18. Saad MF, Khan A, Sharma A, et al. Physiological insulinemia acutely modulates plasma leptin. *Diabetes.* 1998;47: 544–9.
19. Grinspoon SK, Askari H, Landt ML, et al. Effects of fasting and glucose infusion on basal and overnight leptin concentrations in normal-weight women. *Am J Clin Nutr.* 1997;66: 1352–6.
20. Havel PJ, Townsend R, Chaump L, Teff K. High fat meals reduce 24 hour circulating leptin concentrations in women. *Diabetes.* 1999;48:334–41.
21. Gettys TW, Harkness PJ, Watson PM. The beta 3-adrenergic receptor inhibits insulin-stimulated leptin secretion from isolated rats adipocytes. *Endocrinology.* 1996;137:4054–7.
22. Leroy P, Dessolin S, Villageois P, et al. Expression of *ob* gene in adipose cells: regulation by insulin. *J Biol Chem.* 1996;271:2365–8.
23. Yoshida T, Hayashi M, Monkawa T, Saruta T. Regulation of obese mRNA expression by hormonal factors in primary cultures of rat adipocytes. *Eur J Endocrinol.* 1996;135: 619–25.
24. Wabitsch M, Jensen PB, Blum WF, et al. Insulin and cortisol promote leptin production in cultured human fat cells. *Diabetes.* 1996;45:1435–8.
25. Mizuno T, Bergen H, Kleopoulos S, Bauman WA, Mobbs CV. Effects of nutritional status and aging on leptin gene expression in mice: importance of glucose. *Horm Metab Res.* 1996;28:679–84.
26. Mizuno TM, Bergen H, Funabashi T, et al. Obese gene expression: reduction by fasting and stimulation by insulin and glucose in lean mice, and persistent elevation in acquired (diet-induced) and genetic (yellow agouti) obesity. *Proc Natl Acad Sci USA.* 1996;93:3434–8.
27. Havel PJ, Uriu-Hare JY, Stanhope KL, Stern JS, Keen CL, Ahren B. Marked and rapid decrease of circulating leptin in streptozotocin diabetic rats: reversal by insulin. *Am J Physiol.* 1998;274:R1482–R91.
28. Mueller WM, Gregoire FM, Stanhope KL, et al. Evidence that glucose metabolism regulates leptin secretion from isolated adipocytes. *Endocrinology.* 1998;139:551–8.

29. Cusi K, DeFronzo RA. Metformin: a review of its metabolic effects. *Diabetes Rev.* 1998;6:89–131.

30. Sekar N, Li J, Shechter Y. Vanadium salts as insulin substitutes: mechanisms of action, a scientific and therapeutic tool in diabetes mellitus research. *Crit Rev Biochem Mol Biol.* 1996;31:339–59.

31. McNeill JH, Yuen VG, Dai S, Orvig C. Increased potency of vanadium using organic ligands. *Mol Cell Biochem.* 1995;153:175–80.

32. Rodbell M. Metabolism of isolated fat cells. I. Effects of hormones on glucose metabolism and lipolysis. *J Biol Chem.* 1964;239:375–80.

33. Fantus IG, Brosseau R. Mechanism of action of metformin: insulin receptor and postreceptor effects in vitro and in vivo. *J Clin Endocrinol Metab.* 1986;63:898–905.

34. Klip A, Leiter LA. Cellular mechanism of action of metformin. *Diabetes Care.* 1990;13:696–704.

35. Molero JC, Martinez C, Andres A, Satrustegui J, Carrascosa JM. Vanadate fully stimulates insulin receptor substrate-1 associated phosphatidyl inositol 3-kinase activity in adipocytes from young and old rats. *FEBS Lett.* 1998;425:298–304.

36. Nakai M, Watanabe H, Fujiwara C, et al. Mechanism on insulin-like action of vanadyl sulfate: studies on interaction between rat adipocytes and vanadium compounds. *Biol Pharm Bull.* 1995;18:719–25.

37. Landt M, Gingerich RL, Havel PJ, et al. Radioimmunoassay of rat leptin: sexual dimorphism reversed from humans. *Clin Chem.* 1998;44:565–70.

38. Kallen CB, Lazar M. Antidiabetic thiazolidinediones inhibit leptin (*ob*) gene expression in 3T3–L1 adipocytes. *Proc Natl Acad Sci USA.* 1996;93:5793–6.

39. Nolan JJ, Olefsky JM, Nyce MR, Considine RV, Caro JF. Effect of troglitazone on leptin production in vitro and in human subjects. *Diabetes.* 1996;45:1276–8.

40. Scheen AJ. Clinical pharmacokinetics of metformin. *Clin Pharmacokinet.* 1996;30:359–71.

41. Shulman G. Cellular mechanisms of insulin resistance in humans. *Am J Cardiol.* 1999;84:3J–10J.

42. Inzucchi SE, Maggs DG, Spollett GR, et al. Efficacy and metabolic effects of metformin and troglitazone in type II diabetes mellitus. *N Engl J Med.* 1998;338:867–72.

43. Jackson RA, Hawa MI, Jaspan JB, et al. Mechanism of metformin action in non-insulin-dependent diabetes. *Diabetes.* 1987;36:632–40.

44. Pedersen O, Nielson OH, Bak J, et al. The effects of metformin on adipocyte insulin action and metabolic control in obese subjects with type 2 diabetes. *Diabetic Med.* 1989;6:249–56.

45. Fischer Y, Thomas J, Rosen P, Kammermeier H. Action of metformin on glucose transport and glucose transporter GLUT1 and GLUT4 in heart muscle cells from healthy and diabetic rats. *Endocrinology.* 1995;136:412–20.

46. Jacobs DB, Hayes GR, Truglia JA, Lockwood DH. Effects of metformin on insulin receptor tyrosine kinase activity in rat adipocytes. *Diabetologia.* 1986;29:798–801.

47. Di Paolo S. Metformin ameliorates extreme insulin resistance in a patient with anti-insulin receptor antibodies: description of insulin receptor and postreceptor effects in vivo and in vitro. *Acta Endocrinol.* 1992;126:117–23.

48. Kozka IJ, Holman GD. Metformin blocks downregulation of cell surface GLUT4 caused by chronic insulin treatment of rat adipocytes. *Diabetes.* 1993;42:1159–65.

49. Dunn CJ, Peters DH. Metformin: a review of its pharmacological properties and therapeutic use in non-insulin dependent diabetes mellitus. *Drugs.* 1995;49:721–49.

50. DiGirolamo M, Newby FD, Lovejoy J. Lactate production in adipose tissue: a regulated function with extra-adipose implications. *FASEB J.* 1992;6:2405–12.

51. Wang J, Liu R, Hawkins M, Barzilai N, Rossetti L. A nutrient-sensing pathway regulates leptin gene expression in muscle and fat. *Nature.* 1998;393:684–8.

52. Yuen VG, Orvig C, McNeill JH. Effects of bis(maltolato)oxovanadium(IV) are distinct from food restriction in STZ-diabetic rats. *Am J Physiol.* 1997;272:E30–E5.

53. Yuen VG, Orvig C, McNeill JH. Comparison of the glucose-lowering properties of vanadyl sulfate and bis(maltolato)oxovanadium(IV) following acute and chronic administration. *Can J Physiol Pharmacol.* 1995;73:55–64.

54. Cohen N, Halberstam M, Shlimovich P, Chang CJ, Shamoon H, Rossetti L. Oral vanadyl sulfate improves hepatic and peripheral insulin sensitivity in patients with non-insulin-dependent diabetes mellitus. *J Clin Invest.* 1995;95:2501–9.

55. Goldfine AB, Simonson DC, Folli F, Patti ME, Kahn CR. Metabolic effects of sodium metavanadate in humans with insulin-dependent and noninsulin-dependent diabetes mellitus in vivo and in vitro studies. *J Clin Endocrinol Metab.* 1995;80:3311–20.

56. Tsiani E, Fantus IG. Vanadium compounds: biological actions and potential as pharmacological agents. *Trends Endocrinol Metab.* 1997;8:51–8.

Genome-wide Study of Gene Copy Numbers, Transcripts, and Protein Levels in Pairs of Non-invasive and Invasive Human Transitional Cell Carcinomas*

Torben F. Ørntoft‡§, Thomas Thykjaer¶, Frederic M. Waldman||, Hans Wolf**, and Julio E. Celis‡‡

Gain and loss of chromosomal material is characteristic of bladder cancer, as well as malignant transformation in general. The consequences of these changes at both the transcription and translation levels is at present unknown partly because of technical limitations. Here we have attempted to address this question in pairs of non-invasive and invasive human bladder tumors using a combination of technology that included comparative genomic hybridization, high density oligonucleotide array-based monitoring of transcript levels (5600 genes), and high resolution two-dimensional gel electrophoresis. The results showed that there is a gene dosage effect that in some cases superimposes on other regulatory mechanisms. This effect depended ($p < 0.015$) on the magnitude of the comparative genomic hybridization change. In general (18 of 23 cases), chromosomal areas with more than 2-fold gain of DNA showed a corresponding increase in mRNA transcripts. Areas with loss of DNA, on the other hand, showed either reduced or unaltered transcript levels. Because most proteins resolved by two-dimensional gels are unknown it was only possible to compare mRNA and protein alterations in relatively few cases of well focused abundant proteins. With few exceptions we found a good correlation ($p < 0.005$) between transcript alterations and protein levels. The implications, as well as limitations, of the approach are discussed. *Molecular & Cellular Proteomics 1:37–45, 2002.*

Aneuploidy is a common feature of most human cancers (1), but little is known about the genome-wide effect of this

phenomenon at both the transcription and translation levels. High throughput array studies of the breast cancer cell line BT474 has suggested that there is a correlation between DNA copy numbers and gene expression in highly amplified areas (2), and studies of individual genes in solid tumors have revealed a good correlation between gene dose and mRNA or protein levels in the case of c-erb-B2, *cyclin d1*, *ems1*, and N-myc (3–5). However, a high cyclin D1 protein expression has been observed without simultaneous amplification (4), and a low level of c-myc copy number increase was observed without concomitant c-myc protein overexpression (6).

In human bladder tumors, karyotyping, fluorescent *in situ* hybridization, and comparative genomic hybridization (CGH)[1] have revealed chromosomal aberrations that seem to be characteristic of certain stages of disease progression. In the case of non-invasive pTa transitional cell carcinomas (TCCs), this includes loss of chromosome 9 or parts of it, as well as loss of Y in males. In minimally invasive pT1 TCCs, the following alterations have been reported: 2q–, 11p–, 1q+, 11q13+, 17q+, and 20q+ (7–12). It has been suggested that these regions harbor tumor suppressor genes and oncogenes; however, the large chromosomal areas involved often contain many genes, making meaningful predictions of the functional consequences of losses and gains very difficult.

In this investigation we have combined genome-wide technology for detecting genomic gains and losses (CGH) with gene expression profiling techniques (microarrays and proteomics) to determine the effect of gene copy number on transcript and protein levels in pairs of non-invasive and invasive human bladder TCCs.

EXPERIMENTAL PROCEDURES

Material—Bladder tumor biopsies were sampled after informed consent was obtained and after removal of tissue for routine pathology examination. By light microscopy tumors 335 and 532 were staged by an experienced pathologist as pTa (superficial papillary),
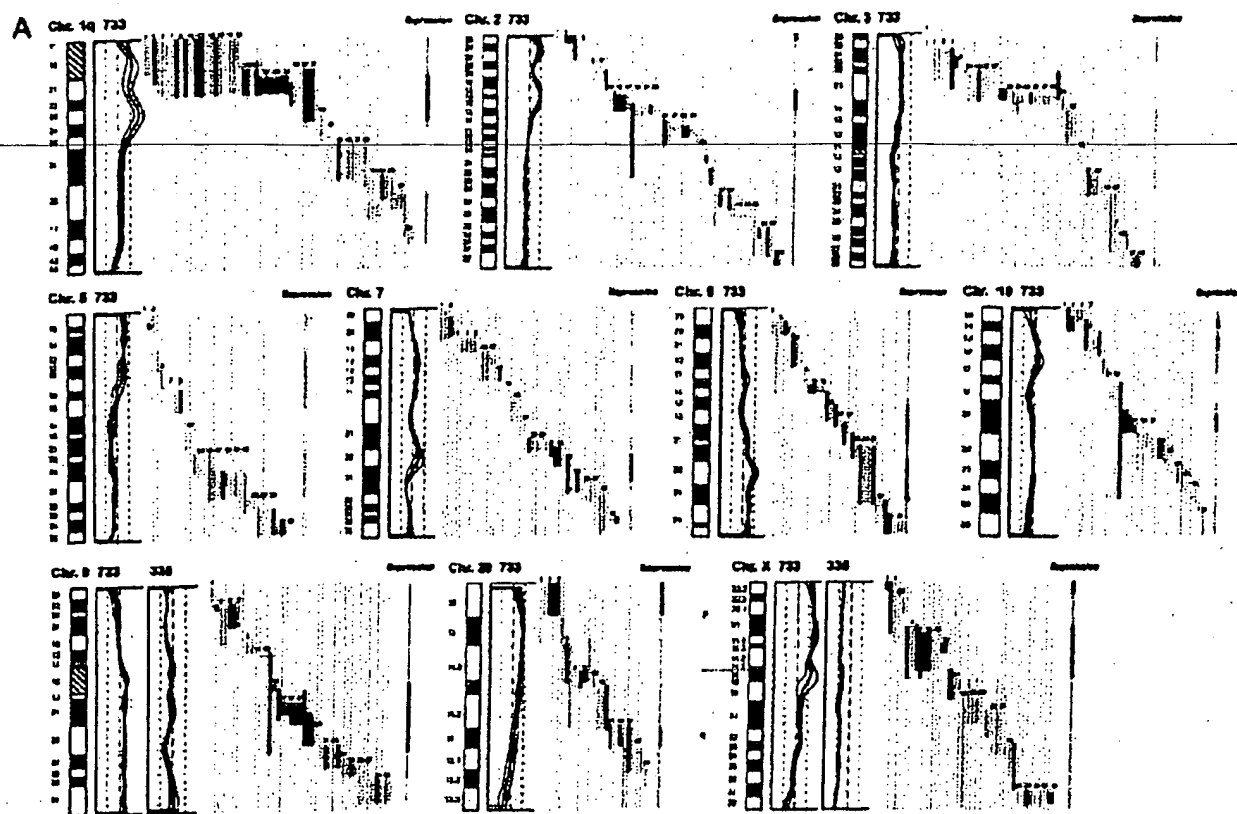
FIG. 1. DNA copy number and mRNA expression level. Shown from *left* to *right* are chromosome (*Chr.*), CGH profiles, gene location and expression level of specific genes, and overall expression level along the chromosome. *A*, expression of mRNA in invasive tumor 733 as compared with the non-invasive counterpart tumor 335. *B*, expression of mRNA in invasive tumor 827 compared with the non-invasive counterpart tumor 532. The average fluorescent signal ratio between tumor DNA and normal DNA is shown along the length of the chromosome (*left*). The *bold curve* in the ratio profile represents a mean of four chromosomes and is surrounded by *thin curves* indicating one standard deviation. The *central vertical line (broken)* indicates a ratio value of 1 (no change), and the *vertical lines* next to it (*dotted*) indicate a ratio of 0.5 (*left*) and 2.0 (*right*). In chromosomes where the non-invasive tumor 335 used for comparison showed alterations in DNA content, the ratio profile of that chromosome is shown to the *right* of the invasive tumor profile. The *colored bars* represents one gene each, identified by the running *numbers* above the *bars* (the name of the gene can be seen at www.MDL.DK/sdata.html). The *bars* indicate the purported location of the gene, and the *colors* indicate the expression level of the gene in the invasive tumor compared with the non-invasive counterpart; >2-fold increase (*black*), >2-fold decrease (*blue*), no significant change (*orange*). The *bar* to the *far right*, entitled *Expression* shows the resulting change in expression along the chromosome; the *colors* indicate that at least half of the genes were up-regulated (*black*), at least half of the genes down-regulated (*blue*), or more than half of the genes are unchanged (*orange*). If a gene was absent in one of the samples and present in another, it was regarded as more than a 2-fold change. A 2-fold level was chosen as this corresponded to one standard deviation in a double determination of ~1800 genes. Centromeres and heterochromatic regions were excluded from data analysis.

grade I and II, respectively, tumors 733 and 827 were staged as pT1 (invasive into submucosa), 733 was staged as solid, and 827 was staged as papillary, both grade III.

mRNA Preparation—Tissue biopsies, obtained fresh from surgery, were embedded immediately in a sodium-guanidinium thiocyanate solution and stored at −80 °C. Total RNA was isolated using the RNAzol B RNA isolation method (WAK-Chemie Medical GMBH). poly(A)⁺ RNA was isolated by an oligo(dT) selection step (Oligotex mRNA kit; Qiagen).

cRNA Preparation—1 µg of mRNA was used as starting material. The first and second strand cDNA synthesis was performed using the SuperScript® choice system (Invitrogen) according to the manufacturer's instructions but using an oligo(dT) primer containing a T7 RNA polymerase binding site. Labeled cRNA was prepared using the ME-GAscrip® in vitro transcription kit (Ambion). Biotin-labeled CTP and

UTP (Enzo) was used, together with unlabeled NTPs in the reaction. Following the in vitro transcription reaction, the unincorporated nucleotides were removed using RNeasy columns (Qiagen).

Array Hybridization and Scanning—Array hybridization and scanning was modified from a previous method (13). 10 µg of cRNA was fragmented at 94 °C for 35 min in buffer containing 40 mM Tris acetate, pH 8.1, 100 mM KOAc, 30 mM MgOAc. Prior to hybridization, the fragmented cRNA in a 6× SSPE-T hybridization buffer (1 M NaCl, 10 mM Tris, pH 7.6, 0.005% Triton), was heated to 95 °C for 5 min, subsequently cooled to 40 °C, and loaded onto the Affymetrix probe array cartridge. The probe array was then incubated for 16 h at 40 °C at constant rotation (60 rpm). The probe array was exposed to 10 washes in 6× SSPE-T at 25 °C followed by 4 washes in 0.5× SSPE-T at 50 °C. The biotinylated cRNA was stained with a streptavidin-phycoerythrin conjugate, 10 µg/ml (Molecular Probes) in 6× SSPE-T
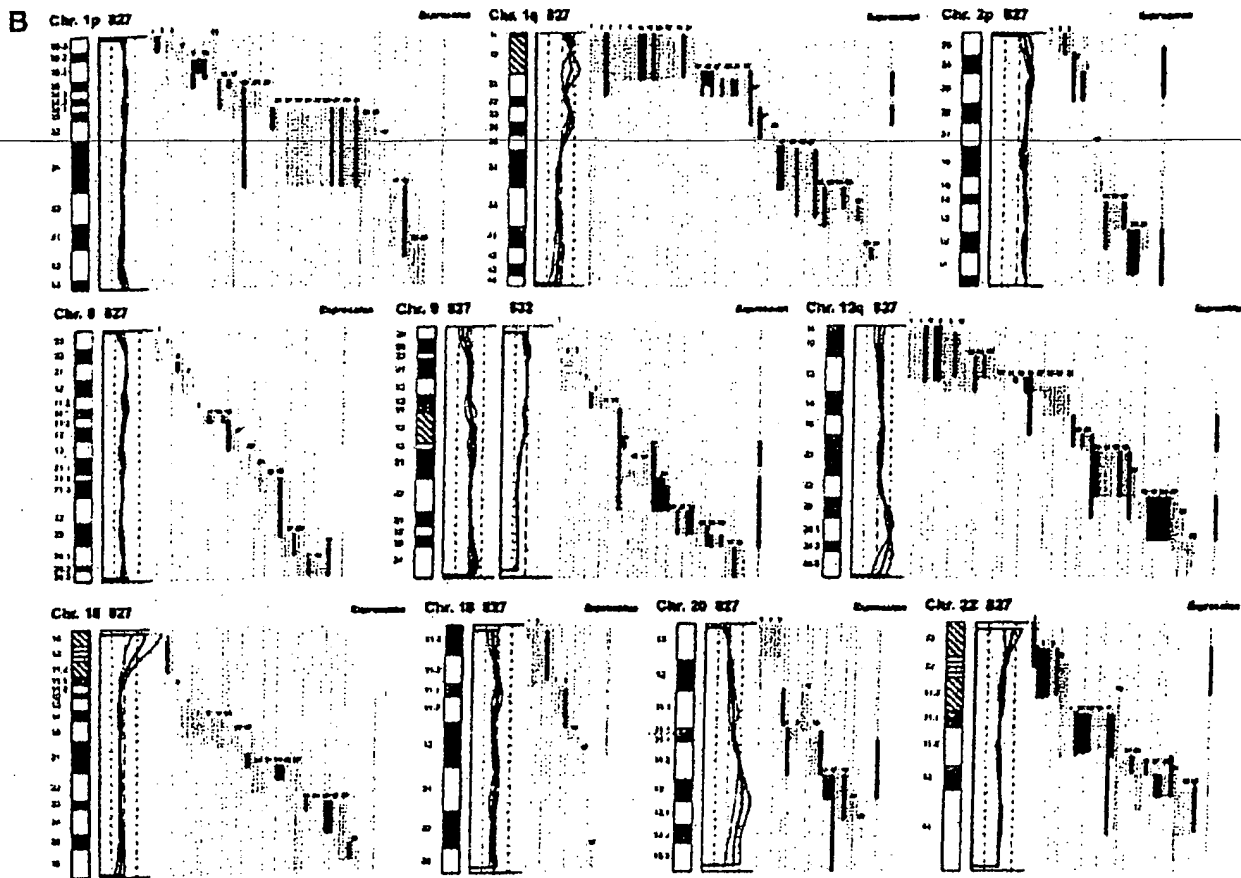
FIG. 1—continued

for 30 min at 25 °C followed by 10 washes in 6× SSPE-T at 25 °C. The probe arrays were scanned at 560 nm using a confocal laser scanning microscope (made for Affymetrix by Hewlett-Packard). The readings from the quantitative scanning were analyzed by Affymetrix gene expression analysis software.

Microsatellite Analysis—Microsatellite Analysis was performed as described previously (14). Microsatellites were selected by use of www.ncbi.nlm.nih.gov/genemap98, and primer sequences were obtained from the genome data base at www.gdb.org. DNA was extracted from tumor and blood and amplified by PCR in a volume of 20 µl for 35 cycles. The amplicons were denatured and electrophoresed for 3 h in an ABI Prism 377. Data were collected in the Gene Scan program for fragment analysis. Loss of heterozygosity was defined as less than 33% of one allele detected in tumor amplicons compared with blood.

Proteomic Analysis—TCCs were minced into small pieces and homogenized in a small glass homogenizer in 0.5 ml of lysis solution. Samples were stored at −20 °C until use. The procedure for 2D gel electrophoresis has been described in detail elsewhere (15, 16). Gels were stained with silver nitrate and/or Coomassie Brilliant Blue. Proteins were identified by a combination of procedures that included microsequencing, mass spectrometry, two-dimensional gel Western immunoblotting, and comparison with the master two-dimensional gel image of human keratinocyte proteins; see biobase.dk/cgi-bin/cells.

CGH—Hybridization of differentially labeled tumor and normal DNA to normal metaphase chromosomes was performed as described previously (10). Fluorescein-labeled tumor DNA (200 ng), Texas Red-

labeled reference DNA (200 ng), and human Cot-1 DNA (20 µg) were denatured at 37 °C for 5 min and applied to denatured normal metaphase slides. Hybridization was at 37 °C for 2 days. After washing, the slides were counterstained with 0.15 µg/ml 4,6-diamidino-2-phenylindole in an anti-fade solution. A second hybridization was performed for all tumor samples using fluorescein-labeled reference DNA and Texas Red-labeled tumor DNA (inverse labeling) to confirm the aberrations detected during the initial hybridization. Each CGH experiment also included a normal control hybridization using fluorescein- and Texas Red-labeled normal DNA. Digital image analysis was used to identify chromosomal regions with abnormal fluorescence ratios, indicating regions of DNA gains and losses. The average green:red fluorescence intensity ratio profiles were calculated using four images of each chromosome (eight chromosomes total) with normalization of the green:red fluorescence intensity ratio for the entire metaphase and background correction. Chromosome identification was performed based on 4,6-diamidino-2-phenylindole banding patterns. Only images showing uniform high intensity fluorescence with minimal background staining were analyzed. All centromeres, p arms of acrocentric chromosomes, and heterochromatic regions were excluded from the analysis.

RESULTS

Comparative Genomic Hybridization—The CGH analysis identified a number of chromosomal gains and losses in the

TABLE I

Correlation between alterations detected by CGH and by expression monitoring

Top, CGH used as independent variable (if CGH alteration — what expression ratio was found); bottom, altered expression used as independent variable (if expression alteration — what CGH deviation was found).

CGH alterations	Tumor 733 vs. 335 Expression change clusters	Concordance	CGH alterations	Tumor 827 vs. 532 Expression change clusters	Concordance
13 Gain	10 Up-regulation 0 Down-regulation 3 No change	77%	10 Gain	8 Up-regulation 0 Down-regulation 2 No change	80%
10 Loss	1 Up-regulation 5 Down-regulation 4 No change	50%	12 Loss	3 Up-regulation 2 Down regulation 7 No change	17%

Expression change clusters	Tumor 733 vs. 335 CGH alterations	Concordance	Expression change clusters	Tumor 827 vs. 532 CGH alterations	Concordance
16 Up-regulation	11 Gain 2 Loss 3 No change	69%	17 Up-regulation	10 Gain 5 Loss 2 No change	59%
21 Down-regulation	1 Gain 8 Loss 12 No change	38%	9 Down-regulation	0 Gain 3 Loss 6 No change	33%
15 No change	3 Gain 3 Loss 9 No change	60%	21 No change	1 Gain 3 Loss 17 No change	81%

two invasive tumors (stage pT1, TCCs 733 and 827), whereas the two non-invasive papillomas (stage pTa, TCCs 335 and 532) showed only 9p−, 9q22-q33−, and X−, and 7+, 9q−, and Y−, respectively. Both invasive tumors showed changes (1q22-24+, 2q14.1-qter−, 3q12-q13.3−, 6q12-q22−, 9q34+, 11q12-q13+, 17+, and 20q11.2-q12+) that are typical for their disease stage, as well as additional alterations, some of which are shown in Fig. 1. Areas with gains and losses deviated from the normal copy number to some extent, and the average numerical deviation from normal was 0.4-fold in the case of TCC 733 and 0.3-fold for TCC 827. The largest changes, amounting to at least a doubling of chromosomal content, were observed at 1q23 in TCC 733 (Fig. 1A) and 20q12 in TCC 827 (Fig. 1B).

mRNA Expression in Relation to DNA Copy Number—The mRNA levels from the two invasive tumors (TCCs 827 and 733) were compared with the two non-invasive counterparts (TCCs 532 and 335). This was done in two separate experiments in which we compared TCCs 733 to 335 and 827 to 532, respectively, using two different scaling settings for the arrays to rule out scaling as a confounding parameter. Approximately 1,800 genes that yielded a signal on the arrays were searched in the Unigene and Genemap data bases for chromosomal location, and those with a known location (1096) were plotted as bars covering their purported locus. In that way it was possible to construct a graphic presentation of DNA copy number and relative mRNA levels along the individual chromosomes (Fig. 1).

For each mRNA a ratio was calculated between the level in the invasive *versus* the non-invasive counterpart. Bars, which represent chromosomal location of a gene, were color-coded according to the expression ratio, and only differences larger

than 2-fold were regarded as informative (Fig. 1). The density of genes along the chromosomes varied, and areas containing only one gene were excluded from the calculations. The resolution of the CGH method is very low, and some of the outlier data may be because of the fact that the boundaries of the chromosomal aberrations are not known at high resolution.

Two sets of calculations were made from the data. For the first set we used CGH alterations as the independent variable and estimated the frequency of expression alterations in these chromosomal areas. In general, areas with a strong gain of chromosomal material contained a cluster of genes having increased mRNA expression. For example, both chromosomes 1q21-q25, 2p and 9q, showed a relative gain of more than 100% in DNA copy number that was accompanied by increased mRNA expression levels in the two tumor pairs (Fig. 1). In most cases, chromosomal gains detected by CGH were accompanied by an increased level of transcripts in both TCCs 733 (77%) and 827 (80%) (Table I, top). Chromosomal losses, on the other hand, were not accompanied by decreased expression in several cases, and were often registered as having unaltered RNA levels (Table I, top). The inability to detect RNA expression changes in these cases was not because of fewer genes mapping to the lost regions (data not shown).

In the second set of calculations we selected expression alterations above 2-fold as the independent variable and estimated the frequency of CGH alterations in these areas. As above, we found that increased transcript expression correlated with gain of chromosomal material (TCC 733, 69% and TCC 827, 59%), whereas reduced expression was often detected in areas with unaltered CGH ratios (Table I, bottom). Furthermore, as a control we looked at areas with no alter-

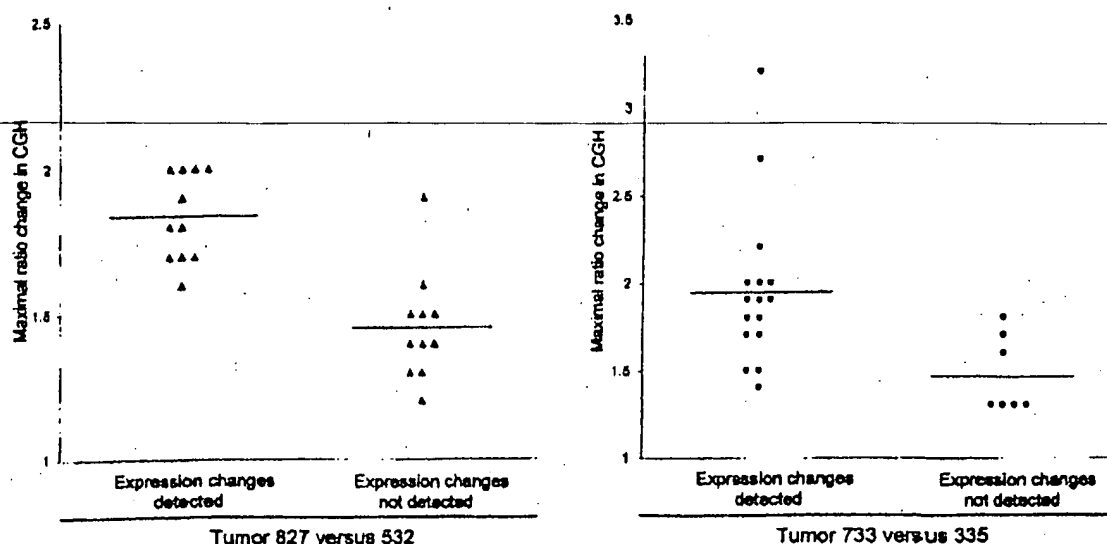Tumor 827 versus 532   Tumor 733 versus 335

FIG. 2. Correlation between maximum CGH aberration and the ability to detect expression change by oligonucleotide array monitoring. The aberration is shown as a numerical -fold change in ratio between invasive tumors 827 (▲) and 733 (♦) and their non-invasive counterparts 532 and 335. The expression change was taken from the *Expression* line to the *right* in Fig. 1, which depicts the resulting expression change for a given chromosomal region. At least half of the mRNAs from a given region have to be either up- or down-regulated to be scored as an expression change. All chromosomal arms in which the CGH ratio plus or minus one standard deviation was outside the ratio value of one were included.

ation in expression. No alteration was detected by CGH in most of these areas (TCC 733, 60% and TCC 827, 81%; see Table I, *bottom*). Because the ability to observe reduced or increased mRNA expression clustering to a certain chromosomal area clearly reflected the extent of copy number changes, we plotted the maximum CGH aberrations in the regions showing CGH changes against the ability to detect a change in mRNA expression as monitored by the oligonucleotide arrays (Fig. 2). For both tumors TCC 733 ($p < 0.015$) and TCC 827 ($p < 0.00003$) a highly significant correlation was observed between the level of CGH ratio change (reflecting the DNA copy number) and alterations detected by the array based technology (Fig. 2). Similar data were obtained when areas with altered expression were used as independent variables. These areas correlated best with CGH when the CGH ratio deviated 1.6- to 2.0-fold (Table I, *bottom*) but mostly did not at lower CGH deviations. These data probably reflect that loss of an allele may only lead to a 50% reduction in expression level, which is at the cut-off point for detection of expression alterations. Gain of chromosomal material can occur to a much larger extent.

Microsatellite-based Detection of Minor Areas of Losses—In TCC 733, several chromosomal areas exhibiting DNA amplification were preceded or followed by areas with a normal CGH but reduced mRNA expression (see Fig. 1, TCC 733 chromosome 1q32, 2p21, and 7q21 and q32, 9q34, and 10q22). To determine whether these results were because of undetected loss of chromosomal material in these regions or because of other non-structural mechanisms regulating transcription, we examined two microsatellites positioned at chromosome 1q25–32 and two at chromosome 2p22. Loss of heterozygosity (LOH) was found at both 1q25 and at 2p22 indicating that minor deleted areas were not detected with the resolution of CGH (Fig. 3). Additionally, chromosome 2p in TCC 733 showed a CGH pattern of gain/no change/gain of DNA that correlated with transcript increase/decrease/increase. Thus, for the areas showing increased expression there was a correlation with the DNA copy number alterations (Fig. 1A). As indicated above, the mRNA decrease observed in the middle of the chromosomal gain was because of LOH, implying that one of the mechanisms for mRNA down-regulation may be regions that have undergone smaller losses of chromosomal material. However, this cannot be detected with the resolution of the CGH method.

In both TCC 733 and TCC 827, the telomeric end of chromosome 11p showed a normal ratio in the CGH analysis; however, clusters of five and three genes, respectively, lost their expression. Two microsatellites (D11S1760, D11S922) positioned close to MUC2, IGF2, and cathepsin D indicated LOH as the most likely mechanism behind the loss of expression (data not shown).

A reduced expression of mRNA observed in TCC 733 at chromosomes 3q24, 11p11, 12p12.2, 12q21.1, and 16q24 and in TCC 827 at chromosome 11p15.5, 12p11, 15q11.2, and 18q12 was also examined for chromosomal losses using microsatellites positioned as close as possible to the gene loci
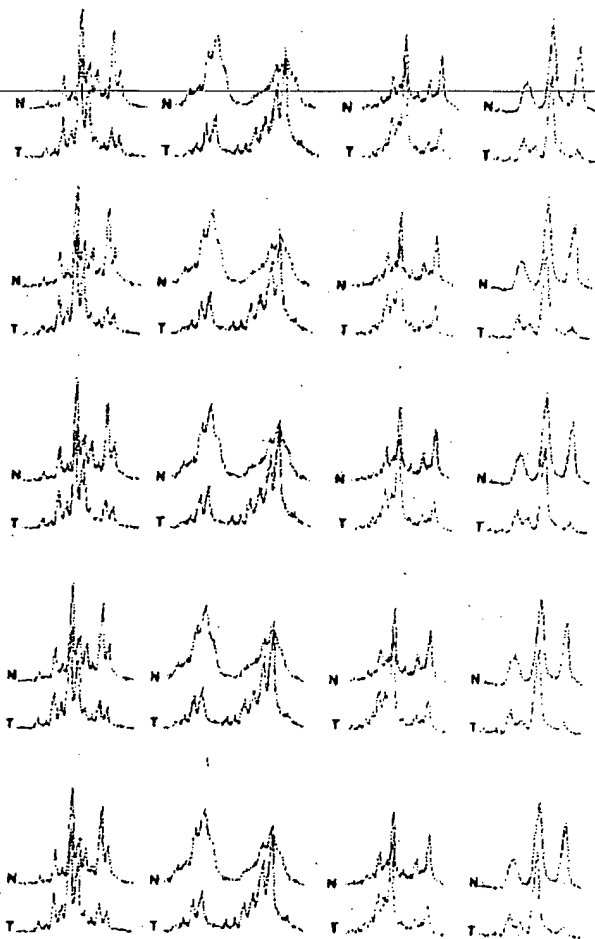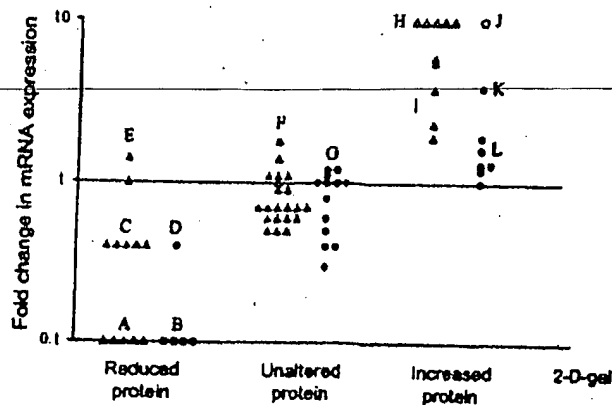
FIG. 4. Correlation between protein levels as judged by 2D-PAGE and transcript ratio. For comparison proteins were divided in three groups, unaltered in level or up- or down-regulated (horizontal axis). The mRNA ratio as determined by oligonucleotide arrays was plotted for each gene (vertical axis). ▲, mRNAs that were scored as present in both tumors used for the ratio calculation; △, mRNAs that were scored as absent in the invasive tumors (along horizontal axis) or as absent in non-invasive reference (top of figure). Two different scalings were used to exclude scaling as a confounder, TCCs 827 and 532 (▲△) were scaled with background suppression, and TCCs 733 and 335 (●○) were scaled without suppression. Both comparisons showed highly significant ($p < 0.005$) differences in mRNA ratios between the groups. Proteins shown were as follows: Group A (from left), phosphoglucomutase 1, glutathione transferase class μ number 4, fatty acid-binding protein homologue, cytokeratin 15, and cytokeratin 13; B (from left), fatty acid-binding protein homologue, 28-kDa heat shock protein, cytokeratin 13, and calcyclin; C (from left), α-enolase, hnRNP B1, 28-kDa heat shock protein, 14-3-3-ε, and pre-mRNA splicing factor; D, mesothelial keratin K7 (type II); E (from top), glutathione S-transferase-π and mesothelial keratin K7 (type II); F (from top and left), adenylyl cyclase-associated protein, E-cadherin, keratin 19, calgizzarin, phosphoglycerate mutase, annexin IV, cytoskeletal γ-actin, hnRNP A1, integral membrane protein calnexin (IP90), hnRNP H, brain-type clathrin light chain-a, hnRNP F, 70-kDa heat shock protein, heterogeneous nuclear ribonucleoprotein A/B, translationally controlled tumor protein, liver glyceraldehyde-3-phosphate dehydrogenase, keratin 8, aldehyde reductase, and Na,K-ATPase β-1 subunit; G, (from top and left), TCP20, calgizzarin, 70-kDa heat shock protein, calnexin, hnRNP H, cytokeratin 15, ATP synthase, keratin 19, triosephosphate isomerase, hnRNP F, liver glyceraldehyde-3-phosphatase dehydrogenase, glutathione S-transferase-π, and keratin 8; H (from left), plasma gelsolin, autoantigen calreticulin, thioredoxin, and NAD+-dependent 15 hydroxyprostaglandin dehydrogenase; I (from top), prolyl 4-hydroxylase β-subunit, cytokeratin 20, cytokeratin 17, prohibition, and fructose 1,6-biphosphatase; J annexin II; K, annexin IV; L (from top and left), 90-kDa heat shock protein, prolyl 4-hydroxylase β-subunit, α-enolase, GRP 78, cyclophilin, and cofilin.

FIG. 3. Microsatellite analysis of loss of heterozygosity. Tumor 733 showing loss of heterozygosity at chromosome 1q25, detected (a) by D1S215 close to Hu class I histocompatibility antigen (gene number 38 in Fig. 1), (b) by D1S2735 close to cathepsin E (gene number 41 in Fig. 1), and (c) at chromosome 2p23 by D2S2251 close to general β-spectrin (gene number 11 on Fig. 1) and of (d) tumor 827 showing loss of heterozygosity at chromosome 18q12 by S18S1118 close to mitochondrial 3-oxoacyl-coenzyme A thiolase (gene number 12 in Fig. 1). The upper curves show the electropherogram obtained from normal DNA from leukocytes (N), and the lower curves show the electropherogram from tumor DNA (T). In all cases one allele is partially lost in the tumor amplicon.

showing reduced mRNA transcripts. Only the microsatellite positioned at 18q12 showed LOH (Fig. 3), suggesting that transcriptional down-regulation of genes in the other regions may be controlled by other mechanisms.

Relation between Changes in mRNA and Protein Levels—2D-PAGE analysis, in combination with Coomassie Brilliant Blue and/or silver staining, was carried out on all four tumors using fresh biopsy material. 40 well resolved abundant known proteins migrating in areas away from the edges of the pH

gradient, and having a known chromosomal location, were selected for analysis in the TCC pair 827/532. Proteins were identified by a combination of methods (see "Experimental Procedures"). In general there was a highly significant correlation ($p < 0.005$) between mRNA and protein alterations (Fig. 4). Only one gene showed disagreement between transcript alteration and protein alteration. Except for a group of cyto-
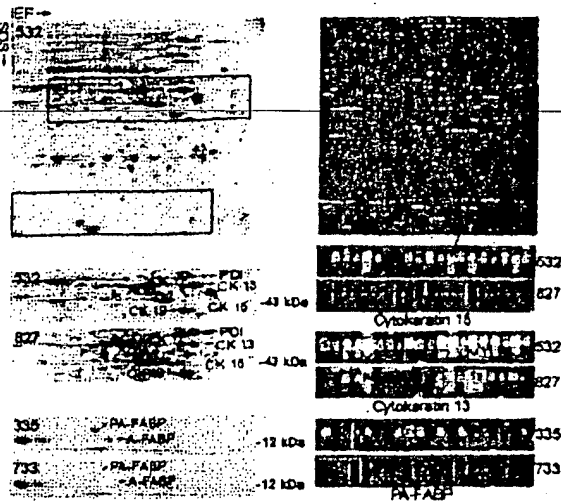
FIG. 5. Comparison of protein and transcript levels in invasive and non-invasive TCCs. The *upper part* of the figure shows a 2D gel (*left*) and the oligonucleotide array (*right*) of TCC 532. The *red rectangles* on the *upper gel* highlight the areas that are compared below. Identical areas of 2D gels of TCCs 532 and 827 are shown below. Clearly, cytokeratins 13 and 15 are strongly down-regulated in TCC 827 (*red annotation*). The tile on the array containing probes for cytokeratin 15 is enlarged *below* the array (*red arrow*) from TCC 532 and is compared with TCC 827. The *upper row* of *squares* in each tile corresponds to perfect match probes; the *lower row* corresponds to mismatch probes containing a mutation (used for correction for unspecific binding). Absence of signal is depicted as *black*, and the higher the signal the lighter the color. A high transcript level was detected in TCC 532 (6151 units) whereas a much lower level was detected in TCC 827 (absence of signals). For cytokeratin 13, a high transcript level was also present in TCC 532 (15659 units), and a much lower level was present in TCC 827 (623 units). The 2D gels at the *bottom* of the figure (*left*) show levels of PA-FABP and adipocyte-FABP in TCCs 335 and 733 (invasive), respectively. Both proteins are down-regulated in the invasive tumor. To the *right* we show the array tiles for the PA-FABP transcript. A medium transcript level was detected in the case of TCC 335 (1277 units) whereas very low levels were detected in TCC 733 (166 units). *IEF*, isoelectric focusing.

keratins encoded by genes on chromosome 17 (Fig. 5) the analyzed proteins did not belong to a particular family. 26 well focused proteins whose genes had a know chromosomal location were detected in TCCs 733 and 335, and of these 19 correlated ($p < 0.005$) with the mRNA changes detected using the arrays (Fig. 4). For example, PA-FABP was highly expressed in the non-invasive TCC 335 but lost in the invasive counterpart (TCC 733; see Fig. 5). The smaller number of proteins detected in both 733 and 335 was because of the smaller size of the biopsies that were available.

11 chromosomal regions where CGH showed aberrations that corresponded to the changes in transcript levels also showed corresponding changes in the protein level (Table II). These regions included genes that encode proteins that are found to be frequently altered in bladder cancer, namely cytokeratins 17 and 20, annexins II and IV, and the fatty acid-binding proteins PA-FABP and FBP1. Four of these proteins were encoded by genes in chromosome 17q, a frequently amplified chromosomal area in invasive bladder cancers.

DISCUSSION

Most human cancers have abnormal DNA content, having lost some chromosomal parts and gained others. The present study provides some evidence as to the effect of these gains and losses on gene expression in two pairs of non-invasive and invasive TCCs using high throughput expression arrays and proteomics, in combination with CGH. In general, the results showed that there is a clear individual regulation of the mRNA expression of single genes, which in some cases was superimposed by a DNA copy number effect. In most cases, genes located in chromosomal areas with gains often exhibited increased mRNA expression, whereas areas showing losses showed either no change or a reduced mRNA expression. The latter might be because of the fact that losses most often are restricted to loss of one allele, and the cut-off point for detection of expression alterations was a 2-fold change, thus being at the border of detection. In several cases, how-

TABLE II
Proteins whose expression level correlates with both mRNA and gene dose changes

Protein	Chromosomal location	Tumor TCC	CGH alteration	Transcript alteration[a]	Protein alteration
Annexin II	1q21	733	Gain	Abs to Pres[b]	Increase
Annexin IV	2p13	733	Gain	3.9-Fold up	Increase
Cytokeratin 17	17q12-q21	827	Gain	3.8-Fold up	Increase
Cytokeratin 20	17q21.1	827	Gain	5.6-Fold up	Increase
(PA-)FABP	8q21.2	827	Loss	10-Fold down	Decrease
FBP1	9q22	827	Gain	2.3-Fold up	Increase
Plasma gelsolin	9q31	827	Gain	Abs to Pres	Increase
Heat shock protein 28	15q12-q13	827	Loss	2.5-Fold up	Decrease
Prohibitin	17q21	827/733	Gain	3.7-/2.5-Fold up[b]	Increase
Prolyl-4-hydroxyl	17q25	827/733	Gain	5.7-/1.6-Fold up	Increase
hnRNPB1	7p15	827	Loss	2.5-Fold down	Decrease

[a] Abs, absent; Pres, present.
[b] In cases where the corresponding alterations were found in both TCCs 827 and 733 these are shown as 827/733.

ever, an increase or decrease in DNA copy number was associated with de novo occurrence or complete loss of transcript, respectively. Some of these transcripts could not be detected in the non-invasive tumor but were present at relatively high levels in areas with DNA amplifications in the invasive tumors (e.g. in TCC 733 transcript from cellular ligand of annexin II gene (chromosome 1q21) from absent to 2670 arbitrary units; in TCC 827 transcript from small proline-rich protein 1 gene (chromosome 1q12-q21.1) from absent to 1326 arbitrary units). It may be anticipated from these data that significant clustering of genes with an increased expression to a certain chromosomal area indicates an increased likelihood of gain of chromosomal material in this area.

Considering the many possible regulatory mechanisms acting at the level of transcription, it seems striking that the gene dose effects were so clearly detectable in gained areas. One hypothetical explanation may lie in the loss of controlled methylation in tumor cells (17-19). Thus, it may be possible that in chromosomes with increased DNA copy numbers two or more alleles could be demethylated simultaneously leading to a higher transcription level, whereas in chromosomes with losses the remaining allele could be partly methylated, turning off the process (20, 21). A recent report has documented a ploidy regulation of gene expression in yeast, but in this case all the genes were present in the same ratio (22), a situation that is not analogous to that of cancer cells, which show marked chromosomal aberrations, as well as gene dosage effects.

Several CGH studies of bladder cancer have shown that some chromosomal aberrations are common at certain stages of disease progression, often occurring in more than 1 of 3 tumors. In pTa tumors, these include 9p−, 9q−, 1q+, Y− (2, 6), and in pT1 tumors, 2q−, 11p−, 11q−, 1q+, 5p+, 8q+, 17q+, and 20q+ (2-4, 6, 7). The pTa tumors studied here showed similar aberrations such as 9p− and 9q22-q33− and 9q− and Y−, respectively. Likewise, the two minimal invasive pT1 tumors showed aberrations that are commonly seen at that stage, and TCC 827 had a remarkable resemblance to the commonly seen pattern of losses and gains, such as 1q22-24 amplification (seen in both tumors), 11q14-q22 loss, the latter often linked to 17 q+ (both tumors), and 1q+ and 9p−, often linked to 20q+ and 11 q13+ (both tumors) (7-9). These observations indicate that the pairs of tumors used in this study exhibit chromosomal changes observed in many tumors, and therefore the findings could be of general importance for bladder cancer.

Considering that the mapping resolution of CGH is of about 20 megabases it is only possible to get a crude picture of chromosomal instability using this technique. Occasionally, we observed reduced transcript levels close to or inside regions with increased copy numbers. Analysis of these regions by positioning heterozygous microsatellites as close as possible to the locus showing reduced gene expression revealed loss of heterozygosity in several cases. It seems likely that multiple and different events occur along each chromosomal arm and that the use of cDNA microarrays for analysis of DNA copy number changes will reach a resolution that can resolve these changes, as has recently been proposed (2). The outlier data were not more frequent at the boundaries of the CGH aberrations. At present we do not know the mechanism behind chromosomal aneuploidy and cannot predict whether chromosomal gains will be transcribed to a larger extent than the two native alleles. A mechanism as genetic imprinting has an impact on the expression level in normal cells and is often reduced in tumors. However, the relation between imprinting and gain of chromosomal material is not known.

We regard it as a strength of this investigation that we were able to compare invasive tumors to benign tumors rather than to normal urothelium, as the tumors studied were biologically very close and probably may represent successive steps in the progression of bladder cancer. Despite the limited amount of fresh tissue available it was possible to apply three different state of the art methods. The observed correlation between DNA copy number and mRNA expression is remarkable when one considers that different pieces of the tumor biopsies were used for the different sets of experiments. This indicate that bladder tumors are relatively homogenous, a notion recently supported by CGH and LOH data that showed a remarkable similarity even between tumors and distant metastasis (10, 23).

In the few cases analyzed, mRNA and protein levels showed a striking correspondence although in some cases we found discrepancies that may be attributed to translational regulation, post-translational processing, protein degradation, or a combination of these. Some transcripts belong to undertranslated mRNA pools, which are associated with few translationally inactive ribosomes; these pools, however, seem to be rare (24). Protein degradation, for example, may be very important in the case of polypeptides with a short half-life (e.g. signaling proteins). A poor correlation between mRNA and protein levels was found in liver cells as determined by arrays and 2D-PAGE (25), and a moderate correlation was recently reported by Ideker et al. (26) in yeast.

Interestingly, our study revealed a much better correlation between gained chromosomal areas and increased mRNA levels than between loss of chromosomal areas and reduced mRNA levels. In general, the level of CGH change determined the ability to detect a change in transcript. One possible explanation could be that by losing one allele the change in mRNA level is not so dramatic as compared with gain of material, which can be rather unlimited and may lead to a severalfold increase in gene copy number resulting in a much higher impact on transcript level. The latter would be much easier to detect on the expression arrays as the cut-off point was placed at a 2-fold level so as not to be biased by noise on the array. Construction of arrays with a better signal to noise ratio may in the future allow detection of lesser than 2-fold alterations in transcript levels, a feature that may facilitate the analysis of the effect of loss of chromosomal areas on transcript levels.

In eleven cases we found a significant correlation between DNA copy number, mRNA expression, and protein level. Four of these proteins were encoded by genes located at a frequently amplified area in chromosome 17q. Whether DNA copy number is one of the mechanisms behind alteration of these eleven proteins is at present unknown and will have to be proved by other methods using a larger number of samples. One factor making such studies complicated is the large extent of protein modification that occurs after translation, requiring immunoidentification and/or mass spectrometry to correctly identify the proteins in the gels.

In conclusion, the results presented in this study exemplify the large body of knowledge that may be possible to gather in the future by combining state of the art techniques that follow the pathway from DNA to protein (26). Here, we used a traditional chromosomal CGH method, but in the future high resolution CGH based on microarrays with many thousand radiation hybrid-mapped genes will increase the resolution and information derived from these types of experiments (2). Combined with expression arrays analyzing transcripts derived from genes with known locations, and 2D gel analysis to obtain information at the post-translational level, a clearer and more developed understanding of the tumor genome will be forthcoming.

REFERENCES

1. Lengauer, C., Kinzler, K. W., and Vogelstein, B. (1998) Genetic instabilities in human cancers. *Nature* 17, 643–649

2. Pollack, J. R., Perou, C. M., Alizadeh, A. A., Eisen, M. B., Pergamenschikov, A., Williams, C. F., Jeffrey, S. S., Botstein, D., and Brown, P. O. (1999) Genome-wide analysis of DNA copy-number changes using cDNA microarrays. *Nat. Genet.* 23, 41–46

3. de Cremoux, P., Martin, E. C., Vincent-Salomon, A., Dieras, V., Barbaroux, C., Liva, S., Pouillart, P., Sastre-Garau, X., and Magdelenat, H. (1999) Quantitative PCR analysis of c-erb B-2 (HER2/neu) gene amplification and comparison with p185(HER2/neu) protein expression in breast cancer drill biopsies. *Int. J. Cancer* 83, 157–161

4. Brungier, P. P., Tamimi, Y., Shuuring, E., and Schalken, J. (1996) Expression of cyclin D1 and EMS1 in bladder tumors; relationship with chromosome 11q13 amplifications. *Oncogene* 12, 1747–1753

5. Slavc, I., Ellenbogen, R., Jung, W. H., Vawter, G. F., Kretschmar, C., Grier, H., and Korf, B. R. (1990) myc gene amplification and expression in primary human neuroblastoma. *Cancer Res.* 50, 1459–1463

6. Sauter, G., Carroll, P., Moch, H., Kallioniemi, A., Kerschmann, R., Narayan,

P., Mihatsch, M. J., and Waldman, F. M. (1995) c-myc copy number gains in bladder cancer detected by fluorescence *in situ* hybridization. *Am. J. Pathol.* 146, 1131–1139

7. Richter, J., Jiang, F., Gorog, J. P., Sartorious, G., Egenter, C., Gasser, T. C., Moch, H., Mihatsch, M. J., and Sauter, G. (1997) Marked genetic differences between stage pTa and stage pT1 papillary bladder cancer detected by comparative genomic hybridization. *Cancer Res.* 57, 2860–2864

8. Richter, J., Beffa, L., Wagner, U., Schraml, P., Gasser, T. C., Moch, H., Mihatsch, M. J., and Sauter, G. (1998) Patterns of chromosomal imbalances in advanced urinary bladder cancer detected by comparative genomic hybridization. *Am. J. Pathol.* 153, 1615–1621

9. Bruch, J., Wohr, G., Hautmann, R., Mattfeldt, T., Bruderlein, S., Moller, P., Sauter, S., Hameister, H., Vogel, W., and Paiss, T. (1998) Chromosomal changes during progression of transitional cell carcinoma of the bladder and delineation of the amplified interval on chromosome arm 8q. *Genes Chromosomes Cancer* 23, 167–174

10. Hovey, R. M., Chu, L., Balazs, M., De Vries, S., Moore, D., Sauter, G., Carroll, P. R., and Waldman, F. M. (1998) Genetic alterations in primary bladder cancers and their metastases. *Cancer Res.* 15, 3555–3560

11. Simon, R., Burger, H., Brinkschmidt, C., Bocker, W., Hertle, L., and Terpe, H. J. (1998) Chromosomal aberrations associated with invasion in papillary superficial bladder cancer. *J. Pathol.* 185, 345–351

12. Koo, S. H., Kwon, K. C., Ihm, C. H., Jeon, Y. M., Park, J. W., and Sul, C. K. (1999) Detection of genetic alterations in bladder tumors by comparative genomic hybridization and cytogenetic analysis. *Cancer Genet. Cytogenet.* 110, 87–93

13. Wodicka, L., Dong, H., Mittmann, M., Ho, M. H., and Lockhart, D. J. (1997) Genome-wide expression monitoring in *Saccharomyces cerevisiae*. *Nat. Biotechnol.* 15, 1359–1367

14. Christensen, M., Sunde, L., Bolund, L., and Orntoft, T. F. (1999) Comparison of three methods of microsatellite detection. *Scand. J. Clin. Lab. Invest.* 59, 167–177

15. Celis, J. E., Ostergaard, M., Basse, B., Celis, A., Lauridsen, J. B., Ratz, G. P., Andersen, I., Hein, B., Wolf, H., Orntoft, T. F., and Rasmussen, H. H. (1996) Loss of adipocyte-type fatty acid binding protein and other protein biomarkers is associated with progression of human bladder transitional cell carcinomas. *Cancer Res.* 56, 4782–4790

16. Celis, J. E., Ratz, G., Basse, B., Lauridsen, J. B., and Celis, A. (1994) In *Cell Biology: A Laboratory Handbook* (Celis, J. E., ed) Vol. 3, pp. 222–230, Academic Press, Orlando, FL

17. Ohlsson, R., Tycko, B., and Sapienza, C. (1998) Monoallelic expression: 'there can only be one'. *Trends Genet.* 14, 435–438

18. Hollander, G. A., Zuklys, S., Morel, C., Mizoguchi, E., Mobisson, K., Simpson, S., Terhorst, C., Wishart, W., Golan, D. E., Bhan, A. K., and Burakoff, S. J. (1998) Monoallelic expression of the interleukin-2 locus. *Science* 279, 2118–2121

19. Brannan, C. I., and Bartolomei, M. S. (1999) Mechanisms of genomic imprinting. *Curr. Opin. Genet. Dev.* 9, 164–170

20. Ohlsson, R., Cui, H., He, L., Pfeifer, S., Malmikumpa, H., Jiang, S., Feinberg, A. P., and Hedborg, F. (1999) Mosaic allelic insulin-like growth factor 2 expression patterns reveal a link between Wilms' tumorigenesis and epigenetic heterogeneity. *Cancer Res.* 59, 3889–3892

21. Cui, H., Hedborg, F., He, L., Nordenskjold, A., Sandstedt, B., Pfeifer-Ohlsson, S., and Ohlsson, R. (1997) Inactivation of H19, an imprinted and putative tumor repressor gene, is a preneoplastic event during Wilms' tumorigenesis. *Cancer Res.* 57, 4469–4473

22. Galitski, T., Saldanha, A. J., Styles, C. A., Lander, E. S., and Fink, G. R. (1999) Ploidy regulation of gene expression. *Science* 285, 251–254

23. Tsao, J., Yatabe, Y., Markl, I. D., Haiyan, K., Jones, P. A., and Shibata, D. (2000) Bladder cancer genotype stability during clinical progression. *Genes Chromosomes Cancer* 29, 26–32

24. Zong, Q., Schummer, M., Hood, L., and Morris, D. R. (1999) Messenger RNA translation state: the second dimension of high-throughput expression screening. *Proc. Natl. Acad. Sci. U. S. A.* 96, 10632–10636

25. Anderson, L., and Seilhamer, J. (1997) Comparison of selected mRNA and protein abundances in human liver. *Electrophoresis* 18, 533–537

26. Ideker, T., Thorsson, V., Ranish, J. A., Christmas, R., Buhler, J., Eng, J. K., Bumgarner, R., Goodlett, D. R., Aebersold, R., and Hood, L. (2001) Integrated genomic and proteomic analyses of a systematically perturbed metabolic network. *Science* 292, 929–934

Impact of DNA Amplification on Gene Expression Patterns in Breast Cancer[1,2]

Elizabeth Hyman,[3] Päivikki Kauraniemi,[3] Sampsa Hautaniemi, Maija Wolf, Spyro Mousses, Ester Rozenblum, Markus Ringnér, Guido Sauter, Outi Monni, Abdel Elkahloun, Olli-P. Kallioniemi, and Anne Kallioniemi[4]

Howard Hughes Medical Institute-NIH Research Scholar, Bethesda, Maryland 20892 [E. H.]; Cancer Genetics Branch, National Human Genome Research Institute, NIH, Bethesda, Maryland 20892 [E. H., P. K., S. H., M. W., S. M., E. R., M. R., A. E., O. K., A. K.]; Laboratory of Cancer Genetics, Institute of Medical Technology, University of Tampere and Tampere University Hospital, FIN-33520 Tampere, Finland [P. K., A. K.]; Signal Processing Laboratory, Tampere University of Technology, FIN-33101 Tampere, Finland [S. H.]; Institute of Pathology, University of Basel, CH-4003 Basel, Switzerland [G. S.]; and Biomedicum Biochip Center, Helsinki University Hospital, Biomedicum Helsinki, FIN-00014 Helsinki, Finland [O. M.]

ABSTRACT

Genetic changes underlie tumor progression and may lead to cancer-specific expression of critical genes. Over 1100 publications have described the use of comparative genomic hybridization (CGH) to analyze the pattern of copy number alterations in cancer, but very few of the genes affected are known. Here, we performed high-resolution CGH analysis on cDNA microarrays in breast cancer and directly compared copy number and mRNA expression levels of 13,824 genes to quantitate the impact of genomic changes on gene expression. We identified and mapped the boundaries of 24 independent amplicons, ranging in size from 0.2 to 12 Mb. Throughout the genome, both high- and low-level copy number changes had a substantial impact on gene expression, with 44% of the highly amplified genes showing overexpression and 10.5% of the highly overexpressed genes being amplified. Statistical analysis with random permutation tests identified 270 genes whose expression levels across 14 samples were systematically attributable to gene amplification. These included most previously described amplified genes in breast cancer and many novel targets for genomic alterations, including the HOXB7 gene, the presence of which in a novel amplicon at 17q21.3 was validated in 10.2% of primary breast cancers and associated with poor patient prognosis. In conclusion, CGH on cDNA microarrays revealed hundreds of novel genes whose overexpression is attributable to gene amplification. These genes may provide insights to the clonal evolution and progression of breast cancer and highlight promising therapeutic targets.

INTRODUCTION

Gene expression patterns revealed by cDNA microarrays have facilitated classification of cancers into biologically distinct categories, some of which may explain the clinical behavior of the tumors (1–6). Despite this progress in diagnostic classification, the molecular mechanisms underlying gene expression patterns in cancer have remained elusive, and the utility of gene expression profiling in the identification of specific therapeutic targets remains limited.

Accumulation of genetic defects is thought to underlie the clonal evolution of cancer. Identification of the genes that mediate the effects of genetic changes may be important by highlighting transcripts that are actively involved in tumor progression. Such transcripts and their encoded proteins would be ideal targets for anticancer therapies, as demonstrated by the clinical success of new therapies against amplified oncogenes, such as ERBB2 and EGFR (7, 8), in breast cancer and other solid tumors. Besides amplifications of known oncogenes, over
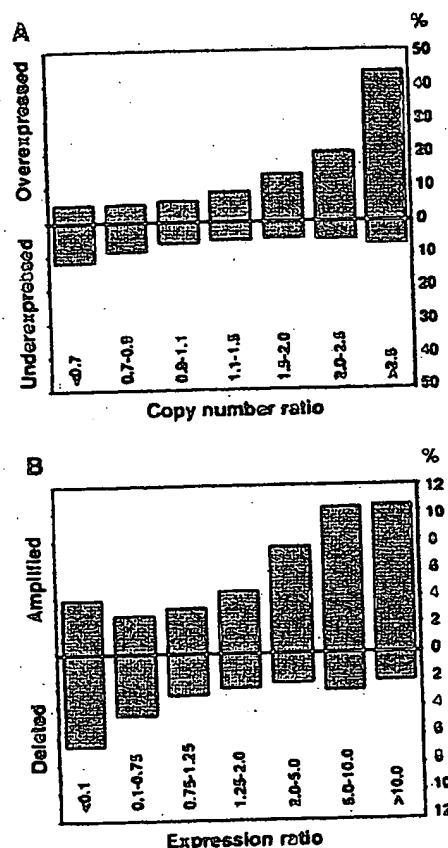

Fig. 1. Impact of gene copy number on global gene expression levels. A, percentage of over- and underexpressed genes (Y axis) according to copy number ratios (X axis). Threshold values used for over- and underexpression were >2.184 (global upper 7% of the cDNA ratios) and <0.4826 (global lower 7% of the expression ratios). B, percentage of amplified and deleted genes according to expression ratios. Threshold values for amplification and deletion were >1.5 and <0.7.

20 recurrent regions of DNA amplification have been mapped in breast cancer by CGH[5] (9, 10). However, these amplicons are often large and poorly defined, and their impact on gene expression remains unknown.

We hypothesized that genome-wide identification of those gene expression changes that are attributable to underlying gene copy number alterations would highlight transcripts that are actively involved in the causation or maintenance of the malignant phenotype. To identify such transcripts, we applied a combination of cDNA and CGH microarrays to: (a) determine the global impact that gene copy number variation plays in breast cancer development and progression; and (b) identify and characterize those genes whose mRNA expres-

[5] The abbreviations used are: CGH, comparative genomic hybridization; FISH, fluorescence in situ hybridization; RT-PCR, reverse transcription-PCR.
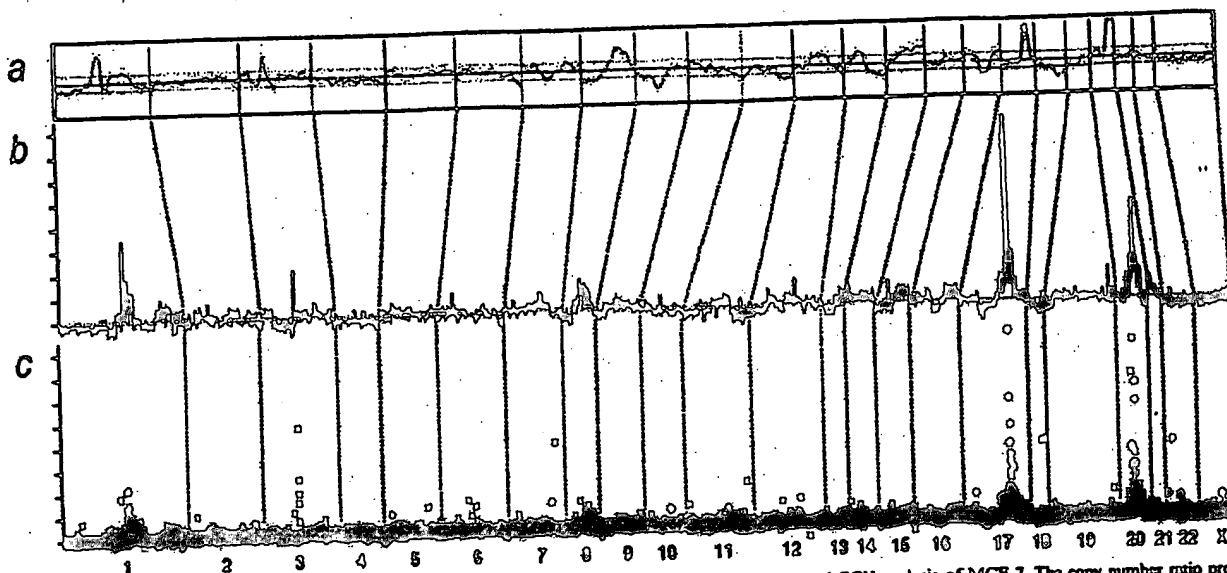
Fig. 2. Genome-wide copy number and expression analysis in the MCF-7 breast cancer cell line. *A*, chromosomal CGH analysis of MCF-7. The copy number ratio profile (*blue line*) across the entire genome from 1p telomere to Xq telomere is shown along with ±1 SD (*orange lines*). The *black horizontal line* indicates a ratio of 1.0; *red line*, a ratio of 0.8; and *green line*, a ratio of 1.2. *B–C*, genome-wide copy number analysis in MCF-7 by CGH on cDNA microarray. The copy number ratios were plotted as a function of the position of the cDNA clones along the human genome. In *B*, individual data points are connected with a line, and a moving median of 10 adjacent clones is shown. *Red horizontal line*, the copy number ratio of 1.0. In *C*, individual data points are labeled by color coding according to cDNA expression ratios. The *bright red dots* indicate the upper 2%, and *dark red dots*, the next 5% of the expression ratios in MCF-7 cells (overexpressed genes); *bright green dots* indicate the lowest 2%, and *dark green dots*, the next 5% of the expression ratios (underexpressed genes); the rest of the observations are shown with *black crosses*. The chromosome numbers are shown at the *bottom* of the figure, and chromosome boundaries are indicated with a *dashed line*.

sion is most significantly associated with amplification of the corresponding genomic template.

MATERIALS AND METHODS

Breast Cancer Cell Lines. Fourteen breast cancer cell lines (BT-20, BT-474, HCC1428, Hs578t, MCF7, MDA-361, MDA-436, MDA-453, MDA-468, SKBR-3, T-47D, UACC812, ZR-75-1, and ZR-75-30) were obtained from the American Type Culture Collection (Manassas, VA). Cells were grown under recommended culture conditions. Genomic DNA and mRNA were isolated using standard protocols.

Copy Number and Expression Analyses by cDNA Microarrays. The preparation and printing of the 13,824 cDNA clones on glass slides were performed as described (11–13). Of these clones, 244 represented uncharacterized expressed sequence tags, and the remainder corresponded to known genes. CGH experiments on cDNA microarrays were done as described (14, 15). Briefly, 20 μg of genomic DNA from breast cancer cell lines and normal human WBCs were digested for 14–18 h with *Alu*I and *Rsa*I (Life Technologies, Inc., Rockville, MD) and purified by phenol/chloroform extraction. Six μg of digested cell line DNAs were labeled with Cy3-dUTP (Amersham Pharmacia) and normal DNA with Cy5-dUTP (Amersham Pharmacia) using the Bioprime Labeling kit (Life Technologies, Inc.). Hybridization (14, 15) and posthybridization washes (13) were done as described. For the expression analyses, a standard reference (Universal Human Reference RNA; Stratagene, La Jolla, CA) was used in all experiments. Forty μg of reference RNA were labeled with Cy3-dUTP and 3.5 μg of test mRNA with Cy5-dUTP, and the labeled cDNAs were hybridized on microarrays as described (13, 15). For both microarray analyses, a laser confocal scanner (Agilent Technologies, Palo Alto, CA) was used to measure the fluorescence intensities at the target locations using the DEARRAY software (16). After background subtraction, average intensities at each clone in the test hybridization were divided by the average intensity of the corresponding clone in the control hybridization. For the copy number analysis, the ratios were normalized on the basis of the distribution of ratios of all targets on the array and for the expression analysis on the basis of 88 housekeeping genes, which were spotted four times onto the array. Low quality measurements (*i.e.*, copy number data with mean reference intensity <100 fluorescent units, and expression data with both test and reference intensity <100 fluorescent units and/or with spot size <50 units)

were excluded from the analysis and were treated as missing values. The distributions of fluorescence ratios were used to define cutpoints for increased/decreased copy number. Genes with CGH ratio >1.43 (representing the upper 5% of the CGH ratios across all experiments) were considered to be amplified, and genes with ratio <0.73 (representing the lower 5%) were considered to be deleted.

Statistical Analysis of CGH and cDNA Microarray Data. To evaluate the influence of copy number alterations on gene expression, we applied the following statistical approach. CGH and cDNA calibrated intensity ratios were log-transformed and normalized using median centering of the values in each cell line. Furthermore, cDNA ratios for each gene across all 14 cell lines were median centered. For each gene, the CGH data were represented by a vector that was labeled 1 for amplification (ratio, >1.43) and 0 for no amplification. Amplification was correlated with gene expression using the signal-to-noise statistics (1). We calculated a weight, w_a, for each gene as follows:

$$w_a = \frac{m_{a1} - m_{a0}}{\sigma_{a1} + \sigma_{a0}}$$

where m_{a1}, σ_{a1} and m_{a0}, σ_{a0} denote the means and SDs for the expression levels for amplified and nonamplified cell lines, respectively. To assess the statistical significance of each weight, we performed 10,000 random permutations of the label vector. The probability that a gene had a larger or equal weight by random permutation than the original weight was denoted by α. A low α (<0.05) indicates a strong association between gene expression and amplification.

Genomic Localization of cDNA Clones and Amplicon Mapping. Each cDNA clone on the microarray was assigned to a Unigene cluster using the Unigene Build 141.[6] A database of genomic sequence alignment information for mRNA sequences was created from the August 2001 freeze of the University of California Santa Cruz's GoldenPath database.[7] The chromosome and bp positions for each cDNA clone were then retrieved by relating these data sets. Amplicons were defined as a CGH copy number ratio >2.0 in at least two adjacent clones in two or more cell lines or a CGH ratio >2.0 in at least three adjacent clones in a single cell line. The amplicon start and end positions were

---

Table 1 *Summary of independent amplicons in 14 breast cancer cell lines by CGH microarray*

Location	Start (Mb)	End (Mb)	Size (Mb)
1p13	132.79	132.94	0.2
1q21	173.92	177.25	3.3
1q22	179.28	179.57	0.3
3p14	71.94	74.66	2.7
7p12.1–7p11.2	55.62	60.95	5.3
7q31	125.73	130.96	5.2
7q32	140.01	140.68	0.7
8q21.11–8q21.13	86.45	92.46	6.0
8q21.3	98.45	103.05	4.6
8q23.3–8q24.14	129.88	142.15	12.3
8q24.22	151.21	152.16	1.0
9p13	38.65	39.25	0.6
13q22–q31	77.15	81.38	4.2
16q22	86.70	87.62	0.9
17q11	29.30	30.85	1.6
17q12–q21.2	39.79	42.80	3.0
17q21.32–q21.33	52.47	55.80	3.3
17q22–q23.3	63.81	69.70	5.9
17q23.3–q24.3	69.93	74.99	5.1
19q13	40.63	41.40	0.8
20q11.22	34.59	35.85	1.3
20q13.12	44.00	45.62	1.6
20q13.12–q13.13	46.45	49.43	3.0
20q13.2–q13.32	51.32	59.12	7.8

CGH were validated, with 1q21, 17q12–q21.2, 17q22–q23, 20q13.1, and 20q13.2 regions being most commonly amplified. Furthermore, the boundaries of these amplicons were precisely delineated. In addition, novel amplicons were identified at 9p13 (38.65–39.25 Mb), and 17q21.3 (52.47–55.80 Mb).

Direct Identification of Putative Amplification Target Genes. The cDNA/CGH microarray technique enables the direct correlation of copy number and expression data on a gene-by-gene basis throughout the genome. We directly annotated high-resolution CGH plots with gene expression data using color coding. Fig. 2C shows that most of the amplified genes in the MCF-7 breast cancer cell line at 1p13, 17q22–q23, and 20q13 were highly overexpressed. A view of chromosome 7 in the MDA-468 cell line implicates *EGFR* as the most highly overexpressed and amplified gene at 7p11–p12 (Fig. 3A). In BT-474, the two known amplicons at 17q12 and 17q22–q23 contained numerous highly overexpressed genes (Fig. 3B). In addition, several genes, including the homeobox genes *HOXB2* and *HOXB7*, were highly amplified in a previously undescribed independent amplicon at 17q21.3. *HOXB7* was systematically amplified (as validated by FISH, Fig. 3B, inset) as well as overexpressed (as verified by RT-PCR, data not shown) in BT-474, UACC812, and ZR-75-30 cells. Furthermore, this novel
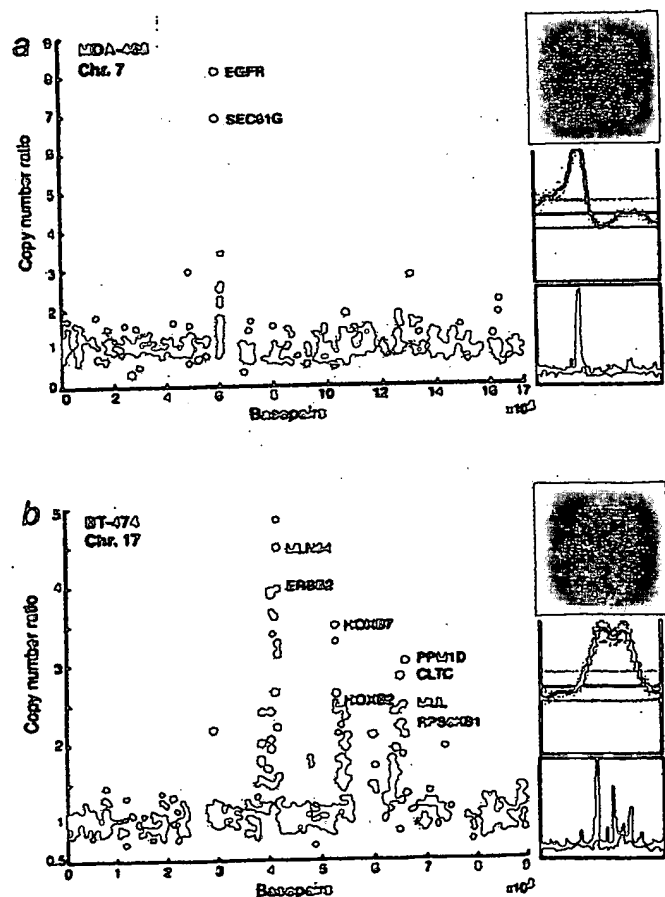
extended to include neighboring nonamplified clones (ratio, <1.5). The amplicon size determination was partially dependent on local clone density.

FISH. Dual-color interphase FISH to breast cancer cell lines was done as described (17). Bacterial artificial chromosome clone RP11-361K8 was labeled with SpectrumOrange (Vysis, Downers Grove, IL), and Spectrum-Orange-labeled probe for *EGFR* was obtained from Vysis. SpectrumGreen-labeled chromosome 7 and 17 centromere probes (Vysis) were used as a reference. A tissue microarray containing 612 formalin-fixed, paraffin-embedded primary breast cancers (17) was applied in FISH analyses as described (18). The use of these specimens was approved by the Ethics Committee of the University of Basel and by the NIH. Specimens containing a 2-fold or higher increase in the number of test probe signals, as compared with corresponding centromere signals, in at least 10% of the tumor cells were considered to be amplified. Survival analysis was performed using the Kaplan-Meier method and the log-rank test.

RT-PCR. The *HOXB7* expression level was determined relative to *GAPDH*. Reverse transcription and PCR amplification were performed using Access RT-PCR System (Promega Corp., Madison, WI) with 10 ng of mRNA as a template. *HOXB7* primers were 5'-GAGCAGAGGGACTCGGACTT-3' and 5'-GCGTCAGGTAGCGATTGTAG-3'.

RESULTS

Global Effect of Copy Number on Gene Expression. 13,824 arrayed cDNA clones were applied for analysis of gene expression and gene copy number (CGH microarrays) in 14 breast cancer cell lines. The results illustrate a considerable influence of copy number on gene expression patterns. Up to 44% of the highly amplified transcripts (CGH ratio, >2.5) were overexpressed (i.e., belonged to the global upper 7% of expression ratios), compared with only 6% for genes with normal copy number levels (Fig. 1A). Conversely, 10.5% of the transcripts with high-level expression (cDNA ratio, >10) showed increased copy number (Fig. 1B). Low-level copy number increases and decreases were also associated with similar, although less dramatic, outcomes on gene expression (Fig. 1).

Identification of Distinct Breast Cancer Amplicons. Base-pair locations obtained for 11,994 cDNAs (86.8%) were used to plot copy number changes as a function of genomic position (Fig. 2, Supplement Fig. A). The average spacing of clones throughout the genome was 267 kb. This high-resolution mapping identified 24 independent breast cancer amplicons, spanning from 0.2 to 12 Mb of DNA (Table 1). Several amplification sites detected previously by chromosomal

Fig. 3. Annotation of gene expression data on CGH microarray profiles. A, genes in the 7p11–p12 amplicon in the MDA-468 cell line are highly expressed (red dots) and include the *EGFR* oncogene. B, several genes in the 17q12, 17q21.3, and 17q23 amplicons in the BT-474 breast cancer cell line are highly overexpressed (red) and include the *HOXB7* gene. The data labels and color coding are as indicated for Fig. 2C. Insets show chromosomal CGH profiles for the corresponding chromosomes and validation of the increased copy number by interphase FISH using *EGFR* (red) and chromosome 7 centromere probe (green) to MDA-468 (A) and *HOXB7*-specific probe (red) and chromosome 17 centromere (green) to BT-474 cells (B).

Copy number ratio   Expression ratio

Fig. 4. List of 50 genes with a statistically significant correlation (α value <0.05) between gene copy number and gene expression. Name, chromosomal location, and the α value for each gene are indicated. The genes have been ordered according to their position in the genome. The color maps on the *right* illustrate the copy number and expression ratio patterns in the 14 cell lines. The key to the color code is shown at the *bottom* of the graph. *Gray squares*, missing values. The complete list of 270 genes is shown in supplemental Fig. B.

amplification was validated to be present in 10.2% of 363 primary breast cancers by FISH to a tissue microarray and was associated with poor prognosis of the patients ($P = 0.001$).

Statistical Identification and Characterization of 270 Highly Expressed Genes in Amplicons. Statistical comparison of expression levels of all genes as a function of gene amplification identified 270 genes whose expression was significantly influenced by copy number across all 14 cell lines (Fig. 4, Supplemental Fig. B). According to the gene ontology data,[*] 91 of the 270 genes represented hypothetical proteins or genes with no functional annotation, whereas 179 had associated functional information available. Of these, 151 (84%) are implicated in apoptosis, cell proliferation, signal transduction, and transcription, whereas 28 (16%) had functional annotations that could not be directly linked with cancer.

DISCUSSION

The importance of recurrent gene and chromosome copy number changes in the development and progression of solid tumors has been characterized in >1000 publications applying CGH[9] (9, 10), as well as in a large number of other molecular cytogenetic, cytogenetic, and molecular genetic studies. The effects of these somatic genetic changes on gene expression levels have remained largely unknown, although a few studies have explored gene expression changes occurring in specific amplicons (15, 19–21). Here, we applied genome-wide cDNA microarrays to identify transcripts whose expression changes were attributable to underlying gene copy number alterations in breast cancer.

The overall impact of copy number on gene expression patterns was substantial with the most dramatic effects seen in the case of high-

level copy number increase. Low-level copy number gains and losses also had a significant influence on expression levels of genes in the regions affected, but these effects were more subtle on a gene-by-gene basis than those of high-level amplifications. However, the impact of low-level gains on the dysregulation of gene expression patterns in cancer may be equally important if not more important than that of high-level amplifications. Aneuploidy and low-level gains and losses of chromosomal arms represent the most common types of genetic alterations in breast and other cancers and, therefore, have an influence on many genes. Our results in breast cancer extend the recent studies on the impact of aneuploidy on global gene expression patterns in yeast cells, acute myeloid leukemia, and a prostate cancer model system (22–24).

The CGH microarray analysis identified 24 independent breast cancer amplicons. We defined the precise boundaries for many amplicons detected previously by chromosomal CGH (9, 10, 25, 26) and also discovered novel amplicons that had not been detected previously, presumably because of their small size (only 1–2 Mb) or close proximity to other larger amplicons. One of these novel amplicons involved the homeobox gene region at 17q21.3 and led to the overexpression of the *HOXB7* and *HOXB2* genes. The homeodomain transcription factors are known to be key regulators of embryonic development and have been occasionally reported to undergo aberrant expression in cancer (27, 28). *HOXB7* transfection induced cell proliferation in melanoma, breast, and ovarian cancer cells and increased tumorigenicity and angiogenesis in breast cancer (29–32). The present results imply that gene amplification may be a prominent mechanism for overexpressing *HOXB7* in breast cancer and suggest that *HOXB7* contributes to tumor progression and confers an aggressive disease phenotype in breast cancer. This view is supported by our finding of amplification of *HOXB7* in 10% of 363 primary breast cancers, as well as an association of amplification with poor prognosis of the patients.

We carried out a systematic search to identify genes whose expression levels across all 14 cell lines were attributable to amplification status. Statistical analysis revealed 270 such genes (representing ~2% of all genes on the array), including not only previously described amplified genes, such as *HER-2*, *MYC*, *EGFR*, ribosomal protein s6 kinase, and *AIB3*, but also numerous novel genes such as *NRAS-related gene* (1p13), *syndecan-2* (8q22), and *bone morphogenic protein* (20q13.1), whose activation by amplification may similarly promote breast cancer progression. Most of the 270 genes have not been implicated previously in breast cancer development and suggest novel pathogenetic mechanisms. Although we would not expect all of them to be causally involved, it is intriguing that 84% of the genes with associated functional information were implicated in apoptosis, cell proliferation, signal transduction, transcription, or other cellular processes that could directly imply a possible role in cancer progression. Therefore, a detailed characterization of these genes may provide biological insights to breast cancer progression and might lead to the development of novel therapeutic strategies.

In summary, we demonstrate application of cDNA microarrays to the analysis of both copy number and expression levels of over 12,000 transcripts throughout the breast cancer genome, roughly once every 267 kb. This analysis provided: (*a*) evidence of a prominent global influence of copy number changes on gene expression levels; (*b*) a high-resolution map of 24 independent amplicons in breast cancer; and (*c*) identification of a set of 270 genes, the overexpression of which was statistically attributable to gene amplification. Characterization of a novel amplicon at 17q21.3 implicated amplification and overexpression of the *HOXB7* gene in breast cancer, including a clinical association

between *HOXB7* amplification and poor patient prognosis. Overall, our results illustrate how the identification of genes activated by gene amplification provides a powerful approach to highlight genes with an important role in cancer as well as to prioritize and validate putative targets for therapy development.

REFERENCES

1. Golub, T. R., Slonim, D. K., Tamayo, P., Huard, C., Gaasenbeek, M., Mesirov, J. P., Coller, H., Loh, M. L., Downing, J. R., Caligiuri, M. A., Bloomfield, C. D., and Lander, E. S. Molecular classification of cancer: class discovery and class prediction by gene expression monitoring. Science (Wash. DC), 286: 531–537, 1999.
2. Alizadeh, A. A., Eisen, M. B., Davis, R. E., Ma, C., Lossos, I. S., Rosenwald, A., Boldrick, J. C., Sabet, H., Tran, T., Yu, X., et al. Distinct types of diffuse large B-cell lymphoma identified by gene expression profiling. Nature (Lond.), 403: 503–511, 2000.
3. Bittner, M., Meltzer, P., Chen, Y., Jiang, Y., Seftor, E., Hendrix, M., Radmacher, M., Simon, R., Yakhini, Z., Ben-Dor, A., et al. Molecular classification of cutaneous malignant melanoma by gene expression profiling. Nature (Lond.), 406: 536–540, 2000.
4. Perou, C. M., Sorlie, T., Eisen, M. B., van de Rijn, M., Jeffrey, S. S., Rees, C. A., Pollack, J. R., Ross, D. T., Johnsen, H., Akslen, L. A., et al. Molecular portraits of human breast tumours. Nature (Lond.), 406: 747–752, 2000.
5. Dhanasekaran, S. M., Barrette, T. R., Ghosh, D., Shah, R., Varambally, S., Kurachi, K., Pienta, K. J., Rubin, M. A., and Chinnaiyan, A. M. Delineation of prognostic biomarkers in prostate cancer. Nature (Lond.), 412: 822–826, 2001.
6. Sorlie, T., Perou, C. M., Tibshirani, R., Aas, T., Geisler, S., Johnsen, H., Hastie, T., Eisen, M. B., van de Rijn, M., Jeffrey, S. S., et al. Gene expression patterns of breast carcinomas distinguish tumor subclasses with clinical implications. Proc. Natl. Acad. Sci. USA, 98: 10869–10874, 2001.
7. Ross, J. S., and Fletcher, J. A. The HER-2/neu oncogene: prognostic factor, predictive factor and target for therapy. Semin. Cancer Biol., 9: 125–138, 1999.
8. Arteaga, C. L. The epidermal growth factor receptor: from mutant oncogene in nonhuman cancers to therapeutic target in human neoplasia. J. Clin. Oncol., 19: 32–40, 2001.
9. Knuutila, S., Bjorkqvist, A. M., Autio, K., Tarkkanen, M., Wolf, M., Monni, O., Szymanska, J., Larramendy, M. L., Tapper, J., Pere, H., El-Rifai, W., et al. DNA copy number amplifications in human neoplasms: review of comparative genomic hybridization studies. Am. J. Pathol., 152: 1107–1123, 1998.
10. Knuutila S., Autio K., and Aalto Y. Online access to CGH data of DNA sequence copy number changes. Am. J. Pathol., 157: 689, 2000.
11. DeRisi, J., Penland, L., Brown, P. O., Bittner, M. L., Meltzer, P. S., Ray, M., Chen, Y., Su, Y. A., and Trent, J. M. Use of a cDNA microarray to analyze gene expression patterns in human cancer. Nat. Genet., 14: 457–460, 1996.
12. Shalon, D., Smith, S. J., and Brown, P. O. A DNA microarray system for analyzing complex DNA samples using two-color fluorescent probe hybridization. Genome Res., 6: 639–645, 1996.
13. Mousses, S., Bittner, M. L., Chen, Y., Dougherty, E. R., Baxevanis, A., Meltzer, P. S., and Trent, J. M. Gene expression analysis by cDNA microarrays. In: F. J. Livesey and S. P. Hunt (eds.), Functional Genomics, pp. 113–137. Oxford: Oxford University Press, 2000.
14. Pollack, J. R., Perou, C. M., Alizadeh, A. A., Eisen, M. B., Pergamenschikov, A., Williams, C. F., Jeffrey, S. S., Botstein, D., and Brown, P. O. Genome-wide analysis of DNA copy-number changes using cDNA microarrays. Nat. Genet., 23: 41–46, 1999.
15. Monni, O., Bärlund, M., Mousses, S., Kononen, J., Sauter, G., Heiskanen, M., Paavola, P., Avela, K., Chen, Y., Bittner, M. L., and Kallioniemi, A. Comprehensive copy number and gene expression profiling of the 17q23 amplicon in human breast cancer. Proc. Natl. Acad. Sci. USA, 98: 5711–5716, 2001.
16. Chen, Y., Dougherty, E. R., and Bittner, M. L. Ratio-based decisions and the quantitative analysis of cDNA microarray images. J. Biomed. Optics, 2: 364–374, 1997.
17. Bärlund, M., Forozan, F., Kononen, J., Bubendorf, L., Chen, Y., Bittner, M. L., Torhorst, J., Haas, P., Bucher, C., Sauter, G., et al. Detecting activation of ribosomal protein S6 kinase by complementary DNA and tissue microarray analysis. J. Natl. Cancer Inst., 92: 1252–1259, 2000.
18. Andersen, C. L., Hostetter, G., Grigoryan, A., Sauter, G., and Kallioniemi, A. Improved procedure for fluorescence in situ hybridization on tissue microarrays. Cytometry, 45: 83–86, 2001.
19. Kauraniemi, P., Bärlund, M., Monni, O., and Kallioniemi, A. New amplified and highly expressed genes discovered in the ERBB2 amplicon in breast cancer by cDNA microarrays. Cancer Res., 61: 8235–8240, 2001.
20. Clark, J., Edwards, S., John, M., Flohr, P., Gordon, T., Maillard, K., Giddings, I., Brown, C., Bagherzadeh, A., Campbell, C., Shipley, J., Wooster, R., and Cooper, C. S. Identification of amplified and expressed genes in breast cancer by comparative hybridization onto microarrays of randomly selected cDNA clones. Genes Chromosomes Cancer, 34: 104–114, 2002.
21. Varis, A., Wolf, M., Monni, O., Vakkari, M. L., Kokkola, A., Moskaluk, C., Frierson, H., Powell, S. M., Knuutila, S., Kallioniemi, A., and El-Rifai, W. Targets of gene amplification and overexpression at 17q in gastric cancer. Cancer Res., 62: 2625–2629, 2002.
22. Hughes, T. R., Roberts, C. J., Dai, H., Jones, A. R., Meyer, M. R., Slade, D., Burchard, J., Dow, S., Ward, T. R., Kidd, M. J., Friend, S. H., and Marton M. J.

Widespread aneuploidy revealed by DNA microarray expression profiling. Nat. Genet., *25:* 333–337, 2000.

23. Virtaneva, K., Wright, F. A., Tanner, S. M., Yuan, B., Lemon, W. J., Caligiuri, M. A., Bloomfield, C. D., de La Chapelle, A., and Krahe, R. Expression profiling reveals fundamental biological differences in acute myeloid leukemia with isolated trisomy 8 and normal cytogenetics. Proc. Natl. Acad. Sci. USA, *98:* 1124–1129, 2001.

24. Phillips, J. L., Hayward, S. W., Wang, Y., Vasselli, J., Pavlovich, C., Padilla-Nash, H., Pezullo, J. R., Ghadimi, B. M., Grossfeld, G. D., Rivera, A., Linehan, W. M., Cunha, G. R., and Ried, T. The consequences of chromosomal aneuploidy on gene expression profiles in a cell line model for prostate carcinogenesis. Cancer Res., *61:* 8143–8149, 2001.

25. Bärlund, M., Tirkkonen, M., Forozan, F., Tanner, M. M., Kallioniemi, O. P., and Kallioniemi, A. Increased copy number at 17q22–q24 by CGH in breast cancer is due to high-level amplification of two separate regions. Genes Chromosomes Cancer, *20:* 372–376, 1997.

26. Tanner, M. M., Tirkkonen, M., Kallioniemi, A., Isola, J., Kuukasjärvi, T., Collins, C., Kowbel, D., Guan, X. Y., Trent, J., Gray, J. W., Meltzer, P., and Kallioniemi O. P. Independent amplification and frequent co-amplification of three nonsyntenic regions

on the long arm of chromosome 20 in human breast cancer. Cancer Res., *56:* 3441–3445, 1996.

27. Cillo, C., Faiella, A., Cantile, M., and Boncinelli, E. Homeobox genes and cancer. Exp. Cell Res., *248:* 1–9, 1999.

28. Cillo, C., Cantile, M., Faiella, A., and Boncinelli, E. Homeobox genes in normal and malignant cells. J. Cell. Physiol., *188:* 161–169, 2001.

29. Care, A., Silvani, A., Meccia, E., Mattia, G., Stoppacciaro, A., Parmiani, G., Peschle, C., and Colombo, M. P. HOXB7 constitutively activates basic fibroblast growth factor in melanomas. Mol. Cell. Biol., *16:* 4842–4851, 1996.

30. Care, A., Silvani, A., Meccia, E., Mattia, G., Peschle, C., and Colombo, M. P. Transduction of the SkBr3 breast carcinoma cell line with the *HOXB7* gene induces bFGF expression, increases cell proliferation and reduces growth factor dependence. Oncogene, *16:* 3285–3289, 1998.

31. Care, A., Felicetti, F., Meccia, E., Bottero, L., Parenza, M., Stoppacciaro, A., Peschle, C., and Colombo, M. P. HOXB7: a key factor for tumor-associated angiogenic switch. Cancer Res., *61:* 6532–6539, 2001.

32. Naora, H., Yang, Y. Q., Montz, F. J., Seidman, J. D., Kurman, R. J., and Roden, R. B. A serologically identified tumor antigen encoded by a homeobox gene promotes growth of ovarian epithelial cells. Proc. Natl. Acad. Sci. USA, *98:* 4060–4065, 2001.

Microarray analysis reveals a major direct role of DNA copy number alteration in the transcriptional program of human breast tumors

Jonathan R. Pollack[o,t,‡], Therese Sørlie[δ], Charles M. Perou[¶], Christian A. Rees[**], Stefanie S. Jeffrey[††], Per E. Lønning[‡‡], Robert Tibshirani[§§], David Botstein[‖], Anne-Lise Børresen-Dale[δ], and Patrick O. Brown[†,m]

Departments of [o]Pathology, [‖]Genetics, [††]Surgery, [§§]Health Research and Policy, and [m]Biochemistry, and [†]Howard Hughes Medical Institute, Stanford University School of Medicine, Stanford, CA 94305; [δ]Department of Genetics, Norwegian Radium Hospital, Montebello, N-0310 Oslo, Norway; [‡‡]Department of Medicine (Oncology), Haukeland University Hospital, N-5021 Bergen, Norway; and [¶]Department of Genetics and Lineberger Comprehensive Cancer Center, University of North Carolina, Chapel Hill, NC 27599

Contributed by Patrick O. Brown, August 6, 2002

Genomic DNA copy number alterations are key genetic events in the development and progression of human cancers. Here we report a genome-wide microarray comparative genomic hybridization (array CGH) analysis of DNA copy number variation in a series of primary human breast tumors. We have profiled DNA copy number alteration across 6,691 mapped human genes, in 44 predominantly advanced, primary breast tumors and 10 breast cancer cell lines. While the overall patterns of DNA amplification and deletion corroborate previous cytogenetic studies, the high-resolution (gene-by-gene) mapping of amplicon boundaries and the quantitative analysis of amplicon shape provide significant improvement in the localization of candidate oncogenes. Parallel microarray measurements of mRNA levels reveal the remarkable degree to which variation in gene copy number contributes to variation in gene expression in tumor cells. Specifically, we find that 62% of highly amplified genes show moderately or highly elevated expression, that DNA copy number influences gene expression across a wide range of DNA copy number alterations (deletion, low-, mid- and high-level amplification), that on average, a 2-fold change in DNA copy number is associated with a corresponding 1.5-fold change in mRNA levels, and that overall, at least 12% of all the variation in gene expression among the breast tumors is directly attributable to underlying variation in gene copy number. These findings provide evidence that widespread DNA copy number alteration can lead directly to global deregulation of gene expression, which may contribute to the development or progression of cancer.

Conventional cytogenetic techniques, including comparative genomic hybridization (CGH) (1), have led to the identification of a number of recurrent regions of DNA copy number alteration in breast cancer cell lines and tumors (2–4). While some of these regions contain known or candidate oncogenes [e.g., FGFR1 (8p11), MYC (8q24), CCND1 (11q13), ERBB2 (17q12), and ZNF217 (20q13)] and tumor suppressor genes [RB1 (13q14) and TP53 (17p13)], the relevant gene(s) within other regions (e.g., gain of 1q, 8q22, and 17q22–24, and loss of 8p) remain to be identified. A high-resolution genome-wide map, delineating the boundaries of DNA copy number alterations in tumors, should facilitate the localization and identification of oncogenes and tumor suppressor genes in breast cancer. In this study, we have created such a map, using array-based CGH (5–7) to profile DNA copy number alteration in a series of breast cancer cell lines and primary tumors.

An unresolved question is the extent to which the widespread DNA copy number changes that we and others have identified in breast tumors alter expression of genes within involved regions. Because we had measured mRNA levels in parallel in the same samples (8), using the same DNA microarrays, we had an opportunity to explore on a genomic scale the relationship between DNA copy number changes and gene expression. From this analysis, we have identified a significant impact of widespread DNA copy number alteration on the transcriptional programs of breast tumors.

Materials and Methods

Tumors and Cell Lines. Primary breast tumors were predominantly large (>3 cm), intermediate-grade, infiltrating ductal carcinomas, with more than 50% being lymph node positive. The fraction of tumor cells within specimens averaged at least 50%. Details of individual tumors have been published (8, 9), and are summarized in Table 1, which is published as supporting information on the PNAS web site, www.pnas.org. Breast cancer cell lines were obtained from the American Type Culture Collection. Genomic DNA was isolated either using Qiagen genomic DNA columns, or by phenol/chloroform extraction followed by ethanol precipitation.

DNA Labeling and Microarray Hybridizations. Genomic DNA labeling and hybridizations were performed essentially as described in Pollack et al. (7), with slight modifications. Two micrograms of DNA was labeled in a total volume of 50 microliters and the volumes of all reagents were adjusted accordingly. "Test" DNA (from tumors and cell lines) was fluorescently labeled (Cy5) and hybridized to a human cDNA microarray containing 6,691 different mapped human genes (i.e., UniGene clusters). The "reference" (labeled with Cy3) for each hybridization was normal female leukocyte DNA from a single donor. The fabrication of cDNA microarrays and the labeling and hybridization of mRNA samples have been described (8).

Data Analysis and Map Positions. Hybridized arrays were scanned on a GenePix scanner (Axon Instruments, Foster City, CA), and fluorescence ratios (test/reference) calculated using SCANALYZE software (available at http://rana.lbl.gov). Fluorescence ratios were normalized for each array by setting the average log fluorescence ratio for all array elements equal to 0. Measurements with fluorescence intensities more than 20% above background were considered reliable. DNA copy number profiles that deviated significantly from background ratios measured in normal genomic DNA control hybridizations were interpreted as evidence of real DNA copy number alteration (see *Estimating Significance of Altered Fluorescence Ratios* in the supporting information). When indicated, DNA copy number profiles are displayed as a moving average (symmetric 5-nearest neighbors). Map positions for arrayed human cDNAs were assigned by
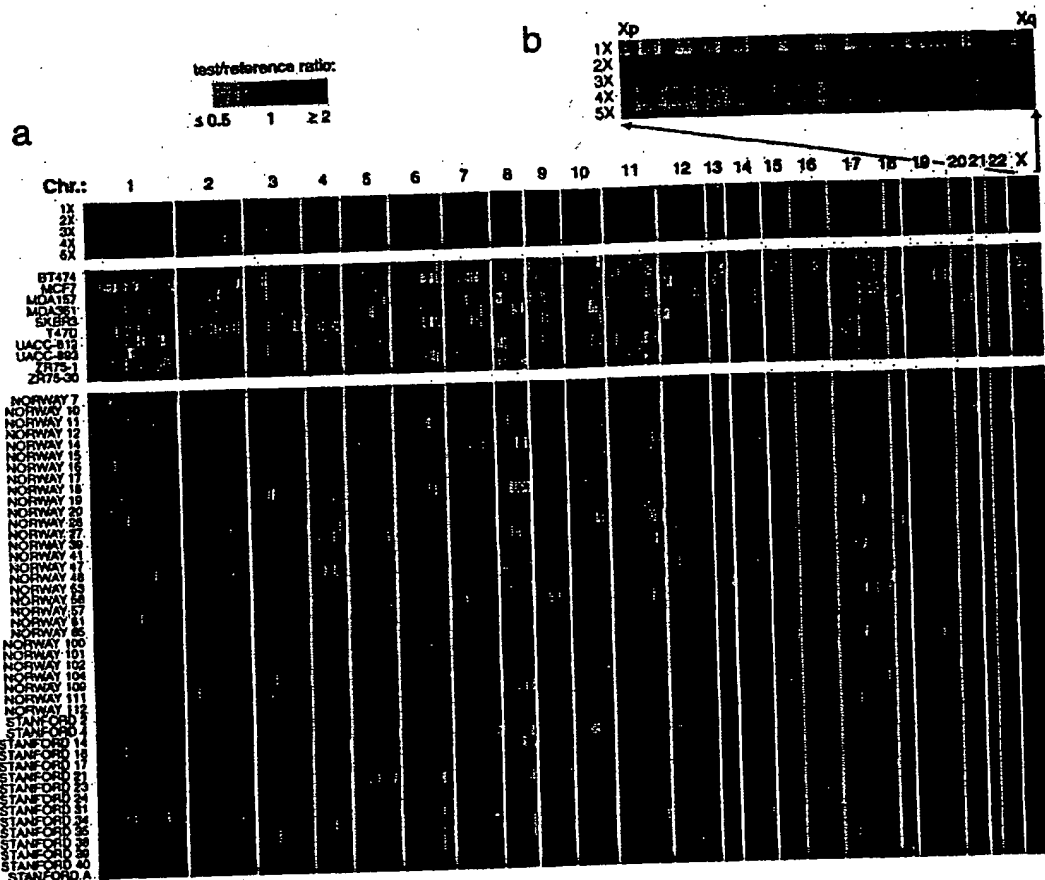
Fig. 1. Genome-wide measurement of DNA copy number alteration by array CGH. (a) DNA copy number profiles are illustrated for cell lines containing different numbers of X chromosomes, for breast cancer cell lines, and for breast tumors. Each row represents a different cell line or tumor, and each column represents one of 6,691 different mapped human genes present on the microarray, ordered by genome map position from 1pter through Xqter. Moving average (symmetric 5-nearest neighbors) fluorescence ratios (test/reference) are depicted using a log₂-based pseudocolor scale (indicated), such that red luminescence reflects fold-amplification, green luminescence reflects fold-deletion, and black indicates no change (gray indicates poorly measured data). (b) Enlarged view of DNA copy number profiles across the X chromosome, shown for cell lines containing different numbers of X chromosomes.

identifying the starting position of the best and longest match of any DNA sequence represented in the corresponding UniGene cluster (10) against the "Golden Path" genome assembly (http://genome.ucsc.edu/; Oct 7, 2000 Freeze). For UniGene clusters represented by multiple arrayed elements, mean fluorescence ratios (for all elements representing the same UniGene cluster) are reported. For mRNA measurements, fluorescence ratios are "mean-centered" (i.e., reported relative to the mean ratio across the 44 tumor samples). The data set described here can be accessed in its entirety in the supporting information.

Results

We performed CGH on 44 predominantly locally advanced, primary breast tumors and 10 breast cancer cell lines, using cDNA microarrays containing 6,691 different mapped human genes (Fig. 1a; also see Materials and Methods for details of microarray hybridizations). To take full advantage of the improved spatial resolution of array CGH, we ordered (fluorescence ratios for) the 6,691 cDNAs according to the "Golden Path" (http://genome.ucsc.edu/) genome assembly of the draft human genome sequences (11). In so doing, arrayed cDNAs not only themselves represent genes of potential interest (e.g., candidate oncogenes within amplicons), but also provide precise genetic landmarks for chromosomal regions of amplification and

deletion. Parallel analysis of DNA from cell lines containing different numbers of X chromosomes (Fig. 1b), as we did before (7), demonstrated the sensitivity of our method to detect single-copy loss (45, XO), and 1.5- (47,XXX), 2- (48,XXXX), or 2.5-fold (49,XXXXX) gains (also see Fig. 5, which is published as supporting information on the PNAS web site). Fluorescence ratios were linearly proportional to copy number ratios, which were slightly underestimated, in agreement with previous observations (7). Numerous DNA copy number alterations were evident in both the breast cancer cell lines and primary tumors (Fig. 1a), detected in the tumors despite the presence of euploid non-tumor cell types; the magnitudes of the observed changes were generally lower in the tumor samples. DNA copy-number alterations were found in every cancer cell line and tumor, and on every human chromosome in at least one sample. Recurrent regions of DNA copy number gain and loss were readily identifiable. For example, gains within 1q, 8q, 17q, and 20q were observed in a high proportion of breast cancer cell lines/tumors (90%/69%, 100%/47%, 100%/60%, and 90%/44%, respectively), as were losses within 1p, 3p, 8p, and 13q (80%/24%, 80%/22%, 80%/22%, and 70%/18%, respectively), consistent with published cytogenetic studies (refs. 2–4; a complete listing of gains/losses is provided in Tables 2 and 3, which are published as supporting information on the PNAS web site). The total
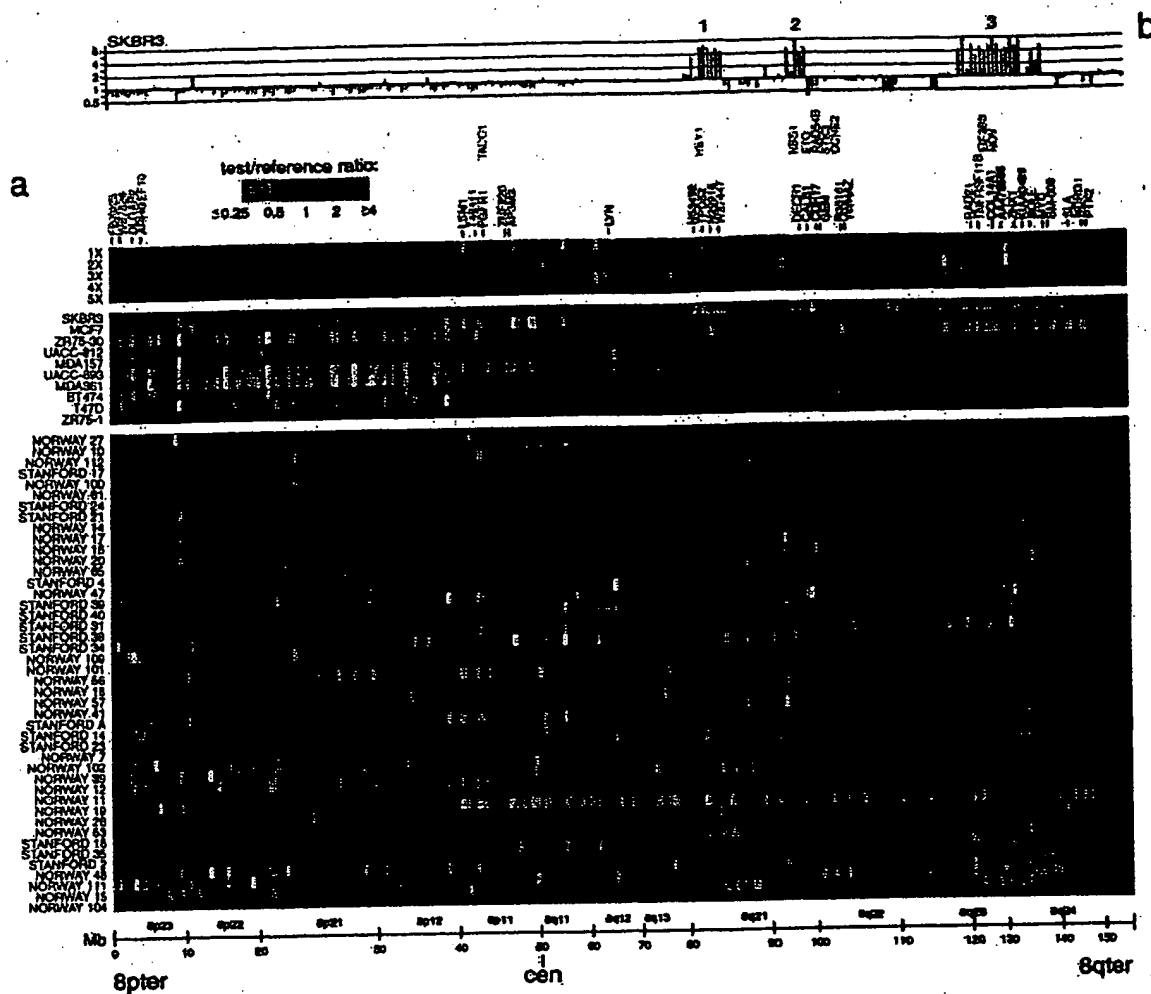
Fig. 2. DNA copy number alteration across chromosome 8 by array CGH. (a) DNA copy number profiles are illustrated for cell lines containing different numbers of X chromosomes, for breast cancer cell lines, and for breast tumors. Breast cancer cell lines and tumors are separately ordered by hierarchical clustering to highlight recurrent copy number changes. The 241 genes present on the microarrays and mapping to chromosome 8 are ordered by position along the chromosome. Fluorescence ratios (test/reference) are depicted by a log₂ pseudocolor scale (indicated). Selected genes are indicated with color-coded text (red, increased; green, decreased; black, no change; gray, not well measured) to reflect correspondingly altered mRNA levels (observed in the majority of the subset of samples displaying the DNA copy number change). The map positions for genes of interest that are not represented on the microarray are indicated in the row above those genes represented on the array. (b) Graphical display of DNA copy number profile for breast cancer cell line SKBR3. Fluorescence ratios (tumor/normal) are plotted on a log₂ scale for chromosome 8 genes, ordered along the chromosome.

number of genomic alterations (gains and losses) was found to be significantly higher in breast tumors that were high grade (P = 0.008), consistent with published CGH data (3), estrogen receptor negative (P = 0.04), and harboring TP53 mutations (P = 0.0006) (see Table 4, which is published as supporting information on the PNAS web site).

The improved spatial resolution of our array CGH analysis is illustrated for chromosome 8, which displayed extensive DNA copy number alteration in our series. A detailed view of the variation in the copy number of 241 genes mapping to chromosome 8 revealed multiple regions of recurrent amplification; each of these potentially harbors a different known or previously uncharacterized oncogene (Fig. 2a). The complexity of amplicon structure is most easily appreciated in the breast cancer cell line SKBR3. Although a conventional CGH analysis of 8q in SKBR3 identified only two distinct regions of amplification (12), we observed three distinct regions of high-level amplification (labeled 1–3 in Fig. 2b). For each of these regions we can define the

boundaries of the interval recurrently amplified in the tumors we examined; in each case, known or plausible candidate oncogenes can be identified (a description of these regions, as well as the recurrently amplified regions on chromosomes 17 and 20, can be found in Figs. 6 and 7, which are published as supporting information on the PNAS web site).

For a subset of breast cancer cell lines and tumors (4 and 37, respectively), and a subset of arrayed genes (6,095), mRNA levels were quantitatively measured in parallel by using cDNA microarrays (8). The parallel assessment of mRNA levels is useful in the interpretation of DNA copy number changes. For example, the highly amplified genes that are also highly expressed are the strongest candidate oncogenes within an amplicon. Perhaps more significantly, our parallel analysis of DNA copy number changes and mRNA levels provides us the opportunity to assess the global impact of widespread DNA copy number alteration on gene expression in tumor cells.

A strong influence of DNA copy number on gene expression is evident in an examination of the pseudocolor representations
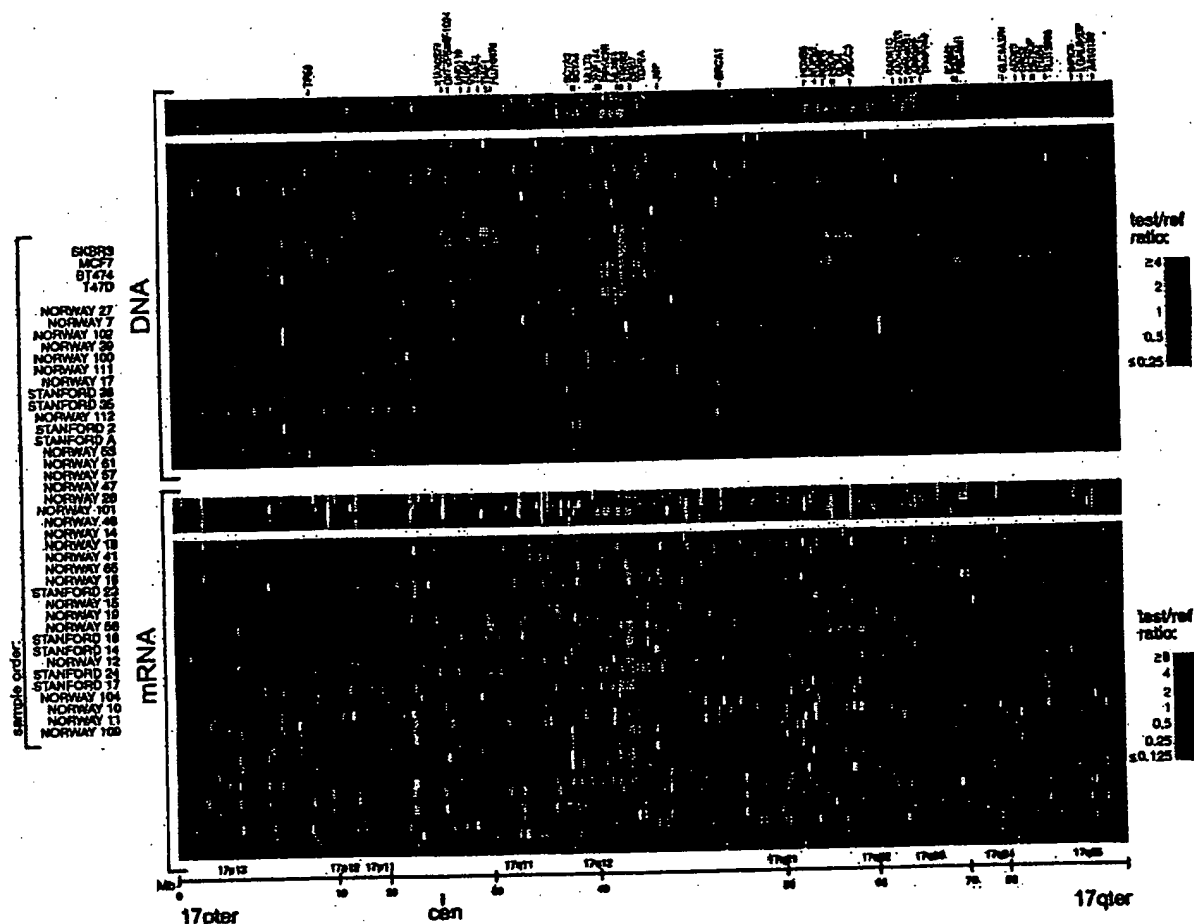
Fig. 3. Concordance between DNA copy number and gene expression across chromosome 17. DNA copy number alteration (*Upper*) and mRNA levels (*Lower*) are illustrated for breast cancer cell lines and tumors. Breast cancer cell lines and tumors are separately ordered by hierarchical clustering (*Upper*), and the identical sample order is maintained (*Lower*). The 354 genes present on the microarrays and mapping to chromosome 17, and for which both DNA copy number and mRNA levels were determined, are ordered by position along the chromosome; selected genes are indicated in color-coded text (see Fig. 2 legend). Fluorescence ratios (test/reference) are depicted by separate log₂ pseudocolor scales (indicated).

of DNA copy number and mRNA levels for genes on chromosome 17 (Fig. 3). The overall patterns of gene amplification and elevated gene expression are quite concordant; i.e., a significant fraction of highly amplified genes appear to be correspondingly highly expressed. The concordance between high-level amplification and increased gene expression is not restricted to chromosome 17. Genome-wide, of 117 high-level DNA amplifications (fluorescence ratios >4, and representing 91 different genes), 62% (representing 54 different genes; see Table 5, which is published as supporting information on the PNAS web site) are found associated with at least moderately elevated mRNA levels (mean-centered fluorescence ratios >2), and 42% (representing 36 different genes) are found associated with comparably highly elevated mRNA levels (mean-centered fluorescence ratios >4).

To determine the extent to which DNA deletion and lower-level amplification (in addition to high-level amplification) are also associated with corresponding alterations in mRNA levels, we performed three separate analyses on the complete data set (4 cell lines and 37 tumors, across 6,095 genes). First, we determined the average mRNA levels for each of five classes of genes, representing DNA deletion, no change, and low-, medium-, and high-level amplification (Fig. 4*a*). For both the

breast cancer cell lines and tumors, average mRNA levels tracked with DNA copy number across all five classes, in a statistically significant fashion (P values for pair-wise Student's t tests comparing adjacent classes: cell lines, 4×10^{-49}, 1×10^{-49}, 5×10^{-5}, 1×10^{-2}; tumors, 1×10^{-43}, 1×10^{-214}, 5×10^{-41}, 1×10^{-4}). A linear regression of the average log(DNA copy number), for each class, against average log(mRNA level) demonstrated that on average, a 2-fold change in DNA copy number was accompanied by 1.4- and 1.5-fold changes in mRNA level for the breast cancer cell lines and tumors, respectively (Fig. 4*a*, regression line not shown). Second, we characterized the distribution of the 6,095 correlations between DNA copy number and mRNA level, each across the 37 tumor samples (Fig. 4*b*). The distribution of correlations forms a normal-shaped curve, but with the peak markedly shifted in the positive direction from zero. This shift is statistically significant, as evidenced in a plot of observed vs. expected correlations (Fig. 4*c*), and reflects a pervasive global influence of DNA copy number alterations on gene expression. Notably, the highest correlations between DNA copy number and mRNA level (the right tail of the distribution in Fig. 4*b*) comprise both amplified and deleted genes (data not shown). Third, we used a linear regression model to estimate the fraction of all variation measured in mRNA levels among the 37
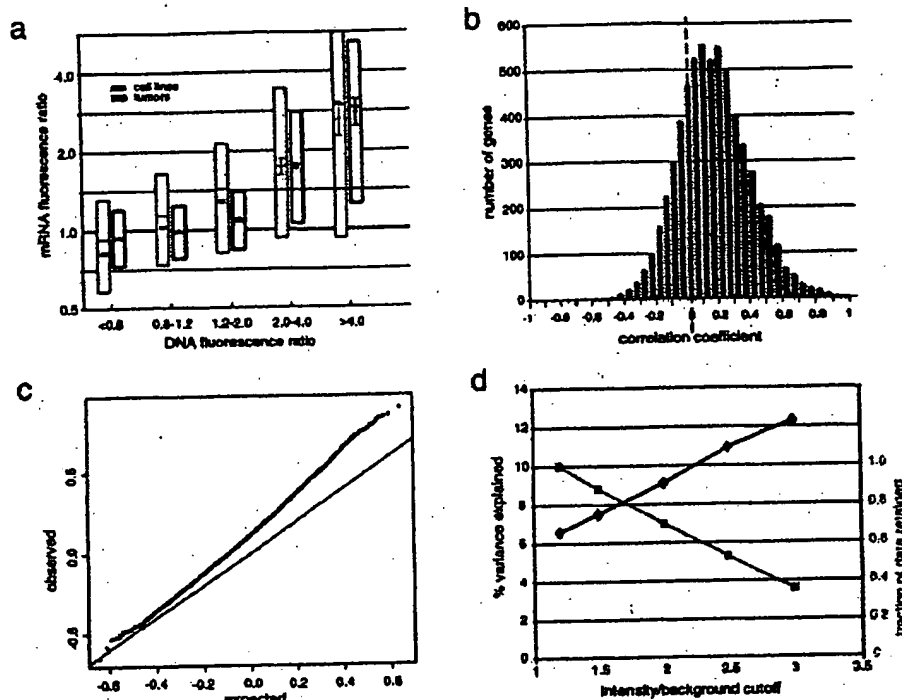
Pollack *et al.*

Fig. 4. Genome-wide influence of DNA copy number alterations on mRNA levels. (a) For breast cancer cell lines (gray) and tumor samples (black), both mean-centered mRNA fluorescence ratio ($\log_2$ scale) quartiles (box plots indicate 25th, 50th, and 75th percentile) and averages (diamonds; Y-value error bars indicate standard errors of the mean) are plotted for each of five classes of genes, representing DNA deletion (tumor/normal ratio < 0.8), no change (0.8–1.2), low- (1.2–2), medium- (2–4), and high-level (>4) amplification. P values for pair-wise Student's t tests, comparing averages between adjacent classes (moving left to right), are 4×10^{-49}, 1×10^{-49}, 5×10^{-5}, 1×10^{-2} (cell lines), and 1×10^{-49}, 1×10^{-214}, 5×10^{-41}, 1×10^{-4} (tumors). (b) Distribution of correlations between DNA copy number and mRNA levels, for 6,095 different human genes across 37 breast tumor samples. (c) Plot of observed versus expected correlation coefficients. The expected values were obtained by randomization of the sample labels in the DNA copy number data set. The line of unity is indicated. (d) Percent variance in gene expression (among tumors) directly explained by variation in gene copy number. Percent variance explained (black line) and fraction of data retained (gray line) are plotted for different fluorescence intensity/background (a rough surrogate for signal/noise) cutoff values. Fraction of data retained is relative to the 1.2 intensity/background cutoff. Details of the linear regression model used to estimate the fraction of variation in gene expression attributable to underlying DNA copy number alteration can be found in the supporting information (see *Estimating the Fraction of Variation in Gene Expression Attributable to Underlying DNA Copy Number Alteration*).

tumors that could be attributed to underlying variation in DNA copy number. From this analysis, we estimate that, overall, about 7% of all of the observed variation in mRNA levels can be explained directly by variation in copy number of the altered genes (Fig. 4d). We can reduce the effects of experimental measurement error on this estimate by using only that fraction of the data most reliably measured (fluorescence intensity/background >3); using that data, our estimate of the percent variation in mRNA levels directly attributed to variation in gene copy number increases to 12% (Fig. 4d). This still undoubtedly represents a significant underestimate, as the observed variation in global gene expression is affected not only by true variation in the expression programs of the tumor cells themselves, but also by the variable presence of non-tumor cell types within clinical samples.

Discussion

This genome-wide, array CGH analysis of DNA copy number alteration in a series of human breast tumors demonstrates the usefulness of defining amplicon boundaries at high resolution (gene-by-gene), and quantitatively measuring amplicon shape, to assist in locating and identifying candidate oncogenes. By analyzing mRNA levels in parallel, we have also discovered that changes in DNA copy number have a large, pervasive, direct effect on global gene expression patterns in both breast cancer

cell lines and tumors. Although the DNA microarrays used in our analysis may display a bias toward characterized and/or highly expressed genes, because we are examining such a large fraction of the genome (approximately 20% of all human genes), and because, as detailed above, we are likely underestimating the contribution of DNA copy number changes to altered gene expression, we believe our findings are likely to be generalizable (but would nevertheless still be remarkable if only applicable to this set of ~6,100 genes).

In budding yeast, aneuploidy has been shown to result in chromosome-wide gene expression biases (13). Two recent studies have begun to examine the global relationship between DNA copy number and gene expression in cancer cells. In agreement with our findings, Phillips *et al.* (14) have shown that with the acquisition of tumorigenicity in an immortalized prostate epithelial cell line, new chromosomal gains and losses resulted in a statistically significant respective increase and decrease in the average expression level of involved genes. In contrast, Platzer *et al.* (15) recently reported that in metastatic colon tumors only ~4% of genes within amplified regions were found more highly (>2-fold) expressed, when compared with normal colonic epithelium. This report differs substantially from our finding that 62% of highly amplified genes in breast cancer exhibit at least 2-fold increased expression. These contrasting findings may reflect methodological differences between the

Pollack et al.

studies. For example, the study of Platzer *et al.* (15) may have systematically under-measured gene expression changes. In this regard it is remarkable that only 14 transcripts of many thousand residing within unamplified chromosomal regions were found to exhibit at least 4-fold altered expression in metastatic colon cancer. Additionally, their reliance on lower-resolution chromosomal CGH may have resulted in poorly delimiting the boundaries of high-complexity amplicons, effectively overcalling regions with amplification. Alternatively, the contrasting findings for amplified genes may represent real biological differences between breast and metastatic colon tumors; resolution of this issue will require further studies.

Our finding that widespread DNA copy number alteration has a large, pervasive and direct effect on global gene expression patterns in breast cancer has several important implications. First, this finding supports a high degree of copy number-dependent gene expression in tumors. Second, it suggests that most genes are not subject to specific autoregulation or dosage compensation. Third, this finding cautions that elevated expression of an amplified gene cannot alone be considered strong independent evidence of a candidate oncogene's role in tumorigenesis. In our study, fully 62% of highly amplified genes demonstrated moderately or highly elevated expression. This highlights the importance of high-resolution mapping of amplicon boundaries and shape [to identify the "driving" gene(s) within amplicons (16)], on a large number of samples, in addition to functional studies. Fourth, this finding suggests that analyzing

the genomic distribution of expressed genes, even within existing microarray gene expression data sets, may permit the inference of DNA copy number aberration, particularly aneuploidy (where gene expression can be averaged across large chromosomal regions; see Fig. 3 and supporting information). Fifth, this finding implies that a substantial portion of the phenotypic uniqueness (and by extension, the heterogeneity in clinical behavior) among patients' tumors may be traceable to underlying variation in DNA copy number. Sixth, this finding supports a possible role for widespread DNA copy number alteration in tumorigenesis (17, 18), beyond the amplification of specific oncogenes and deletion of specific tumor suppressor genes. Widespread DNA copy number alteration, and the concomitant widespread imbalance in gene expression, might disrupt critical stochiometric relationships in cell metabolism and physiology (e.g., proteosome, mitotic spindle), possibly promoting further chromosomal instability and directly contributing to tumor development or progression. Finally, our findings suggest the possibility of cancer therapies that exploit specific or global imbalances in gene expression in cancer.

1. Kallioniemi, A., Kallioniemi, O. P., Sudar, D., Rutovitz, D., Gray, J. W., Waldman, F. & Pinkel, D. (1992) *Science* 258, 818–821.
2. Kallioniemi, A., Kallioniemi, O. P., Piper, J., Tanner, M., Stokke, T., Chen, L., Smith, H. S., Pinkel, D., Gray, J. W. & Waldman, F. M. (1994) *Proc. Natl. Acad. Sci. USA* 91, 2156–2160.
3. Tirkkonen, M., Tanner, M., Karhu, R., Kallioniemi, A., Isola, J. & Kallioniemi, O. P. (1998) *Genes Chromosomes Cancer* 21, 177–184.
4. Forozan, F., Mahlamaki, E. H., Monni, O., Chen, Y., Veldman, R., Jiang, Y., Gooden, G. C., Ethier, S. P., Kallioniemi, A. & Kallioniemi, O. P. (2000) *Cancer Res.* 60, 4519–4525.
5. Solinas-Toldo, S., Lampel, S., Stilgenbauer, S., Nickolenko, J., Benner, A., Dohner, H., Cremer, T. & Lichter, P. (1997) *Genes Chromosomes Cancer* 20, 399–407.
6. Pinkel, D., Segraves, R., Sudar, D., Clark, S., Poole, I., Kowbel, D., Collins, C., Kuo, W. L., Chen, C., Zhai, Y., *et al.* (1998) *Nat. Genet.* 20, 207–211.
7. Pollack, J. R., Perou, C. M., Alizadeh, A. A., Eisen, M. B., Pergamenschikov, A., Williams, C. F., Jeffrey, S. S., Botstein, D. & Brown, P. O. (1999) *Nat. Genet.* 23, 41–46.
8. Perou, C. M., Sorlie, T., Eisen, M. B., van de Rijn, M., Jeffrey, S. S., Rees, C. A., Pollack, J. R., Ross, D. T., Johnsen, H., Akslen, L. A., *et al.* (2000) *Nature (London)* 406, 747–752.
9. Sorlie, T., Perou, C. M., Tibshirani, R., Aas, T., Geisler, S., Johnsen, H., Hastie,

T., Eisen, M. B., van de Rijn, M., Jeffrey, S. S., *et al.* (2001) *Proc. Natl. Acad. Sci. USA* 98, 10869–10874.
10. Schuler, G. D. (1997) *J. Mol. Med.* 75, 694–698.
11. Lander, E. S., Linton, L. M., Birren, B., Nusbaum, C., Zody, M. C., Baldwin, J., Devon, K., Dewar, K., Doyle, M., FitzHugh, W., *et al.* (2001) *Nature (London)* 409, 860–921.
12. Fejzo, M. S., Godfrey, T., Chen, C., Waldman, F. & Gray, J. W. (1998) *Genes Chromosomes Cancer* 22, 105–113.
13. Hughes, T. R., Roberts, C. J., Dai, H., Jones, A. R., Meyer, M. R., Slade, D., Burchard, J., Dow, S., Ward, T. R., Kidd, M. J., *et al.* (2000) *Nat. Genet.* 25, 333–337.
14. Phillips, J. L., Hayward, S. W., Wang, Y., Vasselli, J., Pavlovich, C., Padilla-Nash, H., Pezullo, J. R., Ghadimi, B. M., Grossfeld, G. D., Rivera, A., *et al.* (2001) *Cancer Res.* 61, 8143–8149.
15. Platzer, P., Upender, M. B., Wilson, K., Willis, J., Lutterbaugh, J., Nosrati, A., Willson, J. K., Mack, D., Ried, T. & Markowitz, S. (2002) *Cancer Res.* 62, 1134–1138.
16. Albertson, D. G., Ylstra, B., Segraves, R., Collins, C., Dairkee, S. H., Kowbel, D., Kuo, W. L., Gray, J. W. & Pinkel, D. (2000) *Nat. Genet.* 25, 144–146.
17. Li, R., Yerganian, G., Duesberg, P., Kraemer, A., Willer, A., Rausch, C. & Hehlmann, R. (1997) *Proc. Natl. Acad. Sci. USA* 94, 14506–14511.
18. Rasnick, D. & Duesberg, P. H. (1999) *Biochem. J.* 340, 621–630.

HER-2/neu Breast Cancer Predictive Testing

Julie Sanford Hanna, Ph.D. and Dan Mornin, M.D.

EACH YEAR, OVER 182,000 WOMEN in the United States are diagnosed with breast cancer, and approximately 45,000 die of the disease.[1] Incidence appears to be increasing in the United States at a rate of roughly 2% per year. The reasons for the increase are unclear, but non-genetic risk factors appear to play a large role.[2]

Five-year survival rates range from approximately 65%-85%, depending on demographic group, with a significant percentage of women experiencing recurrence of their cancer within 10 years of diagnosis. One of the factors most predictive for recurrence once a diagnosis of breast cancer has been made is the number of axillary lymph nodes to which tumor has metastasized. Most node-positive women are given adjuvant therapy, which increases their survival. However, 20%-30% of patients without axillary node involvement also develop recurrent disease, and the difficulty lies in how to identify this high-risk subset of patients. These patients could benefit from increased surveillance, early intervention, and treatment.

Prognostic markers currently used in breast cancer recurrence prediction include tumor size, histological grade, steroid hormone receptor status, DNA ploidy, proliferative index, and cathepsin D status. Expression of growth factor receptors and over-expression of the HER-2/neu oncogene have also been identified as having value regarding treatment regimen and prognosis.

HER-2/neu (also known as c-erbB2) is an oncogene that encodes a transmembrane glycoprotein that is homologous to, but distinct from, the epidermal growth factor receptor. Numerous studies have indicated that high levels of expression of this protein are associated with rapid tumor growth, certain forms of therapy resistance, and shorter disease-free survival. The gene has been shown to be amplified and/or overexpressed in 10%-30% of invasive breast cancers and in 40%-60% of intraductal breast carcinoma.[3]

There are two distinct FDA-approved methods by which HER-2/neu status can be evaluated: immunohistochemistry (IHC, HercepTest™) and FISH (fluorescent in situ hybridization, PathVysion™ Kit). Both methods can be performed on archived and current specimens. The first method allows visual assessment of the amount of HER-2/neu protein present on the cell membrane. The latter method allows direct quantification of the level of gene amplification present in the tumor, enabling differentiation between low- versus high-amplification. At least one study has demonstrated a difference in

recurrence risk in women younger than 40 years of age for low- versus high-amplified tumors (54.5% compared to 85.7%); this is compared to a recurrence rate of 16.7% for patients with no HER-2/neu gene amplification.[4] HER-2/neu status may be particularly important to establish in women with small (≤ 1 cm) tumor size.

The choice of methodology for determination of HER-2/neu status depends in part on the clinical setting. FDA approval for the Vysis FISH test was granted based on clinical trials involving 1549 node-positive patients. Patients received one of three different treatments consisting of different doses of cyclophosphamide, Adriamycin, and 5-fluorouracil (CAF). The study showed that patients with amplified HER-2/neu benefited from treatment with higher doses of adriamycin-based therapy, while those with normal HER-2/neu levels did not. The study therefore identified a sub-set of women, who because they did not benefit from more aggressive treatment, did not need to be exposed to the associated side effects. In addition, other evidence indicates that HER-2/neu amplification in node-negative patients can be used as an independent prognostic indicator for early recurrence, recurrent disease at any time and disease-related death.[5] Demonstration of HER-2/neu gene amplification by FISH has also been shown to be of value in predicting response to chemotherapy in stage-2 breast cancer patients.

Selection of patients for Herceptin© (Trastuzumab) monoclonal antibody therapy, however, is based upon demonstration of HER-2/neu protein overexpression using HercepTest™. Studies using Herceptin© in patients with metastatic breast cancer show an increase in time to disease progression, increased response rate to chemotherapeutic agents and a small increase in overall survival rate. The FISH assays have not yet been approved for this purpose, and studies looking at response to Herceptin© in patients with or without gene amplification status determined by FISH are in progress.

In general, FISH and IHC results correlate well. However, subsets of tumors are found which show discordant results; i.e., protein overexpression without gene amplification or lack of protein overexpression with gene amplification. The clinical significance of such results is unclear. Based on the above considerations, HER-2/neu testing at SHMC/PAML will utilize immunohistochemistry (HercepTest©) as a screen, followed by FISH in IHC-negative cases. Alternatively, either method may be ordered individually depending on the clinical setting or clinician preference.

CPT code information

HER-2/neu via IHC

88342   (including interpretive report)

HER-2/neu via FISH

88271×2   Molecular cytogenetics, DNA probe, each
88274   Molecular cytogenetics, interphase in situ hybrid-
          ization, analyze 25-99 cells
88291   Cytogenetics and molecular cytogenetics, interpre-
          tation and report

Procedural Information

Immunohistochemistry is performed using the FDA-approved DAKO antibody kit, Herceptest©. The DAKO kit contains reagents required to complete a two-step immunohisto-chemical staining procedure for routinely processed, paraffin-embedded specimens. Following incubation with the primary rabbit antibody to human HER-2/neu protein, the kit employs a ready-to-use dextran-based visualization reagent. This re-agent consists of both secondary goat anti-rabbit antibody molecules with horseradish peroxidase molecules linked to a common dextran polymer backbone, thus eliminating the need for sequential application of link antibody and peroxidase conjugated antibody. Enzymatic conversion of the subse-quently added chromogen results in formation of visible reaction product at the antigen site. The specimen is then coun-terstained; a pathologist using light-microscopy interprets results.

FISH analysis at SHMC/PAML is performed using the FDA-approved PathVysion™ HER-2/neu DNA probe kit, pro-duced by Vysis, Inc. Formalin fixed, paraffin-embedded breast tissue is processed using routine histological methods, and then slides are treated to allow hybridization of DNA probes to the nuclei present in the tissue section. The Pathvysion™ kit con-tains two direct-labeled DNA probes, one specific for the alphoid repetitive DNA (CEP 17, spectrum orange) present at the chromosome 17 centromere and the second for the HER-2/neu oncogene located at 17q11.2-12 (spectrum green). Enu-meration of the probes allows a ratio of the number of copies of chromosome 17 to the number of copies of HER-2/neu to be obtained; this enables quantification of low versus high amplification levels, and allows an estimate of the percentage of cells with HER-2/neu gene amplification. The clinically relevant distinction is whether the gene amplification is due to increased gene copy number on the two chromosome 17 homologues normally present or an increase in the number of chromosome 17s in the cells. In the majority of cases, ratio equivalents less than 2.0 are indicative of a normal/negative result, ratios of 2.1 and over indicate that amplification is present and to what degree. Interpretation of this data will be performed and reported from the Vysis-certified Cytogenet-ics laboratory at SHMC.

References

1. Wingo, P.A., Tong, T., Bolden, S., "Cancer Statistics", 1995;45:1:8-31.

2. "Cancer Rates and Risks", 4th ed., National Institutes of Health, National Cancer Institute, 1996, p. 120.

3. Slamon, D.J., Clark, G.M., Song, S.G., Levin, W.J., Ullrich, A., McGuire, W.L. "Human breast Cancer: Correlation of relapse and survival with amplification of the her-2/neu oncogene". Science, 235:177-182, 1987.

4. Xing, W.R., Gilchrist, K.W., Harris, C.P., Samson, W., Meisner, L.F. "FISH detection of HER-s/neu oncogene amplification in early onset breast cancer". Breast Cancer Res. And Treatment 39(2):203-212, 1996.

5. Press, M.F. Bernstein, L., Thomas, P.A., Meisner, L.F., Zhou, J.Y., Ma, Y., Hung, G., Robinson, R.A., Harris, C., El-Naggar, A., Slamon, D.J., Phillips, R.N., Ross, J.S., Wolman, S.R., Flom, K.J., "Her-2/neu gene amplification characterized by fluorescence in situ hybridization: poor prognosis in node-negative breast carcinomas", J. Clinical Oncology 15(8):2894-2904, 1997.

IN THE UNITED STATES PATENT AND TRADEMARK OFFICE

In re Application of: Ashkenazi et al.	Group Art Unit: 1647
Serial No.: 09/903,925	Examiner: Fozia Hamid
Filed: July 11, 2001	**CERTIFICATE OF MAILING** I hereby certify that this correspondence is being deposited with the United States Postal Service with sufficient postage as first class mail in an envelope addressed to: Assistant Commissioner of Patents, Washington, D.C. 20231 on
For: SECRETED AND TRANSMEMBRANE POLYPEPTIDES AND NUCLEIC ACIDS	Date

DECLARATION OF AUDREY D. GODDARD, Ph.D UNDER 37 C.F.R. § 1.132

Assistant Commissioner of Patents
Washington, D.C. 20231

Sir:

I, Audrey D. Goddard, Ph.D. do hereby declare and say as follows:

1.   I am a Senior Clinical Scientist at the Experimental Medicine/BioOncology, Medical Affairs Department of Genentech, Inc., South San Francisco, California 94080.

2.   Between 1993 and 2001, I headed the DNA Sequencing Laboratory at the Molecular Biology Department of Genentech, Inc. During this time, my responsibilities included the identification and characterization of genes contributing to the oncogenic process, and determination of the chromosomal localization of novel genes.

3.   My scientific Curriculum Vitae, including my list of publications, is attached to and forms part of this Declaration (Exhibit A).

4.   I am familiar with a variety of techniques known in the art for detecting and quantifying the amplification of oncogenes in cancer, including the quantitative TaqMan PCR (i.e., "gene amplification") assay described in the above captioned patent application.

5.   The TaqMan PCR assay is described, for example, in the following scientific publications: Higuchi et al., Biotechnology 10:413-417 (1992) (Exhibit B); Livak et al., PCR Methods Appl., 4:357-362 (1995) (Exhibit C) and Heid et al., Genome Res. 6:986-994 (1996) (Exhibit D). Briefly, the assay is based on the principle that successful PCR yields a fluorescent signal due to Taq DNA polymerase-mediated exonuclease digestion of a fluorescently labeled oligonucleotide that is homologous to a sequence between two PCR primers. The extent of digestion depends directly on the amount of PCR, and can be quantified accurately by measuring the increment in fluorescence that results from decreased energy transfer. This is an extremely sensitive technique, which allows detection in the exponential phase of the PCR reaction and, as a result, leads to accurate determination of gene copy number.

6.   The quantitative fluorescent TaqMan PCR assay has been extensively and successfully used to characterize genes involved in cancer development and progression. Amplification of protooncogenes has been studied in a variety of human tumors, and is widely considered as having etiological, diagnostic and prognostic significance. This use of the quantitative TaqMan PCR assay is exemplified by the following scientific publications: Pennica et al., Proc. Natl. Acad. Sci. USA 95(25):14717-14722 (1998) (Exhibit E); Pitti et al., Nature 396(6712):699-703 (1998) (Exhibit F) and Bieche et al., Int. J. Cancer 78:661-666 (1998) (Exhibit G), the first two of which I am co-author. In particular, Pennica et al. have used the quantitative TaqMan PCR assay to study relative gene amplification of WISP and c-myc in various cell lines, colorectal tumors and normal mucosa. Pitti et al. studied the genomic amplification of a decoy receptor for Fas ligand in lung and colon cancer, using the quantitative TaqMan PCR assay. Bieche et al. used the assay to study gene amplification in breast cancer.

-2-

7.   It is my personal experience that the quantitative TaqMan PCR technique is technically sensitive enough to detect at least a 2-fold increase in gene copy number relative to control. It is further my considered scientific opinion that an at least 2-fold increase in gene copy number in a tumor tissue sample relative to a normal (i.e., non-tumor) sample is significant and useful in that the detected increase in gene copy number in the tumor sample relative to the normal sample serves as a basis for using relative gene copy number as quantitated by the TaqMan PCR technique as a diagnostic marker for the presence or absence of tumor in a tissue sample of unknown pathology. Accordingly, a gene identified as being amplified at least 2-fold by the quantitative TaqMan PCR assay in a tumor sample relative to a normal sample is useful as a marker for the diagnosis of cancer, for monitoring cancer development and/or for measuring the efficacy of cancer therapy.

8.   I declare further that all statements made herein of my own knowledge are true and that all statements made on information and belief are believed to be true. I declare that these statements were made with the knowledge that willful false statements and the like so made are punishable by fine or imprisonment, or both, under Section 1001 of Title 18 of the United States Code, and that such willful false statements may jeopardize the validity of the application or any patent issuing thereon.

Jan. 16, 2003

Date

Audrey Goddard

Audrey D. Goddard, Ph.D.

AUDREY D. GODDARD, Ph.D.

Genentech, Inc.
1 DNA Way
South San Francisco, CA, 94080
650.225.6429
goddarda@gene.com

110 Congo St.
San Francisco, CA, 94131
415.841.9154
415.819.2247 (mobile)
agoddard@pacbell.net

PROFESSIONAL EXPERIENCE

Genentech, Inc.   **1993-present**
South San Francisco, CA

2001 - present   Senior Clinical Scientist
Experimental Medicine / BioOncology, Medical Affairs

Responsibilities:
- *Companion diagnostic oncology products*
- *Acquisition of clinical samples from Genentech's clinical trials for translational research*
- *Translational research using clinical specimen and data for drug development and diagnostics*
- *Member of Development Science Review Committee, Diagnostic Oversight Team, 21 CFR Part 11 Subteam*

Interests:
- *Ethical and legal implications of experiments with clinical specimens and data*
- *Application of pharmacogenomics in clinical trials*

1998 - 2001   Senior Scientist
Head of the DNA Sequencing Laboratory, Molecular Biology Department, Research

Responsibilities:
- *Management of a laboratory of up to nineteen –including postdoctoral fellow, associate scientist, senior research associate and research assistants/associate levels*
- *Management of a $750K budget*
- *DNA sequencing core facility supporting a 350+ person research facility.*
- *DNA sequencing for high throughput gene discovery, - ESTs, cDNAs, and constructs*
- *Genomic sequence analysis and gene identification*
- *DNA sequence and primary protein analysis*

Research:
- *Chromosomal localization of novel genes*
- *Identification and characterization of genes contributing to the oncogenic process*
- *Identification and characterization of genes contributing to inflammatory diseases*
- *Design and development of schemes for high throughput genomic DNA sequence analysis*
- *Candidate gene prediction and evaluation*

1993 - 1998   Scientist
Head of the DNA Sequencing Laboratory, Molecular Biology Department, Research

Responsibilities
- *DNA sequencing core facility supporting a 350+ person research facility·*
- *Assumed responsibility for a pre-existing team of five technicians and expanded the group into fifteen, introducing a level of middle management and additional areas of research*
- *Participated in the development of the basic plan for high throughput secreted protein discovery program – sequencing strategies, data analysis and tracking, database design*
- *High throughput EST and cDNA sequencing for new gene identification.*
- *Design and implementation of analysis tools required for high throughput gene identification.*
- *Chromosomal localization of genes encoding novel secreted proteins.*

Research:
- *Genomic sequence scanning for new gene discovery.*
- *Development of signal peptide selection methods.*
- *Evaluation of candidate disease genes.*
- *Growth hormone receptor gene SNPs in children with Idiopathic short stature*

Imperial Cancer Research Fund   **1989-1992**
London, UK with Dr. Ellen Solomon

6/89 –12/92 Postdoctoral Fellow
- Cloning and characterization of the genes fused at the acute promyelocytic leukemia translocation breakpoints on chromosomes 17 and 15.
- Prepared a successfully funded European Union multi-center grant application

McMaster University   **1983**
Hamilton, Ontario, Canada with Dr. G. D. Sweeney

5/83 – 8/83: NSERC Summer Student
- *In vitro* metabolism of β-naphthoflavone in C57Bl/6J and DBA mice

EDUCATION

Ph.D.
"Phenotypic and genotypic effects of mutations in the human retinoblastoma gene."
Supervisor: Dr. R. A. Phillips

University of Toronto
Toronto, Ontario, Canada.   1989
Department of Medical
Biophysics.

Honours B.Sc
"The *in vitro* metabolism of the cytochrome P-448 inducer β-naphthoflavone in C57BL/6J mice."
Supervisor: Dr. G. D. Sweeney

McMaster University,
Hamilton, Ontario, Canada.   1983
Department of Biochemistry

ACADEMIC AWARDS

Imperial Cancer Research Fund Postdoctoral Fellowship	1989-1992
Medical Research Council Studentship	1983-1988
NSERC Undergraduate Summer Research Award	1983
Society of Chemical Industry Merit Award (Hons. Biochem.)	1983
Dr. Harry Lyman Hooker Scholarship	1981-1983
J.L.W. Gill Scholarship	1981-1982
Business and Professional Women's Club Scholarship	1980-1981
Wyerhauser Foundation Scholarship	1979-1980

INVITED PRESENTATIONS

Genentech's gene discovery pipeline: High throughput identification, cloning and characterization of novel genes. Functional Genomics: From Genome to Function, Litchfield Park, AZ, USA. October 2000

High throughput identification, cloning and characterization of novel genes. G2K:Back to Science, Advances in Genome Biology and Technology I. Marco Island, FL, USA. February 2000

Quality control in DNA Sequencing: The use of Phred and Phrap. Bay Area Sequencing Users Meeting, Berkeley, CA, USA. April 1999

High throughput secreted protein identification and cloning. Tenth International Genome Sequencing and Analysis Conference, Miami, FL, USA. September 1998

The evolution of DNA sequencing: The Genentech perspective. Bay Area Sequencing Users Meeting, Berkeley, CA, USA. May 1998

Partial Growth Hormone Insensitivity: The role of GH-receptor mutations in Idiopathic Short Stature. Tenth Annual National Cooperative Growth Study Investigators Meeting, San Francisco, CA, USA. October, 1996

Growth hormone (GH) receptor defects are present in selected children with non-GH-deficient short stature: A molecular basis for partial GH-insensitivity. 76th Annual Meeting of The Endocrine Society, Anaheim, CA, USA. June 1994

A previously uncharacterized gene, myl, is fused to the retinoic acid receptor alpha gene in acute promyelocytic leukemia. XV International Association for Comparative Research on Leukemia and Related Disease, Padua, Italy. October 1991

PATENTS

Goddard A, Godowski PJ, Gurney AL. NL2 Tie ligand homologue polypeptide. Patent Number: 6,455,496. Date of Patent: Sept. 24, 2002.

Goddard A, Godowski PJ and Gurney AL. NL3 Tie ligand homologue nucleic acids. Patent Number: 6,426,218. Date of Patent: July 30, 2002.

Godowski P, Gurney A, Hillan KJ, Botstein D, **Goddard A**, Roy M, Ferrara N, Tumas D, Schwall R. NL4 Tie ligand homologue nucleic acid. Patent Number: 6,4137,770. Date of Patent: July 2, 2002.

Ashkenazi A, Fong S, **Goddard A**, Gurney AL, Napier MA, Tumas D, Wood WI. Nucleic acid encoding A-33 related antigen poly peptides. Patent Number: 6,410,708. Date of Patent:: Jun. 25, 2002.

Botstein DA, Cohen RL, **Goddard AD**, Gurney AL, Hillan KJ, Lawrence DA, Levine AJ, Pennica D, Roy MA and Wood WI. WISP polypeptides and nucleic acids encoding same. Patent Number: 6,387,657. Date of Patent: May 14, 2002.

Goddard A, Godowski PJ and Gurney AL. Tie ligands. Patent Number: 6,372,491. Date of Patent: April 16, 2002.

Godowski PJ, Gurney AL, **Goddard A** and Hillan K. TIE ligand homologue antibody. Patent Number: 6,350,450. Date of Patent: Feb. 26, 2002.

Fong S, Ferrara N, **Goddard A**, Godowski PJ, Gurney AL, Hillan K and Williams PM. Tie receptor tyrosine kinase ligand homologues. Patent Number: 6,348,351. Date of Patent: Feb. 19, 2002.

Goddard A, Godowski PJ and Gurney AL. Ligand homologues. Patent Number: 6,348,350. Date of Patent: Feb. 19, 2002.

Attie KM, Carlsson LMS, Gesundheit N and **Goddard A**. Treatment of partial growth hormone insensitivity syndrome. Patent Number: 6,207,640. Date of Patent: March 27, 2001.

Fong S, Ferrara N, **Goddard A**, Godowski PJ, Gurney AL, Hillan K and Williams PM. Nucleic acids encoding NL-3. Patent Number: 6,074,873. Date of Patent: June 13, 2000

Attie K, Carlsson LMS, Gesunheit N and **Goddard A**. Treatment of partial growth hormone insensitivity syndrome. Patent Number: 5,824,642. Date of Patent: October 20, 1998

Attie K, Carlsson LMS, Gesunheit N and **Goddard A**. Treatment of partial growth hormone insensitivity syndrome. Patent Number: 5,646,113. Date of Patent: July 8, 1997

Multiple additional provisional applications filed

PUBLICATIONS

Seshasayee D, Dowd P, Gu Q, Erickson S, **Goddard AD** Comparative sequence analysis of the *HER2* locus in mouse and man. Manuscript in preparation.

Abuzzahab MJ, **Goddard A**, Grigorescu F, Lautier C, Smith RJ and Chernausek SD. Human IGF-1 receptor mutations resulting in pre- and post-natal growth retardation. Manuscript in preparation.

Aggarwal S, Xie, M-H, Foster J, Frantz G, Stinson J, Corpuz RT, Simmons L, Hillan K, Yansura DG, Vandlen RL, **Goddard AD** and Gurney AL. FHFR, a novel receptor for the fibroblast growth factors. Manuscript submitted.

Adams SH, Chui C, Schilbach SL, Yu XX, **Goddard AD**, Grimaldi JC, Lee J, Dowd P, Colman S., Lewin DA. (2001) BFIT, a unique acyl-CoA thioesterase induced in thermogenic brown adipose tissue: Cloning, organization of the human gene, and assessment of a potential link to obesity. *Biochemical Journal* **360**: 135-142.

Lee J. Ho WH. Maruoka M. Corpuz RT. Baldwin DT. Foster JS. **Goddard AD**. Yansura DG. Vandlen RL. Wood WI. Gurney AL. (2001) IL-17E, a novel proinflammatory ligand for the IL-17 receptor homolog IL-17Rh1. *Journal of Biological Chemistry* **276**(2): 1660-1664.

Xie M-H, Aggarwal S, Ho W-H, Foster J, Zhang Z, Stinson J, Wood WI, **Goddard AD** and Gurney AL. (2000) Interleukin (IL)-22, a novel human cytokine that signals through the interferon-receptor related proteins CRF2-4 and IL-22R. *Journal of Biological Chemistry* **275**: 31335-31339.

Weiss GA, Watanabe CK, Zhong A, **Goddard A** and Sidhu SS. (2000) Rapid mapping of protein functional epitopes by combinatorial alanine scanning. *Proc. Natl. Acad. Sci. USA* **97**: 8950-8954.

Guo S, Yamaguchi Y, Schilbach S, Wada T.;Lee J, **Goddard A**, French D , Handa H, Rosenthal A. (2000) A regulator of transcriptional elongation controls vertebrate neuronal development. *Nature* **408**: 366-369.

Yan M, Wang L-C, Hymowitz SG, Schilbach S, Lee J, **Goddard A**, de Vos AM, Gao WQ, Dixit VM. (2000) Two-amino acid molecular switch in an epithelial morphogen that regulates binding to two distinct receptors. *Science* **290**: 523-527.

Sehl PD, Tai JTN, Hillan KJ, Brown LA, **Goddard A**, Yang R, Jin H and Lowe DG. (2000) Application of cDNA microarrays in determining molecular phenotype in cardiac growth, development, and response to injury. *Circulation* **101**: 1990-1999.

Guo S, Brush J, Teraoka H, **Goddard A**, Wilson SW, Mullins MC and Rosenthal A. (1999) Development of noradrenergic neurons in the zebrafish hindbrain requires BMP, FGF8, and the homeodomain protein soulless/Phox2A. *Neuron* **24**: 555-566.

Stone D, Murone, M, Luoh, S, Ye W, Armanini P, Gurney A, Phillips HS, Brush, J, **Goddard A**, de Sauvage FJ and Rosenthal A. (1999) Characterization of the human suppressor of fused; a negative regulator of the zinc-finger transcription factor Gli. *J. Cell Sci.* **112**: 4437-4448.

Xie M-H, Holcomb I, Deuel B, Dowd P, Huang A, Vagts A, Foster J, Liang J, Brush J, Gu Q, Hillan K, **Goddard A** and Gurney, A.L. (1999) FGF-19, a novel fibroblast growth factor with unique specificity for FGFR4. *Cytokine* **11**: 729-735.

Yan M, Lee J, Schilbach S, **Goddard A** and Dixit V. (1999) mE10, a novel caspase recruitment domain-containing proapoptotic molecule. *J. Biol. Chem.* **274**(15): 10287-10292.

Gurney AL, Marsters SA, Huang RM, Pitti RM, Mark DT, Baldwin DT, Gray AM, Dowd P, Brush J, Heldens S, Schow P, **Goddard AD**, Wood WI, Baker KP, Godowski PJ and Ashkenazi A. (1999) Identification of a new member of the tumor necrosis factor family and its receptor, a human ortholog of mouse GITR. *Current Biology* **9**(4): 215-218.

Ridgway JBB, Ng E, Kern JA ,Lee J, Brush J, **Goddard A** and Carter P. (1999) Identification of a human anti-CD55 single-chain Fv by subtractive panning of a phage library using tumor and nontumor cell lines. *Cancer Research* **59**: 2718-2723.

Pitti RM, Marsters SA, Lawrence DA, Roy M, Kischkel FC, Dowd P, Huang A, Donahue CJ, Sherwood SW, Baldwin DT, Godowski PJ, Wood WI, Gurney AL, Hillan KJ, Cohen RL, **Goddard AD**, Botstein D and Ashkenazi A. (1998) Genomic amplification of a decoy receptor for Fas ligand in lung and colon cancer. *Nature* **396**(6712): 699-703.

Pennica D, Swanson TA, Welsh JW, Roy MA, Lawrence DA, Lee J, Brush J, Taneyhill LA, Deuel B, Lew M, Watanabe C, Cohen RL, Melhem MF, Finley GG, Quirke P, **Goddard AD**, Hillan KJ, Gurney AL, Botstein D and Levine AJ. (1998) WISP genes are members of the connective tissue growth factor family that are up-regulated in wnt-1-transformed cells and aberrantly expressed in human colon tumors. *Proc. Natl. Acad. Sci. USA.* **95**(25): 14717-14722.

Yang RB, Mark MR, Gray A, Huang A, Xie MH, Zhang M, **Goddard A**, Wood WI, Gurney AL and Godowski PJ. (1998) Toll-like receptor-2 mediates lipopolysaccharide-induced cellular signalling. *Nature* **395**(6699): 284-288.

Merchant AM, Zhu Z, Yuan JQ, **Goddard A**, Adams CW, Presta LG and Carter P. (1998) An efficient route to human bispecific IgG. *Nature Biotechnology* **16**(7): 677-681.

Marsters SA, Sheridan JP, Pitti RM, Brush J, **Goddard A** and Ashkenazi A. (1998) Identification of a ligand for the death-domain-containing receptor Apo3. *Current Biology* **8**(9): 525-528.

Xie J, Murone M, Luoh SM, Ryan A, Gu Q, Zhang C, Bonifas JM, Lam CW, Hynes M, **Goddard A**, Rosenthal A, Epstein EH Jr. and de Sauvage FJ. (1998) Activating Smoothened mutations in sporadic basal-cell carcinoma. *Nature.* **391**(6662): 90-92.

Marsters SA, Sheridan JP, Pitti RM, Huang A, Skubatch M, Baldwin D, Yuan J, Gurney A, **Goddard AD**, Godowski P and Ashkenazi A. (1997) A novel receptor for Apo2L/TRAIL contains a truncated death domain. *Current Biology.* **7**(12): 1003-1006.

Hynes M, Stone DM, Dowd M, Pitts-Meek S, **Goddard A**, Gurney A and Rosenthal A. (1997) Control of cell pattern in the neural tube by the zinc finger transcription factor *Gli-1*. *Neuron* **19**: 15–26.

Sheridan JP, Marsters SA, Pitti RM, Gurney A., Skubatch M, Baldwin D, Ramakrishnan L, Gray CL, Baker K, Wood WI, **Goddard AD**, Godowski P, and Ashkenazi A. (1997) Control of TRAIL-Induced Apoptosis by a Family of Signaling and Decoy Receptors. *Science* **277** (5327): 818-821.

Goddard AD, Dowd P, Chernausek S, Geffner M, Gertner J, Hintz R, Hopwood N, Kaplan S, Plotnick L, Rogol A, Rosenfield R, Saenger P, Mauras N, Hershkopf R, Angulo M and Attie, K. (1997) Partial growth hormone insensitivity: The role of growth hormone receptor mutations in idiopathic short stature. *J. Pediatr.* **131**: S51-55.

Klein RD, Sherman D, Ho WH, Stone D, Bennett GL, Moffat B, Vandlen R, Simmons L, Gu Q, Hongo JA, Devaux B, Poulsen K, Armanini M, Nozaki C, Asai N, **Goddard A**, Phillips H, Henderson CE, Takahashi M and Rosenthal A. (1997) A GPI-linked protein that interacts with Ret to form a candidate neurturin receptor. *Nature.* **387**(6634): 717-21.

Stone DM, Hynes M, Armanini M, Swanson TA, Gu Q, Johnson RL, Scott MP, Pennica D, **Goddard A**, Phillips H, Noll M, Hooper JE, de Sauvage F and Rosenthal A. (1996) The tumour-suppressor gene patched encodes a candidate receptor for Sonic hedgehog. *Nature* **384**(6605): 129-34.

Marsters SA, Sheridan JP, Donahue CJ, Pitti RM, Gray CL, **Goddard AD**, Bauer KD and Ashkenazi A. (1996) Apo-3, a new member of the tumor necrosis factor receptor family, contains a death domain and activates apoptosis and NF-kappa β. *Current Biology* **6**(12): 1669-76.

Rothe M, Xiong J, Shu HB, Williamson K, **Goddard A** and Goeddel DV. (1996) I-TRAF is a novel TRAF-interacting protein that regulates TRAF-mediated signal transduction. *Proc. Natl. Acad. Sci. USA* **93**: 8241-8246.

Yang M, Luoh SM, **Goddard A**, Reilly D, Henzel W and Bass S. (1996) The bglX gene located at 47.8 min on the Escherichia coli chromosome encodes a periplasmic beta-glucosidase. *Microbiology* **142**: 1659-65.

Goddard AD and Black DM. (1996) Familial Cancer in <u>Molecular Endocrinology of Cancer.</u> Waxman, J. Ed. Cambridge University Press, Cambridge UK, pp.187-215.

Treanor JJS, Goodman L, de Sauvage F, Stone DM, Poulson KT, Beck CD, Gray C, Armanini MP, Pollocks RA, Hefti F, Phillips HS, **Goddard A**, Moore MW, Buj-Bello A, Davis AM, Asai N, Takahashi M, Vandlen R, Henderson CE and Rosenthal A. (1996) Characterization of a receptor for GDNF. *Nature* **382**: 80-83.

Klein RD, Gu Q, **Goddard A** and Rosenthal A. (1996) Selection for genes encoding secreted proteins and receptors. *Proc. Natl. Acad. Sci. USA* **93**: 7108-7113.

Winslow JW, Moran P, Valverde J, Shih A, Yuan JQ, Wong SC, Tsai SP, **Goddard A**, Henzel WJ, Hefti F and Caras I. (1995) Cloning of AL-1, a ligand for an Eph-related tyrosine kinase receptor involved in axon bundle formation. *Neuron* **14**: 973-981.

Bennett BD, Zeigler FC, Gu Q, Fendly B, **Goddard AD**, Gillett N and Matthews W. (1995) Molecular cloning of a ligand for the EPH-related receptor protein-tyrosine kinase Htk. *Proc. Natl. Acad. Sci. USA* **92**: 1866-1870.

Huang X, Yuang J, **Goddard A**, Foulis A, James RF, Lernmark A, Pujol-Borrell R, Rabinovitch A, Somoza N and Stewart TA. (1995) Interferon expression in the pancreases of patients with type I diabetes. *Diabetes* **44**: 658-664.

Goddard AD, Yuan JQ, Fairbairn L, Dexter M, Borrow J, Kozak C and Solomon E. (1995) Cloning of the murine homolog of the leukemia-associated PML gene. *Mammalian Genome* **6**: 732-737.

Goddard AD, Covello R, Luoh SM, Clackson T, Attie KM, Gesundheit N, Rundle AC, Wells JA, Carlsson LMTI and The Growth Hormone Insensitivity Study Group. (1995) Mutations of the growth hormone receptor in children with idiopathic short stature. *N. Engl. J. Med.* **333**: 1093-1098.

Kuo SS, Moran P, Gripp J, Armanini M, Phillips HS, **Goddard A** and Caras IW. (1994) Identification and characterization of Batk, a predominantly brain-specific non-receptor protein tyrosine kinase related to Csk. *J. Neurosci. Res.* **38**: 705-715.

Mark MR, Scadden DT, Wang Z, Gu Q, **Goddard A** and Godowski PJ. (1994) Rse, a novel receptor-type tyrosine kinase with homology to Axl/Ufo, is expressed at high levels in the brain. *Journal of Biological Chemistry* **269**: 10720-10728.

Borrow J, Shipley J, Howe K, Kiely F, **Goddard A**, Sheer D, Srivastava A, Antony AC, Fioretos T, Mitelman F and Solomon E. (1994) Molecular analysis of simple variant translocations in acute promyelocytic leukemia. *Genes Chromosomes Cancer* **9**: 234-243.

Goddard AD and Solomon E. (1993) Genetics of Cancer. *Adv. Hum. Genet.* **21**: 321-376.

Borrow J, **Goddard AD**, Gibbons B, Katz F, Swirsky D, Fioretos T, Dube I, Winfield DA, Kingston J, Hagemeijer A, Rees JKH, Lister AT and Solomon E. (1992) Diagnosis of acute promyelocytic leukemia by RT-PCR: Detection of *PML-RARA* and *RARA-PML* fusion transcripts. *Br. J. Haematol.* **82**: 529-540.

Goddard AD, Borrow J and Solomon E. (1992) A previously uncharacterized gene, PML, is fused to the retinoic acid receptor alpha gene in acute promyelocytic leukemia. *Leukemia* **6 Suppl 3**: 117S–119S.

Zhu X, Dunn JM, **Goddard AD**, Squire JA, Becker A, Phillips RA and Gallie BL. (1992) Mechanisms of loss of heterozygosity in retinoblastoma. *Cytogenet. Cell. Genet.* **59**: 248-252.

Foulkes W, **Goddard A** and Patel K. (1991) Retinoblastoma linked with Seascale [letter]. *British Med. J.* **302**: 409.

Goddard AD, Borrow J, Freemont PS and Solomon E. (1991) Characterization of a novel zinc finger gene disrupted by the t(15;17) in acute promyelocytic leukemia. *Science* **254**: 1371-1374.

Solomon E, Borrow J and **Goddard AD**. (1991) Chromosomal aberrations in cancer. *Science* **254**: 1153-1160.

Pajunen L, Jones TA, **Goddard A**, Sheer D, Solomon E, Pihlajaniemi T and Kivirikko KI. (1991) Regional assignment of the human gene coding for a multifunctional peptide (P4HB) acting as the β–subunit of prolyl-4-hydroxylase and the enzyme protein disulfide isomerase to 17q25. *Cytogenet. Cell. Genet.* **56**: 165-168.

Borrow J, Black DM, **Goddard AD**, Yagle MK, Frischauf A.-M and Solomon E. (1991) Construction and regional localization of a *Not*I linking library from human chromosome 17q. *Genomics* **10**: 477–480.

Borrow J, **Goddard AD**, Sheer D and Solomon E. (1990) Molecular analysis of acute promyelocytic leukemia breakpoint cluster region on chromosome 17. *Science* **249**: 1577-1580.

Myers JC, Jones TA, Pohjolainen E-R, Kadri AS, **Goddard AD**, Sheer D, Solomon E and Pihlajaniemi T. (1990) Molecular cloning of 5(IV) collagen and assignment of the gene to the region of the region of the X-chromosome containing the Alport Syndrome locus. *Am. J. Hum. Genet.* **46**: 1024-1033.

Gallie BL, Squire JA, **Goddard A**, Dunn JM, Canton M, Hinton D, Zhu X and Phillips RA. (1990) Mechanisms of oncogenesis in retinoblastoma. *Lab. Invest.* **62**: 394-408.

Goddard AD, Phillips RA, Greger V, Passarge E, Hopping W, Gallie BL and Horsthemke B. (1990) Use of the RB1 cDNA as a diagnostic probe in retinoblastoma families. *Clinical Genetics* **37**: 117-126.

Zhu XP, Dunn JM, Phillips RA, **Goddard AD**, Paton KE, Becker A and Gallie BL. (1989) Germline, but not somatic, mutations of the RB1 gene preferentially involve the paternal allele. *Nature* **340**: 312-314.

Gallie BL, Dunn JM, **Goddard A**, Becker A and Phillips RA. (1988) Identification of mutations in the putative retinoblastoma gene. In Molecular Biology of The Eye: Genes, Vision and Ocular Disease. UCLA Symposia on Molecular and Cellular Biology, New Series, Volume 88. J. Piatigorsky, T. Shinohara and P.S. Zelenka, Eds. Alan R. Liss, Inc., New York, 1988, pp. 427-436.

Goddard AD, Balakier H, Canton M, Dunn J, Squire J, Reyes E, Becker A, Phillips RA and Gallie BL. (1988) Infrequent genomic rearrangement and normal expression of the putative RB1 gene in retinoblastoma tumors. *Mol. Cell. Biol.* **8**: 2082-2088.

Squire J, Dunn J, **Goddard A**, Hoffman T, Musarella M, Willard HF, Becker AJ, Gallie BL and Phillips RA. (1986) Cloning of the esterase D gene: A polymorphic gene probe closely linked to the retinoblastoma locus on chromosome 13. *Proc. Natl. Acad. Sci.* USA **83**: 6573-6577.

Squire J, **Goddard AD**, Canton M, Becker A, Phillips RA and Gallie BL (1986) Tumour induction by the retinoblastoma mutation is independent of N-*myc* expression. *Nature* **322**: 555-557.

Goddard AD, Heddle JA, Gallie BL and Phillips RA. (1985) Radiation sensitivity of fibroblasts of bilateral retinoblastoma patients as determined by micronucleus induction *in vitro*. *Mutation Research* **152**: 31-38.

RESEARCH/

SIMULTANEOUS AMPLIFICATION AND DETECTION OF SPECIFIC DNA SEQUENCES

Russell Higuchi*, Gavin Dollinger[1], P. Sean Walsh and Robert Griffith

Roche Molecular Systems, Inc., 1400 53rd St., Emeryville, CA 94608. [1]Chiron Corporation, 1400 53rd St., Emeryville, CA 94608. *Corresponding author.

We have enhanced the polymerase chain reaction (PCR) such that specific DNA sequences can be detected without opening the reaction tube. This enhancement requires the addition of ethidium bromide (EtBr) to a PCR. Since the fluorescence of EtBr increases in the presence of double-stranded (ds) DNA an increase in fluorescence in such a PCR indicates a positive amplification, which can be easily monitored externally. In fact, amplification can be continuously monitored in order to follow its progress. The ability to simultaneously amplify specific DNA sequences and detect the product of the amplification both simplifies and improves PCR and may facilitate its automation and more widespread use in the clinic or in other situations requiring high sample throughput.

Although the potential benefits of PCR[1] to clinical diagnostics are well known[2,3], it is still not widely used in this setting, even though it is four years since thermostable DNA polymerases[4] made PCR practical. Some of the reasons for its slow acceptance are high cost, lack of automation of pre- and post-PCR processing steps, and false positive results from carryover-contamination. The first two points are related in that labor is the largest contributor to cost at the present stage of PCR development. Most current assays require some form of "downstream" processing once thermocycling is done in order to determine whether the target DNA sequence was present and has amplified. These include DNA hybridization[3,6], gel electrophoresis with or without use of restriction digestion[7,8], HPLC[9], or capillary electrophoresis[10]. These methods are labor-intense, have low throughput, and are difficult to automate. The third point is also closely related to downstream processing. The handling of the PCR product in these downstream processes increases the chances that amplified DNA will spread through the typing lab, resulting in a risk of

"carryover" false positives in subsequent testing[11].

These downstream processing steps would be eliminated if specific amplification and detection of amplified DNA took place simultaneously within an unopened reaction vessel. Assays in which such different processes take place without the need to separate reaction components have been termed "homogeneous". No truly homogeneous PCR assay has been demonstrated to date, although progress towards this end has been reported. Chehab, et al.[12], developed a PCR product detection scheme using fluorescent primers that resulted in a fluorescent PCR product. Allele-specific primers, each with different fluorescent tags, were used to indicate the genotype of the DNA. However, the unincorporated primers must still be removed in a downstream process in order to visualize the result. Recently, Holland, et al.[13], developed an assay in which the endogenous 5′ exonuclease assay of Taq DNA polymerase was exploited to cleave a labeled oligonucleotide probe. The probe would only cleave if PCR amplification had produced its complementary sequence. In order to detect the cleavage products, however, a subsequent process is again needed.

We have developed a truly homogeneous assay for PCR and PCR product detection based upon the greatly increased fluorescence that ethidium bromide and other DNA binding dyes exhibit when they are bound to ds-DNA[14-16]. As outlined in Figure 1, a prototypic PCR
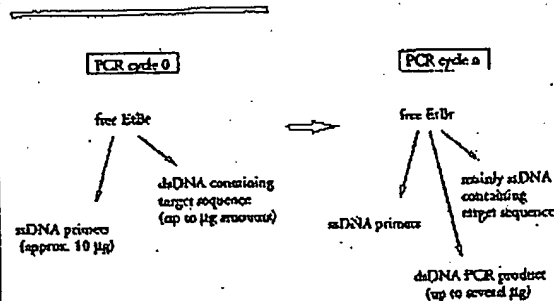

FIGURE 1 Principle of simultaneous amplification and detection of PCR product. The components of a PCR containing EtBr that are fluorescent are listed—EtBr itself, EtBr bound to either ssDNA or dsDNA. There is a large fluorescence enhancement when EtBr is bound to DNA and binding is greatly enhanced when DNA is double-stranded. After sufficient (n) cycles of PCR, the net increase in dsDNA results in additional EtBr binding, and a net increase in total fluorescence.
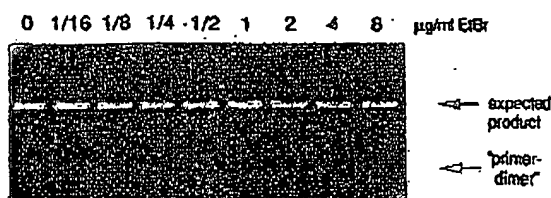
0 1/16 1/8 1/4 ·1/2 1   2   4   8 · µg/ml EtBr

←◁— expected
product

←◁— "primer-
dimer"

FIGURE 2 Gel electrophoresis of PCR amplification products of the human, nuclear gene, HLA DQα, made in the presence of increasing amounts of EtBr (up to 8 µg/ml). The presence of EtBr has no obvious effect on the yield or specificity of amplification.
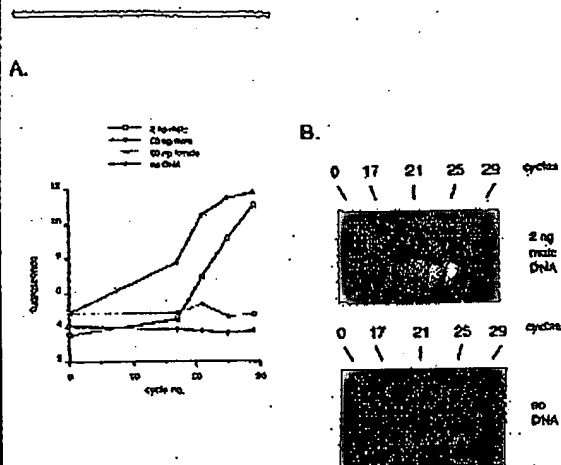
A.

B.

0   17 21 25 29 cycles
 \   \   I   /   /

2 ng
male
DNA

0   17 21 25 29 cycles
 \   \   I   /   /

no
DNA

FIGURE 3 (A) Fluorescence measurements from PCRs that contain 0.5 µg/ml EtBr and that are specific for Y-chromosome repeat sequences. Five replicate PCRs were begun containing each of the DNAs specified. At each indicated cycle, one of the five replicate PCRs for each DNA was removed from thermocycling and its fluorescence measured. Units of fluorescence are arbitrary. (B) UV photography of PCR tubes (0.5 ml Eppendorf-style, polypropylene micro-centrifuge tubes) containing reactions, those starting from 2 ng male DNA and control reactions without any DNA, from (A).

begins with primers that are single-stranded DNA (ss-DNA), dNTPs, and DNA polymerase. An amount of dsDNA containing the target sequence (target DNA) is also typically present. This amount can vary, depending on the application, from single-cell amounts of DNA[17] to micrograms per PCR[18]. If EtBr is present, the reagents that will fluoresce, in order of increasing fluorescence, are free EtBr itself, and EtBr bound to the single-stranded DNA primers and to the double-stranded target DNA (by its intercalation between the stacked bases of the DNA double-helix). After the first denaturation cycle, target DNA will be largely single-stranded. After a PCR is completed, the most significant change is the increase in the amount of dsDNA (the PCR product itself) of up to several micrograms. Formerly free EtBr is bound to the additional dsDNA, resulting in an increase in fluorescence. There is also some decrease in the amount of ssDNA primer, but because the binding of EtBr to ssDNA is much less than to dsDNA, the effect of this change on the total fluorescence of the sample is small. The fluorescence increase can be measured by directing excitation illumination through the walls of the amplification vessel

before and after, or even continuously during, thermocycling.

RESULTS

PCR in the presence of EtBr. In order to assess the affect of EtBr in PCR, amplifications of the human HLA DQα gene[19] were performed with the dye present at concentrations from 0.06 to 8.0 µg/ml (a typical concentration of EtBr used in staining of nucleic acids following gel electrophoresis is 0.5 µg/ml). As shown in Figure 2, gel electrophoresis revealed little or no difference in the yield or quality of the amplification product whether EtBr was absent or present at any of these concentrations, indicating that EtBr does not inhibit PCR.

Detection of human Y-chromosome specific sequences. Sequence-specific, fluorescence enhancement of EtBr as a result of PCR was demonstrated in a series of amplifications containing 0.5 µg/ml EtBr and primers specific to repeat DNA sequences found on the human Y-chromosome[20]. These PCRs initially contained either 60 ng male, 60 ng female, 2 ng male human or no DNA. Five replicate PCRs were begun for each DNA. After 0, 17, 21, 24 and 29 cycles of thermocycling, a PCR for each DNA was removed from the thermocycler, and its fluorescence measured in a spectrofluorometer and plotted vs. amplification cycle number (Fig. 3A). The shape of this curve reflects the fact that by the time an increase in fluorescence can be detected, the increase in DNA is becoming linear and not exponential with cycle number. As shown, the fluorescence increased about three-fold over the background fluorescence for the PCRs containing human male DNA, but did not significantly increase for negative control PCRs, which contained either no DNA or human female DNA. The more male DNA present to begin with—60 ng versus 2 ng—the fewer cycles were needed to give a detectable increase in fluorescence. Gel electrophoresis on the products of these amplifications showed that DNA fragments of the expected size were made in the male DNA containing reactions and that little DNA synthesis took place in the control samples.

In addition, the increase in fluorescence was visualized by simply laying the completed, unopened PCRs on a UV transilluminator and photographing them through a red filter. This is shown in figure 3B for the reactions that began with 2 ng male DNA and those with no DNA.

Detection of specific alleles of the human β-globin gene. In order to demonstrate that this approach has adequate specificity to allow genetic screening, a detection of the sickle-cell anemia mutation was performed. Figure 4 shows the fluorescence from completed amplifications containing EtBr (0.5 µg/ml) as detected by photography of the reaction tubes on a UV transilluminator. These reactions were performed using primers specific for either the wild-type or sickle-cell mutation of the human β-globin gene[21]. The specificity for each allele is imparted by placing the sickle-mutation site at the terminal 3′ nucleotide of one primer. By using an appropriate primer annealing temperature, primer extension—and thus amplification—can take place only if the 3′ nucleotide of the primer is complementary to the β-globin allele present[21,22].

Each pair of amplifications shown in Figure 4 consists of a reaction with either the wild-type allele specific (left tube) or sickle-allele specific (right tube) primers. Three different DNAs were typed: DNA from a homozygous, wild-type β-globin individual (AA); from a heterozygous sickle β-globin individual (AS); and from a homozygous sickle β-globin individual (SS). Each DNA (50 ng genomic DNA to start each PCR) was analyzed in triplicate (3 pairs

of reactions each). The DNA type was reflected in the relative fluorescence intensities in each pair of completed amplifications. There was a significant increase in fluorescence only where a β-globin allele DNA matched the primer set. When measured on a spectrofluorometer (data not shown), this fluorescence was about three times that present in a PCR where both β-globin alleles were mismatched to the primer set. Gel electrophoresis (not shown) established that this increase in fluorescence was due to the synthesis of nearly a microgram of a DNA fragment of the expected size for β-globin. There was little synthesis of dsDNA in reactions in which the allele-specific primer was mismatched to both alleles.

Continuous monitoring of a PCR. Using a fiber optic device, it is possible to direct excitation illumination from a spectrofluorometer to a PCR undergoing thermocycling and to return its fluorescence to the spectrofluorometer. The fluorescence readout of such an arrangement, directed at an EtBr-containing amplification of Y-chromosome specific sequences from 25 ng of human male DNA, is shown in Figure 5. The readout from a control PCR with no target DNA is also shown. Thirty cycles of PCR were monitored for each.

The fluorescence trace as a function of time clearly shows the effect of the thermocycling. Fluorescence intensity rises and falls inversely with temperature. The fluorescence intensity is minimum at the denaturation temperature (94°C) and maximum at the annealing/extension temperature (50°C). In the negative-control PCR, these fluorescence maxima and minima do not change significantly over the thirty thermocycles, indicating that there is little dsDNA synthesis without the appropriate target DNA, and there is little if any bleaching of EtBr during the continuous illumination of the sample.

In the PCR containing male DNA, the fluorescence maxima at the annealing/extension temperature begin to increase at about 4000 seconds of thermocycling, and continue to increase with time, indicating that dsDNA is being produced at a detectable level. Note that the fluorescence minima at the denaturation temperature do not significantly increase, presumably because at this temperature there is no dsDNA for EtBr to bind. Thus the course of the amplification is followed by tracking the fluorescence increase at the annealing temperature. Analysis of the products of these two amplifications by gel electrophoresis showed a DNA fragment of the expected size for the male DNA containing sample and no detectable DNA synthesis for the control sample.

DISCUSSION

Downstream processes such as hybridization to a sequence-specific probe can enhance the specificity of DNA detection by PCR. The elimination of these processes means that the specificity of this homogeneous assay depends solely on that of PCR. In the case of sickle-cell disease, we have shown that PCR alone has sufficient DNA sequence specificity to permit genetic screening. Using appropriate amplification conditions, there is little nonspecific production of dsDNA in the absence of the appropriate target allele.

The specificity required to detect pathogens can be more or less than that required to do genetic screening, depending on the number of pathogens in the sample and the amount of other DNA that must be taken with the sample. A difficult target is HIV, which requires detection of a viral genome that can be at the level of a few copies per thousands of host cells[6]. Compared with genetic screening, which is performed on cells containing at least one copy of the target sequence, HIV detection requires both more specificity and the input of more total
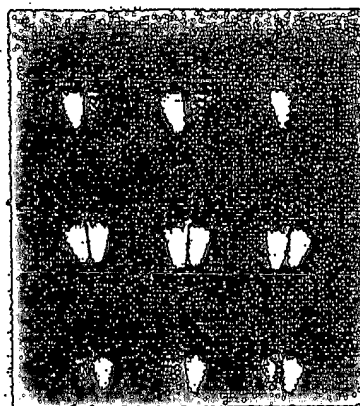

FIGURE 4 UV photography of PCR tubes containing amplifications using EtBr that are specific to wild-type (A) or sickle (S) alleles of the human β-globin gene. The left of each pair of tubes contains allele-specific primers to the wild-type alleles, the right tube primers to the sickle allele. The photograph was taken after 30 cycles of PCR, and the input DNAs and the alleles they contain are indicated. Fifty ng of DNA was used to begin PCR. Typing was done in triplicate (3 pairs of PCRs) for each input DNA.
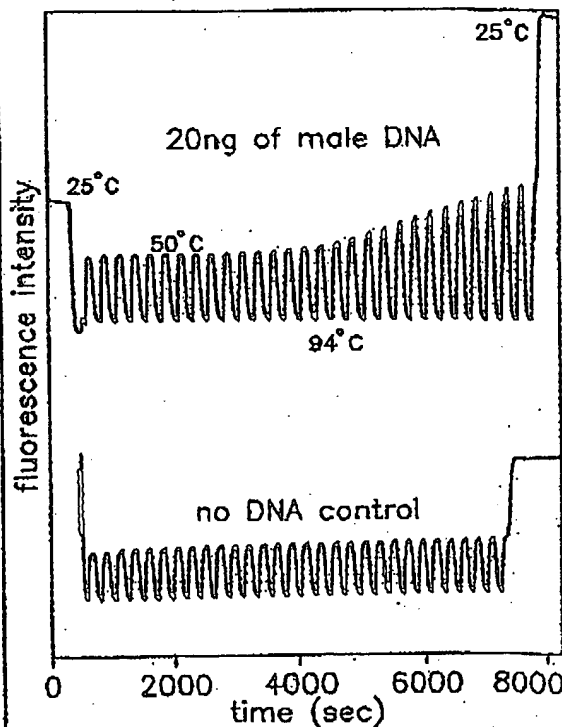

FIGURE 5 Continuous, real-time monitoring of a PCR. A fiber optic was used to carry excitation light to a PCR in progress and also emitted light back to a fluorometer (see Experimental Protocol). Amplification using human male-DNA specific primers in a PCR starting with 20 ng of human male DNA (top), or in a control PCR without DNA (bottom), were monitored. Thirty cycles of PCR were followed for each. The temperature cycled between 94°C (denaturation) and 50°C (annealing and extension). Note in the male DNA PCR, the cycle (time) dependent increase in fluorescence at the annealing/extension temperature.

DNA—up to microgram amounts—in order to have sufficient numbers of target sequences. This large amount of starting DNA in an amplification significantly increases the background fluorescence over which any additional fluorescence produced by PCR must be detected. An additional complication that occurs with targets in low copy-number is the formation of the "primer-dimer" artifact. This is the result of the extension of one primer using the other primer as a template. Although this occurs infrequently, once it occurs the extension product is a substrate for PCR amplification, and can compete with true PCR targets if those targets are rare. The primer-dimer product is of course dsDNA and thus is a potential source of false signal in this homogeneous assay.

To increase PCR specificity and reduce the effect of primer-dimer amplification, we are investigating a number of approaches, including the use of nested-primer amplifications that take place in a single tube[6], and the "hot-start", in which nonspecific amplification is reduced by raising the temperature of the reaction before DNA synthesis begins[23]. Preliminary results using these approaches suggest that primer-dimer is effectively reduced and it is possible to detect the increase in EtBr fluorescence in a PCR instigated by a single HIV genome in a background of 10^5 cells. With larger numbers of cells, the background fluorescence contributed by genomic DNA becomes problematic. To reduce this background, it may be possible to use sequence-specific DNA-binding dyes that can be made to preferentially bind PCR product over genomic DNA by incorporating the dye-binding DNA sequence into the PCR product through a 5' "add-on" to the oligonucleotide primer[24].

We have shown that the detection of fluorescence generated by an EtBr-containing PCR is straightforward, both once PCR is completed and continuously during thermocycling. The ease with which automation of specific DNA detection can be accomplished is the most promising aspect of this assay. The fluorescence analysis of completed PCRs is already possible with existing instrumentation in 96-well format[25]. In this format, the fluorescence in each PCR can be quantitated before, after, and even at selected points during thermocycling by moving the rack of PCRs to a 96-microwell plate fluorescence reader[26].

The instrumentation necessary to continuously monitor multiple PCRs simultaneously is also simple in principle. A direct extension of the apparatus used here is to have multiple fiberoptics transmit the excitation light and fluorescent emissions to and from multiple PCRs. The ability to monitor multiple PCRs continuously may allow quantitation of target DNA copy number. Figure 3 shows that the larger the amount of starting target DNA, the sooner during PCR a fluorescence increase is detected. Preliminary experiments (Higuchi and Dollinger, manuscript in preparation) with continuous monitoring have shown a sensitivity to two-fold differences in initial target DNA concentration.

Conversely, if the number of target molecules is known—as it can be in genetic screening—continuous monitoring may provide a means of detecting false positive and false negative results. With a known number of target molecules, a true positive would exhibit detectable fluorescence by a predictable number of cycles of PCR. Increases in fluorescence detected before or after that cycle would indicate potential artifacts. False negative results due to, for example, inhibition of DNA polymerase, may be detected by including within each PCR an inefficiently amplifying marker. This marker results in a fluorescence increase only after a large number of cycles—many more than are necessary to detect a true

positive. If a sample fails to have a fluorescence increase after this many cycles, inhibition may be suspected. Since, in this assay, conclusions are drawn based on the presence or absence of fluorescence signal alone, such controls may be important. In any event, before any test based on this principle is ready for the clinic, an assessment of its false positive/false negative rates will need to be obtained using a large number of known samples.

In summary, the inclusion in PCR of dyes whose fluorescence is enhanced upon binding dsDNA makes it possible to detect specific DNA amplification from outside the PCR tube. In the future, instruments based upon this principle may facilitate the more widespread use of PCR in applications that demand the high throughput of samples.

EXPERIMENTAL PROTOCOL

Human HLA-DQα gene amplifications containing EtBr. PCRs were set up in 100 µl volumes containing 10 mM Tris-HCl, pH 8.3; 50 mM KCl; 4 mM $MgCl_2$; 2.5 units of Taq DNA polymerase (Perkin-Elmer Cetus, Norwalk, CT); 20 pmole each of human HLA-DQα gene specific oligonucleotide primers (GH26 and GH27[19] and approximately 10^7 copies of DQα PCR product diluted from a previous reaction. Ethidium bromide (EtBr; Sigma) was used at the concentrations indicated in Figure 2. Thermocycling proceeded for 20 cycles in a model 480 thermocycler (Perkin-Elmer Cetus, Norwalk, CT) using a "step-cycle" program of 94°C for 1 min. denaturation and 60°C for 30 sec. annealing and 72°C for 30 sec. extension.

Y-chromosome specific PCR. PCRs (100 µl total reaction volume) containing 0.5 µg/ml EtBr were prepared as described for HLA-DQα, except with different primers and target DNAs. These PCRs contained 15 pmole each male DNA-specific primers Y1.1 and Y1.2[20], and either 60 ng male, 60 ng female, 2 ng male, or no human DNA. Thermocycling was 94°C for 1 min. and 60°C for 1 min using a "step-cycle" program. The number of cycles for a sample were as indicated in Figure 3. Fluorescence measurement is described below.

Allele-specific, human β-globin gene PCR. Amplifications of 100 µl volume using 0.5 µg/ml of EtBr were prepared as described for HLA-DQα above except with different primers and target DNAs. These PCRs contained either primer pair HGP2/Hβ14A (wild-type globin specific primers) or HGP2/Hβ14S (sickle-globin specific primers) at 10 pmole each primer per PCR. These primers were developed by Wu et al[21]. Three different target DNAs were used in separate amplifications—50 ng each of human DNA that was homozygous for the sickle trait (SS), DNA that was heterozygous for the sickle trait (AS), or DNA that was homozygous for the w.t. globin (AA). Thermocycling was for 30 cycles at 94°C for 1 min. and 55°C for 1 min. using a "step-cycle" program. An annealing temperature of 55°C had been shown by Wu et al[21] to provide allele-specific amplification. Completed PCRs were photographed through a red filter (Wratten 23A) after placing the reaction tubes atop a model TM-36 transilluminator (UV-products San Gabriel, CA).

Fluorescence measurement. Fluorescence measurements were made on PCRs containing EtBr in a Fluorolog-2 fluorometer (SPEX, Edison, NJ). Excitation was at the 500 nm band with about 2 nm bandwidth with a GG 435 nm cut-off filter (Melles Griot, Inc., Irvine, CA) to exclude second-order light. Emitted light was detected at 570 nm with a bandwidth of about 7 nm. An OG 530 nm cut-off filter was used to remove the excitation light.

Continuous fluorescence monitoring of PCR. Continuous monitoring of a PCR in progress was accomplished using the spectrofluorometer and settings described above as well as a fiberoptic accessory (SPEX cat. no. 1950) to both send excitation light to, and receive emitted light from, a PCR placed in a well of a model 480 thermocycler (Perkin-Elmer Cetus). The probe end of the fiberoptic cable was attached with "5 minute-epoxy" to the open top of a PCR tube (a 0.5 ml polypropylene centrifuge tube with its cap removed) effectively sealing it. The exposed top of the PCR tube and the end of the fiberoptic cable were shielded from room light and the room lights were kept dimmed during each run. The monitored PCR was an amplification of Y-chromosome-specific repeat sequences as described above, except using an annealing/extension temperature of 50°C. The reaction was covered with mineral oil (2 drops) to prevent evaporation. Thermocycling and fluorescence measurement were started simultaneously. A time-base scan with a 10 second integration time

was used and the emission signal was ratioed to the excitation signal to control for changes in light-source intensity. Data were collected using the dm3000f, version 2.5 (SPEX) data system.

Acknowledgments

We thank Bob Jones for help with the spectrofluormetric measurements and Heatherbell Fong for editing this manuscript.
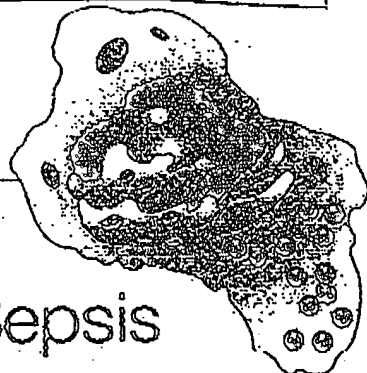
References

1. Mullis, K., Faloona, F., Scharf, S., Saiki, R., Horn, G. and Erlich, H. 1986. Specific enzymatic amplification of DNA in vitro: The polymerase chain reaction. CSHSQB 51:263–273.
2. White, T. J., Arnheim, N. and Erlich, H. A. 1989. The polymerase chain reaction. Trends Genet. 5:185–189.
3. Erlich, H. A., Gelfand, D. and Sninsky, J. J. 1991. Recent advances in the polymerase chain reaction. Science 252:1643–1651.
4. Saiki, R. K., Gelfand, D. H., Stoffel, S., Scharf, S. J., Higuchi, R., Horn, G. T., Mullis, K. B. and Erlich, H. A. 1988. Primer-directed enzymatic amplification of DNA with a thermostable DNA polymerase. Science 239:487–491.
5. Saiki, R. K., Walsh, P. S., Levenson, C. H. and Erlich, H. A. 1989. Genetic analysis of amplified DNA with immobilized sequence-specific oligonucleotide probes. Proc. Natl. Acad. Sci. USA 86:6230–6234.
6. Kwok, S. Y., Mack, D. H., Mullis, K. B., Poiesz, B. J., Ehrlich, G. D., Blair, D. and Friedman-Kien, A. S. 1987. Identification of human immunodeficiency virus sequences by using in vitro enzymatic amplification and oligomer cleavage detection. J. Virol. 61:1690–1694.
7. Chehab, F. F., Doherty, M., Cai, S. P., Kan, Y. W., Cooper, S. and Rubin, E. M. 1987. Detection of sickle cell anemia and thalassemia. Nature 329:293–294.
8. Horn, G. T., Richards, B. and Klinger, K. W. 1989. Amplification of a highly polymorphic VNTR segment by the polymerase chain reaction. Nuc. Acids Res. 16:2140.
9. Katz, E. D. and Dong, M. W. 1990. Rapid analysis and purification of polymerase chain reaction products by high-performance liquid chromatography. Biotechniques 8:546–555.
10. Heiger, D. N., Cohen, A. S. and Karger, B. L. 1990. Separation of DNA restriction fragments by high performance capillary electrophoresis with low and zero crosslinked polyacrylamide using continuous and pulsed electric fields. J. Chromatogr. 516:33–48.
11. Kwok, S. Y. and Higuchi, R. G. 1989. Avoiding false positives with PCR. Nature 339:237–238.
12. Chehab, F. F. and Kan, Y. W. 1989. Detection of specific DNA sequences by fluorescence amplification: a color complementation assay. Proc. Natl. Acad. Sci. USA 86:9178–9182.
13. Holland, P. M., Abramson, R. D., Watson, R. and Gelfand, D. H.
14. 1991. Detection of specific polymerase chain reaction product by utilizing the 5′ to 3′ exonuclease activity of Thermus aquaticus DNA polymerase. Proc. Natl. Acad. Sci. USA 88:7276–7280.
14. Markovits, J., Roques, B. P. and Le Pecq, J. B. 1979. Ethidium dimer: a new reagent for the fluorimetric determination of nucleic acids. Anal. Biochem. 94:259–264.
15. Kapuscinski, J. and Szer, W. 1979. Interactions of 4′,6-diamidine-2-phenylindole with synthetic polynucleotides. Nuc. Acids Res. 6:3519–3534.
16. Searle, M. S. and Embrey, K. J. 1990. Sequence-specific interaction of Hoechst 33258 with the minor groove of an adenine-tract DNA duplex studied in solution by ¹H NMR spectroscopy. Nuc. Acids Res. 18:3753–3762.
17. Li, H. H., Gyllensten, U. B., Cui, X. F., Saiki, R. K., Erlich, H. A. and Arnheim, N. 1988. Amplification and analysis of DNA sequences in single human sperm and diploid cells. Nature 335:414–417.
18. Abbott, M. A., Poiesz, B. J., Byrne, B. C., Kwok, S. Y., Sninsky, J. J. and Erlich, H. A. 1988. Enzymatic gene amplification: qualitative and quantitative methods for detecting proviral DNA amplified in vitro. J. Infect. Dis. 158:1158.
19. Saiki, R. K., Bugawan, T. L., Horn, G. T., Mullis, K. B. and Erlich, H. A. 1986. Analysis of enzymatically amplified β-globin and HLA-DQα DNA with allele-specific oligonucleotide probes. Nature 324:163–166.
20. Kogan, S. C., Doherty, M. and Gitschier, J. 1987. An improved method for prenatal diagnosis of genetic disease by analysis of amplified DNA sequences. N. Engl. J. Med. 317:985–990.
21. Wu, D. Y., Ugozzoli, L., Pal, B. K. and Wallace, R. B. 1989. Allele-specific enzymatic amplification of β-globin genomic DNA for diagnosis of sickle cell anemia. Proc. Natl. Acad. Sci. USA 86:2757–2760.
22. Kwok, S., Kellogg, D. E., McKinney, N., Spasic, D., Goda, L., Levenson, C. and Sninsky, J. J. 1990. Effects of primer-template mismatches on the polymerase chain reaction: Human immunodeficiency virus type 1 model studies. Nuc. Acids Res. 18:999–1005.
23. Chou, Q., Russell, M., Birch, D., Raymond, J. and Bloch, W. 1992. Prevention of pre-PCR mis-priming and primer dimerization improves low-copy-number amplifications: Submitted.
24. Higuchi, R. 1989. Using PCR to engineer DNA. p. 61–70. In: PCR Technology. H. A. Erlich (Ed.). Stockton Press, New York, N.Y.
25. Haff, L., Atwood, J. G., DiCesare, J., Katz, E., Picozza, E., Williams, J. F. and Woudenberg, T. 1991. A high-performance system for automation of the polymerase chain reaction. Biotechniques 10:102–103, 106–112.
26. Tumosa, N. and Kahan, L. 1989. Fluorescent EIA screening of monoclonal antibodies to cell surface antigens. J. Immun. Meth. 116:59–63.

IIIIIResearch

Oligonucleotides with Fluorescent Dyes at Opposite Ends Provide a Quenched Probe System Useful for Detecting PCR Product and Nucleic Acid Hybridization

Kenneth J. Livak, Susan J.A. Flood, Jeffrey Marmaro, William Giusti, and Karin Deetz

Perkin-Elmer, Applied Biosystems Division, Foster City, California 94404

The 5' nuclease PCR assay detects the accumulation of specific PCR product by hybridization and cleavage of a double-labeled fluorogenic probe during the amplification reaction. The probe is an oligonucleotide with both a reporter fluorescent dye and a quencher dye attached. An increase in reporter fluorescence intensity indicates that the probe has hybridized to the target PCR product and has been cleaved by the 5'→3' nucleolytic activity of *Taq* DNA polymerase. In this study, probes with the quencher dye attached to an internal nucleotide were compared with probes with the quencher dye attached to the 3'-end nucleotide. In all cases, the reporter dye was attached to the 5' end. All intact probes showed quenching of the reporter fluorescence. In general, probes with the quencher dye attached to the 3'-end nucleotide exhibited a larger signal in the 5' nuclease PCR assay than the internally labeled probes. It is proposed that the larger signal is caused by increased likelihood of cleavage by *Taq* DNA polymerase when the probe is hybridized to a template strand during PCR. Probes with the quencher dye attached to the 3'-end nucleotide also exhibited an increase in reporter fluorescence intensity when hybridized to a complementary strand. Thus, oligonucleotides with reporter and quencher dyes attached at opposite ends can be used as homogeneous hybridization probes.

A homogeneous assay for detecting the accumulation of specific PCR product that uses a double-labeled fluorogenic probe was described by Lee et al.[1] The assay exploits the 5'→3' nucleolytic activity of *Taq* DNA polymerase[2,3] and is diagramed in Figure 1. The fluorogenic probe consists of an oligonucleotide with a reporter fluorescent dye, such as a fluorescein, attached to the 5' end; and a quencher dye, such as a rhodamine, attached internally. When the fluorescein is excited by irradiation, its fluorescent emission will be quenched if the rhodamine is close enough to be excited through the process of fluorescence energy transfer (FET).[4,5] During PCR, if the probe is hybridized to a template strand, *Taq* DNA polymerase will cleave the probe because of its inherent 5'→3' nucleolytic activity. If the cleavage occurs between the fluorescein and rhodamine dyes, it causes an increase in fluorescein fluorescence intensity because the fluorescein is no longer quenched. The increase in fluorescein fluorescence intensity indicates that the probe-specific PCR product has been generated. Thus, FET between a reporter dye and a quencher dye is critical to the performance of the probe in the 5' nuclease PCR assay.

Quenching is completely dependent on the physical proximity of the two dyes.[6] Because of this, it has been assumed that the quencher dye must be attached near the 5' end. Surprisingly, we have found that attaching a rhodamine dye at the 3' end of a probe still provides adequate quenching for the probe to perform in the 5' nuclease

PCR assay. Furthermore, cleavage of this type of probe is not required to achieve some reduction in quenching. Oligonucleotides with a reporter dye on the 5' end and a quencher dye on the 3' end exhibit a much higher reporter fluorescence when double-stranded as compared with single-stranded. This should make it possible to use this type of double-labeled probe for homogeneous detection of nucleic acid hybridization.

MATERIALS AND METHODS

Oligonucleotides

Table 1 shows the nucleotide sequence of the oligonucleotides used in this study. Linker arm nucleotide (LAN) phosphoramidite was obtained from Glen Research. The standard DNA phosphoramidites, 6-carboxyfluorescein (6-FAM) phosphoramidite, 6-carboxytetramethylrhodamine succinimidyl ester (TAMRA NHS ester), and Phosphalink for attaching a 3'-blocking phosphate, were obtained from Perkin-Elmer, Applied Biosystems Division. Oligonucleotide synthesis was performed using an ABI model 394 DNA synthesizer (Applied Biosystems). Primer and complement oligonucleotides were purified using Oligo Purification Cartridges (Applied Biosystems). Double-labeled probes were synthesized with 6-FAM-labeled phosphoramidite at the 5' end, LAN replacing one of the T's in the sequence, and Phosphalink at the 3' end. Following deprotection and ethanol precipitation, TAMRA NHS ester was coupled to the LAN-containing oligonucleotide in 250
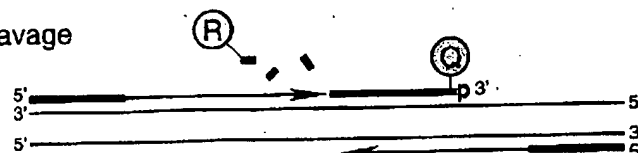
Research▮▮▮▮▮▮ ▮▮ ▮ ▮▮▮ ▮ ▮▮▮▮

Polymerization
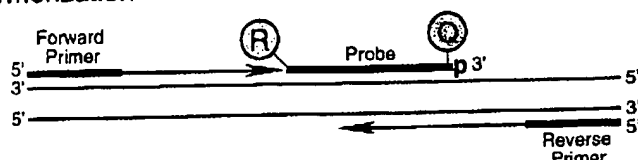
Strand displacement
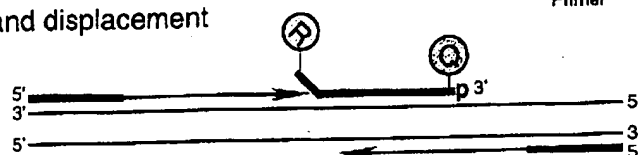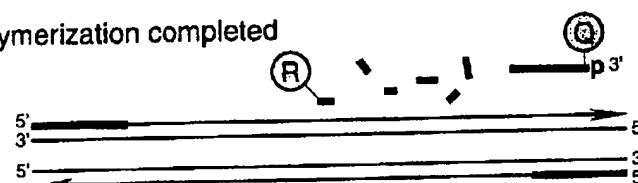
Cleavage

Polymerization completed

FIGURE 1 Diagram of 5' nuclease assay. Stepwise representation of the 5' → 3' nucleolytic activity of *Taq* DNA polymerase acting on a fluorogenic probe during one extension phase of PCR.

mM Na-bicarbonate buffer (pH 9.0) at room temperature. Unreacted dye was removed by passage over a PD-10 Sephadex column. Finally, the double-labeled probe was purified by preparative high-performance liquid chromatography (HPLC) using an Aquapore C_8 220×4.6-mm column with 7-μm particle size. The column was developed with a 24-min linear gradient of 8–20% acetonitrile in 0.1 M TEAA (triethylamine acetate). Probes are named by designating the sequence from Table 1 and the position of the LAN–TAMRA moiety. For example, probe A1-7 has sequence A1 with LAN–TAMRA at nucleotide position 7 from the 5' end.

PCR Systems

All PCR amplifications were performed in the Perkin-Elmer GeneAmp PCR System 9600 using 50-μl reactions that contained 10 mM Tris-HCl (pH 8.3), 50 mM KCl, 200 μM dATP, 200 μM dCTP, 200 μM dGTP, 400 μM dUTP, 0.5 unit of AmpErase uracil N-glycosylase (Perkin-Elmer), and 1.25 unit of AmpliTaq DNA polymerase (Perkin-Elmer). A 295-bp segment from exon 3 of the human β-actin

gene (nucleotides 2141–2435 in the sequence of Nakajima-Iijima et al.)[7] was amplified using primers AFP and ARP (Table 1), which are modified slightly from those of du Breuil et al.[8] Actin amplification reactions contained 4 mM $MgCl_2$, 20 ng of human genomic DNA, 50 nM A1 or A3 probe, and 300 nM each

primer. The thermal regimen was 50°C (2 min), 95°C (10 min), 40 cycles of 95°C (20 sec), 60°C (1 min), and hold at 72°C. A 515-bp segment was amplified from a plasmid that consists of a segment of λ DNA (nucleotides 32,220–32,747) inserted in the SmaI site of vector pUC119. These reactions contained 3.5 mM $MgCl_2$, 1 ng of plasmid DNA, 50 nM P2 or P5 probe, 200 nM primer F119, and 200 nM primer R119. The thermal regimen was 50°C (2 min), 95°C (10 min), 25 cycles of 95°C (20 sec), 57°C (1 min), and hold at 72°C.

Fluorescence Detection

For each amplification reaction, a 40-μl aliquot of a sample was transferred to an individual well of a white, 96-well microtiter plate (Perkin-Elmer). Fluorescence was measured on the Perkin-Elmer Taq-Man LS-50B System, which consists of a luminescence spectrometer with plate reader assembly, a 485-nm excitation filter, and a 515-nm emission filter. Excitation was at 488 nm using a 5-nm slit width. Emission was measured at 518 nm for 6-FAM (the reporter or R value) and 582 nm for TAMRA (the quencher or Q value) using a 10-nm slit width. To determine the increase in reporter emission that is caused by cleavage of the probe during PCR, three normalizations are applied to the raw emission data. First, emission intensity of a buffer blank is subtracted for each wavelength. Second, emission intensity of the reporter is

TABLE 1 Sequences of Oligonucleotides

Name	Type	Sequence
F119	primer	ACCCACAGGAACTGATCACCACTC
R119	primer	ATGTCGCGTTCCGGCTGACGTTCTGC
P2	probe	TCGCATTACTGATCGTTGCCAACCAGTp
P2C	complement	GTACTGGTTGGCAACGATCAGTAATGCGATG
P5	probe	CGGATTTGCTGGTATCTATGACAAGGATp
P5C	complement	TTCATCCTTGTCATAGATACCAGCAAATCCG
AFP	primer	TCACCCACACTGTGCCCATCTACGA
ARP	primer	CAGCGGAACCGCTCATTGCCAATGG
A1	probe	ATGCCCTCCCCCCATGCCATCCTGCGTp
A1C	complement	AGACGCAGGATGGCATGGGGGAGGGCATAC
A3	probe	CGCCCTGGACTTCGAGCAAGAGATp
A3C	complement	CCATCTCTTGCTCGAAGTCCAGGGCGAC

For each oligonucleotide used in this study, the nucleic acid sequence is given, written in the 5' → 3' direction. There are three types of oligonucleotides: PCR primer, fluorogenic probe used in the 5' nuclease assay, and complement used to hybridize to the corresponding probe. For the probes, the underlined base indicates a position where LAN with TAMRA attached was substituted for a T. (p) The presence of a 3' phosphate on each probe.

■■■■■■■■■■■■IIIIIResearch

A1-2	RAQGCCCTCCCCCATGCCATCCTGCGTp
A1-7	RATGCCCQCCCCCATGCCATCCTGCGTp
A1-14	RATGCCCTCCCCCAQGCCATCCTGCGTp
A1-19	RATGCCCTCCCCCATGCCAQCCTGCGTp
A1-22	RATGCCCTCCCCCATGCCATCCQGCGTp
A1-26	RATGCCCTCCCCCATGCCATCCTGCGQp

| Probe | 518 nm | | 582 nm | | RQ⁻ | RQ⁺ | ΔRQ |
	no temp.	+ temp.	no temp.	+ temp.			
A1-2	25.5 ± 2.1	32.7 ± 1.9	38.2 ± 3.0	38.2 ± 2.0	0.67 ± 0.01	0.86 ± 0.06	0.19 ± 0.06
A1-7	53.5 ± 4.3	395.1 ± 21.4	108.5 ± 6.3	110.3 ± 5.3	0.49 ± 0.03	3.58 ± 0.17	3.09 ± 0.18
A1-14	127.0 ± 4.9	403.5 ± 19.1	109.7 ± 5.3	93.1 ± 6.3	1.16 ± 0.02	4.34 ± 0.15	3.18 ± 0.15
A1-19	187.5 ± 17.9	422.7 ± 7.7	70.3 ± 7.4	73.0 ± 2.8	2.67 ± 0.05	5.80 ± 0.15	3.13 ± 0.16
A1-22	224.6 ± 9.4	482.2 ± 43.6	100.0 ± 4.0	96.2 ± 9.6	2.25 ± 0.03	5.02 ± 0.11	2.77 ± 0.12
A1-26	160.2 ± 8.9	454.1 ± 18.4	93.1 ± 5.4	90.7 ± 3.2	1.72 ± 0.02	5.01 ± 0.08	3.29 ± 0.08

FIGURE 2 Results of 5' nuclease assay comparing β-actin probes with TAMRA at different nucleotide positions. As described in Materials and Methods, PCR amplifications containing the indicated probes were performed, and the fluorescence emission was measured at 518 and 582 nm. Reported values are the average ± 1 s.D. for six reactions run without added template (no temp.) and six reactions run with template (+ temp.). The RQ ratio was calculated for each individual reaction and averaged to give the reported RQ⁻ and RQ⁺ values.

divided by the emission intensity of the quencher to give an RQ ratio for each reaction tube. This normalizes for well-to-well variations in probe concentration and fluorescence measurement. Finally, ΔRQ is calculated by subtracting the RQ value of the no-template control (RQ⁻) from the RQ value for the complete reaction including template (RQ⁺).

RESULTS

A series of probes with increasing distances between the fluorescein reporter and rhodamine quencher were tested to investigate the minimum and maximum spacing that would give an acceptable performance in the 5' nuclease PCR assay. These probes hybridize to a target

sequence in the human β-actin gene. Figure 2 shows the results of an experiment in which these probes were included in PCR that amplified a segment of the β-actin gene containing the target sequence. Performance in the 5' nuclease PCR assay is monitored by the magnitude of ΔRQ, which is a measure of the increase in reporter fluorescence caused by PCR amplification of the probe target. Probe A1-2 has a ΔRQ value that is close to zero, indicating that the probe was not cleaved appreciably during the amplification reaction. This suggests that with the quencher dye on the second nucleotide from the 5' end, there is insufficient room for Taq polymerase to cleave efficiently between the reporter and quencher. The other five probes exhibited comparable ΔRQ values that are

clearly different from zero. Thus, all five probes are being cleaved during PCR amplification resulting in a similar increase in reporter fluorescence. It should be noted that complete digestion of a probe produces a much larger increase in reporter fluorescence than that observed in Figure 2 (data not shown). Thus, even in reactions where amplification occurs, the majority of probe molecules remain uncleaved. It is mainly for this reason that the fluorescence intensity of the quencher dye TAMRA changes little with amplification of the target. This is what allows us to use the 582-nm fluorescence reading as a normalization factor.

The magnitude of RQ⁻ depends mainly on the quenching efficiency inherent in the specific structure of the probe and the purity of the oligonucleotide. Thus, the larger RQ⁻ values indicate that probes A1-14, A1-19, A1-22, and A1-26 probably have reduced quenching as compared with A1-7. Still, the degree of quenching is sufficient to detect a highly significant increase in reporter fluorescence when each of these probes is cleaved during PCR.

To further investigate the ability of TAMRA on the 3' end to quench 6-FAM on the 5' end, three additional pairs of probes were tested in the 5' nuclease PCR assay. For each pair, one probe has TAMRA attached to an internal nucleotide and the other has TAMRA attached to the 3' end nucleotide. The results are shown in Table 2. For all three sets, the probe with the 3' quencher exhibits a ΔRQ value that is considerably higher than for the probe with the internal quencher. The RQ⁻ values suggest that differences in quenching are not as great as those observed with some of the A1 probes. These results demonstrate that a quencher dye on the 3' end of an oligonucleotide can quench efficiently the

TABLE 2 Results of 5' Nuclease Assay Comparing Probes with TAMRA Attached to an Internal or 3'-terminal Nucleotide

| Probe | 518 nm | | 582 nm | | RQ⁻ | RQ⁺ | ΔRQ |
	no temp.	+ temp.	no temp.	+ temp.			
A3-6	54.6 ± 3.2	84.8 ± 3.7	116.2 ± 6.4	115.6 ± 2.5	0.47 ± 0.02	0.73 ± 0.03	0.26 ± 0.04
A3-24	72.1 ± 2.9	236.5 ± 11.1	84.2 ± 4.0	90.2 ± 3.8	0.86 ± 0.02	2.62 ± 0.05	1.76 ± 0.05
P2-7	82.8 ± 4.4	384.0 ± 34.1	105.1 ± 6.4	120.4 ± 10.2	0.79 ± 0.02	3.19 ± 0.16	2.40 ± 0.16
P2-27	113.4 ± 6.6	555.4 ± 14.1	140.7 ± 8.5	118.7 ± 4.8	0.81 ± 0.01	4.68 ± 0.10	3.88 ± 0.10
P5-10	77.5 ± 6.5	244.4 ± 15.9	86.7 ± 4.3	95.8 ± 6.7	0.89 ± 0.05	2.55 ± 0.06	1.66 ± 0.08
P5-28	64.0 ± 5.2	333.6 ± 12.1	100.6 ± 6.1	94.7 ± 6.3	0.63 ± 0.02	3.53 ± 0.12	2.89 ± 0.13

Reactions containing the indicated probes and calculations were performed as described in Material and Methods and in the legend to Fig. 2.

Research

fluorescence of a reporter dye on the 5' end. The degree of quenching is sufficient for this type of oligonucleotide to be used as a probe in the 5' nuclease PCR assay.

To test the hypothesis that quenching by a 3' TAMRA depends on the flexibility of the oligonucleotide, fluorescence was measured for probes in the single-stranded and double-stranded states. Table 3 reports the fluorescence observed at 518 and 582 nm. The relative degree of quenching is assessed by calculating the RQ ratio. For probes with TAMRA 6–10 nucleotides from the 5' end, there is little difference in the RQ values when comparing single-stranded with double-stranded oligonucleotides. The results for probes with TAMRA at the 3' end are much different. For these probes, hybridization to a complementary strand causes a dramatic increase in RQ. We propose that this loss of quenching is caused by the rigid structure of double-stranded DNA, which prevents the 5' and 3' ends from being in proximity.

When TAMRA is placed toward the 3' end, there is a marked Mg^{2+} effect on quenching. Figure 3 shows a plot of observed RQ values for the A1 series of probes as a function of Mg^{2+} concentration. With TAMRA attached near the 5' end (probe A1-2 or A1-7), the RQ value at 0 mM Mg^{2+} is only slightly higher than RQ at 10 mM Mg^{2+}. For probes A1-19, A1-22, and A1-26, the RQ values at 0 mM Mg^{2+} are very high, indicating a much

reduced quenching efficiency. For each of these probes, there is a marked decrease in RQ at 1 mM Mg^{2+} followed by a gradual decline as the Mg^{2+} concentration increases to 10 mM. Probe A1-14 shows an intermediate RQ value at 0 mM Mg^{2+} with a gradual decline at higher Mg^{2+} concentrations. In a low-salt environment with no Mg^{2+} present, a single-stranded oligonucleotide would be expected to adopt an extended conformation because of electrostatic repulsion. The binding of Mg^{2+} ions acts to shield the negative charge of the phosphate backbone so that the oligonucleotide can adopt conformations where the 3' end is close to the 5' end. Therefore, the observed Mg^{2+} effects support the notion that quenching of a 5' reporter dye by TAMRA at or near the 3' end depends on the flexibility of the oligonucleotide.

DISCUSSION

The striking finding of this study is that it seems the rhodamine dye TAMRA, placed at any position in an oligonucleotide, can quench the fluorescent emission of a fluorescein (6-FAM) placed at the 5' end. This implies that a single-stranded, double-labeled oligonucleotide must be able to adopt conformations where the TAMRA is close to the 5' end. It should be noted that the decay of 6-FAM in the excited state requires a certain amount of time. Therefore, what

matters for quenching is not the average distance between 6-FAM and TAMRA but, rather, how close TAMRA can get to 6-FAM during the lifetime of the 6-FAM excited state. As long as the decay time of the excited state is relatively long compared with the molecular motions of the oligonucleotide, quenching can occur. Thus, we propose that TAMRA at the 3' end, or any other position, can quench 6-FAM at the 5' end because TAMRA is in proximity to 6-FAM often enough to be able to accept energy transfer from an excited 6-FAM.

Details of the fluorescence measurements remain puzzling. For example, Table 3 shows that hybridization of probes A1-26, A3-24, and P5-28 to their complementary strands not only causes a large increase in 6-FAM fluorescence at 518 nm but also causes a modest increase in TAMRA fluorescence at 582 nm. If TAMRA is being excited by energy transfer from quenched 6-FAM, then loss of quenching attributable to hybridization should cause a decrease in the fluorescence emission of TAMRA. The fact that the fluorescence emission of TAMRA increases indicates that the situation is more complex. For example, we have anecdotal evidence that the bases of the oligonucleotide, especially G, quench the fluorescence of both 6-FAM and TAMRA to some degree. When double-stranded, base-pairing may reduce the ability of the bases to quench. The primary factor causing the quenching of 6-FAM in an intact probe is the TAMRA dye. Evidence for the importance of TAMRA is that 6-FAM fluorescence remains relatively unchanged when probes labeled only with 6-FAM are used in the 5' nuclease PCR assay (data not shown). Secondary effectors of fluorescence, both before and after cleavage of the probe, need to be explored further.

Regardless of the physical mechanism, the relative independence of position and quenching greatly simplifies the design of probes for the 5' nuclease PCR assay. There are three main factors that determine the performance of a double-labeled fluorescent probe in the 5' nuclease PCR assay. The first factor is the degree of quenching observed in the intact probe. This is characterized by the value of RQ^-, which is the ratio of reporter to quencher fluorescent emissions for a no template control PCR. Influences on the value of RQ^- include the particular reporter and quencher

TABLE 3 Comparison of Fluorescence Emissions of Single-stranded and Double-stranded Fluorogenic Probes

Probe	518 nm		582 nm		RQ	
	ss	ds	ss	ds	ss	ds
A1-7	27.75	68.53	61.08	138.18	0.45	0.50
A1-26	43.31	509.38	53.50	93.86	0.81	5.43
A3-6	16.75	62.88	39.33	165.57	0.43	0.38
A3-24	30.05	578.64	67.72	140.25	0.45	3.21
P2-7	35.02	70.13	54.63	121.09	0.64	0.58
P2-27	39.89	320.47	65.10	61.13	0.61	5.25
P5-10	27.34	144.85	61.95	165.54	0.44	0.87
P5-28	33.65	462.29	72.39	104.61	0.46	4.43

(ss) Single-stranded. The fluorescence emissions at 518 or 582 nm for solutions containing a final concentration of 50 nM indicated probe, 10 mM Tris-HCl (pH 8.3), 50 mM KCl, and 10 mM $MgCl_2$. (ds) Double-stranded. The solutions contained, in addition, 100 nM A1C for probes A1-7 and A1-26, 100 nM A3C for probes A3-6 and A3-24, 100 nM P2C for probes P2-7 and P2-27, or 100 nM P5C for probes P5-10 and P5-28. Before the addition of $MgCl_2$, 120 μl of each sample was heated at 95°C for 5 min. Following the addition of 80 μl of 25 mM $MgCl_2$, each sample was allowed to cool to room temperature and the fluorescence emissions were measured. Reported values are the average of three determinations.
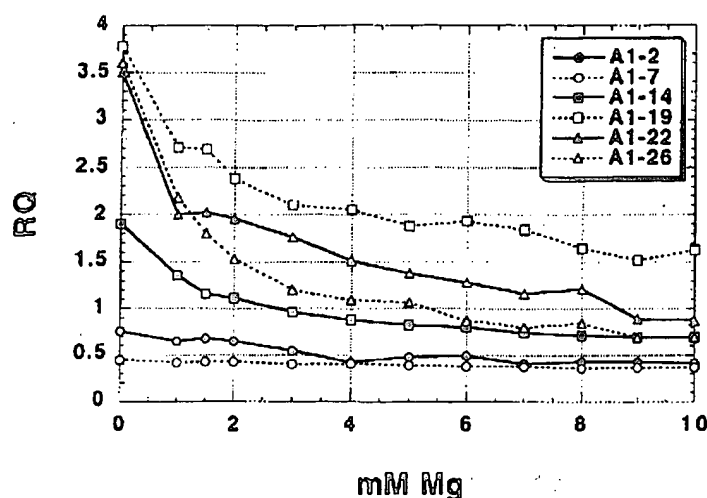
360   PCR Methods and Applications

IIIIIResearch

FIGURE 3 Effect of Mg^{2+} concentration on RQ ratio for the A1 series of probes. The fluorescence emission intensity at 518 and 582 nm was measured for solutions containing 50 nM probe, 10 mM Tris-HCl (pH 8.3), 50 mM KCl, and varying amounts (0–10 mM) of $MgCl_2$. The calculated RQ ratios (518 nm intensity divided by 582 nm intensity) are plotted vs. $MgCl_2$ concentration (mM Mg). The key (*upper right*) shows the probes examined.

dyes used, spacing between reporter and quencher dyes, nucleotide sequence context effects, presence of structure or other factors that reduce flexibility of the oligonucleotide, and purity of the probe. The second factor is the efficiency of hybridization, which depends on probe T_m, presence of secondary structure in probe or template, annealing temperature, and other reaction conditions. The third factor is the efficiency at which *Taq* DNA polymerase cleaves the bound probe between the reporter and quencher dyes. This cleavage is dependent on sequence complementarity between probe and template as shown by the observation that mismatches in the segment between reporter and quencher dyes drastically reduce the cleavage of probe.[1]

The rise in RQ^- values for the A1 series of probes seems to indicate that the degree of quenching is reduced somewhat as the quencher is placed toward the 3' end. The lowest apparent quenching is observed for probe A1-19 (see Fig. 3) rather than for the probe where the TAMRA is at the 3' end (A1-26). This is understandable, as the conformation of the 3' end position would be expected to be less restricted than the conformation of an internal position. In effect, a quencher at the 3' end is freer to adopt conformations close to the 5' reporter dye than is an internally placed quencher. For the other three sets of

probes, the interpretation of RQ^- values is less clear-cut. The A3 probes show the same trend as A1, with the 3' TAMRA probe having a larger RQ^- than the internal TAMRA probe. For the P2 pair, both probes have about the same RQ^- value. For the P5 probes, the RQ^- for the 3' probe is less than for the internally labeled probe. Another factor that may explain some of the observed variation is that purity affects the RQ^- value. Although all probes are HPLC purified, a small amount of contamination with unquenched reporter can have a large effect on RQ^-.

Although there may be a modest effect on degree of quenching, the position of the quencher apparently can have a large effect on the efficiency of probe cleavage. The most drastic effect is observed with probe A1-2, where placement of the TAMRA on the second nucleotide reduces the efficiency of cleavage to almost zero. For the A3, P2, and P5 probes, ΔRQ is much greater for the 3' TAMRA probes as compared with the internal TAMRA probes. This is explained most easily by assuming that probes with TAMRA at the 3' end are more likely to be cleaved between reporter and quencher than are probes with TAMRA attached internally. For the A1 probes, the cleavage efficiency of probe A1-7 must already be quite high, as ΔRQ does not increase when the quencher is placed closer to the 3' end. This illus-

trates the importance of being able to use probes with a quencher on the 3' end in the 5' nuclease PCR assay. In this assay, an increase in the intensity of reporter fluorescence is observed only when the probe is cleaved between the reporter and quencher dyes. By placing the reporter and quencher dyes on the opposite ends of an oligonucleotide probe, any cleavage that occurs will be detected. When the quencher is attached to an internal nucleotide, sometimes the probe works well (A1-7) and other times not so well (A3-6). The relatively poor performance of probe A3-6 presumably means the probe is being cleaved 3' to the quencher rather than between the reporter and quencher. Therefore, the best chance of having a probe that reliably detects accumulation of PCR product in the 5' nuclease PCR assay is to use a probe with the reporter and quencher dyes on opposite ends.

Placing the quencher dye on the 3' end may also provide a slight benefit in terms of hybridization efficiency. The presence of a quencher attached to an internal nucleotide might be expected to disrupt base-pairing and reduce the T_m of a probe. In fact, a 2°C–3°C reduction in T_m has been observed for two probes with internally attached TAMRAs.[9] This disruptive effect would be minimized by placing the quencher at the 3' end. Thus, probes with 3' quenchers might exhibit slightly higher hybridization efficiencies than probes with internal quenchers.

The combination of increased cleavage and hybridization efficiencies means that probes with 3' quenchers probably will be more tolerant of mismatches between probe and target as compared with internally labeled probes. This tolerance of mismatches can be advantageous, as when trying to use a single probe to detect PCR-amplified products from samples of different species. Also, it means that cleavage of probe during PCR is less sensitive to alterations in annealing temperature or other reaction conditions. The one application where tolerance of mismatches may be a disadvantage is for allelic discrimination. Lee et al.[1] demonstrated that allele-specific probes were cleaved between reporter and quencher only when hybridized to a perfectly complementary target. This allowed them to distinguish the normal human cystic fibrosis allele from the ΔF508 mutant. Their probes had TAMRA attached to the seventh nucleotide from

Research▊▊▊

the 5' end and were designed so that any mismatches were between the reporter and quencher. Increasing the distance between reporter and quencher would lessen the disruptive effect of mismatches and allow cleavage of the probe on the incorrect target. Thus, probes with a quencher attached to an internal nucleotide may still be useful for allelic discrimination.

· In this study loss of quenching upon hybridization was used to show that quenching by a 3' TAMRA is dependent on the flexibility of a single-stranded oligonucleotide. The increase in reporter fluorescence intensity, though, could also be used to determine whether hybridization has occurred or not. Thus, oligonucleotides with reporter and quencher dyes attached at opposite ends should also be useful as hybridization probes. The ability to detect hybridization in real time means that these probes could be used to measure hybridization kinetics. Also, this type of probe could be used to develop homogeneous hybridization assays for diagnostics or other applications. Bagwell et al.[10] describe just this type of homogeneous assay where hybridization of a probe causes an increase in fluorescence caused by a loss of quenching. However, they utilized a complex probe design that requires adding nucleotides to both ends of the probe sequence to form two imperfect hairpins. The results presented here demonstrate that the simple addition of a reporter dye to one end of an oligonucleotide and a quencher dye to the other end generates a fluorogenic probe that can detect hybridization or PCR amplification.

ACKNOWLEDGMENTS

REFERENCES

1. Lee, L.G., C.R. Connell, and W. Bloch. 1993. Allelic discrimination by nick-translation PCR with fluorogenic probes. *Nucleic Acids Res.* **21**: 3761–3766.
2. Holland, P.M., R.D. Abramson, R. Watson, and D.H. Gelfand. 1991. Detection of specific polymerase chain reaction product by utilizing the 5' to 3' exonuclease activity of *Thermus aquaticus* DNA polymerase. *Proc. Natl. Acad. Sci.* **88**: 7276–7280.
3. Lyamichev, V., M.A.D. Brow, and J.E. Dahlberg. 1993. Structure-specific endonucleolytic cleavage of nucleic acids by eubacterial DNA polymerases. *Science* **260**: 778–783.
4. Förster, V.Th. 1948. Zwischenmolekulare Energiewanderung und Fluoreszenz. *Ann. Phys. (Leipzig)* **2**: 55–75.
5. Lakowicz, J.R. 1983. Energy transfer. In *Principles of fluorescent spectroscopy*, pp. 303–339. Plenum Press, New York, NY.
6. Stryer, L. and R.P. Haugland. 1967. Energy transfer: A spectroscopic ruler. *Proc. Natl. Acad. Sci.* **58**: 719–726.
7. Nakajima-Iijima, S., H. Hamada, P. Reddy, and T. Kakunaga. 1985. Molecular structure of the human cytoplasmic beta-actin gene: Inter-species homology of sequences in the introns. *Proc. Natl. Acad. Sci.* **82**: 6133–6137.
8. du Breuil, R.M., J.M. Patel, and B.V. Mendelow. 1993. Quantitation of β-actin-specific mRNA transcripts using xeno-competitive PCR. *PCR Methods Applic.* **3**: 57–59.
9. Livak, K.J. (unpubl.).
10. Bagwell, C.B., M.E. Munson, R.L. Christensen, and E.J. Lovett. 1994. A new homogeneous assay system for specific nucleic acid sequences: Poly-dA and poly-A detection. *Nucleic Acids Res.* **22**: 2424–2425.

GENOME METHODS

Real Time Quantitative PCR

Christian A. Heid,[1] Junko Stevens,[2] Kenneth J. Livak,[2] and P. Mickey Williams[1,3]

[1]BioAnalytical Technology Department, Genentech, Inc., South San Francisco, California 94080;
[2]Applied BioSystems Division of Perkin Elmer Corp., Foster City, California 94404

We have developed a novel "real time" quantitative PCR method. The method measures PCR product accumulation through a dual-labeled fluorogenic probe (i.e., TaqMan Probe). This method provides very accurate and reproducible quantitation of gene copies. Unlike other quantitative PCR methods, real-time PCR does not require post-PCR sample handling, preventing potential PCR product carry-over contamination and resulting in much faster and higher throughput assays. The real-time PCR method has a very large dynamic range of starting target molecule determination (at least five orders of magnitude). Real-time quantitative PCR is extremely accurate and less-labor-intensive than current quantitative PCR methods.

Quantitative nucleic acid sequence analysis has had an important role in many fields of biological research. Measurement of gene expression (RNA) has been used extensively in monitoring biological responses to various stimuli (Tan et al. 1994; Huang et al. 1995a,b; Prud'homme et al. 1995). Quantitative gene analysis (DNA) has been used to determine the genome quantity of a particular gene, as in the case of the human HER2 gene, which is amplified in ~30% of breast tumors (Slamon et al. 1987). Gene and genome quantitation (DNA and RNA) also have been used for analysis of human immunodeficiency virus (HIV) burden demonstrating changes in the levels of virus throughout the different phases of the disease (Connor et al. 1993; Piatak et al. 1993b; Furtado et al. 1995).

Many methods have been described for the quantitative analysis of nucleic acid sequences (both for RNA and DNA; Southern 1975; Sharp et al. 1980; Thomas 1980). Recently, PCR has proven to be a powerful tool for quantitative nucleic acid analysis. PCR and reverse transcriptase (RT)–PCR have permitted the analysis of minimal starting quantities of nucleic acid (as little as one cell equivalent). This has made possible many experiments that could not have been performed with traditional methods. Although PCR has provided a powerful tool, it is imperative

that it be used properly for quantitation (Raeymaekers 1995). Many early reports of quantitative PCR and RT–PCR described quantitation of the PCR product but did not measure the initial target sequence quantity. It is essential to design proper controls for the quantitation of the initial target sequences (Ferre 1992; Clementi et al. 1993).

Researchers have developed several methods of quantitative PCR and RT–PCR. One approach measures PCR product quantity in the log phase of the reaction before the plateau (Kellogg et al. 1990; Pang et al. 1990). This method requires that each sample has equal input amounts of nucleic acid and that each sample under analysis amplifies with identical efficiency up to the point of quantitative analysis. A gene sequence (contained in all samples at relatively constant quantities, such as β-actin) can be used for sample amplification efficiency normalization. Using conventional methods of PCR detection and quantitation (gel electrophoresis or plate capture hybridization), it is extremely laborious to assure that all samples are analyzed during the log phase of the reaction (for both the target gene and the normalization gene). Another method, quantitative competitive (QC)–PCR, has been developed and is used widely for PCR quantitation. QC–PCR relies on the inclusion of an internal control competitor in each reaction (Becker-Andre 1991; Piatak et al. 1993a,b). The efficiency of each reaction is normalized to the internal competitor. A known amount of internal competitor can be

[3]Corresponding author.

added to each sample. To obtain relative quantitation, the unknown target PCR product is compared with the known competitor PCR product. Success of a quantitative competitive PCR assay relies on developing an internal control that amplifies with the same efficiency as the target molecule. The design of the competitor and the validation of amplification efficiencies require a dedicated effort. However, because QC-PCR does not require that PCR products be analyzed during the log phase of the amplification, it is the easier of the two methods to use.

Several detection systems are used for quantitative PCR and RT-PCR analysis: (1) agarose gels, (2) fluorescent labelling of PCR products and detection with laser-induced fluorescence using capillary electrophoresis (Fasco et al. 1995; Williams et al. 1996) or acrylamide gels, and (3) plate capture and sandwich probe hybridization (Mulder et al. 1994). Although these methods proved successful, each method requires post-PCR manipulations that add time to the analysis and may lead to laboratory contamination. The sample throughput of these methods is limited (with the exception of the plate capture approach), and, therefore, these methods are not well suited for uses demanding high sample throughput (i.e., screening of large numbers of biomolecules or analyzing samples for diagnostics or clinical trials).

Here we report the development of a novel assay for quantitative DNA analysis. The assay is based on the use of the 5′ nuclease assay first described by Holland et al. (1991). The method uses the 5′ nuclease activity of Taq polymerase to cleave a nonextendible hybridization probe during the extension phase of PCR. The approach uses dual-labeled fluorogenic hybridization probes (Lee et al. 1993; Bassler et al. 1995; Livak et al. 1995a,b). One fluorescent dye serves as a reporter [FAM (i.e., 6-carboxyfluorescein)] and its emission spectra is quenched by the second fluorescent dye, TAMRA (i.e., 6-carboxy-tetramethylrhodamine). The nuclease degradation of the hybridization probe releases the quenching of the FAM fluorescent emission, resulting in an increase in peak fluorescent emission at 518 nm. The use of a sequence detector (ABI Prism) allows measurement of fluorescent spectra of all 96 wells of the thermal cycler continuously during the PCR amplification. Therefore, the reactions are monitored in real time. The output data is described and quantitative analysis of input target DNA sequences is discussed below.

RESULTS

PCR Product Detection in Real Time

The goal was to develop a high-throughput, sensitive, and accurate gene quantitation assay for use in monitoring lipid mediated therapeutic gene delivery. A plasmid encoding human factor VIII gene sequence, pF8TM (see Methods), was used as a model therapeutic gene. The assay uses fluorescent Taqman methodology and an instrument capable of measuring fluorescence in real time (ABI Prism 7700 Sequence Detector). The Taqman reaction requires a hybridization probe labeled with two different fluorescent dyes. One dye is a reporter dye (FAM), the other is a quenching dye (TAMRA). When the probe is intact, fluorescent energy transfer occurs and the reporter dye fluorescent emission is absorbed by the quenching dye (TAMRA). During the extension phase of the PCR cycle, the fluorescent hybridization probe is cleaved by the 5′-3′ nucleolytic activity of the DNA polymerase. On cleavage of the probe, the reporter dye emission is no longer transferred efficiently to the quenching dye, resulting in an increase of the reporter dye fluorescent emission spectra. PCR primers and probes were designed for the human factor VIII sequence and human β-actin gene (as described in Methods). Optimization reactions were performed to choose the appropriate probe and magnesium concentrations yielding the highest intensity of reporter fluorescent signal without sacrificing specificity. The instrument uses a charge-coupled device (i.e., CCD camera) for measuring the fluorescent emission spectra from 500 to 650 nm. Each PCR tube was monitored sequentially for 25 msec with continuous monitoring throughout the amplification. Each tube was re-examined every 8.5 sec. Computer software was designed to examine the fluorescent intensity of both the reporter dye (FAM) and the quenching dye (TAMRA). The fluorescent intensity of the quenching dye, TAMRA, changes very little over the course of the PCR amplification (data not shown). Therefore, the intensity of TAMRA dye emission serves as an internal standard with which to normalize the reporter dye (FAM) emission variations. The software calculates a value termed ΔRn (or ΔRQ) using the following equation: $\Delta Rn = (Rn^+) (Rn^-)$, where Rn^+ = emission intensity of reporter/emission intensity of quencher at any given time in a reaction tube, and Rn^- = emission intensity of re-

HLID ET AL.

porter/emission intensity of quencher measured prior to PCR amplification in that same reaction tube. For the purpose of quantitation, the last three data points (ΔRns) collected during the extension step for each PCR cycle were analyzed. The nucleolytic degradation of the hybridization probe occurs during the extension phase of PCR, and, therefore, reporter fluorescent emission increases during this time. The three data points were averaged for each PCR cycle and the mean value for each was plotted in an "amplification plot" shown in Figure 1A. The ΔRn mean value is plotted on the y-axis, and time, represented by cycle number, is plotted on the x-axis. During the early cycles of the PCR amplification, the ΔRn

value remains at base line. When sufficient hybridization probe has been cleaved by the Taq polymerase nuclease activity, the intensity of reporter fluorescent emission increases. Most PCR amplifications reach a plateau phase of reporter fluorescent emission if the reaction is carried out to high cycle numbers. The amplification plot is examined early in the reaction, at a point that represents the log phase of product accumulation. This is done by assigning an arbitrary threshold that is based on the variability of the base-line data. In Figure 1A, the threshold was set at 10 standard deviations above the mean of base line emission calculated from cycles 1 to 15. Once the threshold is chosen, the point at which

A

B   C
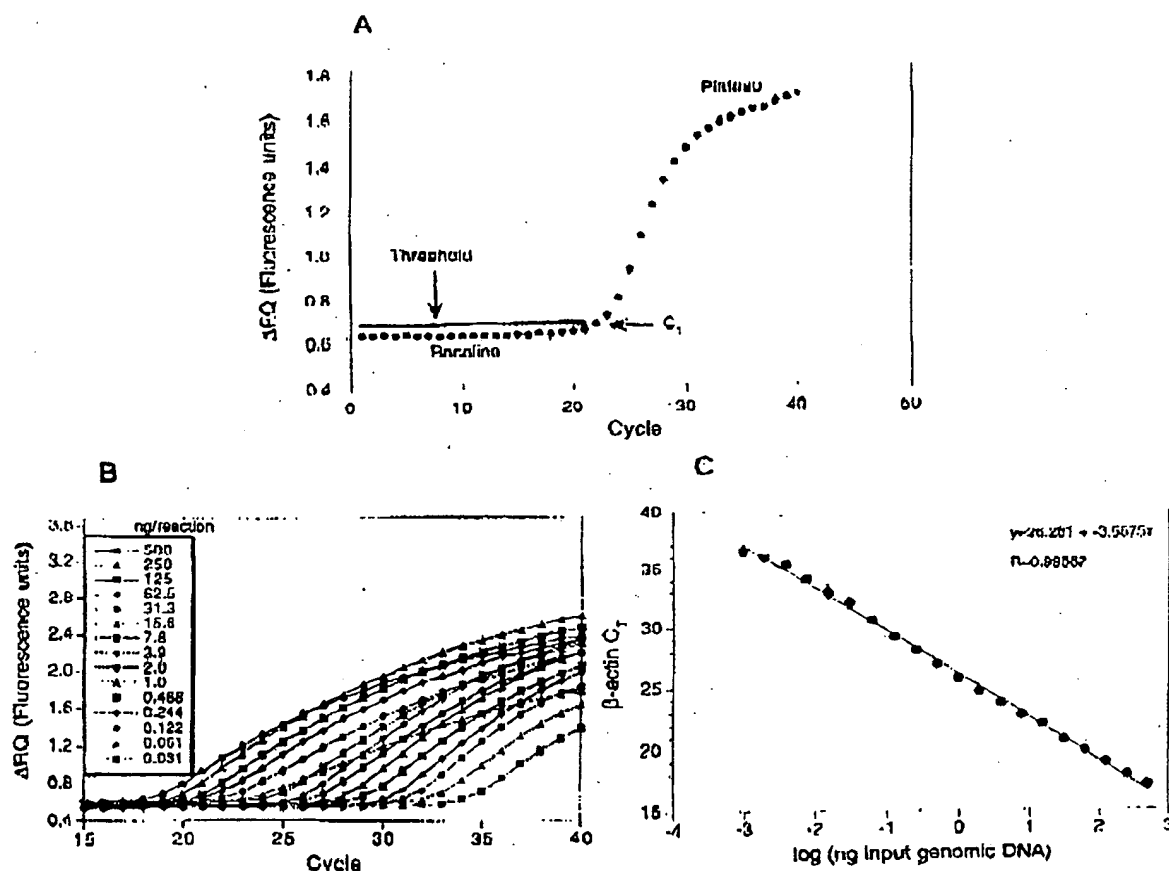
Figure 1 PCR product detection in real time. (A) The Model 7700 software will construct amplification plots from the extension phase fluorescent emission data collected during the PCR amplification. The standard deviation is determined from the data points collected from the base line of the amplification plot. C_T values are calculated by determining the point at which the fluorescence exceeds a threshold limit (usually 10 times the standard deviation of the base line). (B) Overlay of amplification plots of serially (1:2) diluted human genomic DNA samples amplified with β-actin primers. (C) Input DNA concentration of the samples plotted versus C_T. All

the amplification plot crosses the threshold is defined as C_T. C_T is reported as the cycle number at this point. As will be demonstrated, the C_T value is predictive of the quantity of input target.

C_T Values Provide a Quantitative Measurement of Input Target Sequences

Figure 1B shows amplification plots of 15 different PCR amplifications overlaid. The amplifications were performed on a 1:2 serial dilution of human genomic DNA. The amplified target was human β actin. The amplification plots shift to the right (to higher threshold cycles) as the input target quantity is reduced. This is expected because reactions with fewer starting copies of the target molecule require greater amplification to degrade enough probe to attain the threshold fluorescence. An arbitrary threshold of 10 standard deviations above the base line was used to determine the C_T values. Figure 1C represents the C_T values plotted versus the sample dilution value. Each dilution was amplified in triplicate PCR amplifications and plotted as mean values with error bars representing one standard deviation. The C_T values decrease linearly with increasing target quantity. Thus, C_T values can be used as a quantitative measurement of the input target number. It should be noted that the amplification plot for the 15.6-ng sample shown in Figure 1B does not reflect the same fluorescent rate of increase exhibited by most of the other samples. The 15.6-ng sample also achieves endpoint plateau at a lower fluorescent value than would be expected based on the input DNA. This phenomenon has been observed occasionally with other samples (data not shown) and may be attributable to late cycle inhibition; this hypothesis is still under investigation. It is important to note that the flattened slope and early plateau do not impact significantly the calculated C_T value as demonstrated by the fit on the line shown in Figure 1C. All triplicate amplifications resulted in very similar C_T values—the standard deviation did not exceed 0.5 for any dilution. This experiment contains a >100,000-fold range of input target molecules. Using C_T values for quantitation permits a much larger assay range than directly using total fluorescent emission intensity for quantitation. The linear range of fluorescent intensity measurement of the ABI Prism 7700 Se-

ments over a very large range of relative starting target quantities.

Sample Preparation Validation

Several parameters influence the efficiency of PCR amplification: magnesium and salt concentrations, reaction conditions (i.e., time and temperature), PCR target size and composition, primer sequences, and sample purity. All of the above factors are common to a single PCR assay, except sample to sample purity. In an effort to validate the method of sample preparation for the factor VIII assay, PCR amplification reproducibility and efficiency of 10 replicate sample preparations were examined. After genomic DNA was prepared from the 10 replicate samples, the DNA was quantitated by ultraviolet spectroscopy. Amplifications were performed analyzing β-actin gene content in 100 and 25 ng of total genomic DNA. Each PCR amplification was performed in triplicate. Comparison of C_T values for each triplicate sample show minimal variation based on standard deviation and coefficient of variance (Table 1). Therefore, each of the triplicate PCR amplifications was highly reproducible, demonstrating that real time PCR using this instrumentation introduces minimal variation into the quantitative PCR analysis. Comparison of the mean C_T values of the 10 replicate sample preparations also showed minimal variability, indicating that each sample preparation yielded similar results for β-actin gene quantity. The highest C_T difference between any of the samples was 0.85 and 0.71 for the 100 and 25 ng samples, respectively. Additionally, the amplification of each sample exhibited an equivalent rate of fluorescent emission intensity change per amount of DNA target analyzed as indicated by similar slopes derived from the sample dilutions (Fig. 2). Any sample containing an excess of a PCR inhibitor would exhibit a greater measured β-actin C_T value for a given quantity of DNA. In addition, the inhibitor would be diluted along with the sample in the dilution analysis (Fig. 2), altering the expected C_T value change. Each sample amplification yielded a similar result in the analysis, demonstrating that this method of sample preparation is highly reproducible with regard to sample purity.

Quantitative Analysis of a Plasmid After

HUDHAL

Table 1. Reproducibility of Sample Preparation Method

Sample no.	100 ng				25 ng			
	C_T	mean	standard deviation	CV	C_T	mean	standard deviation	CV
1	18.24				20.48			
	18.23				20.55			
	18.33	18.27	0.06	0.32	20.5	20.51	0.03	0.17
2	18.33				20.61			
	18.35				20.59			
	18.44	18.37	0.06	0.32	20.41	20.54	0.11	0.54
3	18.3				20.54			
	18.3				20.6			
	18.42	18.34	0.07	0.36	20.49	20.54	0.06	0.28
4	18.15				20.48			
	18.23				20.44			
	18.32	18.23	0.08	0.46	20.38	20.43	0.05	0.26
5	18.4				20.68			
	18.38				20.87			
	18.46	18.42	0.04	0.23	20.63	20.73	0.13	0.61
6	18.54				21.09			
	18.67				21.04			
	19	18.74	0.24	1.26	21.04	21.06	0.03	0.15
7	18.28				20.67			
	18.36				20.73			
	18.52	18.39	0.12	0.66	20.65	20.68	0.04	0.2
8	18.45				20.98			
	18.7				20.84			
	18.73	18.63	0.16	0.83	20.75	20.86	0.12	0.57
9	18.18				20.46			
	18.34				20.54			
	18.36	18.29	0.1	0.55	20.48	20.51	0.07	0.32
10	18.42				20.79			
	18.57				20.78			
	18.66	18.55	0.12	0.65	20.62	20.73	0.1	0.16
Mean	(1 10)	18.42	0.17	0.90		20.66	0.19	0.94

tor containing a partial cDNA for human factor VIII, pF8TM. A series of transfections was set up using a decreasing amount of the plasmid (40, 4, 0.5, and 0.1 μg). Twenty-four hours posttransfection, total DNA was purified from each flask of cells. β-Actin gene quantity was chosen as a value for normalization of genomic DNA concentration from each sample. In this experiment, β-actin gene content should remain constant relative to total genomic DNA. Figure 3 shows the result of the β-actin DNA measurement (100 ng total DNA determined by ultraviolet spectroscopy) of each sample. Each sample was analyzed in triplicate and the mean β-actin C_T values of the triplicates were plotted (error bars represent one standard deviation). The highest difference

between any two sample means was 0.95 C_T. Ten nanograms of total DNA of each sample were also examined for β-actin. The results again showed that very similar amounts of genomic DNA were present; the maximum mean β actin C_T value difference was 1.0. As Figure 3 shows, the rate of β-actin C_T change between the 100 and 10-ng samples was similar (slope values range between 3.56 and 3.45). This verifies again that the method of sample preparation yields samples of identical PCR integrity (i.e., no sample contained an excessive amount of a PCR inhibitor). However, these results indicate that each sample contained slight differences in the actual amount of genomic DNA analyzed. Determination of actual genomic DNA concentration was accomplished
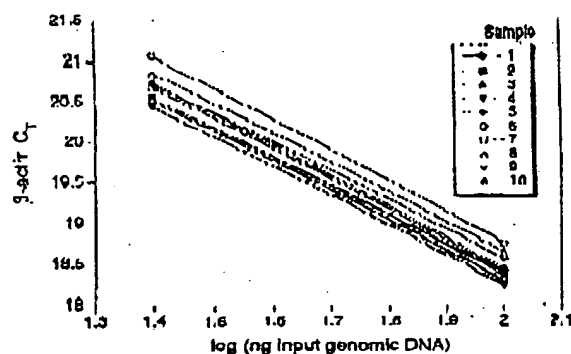
Figure 2 Sample preparation purity. The replicate samples shown in Table 1 were also amplified in triplicate using 25 ng of each DNA sample. The figure shows the input DNA concentration (100 and 25 ng) vs. C_t. In the figure, the 100 and 25 ng points for each sample are connected by a line.

by plotting the mean β-actin C_t value obtained for each 100-ng sample on a β-actin standard curve (shown in Fig. 4C). The actual genomic DNA concentration of each sample, a, was obtained by extrapolation to the x-axis.

Figure 4A shows the measured (i.e., non-normalized) quantities of factor VIII plasmid DNA (pF8TM) from each of the four transient cell transfections. Each reaction contained 100 ng of total sample DNA (as determined by UV spectroscopy). Each sample was analyzed in triplicate
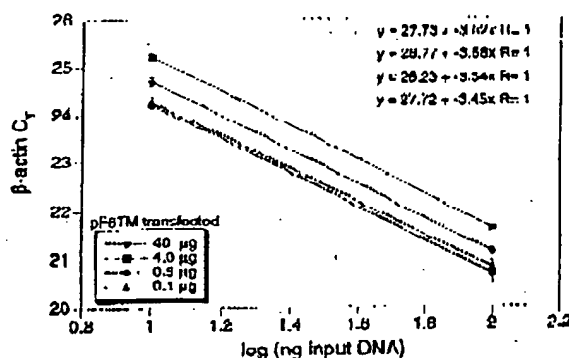
Figure 3 Analysis of transfected cell DNA quantity and purity. The DNA preparations of the four 293 cell transfections (40, 4, 0.5, and 0.1 μg of pF8TM) were analyzed for the β-actin gene. 100 and 10 ng (determined by ultraviolet spectroscopy) of each sample were amplified in triplicate. For each amount of pF8TM that was transfected, the β-actin C_t values are plotted versus the total input DNA concentration.

PCR amplifications. As shown, pF8TM purified from the 293 cells decreases (mean C_t values increase) with decreasing amounts of plasmid transfected. The mean C_t values obtained for pF8TM in Figure 4A were plotted on a standard curve comprised of serially diluted pF8TM, shown in Figure 4B. The quantity of pF8TM, b, found in each of the four transfections was determined by extrapolation to the x axis of the standard curve in Figure 4B. These uncorrected values, b, for pF8TM were normalized to determine the actual amount of pF8TM found per 100 ng of genomic DNA by using the equation:

$$\frac{b \times 100 \text{ ng}}{a} = \frac{\text{actual pF8TM copies per}}{100 \text{ ng of genomic DNA}}$$

where a = actual genomic DNA in a sample and b = pF8TM copies from the standard curve. The normalized quantity of pF8TM per 100 ng of genomic DNA for each of the four transfections is shown in Figure 4D. These results show that the quantity of factor VIII plasmid associated with the 293 cells, 24 hr after transfection, decreases with decreasing plasmid concentration used in the transfection. The quantity of pF8TM associated with 293 cells, after transfection with 40 μg of plasmid, was 35 pg per 100 ng genomic DNA. This results in ~520 plasmid copies per cell.

DISCUSSION

We have described a new method for quantitating gene copy numbers using real-time analysis of PCR amplifications. Real-time PCR is compatible with either of the two PCR (RT-PCR) approaches: (1) quantitative competitive where an internal competitor for each target sequence is used for normalization (data not shown) or (2) quantitative comparative PCR using a normalization gene contained within the sample (i.e., β-actin) or a "housekeeping" gene for RT-PCR. If equal amounts of nucleic acid are analyzed for each sample and if the amplification efficiency before quantitative analysis is identical for each sample, the internal control (normalization gene or competitor) should give equal signals for all samples.

The real-time PCR method offers several advantages over the other two methods currently employed (see the Introduction). First, the real-time PCR method is performed in a closed-tube system and requires no post-PCR manipulation
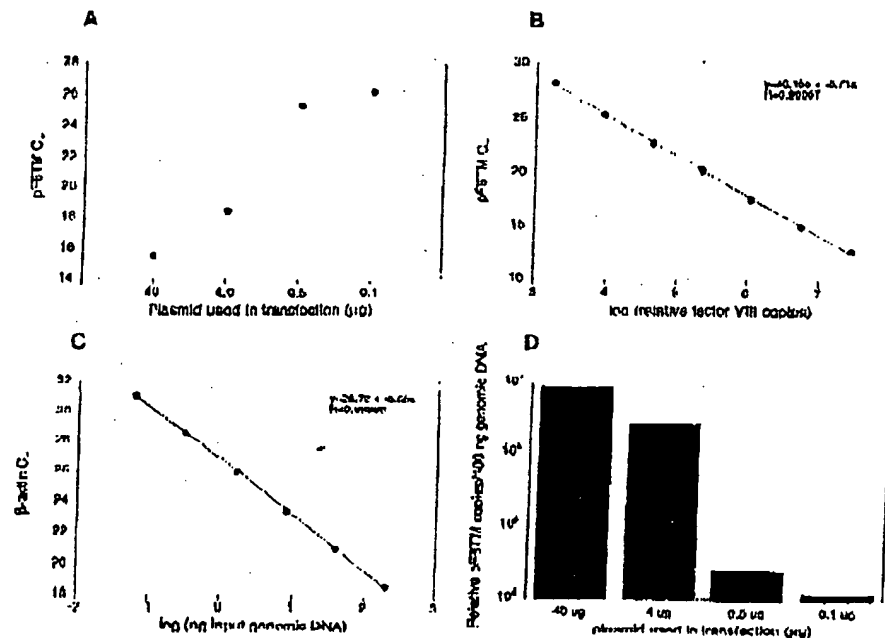
HLID LT AL.

Figure 4 Quantitative analysis of pF8TM in transfected cells. (A) Amount of plasmid DNA used for the transfection plotted against the mean C_t value determined for pF8TM remaining 24 hr after transfection. (B,C) Standard curves of pF8TM and β-actin, respectively. pF8TM DNA (B) and genomic DNA (C) were diluted serially 1:5 before amplification with the appropriate primers. The β-actin standard curve was used to normalize the results of A to 100 ng of genomic DNA. (D) The amount of pF8TM present per 100 ng of genomic DNA.

of sample. Therefore, the potential for PCR contamination in the laboratory is reduced because amplified products can be analyzed and disposed of without opening the reaction tubes. Second, this method supports the use of a normalization gene (i.e., β-actin) for quantitative PCR or housekeeping genes for quantitative RT-PCR controls. Analysis is performed in real time during the log phase of product accumulation. Analysis during log phase permits many different genes (over a wide input target range) to be analyzed simultaneously, without concern of reaching reaction plateau at different cycles. This will make multigene analysis assays much easier to develop, because individual internal competitors will not be needed for each gene under analysis. Third, sample throughput will increase dramatically with the new method because there is no post-PCR processing time. Additionally, working in a 96-well format is highly compatible with automation technology.

The real-time PCR method is highly reproducible. Replicate amplifications can be analyzed

for each sample minimizing potential error. The system allows for a very large assay dynamic range (approaching 1,000,000-fold starting target). Using a standard curve for the target of interest, relative copy number values can be determined for any unknown sample. Fluorescent threshold values, C_t, correlate linearly with relative DNA copy numbers. Real time quantitative RT-PCR methodology (Gibson et al., this issue) has also been developed. Finally, real time quantitative PCR methodology can be used to develop high-throughput screening assays for a variety of applications [quantitative gene expression (RT-PCR), gene copy assays (Her2, HIV, etc.), genotyping (knockout mouse analysis), and Immuno-PCR].

Real-time PCR may also be performed using intercalating dyes (Higuchi et al. 1992) such as ethidium bromide. The fluorogenic probe method offers a major advantage over intercalating dyes--greater specificity (i.e., primer dimers and nonspecific PCR products are not detected).

METHODS

Generation of a Plasmid Containing a Partial cDNA for Human Factor VIII

Total RNA was harvested (RNAzol B from Tel Test, Inc., Friendswood, TX) from cells transfected with a factor VIII expression vector, pCIS2.8c25D (Eaton et al. 1986; Gorman et al. 1990). A factor VIII partial cDNA sequence was generated by RT-PCR [GeneAmp EZ rTth RNA PCR Kit (part N808-0179, PE Applied Biosystems, Foster City, CA)] using the PCR primers F8for and F8rev (primer sequences are shown below). The amplicon was reamplified using modified F8for and F8rev primers (appended with *Bam*HI and *Hind*III restriction site sequences at the 5' end) and cloned into pGEM-3Z (Promega Corp., Madison, WI). The resulting clone, pF8TM, was used for transient transfection of 293 cells.

Amplification of Target DNA and Detection of Amplicon Factor VIII Plasmid DNA

(pF8TM) was amplified with the primers F8for 5'-CCC-GTGCCAAGAGTGACATGTC-3' and F8rev 5'-AAACCT-CAGCCTGGATGGTACG-3'. The reaction produced a 422-bp PCR product. The forward primer was designed to recognize a unique sequence found in the 5' untranslated region of the parent pCIS2.8c25D plasmid and therefore does not recognize and amplify the human factor VIII gene. Primers were chosen with the assistance of the computer program Oligo 4.0 (National Biosciences, Inc., Plymouth, MN). The human β-actin gene was amplified with the primers β-actin forward primer 5'-TCACCCACACTGT GCCCATCTACGA-3' and β-actin reverse primer 5'-CAG-CGGAACCGCTCATTGCCAATGG-3'. The reaction produced a 295-bp PCR product.

Amplification reactions (50 µl) contained a DNA sample, 10× PCR Buffer II (5 µl), 200 µM dATP, dCTP, dGTP, and 400 µM dUTP, 4 mM $MgCl_2$, 1.25 Units Ampli Taq DNA polymerase, 0.5 unit AmpErase uracil N-glycosylase (UNG), 50 pmole of each factor VIII primer, and 15 pmole of each β-actin primer. The reactions also contained one of the following detection probes (100 nM each): F8probe 5'(FAM)AGCTCTCCACCTGCTTCTTTCTGT-GCCTT(TAMRA)p 3' and β-actin probe 5' (FAM)ATGCCC-X(TAMRA)CCCCCATGCCATCp-3' where p indicates phosphorylation and X indicates a linker arm nucleotide. Reaction tubes were MicroAmp Optical Tubes (part number N801 0933, Perkin Elmer) that were frosted (at Perkin Elmer) to prevent light from reflecting. Tube caps were similar to MicroAmp Caps but specially designed to prevent light scattering. All of the PCR consumables were supplied by PE Applied Biosystems (Foster City, CA) except the factor VIII primers, which were synthesized at Genentech, Inc. (South San Francisco, CA). Probes were designed using the Oligo 4.0 software, following guidelines suggested in the Model 7700 Sequence Detector Instrument manual. Briefly, probe T_m should be at least 5°C higher than the annealing temperature used during thermal cycling; primers should not form stable duplexes with the probe.

The thermal cycling conditions included 2 min at 50°C and 10 min at 95°C. Thermal cycling proceeded with

reactions were performed in the Model 7700 Sequence Detector (PE Applied Biosystems), which contains a Gene-Amp PCR System 9600. Reaction conditions were programmed on a Power Macintosh 7100 (Apple Computer, Santa Clara, CA) linked directly to the Model 7700 Sequence Detector. Analysis of data was also performed on the Macintosh computer. Collection and analysis software was developed at PE Applied Biosystems.

Transfection of Cells with Factor VIII Construct

Four T175 flasks of 293 cells (ATCC CRL 1573), a human fetal kidney suspension cell line, were grown to 80% confluency and transfected pF8TM. Cells were grown in the following media: 50% HAM'S F12 without GHT, 50% low glucose Dulbecco's modified Eagle medium (DMEM) without glycine with sodium bicarbonate, 10% fetal bovine serum, 2 mM L-glutamine, and 1% penicillin-streptomycin. The media was changed 30 min before the transfection. pF8TM DNA amounts of 40, 4, 0.5, and 0.1 µg were added to 1.5 ml of a solution containing 0.125 M $CaCl_2$ and 1× HEPES. The four mixtures were left at room temperature for 10 min and then added dropwise to the cells. The flasks were incubated at 37°C and 5% CO_2 for 24 hr, washed with PBS, and resuspended in PBS. The resuspended cells were divided into aliquots and DNA was extracted immediately using the QIAamp Blood Kit (Qiagen, Chatsworth, CA). DNA was eluted into 200 µl of 20 mM Tris-HCl at pH 8.0.

ACKNOWLEDGMENTS

REFERENCES

Bassler, H.A., S.J. Flood, K.J. Livak, J. Marmaro, R. Knorr, and C.A. Batt. 1995. Use of a fluorogenic probe in a PCR-based assay for the detection of Listeria monocytogenes. *App. Environ. Microbiol.* **61**: 3724–3728.

Becker-Andre, M. 1991. Quantitative evaluation of mRNA levels. *Meth. Mol. Cell. Biol.* **2**: 189–201.

Clementi, M., S. Menzo, P. Bagnarelli, A. Manzin, A. Valenza, and P.E. Varaldo. 1993. Quantitative PCR and RT-PCR in virology. [Review]. *PCR Methods Applic.* **2**: 191–196.

Connor, R.I., H. Mohri, Y. Cao, and D.D. Ho. 1993. Increased viral burden and cytopathicity correlate temporally with CD4+ T-lymphocyte decline and clinical progression in human immunodeficiency virus type 1-infected individuals. *J. Virol.* **67**: 1772–1777.

Eaton, D.L., W.I. Wood, D. Eaton, P.E. Hass, P.

HEID LI AL.

Vehar, and C. Gorman. 1986. Construction and characterization of an active factor VIII variant lacking the central one third of the molecule. *Biochemistry* 25: 8343–8347.

Fasco, M.J., C.P. Treanor, S. Spivack, H.L. Figge, and L.S. Kaminsky. 1995. Quantitative RNA-polymerase chain reaction-DNA analysis by capillary electrophoresis and laser-induced fluorescence. *Anal. Biochem.* 224: 140–147.

Ferre, F. 1992. Quantitative or semi-quantitative PCR: Reality versus myth. *PCR Methods Applic.* 2: 1–9.

Furtado, M.R., L.A. Kingsley, and S.M. Wolinsky. 1995. Changes in the viral mRNA expression pattern correlate with a rapid rate of CD4+ T-cell number decline in human immunodeficiency virus type 1-infected individuals. *J. Virol.* 69: 2092–2100.

Gibson, U.E.M., C.A. Heid, and P.M. Williams. 1996. A novel method for real time quantitative competitive RT-PCR. *Genome Res.* (this issue).

Gorman, C.M., D.R. Gies, and G. McCray. 1990. Transient production of proteins using an adenovirus transformed cell line. *DNA Prot. Engin. Tech.* 2: 3–10.

Higuchi, R., G. Dollinger, P.S. Walsh, and R. Griffith. 1992. Simultaneous amplification and detection of specific DNA sequences. *Biotechnology* 10: 413–417.

Holland, P.M., R.D. Abramson, R. Watson, and D.H. Gelfand. 1991. Detection of specific polymerase chain reaction product by utilizing the 5'—3' exonuclease activity of *Thermus aquaticus* DNA polymerase. *Proc. Natl. Acad. Sci.* 88: 7276–7280.

Huang, S.K., H.Q. Xiao, T.J. Kleine, G. Paciotti, H.G. Marsh, L.M. Lichtenstein, and M.C. Liu. 1995a. IL-13 expression at the sites of allergen challenge in patients with asthma. *J. Immun.* 155: 2688–2694.

Huang, S.K., M. Yi, E. Palmer, and D.G. Marsh. 1995b. A dominant T cell receptor beta-chain in response to a short ragweed allergen, Amb a 5. *J. Immun.* 154: 6157–6162.

Kellogg, D.E., J.J. Sninsky, and S. Kowk. 1990. Quantitation of HIV-1 proviral DNA relative to cellular DNA by the polymerase chain reaction. *Anal. Biochem.* 189: 202–208.

Lee, L.G., C.R. Connell, and W. Bloch. 1993. Allelic discrimination by nick-translation PCR with fluorogenic probes. *Nucleic Acids Res.* 21: 3761–3766.

Livak, K.J., S.J. Flood, J. Marmaro, W. Giusti, and K. Deetz. 1995a. Oligonucleotides with fluorescent dyes at opposite ends provide a quenched probe system useful for detecting PCR product and nucleic acid hybridization. *PCR Methods Applic.* 4: 357–362.

Livak, K.J., J. Marmaro, and J.A. Todd. 1995b. Towards fully automated genome-wide polymorphism screening. [Letter] *Nature Genet.* 9: 341–342.

Mulder, J., N. McKinney, C. Christopherson, J. Sninsky, L. Greenfield, and S. Kwok. 1994. Rapid and simple PCR assay for quantitation of human immunodeficiency virus type 1 RNA in plasma: Application to acute retroviral infection. *J. Clin. Microbiol.* 32: 292–300.

Pang, S., Y. Koyanagi, S. Miles, C. Wiley, H.V. Vinters, and I.S. Chen. 1990. High levels of unintegrated HIV-1 DNA in brain tissue of AIDS dementia patients. *Nature* 343: 85–89.

Piatak, M.J., K.C. Luk, B. Williams, and J.D. Lifson. 1993a. Quantitative competitive polymerase chain reaction for accurate quantitation of HIV DNA and RNA species. *BioTechniques* 14: 70–81.

Piatak, M.J., M.S. Saag, L.C. Yang, S.J. Clark, J.C. Kappes, K.C. Luk, B.H. Hahn, G.M. Shaw, and J.D. Lifson. 1993b. High levels of HIV-1 in plasma during all stages of infection determined by competitive PCR [see Comments]. *Science* 259: 1749–1754.

Prud'homme, G.J., D.H. Kono, and A.N. Theofilopoulos. 1995. Quantitative polymerase chain reaction analysis reveals marked overexpression of interleukin-1 beta, interleukin-1 and interferon-gamma mRNA in the lymph nodes of lupus-prone mice. *Mol. Immunol.* 32: 495–503.

Raeymaekers, L. 1995. A commentary on the practical applications of competitive PCR. *Genome Res.* 5: 91–94.

Sharp, P.A., A.J. Berk, and S.M. Berget. 1980. Transcription maps of adenovirus. *Methods Enzymol.* 65: 750–768.

Slamon, D.J., G.M. Clark, S.G. Wong, W.J. Levin, A. Ullrich, and W.L. McGuire. 1987. Human breast cancer: Correlation of relapse and survival with amplification of the HER-2/neu oncogene. *Science* 235: 177–182.

Southern, E.M. 1975. Detection of specific sequences among DNA fragments separated by gel electrophoresis. *J. Mol. Biol.* 98: 503–517.

Tan, X., X. Sun, C.F. Gonzalez, and W. Hsueh. 1994. PAF and TNF increase the precursor of NF-kappa B p50 mRNA in mouse intestine: Quantitative analysis by competitive PCR. *Biochim. Biophys. Acta* 1215: 157–162.

Thomas, P.S. 1980. Hybridization of denatured RNA and small DNA fragments transferred to nitrocellulose. *Proc. Natl. Acad. Sci.* 77: 5201–5205.

Williams, S., C. Schwer, A. Krishnarao, C. Heid, B. Karger, and P.M. Williams. 1996. Quantitative competitive PCR: Analysis of amplified products of the HIV-1 gag gene by capillary electrophoresis with laser induced fluorescence detection. *Anal. Biochem.* (in press).

WISP genes are members of the connective tissue growth factor family that are up-regulated in Wnt-1-transformed cells and aberrantly expressed in human colon tumors

DIANE PENNICA*†, TODD A. SWANSON*, JAMES W. WELSH*, MARGARET A. ROY‡, DAVID A. LAWRENCE*, JAMES LEE‡, JENNIFER BRUSH‡, LISA A. TANEYHILL§, BETHANNE DEUEL‡, MICHAEL LEW¶, COLIN WATANABE‖, ROBERT L. COHEN*, MONA F. MELHEM**, GENE G. FINLEY**, PHIL QUIRKE††, AUDREY D. GODDARD‡, KENNETH J. HILLAN¶, AUSTIN L. GURNEY‡, DAVID BOTSTEIN‡,‡‡, AND ARNOLD J. LEVINE§

Departments of *Molecular Oncology, ‡Molecular Biology, ‖Scientific Computing, and ¶Pathology, Genentech Inc., 1 DNA Way, South San Francisco, CA 94080; **University of Pittsburgh School of Medicine, Veterans Administration Medical Center, Pittsburgh, PA 15240; ††University of Leeds, Leeds, LS29JT United Kingdom; ‡‡Department of Genetics, Stanford University, Palo Alto, CA 94305; and §Department of Molecular Biology, Princeton University, Princeton, NJ 08544

ABSTRACT   Wnt family members are critical to many developmental processes, and components of the Wnt signaling pathway have been linked to tumorigenesis in familial and sporadic colon carcinomas. Here we report the identification of two genes, *WISP-1* and *WISP-2*, that are up-regulated in the mouse mammary epithelial cell line C57MG transformed by Wnt-1, but not by Wnt-4. Together with a third related gene, *WISP-3*, these proteins define a subfamily of the connective tissue growth factor family. Two distinct systems demonstrated *WISP* induction to be associated with the expression of Wnt-1. These included (*i*) C57MG cells infected with a Wnt-1 retroviral vector or expressing Wnt-1 under the control of a tetracyline repressible promoter, and (*ii*) Wnt-1 transgenic mice. The *WISP-1* gene was localized to human chromosome 8q24.1–8q24.3. *WISP-1* genomic DNA was amplified in colon cancer cell lines and in human colon tumors and its RNA overexpressed (2- to >30-fold) in 84% of the tumors examined compared with patient-matched normal mucosa. *WISP-3* mapped to chromosome 6q22–6q23 and also was overexpressed (4- to >40-fold) in 63% of the colon tumors analyzed. In contrast, *WISP-2* mapped to human chromosome 20q12–20q13 and its DNA was amplified, but RNA expression was reduced (2- to >30-fold) in 79% of the tumors. These results suggest that the *WISP* genes may be downstream of Wnt-1 signaling and that aberrant levels of *WISP* expression in colon cancer may play a role in colon tumorigenesis.

Wnt-1 is a member of an expanding family of cysteine-rich, glycosylated signaling proteins that mediate diverse developmental processes such as the control of cell proliferation, adhesion, cell polarity, and the establishment of cell fates (1, 2). Wnt-1 originally was identified as an oncogene activated by the insertion of mouse mammary tumor virus in virus-induced mammary adenocarcinomas (3, 4). Although Wnt-1 is not expressed in the normal mammary gland, expression of Wnt-1 in transgenic mice causes mammary tumors (5).

In mammalian cells, Wnt family members initiate signaling by binding to the seven-transmembrane spanning Frizzled receptors and recruiting the cytoplasmic protein Dishevelled (Dsh) to the cell membrane (1, 2, 6). Dsh then inhibits the kinase activity of the normally constitutively active glycogen synthase kinase-3β (GSK-3β) resulting in an increase in β-catenin levels. Stabilized β-catenin interacts with the transcription factor TCF/Lef1, forming a complex that appears in the nucleus and binds TCF/Lef1 target DNA elements to activate transcription (7, 8). Other experiments suggest that the adenomatous polyposis coli (APC) tumor suppressor gene also plays an important role in Wnt signaling by regulating β-catenin levels (9). APC is phosphorylated by GSK-3β, binds to β-catenin, and facilitates its degradation. Mutations in either APC or β-catenin have been associated with colon carcinomas and melanomas, suggesting these mutations contribute to the development of these types of cancer, implicating the Wnt pathway in tumorigenesis (1).

Although much has been learned about the Wnt signaling pathway over the past several years, only a few of the transcriptionally activated downstream components activated by Wnt have been characterized. Those that have been described cannot account for all of the diverse functions attributed to Wnt signaling. Among the candidate Wnt target genes are those encoding the nodal-related 3 gene, *Xnr3*, a member of the transforming growth factor (TGF)-β superfamily, and the homeobox genes, *engrailed*, *goosecoid*, *twin* (*Xtwn*), and *siamois* (2). A recent report also identifies c-*myc* as a target gene of the Wnt signaling pathway (10).

To identify additional downstream genes in the Wnt signaling pathway that are relevant to the transformed cell phenotype, we used a PCR-based cDNA subtraction strategy, suppression subtractive hybridization (SSH) (11), using RNA isolated from C57MG mouse mammary epithelial cells and C57MG cells stably transformed by a Wnt-1 retrovirus. Overexpression of Wnt-1 in this cell line is sufficient to induce a partially transformed phenotype, characterized by elongated and refractile cells that lose contact inhibition and form a multilayered array (12, 13). We reasoned that genes differentially expressed between these two cell lines might contribute to the transformed phenotype.

In this paper, we describe the cloning and characterization of two genes up-regulated in Wnt-1 transformed cells, *WISP-1* and *WISP-2*, and a third related gene, *WISP-3*. The *WISP* genes are members of the CCN family of growth factors, which includes connective tissue growth factor (CTGF), Cyr61, and *nov*, a family not previously linked to Wnt signaling.

MATERIALS AND METHODS

SSH. SSH was performed by using the PCR-Select cDNA Subtraction Kit (CLONTECH). Tester double-stranded

---

---

cDNA was synthesized from 2 μg of poly(A)$^+$ RNA isolated from the C57MG/Wnt-1 cell line and driver cDNA from 2 μg of poly(A)$^+$ RNA from the parent C57MG cells. The subtracted cDNA library was subcloned into a pGEM-T vector for further analysis.

cDNA Library Screening. Clones encoding full-length mouse *WISP-1* were isolated by screening a λgt10 mouse embryo cDNA library (CLONTECH) with a 70-bp probe from the original partial clone 568 sequence corresponding to amino acids 128–169. Clones encoding full-length human *WISP-1* were isolated by screening λgt10 lung and fetal kidney cDNA libraries with the same probe at low stringency. Clones encoding full-length mouse and human *WISP-2* were isolated by screening a C57MG/Wnt-1 or human fetal lung cDNA library with a probe corresponding to nucleotides 1463–1512. Full-length cDNAs encoding *WISP-3* were cloned from human bone marrow and fetal kidney libraries.

Expression of Human WISP RNA. PCR amplification of first-strand cDNA was performed with human Multiple Tissue cDNA panels (CLONTECH) and 300 μM of each dNTP at 94°C for 1 sec, 62°C for 30 sec, 72°C for 1 min, for 22–32 cycles. *WISP* and glyceraldehyde-3-phosphate dehydrogenase primer sequences are available on request.

In Situ Hybridization. ^{33}P-labeled sense and antisense riboprobes were transcribed from an 897-bp PCR product corresponding to nucleotides 601–1440 of mouse *WISP-1* or a 294-bp PCR product corresponding to nucleotides 82–375 of mouse *WISP-2*. All tissues were processed as described (40).

Radiation Hybrid Mapping. Genomic DNA from each hybrid in the Stanford G3 and Genebridge4 Radiation Hybrid Panels (Research Genetics, Huntsville, AL) and human and hamster control DNAs were PCR-amplified, and the results were submitted to the Stanford or Massachusetts Institute of Technology web servers.

Cell Lines, Tumors, and Mucosa Specimens. Tissue specimens were obtained from the Department of Pathology (University of Pittsburgh) for patients undergoing colon resection and from the University of Leeds, United Kingdom. Genomic DNA was isolated (Qiagen) from the pooled blood of 10 normal human donors, surgical specimens, and the following ATCC human cell lines: SW480, COLO 320DM, HT-29, WiDr, and SW403 (colon adenocarcinomas), SW620 (lymph node metastasis, colon adenocarcinoma), HCT 116 (colon carcinoma), SK-CO-1 (colon adenocarcinoma, ascites), and HM7 (a variant of ATCC colon adenocarcinoma cell line LS 174T). DNA concentration was determined by using Hoechst dye 33258 intercalation fluorimetry. Total RNA was prepared by homogenization in 7 M GuSCN followed by centrifugation over CsCl cushions or prepared by using RNAzol.

Gene Amplification and RNA Expression Analysis. Relative gene amplification and RNA expression of *WISP*s and c-*myc* in the cell lines, colorectal tumors, and normal mucosa were determined by quantitative PCR. Gene-specific primers and fluorogenic probes (sequences available on request) were designed and used to amplify and quantitate the genes. The relative gene copy number was derived by using the formula $2^{(\Delta ct)}$ where ΔCt represents the difference in amplification cycles required to detect the *WISP* genes in peripheral blood lymphocyte DNA compared with colon tumor DNA or colon tumor RNA compared with normal mucosal RNA. The ∂-method was used for calculation of the SE of the gene copy number or RNA expression level. The *WISP*-specific signal was normalized to that of the glyceraldehyde-3-phosphate dehydrogenase housekeeping gene. All TaqMan assay reagents were obtained from Perkin–Elmer Applied Biosystems.

RESULTS

Isolation of *WISP-1* and *WISP-2* by SSH. To identify Wnt-1-inducible genes, we used the technique of SSH using the

mouse mammary epithelial cell line C57MG and C57MG cells that stably express Wnt-1 (11). Candidate differentially expressed cDNAs (1,384 total) were sequenced. Thirty-nine percent of the sequences matched known genes or homologues, 32% matched expressed sequence tags, and 29% had no match. To confirm that the transcript was differentially expressed, semiquantitative reverse transcription–PCR and Northern analysis were performed by using mRNA from the C57MG and C57MG/Wnt-1 cells.

Two of the cDNAs, *WISP-1* and *WISP-2*, were differentially expressed, being induced in the C57MG/Wnt-1 cell line, but not in the parent C57MG cells or C57MG cells overexpressing Wnt-4 (Fig. 1 *A* and *B*). Wnt-4, unlike Wnt-1, does not induce the morphological transformation of C57MG cells and has no effect on β-catenin levels (13, 14). Expression of *WISP-1* was up-regulated approximately 3-fold in the C57MG/Wnt-1 cell line and *WISP-2* by approximately 5-fold by both Northern analysis and reverse transcription–PCR.

An independent, but similar, system was used to examine *WISP* expression after Wnt-1 induction. C57MG cells expressing the *Wnt-1* gene under the control of a tetracycline-repressible promoter produce low amounts of Wnt-1 in the repressed state but show a strong induction of *Wnt-1* mRNA and protein within 24 hr after tetracycline removal (8). The levels of Wnt-1 and *WISP* RNA isolated from these cells at various times after tetracycline removal were assessed by quantitative PCR. Strong induction of Wnt-1 mRNA was seen as early as 10 hr after tetracycline removal. Induction of *WISP* mRNA (2- to 6-fold) was seen at 48 and 72 hr (data not shown). These data support our previous observations that show that *WISP* induction is correlated with Wnt-1 expression. Because the induction is slow, occurring after approximately 48 hr, the induction of *WISP*s may be an indirect response to Wnt-1 signaling.

cDNA clones of human *WISP-1* were isolated and the sequence compared with mouse *WISP-1*. The cDNA sequences of mouse and human *WISP-1* were 1,766 and 2,830 bp in length, respectively, and encode proteins of 367 aa, with predicted relative molecular masses of ≈40,000 (M_r 40 K). Both have hydrophobic N-terminal signal sequences, 38 conserved cysteine residues, and four potential N-linked glycosylation sites and are 84% identical (Fig. 2A).

Full-length cDNA clones of mouse and human *WISP-2* were 1,734 and 1,293 bp in length, respectively, and encode proteins of 251 and 250 aa, respectively, with predicted relative molecular masses of ≈27,000 (M_r 27 K) (Fig. 2B). Mouse and human *WISP-2* are 73% identical. Human *WISP-2* has no potential N-linked glycosylation sites, and mouse *WISP-2* has one at
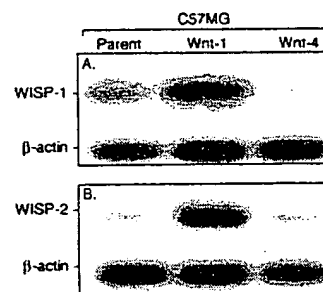

Fig. 1.   *WISP-1* and *WISP-2* are induced by Wnt-1, but not Wnt-4, expression in C57MG cells. Northern analysis of *WISP-1* (*A*) and *WISP-2* (*B*) expression in C57MG, C57MG/Wnt-1, and C57MG/Wnt-4 cells. Poly(A)$^+$ RNA (2 μg) was subjected to Northern blot analysis and hybridized with a 70-bp mouse *WISP-1*-specific probe (amino acids 278–300) or a 190-bp *WISP-2*-specific probe (nucleotides 1438–1627) in the 3' untranslated region. Blots were rehybridized with human β-actin probe.
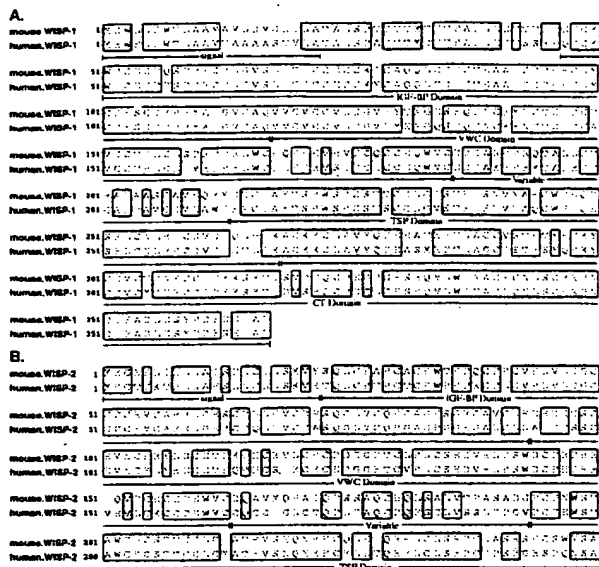
Cell Biology, Medical Sciences: Pennica *et al.*

Proc. Natl. Acad. Sci. USA 95 (1998)   14719

FIG. 2. Encoded amino acid sequence alignment of mouse and human *WISP-1* (*A*) and mouse and human *WISP-2* (*B*). The potential signal sequence, insulin-like growth factor-binding protein (IGF-BP), VWC, thrombospondin (TSP), and C-terminal (CT) domains are underlined.

FIG. 3. (*A*) Encoded amino acid sequence alignment of human WISPs. The cysteine residues of WISP-1 and WISP-2 that are not present in WISP-3 are indicated with a dot. (*B*) Schematic representation of the WISP proteins showing the domain structure and cysteine residues (vertical lines). The four cysteine residues in the VWC domain that are absent in WISP-3 are indicated with a dot. (*C*) Expression of *WISP* mRNA in human tissues. PCR was performed on human multiple-tissue cDNA panels (CLONTECH) from the indicated adult and fetal tissues.

position 197. *WISP-2* has 28 cysteine residues that are conserved among the 38 cysteines found in *WISP-1*.

Identification of *WISP-3*. To search for related proteins, we screened expressed sequence tag (EST) databases with the WISP-1 protein sequence and identified several ESTs as potentially related sequences. We identified a homologous protein that we have called WISP-3. A full-length human *WISP-3* cDNA of 1,371 bp was isolated corresponding to those ESTs that encode a 354-aa protein with a predicted molecular mass of 39,293. WISP-3 has two potential N-linked glycosylation sites and 36 cysteine residues. An alignment of the three human WISP proteins shows that WISP-1 and WISP-3 are the most similar (42% identity), whereas WISP-2 has 37% identity with WISP-1 and 32% identity with WISP-3 (Fig. 3*A*).

***WISPs* Are Homologous to the CTGF Family of Proteins.** Human *WISP-1*, *WISP-2*, and *WISP-3* are novel sequences; however, mouse *WISP-1* is the same as the recently identified *Elm1* gene. *Elm1* is expressed in low, but not high, metastatic mouse melanoma cells, and suppresses the *in vivo* growth and metastatic potential of K-1735 mouse melanoma cells (15). Human and mouse *WISP-2* are homologous to the recently described rat gene, *rCop-1* (16). Significant homology (36–44%) was seen to the CCN family of growth factors. This family includes three members, CTGF, Cyr61, and the protooncogene *nov*. CTGF is a chemotactic and mitogenic factor for fibroblasts that is implicated in wound healing and fibrotic disorders and is induced by TGF-β (17). Cyr61 is an extracellular matrix signaling molecule that promotes cell adhesion, proliferation, migration, angiogenesis, and tumor growth (18, 19). *nov* (nephroblastoma overexpressed) is an immediate early gene associated with quiescence and found altered in Wilms tumors (20). The proteins of the CCN family share functional, but not sequence, similarity to Wnt-1. All are secreted, cysteine-rich heparin binding glycoproteins that associate with the cell surface and extracellular matrix.

WISP proteins exhibit the modular architecture of the CCN family, characterized by four conserved cysteine-rich domains (Fig. 3*B*) (21). The N-terminal domain, which includes the first 12 cysteine residues, contains a consensus sequence (GCGC-CXXC) conserved in most insulin-like growth factor (IGF)-
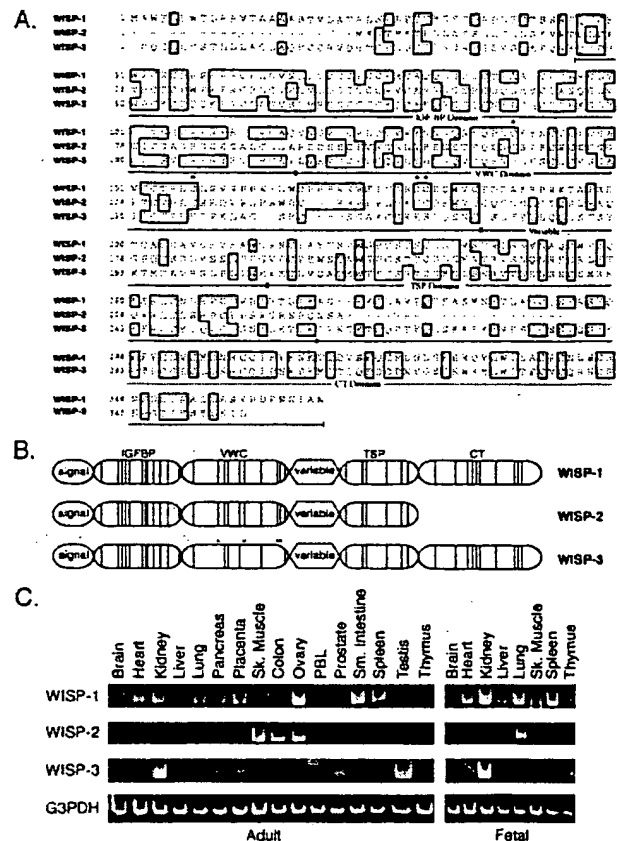
binding proteins (BP). This sequence is conserved in WISP-2 and WISP-3, whereas WISP-1 has a glutamine in the third position instead of a glycine. CTGF recently has been shown to specifically bind IGF (22) and a truncated *nov* protein lacking the IGF-BP domain is oncogenic (23). The von Willebrand factor type C module (VWC), also found in certain collagens and mucins, covers the next 10 cysteine residues, and is thought to participate in protein complex formation and oligomerization (24). The VWC domain of WISP-3 differs from all CCN family members described previously, in that it contains only six of the 10 cysteine residues (Fig. 3 *A* and *B*). A short variable region follows the VWC domain. The third module, the thrombospondin (TSP) domain is involved in binding to sulfated glycoconjugates and contains six cysteine residues and a conserved WSxCSxxCG motif first identified in thrombospondin (25). The C-terminal (CT) module containing the remaining 10 cysteines is thought to be involved in dimerization and receptor binding (26). The CT domain is present in all CCN family members described to date but is absent in WISP-2 (Fig. 3*A* and *B*). The existence of a putative signal sequence and the absence of a transmembrane domain suggest that WISPs are secreted proteins, an observation supported by an analysis of their expression and secretion from mammalian cell and baculovirus cultures (data not shown).

Expression of *WISP* mRNA in Human Tissues. Tissue-specific expression of human *WISPs* was characterized by PCR

analysis on adult and fetal multiple tissue cDNA panels. *WISP-1* expression was seen in the adult heart, kidney, lung, pancreas, placenta, ovary, small intestine, and spleen (Fig. 3*C*). Little or no expression was detected in the brain, liver, skeletal muscle, colon, peripheral blood leukocytes, prostate, testis, or thymus. *WISP-2* had a more restricted tissue expression and was detected in adult skeletal muscle, colon, ovary, and fetal lung. Predominant expression of *WISP-3* was seen in adult kidney and testis and fetal kidney. Lower levels of *WISP-3* expression were detected in placenta, ovary, prostate, and small intestine.

In Situ **Localization of *WISP-1* and *WISP-2*.** Expression of *WISP-1* and *WISP-2* was assessed by *in situ* hybridization in mammary tumors from Wnt-1 transgenic mice. Strong expression of *WISP-1* was observed in stromal fibroblasts lying within the fibrovascular tumor stroma (Fig. 4 *A–D*). However, low-level *WISP-1* expression also was observed focally within tumor cells (data not shown). No expression was observed in normal breast. Like *WISP-1*, *WISP-2* expression also was seen in the tumor stroma in breast tumors from Wnt-1 transgenic animals (Fig. 4 *E–H*). However, *WISP-2* expression in the stroma was in spindle-shaped cells adjacent to capillary vessels, whereas

FIG. 4.   (*A*, *C*, *E*, and *G*) Representative hematoxylin/eosin-stained images from breast tumors in Wnt-1 transgenic mice. The corresponding dark-field images showing *WISP-1* expression are shown in *B* and *D*. The tumor is a moderately well-differentiated adenocarcinoma showing evidence of adenoid cystic change. At low power (*A* and *B*), expression of *WISP-1* is seen in the delicate branching fibrovascular tumor stroma (arrowhead). At higher magnification, expression is seen in the stromal(s) fibroblasts (*C* and *D*), and tumor cells are negative. Focal expression of *WISP-1*, however, was observed in tumor cells in some areas. Images of *WISP-2* expression are shown in *E–H*. At low power (*E* and *F*), expression of WISP-2 is seen in cells lying within the fibrovascular tumor stroma. At higher magnification, these cells appeared to be adjacent to capillary vessels whereas tumor cells are negative (*G* and *H*).

the predominant cell type expressing *WISP-1* was the stromal fibroblasts.

Chromosome Localization of the *WISP* Genes. The chromosomal location of the human *WISP* genes was determined by radiation hybrid mapping panels. *WISP-1* is approximately 3.48 cR from the meiotic marker AFM259xc5 [logarithm of odds (lod) score 16.31] on chromosome 8q24.1 to 8q24.3, in the same region as the human locus of the *nov*H family member (27) and roughly 4 Mbs distal to c-*myc* (28). Preliminary fine mapping indicates that *WISP-1* is located near D8S1712 STS. *WISP-2* is linked to the marker SHGC-33922 (lod = 1,000) on chromosome 20q12–20q13.1. Human *WISP-3* mapped to chromosome 6q22–6q23 and is linked to the marker AFM211ze5 (lod = 1,000). *WISP-3* is approximately 18 Mbs proximal to CTGF and 23 Mbs proximal to the human cellular oncogene *MYB* (27, 29).

Amplification and Aberrant Expression of *WISPs* in Human Colon Tumors. Amplification of protooncogenes is seen in many human tumors and has etiological and prognostic significance. For example, in a variety of tumor types, c-*myc* amplification has been associated with malignant progression and poor prognosis (30). Because *WISP-1* resides in the same general chromosomal location (8q24) as c-*myc*, we asked whether it was a target of gene amplification, and, if so, whether this amplification was independent of the c-*myc* locus. Genomic DNA from human colon cancer cell lines was assessed by quantitative PCR and Southern blot analysis. (Fig. 5 *A* and *B*). Both methods detected similar degrees of *WISP-1* amplification. Most cell lines showed significant (2- to 4-fold) amplification, with the HT-29 and WiDr cell lines demonstrating an 8-fold increase. Significantly, the pattern of amplification observed did not correlate with that observed for c-*myc*, indicating that the c-*myc* gene is not part of the amplicon that involves the *WISP-1* locus.

We next examined whether the *WISP* genes were amplified in a panel of 25 primary human colon adenocarcinomas. The relative *WISP* gene copy number in each colon tumor DNA was compared with pooled normal DNA from 10 donors by quantitative PCR (Fig. 6). The copy number of *WISP-1* and *WISP-2* was significantly greater than one, approximately 2-fold for *WISP-1* in about 60% of the tumors and 2- to 4-fold for *WISP-2* in 92% of the tumors (*P* < 0.001 for each). The copy number for *WISP-3* was indistinguishable from one (*P* = 0.166). In addition, the copy number of *WISP-2* was significantly higher than that of *WISP-1* (*P* < 0.001).

The levels of *WISP* transcripts in RNA isolated from 19 adenocarcinomas and their matched normal mucosa were
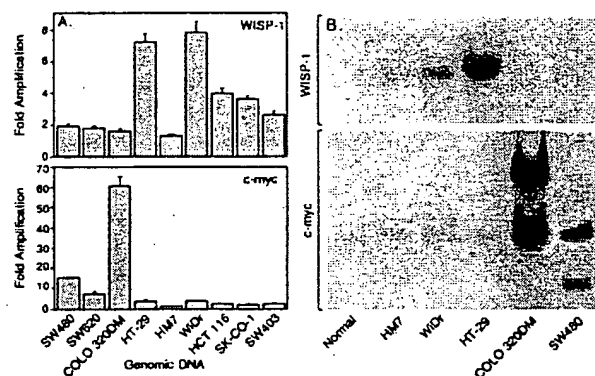

FIG. 5.   Amplification of *WISP-1* genomic DNA in colon cancer cell lines. (*A*) Amplification in cell line DNA was determined by quantitative PCR. (*B*) Southern blots containing genomic DNA (10 μg) digested with *Eco*RI (*WISP-1*) or *Xba*I (c-*myc*) were hybridized with a 100-bp human *WISP-1* probe (amino acids 186–219) or a human c-*myc* probe (located at bp 1901–2000). The *WISP* and *myc* genes are detected in normal human genomic DNA after a longer film exposure.
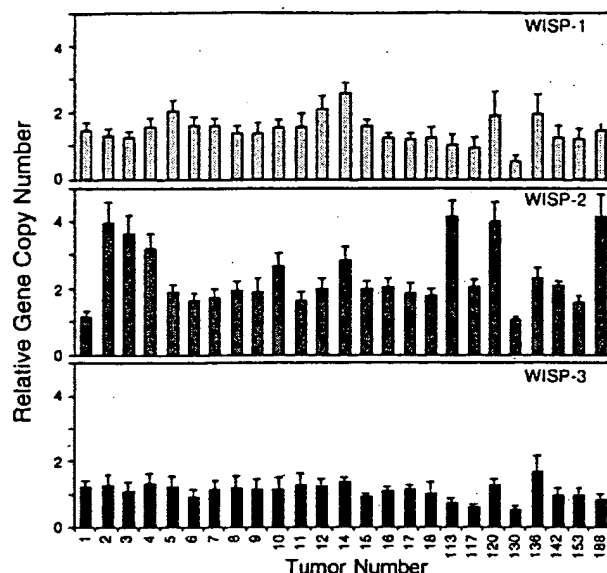
FIG. 6. Genomic amplification of *WISP* genes in human colon tumors. The relative gene copy number of the *WISP* genes in 25 adenocarcinomas was assayed by quantitative PCR, by comparing DNA from primary human tumors with pooled DNA from 10 healthy donors. The data are means ± SEM from one experiment done in triplicate. The experiment was repeated at least three times.

assessed by quantitative PCR (Fig. 7). The level of *WISP-1* RNA present in tumor tissue varied but was significantly increased (2- to >25-fold) in 84% (16/19) of the human colon tumors examined compared with normal adjacent mucosa. Four of 19 tumors showed greater than 10-fold overexpression. In contrast, in 79% (15/19) of the tumors examined, *WISP-2* RNA expression was significantly lower in the tumor than the mucosa. Similar to *WISP-1*, *WISP-3* RNA was overexpressed in 63% (12/19) of the colon tumors compared with the normal

FIG. 7. *WISP* RNA expression in primary human colon tumors relative to expression in normal mucosa from the same patient. Expression of *WISP* mRNA in 19 adenocarcinomas was assayed by quantitative PCR. The Dukes stage of the tumor is listed under the sample number. The data are means ± SEM from one experiment done in triplicate. The experiment was repeated at least twice.

mucosa. The amount of overexpression of *WISP-3* ranged from 4- to >40-fold.

DISCUSSION

One approach to understanding the molecular basis of cancer is to identify differences in gene expression between cancer cells and normal cells. Strategies based on assumptions that steady-state mRNA levels will differ between normal and malignant cells have been used to clone differentially expressed genes (31). We have used a PCR-based selection strategy, SSH, to identify genes selectively expressed in C57MG mouse mammary epithelial cells transformed by Wnt-1.

Three of the genes isolated, *WISP-1*, *WISP-2*, and *WISP-3*, are members of the CCN family of growth factors, which includes CTGF, Cyr61, and *nov*, a family not previously linked to Wnt signaling.

Two independent experimental systems demonstrated that *WISP* induction was associated with the expression of Wnt-1. The first was C57MG cells infected with a Wnt-1 retroviral vector or C57MG cells expressing Wnt-1 under the control of a tetracyline-repressible promoter, and the second was in Wnt-1 transgenic mice, where breast tissue expresses Wnt-1, whereas normal breast tissue does not. No *WISP* RNA expression was detected in mammary tumors induced by polyoma virus middle T antigen (data not shown). These data suggest a link between Wnt-1 and *WISP*s in that in these two situations, *WISP* induction was correlated with Wnt-1 expression.

It is not clear whether the *WISP*s are directly or indirectly induced by the downstream components of the Wnt-1 signaling pathway (i.e., β-catenin-TCF-1/Lef1). The increased levels of *WISP* RNA were measured in Wnt-1-transformed cells, hours or days after Wnt-1 transformation. Thus, *WISP* expression could result from Wnt-1 signaling directly through β-catenin transcription factor regulation or alternatively through Wnt-1 signaling turning on a transcription factor, which in turn regulates *WISP*s.

The *WISP*s define an additional subfamily of the CCN family of growth factors. One striking difference observed in the protein sequence of WISP-2 is the absence of a CT domain, which is present in CTGF, Cyr61, *nov*, WISP-1, and WISP-3. This domain is thought to be involved in receptor binding and dimerization. Growth factors, such as TGF-β, platelet-derived growth factor, and nerve growth factor, which contain a cystine knot motif exist as dimers (32). It is tempting to speculate that WISP-1 and WISP-3 may exist as dimers, whereas WISP-2 exists as a monomer. If the CT domain is also important for receptor binding, WISP-2 may bind its receptor through a different region of the molecule than the other CCN family members. No specific receptors have been identified for CTGF or *nov*. A recent report has shown that integrin $\alpha_v\beta_3$ serves as an adhesion receptor for Cyr61 (33).

The strong expression of *WISP-1* and *WISP-2* in cells lying within the fibrovascular tumor stroma in breast tumors from Wnt-1 transgenic animals is consistent with previous observations that transcripts for the related CTGF gene are primarily expressed in the fibrous stroma of mammary tumors (34). Epithelial cells are thought to control the proliferation of connective tissue stroma in mammary tumors by a cascade of growth factor signals similar to that controlling connective tissue formation during wound repair. It has been proposed that mammary tumor cells or inflammatory cells at the tumor interstitial interface secrete TGF-β1, which is the stimulus for stromal proliferation (34). TGF-β1 is secreted by a large percentage of malignant breast tumors and may be one of the growth factors that stimulates the production of CTGF and WISPs in the stroma.

It was of interest that *WISP-1* and *WISP-2* expression was observed in the stromal cells that surrounded the tumor cells

(epithelial cells) in the Wnt-1 transgenic mouse sections of breast tissue. This finding suggests that paracrine signaling could occur in which the stromal cells could supply WISP-1 and WISP-2 to regulate tumor cell growth on the WISP extracellular matrix. Stromal cell-derived factors in the extracellular matrix have been postulated to play a role in tumor cell migration and proliferation (35). The localization of *WISP-1* and *WISP-2* in the stromal cells of breast tumors supports this paracrine model.

An analysis of *WISP-1* gene amplification and expression in human colon tumors showed a correlation between DNA amplification and overexpression, whereas overexpression of *WISP-3* RNA was seen in the absence of DNA amplification. In contrast, *WISP-2* DNA was amplified in the colon tumors, but its mRNA expression was significantly reduced in the majority of tumors compared with the expression in normal colonic mucosa from the same patient. The gene for human *WISP-2* was localized to chromosome 20q12–20q13, at a region frequently amplified and associated with poor prognosis in node negative breast cancer and many colon cancers, suggesting the existence of one or more oncogenes at this locus (36–38). Because the center of the 20q13 amplicon has not yet been identified, it is possible that the apparent amplification observed for *WISP-2* may be caused by another gene in this amplicon.

A recent manuscript on *rCop-1*, the rat orthologue of *WISP-2*, describes the loss of expression of this gene after cell transformation, suggesting it may be a negative regulator of growth in cell lines (16). Although the mechanism by which *WISP-2* RNA expression is down-regulated during malignant transformation is unknown, the reduced expression of *WISP-2* in colon tumors and cell lines suggests that it may function as a tumor suppressor. These results show that the *WISP* genes are aberrantly expressed in colon cancer and suggest that their altered expression may confer selective growth advantage to the tumor.

Members of the Wnt signaling pathway have been implicated in the pathogenesis of colon cancer, breast cancer, and melanoma, including the tumor suppressor gene adenomatous polyposis coli and β-catenin (39). Mutations in specific regions of either gene can cause the stabilization and accumulation of cytoplasmic β-catenin, which presumably contributes to human carcinogenesis through the activation of target genes such as the *WISP*s. Although the mechanism by which Wnt-1 transforms cells and induces tumorigenesis is unknown, the identification of *WISP*s as genes that may be regulated downstream of Wnt-1 in C57MG cells suggests they could be important mediators of Wnt-1 transformation. The amplification and altered expression patterns of the *WISP*s in human colon tumors may indicate an important role for these genes in tumor development.

1. Cadigan, K. M. & Nusse, R. (1997) *Genes Dev.* 11, 3286–3305.
2. Dale, T. C. (1998) *Biochem. J.* 329, 209–223.
3. Nusse, R. & Varmus, H. E. (1982) *Cell* 31, 99–109.
4. van Ooyen, A. & Nusse, R. (1984) *Cell* 39, 233–240.
5. Tsukamoto, A. S., Grosschedl, R., Guzman, R. C., Parslow, T. & Varmus, H. E. (1988) *Cell* 55, 619–625.
6. Brown, J. D. & Moon, R. T. (1998) *Curr. Opin. Cell. Biol.* 10, 182–187.
7. Molenaar, M., van de Wetering, M., Oosterwegel, M., Peterson-Maduro, J., Godsave, S., Korinek, V., Roose, J., Destree, O. & Clevers, H. (1996) *Cell* 86, 391–399.
8. Korinek, V., Barker, N., Willert, K., Molenaar, M., Roose, J., Wagenaar, G., Markman, M., Lamers, W., Destree, O. & Clevers, H. (1998) *Mol. Cell. Biol.* 18, 1248–1256.
9. Munemitsu, S., Albert, I., Souza, B., Rubinfeld, B. & Polakis, P. (1995) *Proc. Natl. Acad. Sci. USA* 92, 3046–3050.
10. He, T. C., Sparks, A. B., Rago, C., Hermeking, H., Zawel, L., da Costa, L. T., Morin, P. J., Vogelstein, B. & Kinzler, K. W. (1998) *Science* 281, 1509–1512.
11. Diatchenko, L., Lau, Y. F., Campbell, A. P., Chenchik, A., Moqadam, F., Huang, B., Lukyanov, S., Lukyanov, K., Gurskaya, N., Sverdlov, E. D. & Siebert, P. D. (1996) *Proc. Natl. Acad. Sci. USA* 93, 6025–6030.
12. Brown, A. M., Wildin, R. S., Prendergast, T. J. & Varmus, H. E. (1986) *Cell* 46, 1001–1009.
13. Wong, G. T., Gavin, B. J. & McMahon, A. P. (1994) *Mol. Cell. Biol.* 14, 6278–6286.
14. Shimizu, H., Julius, M. A., Giarre, M., Zheng, Z., Brown, A. M. & Kitajewski, J. (1997) *Cell Growth Differ.* 8, 1349–1358.
15. Hashimoto, Y., Shindo-Okada, N., Tani, M., Nagamachi, Y., Takeuchi, K., Shiroishi, T., Toma, H. & Yokota, J. (1998) *J. Exp. Med.* 187, 289–296.
16. Zhang, R., Averboukh, L., Zhu, W., Zhang, H., Jo, H., Dempsey, P. J., Coffey, R. J., Pardee, A. B. & Liang, P. (1998) *Mol. Cell. Biol.* 18, 6131–6141.
17. Grotendorst, G. R. (1997) *Cytokine Growth Factor Rev.* 8, 171–179.
18. Kireeva, M. L., Mo, F. E., Yang, G. P. & Lau, L. F. (1996) *Mol. Cell. Biol.* 16, 1326–1334.
19. Babic, A. M., Kireeva, M. L., Kolesnikova, T. V. & Lau, L. F. (1998) *Proc. Natl. Acad. Sci. USA* 95, 6355–6360.
20. Martinerie, C., Huff, V., Joubert, I., Badzioch, M., Saunders, G., Strong, L. & Perbal, B. (1994) *Oncogene* 9, 2729–2732.
21. Bork, P. (1993) *FEBS Lett.* 327, 125–130.
22. Kim, H. S., Nagalla, S. R., Oh, Y., Wilson, E., Roberts, C. T., Jr. & Rosenfeld, R. G. (1997) *Proc. Natl. Acad. Sci. USA* 94, 12981–12986.
23. Joliot, V., Martinerie, C., Dambrine, G., Plassiart, G., Brisac, M., Crochet, J. & Perbal, B. (1992) *Mol. Cell. Biol.* 12, 10–21.
24. Mancuso, D. J., Tuley, E. A., Westfield, L. A., Worrall, N. K., Shelton-Inloes, B. B., Sorace, J. M., Alevy, Y. G. & Sadler, J. E. (1989) *J. Biol. Chem.* 264, 19514–19527.
25. Holt, G. D., Pangburn, M. K. & Ginsburg, V. (1990) *J. Biol. Chem.* 265, 2852–2855.
26. Voorberg, J., Fontijn, R., Calafat, J., Janssen, H., van Mourik, J. A. & Pannekoek, H. (1991) *J. Cell. Biol.* 113, 195–205.
27. Martinerie, C., Viegas-Pequignot, E., Guenard, I., Dutrillaux, B., Nguyen, V. C., Bernheim, A. & Perbal, B. (1992) *Oncogene* 7, 2529–2534.
28. Takahashi, E., Hori, T., O'Connell, P., Leppert, M. & White, R. (1991) *Cytogenet. Cell. Genet.* 57, 109–111.
29. Meese, E., Meltzer, P. S., Witkowski, C. M. & Trent, J. M. (1989) *Genes Chromosomes Cancer* 1, 88–94.
30. Garte, S. J. (1993) *Crit. Rev. Oncog.* 4, 435–449.
31. Zhang, L., Zhou, W., Velculescu, V. E., Kern, S. E., Hruban, R. H., Hamilton, S. R., Vogelstein, B. & Kinzler, K. W. (1997) *Science* 276, 1268–1272.
32. Sun, P. D. & Davies, D. R. (1995) *Annu. Rev. Biophys. Biomol. Struct.* 24, 269–291.
33. Kireeva, M. L., Lam, S. C. T. & Lau, L. F. (1998) *J. Biol. Chem.* 273, 3090–3096.
34. Frazier, K. S. & Grotendorst, G. R. (1997) *Int. J. Biochem. Cell. Biol.* 29, 153–161.
35. Wernert, N. (1997) *Virchows Arch.* 430, 433–443.
36. Tanner, M. M., Tirkkonen, M., Kallioniemi, A., Collins, C., Stokke, T., Karhu, R., Kowbel, D., Shadravan, F., Hintz, M., Kuo, W. L., *et al.* (1994) *Cancer Res.* 54, 4257–4260.
37. Brinkmann, U., Gallo, M., Polymeropoulos, M. H. & Pastan, I. (1996) *Genome Res.* 6, 187–194.
38. Bischoff, J. R., Anderson, L., Zhu, Y., Mossie, K., Ng, L., Souza, B., Schryver, B., Flanagan, P., Clairvoyant, F., Ginther, C., *et al.* (1998) *EMBO J.* 17, 3052–3065.
39. Morin, P. J., Sparks, A. B., Korinek, V., Barker, N., Clevers, H., Vogelstein, B. & Kinzler, K. W. (1997) *Science* 275, 1787–1790.
40. Lu, L. H. & Gillett, N. (1994) *Cell Vision* 1, 169–176.

methods. Peptides AENK or AEQK were dissolved in water, made isotonic with NaCl and diluted into RPMI growth medium. T-cell-proliferation assays were done essentially as described[20,21]. Briefly, after antigen pulsing (30 μg ml^{-1} TTCF) with tetrapeptides (1–2 mg ml^{-1}), PBMCs or EBV-B cells were washed in PBS and fixed for 45 s in 0.05% glutaraldehyde. Glycine was added to a final concentration of 0.1M and the cells were washed five times in RPMI 1640 medium containing 1% FCS before co-culture with T-cell clones in round-bottom 96-well microtitre plates. After 48 h, the cultures were pulsed with 1 μCi of ^{3}H-thymidine and harvested for scintillation counting 16 h later. Predigestion of native TTCF was done by incubating 200 μg TTCF with 0.25 μg pig kidney legumain in 500 μl 50 mM citrate buffer, pH 5.5, for 1 h at 37 °C.

Glycopeptide digestions. The peptides HIDNEEDI, HIDN(N-glucosamine) EEDI and HIDNESDI, which are based on the TTCF sequence, and QQQHLFGSNVTDCSGNFCLFR(KKK), which is based on human transferrin, were obtained by custom synthesis. The three C-terminal lysine residues were added to the natural sequence to aid solubility. The transferrin glycopeptide QQQHLFGSNVTDCSGNFCLFR was prepared by tryptic (Promega) digestion of 5 mg reduced, carboxy-methylated human transferrin followed by concanavalin A chromatography[11]. Glycopeptides corresponding to residues 622–642 and 421–452 were isolated by reverse-phase HPLC and identified by mass spectrometry and N-terminal sequencing. The lyophilized transferrin-derived peptides were redissolved in 50 mM sodium acetate, pH 5.5, 10 mM dithiothreitol, 20% methanol. Digestions were performed for 3 h at 30 °C with 5–50 mU ml^{-1} pig kidney legumain or B-cell AEP. Products were analysed by HPLC or MALDI-TOF mass spectrometry using a matrix of 10 mg ml^{-1} α-cyanocinnamic acid in 50% acetonitrile/0.1% TFA and a PerSeptive Biosystems Elite STR mass spectrometer set to linear or reflector mode. Internal standardization was obtained with a matrix ion of 568.13 mass units.

1. Chen, J. M. et al. Cloning, isolation, and characterisation of mammalian legumain, an asparaginyl endopeptidase. J. Biol. Chem. 272, 8090–8098 (1997).
2. Kembhavi, A. A., Buttle, D. J., Knight, C. G. & Barrett, A. J. The two cysteine endopeptidases of legume seeds: purification and characterization by use of specific fluorometric assays. Arch. Biochem. Biophys. 303, 208–213 (1993).
3. Dalton, J. P., Hola Jamriska, L. & Bridley, P. J. Asparaginyl endopeptidase activity in adult Schistosoma mansoni. Parasitology 111, 575–580 (1995).
4. Bennett, K. et al. Antigen processing for presentation by class II major histocompatibility complex requires cleavage by cathespin E. Eur. J. Immunol. 22, 1519–1524 (1992).
5. Riese, R. J. et al. Essential role for cathepsin S in MHC class II-associated invariant chain processing and peptide loading. Immunity 4, 357–366 (1996).
6. Rodriguez, G. M. & Diment, S. Role of cathepsin D in antigen presentation of ovalbumin. J. Immunol. 149, 2894–2898 (1992).
7. Hewitt, E. W. et al. Natural processing sites for human cathepsin E and cathepsin D in tetanus toxin: implications for T cell epitope generation. J. Immunol. 159, 4693–4699 (1997).
8. Watts, C. Capture and processing of exogenous antigens for presentation on MHC molecules. Annu. Rev. Immunol. 15, 821–850 (1997).
9. Chapman, H. A. Endosomal proteases and MHC class II function. Curr. Opin. Immunol. 10, 93–102 (1998).
10. Fineschi, B. & Miller, J. Endosomal proteases and antigen processing. Trends Biochem. Sci. 22, 377–382 (1997).
11. Lu, J. & van Halbeek, H. Complete ¹H and ¹³C resonance assignments of a 21-amino acid glycopeptide prepared from human serum transferrin. Carbohydr. Res. 296, 1–21 (1996).
12. Fearon, D. T. & Locksley, R. M. The instructive role of innate immunity in the acquired immune response. Science 272, 50–54 (1996).
13. Medzhitov, R. & Janeway, C. A. J. Innate immunity: the virtues of a nonclonal system of recognition. Cell 91, 295–298 (1997).
14. Wyatt, R. et al. The antigenic structure of the HIV gp120 envelope glycoprotein. Nature 393, 705–711 (1998).
15. Botarelli, P. et al. N-glycosylation of HIV gp120 may constrain recognition by T lymphocytes. J. Immunol. 147, 3128–3132 (1991).
16. Davidson, H. W., West, M. A. & Watts, C. Endocytosis, intracellular trafficking, and processing of membrane IgG and monovalent antigen/membrane IgG complexes in B lymphocytes. J. Immunol. 144, 4101–4109 (1990).
17. Barrett, A. J. & Kirschke, H. Cathepsin B, cathepsin H and cathepsin L. Methods Enzymol. 80, 535–559 (1981).
18. Makoff, A. J., Ballantine, S. P., Smallwood, A. E. & Fairweather, N. F. Expression of tetanus toxin fragment C in E. coli: its purification and potential use as a vaccine. Biotechnology 7, 1043–1046 (1989).
19. Lane, D. P. & Harlow, E. Antibodies: A Laboratory Manual (Cold Spring Harbor Laboratory Press, 1988).
20. Lanzavecchia, A. Antigen-specific interaction between T and B cells. Nature 314, 537–539 (1985).
21. Pond, L. & Watts, C. Characterization of transport of newly assembled, T cell-stimulatory MHC class II-peptide complexes from MHC class II compartments to the cell surface. J. Immunol. 159, 543–553 (1997).

Genomic amplification of a decoy receptor for Fas ligand in lung and colon cancer

Robert M. Pitti*†, Scot A. Marsters*†, David A. Lawrence*†, Margaret Roy*, Frank C. Kischkel*, Patrick Dowd*, Arthur Huang*, Christopher J. Donahue*, Steven W. Sherwood*, Daryl T. Baldwin*, Paul J. Godowski*, William I. Wood*, Austin L. Gurney*, Kenneth J. Hillan*, Robert L. Cohen*, Audrey D. Goddard*, David Botstein‡ & Avi Ashkenazi*

* Departments of Molecular Oncology, Molecular Biology, and Immunology, Genentech Inc., 1 DNA Way, South San Francisco, California 94080, USA
‡ Department of Genetics, Stanford University, Stanford, California 94305, USA
† These authors contributed equally to this work

Fas ligand (FasL) is produced by activated T cells and natural killer cells and it induces apoptosis (programmed cell death) in target cells through the death receptor Fas/Apo1/CD95 (ref. 1). One important role of FasL and Fas is to mediate immune-cytotoxic killing of cells that are potentially harmful to the organism, such as virus-infected or tumour cells[1]. Here we report the discovery of a soluble decoy receptor, termed decoy receptor 3 (DcR3), that binds to FasL and inhibits FasL-induced apoptosis. The DcR3 gene was amplified in about half of 35 primary lung and colon tumours studied, and DcR3 messenger RNA was expressed in malignant tissue. Thus, certain tumours may escape FasL-dependent immune-cytotoxic attack by expressing a decoy receptor that blocks FasL.

By searching expressed sequence tag (EST) databases, we identified a set of related ESTs that showed homology to the tumour necrosis factor (TNF) receptor (TNFR) gene superfamily[2]. Using the overlapping sequence, we isolated a previously unknown full-length complementary DNA from human fetal lung. We named the protein encoded by this cDNA decoy receptor 3 (DcR3). The cDNA encodes a 300-amino-acid polypeptide that resembles members of the TNFR family (Fig. 1a): the amino terminus contains a leader sequence, which is followed by four tandem cysteine-rich domains (CRDs). Like one other TNFR homologue, osteoprotegerin (OPG)[3], DcR3 lacks an apparent transmembrane sequence, which indicates that it may be a secreted, rather than a membrane-asscociated, molecule. We expressed a recombinant, histidine-tagged form of DcR3 in mammalian cells; DcR3 was secreted into the cell culture medium, and migrated on polyacrylamide gels as a protein of relative molecular mass 35,000 (data not shown). DcR3 shares sequence identity in particular with OPG (31%) and TNFR2 (29%), and has relatively less homology with Fas (17%). All of the cysteines in the four CRDs of DcR3 and OPG are conserved; however, the carboxy-terminal portion of DcR3 is 101 residues shorter.

We analysed expression of DcR3 mRNA in human tissues by northern blotting (Fig. 1b). We detected a predominant 1.2-kilobase transcript in fetal lung, brain, and liver, and in adult spleen, colon and lung. In addition, we observed relatively high DcR3 mRNA expression in the human colon carcinoma cell line SW480.

To investigate potential ligand interactions of DcR3, we generated a recombinant, Fc-tagged DcR3 protein. We tested binding of DcR3–Fc to human 293 cells transfected with individual TNF-family ligands, which are expressed as type 2 transmembrane proteins (these transmembrane proteins have their N termini in the cytosol). DcR3–Fc showed a significant increase in binding to cells transfected with FasL[4] (Fig. 2a), but not to cells transfected with TNF[5], Apo2L/TRAIL[6,7], Apo3L/TWEAK[8,9], or OPGL/TRANCE/

RANKL[10-12] (data not shown). DcR3–Fc immunoprecipitated shed FasL from FasL-transfected 293 cells (Fig. 2b) and purified soluble FasL (Fig. 2c), as did the Fc-tagged ectodomain of Fas but not TNFR1. Gel-filtration chromatography showed that DcR3–Fc and soluble FasL formed a stable complex (Fig. 2d). Equilibrium analysis indicated that DcR3–Fc and Fas–Fc bound to soluble FasL with a comparable affinity ($K_d = 0.8 \pm 0.2$ and 1.1 ± 0.1 nM, respectively; Fig. 2e), and that DcR3–Fc could block nearly all of the binding of soluble FasL to Fas–Fc (Fig. 2e, inset). Thus, DcR3 competes with Fas for binding to FasL.

To determine whether binding of DcR3 inhibits FasL activity, we tested the effect of DcR3–Fc on apoptosis induction by soluble FasL in Jurkat T leukaemia cells, which express Fas (Fig. 3a). DcR3–Fc and Fas–Fc blocked soluble-FasL-induced apoptosis in a similar dose-dependent manner, with half-maximal inhibition at ~0.1 µg ml^{-1}. Time-course analysis showed that the inhibition did not merely delay cell death, but rather persisted for at least 24 hours (Fig. 3b). We also tested the effect of DcR3–Fc on activation-induced cell death (AICD) of mature T lymphocytes, a FasL-dependent process[1]. Consistent with previous results[13], activation of interleukin-2-stimulated CD4-positive T cells with anti-CD3 antibody increased the level of apoptosis twofold, and Fas–Fc blocked this effect substantially (Fig. 3c); DcR3–Fc blocked the

induction of apoptosis to a similar extent. Thus, DcR3 binding blocks apoptosis induction by FasL.

FasL-induced apoptosis is important in elimination of virus-infected cells and cancer cells by natural killer cells and cytotoxic T lymphocytes; an alternative mechanism involves perforin and granzymes[1,14-16]. Peripheral blood natural killer cells triggered marked cell death in Jurkat T leukaemia cells (Fig. 3d); DcR3–Fc and Fas–Fc each reduced killing of target cells from ~65% to ~30%, with half-maximal inhibition at ~1 µg ml^{-1}; the residual killing was probably mediated by the perforin/granzyme pathway. Thus, DcR3 binding blocks FasL-dependent natural killer cell activity. Higher DcR3–Fc and Fas–Fc concentrations were required to block natural killer cell activity compared with those required to block soluble FasL activity, which is consistent with the greater potency of membrane-associated FasL compared with soluble FasL[17].

Given the role of immune-cytotoxic cells in elimination of tumour cells and the fact that DcR3 can act as an inhibitor of FasL, we proposed that DcR3 expression might contribute to the ability of some tumours to escape immune-cytotoxic attack. As genomic amplification frequently contributes to tumorigenesis, we investigated whether the DcR3 gene is amplified in cancer. We analysed DcR3 gene-copy number by quantitative polymerase chain
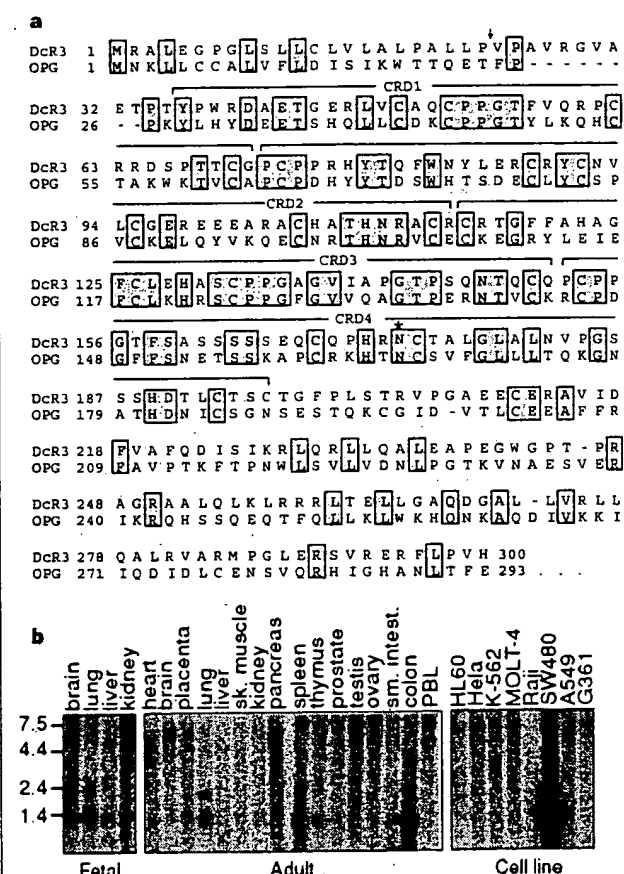

Figure 1 Primary structure and expression of human DcR3. **a**, Alignment of the amino-acid sequences of DcR3 and of osteoprotegerin (OPG); the C-terminal 101 residues of OPG are not shown. The putative signal cleavage site (arrow), the cysteine-rich domains (CRD 1–4), and the N-linked glycosylation site (asterisk) are shown. **b**, Expression of DcR3 mRNA. Northern hybridization analysis was done using the DcR3 cDNA as a probe and blots of poly(A)+ RNA (Clontech) from human fetal and adult tissues or cancer cell lines. PBL, peripheral blood lymphocyte.
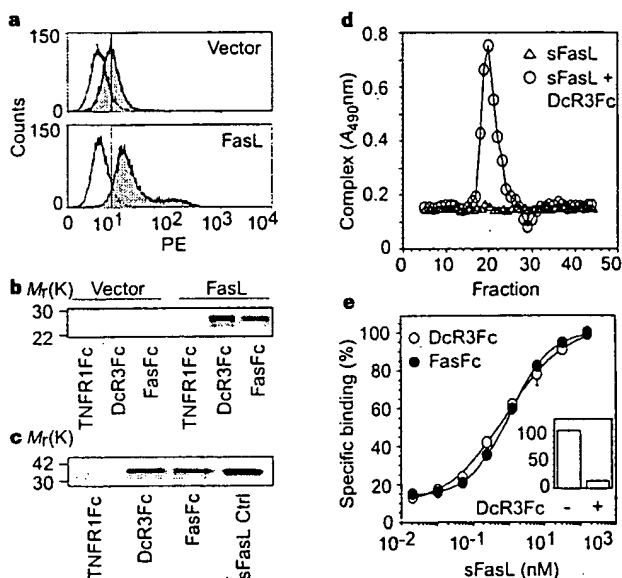

Figure 2 Interaction of DcR3 with FasL. **a**, 293 cells were transfected with pRK5 vector (top) or with pRK5 encoding full-length FasL (bottom), incubated with DcR3-Fc (solid line, shaded area), TNFR1-Fc (dotted line) or buffer control (dashed line) (the dashed and dotted lines overlap), and analysed for binding by FACS. Statistical analysis showed a significant difference ($P < 0.001$) between the binding of DcR3-Fc to cells transfected with FasL or pRK5. PE, phycoerythrin-labelled cells. **b**, 293 cells were transfected as in a and metabolically labelled, and cell supernatants were immunoprecipitated with Fc-tagged TNFR1, DcR3 or Fas. **c**, Purified soluble FasL (sFasL) was immunoprecipitated with TNFR1-Fc, DcR3-Fc or Fas-Fc and visualized by immunoblot with anti-FasL antibody. sFasL was loaded directly for comparison in the right-hand lane. **d**, Flag-tagged sFasL was incubated with DcR3-Fc or with buffer and resolved by gel filtration; column fractions were analysed in an assay that detects complexes containing DcR3-Fc and sFasL-Flag. **e**, Equilibrium binding of DcR3-Fc or Fas-Fc to sFasL-Flag. Inset, competition of DcR3-Fc with Fas-Fc for binding to sFasL-Flag.

reaction (PCR)[18] in genomic DNA from 35 primary lung and colon tumours, relative to pooled genomic DNA from peripheral blood leukocytes (PBLs) of 10 healthy donors. Eight of 18 lung tumours and 9 of 17 colon tumours showed DcR3 gene amplification, ranging from 2- to 18-fold (Fig. 4a, b). To confirm this result, we analysed the colon tumour DNAs with three more, independent sets of DcR3-based PCR primers and probes; we observed nearly the same amplification (data not shown).

We then analysed DcR3 mRNA expression in primary tumour tissue sections by in situ hybridization. We detected DcR3 expression in 6 out of 15 lung tumours, 2 out of 2 colon tumours, 2 out of 5 breast tumours, and 1 out of 1 gastric tumour (data not shown). A section through a squamous-cell carcinoma of the lung is shown in Fig. 4c. DcR3 mRNA was localized to infiltrating malignant epithelium, but was essentially absent from adjacent stroma, indicating tumour-specific expression. Although the individual tumour specimens that we analysed for mRNA expression and gene amplification were different, the in situ hybridization results are consistent with the finding that the DcR3 gene is amplified frequently in tumours. SW480 colon carcinoma cells, which showed abundant DcR3 mRNA expression (Fig. 1b), also had marked DcR3 gene amplification, as shown by quantitative PCR (fourfold) and by Southern blot hybridization (fivefold) (data not shown).

If DcR3 amplification in cancer is functionally relevant, then DcR3 should be amplified more than neighbouring genomic regions that are not important for tumour survival. To test this,

we mapped the human DcR3 gene by radiation-hybrid analysis; DcR3 showed linkage to marker AFM218xe7 (T160), which maps to chromosome position 20q13. Next, we isolated from a bacterial artificial chromosome (BAC) library a human genomic clone that carries DcR3, and sequenced the ends of the clone's insert. We then determined, from the nine colon tumours that showed twofold or greater amplification of DcR3, the copy number of the DcR3-flanking sequences (reverse and forward) from the BAC, and of seven genomic markers that span chromosome 20 (Fig. 4d). The DcR3-linked reverse marker showed an average amplification of roughly threefold, slightly less than the approximately fourfold amplification of DcR3; the other markers showed little or no amplification. These data indicate that DcR3 may be at the 'epicentre' of a distal chromosome 20 region that is amplified in colon cancer, consistent with the possibility that DcR3 amplification promotes tumour survival.

Our results show that DcR3 binds specifically to FasL and inhibits FasL activity. We did not detect DcR3 binding to several other TNF-ligand-family members; however, this does not rule out the possibility that DcR3 interacts with other ligands, as do some other TNFR family members, including OPG[2,19].

FasL is important in regulating the immune response; however, little is known about how FasL function is controlled. One mechanism involves the molecule cFLIP, which modulates apoptosis signalling downstream of Fas[20]. A second mechanism involves proteolytic shedding of FasL from the cell surface[17]. DcR3 competes with Fas for
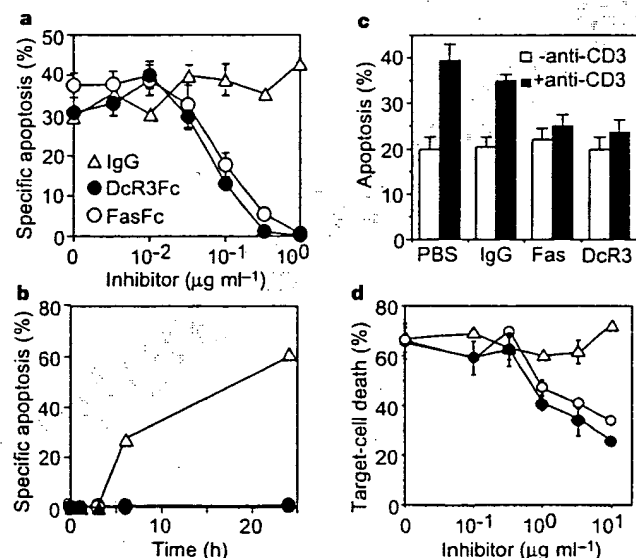

Figure 3 Inhibition of FasL activity by DcR3. **a**, Human Jurkat T leukaemia cells were incubated with Flag-tagged soluble FasL (sFasL; 5 ng ml⁻¹) oligomerized with anti-Flag antibody (0.1 μg ml⁻¹) in the presence of the proposed inhibitors DcR3-Fc, Fas-Fc or human IgG1 and assayed for apoptosis (mean ± s.e.m. of triplicates). **b**, Jurkat cells were incubated with sFasL-Flag plus anti-Flag antibody as in **a**, in presence of 1 μg ml⁻¹ DcR3-Fc (filled circles), Fas-Fc (open circles) or human IgG1 (triangles), and apoptosis was determined at the indicated time points. **c**, Peripheral blood T cells were stimulated with PHA and interleukin-2, followed by control (white bars) or anti-CD3 antibody (filled bars), together with phosphate-buffered saline (PBS), human IgG1, Fas-Fc, or DcR3-Fc (10 μg ml⁻¹). After 16 h, apoptosis of CD4⁺ cells was determined (mean ± s.e.m. of results from five donors). **d**, Peripheral blood natural killer cells were incubated with ⁵¹Cr-labelled Jurkat cells in the presence of DcR3-Fc (filled circles), Fas-Fc (open circles) or human IgG1 (triangles), and target-cell death was determined by release of ⁵¹Cr (mean ± s.d. for two donors, each in triplicate).
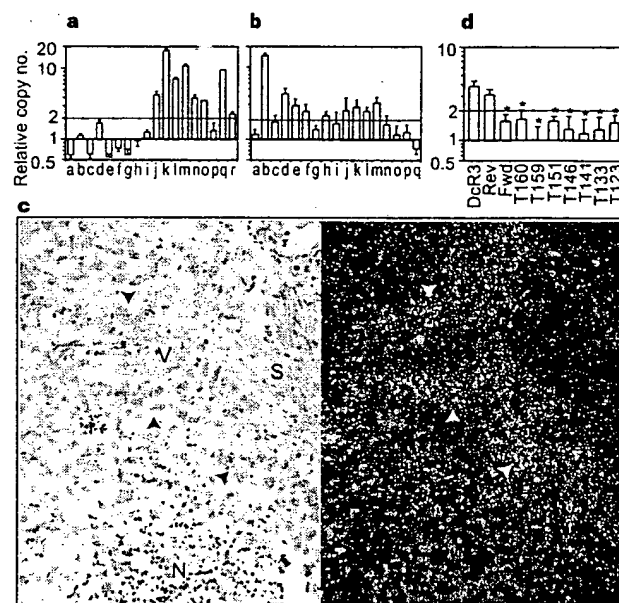
Figure 4 Genomic amplification of DcR3 in tumours. **a**, Lung cancers, comprising eight adenocarcinomas (c, d, f, g, h, j, k, r), seven squamous-cell carcinomas (a, e, m, n, o, p, q), one non-small-cell carcinoma (b), one small-cell carcinoma (i), and one bronchial adenocarcinoma (l). The data are means ± s.d. of 2 experiments done in duplicate. **b**, Colon tumours, comprising 17 adenocarcinomas. Data are means ± s.e.m. of five experiments done in duplicate. **c**, In situ hybridization analysis of DcR3 mRNA expression in a squamous-cell carcinoma of the lung. A representative bright-field image (left) and the corresponding dark-field image (right) show DcR3 mRNA over infiltrating malignant epithelium (arrowheads). Adjacent non-malignant stroma (S), blood vessel (V) and necrotic tumour tissue (N) are also shown. **d**, Average amplification of DcR3 compared with amplification of neighbouring genomic regions (reverse and forward, Rev and Fwd), the DcR3-linked marker T160, and other chromosome-20 markers, in the nine colon tumours showing DcR3 amplification of twofold or more (**b**). Data are from two experiments done in duplicate. Asterisk indicates P < 0.01 for a Student's t-test comparing each marker with DcR3.

FasL binding; hence, it may represent a third mechanism of extracellular regulation of FasL activity. A decoy receptor that modulates the function of the cytokine interleukin-1 has been described[21]. In addition, two decoy receptors that belong to the TNFR family, DcR1 and DcR2, regulate the FasL-related apoptosis-inducing molecule Apo2L[22]. Unlike DcR1 and DcR2, which are membrane-associated proteins, DcR3 is directly secreted into the extracellular space. One other secreted TNFR-family member is OPG[3], which shares greater sequence homology with DcR3 (31%) than do DcR1 (17%) or DcR2 (19%); OPG functions as a third decoy for Apo2L[19]. Thus, DcR3 and OPG define a new subset of TNFR-family members that function as secreted decoys to modulate ligands that induce apoptosis. Pox viruses produce soluble TNFR homologues that neutralize specific TNF-family ligands, thereby modulating the antiviral immune response[2]. Our results indicate that a similar mechanism, namely, production of a soluble decoy receptor for FasL, may contribute to immune evasion by certain tumours. □

Methods

Isolation of DcR3 cDNA. Several overlapping ESTs in GenBank (accession numbers AA025672, AA025673 and W67560) and in Lifeseq™ (Incyte Pharmaceuticals; accession numbers 1339238, 1533571, 1533650, 1542861, 1789372 and 2207027) showed similarity to members of the TNFR family. We screened human cDNA libraries by PCR with primers based on the region of EST consensus; fetal lung was positive for a product of the expected size. By hybridization to a PCR-generated probe based on the ESTs, one positive clone (DNA30942) was identified. When searching for potential alternatively spliced forms of DcR3 that might encode a transmembrane protein, we isolated 50 more clones; the coding regions of these clones were identical in size to that of the initial clone (data not shown).

Fc-fusion proteins (immunoadhesins). The entire DcR3 sequence, or the ectodomain of Fas or TNFR1, was fused to the hinge and Fc region of human IgG1, expressed in insect SF9 cells or in human 293 cells, and purified as described[23].

Fluorescence-activated cell sorting (FACS) analysis. We transfected 293 cells using calcium phosphate or Effectene (Qiagen) with pRK5 vector or pRK5 encoding full-length human FasL[4] (2 µg), together with pRK5 encoding CrmA (2 µg) to prevent cell death. After 16 h, the cells were incubated with biotinylated DcR3–Fc or TNFR1–Fc and then with phycoerythrin-conjugated streptavidin (GibcoBRL), and were assayed by FACS. The data were analysed by Kolmogorov–Smirnov statistical analysis. There was some detectable staining of vector-transfected cells by DcR3–Fc; as these cells express little FasL (data not shown), it is possible that DcR3 recognized some other factor that is expressed constitutively on 293 cells.

Immunoprecipitation. Human 293 cells were transfected as above, and metabolically labelled with [35S]cysteine and [35S]methionine (0.5 mCi; Amersham). After 16 h of culture in the presence of z-VAD-fmk (10 µM), the medium was immunoprecipitated with DcR3–Fc, Fas–Fc or TNFR1–Fc (5 µg), followed by protein A–Sepharose (Repligen). The precipitates were resolved by SDS–PAGE and visualized on a phosphorimager (Fuji BAS2000). Alternatively, purified, Flag-tagged soluble FasL (1 µg) (Alexis) was incubated with each Fc-fusion protein (1 µg), precipitated with protein A–Sepharose, resolved by SDS–PAGE and visualized by immunoblotting with rabbit anti-FasL antibody (Oncogene Research).

Analysis of complex formation. Flag-tagged soluble FasL (25 µg) was incubated with buffer or with DcR3–Fc (40 µg) for 1.5 h at 24 °C. The reaction was loaded onto a Superdex 200 HR 10/30 column (Pharmacia) and developed with PBS; 0.6-ml fractions were collected. The presence of DcR3–Fc–FasL complex in each fraction was analysed by placing 100 µl aliquots into microtitre wells precoated with anti-human IgG (Boehringer) to capture DcR3–Fc, followed by detection with biotinylated anti-Flag antibody Bio M2 (Kodak) and streptavidin–horseradish peroxidase (Amersham). Calibration of the column indicated an apparent relative molecular mass of the complex of 420K (data not shown), which is consistent with a stoichiometry of two DcR3–Fc homodimers to two soluble FasL homotrimers.

Equilibrium binding analysis. Microtitre wells were coated with anti-human IgG, blocked with 2% BSA in PBS. DcR3–Fc or Fas–Fc was added, followed by serially diluted Flag-tagged soluble FasL. Bound ligand was detected with anti-Flag antibody as above. In the competition assay, Fas–Fc was immobilized as above, and the wells were blocked with excess IgG1 before addition of Flag-tagged soluble FasL plus DcR3–Fc.

T-cell AICD. CD3+ lymphocytes were isolated from peripheral blood of individual donors using anti-CD3 magnetic beads (Miltenyi Biotech), stimulated with phytohaemagglutinin (PHA; 2 µg ml⁻¹) for 24 h, and cultured in the presence of interleukin-2 (100 U ml⁻¹) for 5 days. The cells were plated in wells coated with anti-CD3 antibody (Pharmingen) and analysed for apoptosis 16 h later by FACS analysis of annexin-V-binding of CD4+ cells[24].

Natural killer cell activity. Natural killer cells were isolated from peripheral blood of individual donors using anti-CD56 magnetic beads (Miltenyi Biotech), and incubated for 16 h with 51Cr-loaded Jurkat cells at an effector-to-target ratio of 1:1 in the presence of DcR3–Fc, Fas–Fc or human IgG1. Target-cell death was determined by release of 51Cr in effector–target co-cultures relative to release of 51Cr by detergent lysis of equal numbers of Jurkat cells.

Gene-amplification analysis. Surgical specimens were provided by J. Kern (lung tumours) and P. Quirke (colon tumours). Genomic DNA was extracted (Qiagen) and the concentration was determined using Hoechst dye 33258 intercalation fluorometry. Amplification was determined by quantitative PCR[18] using a TaqMan instrument (ABI). The method was validated by comparison of PCR and Southern hybridization data for the Myc and HER-2 oncogenes (data not shown). Gene-specific primers and fluorogenic probes were designed on the basis of the sequence of DcR3 or of nearby regions identified on a BAC carrying the human DcR3 gene; alternatively, primers and probes were based on Stanford Human Genome Center marker AFM218xe7 (T160), which is linked to DcR3 (likelihood score = 5.4), SHGC-36268 (T159), the nearest available marker which maps to ~500 kilobases from T160, and five extra markers that span chromosome 20. The DcR3-specific primer sequences were 5′-CTTCTTCGCGCACGCTG-3′ and 5′-ATCACGCCGGCACCAG-3′ and the fluorogenic probe sequence was 5′-(FAM-ACACGATGCGTGCTCCAAGCAG AAp-(TAMARA), where FAM is 5′-fluorescein phosphoramidite. Relative gene-copy numbers were derived using the formula $2^{(\Delta CT)}$, where ΔCT is the difference in amplification cycles required to detect DcR3 in peripheral blood lymphocyte DNA compared to test DNA.

1. Nagata, S. Apoptosis by death factor. *Cell* 88, 355–365 (1997).
2. Smith, C. A., Farrah, T. & Goodwin, R. G. The TNF receptor superfamily of cellular and viral proteins: activation, costimulation, and death. *Cell* 76, 959–962 (1994).
3. Simonet, W. S. *et al.* Osteoprotegerin: a novel secreted protein involved in the regulation of bone density. *Cell* 89, 309–319 (1997).
4. Suda, T., Takahashi, T., Golstein, P. & Nagata, S. Molecular cloning and expression of Fas ligand, a novel member of the TNF family. *Cell* 75, 1169–1178 (1993).
5. Pennica, D. *et al.* Human tumour necrosis factor: precursor structure, expression and homology to lymphotoxin. *Nature* 312, 724–729 (1984).
6. Pitti, R. M. *et al.* Induction of apoptosis by Apo-2 ligand, a new member of the tumor necrosis factor receptor family. *J. Biol. Chem.* 271, 12687–12690 (1996).
7. Wiley, S. R. *et al.* Identification and characterization of a new member of the TNF family that induces apoptosis. *Immunity* 3, 673–682 (1995).
8. Marsters, S. A. *et al.* Identification of a ligand for the death-domain-containing receptor Apo3. *Curr. Biol.* 8, 525–528 (1998).
9. Chicheportiche, Y. *et al.* TWEAK, a new secreted ligand in the TNF family that weakly induces apoptosis. *J. Biol. Chem.* 272, 32401–32410 (1997).
10. Wong, B. R. *et al.* TRANCE is a novel ligand of the TNFR family that activates c-Jun-N-terminal kinase in T cells. *J. Biol. Chem.* 272, 25190–25194 (1997).
11. Anderson, D. M. *et al.* A homolog of the TNF receptor and its ligand enhance T-cell growth and dendritic-cell function. *Nature* 390, 175–179 (1997).
12. Lacey, D. L. *et al.* Osteoprotegerin ligand is a cytokine that regulates osteoclast differentiation and activation. *Cell* 93, 165–176 (1998).
13. Dhein, J., Walczak, H., Baumler, C., Debatin, K. M. & Krammer, P. H. Autocrine T-cell suicide mediated by Apo1/(Fas/CD95). *Nature* 373, 438–441 (1995).
14. Arase, H., Arase, N. & Saito, T. Fas-mediated cytotoxicity by freshly isolated natural killer cells. *J. Exp. Med.* 181, 1235–1238 (1995).
15. Medvedev, A. E. *et al.* Regulation of Fas and Fas ligand expression in NK cells by cytokines and the involvement of Fas ligand in NK/LAK cell-mediated cytotoxicity. *Cytokine* 9, 394–404 (1997).
16. Moretta, A. Mechanisms in cell-mediated cytotoxicity. *Cell* 90, 13–18 (1997).
17. Tanaka, M., Itai, T., Adachi, M. & Nagata, S. Downregualtion of Fas ligand by shedding. *Nature Med.* 4, 31–36 (1998).
18. Gelmini, S. *et al.* Quantitative PCR-based homogeneous assay with fluorogenic probes to measure c-erbB-2 oncogene amplification. *Clin. Chem.* 43, 752–758 (1997).
19. Emery, J. G. *et al.* Osteoprotegerin is a receptor for the cytotoxic ligand TRAIL. *J. Biol. Chem.* 273, 14363–14367 (1998).
20. Wallach, D. Placing death under control. *Nature* 388, 123–125 (1997).
21. Collota, F. *et al.* Interleukin-1 type II receptor: a decoy target for IL-1 that is regulated by IL-4. *Science* 261, 472–475 (1993).

22. Ashkenazi, A. & Dixit, V. M..Death receptors: signaling and modulation. *Science* 281, 1305–1308 (1998).
23. Ashkenazi, A. & Chamow, S. M. Immunoadhesins as research tools and therapeutic agents. *Curr. Opin. Immunol.* 9, 195–200 (1997).
24. Marsters, S. *et al.* Activation of apoptosis by Apo-2 ligand is independent of FADD but blocked by CrmA. *Curr. Biol.* 6, 750–752 (1996).

Crystal structure of the ATP-binding subunit of an ABC transporter

Li-Wei Hung*, Iris Xiaoyan Wang†, Kishiko Nikaido,· Pei-Qi Liu†, Giovanna Ferro-Luzzi Ames† & Sung-Hou Kim*‡

* E. O. Lawrence Berkeley National Laboratory, † Department of Molecular and Cell Biology, and ‡ Department of Chemistry, University of California at Berkeley, Berkeley, California 94720, USA

ABC transporters (also known as traffic ATPases) form a large family of proteins responsible for the translocation of a variety of compounds across membranes of both prokaryotes and eukaryotes[1]. The recently completed *Escherichia coli* genome sequence revealed that the largest family of paralogous *E. coli* proteins is composed of ABC transporters[2]. Many eukaryotic proteins of medical significance belong to this family, such as the cystic fibrosis transmembrane conductance regulator (CFTR), the P-glycoprotein (or multidrug-resistance protein) and the heterodimeric transporter associated with antigen processing (Tap1–Tap2). Here we report the crystal structure at 1.5 Å resolution of HisP, the ATP-binding subunit of the histidine permease, which is an ABC transporter from *Salmonella typhimurium*. We correlate the details of this structure with the biochemical, genetic and biophysical properties of the wild-type and several mutant HisP proteins. The structure provides a basis for understanding properties of ABC transporters and of defective CFTR proteins.

ABC transporters contain four structural domains: two nucleotide-binding domains (NBDs), which are highly conserved throughout the family, and two transmembrane domains[1]. In prokaryotes these domains are often separate subunits which are assembled into a membrane-bound complex; in eukaryotes the domains are generally fused into a single polypeptide chain. The periplasmic histidine permease of *S. typhimurium* and *E. coli*[1,3–8] is a well-characterized ABC transporter that is a good model for this superfamily. It consists of a membrane-bound complex, HisQMP₂, which comprises integral membrane subunits, HisQ and HisM, and two copies of HisP, the ATP-binding subunit. HisP, which has properties intermediate between those of integral and peripheral membrane proteins[9], is accessible from both sides of the membrane, presumably by its interaction with HisQ and HisM[6]. The two HisP subunits form a dimer, as shown by their cooperativity in ATP hydrolysis[5], the requirement for both subunits to be present for activity[8], and the formation of a HisP dimer upon chemical cross-linking. Soluble HisP also forms a dimer[3]. HisP has been purified and characterized in an active soluble form[3] which can be reconstituted into a fully active membrane-bound complex[8].

The overall shape of the crystal structure of the HisP monomer is that of an 'L' with two thick arms (arm I and arm II); the ATP-binding pocket is near the end of arm I (Fig. 1). A six-stranded β-sheet (β3 and β8–β12) spans both arms of the L, with a domain of α- plus β-type structure (β1, β2, β4–β7, α1 and α2) on one side (within arm I) and a domain of mostly α-helices (α3–α9) on the
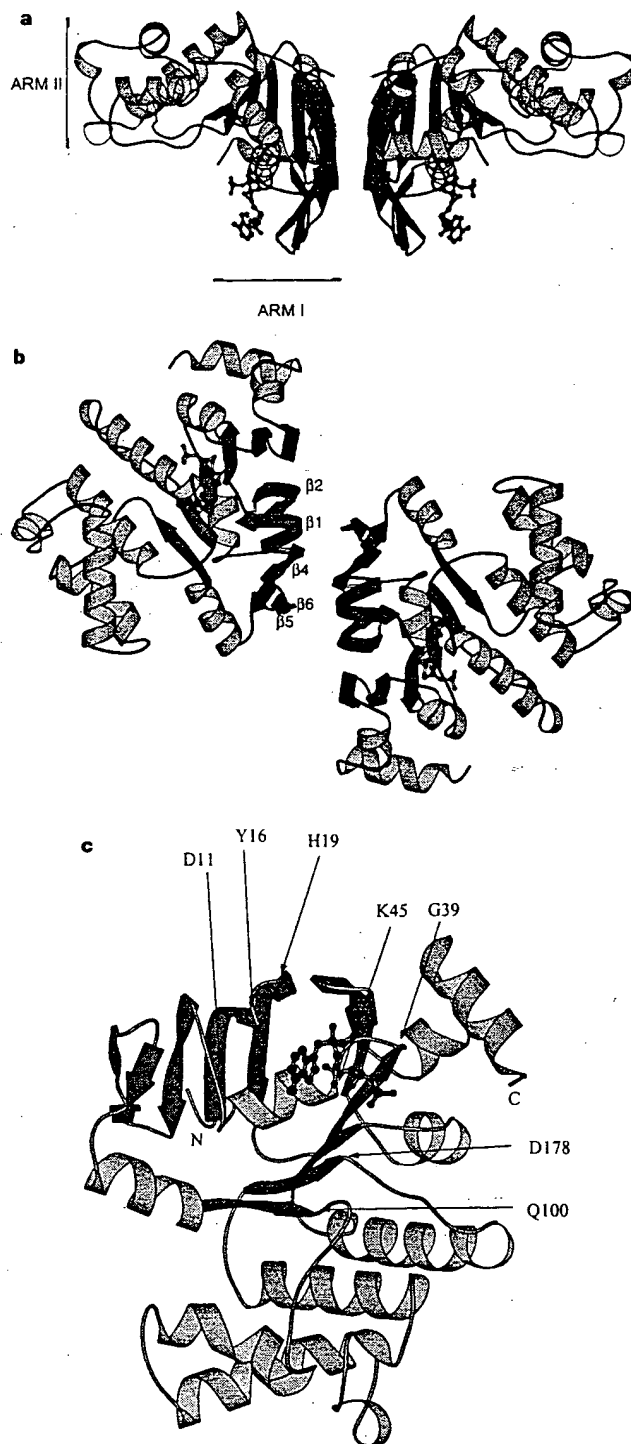

Figure 1 Crystal structure of HisP. **a**, View of the dimer along an axis perpendicular to its two-fold axis. The top and bottom of the dimer are suggested to face towards the periplasmic and cytoplasmic sides, respectively (see text). The thickness of arm II is about 25 Å, comparable to that of membrane. α-Helices are shown in orange and β-sheets in green. **b**, View along the two-fold axis of the HisP dimer, showing the relative displacement of the monomers not apparent in **a**. The β-strands at the dimer interface are labelled. **c**, View of one monomer from the bottom of arm I, as shown in **a**, towards arm II, showing the ATP-binding pocket. **a–c**, The protein and the bound ATP are in 'ribbon' and 'ball-and-stick' representations, respectively. Key residues discussed in the text are indicated in **c**. These figures were prepared with MOLSCRIPT[29]. N, amino terminus; C, C terminus.

NOVEL APPROACH TO QUANTITATIVE POLYMERASE CHAIN REACTION USING REAL-TIME DETECTION: APPLICATION TO THE DETECTION OF GENE AMPLIFICATION IN BREAST CANCER

Ivan Bièche[1,2], Martine Olivi[1], Marie-Hélène Champème[2], Dominique Vidaud[1], Rosette Lidereau[2] and Michel Vidaud[1]*

[1]*Laboratoire de Génétique Moléculaire, Faculté des Sciences Pharmaceutiques et Biologiques de Paris, Paris, France*
[2]*Laboratoire d'Oncogénétique, Centre René Huguenin, St-Cloud, France*

Gene amplification is a common event in the progression of human cancers, and amplified oncogenes have been shown to have diagnostic, prognostic and therapeutic relevance. A kinetic quantitative polymerase-chain-reaction (PCR) method, based on fluorescent TaqMan methodology and a new instrument (ABI Prism 7700 Sequence Detection System) capable of measuring fluorescence in real-time, was used to quantify gene amplification in tumor DNA. Reactions are characterized by the point during cycling when PCR amplification is still in the exponential phase, rather than the amount of PCR product accumulated after a fixed number of cycles. None of the reaction components is limited during the exponential phase, meaning that values are highly reproducible in reactions starting with the same copy number. This greatly improves the precision of DNA quantification. Moreover, real-time PCR does not require post-PCR sample handling, thereby preventing potential PCR-product carry-over contamination; it possesses a wide dynamic range of quantification and results in much faster and higher sample throughput. The real-time PCR method, was used to develop and validate a simple and rapid assay for the detection and quantification of the 3 most frequently amplified genes (*myc, ccnd1* and *erbB2*) in breast tumors. Extra copies of *myc, ccnd1* and *erbB2* were observed in 10, 23 and 15%, respectively, of 108 breast-tumor DNA; the largest observed numbers of gene copies were 4.6, 18.6 and 15.1, respectively. These results correlated well with those of Southern blotting. The use of this new semi-automated technique will make molecular analysis of human cancers simpler and more reliable, and should find broad applications in clinical and research settings. *Int. J. Cancer* **78:661–666, 1998.**
© *1998 Wiley-Liss, Inc.*

Gene amplification plays an important role in the pathogenesis of various solid tumors, including breast cancer, probably because over-expression of the amplified target genes confers a selective advantage. The first technique used to detect genomic amplification was cytogenetic analysis. Amplification of several chromosome regions, visualized either as extrachromosomal double minutes (dmins) or as integrated homogeneously staining regions (HSRs), are among the main visible cytogenetic abnormalities in breast tumors. Other techniques such as comparative genomic hybridization (CGH) (Kallioniemi *et al.*, 1994) have also been used in broad searches for regions of increased DNA copy numbers in tumor cells, and have revealed some 20 amplified chromosome regions in breast tumors. Positional cloning efforts are underway to identify the critical gene(s) in each amplified region. To date, genes known to be amplified frequently in breast cancers include *myc* (8q24), *ccnd1* (11q13), and *erbB2* (17q12-q21) (for review, see Bièche and Lidereau, 1995).

Amplification of the *myc, ccnd1,* and *erbB2* proto-oncogenes should have clinical relevance in breast cancer, since independent studies have shown that these alterations can be used to identify sub-populations with a worse prognosis (Berns *et al.*, 1992; Schuuring *et al.*, 1992; Slamon *et al.*, 1987). Muss *et al.* (1994) suggested that these gene alterations may also be useful for the prediction and assessment of the efficacy of adjuvant chemotherapy and hormone therapy.

However, published results diverge both in terms of the frequency of these alterations and their clinical value. For instance, over 500 studies in 10 years have failed to resolve the controversy surrounding the link suggested by Slamon *et al.* (1987) between *erbB2* amplification and disease progression. These discrepancies are partly due to the clinical, histological and ethnic heterogeneity of breast cancer, but technical considerations are also probably involved.

Specific genes (DNA) were initially quantified in tumor cells by means of blotting procedures such as Southern and slot blotting. These batch techniques require large amounts of DNA (5–10 µg/reaction) to yield reliable quantitative results. Furthermore, meticulous care is required at all stages of the procedures to generate blots of sufficient quality for reliable dosage analysis. Recently, PCR has proven to be a powerful tool for quantitative DNA analysis, especially with minimal starting quantities of tumor samples (small, early-stage tumors and formalin-fixed, paraffin-embedded tissues).

Quantitative PCR can be performed by evaluating the amount of product either after a given number of cycles (end-point quantitative PCR) or after a varying number of cycles during the exponential phase (kinetic quantitative PCR). In the first case, an internal standard distinct from the target molecule is required to ascertain PCR efficiency. The method is relatively easy but implies generating, quantifying and storing an internal standard for each gene studied. Nevertheless, it is the most frequently applied method to date.

One of the major advantages of the kinetic method is its rapidity in quantifying a new gene, since no internal standard is required (an external standard curve is sufficient). Moreover, the kinetic method has a wide dynamic range (at least 5 orders of magnitude), giving an accurate value for samples differing in their copy number. Unfortunately, the method is cumbersome and has therefore been rarely used. It involves aliquot sampling of each assay mix at regular intervals and quantifying, for each aliquot, the amplification product. Interest in the kinetic method has been stimulated by a novel approach using fluorescent TaqMan methodology and a new instrument (ABI Prism 7700 Sequence Detection System) capable of measuring fluorescence in real time (Gibson *et al.*, 1996; Heid *et al.*, 1996). The TaqMan reaction is based on the 5' nuclease assay first described by Holland *et al.* (1991). The latter uses the 5' nuclease activity of Taq polymerase to cleave a specific fluorogenic oligonucleotide probe during the extension phase of PCR. The approach uses dual-labeled fluorogenic hybridization probes (Lee *et al.*, 1993). One fluorescent dye, co-valently linked to the 5' end of the oligonucleotide, serves as a reporter [FAM (*i.e.*, 6-carboxy-fluorescein)] and its emission spectrum is quenched by a second fluorescent dye, TAMRA (*i.e.*, 6-carboxy-tetramethyl-rhodamine) attached to the 3' end. During the extension phase of the PCR

cycle, the fluorescent hybridization probe is hydrolyzed by the 5'-3' nucleolytic activity of DNA polymerase. Nuclease degradation of the probe releases the quenching of FAM fluorescence emission, resulting in an increase in peak fluorescence emission. The fluorescence signal is normalized by dividing the emission intensity of the reporter dye (FAM) by the emission intensity of a reference dye (*i.e.*, ROX, 6-carboxy-X-rhodamine) included in TaqMan buffer, to obtain a ratio defined as the Rn (normalized reporter) for a given reaction tube. The use of a sequence detector enables the fluorescence spectra of all 96 wells of the thermal cycler to be measured continuously during PCR amplification.

The real-time PCR method offers several advantages over other current quantitative PCR methods (Celi *et al.*, 1994): *(i)* the probe-based homogeneous assay provides a real-time method for detecting only specific amplification products, since specific hybridation of both the primers and the probe is necessary to generate a signal; *(ii)* the C_t (threshold cycle) value used for quantification is measured when PCR amplification is still in the log phase of PCR product accumulation. This is the main reason why C_t is a more reliable measure of the starting copy number than are end-point measurements, in which a slight difference in a limiting component can have a drastic effect on the amount of product; *(iii)* use of C_t values gives a wider dynamic range (at least 5 orders of magnitude), reducing the need for serial dilution; *(iv)* The real-time PCR method is run in a closed-tube system and requires no post-PCR sample handling, thus avoiding potential contamination; *(v)* the system is highly automated, since the instrument continuously measures fluorescence in all 96 wells of the thermal cycler during PCR amplification and the corresponding software processes and analyzes the fluorescence data; *(vi)* the assay is rapid, as results are available just one minute after thermal cycling is complete; *(vii)* the sample throughput of the method is high, since 96 reactions can be analyzed in 2 hr.

Here, we applied this semi-automated procedure to determine the copy numbers of the 3 most frequently amplified genes in breast tumors (*myc, ccnd1* and *erb*B2), as well as 2 genes (*alb* and *app*) located in a chromosome region in which no genetic changes have been observed in breast tumors. The results for 108 breast tumors were compared with previous Southern-blot data for the same samples.

MATERIAL AND METHODS

Tumor and blood samples

Samples were obtained from 108 primary breast tumors removed surgically from patients at the Centre René Huguenin; none of the patients had undergone radiotherapy or chemotherapy. Immediately after surgery, the tumor samples were placed in liquid nitrogen until extraction of high-molecular-weight DNA. Patients were included in this study if the tumor sample used for DNA preparation contained more than 60% of tumor cells (histological analysis). A blood sample was also taken from 18 of the same patients.

DNA was extracted from tumor tissue and blood leukocytes according to standard methods.

Real-time PCR

Theoretical basis. Reactions are characterized by the point during cycling when amplification of the PCR product is first detected, rather than by the amount of PCR product accumulated after a fixed number of cycles. The higher the starting copy number of the genomic DNA target, the earlier a significant increase in fluorescence is observed. The parameter C_t (threshold cycle) is defined as the fractional cycle number at which the fluorescence generated by cleavage of the probe passes a fixed threshold above baseline. The target gene copy number in unknown samples is quantified by measuring C_t and by using a standard curve to determine the starting copy number. The precise amount of genomic DNA (based on optical density) and its quality (*i.e.*, lack

of extensive degradation) are both difficult to assess. We therefore also quantified a control gene *(alb)* mapping to chromosome region 4q11-q13, in which no genetic alterations have been found in breast-tumor DNA by means of CGH (Kallioniemi *et al.*, 1994).

Thus, the ratio of the copy number of the target gene to the copy number of the *alb* gene normalizes the amount and quality of genomic DNA. The ratio defining the level of amplification is termed "N", and is determined as follows:

$$N = \frac{\text{copy number of target gene } (app, myc, ccnd1, erbB2)}{\text{copy number of reference gene } (alb)}.$$

Primers, probes, reference human genomic DNA and PCR consumables. Primers and probes were chosen with the assistance of the computer programs Oligo 4.0 (National Biosciences, Plymouth, MN), EuGene (Daniben Systems, Cincinnati, OH) and Primer Express (Perkin-Elmer Applied Biosystems, Foster City, CA).

Primers were purchased from DNAgency (Malvern, PA) and probes from Perkin-Elmer Applied Biosystems.

Nucleotide sequences for the oligonucleotide hybridization probes and primers are available on request.

The TaqMan PCR Core reagent kit, MicroAmp optical tubes, and MicroAmp caps were from Perkin-Elmer Applied Biosystems.

Standard-curve construction. The kinetic method requires a standard curve. The latter was constructed with serial dilutions of specific PCR products, according to Piatak *et al.* (1993). In practice, each specific PCR product was obtained by amplifying 20 ng of a standard human genomic DNA (Boehringer, Mannheim, Germany) with the same primer pairs as those used later for real-time quantitative PCR. The 5 PCR products were purified using MicroSpin S-400 HR columns (Pharmacia, Uppsala, Sweden) electrophorezed through an acrylamide gel and stained with ethidium bromide to check their quality. The PCR products were then quantified spectrophotometrically and pooled, and serially diluted 10-fold in mouse genomic DNA (Clontech, Palo Alto, CA) at a constant concentration of 2 ng/µl. The standard curve used for real-time quantitative PCR was based on serial dilutions of the pool of PCR products ranging from 10^{-7} (10^5 copies of each gene) to 10^{-10} (10^2 copies). This series of diluted PCR products was aliquoted and stored at $-80°C$ until use.

The standard curve was validated by analyzing 2 known quantities of calibrator human genomic DNA (20 ng and 50 ng).

PCR amplification. Amplification mixes (50 µl) contained the sample DNA (around 20 ng, around 6600 copies of disomic genes), $10\times$ TaqMan buffer (5 µl), 200 µM dATP, dCTP, dGTP, and 400 µM dUTP, 5 mM MgCl$_2$, 1.25 units of AmpliTaq Gold, 0.5 units of AmpErase uracil N-glycosylase (UNG), 200 nM each primer and 100 nM probe. The thermal cycling conditions comprised 2 min at 50°C and 10 min at 95°C. Thermal cycling consisted of 40 cycles at 95°C for 15 s and 65°C for 1 min. Each assay included: a standard curve (from 10^5 to 10^2 copies) in duplicate, a no-template control, 20 ng and 50 ng of calibrator human genomic DNA (Boehringer) in triplicate, and about 20 ng of unknown genomic DNA in triplicate (26 samples can thus be analyzed on a 96-well microplate). All samples with a coefficient of variation (CV) higher than 10% were retested.

All reactions were performed in the ABI Prism 7700 Sequence Detection System (Perkin-Elmer Applied Biosystems), which detects the signal from the fluorogenic probe during PCR.

Equipment for real-time detection. The 7700 system has a built-in thermal cycler and a laser directed via fiber optical cables to each of the 96 sample wells. A charge-coupled-device (CDD) camera collects the emission from each sample and the data are analyzed automatically. The software accompanying the 7700 system calculates C_t and determines the starting copy number in the samples.

Determination of gene amplification. Gene amplification was calculated as described above. Only samples with an N value higher than 2 were considered to be amplified.

RESULTS

To validate the method, real-time PCR was performed on genomic DNA extracted from 108 primary breast tumors, and 18 normal leukocyte DNA samples from some of the same patients. The target genes were the *myc, ccnd1.* and *erb*B2 proto-oncogenes, and the β-amyloid precursor protein gene (*app*), which maps to a chromosome region (21q21.2) in which no genetic alterations have been found in breast tumors (Kallioniemi *et al.,* 1994). The reference disomic gene was the albumin gene (*alb,* chromosome 4q11-q13).

Validation of the standard curve and dynamic range of real-time PCR

The standard curve was constructed from PCR products serially diluted in genomic mouse DNA at a constant concentration of 2 ng/μl. It should be noted that the 5 primer pairs chosen to analyze the 5 target genes do not amplify genomic mouse DNA (data not shown). Figure 1 shows the real-time PCR standard curve for the *alb* gene. The dynamic range was wide (at least 4 orders of magnitude), with samples containing as few as 10^2 copies or as many as 10^5 copies.

*Copy-number ratio of the 2 reference genes (*app *and* alb*)*

The *app* to *alb* copy-number ratio was determined in 18 normal leukocyte DNA samples and all 108 primary breast-tumor DNA
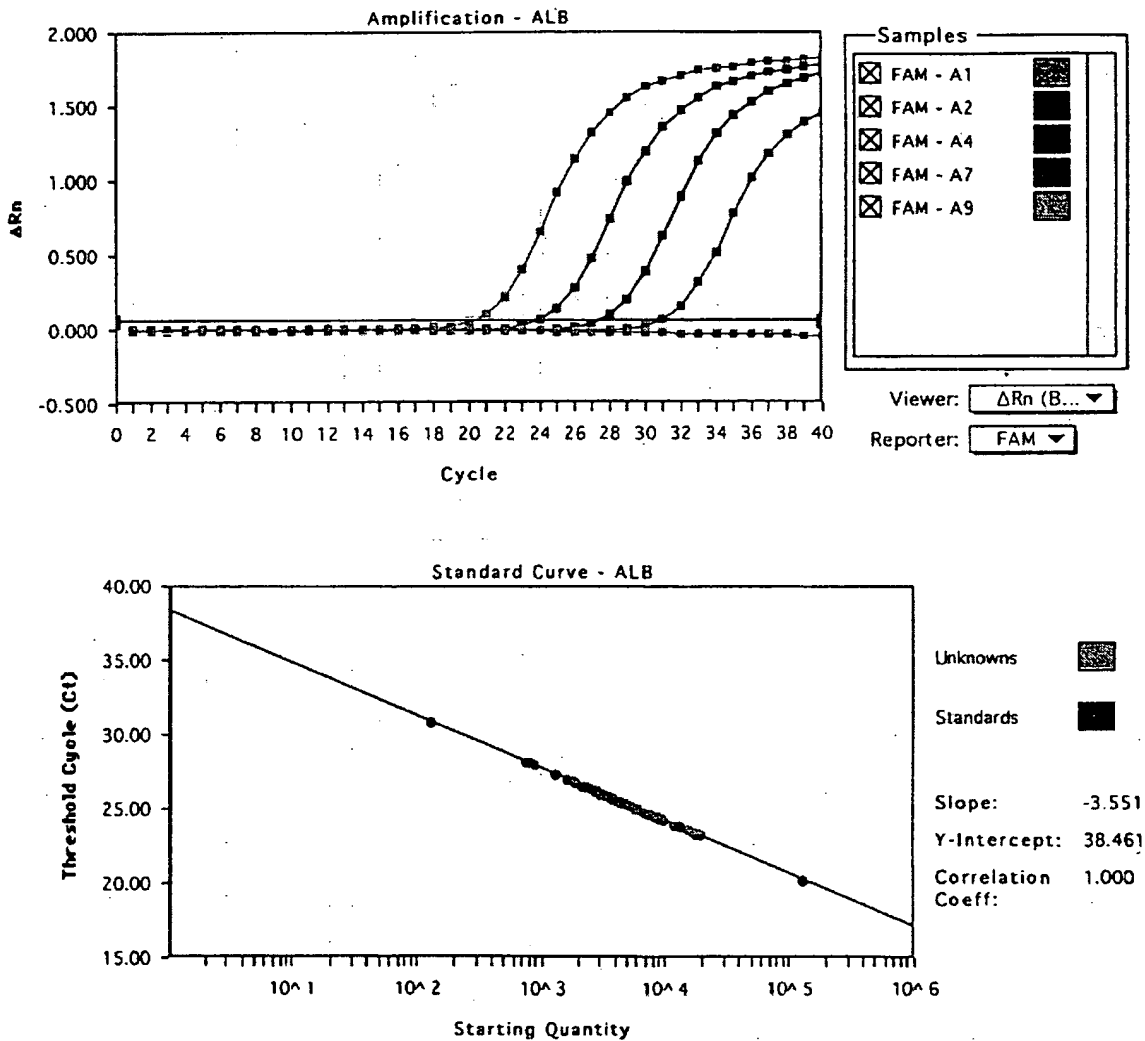

FIGURE 1 – Albumin (*alb*) gene dosage by real-time PCR. Top: Amplification plots for reactions with starting *alb* gene copy number ranging from 10^5 (A9), 10^4 (A7), 10^3 (A4) to 10^2 (A2) and a no-template control (A1). Cycle number is plotted *vs.* change in normalized reporter signal (ΔRn). For each reaction tube, the fluorescence signal of the reporter dye (FAM) is divided by the fluorescence signal of the passive reference dye (ROX), to obtain a ratio defined as the normalized reporter signal (Rn). ΔRn represents the normalized reporter signal (Rn) minus the baseline signal established in the first 15 PCR cycles. ΔRn increases during PCR as *alb* PCR product copy number increases until the reaction reaches a plateau. C_t (threshold cycle) represents the fractional cycle number at which a significant increase in Rn above a baseline signal (horizontal black line) can first be detected. Two replicate plots were performed for each standard sample, but the data for only one are shown here. Bottom: Standard curve plotting log starting copy number *vs.* C_t (threshold cycle). The black dots represent the data for standard samples plotted in duplicate and the red dots the data for unknown genomic DNA samples plotted in triplicate. The standard curve shows 4 orders of linear dynamic range.

samples. We selected these 2 genes because they are located in 2 chromosome regions (*app*, 21q21.2; *alb*, 4q11-q13) in which no obvious genetic changes (including gains or losses) have been observed in breast cancers (Kallioniemi *et al.*, 1994). The ratio for the 18 normal leukocyte DNA samples fell between 0.7 and 1.3 (mean 1.02 ± 0.21), and was similar for the 108 primary breast-tumor DNA samples (0.6 to 1.6, mean 1.06 ± 0.25), confirming that *alb* and *app* are appropriate reference disomic genes for breast-tumor DNA. The low range of the ratios also confirmed that the nucleotide sequences chosen for the primers and probes were not polymorphic, as mismatches of their primers or probes with the subject's DNA would have resulted in differential amplification.

myc, ccnd1 *and* erbB2 *gene dose in normal leukocyte DNA*

To determine the cut-off point for gene amplification in breast-cancer tissue, 18 normal leukocyte DNA samples were tested for the gene dose (N), calculated as described in "Material and Methods". The N value of these samples ranged from 0.5 to 1.3 (mean 0.84 ± 0.22) for *myc*; 0.7 to 1.6 (mean 1.06 ± 0.23) for *ccnd1* and 0.6 to 1.3 (mean 0.91 ± 0.19) for *erbB2*. Since N values for *myc*, *ccnd1* and *erbB2* in normal leukocyte DNA consistently fell between 0.5 and 1.6, values of 2 or more were considered to represent gene amplification in tumor DNA.

myc, ccnd1 *and* erbB2 *gene dose in breast-tumor DNA*

myc, *ccnd1* and *erbB2* gene copy numbers in the 108 primary breast tumors are reported in Table I. Extra copies of *ccnd1* were more frequent (23%, 25/108) than extra copies of *erbB2* (15%, 16/108) and *myc* (10%, 11/108), and ranged from 2 to 18.6 for *ccnd1*, 2 to 15.1 for *erbB2*, and only 2 to 4.6 for the *myc* gene. Figure 2 and Table II represent tumors in which the *ccnd1* gene was amplified 16-fold (T145), 6-fold (T133) and non-amplified (T118). The 3 genes were never found to be co-amplified in the same tumor. *erbB2* and *ccnd1* were co-amplified in only 3 cases, *myc* and *ccnd1* in 2 cases and *myc* and *erbB2* in 1 case. This favors the hypothesis that gene amplifications are independent events in breast cancer. Interestingly, 5 tumors showed a decrease of at least 50% in the *erbB2* copy number (N < 0.5), suggesting that they bore deletions of the 17q21 region (the site of *erbB2*). No such decrease in copy number was observed with the other 2 proto-oncogenes.

Comparison of gene dose determined by real-time quantitative PCR and Southern-blot analysis

Southern-blot analysis of *myc*, *ccnd1* and *erbB2* amplifications had previously been done on the same 108 primary breast tumors. A perfect correlation between the results of real-time PCR and Southern blot was obtained for tumors with high copy numbers (N ≥ 5). However, there were cases (1 *myc*, 6 *ccnd1* and 4 *erbB2*) in which real-time PCR showed gene amplification whereas Southern-blot did not, but these were mainly cases with low extra copy numbers (N from 2 to 2.9).

DISCUSSION

The clinical applications of gene amplification assays are currently limited, but would certainly increase if a simple, standardized and rapid method were perfected. Gene amplification status has been studied mainly by means of Southern blotting, but this method is not sensitive enough to detect low-level gene amplification nor accurate enough to quantify the full range of amplification values. Southern blotting is also time-consuming, uses radioactive

TABLE I – DISTRIBUTION OF AMPLIFICATION LEVEL (N) FOR *myc*, *ccnd1* AND *erbB2* GENES IN 108 HUMAN BREAST TUMORS

Gene	Amplification level (N)			
	<0.5	0.5–1.9	2–4.9	≥5
myc	0	97 (89.8%)	11 (10.2%)	0
ccnd1	0	83 (76.9%)	17 (15.7%)	8 (7.4%)
erbB2	5 (4.6%)	87 (80.6%)	8 (7.4%)	8 (7.4%)

reagents and requires relatively large amounts of high-quality genomic DNA, which means it cannot be used routinely in many laboratories. An amplification step is therefore required to determine the copy number of a given target gene from minimal quantities of tumor DNA (small early-stage tumors, cytopuncture specimens or formalin-fixed, paraffin-embedded tissues).
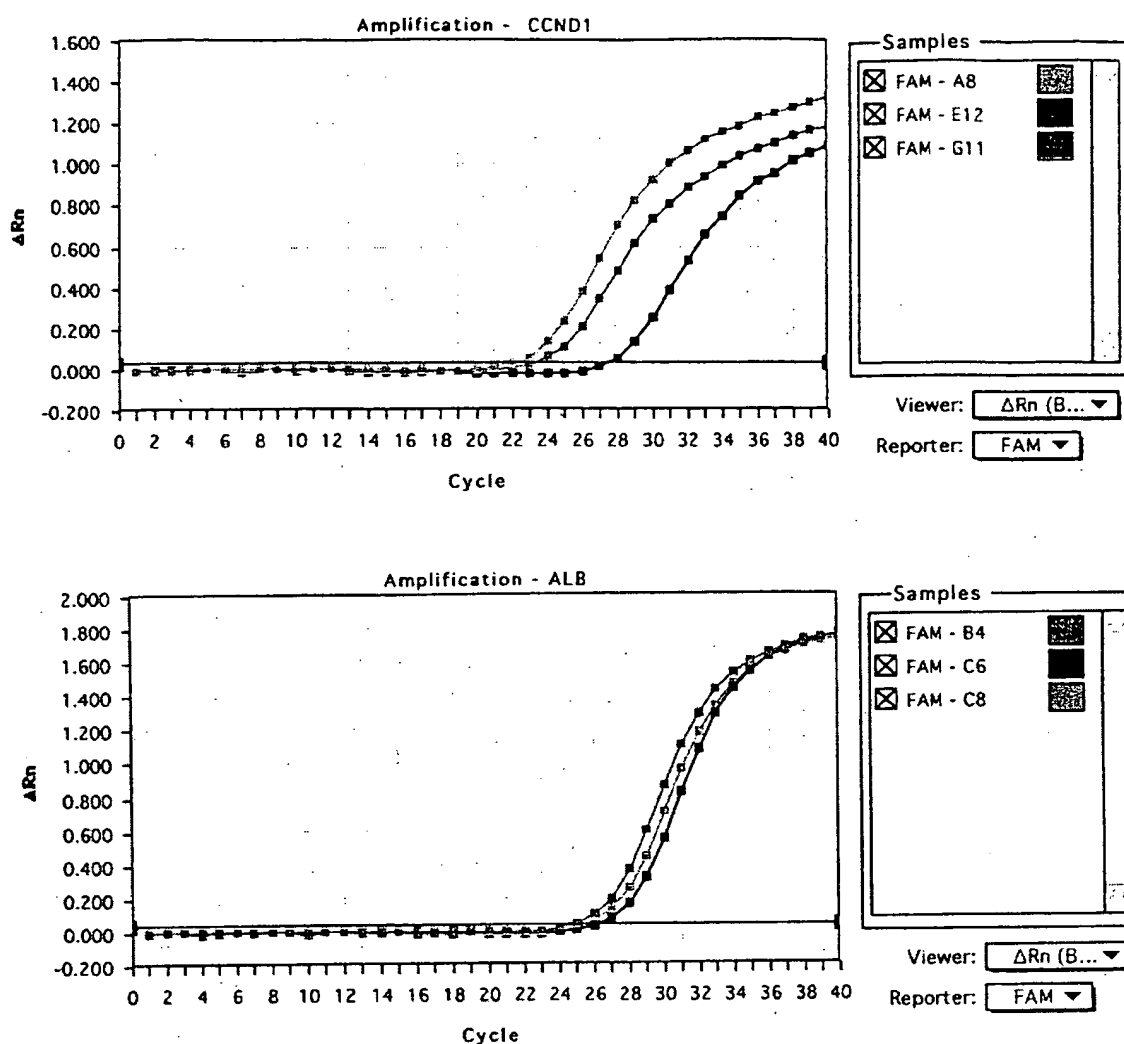
In this study, we validated a PCR method developed for the quantification of gene over-representation in tumors. The method, based on real-time analysis of PCR amplification, has several advantages over other PCR-based quantitative assays such as competitive quantitative PCR (Celi *et al.*, 1994). First, the real-time PCR method is performed in a closed-tube system, avoiding the risk of contamination by amplified products. Re-amplification of carryover PCR products in subsequent experiments can also be prevented by using the enzyme uracil N-glycosylase (UNG) (Longo *et al.*, 1990). The second advantage is the simplicity and rapidity of sample analysis, since no post-PCR manipulations are required. Our results show that the automated method is reliable. We found it possible to determine, in triplicate, the number of copies of a target gene in more than 100 tumors per day. Third, the system has a linear dynamic range of at least 4 orders of magnitude, meaning that samples do not have to contain equal starting amounts of DNA. This technique should therefore be suitable for analyzing formalin-fixed, paraffin-embedded tissues. Fourth, and above all, real-time PCR makes DNA quantification much more precise and reproducible, since it is based on C_t values rather than end-point measurement of the amount of accumulated PCR product. Indeed, the ABI Prism 7700 Sequence Detection System enables C_t to be calculated when PCR amplification is still in the exponential phase and when none of the reaction components is rate-limiting. The within-run CV of the C_t value for calibrator human DNA (5 replicates) was always below 5%, and the between-assay precision in 5 different runs was always below 10% (data not shown). In addition, the use of a standard curve is not absolutely necessary, since the copy number can be determined simply by comparing the C_t ratio of the target gene with that of reference genes. The results obtained by the 2 methods (with and without a standard curve) are similar in our experiments (data not shown). Moreover, unlike competitive quantitative PCR, real-time PCR does not require an internal control (the design and storage of internal controls and the validation of their amplification efficiency is laborious).

The only potential disavantage of real-time PCR, like all other PCR-based methods and solid-matrix blotting techniques (Southern blots and dot blots) is that is cannot avoid dilution artifacts inherent in the extraction of DNA from tumor cells contained in heterogeneous tissue specimens. Only FISH and immunohistochemistry can measure alterations on a cell-by-cell basis (Pauletti *et al.*, 1996; Slamon *et al.*, 1989). However, FISH requires expensive equipment and trained personnel and is also time-consuming. Moreover, FISH does not assess gene expression and therefore cannot detect cases in which the gene product is over-expressed in the absence of gene amplification, which will be possible in the future by real-time quantitative RT-PCR. Immunohistochemistry is subject to considerable variations in the hands of different teams, owing to alterations of target proteins during the procedure, the different primary antibodies and fixation methods used and the criteria used to define positive staining.

The results of this study are in agreement with those reported in the literature. (i) Chromosome regions 4q11-q13 and 21q21.2 (which bear *alb* and *app*, respectively) showed no genetic alterations in the breast-cancer samples studied here, in keeping with the results of CGH (Kallioniemi *et al.*, 1994). (ii) We found that amplifications of these 3 oncogenes were independent events, as reported by other teams (Berns *et al.*, 1992; Borg *et al.*, 1992). (iii) The frequency and degree of *myc* amplification in our breast tumor DNA series were lower than those of *ccnd1* and *erbB2* amplification, confirming the findings of Borg *et al.* (1992) and Courjal *et al.* (1997). (iv) The maxima of *ccnd1* and *erbB2* over-representation were 18-fold and 15-fold, also in keeping with earlier results (about

Figure 2 – *ccnd1* and *alb* gene dosage by real-time PCR in 3 breast tumor samples: T118 (E12, C6, black squares), T133 (G11, B4, red squares) and T145 (A8, C8, blue squares). Given the C, of each sample, the initial copy number is inferred from the standard curve obtained during the same experiment. Triplicate plots were performed for each tumor sample, but the data for only one are shown here. The results are shown in Table II.

30-fold maximum) (Berns *et al.*, 1992; Borg *et al.*, 1992; Courjal *et al.*, 1997). (*v*) The *erb*B2 copy numbers obtained with real-time PCR were in good agreement with data obtained with other quantitative PCR-based assays in terms of the frequency and degree of amplification (An *et al.*, 1995; Deng *et al.*, 1996; Valéron

et al., 1996). Our results also correlate well with those recently published by Gelmini *et al.* (1997), who used the TaqMan system to measure *erb*B2 amplification in a small series of breast tumors (n = 25), but with an instrument (LS-50B luminescence spectrometer, Perkin-Elmer Applied Biosystems) which only allows end-

TABLE II – EXAMPLES OF ccnd1 GENE DOSAGE RESULTS
FROM 3 BREAST TUMORS[1]

Tumor	ccnd1			alb			Nccnd1/alb
	Copy number	Mean	SD	Copy number	Mean	SD	
T118	4525			4223			
	4605	4603	77	4365	4325	89	1.06
	4678			4387			
T133	59821			9787			
	61659	61100	1111	10092	10137	375	6.03
	61821			10533			
T145	128563			7321			
	125892	125392	3448	7762	7672	316	16.34
	121722			7933			

[1]For each sample, 3 replicate experiments were performed and the mean
and the standard deviation (SD) was determined. The level of ccnd1 gene
amplification (Nccnd1/alb) is determined by dividing the average ccnd1
copy number value by the average alb copy number value.

point measurement of fluorescence intensity. Here we report myc
and ccnd1 gene dosage in breast cancer by means of quantitative
PCR. (vi) We found a high degree of concordance between
real-time quantitative PCR and Southern blot analysis in terms of
gene amplification, especially for samples with high copy numbers
(≥5-fold). The slightly higher frequency of gene amplification
(especially ccnd1 and erbB2) observed by means of real-time
quantitative PCR as compared with Southern-blot analysis may be
explained by the higher sensitivity of the former method. However,
we cannot rule out the possibility that some tumors with a few extra

gene copies observed in real-time PCR had additional copies of an
arm or a whole chromosome (trisomy, tetrasomy or polysomy)
rather than true gene amplification. These 2 types of genetic
alteration (polysomy and gene amplification) could be easily
distinguished in the future by using an additional probe located on
the same chromosome arm, but some distance from the target gene.
It is noteworthy that high gene copy numbers have the greatest
prognostic significance in breast carcinoma (Borg et al., 1992;
Slamon et al., 1987).

Finally, this technique can be applied to the detection of gene
deletion as well as gene amplification. Indeed, we found a
decreased copy number of erbB2 (but not of the other 2 proto-
oncogenes) in several tumors; erbB2 is located in a chromosome
region (17q21) reported to contain both deletions and amplifica-
tions in breast cancer (Bièche and Lidereau, 1995).

In conclusion, gene amplification in various cancers can be used
as a marker of pre-neoplasia, also for early diagnosis of cancer,
staging, prognostication and choice of treatment. Southern blotting
is not sufficiently sensitive, and FISH is lengthy and complex.
Real-time quantitative PCR overcomes both these limitations, and
is a sensitive and accurate method of analyzing large numbers of
samples in a short time. It should find a place in routine clinical
gene dosage.

ACKNOWLEDGEMENTS

REFERENCES

AN, H.X., NIEDERACHER, D., BECKMANN, M.W., GÖHRING, U.J., SCHARL, A.,
PICARD, F., VAN ROEYEN, C., SCHNÜRCH, H.G. and BENDER, H.G., erbB2
gene amplification detected by fluorescent differential polymerase chain
reaction in paraffin-embedded breast carcinoma tissues. Int. J. Cancer
(Pred. Oncol.), 64, 291–297 (1995).

BERNS, E.M.J.J., KLIJN, J.G.M., VAN PUTTEN, W.L.J., VAN STAVEREN, I.L.,
PORTENGEN, H. and FOEKENS, J.A., c-myc amplification is a better prognos-
tic factor than HER2/neu amplification in primary breast cancer. Cancer
Res., 52, 1107–1113 (1992).

BIÈCHE, I. and LIDEREAU, R., Genetic alterations in breast cancer. Genes
Chrom. Cancer, 14, 227–251 (1995).

BORG, A., BALDETORP, B., FERNO, M., OLSSON, H. and SIGURDSSON, H.,
c-myc amplification is an independent prognostic factor in post-menopausal
breast cancer. Int. J. Cancer, 51, 687–691 (1992).

CÉLI, F.S., COHEN, M.M., ANTONARAKIS, S.E., WERTHEIMER, E., ROTH, J.
and SHULDINER, A.R., Determination of gene dosage by a quantitative
adaptation of the polymerase chain reaction (gd-PCR): rapid detection of
deletions and duplications of gene sequences. Genomics, 21, 304–310
(1994).

COURJAL, F., CUNY, M., SIMONY-LAFONTAINE, J., LOUASSON, G., SPEISER, P.,
ZEILLINGER, R., RODRIGUEZ, C. and THEILLET, C., Mapping of DNA
amplifications at 15 chromosomal localizations in 1875 breast tumors:
definition of phenotypic groups. Cancer Res., 57, 4360–4367 (1997).

DENG, G., YU, M., CHEN, L.C., MOORE, D., KURISU, W., KALLIONIEMI, A.,
WALDMAN, F.M., COLLINS, C. and SMITH, H.S., Amplifications of oncogene
erbB-2 and chromosome 20q in breast cancer determined by differentially
competitive polymerase chain reaction. Breast Cancer Res. Treat., 40,
271–281 (1996).

GELMINI, S., ORLANDO, C., SESTINI, R., VONA, G., PINZANI, P., RUOCCO, L.
and PAZZAGLI, M., Quantitative polymerase chain reaction-based homoge-
neous assay with fluorogenic probes to measure c-erB-2 oncogene amplifi-
cation. Clin. Chem., 43, 752–758 (1997).

GIBSON, U.E.M., HEID, C.A. and WILLIAMS, P.M., A novel method for
real-time quantitative RT-PCR. Genome Res., 6, 995–1001 (1996).

HEID, C.A., STEVENS, J., LIVAK, K.J. and WILLIAMS, P.M., Real-time
quantitative PCR. Genome Res., 6, 986–994 (1996).

HOLLAND, P.M., ABRAMSON, R.D., WATSON, R. and GELFAND, D.H.,
Detection of specific polymerase chain reaction product by utilizing the 5'
to 3' exonuclease activity of Thermus aquaticus DNA polymerase. Proc.
nat. Acad. Sci. (Wash.), 88, 7276–7280 (1991).

KALLIONIEMI, A., KALLIONIEMI, O.P., PIPER, J., TANNER, M., STOKKES, T.,
CHEN, L., SMITH, H.S., PINKEL, D., GRAY, J.W. and WALDMAN, F.M.,
Detection and mapping of amplified DNA sequences in breast cancer by
comparative genomic hybridization. Proc. nat. Acad. Sci. (Wash.), 91,
2156–2160 (1994).

LEE, L.G., CONNELL, C.R. and BIOCH, W., Allelic discrimination by
nick-translation PCR with fluorogenic probe. Nucleic Acids Res., 21,
3761–3766 (1993).

LONGO, N., BERNINGER, N.S. and HARTLEY, J.L., Use of uracil DNA
glycosylase to control carry-over contamination in polymerase chain
reactions. Gene, 93, 125–128 (1990).

MUSS, H.B., THOR, A.D., BERRY, D.A., KUTE, T., LIU, E.T., KOERNER, F.,
CIRRINCIONE, C.T., BUDMAN, D.R., WOOD, W.C., BARCOS, M. and HENDER-
SON, I.C., c-erbB-2 expression and response to adjuvant therapy in women
with node-positive early breast cancer. New Engl. J. Med., 330, 1260–1266
(1994).

PAULETTI, G., GODOLPHIN, W., PRESS, M.F. and SALMON, D.J., Detection and
quantification of HER-2/neu gene amplification in human breast cancer
archival material using fluorescence in situ hybridization. Oncogene, 13,
63–72 (1996).

PIATAK, M., LUK, K.C., WILLIAMS, B. and LIFSON, J.D., Quantitative
competitive polymerase chain reaction for accurate quantitation of HIV
DNA and RNA species. Biotechniques, 14, 70–80 (1993).

SCHUURING, E., VERHOEVEN, E., VAN TINTEREN, H., PETERSE, J.L., NUNNIK,
B., THUNNISSEN, F.B.J.M., DEVILEE, P., CORNELISSE, C.J., VAN DE VIJVER,
M.J., MOOI, W.J. and MICHALIDES, R.J.A.M., Amplification of genes within
the chromosome 11q13 region is indicative of poor prognosis in patients
with operable breast cancer. Cancer Res., 52, 5229–5234 (1992).

SLAMON, D.J., CLARK, G.M., WONG, S.G., LEVIN, W.S., ULLRICH, A. and
McGUIRE, W.L., Human breast cancer: correlation of relapse and survival
with amplification of the HER-2/neu oncogene. Science, 235, 177–182
(1987).

SLAMON, D.J., GODOLPHIN, W., JONES, L.A., HOLT, J.A., WONG, S.G., KEITH,
D.E., LEVIN, W.J., STUART, S.G., UDOVE, J., ULLRICH, A. and PRESS, M.F.,
Studies of the HER-2/neu proto-oncogene in human breast and ovarian
cancer. Science, 244, 707–712 (1989).

VALERON, P.F., CHIRINO, R., FERNANDEZ, L., TORRES, S., NAVARRO, D.,
AGUIAR, J., CABRERA, J.J., DIAZ-CHICO, B.N. and DIAZ-CHICO, J.C.,
Validation of a differential PCR and an ELISA procedure in studying
HER-2/neu status in breast cancer. Int. J. Cancer, 65, 129–133 (1996).

DECLARATION OF PAUL POLAKIS, Ph.D.

I, Paul Polakis, Ph.D., declare and say as follows:

1.   I was awarded a Ph.D. by the Department of Biochemistry of the Michigan State University in 1984. My scientific Curriculum Vitae is attached to and forms part of this Declaration (Exhibit A).

2.   I am currently employed by Genentech, Inc. where my job title is Staff Scientist. Since joining Genentech in 1999, one of my primary responsibilities has been leading Genentech's Tumor Antigen Project, which is a large research project with a primary focus on identifying tumor cell markers that find use as targets for both the diagnosis and treatment of cancer in humans.

3.   As part of the Tumor Antigen Project, my laboratory has been analyzing differential expression of various genes in tumor cells relative to normal cells. The purpose of this research is to identify proteins that are abundantly expressed on certain tumor cells and that are either (i) not expressed, or (ii) expressed at lower levels, on corresponding normal cells. We call such differentially expressed proteins "tumor antigen proteins". When such a tumor antigen protein is identified, one can produce an antibody that recognizes and binds to that protein. Such an antibody finds use in the diagnosis of human cancer and may ultimately serve as an effective therapeutic in the treatment of human cancer.

4.   In the course of the research conducted by Genentech's Tumor Antigen Project, we have employed a variety of scientific techniques for detecting and studying differential gene expression in human tumor cells relative to normal cells, at genomic DNA, mRNA and protein levels. An important example of one such technique is the well known and widely used technique of microarray analysis which has proven to be extremely useful for the identification of mRNA molecules that are differentially expressed in one tissue or cell type relative to another. In the course of our research using microarray analysis, we have identified approximately 200 gene transcripts that are present in human tumor cells at significantly higher levels than in corresponding normal human cells. To date, we have generated antibodies that bind to about 30 of the tumor antigen proteins expressed from these differentially expressed gene transcripts and have used these antibodies to quantitatively determine the level of production of these tumor antigen proteins in both human cancer cells and corresponding normal cells. We have then compared the levels of mRNA and protein in both the tumor and normal cells analyzed.

5.   From the mRNA and protein expression analyses described in paragraph 4 above, we have observed that there is a strong correlation between changes in the level of mRNA present in any particular cell type and the level of protein

expressed from that mRNA in that cell type. In approximately 80% of our observations we have found that increases in the level of a particular mRNA correlates with changes in the level of protein expressed from that mRNA when human tumor cells are compared with their corresponding normal cells.

6.   Based upon my own experience accumulated in more than 20 years of research, including the data discussed in paragraphs 4 and 5 above and my knowledge of the relevant scientific literature, it is my considered scientific opinion that for human genes, an increased level of mRNA in a tumor cell relative to a normal cell typically correlates to a similar increase in abundance of the encoded protein in the tumor cell relative to the normal cell. In fact, it remains a central dogma in molecular biology that increased mRNA levels are predictive of corresponding increased levels of the encoded protein. While there have been published reports of genes for which such a correlation does not exist, it is my opinion that such reports are exceptions to the commonly understood general rule that increased mRNA levels are predictive of corresponding increased levels of the encoded protein.

7.   I hereby declare that all statements made herein of my own knowledge are true and that all statements made on information or belief are believed to be true, and further that these statements were made with the knowledge that willful false statements and the like so made are punishable by fine or imprisonment, or both, under Section 1001 of Title 18 of the United States Code and that such willful statements may jeopardize the validity of the application or any patent issued thereon.

Dated:_5/07/04_   By:_Paul Polakis_

                                               Paul Polakis, Ph.D.

2

CURRICULUM VITAE

PAUL G. POLAKIS
Staff Scientist
Genentech, Inc
1 DNA Way, MS#40
S. San Francisco, CA 94080

EDUCATION:

Ph.D., Biochemistry, Department of Biochemistry,
Michigan State University (1984)

B.S., Biology. College of Natural Science, Michigan State University (1977)

PROFESSIONAL EXPERIENCE:

2002-present	Staff Scientist, Genentech, Inc S. San Francisco, CA
1999- 2002	Senior Scientist, Genentech, Inc., S. San Francisco, CA
1997 -1999	Research Director Onyx Pharmaceuticals, Richmond, CA
1992- 1996	Senior Scientist, Project Leader, Onyx Pharmaceuticals, Richmond, CA
1991-1992	Senior Scientist, Chiron Corporation, Emeryville, CA.
1989-1991	Scientist, Cetus Corporation, Emeryville CA.
1987-1989	Postdoctoral Research Associate, Genentech, Inc., South SanFrancisco, CA.
1985-1987	Postdoctoral Research Associate, Department of Medicine, Duke University Medical Center, Durham, NC

1984-1985	Assistant Professor, Department of Chemistry, Oberlin College, Oberlin, Ohio
1980-1984	Graduate Research Assistant, Department of Biochemistry, Michigan State University East Lansing, Michigan

PUBLICATIONS:

1. Polakis, P G. and Wilson, J. E. 1982 Purification of a Highly Bindable Rat Brain Hexokinase by High Performance Liquid Chromatography. Biochem. Biophys. Res. Commun. 107, 937-943.

2. Polakis, P.G. and Wilson, J. E. 1984 Proteolytic Dissection of Rat Brain Hexokinase: Determination of the Cleavage Pattern during Limited Digestion with Trypsin. Arch. Biochem. Biophys. 234, 341-352.

3. Polakis, P. G. and Wilson, J. E. 1985 An Intact Hydrophobic N-Terminal Sequence is Required for the Binding Rat Brain Hexokinase to Mitochondria. Arch. Biochem. Biophys. 236, 328-337.

4. Uhing, R.J., Polakis,P.G. and Snyderman, R. 1987 Isolaton of GTP-binding Proteins from Myeloid HL60 Cells. J. Biol. Chem. 262, 15575-15579.

5. Polakis, P.G., Uhing, R.J. and Snyderman, R. 1988 The Formylpeptide Chemoattractant Receptor Copurifies with a GTP-binding Protein Containing a Distinct 40 kDa Pertussis Toxin Substrate. J. Biol. Chem. 263, 4969-4979.

6. Uhing, R. J., Dillon, S., Polakis, P. G., Truett, A. P. and Snyderman, R. 1988 Chemoattractant Receptors and Signal Transduction Processes in Cellular and Molecular Aspects of Inflammation (Poste, G. and Crooke, S. T. eds.) pp 335-379.

7. Polakis, P.G., Evans, T. and Snyderman 1989 Multiple Chromatographic Forms of the Formylpeptide Chemoattractant Receptor and their Relationship to GTP-binding Proteins. Biochem. Biophys. Res. Commun. 161, 276-283.

8. Polakis, P. G., Snyderman, R. and Evans, T. 1989 Characterization of G25K, a GTP-binding Protein Containing a Novel Putative Nucleotide Binding Domain. Biochem. Biophys. Res. Comun. 160, 25-32.

9. Polakis, P., Weber,R.F., Nevins,B., Didsbury, J. Evans,T. and Snyderman, R. 1989 Identification of the ral and rac1 Gene Products, Low Molecular Mass GTP-binding Proteins from Human Platelets. J. Biol. Chem. 264, 16383-16389.

10. Snyderman, R., Perianin, A., Evans, T., Polakis, P. and Didsbury, J. 1989 G Proteins and Neutrophil Function. In ADP-Ribosylating Toxins and G Proteins: Insights into Signal Transduction. (J. Moss and M. Vaughn, eds.) Amer. Soc. Microbiol. pp. 295-323.

11. Hart, M.J., Polakis, P.G., Evans, T. and Cerrione, R.A. 1990 The Identification and Charaterization of an Epidermal Growth Factor-Stimulated Phosphorylation of a Specific Low Molecular Mass GTP-binding Protein in a Reconstituted Phospholipid Vesicle System. J. Biol. Chem. 265, 5990-6001.

12. Yatani, A., Okabe, K., Polakis, P. Halenbeck, R. McCormick, F. and Brown, A. M. 1990 ras p21 and GAP Inhibit Coupling of Muscarinic Receptors to Atrial K^+ Channels. Cell. 61, 769-776.

13. Munemitsu, S., Innis, M.A., Clark, R., McCormick, F., Ullrich, A. and Polakis, P.G. 1990 Molecular Cloning and Expression of a G25K cDNA, the Human Homolog of the Yeast Cell Cycle Gene CDC42. Mol. Cell. Biol. 10, 5977-5982.

14. Polakis, P.G. Rubinfeld, B. Evans, T. and McCormick, F. 1991 Purification of Plasma Membrane-Associated GTPase Activating Protein (GAP) Specific for rap-1/krev-1 from HL60 Cells. Proc. Natl. Acad. Sci. USA 88, 239-243.

15. Moran, M. F., Polakis, P., McCormick, F., Pawson, T. and Ellis, C. 1991 Protein Tyrosine Kinases Regulate the Phosphorylation, Protein Interactions, Subcellular Distribution, and Activity of p21ras GTPase Activating Protein. Mol. Cell. Biol. 11, 1804-1812

16. Rubinfeld, B., Wong, G., Bekesi, E. Wood, A. McCormick, F. and Polakis, P. G. 1991 A Synthetic Peptide Corresponding to a Sequence in the GTPase Activating Protein Inhibits p21[ras] Stimulation and Promotes Guanine Nucleotide Exchange. Internatl. J. Peptide and Prot. Res. 38, 47-53.

17. Rubinfeld, B., Munemitsu, S., Clark, R., Conroy, L., Watt, K., Crosier, W., McCormick, F., and Polakis, P. 1991 Molecular Cloning of a GTPase Activating Protein Specific for the Krev-1 Protein p21[rap1]. Cell 65, 1033-1042.

18. Zhang, K. Papageorge, A., G., Martin, P., Vass, W. C., Olah, Z., Polakis, P., McCormick, F. and Lowy, D, R. 1991 Heterogenous Amino Acids in RAS and Rap1A Specifying Sensitivity to GAP Proteins. Science 254, 1630-1634.

19. Martin, G., Yatani, A., Clark, R., Polakis, P., Brown, A. M. and McCormick, F. 1992 GAP Domains Responsible for p21[ras]-dependent Inhibition of Muscarinic Atrial K^+ Channel Currents. Science 255, 192-194.

20. McCormick, F., Martin, G. A., Clark, R., Bollag, G. and Polakis, P . 1992 Regulation of p21ras by GTPase Activating Proteins. Cold Spring Harbor Symposia on Quantitative Biology. Vol. 56, 237-241.

21. Pronk, G. B., Polakis, P., Wong, G., deVries-Smits, A. M., Bos J. L. and McCormick, F. 1992 p60[v-src] Can Associate with and Phosphorylate the p21[ras] GTPase Activating Protein. Oncogene 7,389-394.

22. Polakis P. and McCormick, F. 1992 Interactions Between p21[ras] Proteins and Their GTPase Activating Proteins. In Cancer Surveys (Franks, L. M., ed.) 12, 25-42.

23. Wong, G., Muller, O., Clark, R., Conroy, L., Moran, M., Polakis,P. and McCormick, F. 1992 Molecular coloning and nucleic acid binding properties of the GAP-associated tyrosine phosphoprotein p62. Cell 69, 551-558.

24. Polakis, P., Rubinfeld, B. and McCormick, F. 1992 Phosphorylation of rap1GAP in vivo and by cAMP-dependent Kinase and the Cell Cycle p34[cdc2] Kinase in vitro. J. Biol. Chem. 267, 10780-10785.

25. McCabe, P.C., Haubrauck, H., Polakis, P., McCormick, F., and Innis, M. A., 1992 Functional Interactions Between p21[rap1A] and Components of the Budding pathway of *Saccharomyces cerevisiae*. Mol. Cell. Biol. 12, 4084-4092.

26. Rubinfeld, B., Crosier, W.J., Albert, I., Conroy,L., Clark, R., McCormick, F. and Polakis, P. 1992 Localization of the rap1GAP Catalytic Domain and Sites of Phosphorylation by Mutational Analysis. Mol. Cell . Biol. 12, 4634-4642.

27. Ando, S., Kaibuchi, K., Sasaki, K., Hiraoka, T., Nishiyama, T., Mizuno, T., Asada, M., Nunoi, H., Matsuda, I., Matsuura, Y., Polakis, P., McCormick, F. and Takai, Y. 1992 Post-translational processing of rac p21s is important both for their interaction with the GDP/GTP exchange proteins and for their activation of NADPH oxidase. J. Biol. Chem. 267, 25709-25713.

28. Janoueix-Lerosey, I., Polakis, P., Tavitian, A. and deGunzberg, J. 1992 Regulation of the GTPase activity of the ras-related rap2 protein. Biochem. Biophys. Res. Commun. 189, 455-464.

29. Polakis, P. 1993 GAPs Specific for the rap1/Krev-1 Protein. in GTP-binding Proteins: the *ras*-superfamily. (J.C. LaCale and F. McCormick, eds.) 445-452.

30. Polakis, P. and McCormick, F. 1993 Structural requirements for the interaction of p21[ras] with GAP, exchange factors, and its bological effector target. J. Biol Chem. 268, 9157-9160.

31. Rubinfeld, B., Souza, B. Albert, I., Muller, O., Chamberlain, S., Masiarz, F., Munemitsu, S. and Polakis, P. 1993 Association of the APC gene product with beta- catenin. Science 262, 1731-1734.

32. Weiss, J., Rubinfeld, B., Polakis, P., McCormick, F. Cavenee, W. A. and Arden, K. 1993 The gene for human rap1-GTPase activating protein (rap1GAP) maps to chromosome 1p35-1p36.1. Cytogenet. Cell Genet. 66, 18-21.

33. Sato, K. Y., Polakis, P., Haubruck, H., Fasching, C. L., McCormick, F. and Stanbridge, E. J. 1994 Analysis of the tumor suppressor acitvity of the K-rev gene in human tumor cell lines. Cancer Res. 54, 552-559.

34. Janoueix-Lerosey, I., Fontenay, M., Tobelem, G., Tavitian, A., Polakis, P. and DeGunzburg, J. 1994 Phosphorylation of rap1GAP during the cell cycle. Biochem. Biophys. Res. Commun. 202, 967-975

35. Munemitsu, S., Souza, B., Mueller, O., Albert, I., Rubinfeld, B., and Polakis, P. 1994 The APC gene product associates with microtubules in vivo and affects their assembly in vitro. Cancer Res. 54, 3676-3681.

36. Rubinfeld, B. and Polakis, P. 1995 Purification of baculovirus produced rap1GAP. Methods Enz. 255,31

37. Polakis, P. 1995 Mutations in the APC gene and their implications for protein structure and function. Current Opinions in Genetics and Development 5, 66-71

38. Rubinfeld, B., Souza, B., Albert, I., Munemitsu, S. and Polakis P. 1995 The APC protein and E-cadherin form similar but independent complexes with α-catenin, β-catenin and Plakoglobin. J. Biol. Chem. 270, 5549-5555

39. Munemitsu, S., Albert, I., Souza, B., Rubinfeld, B., and Polakis, P. 1995 Regulation of intracellular β-catenin levels by the APC tumor suppressor gene. Proc. Natl. Acad. Sci. 92, 3046-3050.

40. Lock, P., Fumagalli, S., Polakis, P. McCormick, F. and Courtneidge, S. A. 1996 The human p62 cDNA encodes Sam68 and not the rasGAP-associated p62 protein. Cell 84, 23-24.

41. Papkoff, J., Rubinfeld, B., Schryver, B. and Polakis, P. 1996 Wnt-1 regulates free pools of catenins and stabilizes APC-catenin complexes. Mol. Cell. Biol. 16, 2128-2134.

42. Rubinfeld, B., Albert, I., Porfiri, E., Fiol, C., Munemitsu, S. and Polakis, P. 1996 Binding of GSK3β to the APC-β-catenin complex and regulation of complex assembly. Science 272, 1023-1026.

43. Munemitsu, S., Albert, I., Rubinfeld, B. and Polakis, P. 1996 Deletion of amino-terminal structure stabilizes β-catenin in vivo and promotes the hyperphosphorylation of the APC tumor suppressor protein. Mol. Cell. Biol.16, 4088-4094.

44. Hart, M. J., Callow, M. G., Sousa, B. and Polakis P. 1996 IQGAP1, a calmodulin binding protein witha rasGAP related domain, is a potential effector for cdc42Hs. EMBO J. 15, 2997-3005.

45. Nathke, I. S., Adams, C. L., Polakis, P., Sellin, J. and Nelson, W. J. 1996 The adenomatous polyposis coli (APC) tumor suppressor protein is localized to plasma membrane sites involved in active epithelial cell migration. J. Cell. Biol. 134, 165-180.

46. Hart, M. J., Sharma, S., elMasry, N., Qui, R-G., McCabe, P., Polakis, P. and Bollag, G. 1996 Identification of a novel guanine nucleotide exchange factor for the rho GTPase. J. Biol. Chem. 271, 25452.

47. Thomas JE, Smith M, Rubinfeld B, Gutowski M, Beckmann RP, and Polakis P. 1996 Subcellular localization and analysis of apparent 180-kDa and 220-kDa proteins of the breast cancer susceptibility gene, BRCA1. J. Biol. Chem. 1996 271, 28630-28635

48. Hayashi, S., Rubinfeld, B., Souza, B., Polakis, P., Wieschaus, E., and Levine, A. 1997 A Drosophila homolog of the tumor suppressor adenomatous polyposis coli

down-regulates β -catenin but its zygotic expression is not essential for the regulation of armadillo. Proc. Natl. Acad. Sci. 94, 242-247.

49. Vleminckx, K., Rubinfeld, B., Polakis, P. and Gumbiner, B. 1997 The APC tumor suppressor protein induces a new axis in Xenopus embryos. J. Cell. Biol. 136, 411-420.

50. Rubinfeld, B., Robbins, P., El-Gamil, M., Albert, I., Porfiri, P. and Polakis, P. 1997 Stabilization of β-catenin by genetic defects in melanoma cell lines. Science 275, 1790-1792.

51. Polakis, P. The adenomatous polyposis coli (APC) tumor suppressor. 1997 Biochem. Biophys. Acta, 1332, F127-F147.

52. Rubinfeld, B., Albert, I., Porfiri, E., Munemitsu, S., and Polakis, P 1997 Loss of β-catenin regulation by the APC tumor suppressor protein correlates with loss of structure due to common somatic mutations of the gene. Cancer Res. 57, 4624-4630.

53. Porfiri, E., Rubinfeld, B., Albert, I., Hovanes. K., Waterman, M., and Polakis, P. 1997 Induction of a β-catenin-LEF-1 complex by wnt-1 and transforming mutants of β-catenin. Oncogene 15, 2833-2839.

54. Thomas JE, Smith M, Tonkinson JL, Rubinfeld B, and Polakis P., 1997 Induction of phosphorylation on BRCA1 during the cell cycle and after DNA damage. Cell Growth Differ. 8, 801-809.

55. Hart, M., de los Santos, R., Albert, I., Rubinfeld, B., and Polakis P., 1998 Down regulation of β-catenin by human Axin and its association with the adenomatous polyposis coli (APC) tumor suppressor, β-catenin and glycogen synthase kinase 3β. Current Biology 8, 573-581.

56. Polakis, P. 1998 The oncogenic activation of β-catenin. Current Opinions in Genetics and Development 9, 15-21

57. Matt Hart, Jean-Paul Concordet, Irina Lassot, Iris Albert, Rico del los Santos, Herve Durand, Christine Perret, Bonnee Rubinfled, Florence Margottin, Richard Benarous and Paul Polakis. 1999 The F-box protein β–TrCP associates with phosphorylated β–catenin and regulates its activity in the cell. Current Biology 9, 207-10.

58. Howard C. Crawford, Barbara M. Fingleton, Bonnee Rubinfeld, Paul Polakis and Lynn M. Matrisian 1999 The metalloproteinase matrilysin is a target of β–catenin transactivation in intestinal tumours. Oncogene 18, 2883-91.

59. Meng J, Glick JL, Polakis P, Casey PJ. 1999 Functional interaction between Galpha(z) and Rap1GAP suggests a novel form of cellular cross-talk. J Biol Chem. 17, 36663-9

60. Vijayasurian Easwaran, Virginia Song, **Paul Polakis** and Steve Byers 1999 The ubiquitin-proteosome pathway and serine kinase activity modulate APC mediated regulation of β-catenin-LEF signaling. **J. Biol. Chem**. 274(23):16641-5.

61 **Polakis P**, Hart M and Rubinfeld B. 1999 Defects in the regulation of beta-catenin
in colorectal cancer. **Adv Exp Med Biol**. 470, 23-32

62 Shen Z, Batzer A, Koehler JA, **Polakis P**, Schlessinger J, Lydon NB, Moran MF. 1999 Evidence for SH3 domain directed binding and phosphorylation of Sam68 by Src. **Oncogene**. 18, 4647-53

64. Thomas GM, Frame S, Goedert M, Nathke I, **Polakis P**, Cohen P. 1999 A GSK3- binding peptide from FRAT1 selectively inhibits the GSK3-catalysed phosphorylation of axin and beta-catenin. **FEBS Lett**. 458, 247-51.

65. Peifer M, **Polakis P**. 2000 Wnt signaling in oncogenesis and embryogenesis--a look outside the nucleus. **Science** 287,1606-9.

66. **Polakis P.** 2000 Wnt signaling and cancer. **Genes Dev;**14, 1837-1851.

67. Spink KE, **Polakis P**, Weis WI 2000 Structural basis of the Axin-adenomatous polyposis coli interaction. **EMBO J** 19, 2270-2279.

68. Szeto , W., Jiang, W., Tice, D.A., Rubinfeld, B., Hollingshead, P.G., Fong, S.E., Dugger, D.L., Pham, T., Yansura, D.E., Wong, T.A., Grimaldi, J.C., Corpuz, R.T., Singh J.S., Frantz, G.D., Devaux, B., Crowley, C.W., Schwall, R.H., Eberhard, D.A.,
Rastelli, L., **Polakis, P.** and Pennica, D. 2001 Overexpression of the Retinoic Acid-
Responsive Gene Stra6 in Human Cancers and its Synergistic Induction by Wnt-1 and
Retinoic Acid. **Cancer Res** 61, 4197-4204.

69. Rubinfeld B, Tice DA, **Polakis P**. 2001 Axin dependent phosphorylation of the adenomatous polyposis coli protein mediated by casein kinase 1 epsilon. **J Biol Chem**
276, 39037-39045.

70. **Polakis P**. 2001 More than one way to skin a catenin. **Cell** 2001 105, 563-566.

71. Tice DA, Soloviev I, **Polakis P**. 2002 Activation of the Wnt Pathway Interferes withSerum Response Element-driven Transcription of Immediate Early Genes. **J Biol.**
Chem. 277, 6118-6123.

72. Tice DA, Szeto W, Soloviev I, Rubinfeld B, Fong SE, Dugger DL, Winer J,

Williams PM, Wieand D, Smith V, Schwall RH, Pennnica D, **Polakis P**. 2002
Synergistic activation of tumor antigens by wnt-1 signaling and retinoic acid revealed
by gene expression profiling. **J Biol Chem**. 277,14329-14335.

73. **Polakis, P**. 2002 Casein kinase I: A wnt'er of disconnect. **Curr. Biol**. 12, R499.

74. Mao,W. , Luis, E., Ross, S., Silva, J., Tan, C., Crowley, C., Chui, C., Franz, G.,
Senter, P., Koeppen, H., **Polakis, P**. 2004 EphB2 as a therapeutic antibody drug
target for the treatment of colorectal cancer. **Cancer Res**. 64, 781-788.

75. Shibamoto, S., Winer, J., Williams, M., Polakis, P. 2003 A Blockade in Wnt
signaling is activated following the differentiation of F9 teratocarcinoma cells. **Exp.
Cell Res.** 29211-20.

76. Zhang Y, Eberhard DA, Frantz GD, Dowd P, Wu TD, Zhou Y, Watanabe C, Luoh SM, **Polakis P,**
Hillan KJ, Wood WI, Zhang Z. 2004 GEPIS--quantitative gene expression profiling in normal and
cancer tissues. **Bioinformatics**, April 8

IN THE UNITED STATES PATENT AND TRADEMARK OFFICE

Applicant	:	Ashkenazi et al.
App. No.	:	09/903,925
Filed	:	July 11, 2001
For	:	SECRETED AND TRANSMEMBRANE POLYPEPTIDES AND NUCLEIC ACIDS ENCODING THE SAME
Examiner	:	Hamud, Fozia M

Group Art Unit 1647

Commissioner of Patents
P.O. Box 1450
Alexandria, VA 22313-1450

DECLARATION OF AVI ASHKENAZI, Ph.D UNDER 37 C.F.R. § 1.132

I, Avi Ashkenazi, Ph.D. declare and say as follows: -

1.   I am Director and Staff Scientist at the Molecular Oncology Department of Genentech, Inc., South San Francisco, CA 94080.

2.   I joined Genentech in 1988 as a postdoctoral fellow. Since then, I have investigated a variety of cellular signal transduction mechanisms, including apoptosis, and have developed technologies to modulate such mechanisms as a means of therapeutic intervention in cancer and autoimmune disease. I am currently involved in the investigation of a series of secreted proteins over-expressed in tumors, with the aim to identify useful targets for the development of therapeutic antibodies for cancer treatment.

3.   My scientific Curriculum Vitae, including my list of publications, is attached to and forms part of this Declaration (Exhibit A).

4.   Gene amplification is a process in which chromosomes undergo changes to contain multiple copies of certain genes that normally exist as a single copy, and is an important factor in the pathophysiology of cancer. Amplification of certain genes (e.g., Myc or Her2/Neu)

gives cancer cells a growth or survival advantage relative to normal cells, and might also provide a mechanism of tumor cell resistance to chemotherapy or radiotherapy.

5. If gene amplification results in over-expression of the mRNA and the corresponding gene product, then it identifies that gene product as a promising target for cancer therapy, for example by the therapeutic antibody approach. Even in the absence of over-expression of the gene product, amplification of a cancer marker gene - as detected, for example, by the reverse transcriptase TaqMan® PCR or the fluorescence *in situ* hybridization (FISH) assays -is useful in the diagnosis or classification of cancer, or in predicting or monitoring the efficacy of cancer therapy. An increase in gene copy number can result not only from intrachromosomal changes but also from chromosomal aneuploidy. It is important to understand that detection of gene amplification can be used for cancer diagnosis even if the determination includes measurement of chromosomal aneuploidy. Indeed, as long as a significant difference relative to normal tissue is detected, it is irrelevant if the signal originates from an increase in the number of gene copies per chromosome and/or an abnormal number of chromosomes.

6. I understand that according to the Patent Office, absent data demonstrating that the increased copy number of a gene in certain types of cancer leads to increased expression of its product, gene amplification data are insufficient to provide substantial utility or well established utility for the gene product (the encoded polypeptide), or an antibody specifically binding the encoded polypeptide. However, even when amplification of a cancer marker gene does not result in significant over-expression of the corresponding gene product, this very absence of gene product over-expression still provides significant information for cancer diagnosis and treatment. Thus, if over-expression of the gene product does not parallel gene amplification in certain tumor types but does so in others, then parallel monitoring of gene amplification and gene product over-expression enables more accurate tumor classification and hence better determination of suitable therapy. In addition, absence of over-expression is crucial information for the practicing clinician. If a gene is amplified but the corresponding gene product is not over-expressed, the clinician accordingly will decide not to treat a patient with agents that target that gene product.

7. I hereby declare that all statements made herein of my own knowledge are true and that all statements made on information or belief are believed to be true, and further that these statements were made with the knowledge that willful false statements and the like so

made are punishable by fine or imprisonment, or both, under Section 1001 of Title 18 of the United States Code and that such willful statements may jeopardize the validity of the application or any patent issued thereon.

By: ~Avi Ashkenazi~   Date: 9/15/03
    Avi Ashkenazi, Ph.D.

SV 455281 v1
9/12/03 3:06 PM (39780.7000)

CURRICULUM VITAE
Avi Ashkenazi
July 2003

Personal:

Date of birth:	29 November, 1956
Address:	1456 Tarrytown Street, San Mateo, CA 94402
Phone:	(650) 578-9199 (home); (650) 225-1853 (office)
Fax:	(650) 225-6443 (office)
Email:	aa@gene.com

Education:

1983:	B.S. in Biochemistry, with honors, Hebrew University, Israel
1986:	Ph.D. in Biochemistry, Hebrew University, Israel

Employment:

1983-1986:	Teaching assistant, undergraduate level course in Biochemistry
1985-1986:	Teaching assistant, graduate level course on Signal Transduction
1986 - 1988:	Postdoctoral fellow, Hormone Research Dept., UCSF, and Developmental Biology Dept., Genentech, Inc., with J. Ramachandran
1988 - 1989:	Postdoctoral fellow, Molecular Biology Dept., Genentech, Inc., with D. Capon
1989 - 1993:	Scientist, Molecular Biology Dept., Genentech, Inc.
1994 -1996:	Senior Scientist, Molecular Oncology Dept., Genentech, Inc.
1996-1997:	Senior Scientist and Interim director, Molecular Oncology Dept., Genentech, Inc.
1997-1990:	Senior Scientist and preclinical project team leader, Genentech, Inc.
1999 -2002:	Staff Scientist in Molecular Oncology, Genentech, Inc.
2002-present:	Staff Scientist and Director in Molecular Oncology, Genentech, Inc.

Awards:

1988:	First prize, The Boehringer Ingelheim Award

Editorial:

Editorial Board Member: Current Biology

Associate Editor, Clinical Cancer Research.

Associate Editor, Cancer Biology and Therapy.

Refereed papers:

1.   Gertler, A., Ashkenazi, A., and Madar, Z. Binding sites for human growth hormone and ovine and bovine prolactins in the mammary gland and liver of the lactating cow. *Mol. Cell. Endocrinol.* 34, 51-57 (1984).

2.   Gertler, A., Shamay, A., Cohen, N., Ashkenazi, A., Friesen, H., Levanon, A., Gorecki, M., Aviv, H., Hadari, D., and Vogel, T. Inhibition of lactogenic activities of ovine prolactin and human growth hormone (hGH) by a novel form of a modified recombinant hGH. *Endocrinology* 118, 720-726 (1986).

3.   Ashkenazi, A., Madar, Z., and Gertler, A. Partial purification and characterization of bovine mammary gland prolactin receptor. *Mol. Cell. Endocrinol.* 50, 79-87 (1987).

4.   Ashkenazi, A., Pines, M., and Gertler, A. Down-regulation of lactogenic hormone receptors in Nb2 lymphoma cells by cholera toxin. *Biochemistry Internatl.* 14, 1065-1072 (1987).

5.   Ashkenazi, A., Cohen, R., and Gertler, A. Characterization of lactogen receptors in lactogenic hormone-dependent and independent Nb2 lymphoma cell lines. *FEBS Lett.* 210, 51-55 (1987).

6.   Ashkenazi, A., Vogel, T., Barash, I., Hadari, D., Levanon, A., Gorecki, M., and Gertler, A. Comparative study on in vitro and in vivo modulation of lactogenic and somatotropic receptors by native human growth hormone and its modified recombinant analog. *Endocrinology* 121, 414-419 (1987).

7.   Peralta, E., Winslow, J., Peterson, G., Smith, D., Ashkenazi, A., Ramachandran, J., Schimerlik, M., and Capon, D. Primary structure and biochemical properties of an M2 muscarinic receptor. *Science* 236, 600-605 (1987).

8.   Peralta, E. Ashkenazi, A., Winslow, J., Smith, D., Ramachandran, J., and Capon, D. J. Distinct primary structures, ligand-binding properties and tissue-specific expression of four human muscarinic acetylcholine receptors. *EMBO J.* 6, 3923-3929 (1987).

9.   Ashkenazi, A., Winslow, J., Peralta, E., Peterson, G., Schimerlik, M., Capon, D., and Ramachandran, J. An M2 muscarinic receptor subtype coupled to both adenylyl cyclase and phosphoinositide turnover. *Science* 238, 672-675 (1987).

10. Pines, M., Ashkenazi, A., Cohen-Chapnik, N., Binder, L., and Gertler, A. Inhibition of the proliferation of Nb2 lymphoma cells by femtomolar concentrations of cholera toxin and partial reversal of the effect by 12-o-tetradecanoyl-phorbol-13-acetate. *J. Cell. Biochem.* 37, 119-129 (1988).

11. Peralta, E. Ashkenazi, A., Winslow, J. Ramachandran, J., and Capon, D. Differential regulation of PI hydrolysis and adenylyl cyclase by muscarinic receptor subtypes. *Nature* 334, 434-437 (1988).

12. Ashkenazi., A. Peralta, E., Winslow, J., Ramachandran, J., and Capon, D. Functionally distinct G proteins couple different receptors to PI hydrolysis in the same cell. *Cell* 56, 487-493 (1989).

13. Ashkenazi, A., Ramachandran, J., and Capon, D. Acetylcholine analogue stimulates DNA synthesis in brain-derived cells via specific muscarinic acetylcholine receptor subtypes. *Nature* 340, 146-150 (1989).

14. Lammare, D., Ashkenazi, A., Fleury, S., Smith, D., Sekaly, R., and Capon, D. The MHC-binding and gp120-binding domains of CD4 are distinct and separable. *Science* 245, 743-745 (1989).

15. Ashkenazi., A., Presta, L., Marsters, S., Camerato, T., Rosenthal, K., Fendly, B., and Capon, D. Mapping the CD4 binding site for human immunodefficiency virus type 1 by alanine-scanning mutagenesis. *Proc. Natl. Acad. Sci. USA.* 87, 7150-7154 (1990).

16. Chamow, S., Peers, D., Byrn, R., Mulkerrin, M., Harris, R., Wang, W., Bjorkman, P., Capon, D., and Ashkenazi, A. Enzymatic cleavage of a CD4 immunoadhesin generates crystallizable, biologically active Fd-like fragments. *Biochemistry* 29, 9885-9891 (1990).

17. Ashkenazi, A., Smith, D., Marsters, S., Riddle, L., Gregory, T., Ho, D., and Capon, D. Resistance of primary isolates of human immunodefficiency virus type 1 to soluble CD4 is independent of CD4-rgp120 binding affinity. *Proc. Natl. Acad. Sci. USA.* 88, 7056-7060 (1991).

18. Ashkenazi, A., Marsters, S., Capon, D., Chamow, S., Figari., I., Pennica, D., Goeddel., D., Palladino, M., and Smith, D. Protection against endotoxic shock by a tumor necrosis factor receptor immunoadhesin. *Proc. Natl. Acad. Sci. USA.* 88, 10535-10539 (1991).

19. Moore, J., McKeating, J., Huang, Y., Ashkenazi, A., and Ho, D. Virions of primary HIV-1 isolates resistant to sCD4 neutralization differ in sCD4 affinity and glycoprotein gp120 retention from sCD4-sensitive isolates. *J. Virol.* 66, 235-243 (1992).

20. Jin, H., Oksenberg, D., Ashkenazi, A., Peroutka, S., Duncan, A., Rozmahel., R., Yang, Y., Mengod, G., Palacios, J., and O'Dowd, B. Characterization of the human 5-hydroxytryptamine$_{1B}$ receptor. *J. Biol. Chem.* 267, 5735-5738 (1992).

21. Marsters, A., Frutkin, A., Simpson, N., Fendly, B. and Ashkenazi, A. Identification of cysteine-rich domains of the type 1 tumor necrosis receptor involved in ligand binding. *J. Biol. Chem.* 267, 5747-5750 (1992).

22. Chamow, S., Kogan, T., Peers, D., Hastings, R., Byrn, R., and Ashkenazi, A. Conjugation of sCD4 without loss of biological activity via a novel carbohydrate-directed cross-linking reagent. *J. Biol. Chem.* 267, 15916-15922 (1992).

23. Oksenberg, D., Marsters, A., O'Dowd, B., Jin, H., Havlik, S., Peroutka, S., and Ashkenazi, A. A single amino-acid difference confers major pharmacologic variation between human and rodent 5-HT$_{1B}$ receptors. *Nature* 360, 161-163 (1992).

24. Haak-Frendscho, M., Marsters, S., Chamow, S., Peers, D., Simpson, N., and Ashkenazi, A. Inhibition of interferon γ by an interferon γ receptor immunoadhesin. *Immunology* 79, 594-599 (1993).

25. Penica, D., Lam, V., Weber, R., Kohr, W., Basa, L., Spellman, M., Ashkenazi, Shire, S., and Goeddel, D. Biochemical characterization of the extracellular domain of the 75-kd tumor necrosis factor receptor. *Biochemistry* 32, 3131-3138. (1993).

26. Barfod, L., Zheng, Y., Kuang, W., Hart, M., Evans, T., Cerione, R., and Ashkenazi, A. Cloning and expression of a human CDC42 GTPase Activating Protein reveals a functional SH3-binding domain. *J. Biol. Chem.* 268, 26059-26062 (1993).

27. Chamow, S., Zhang, D., Tan, X., Mhtre, S., Marsters, S., Peers, D., Byrn, R., Ashkenazi, A., and Yunghans, R. A humanized bispecific immunoadhesin-antibody that retargets CD3+ effectors to kill HIV-1-infected cells. *J. Immunol.* 153, 4268-4280 (1994).

28. Means, R., Krantz, S., Luna, J., Marsters, S., and Ashkenazi, A. Inhibition of murine erythroid colony formation in vitro by iterferon γ and correction by interferon γ receptor immunoadhesin. *Blood* 83, 911-915 (1994).

29. Haak-Frendscho, M., Marsters, S., Mordenti, J., Gillet, N., Chen, S., andAshkenazi, A. Inhibition of TNF by a TNF receptor immunoadhesin: comparison with an anti-TNF mAb. *J. Immunol.* 152, 1347-1353 (1994).

30. Chamow, S., Kogan, T., Venuti, M., Gadek, T., Peers, D., Mordenti, J., Shak, S., and Ashkenazi, A. Modification of CD4 immunoadhesin with monomethoxy-PEG aldehyde via reductive alkilation. *Bioconj. Chem.* 5, 133-140 (1994).

31. Jin, H., Yang, R., Marsters, S., Bunting, S., Wurm, F., Chamow, S., and Ashkenazi, A. Protection against rat endotoxic shock by p55 tumor necrosis factor (TNF) receptor immunoadhesin: comparison to anti-TNF monoclonal antibody. *J. Infect. Diseases* 170, 1323-1326 (1994).

32. Beck, J., Marsters, S., Harris, R., Ashkenazi, A., and Chamow, S. Generation of soluble interleukin-1 receptor from an immunoadhesin by specific cleavage. *Mol. Immunol.* 31, 1335-1344 (1994).

33. Pitti, B., Marsters, M., Haak-Frendscho, M., Osaka, G., Mordenti, J., Chamow, S., and Ashkenazi, A. Molecular and biological properties of an interleukin-1 receptor immunoadhesin. *Mol. Immunol.* 31, 1345-1351 (1994).

34. Oksenberg, D., Havlik, S., Peroutka, S., and Ashkenazi, A. The third intracellular loop of the 5-HT2 receptor specifies effector coupling. *J. Neurochem.* 64, 1440-1447 (1995).

35. Bach, E., Szabo, S., Dighe, A., Ashkenazi, A., Aguet, M., Murphy, K., and Schreiber, R. Ligand-induced autoregulation of IFN-γ receptor β chain expression in T helper cell subsets. *Science* 270, 1215-1218 (1995).

36. Jin, H., Yang, R., Marsters, S., Ashkenazi, A., Bunting, S., Marra, M., Scott, R., and Baker, J. Protection against endotoxic shock by bactericidal/permeability-increasing protein in rats. *J. Clin. Invest.* 95, 1947-1952 (1995).

37. Marsters, S., Penica, D., Bach, E., Schreiber, R., and Ashkenazi, A. Interferon γ signals via a high-affinity multisubunit receptor complex that contains two types of polypeptide chain. *Proc. Natl. Acad. Sci. USA.* 92, 5401-5405 (1995).

38. Van Zee, K., Moldawer, L., Oldenburg, H., Thompson, W., Stackpole, S., Montegut, W., Rogy, M., Meschter, C., Gallati, H., Schiller, C., Richter, W., Loetcher, H., Ashkenazi, A., Chamow, S., Wurm, F., Calvano, S., Lowry, S., and Lesslauer, W. Protection against lethal E. coli bacteremia in baboons by pretreatment with a 55-kDa TNF receptor-Ig fusion protein, Ro45-2081. *J. Immunol.* 156, 2221-2230 (1996).

39. Pitti, R., Marsters, S., Ruppert, S., Donahue, C., Moore, A., and Ashkenazi, A. Induction of apoptosis by Apo-2 Ligand, a new member of the tumor necrosis factor cytokine family. *J. Biol. Chem.* 271, 12687-12690 (1996).

40. Marsters, S., Pitti, R., Donahue, C., Rupert, S., Bauer, K., and Ashkenazi, A. Activation of apoptosis by Apo-2 ligand is independent of FADD but blocked by CrmA. *Curr. Biol.* 6, 1669-1676 (1996).

41. Marsters, S., Skubatch, M., Gray, C., and Ashkenazi, A. Herpesvirus entry mediator, a novel member of the tumor necrosis factor receptor family, activates the NF-κB and AP-1 transcription factors. *J. Biol. Chem.* 272, 14029-14032 (1997).

42. Sheridan, J., Marsters, S., Pitti, R., Gurney, A., Skubatch, M., Baldwin, D., Ramakrishnan, L., Gray, C., Baker, K., Wood, W.I., Goddard, A., Godowski, P., and Ashkenazi, A. Control of TRAIL-induced apoptosis by a family of signaling and decoy receptors. *Science* 277, 818-821 (1997).

43. Marsters, S., Sheridan, J., Pitti, R., Gurney, A., Skubatch, M., Balswin, D., Huang, A., Yuan, J., Goddard, A., Godowski, P., and Ashkenazi, A. A novel receptor for Apo2L/TRAIL contains a truncated death domain. *Curr. Biol.* 7, 1003-1006 (1997).

44. Marsters, A., Sheridan, J., Pitti, R., Brush, J., Goddard, A., and Ashkenazi, A. Identification of a ligand for the death-domain-containing receptor Apo3. *Curr. Biol.* 8, 525-528 (1998).

45. Rieger, J., Naumann, U., Glaser, T., Ashkenazi, A., and Weller, M. Apo2 ligand: a novel weapon against malignant glioma? *FEBS Lett.* 427, 124-128 (1998).

46. Pender, S., Fell, J., Chamow, S., Ashkenazi, A., and MacDonald, T. A p55 TNF receptor immunoadhesin prevents T cell mediated intestinal injury by inhibiting matrix metalloproteinase production. *J. Immunol.* 160, 4098-4103 (1998).

47. Pitti, R., Marsters, S., Lawrence, D., Roy, Kischkel, F., M., Dowd, P., Huang, A., Donahue, C., Sherwood, S., Baldwin, D., Godowski, P., Wood, W., Gurney, A., Hillan, K., Cohen, R., Goddard, A., Botstein, D., and Ashkenazi, A. Genomic amplification of a decoy receptor for Fas ligand in lung and colon cancer. *Nature* 396, 699-703 (1998).

48. Mori, S., Marakami-Mori, K., Nakamura, S., Ashkenazi, A., and Bonavida, B. Sensitization of AIDS Kaposi's sarcoma cells to Apo-2 ligand-induced apoptosis by actinomycin D. *J. Immunol.* 162, 5616-5623 (1999).

49. Gurney, A. Marsters, S., Huang, A., Pitti, R., Mark, M., Baldwin, D., Gray, A., Dowd, P., Brush, J., Heldens, S., Schow, P., Goddard, A., Wood, W., Baker, K., Godowski, P., and Ashkenazi, A. Identification of a new member of the tumor necrosis factor family and its receptor, a human ortholog of mouse GITR. *Curr. Biol.* 9, 215-218 (1999).

50. Ashkenazi, A., Pai, R., Fong, s., Leung, S., Lawrence, D., Marsters, S., Blackie, C., Chang, L., McMurtrey, A., Hebert, A., DeForge, L., Khoumenis, I., Lewis, D., Harris, L., Bussiere, J., Koeppen, H., Shahrokh, Z., and Schwall, R. Safety and anti-tumor activity of recombinant soluble Apo2 ligand. *J. Clin. Invest.* 104, 155-162 (1999).

51. Chuntharapai, A., Gibbs, V., Lu, J., Ow, A., Marsters, S., Ashkenazi, A., De Vos, A., Kim, K.J. Determination of residues involved in ligand binding and signal transmissiion in the human IFN-α receptor 2. *J. Immunol.* 163, 766-773 (1999).

52. Johnsen, A.-C., Haux, J., Steinkjer, B., Nonstad, U., Egeberg, K., Sundan, A., Ashkenazi, A., and Espevik, T. Regulation of Apo2L/TRAIL expression in NK cells – involvement in NK cell-mediated cytotoxicity. *Cytokine* 11, 664-672 (1999).

53. Roth, W., Isenmann, S., Naumann, U., Kugler, S., Bahr, M., Dichgans, J., Ashkenazi, A., and Weller, M. Eradication of intracranial human malignant glioma xenografts by Apo2L/TRAIL. *Biochem. Biophys. Res. Commun.* 265, 479-483 (1999).

54. Hymowitz, S.G., Christinger, H.W., Fuh, G., Ultsch, M., O'Connell, M., Kelley, R.F., Ashkenazi, A. and de Vos, A.M. Triggering Cell Death: The Crystal Structure of Apo2L/TRAIL in a Complex with Death Receptor 5. *Molec. Cell* 4, 563–571 (1999).

55. Hymowitz, S.G., O'Connel, M.P., Utsch, M.H., Hurst, A., Totpal, K., Ashkenazi, A., de Vos, A.M., Kelley, R.F. A unique zinc-binding site revealed by a high-resolution X-ray structure of homotrimeric Apo2L/TRAIL. *Biochemistry* 39, 633-640 (2000).

56. Zhou, Q., Fukushima, P., DeGraff, W., Mitchell, J.B., Stetler-Stevenson, M., Ashkenazi, A., and Steeg, P.S. Radiation and the Apo2L/TRAIL apoptotic pathway preferentially inhibit the colonization of premalignant human breast cancer cells overexpressing cyclin D1. *Cancer Res.* 60, 2611-2615 (2000).

57. Kischkel, F.C., Lawrence, D. A., Chuntharapai, A., Schow, P., Kim, J., and Ashkenazi, A. Apo2L/TRAIL-dependent recruitment of endogenous FADD and Caspase-8 to death receptors 4 and 5. *Immunity* 12, 611-620 (2000).

58. Yan, M., Marsters, S.A., Grewal, I.S., Wang, H., *Ashkenazi, A., and *Dixit, V.M. Identification of a receptor for BlyS demonstrates a crucial role in humoral immunity. *Nature Immunol.* 1, 37-41 (2000).

59.   Marsters, S.A., Yan, M., Pitti, R.M., Haas, P.E., Dixit, V.M., and Ashkenazi, A. Interaction of the TNF homologues BLyS and APRIL with the TNF receptor homologues BCMA and TACI. *Curr. Biol.* 10, 785-788 (2000).

60.   Kischkel, F.C., and Ashkenazi, A. Combining enhanced metabolic labeling with immunoblotting to detect interactions of endogenous cellular proteins. *Biotechniques* 29, 506-512 (2000).

61.   Lawrence, D., Shahrokh, Z., Marsters, S., Achilles, K., Shih, D. Mounho, B., Hillan, K., Totpal, K. DeForge, L., Schow, P., Hooley, J., Sherwood, S., Pai, R., Leung, S., Khan, L., Gliniak, B., Bussiere, J., Smith, C., Strom, S., Kelley, S., Fox, J., Thomas, D., and Ashkenazi, A. Differential hepatocyte toxicity of recombinant Apo2L/TRAIL versions. *Nature Med.* 7, 383-385 (2001).

62.   Chuntharapai, A., Dodge, K., Grimmer, K., Schroeder, K., Martsters, S.A., Koeppen, H., Ashkenazi, A., and Kim, K.J. Isotype-dependent inhibition of tumor growth in vivo by monoclonal antibodies to death receptor 4. *J. Immunol.* 166, 4891-4898 (2001).

63.   Pollack, I.F., Erff, M., and Ashkenazi, A. Direct stimulation of apoptotic signaling by soluble Apo2L/tumor necrosis factor-related apoptosis-inducing ligand leads to selective killing of glioma cells. *Clin. Cancer Res.* 7, 1362-1369 (2001).

64.   Wang, H., Marsters, S.A., Baker, T., Chan, B., Lee, W.P., Fu, L., Tumas, D., Yan, M., Dixit, V.M., *Ashkenazi, A., and *Grewal, I.S. TACI-ligand interactions are required for T cell activation and collagen-induced arthritis in mice. *Nature Immunol.* 2, 632-637 (2001).

65.   Kischkel, F.C., Lawrence, D. A., Tinel, A., Virmani, A., Schow, P., Gazdar, A., Blenis, J., Arnott, D., and Ashkenazi, A. Death receptor recruitment of endogenous caspase-10 and apoptosis initiation in the absence of caspase-8. *J. Biol. Chem.* 276, 46639-46646 (2001).

66.   LeBlanc, H., Lawrence, D.A., Varfolomeev, E., Totpal, K., Morlan, J., Schow, P., Fong, S., Schwall, R., Sinicropi, D., and Ashkenazi, A Tumor cell resistance to death receptor induced apoptosis through mutational inactivation of the proapoptotitc Bcl-2 homolog Bax. *Nature Med.* 8, 274-281 (2002).

67.   Miller, K., Meng, G., Liu, J., Hurst, A., Hsei, V., Wong, W-L., Ekert, R., Lawrence, D., Sherwood, S., DeForge, L., Gaudreault., Keller, G., Sliwkowski, M., Ashkenazi, A., and Presta, L. Design, Construction, and analyses of multivalent antibodies. *J. Immunol.* 170, 4854-4861 (2003).

68.   Varfolomeev, E., Kischkel, F., Martin, F., Wanh, H., Lawrence, D., Olsson, C., Tom, L., Erickson, S., French, D., Schow, P., Grewal, I. and Ashkenazi, A. Immune system development in APRIL knockout mice. Submitted.

Review articles:

1.   Ashkenazi, A., Peralta, E., Winslow, J., Ramachandran, J., and Capon, D., J. Functional role of muscarinic acetylcholine receptor subtype diversity. *Cold Spring Harbor Symposium on Quantitative Biology.* LIII, 263-272 (1988).

2.   Ashkenazi, A., Peralta, E., Winslow, J., Ramachandran, J., and Capon, D. Functional diversity of muscarinic receptor subtypes in cellular signal transduction and growth. *Trends Pharmacol. Sci.* Dec Supplement, 12-21 (1989).

3.   Chamow, S., Duliege, A., Ammann, A., Kahn, J., Allen, D., Eichberg, J., Byrn, R., Capon, D., Ward, R., and Ashkenazi, A. CD4 immunoadhesins in anti-HIV therapy: new developments. *Int. J. Cancer* Supplement 7, 69-72 (1992).

4.   Ashkenazi, A., Capon, and D. Ward, R. Immunoadhesins. *Int. Rev. Immunol.* 10, 217-225 (1993).

5.   Ashkenazi, A., and Peralta, E. Muscarinic Receptors. In *Handbook of Receptors and Channels.* (S. Peroutka, ed.), CRC Press, Boca Raton, Vol. I, p. 1-27, (1994).

6.   Krantz, S. B., Means, R. T., Jr., Lina, J., Marsters, S. A., and Ashkenazi, A. Inhibition of erythroid colony formation in vitro by gamma interferon. In *Molecular Biology of Hematopoiesis* (N. Abraham, R. Shadduck, A. Levine F. Takaku, eds.) Intercept Ltd. Paris, Vol. 3, p. 135-147 (1994).

7.   Ashkenazi, A. Cytokine neutralization as a potential therapeutic approach for SIRS and shock. *J. Biotechnology in Healthcare* 1, 197-206 (1994).

8.   Ashkenazi, A., and Chamow, S. M. Immunoadhesins: an alternative to human monoclonal antibodies. *Immunomethods: A companion to Methods in Enzimology* 8, 104-115 (1995).

9.   Chamow, S., and Ashkenazi, A. Immunoadhesins: Principles and Applications. *Trends Biotech.* 14, 52-60 (1996).

10.   Ashkenazi, A., and Chamow, S. M. Immunoadhesins as research tools and therapeutic agents. *Curr. Opin. Immunol.* 9, 195-200 (1997).

11.   Ashkenazi, A., and Dixit, V. Death receptors: signaling and modulation. *Science* 281, 1305-1308 (1998).

12.   Ashkenazi, A., and Dixit, V. Apoptosis control by death and decoy receptors. *Curr. Opin. Cell. Biol.* 11, 255-260 (1999).

9

13. <u>Ashkenazi, A.</u> Chapters on Apo2L/TRAIL; DR4, DR5, DcR1, DcR2; and DcR3. Online Cytokine Handbook (<u>www.apnet.com/cytokinereference/</u>).

14. <u>Ashkenazi, A.</u> Targeting death and decoy receptors of the tumor necrosis factor superfamily. *Nature Rev. Cancer* 2, 420-430 (2002).

15. LeBlanc, H. and <u>Ashkenazi, A.</u> Apoptosis signaling by Apo2L/TRAIL. *Cell Death and Differentiation* 10, 66-75 (2003).

16. Almasan, A. and <u>Ashkenazi, A.</u> Apo2L/TRAIL: apoptosis signaling, biology, and potential for cancer therapy. Cytokine and Growth Factor Reviews 14, 337-348 (2003).

Book:

Antibody Fusion Proteins (Chamow, S., and <u>Ashkenazi, A.</u>, eds., John Wiley and Sons Inc.) (1999).

Talks:

1. Resistance of primary HIV isolates to CD4 is independent of CD4-gp120 binding affinity. UCSD Symposium, HIV Disease: Pathogenesis and Therapy. Greenelefe, FL, March 1991.

2. Use of immuno-hybrids to extend the half-life of receptors. IBC conference on Biopharmaceutical Halflife Extension. New Orleans, LA, June 1992.

3. Results with TNF receptor Immunoadhesins for the Treatment of Sepsis. IBC conference on Endotoxemia and Sepsis. Philadelphia, PA, June 1992.

4. Immunoadhesins: an alternative to human antibodies. IBC conference on Antibody Engineering. San Diego, CA, December 1993.

5. Tumor necrosis factor receptor: a potential therapeutic for human septic shock. American Society for Microbiology Meeting, Atlanta, GA, May 1993.

6. Protective efficiacy of TNF receptor immunoadhesin vs anti-TNF monoclonal antibody in a rat model for endotoxic shock. 5th International Congress on TNF. Asilomar, CA, May 1994.

7. Interferon-γ signals via a multisubunit receptor complex that contains two types of polypeptide chain. American Association of Immunologists Conference. San Franciso, CA, July 1995.

8. Immunoadhesins: Principles and Applications. Gordon Research Conference on Drug Delivery in Biology and Medicine. Ventura, CA, February 1996.

9. Apo-2 Ligand, a new member of the TNF family that induces apoptosis in tumor cells. Cambridge Symposium on TNF and Related Cytokines in Treatment of Cancer. Hilton-Head, NC, March 1996.

10. Induction of apoptosis by Apo2 Ligand. American Society for Biochemistry and Molecular Biology, Symposium on Growth Factors and Cytokine Receptors. New Orleans, LA, June, 1996.

11. Apo2 ligand, an extracellular trigger of apoptosis. 2nd Clontech Symposium, Palo Alto, CA, October 1996.

12. Regulation of apoptosis by members of the TNF ligand and receptor families. Stanford University School of Medicine, Palo Alto, CA, December 1996.

13. Apo-3: a novel receptor that regulates cell death and inflammation. 4th International Congress on Immune Consequences of Trauma, Shock, and Sepsis. Munich, Germany, March 1997.

14. New members of the TNF ligand and receptor families that regulate apoptosis, inflammation, and immunity. UCLA School of Medicine, LA, CA, March 1997.

15. Immunoadhesins: an alternative to monoclonal antibodies. 5th World Conference on Bispecific Antibodies. Volendam, Holland, June 1997.

16. Control of Apo2L signaling. Cold Spring Harbor Laboratory Symposium on Programmed Cell Death. Cold Spring Harbor, New York. September, 1997.

17. Chairman and speaker, Apoptosis Signaling session. IBC's 4th Annual Conference on Apoptosis. San Diego, CA., October 1997.

18. Control of Apo2L signaling by death and decoy receptors. American Association for the Advancement of Science. Philladelphia, PA, February 1998.

19. Apo2 ligand and its receptors. American Society of Immunologists. San Francisco, CA, April 1998.

20. Death receptors and ligands. 7th International TNF Congress. Cape Cod, MA, May 1998.

21. Apo2L as a potential therapeutic for cancer. UCLA School of Medicine. LA, CA, June 1998.

22. Apo2L as a potential therapeutic for cancer. Gordon Research Conference on Cancer Chemotherapy. New London, NH, July 1998.

23. Control of apoptosis by Apo2L. Endocrine Society Conference, Stevenson, WA, August 1998.

24. Control of apoptosis by Apo2L. International Cytokine Society Conference, Jerusalem, Israel, October 1998.

25. Apoptosis control by death and decoy receptors. American Association for Cancer Research Conference, Whistler, BC, Canada, March 1999.

26. Apoptosis control by death and decoy receptors. American Society for Biochemistry and Molecular Biology Conference, San Francisco, CA, May 1999.

27. Apoptosis control by death and decoy receptors. Gordon Research Conference on Apoptosis, New London, NH, June 1999.

28. Apoptosis control by death and decoy receptors. Arthritis Foundation Research Conference, Alexandria GA, Aug 1999.

29. Safety and anti-tumor activity of recombinant soluble Apo2L/TRAIL. Cold Spring Harbor Laboratory Symposium on Programmed Cell Death. . Cold Spring Harbor, NY, September 1999.

30. The Apo2L/TRAIL system: therapeutic potential. American Association for Cancer Research, Lake Tahoe, NV, Feb 2000.

31. Apoptosis and cancer therapy. Stanford University School of Medicine, Stanford, CA, Mar 2000.

32. Apoptosis and cancer therapy. University of Pennsylvania School of Medicine, Philladelphia, PA, Apr 2000.

33. Apoptosis signaling by Apo2L/TRAIL. International Congress on TNF. Trondheim, Norway, May 2000.

34. The Apo2L/TRAIL system: therapeutic potential. Cap-CURE summit meeting. Santa Monica, CA, June 2000.

35. The Apo2L/TRAIL system: therapeutic potential. MD Anderson Cancer Center. Houston, TX, June 2000.

36. Apoptosis signaling by Apo2L/TRAIL. The Protein Society, 14th Symposium. San Diego, CA, August 2000.

37. Anti-tumor activity of Apo2L/TRAIL. AAPS annual meeting. Indianapolis, IN Aug 2000.

38. Apoptosis signaling and anti-cancer potential of Apo2L/TRAIL. Cancer Research Institute, UC San Francisco, CA, September 2000.

39. Apoptosis signaling by Apo2L/TRAIL. Kenote address, TNF family Minisymposium, NIH. Bethesda, MD, September 2000.

40. Death receptors: signaling and modulation. Keystone symposium on the Molecular basis of cancer. Taos, NM, Jan 2001.

41. Preclinical studies of Apo2L/TRAIL in cancer. Symposium on Targeted therapies in the treatment of lung cancer. Aspen, CO, Jan 2001.

42. Apoptosis signaling by Apo2L/TRAIL. Wiezmann Institute of Science, Rehovot, Israel, March 2001.

43. Apo2L/TRAIL: Apoptosis signaling and potential for cancer therapy. Weizmann Institute of Science, Rehovot, Israel, March 2001.

44. Targeting death receptors in cancer with Apo2L/TRAIL. Cell Death and Disease conference, North Falmouth, MA, Jun 2001.

45. Targeting death receptors in cancer with Apo2L/TRAIL. Biotechnology Organization conference, San Diego, CA, Jun 2001.

46. Apo2L/TRAIL signaling and apoptosis resistance mechanisms. Gordon Research Conference on Apoptosis, Oxford, UK, July 2001.

47. Apo2L/TRAIL signaling and apoptosis resistance mechanisms. Cleveland Clinic Foundation, Cleveland, OH, Oct 2001.

48. Apoptosis signaling by death receptors: overview. International Society for Interferon and Cytokine Research conference, Cleveland, OH, Oct 2001.

49. Apoptosis signaling by death receptors. American Society of Nephrology Conference. San Francisco, CA, Oct 2001.

50. Targeting death receptors in cancer. Apoptosis: commercial opportunities. San Diego, CA, Apr 2002.

51. Apo2L/TRAIL signaling and apoptosis resistance mechanisms. Kimmel Cancer Research Center, Johns Hopkins University, Baltimore MD. May 2002.

52. Apoptosis control by Apo2L/TRAIL. (Keynote Address) University of Alabama Cancer Center Retreat, Birmingham, Ab. October 2002.

53. Apoptosis signaling by Apo2L/TRAIL. (Session co-chair) TNF international conference. San Diego, CA. October 2002.

54. Apoptosis signaling by Apo2L/TRAIL. Swiss Institute for Cancer Research (ISREC). Lausanne, Swizerland. Jan 2003.

55. Apoptosis induction with Apo2L/TRAIL. Conference on New Targets and Innovative Strategies in Cancer Treatment. Monte Carlo. February 2003.

56. Apoptosis signaling by Apo2L/TRAIL. Hermelin Brain Tumor Center Symposium on Apoptosis. Detroit, MI. April 2003.

57. Targeting apoptosis through death receptors. Sixth Annual Conference on Targeted Therapies in the Treatment of Breast Cancer. Kona, Hawaii. July 2003.

58. Targeting apoptosis through death receptors. Second International Conference on Targeted Cancer Therapy. Washington, DC. Aug 2003.

Issued Patents:

1. Ashkenazi, A., Chamow, S. and Kogan, T. Carbohydrate-directed crosslinking reagents. US patent 5,329,028 (Jul 12, 1994).

2. Ashkenazi, A., Chamow, S. and Kogan, T. Carbohydrate-directed crosslinking reagents. US patent 5,605,791 (Feb 25, 1997).

3. Ashkenazi, A., Chamow, S. and Kogan, T. Carbohydrate-directed crosslinking reagents. US patent 5,889,155 (Jul 27, 1999).

4. Ashkenazi, A., APO-2 Ligand. US patent 6,030,945 (Feb 29, 2000).

5. Ashkenazi, A., Chuntharapai, A., Kim, J., APO-2 ligand antibodies. US patent 6,046,048 (Apr 4, 2000).

6. Ashkenazi, A., Chamow, S. and Kogan, T. Carbohydrate-directed crosslinking reagents. US patent 6,124,435 (Sep 26, 2000).

7. Ashkenazi, A., Chuntharapai, A., Kim, J., Method for making monoclonal and cross-reactive antibodies. US patent 6,252,050 (Jun 26, 2001).

8. Ashkenazi, A. APO-2 Receptor. US patent 6,342,369 (Jan 29, 2002).

9. Ashkenazi, A. Fong, S., Goddard, A., Gurney, A., Napier, M., Tumas, D., Wood, W. A-33 polypeptides. US patent 6,410,708 (Jun 25, 2002).

10. Ashkenazi, A. APO-3 Receptor. US patent 6,462,176 B1 (Oct 8, 2002).

11. Ashkenazi, A. APO-2LI and APO-3 polypeptide antibodies. US patent 6,469,144 B1 (Oct 22, 2002).

12. Ashkenazi, A., Chamow, S. and Kogan, T. Carbohydrate-directed crosslinking reagents. US patent 6,582,928B1 (Jun 24, 2003).

Variable expression of the translocated c-*abl* oncogene in Philadelphia-chromosome-positive B-lymphoid cell lines from chronic myelogenous leukemia patients

James B. Konopka[*‡], Steven Clark[*], Jami McLaughlin[*], Masakuzu Nitta[†], Yoshiro Kato[†], Annabel Strife[†], Bayard Clarkson[†], and Owen N. Witte[*§]

*Department of Microbiology and Molecular Biology Institute, University of California, Los Angeles, 405 Hilgard Avenue, Los Angeles, CA 90024; and †The Laboratory of Hematopoietic Cell Kinetics and The Laboratory of Cancer Genetics and Cytogenetics, Memorial Sloan-Kettering Cancer Center, 1275 York Avenue, New York, NY 10021

ABSTRACT   The consistent cytogenetic translocation of chronic myelogenous leukemia (the Philadelphia chromosome, Ph[1]) has been observed in cells of multiple hematopoietic lineages. This translocation creates a chimeric gene composed of breakpoint-cluster-region (*bcr*) sequences from chromosome 22 fused to a portion of the *abl* oncogene on chromosome 9. The resulting gene product (P210^c-abl) resembles the transforming protein of the Abelson murine leukemia virus in its structure and tyrosine kinase activity. P210^c-abl is expressed in Ph[1]-positive cell lines of myeloid lineage and in clinical specimens with myeloid predominance. We show here that Epstein–Barr virus-transformed B-lymphocyte lines that retain Ph[1] can express P210^c-abl. The level of expression in these B-cell lines is generally lower and more variable than that observed for myeloid lines. Protein expression is not related to amplification of the *abl* gene but to variation in the level of *bcr-abl* mRNA produced from a single Ph[1] template.

Chronic myelogenous leukemia (CML) is a disease of the pluripotent stem cell (1). In greater than 95% of patients, the leukemic cells contain the cytogenetic marker known as the Philadelphia chromosome, or Ph[1] (2). This reciprocal translocation event between the long arms of chromosomes 9 and 22 has been used as a disease-specific marker for diagnosis and evaluation of therapy. Multiple hematopoietic lineages, including myeloid and B-lymphoid, contain Ph[1] in early or chronic phase, as well as in the more acute accelerated and blast crisis phases of the disease.

One molecular consequence of Ph[1] is the translocation of the chromosomal arm containing the c-*abl* gene on chromosome 9 into the middle of the breakpoint-cluster region (*bcr*) gene on chromosome 22 (3–6). Although the precise translocation breakpoints are variable, an RNA-splicing mechanism generates a very similar 8-kilobase (kb) mRNA in each case (5–9). The hybrid *bcr-abl* message encodes a structurally altered form of the *abl* oncogene product, called P210^c-abl (10–13), with an amino-terminal segment derived from a portion of the exons of *bcr* on chromosome 22 and a carboxyl-terminal segment derived from a major portion of the exons of the c-*abl* gene on chromosome 9. The chimeric structure of *bcr-abl* and the resulting P210^c-abl is similar to the structure of the Abelson murine leukemia virus *gag-abl* genome and resulting P160^v-abl transforming gene product. Both proteins have very similar tyrosine kinase activities (10, 11, 14) which can be distinguished by their relative stability to denaturing detergents and by their ATP requirements from the recently described tyrosine kinase activity of the c-*abl* gene product (15).

In concert with structural modification of the amino-terminal portion of the *abl* gene, increased level of expression has been implicated in activation of c-*abl* oncogenic potential. Myeloid and erythroid cell lines and clinical samples derived from acute-phase CML patients contain about 10-fold higher levels of the 8-kb *bcr-abl* mRNA and P210^c-abl than the c-*abl* mRNA forms (6 and 7 kb) and P145^c-abl gene product (5, 8, 9, 11). The higher level of expression of the chimeric *bcr-abl* message in acute-phase cells is not likely to be solely due to the presence of the *bcr* promoter sequences at the 5' end of the gene, since the normal 4.5-kb and 6.7-kb *bcr*-encoded mRNA species are expressed at an even lower level than the normal c-*abl* messages (5, 6).

We have analyzed a series of Epstein–Barr virus-immortalized B-lymphoid cell lines derived from CML patients (16). With such *in vitro* clonal cell lines, we can evaluate whether the presence of Ph[1] always results in synthesis of the chimeric *bcr-abl* message and protein, and whether the quantitative expression varies for cells of B-lymphoid lineage as compared to previously examined myeloid cell lines. Our results show that cell lines that retain Ph[1] do express *bcr-abl* message and protein, but that the level is generally lower and more variable than previously seen for myeloid cell lines. The demonstration that the Ph[1] chromosomal template can vary in its level of expression of P210^c-abl suggests that secondary mechanisms, beyond the translocation itself, contribute to the regulation of the *bcr-abl* gene in different cell types or subclones that derive from the affected stem cell.

MATERIALS AND METHODS

Cells and Cell Labelings. Epstein–Barr virus-transformed B-lymphoid cell lines were established from peripheral blood samples of chronic- and acute-phase CML patients as reported (16). The cell lines are designated according to patient number, karyotype, and lineage. For example, SK-CML7Bt(9,22)-33 refers to CML patient 7, B-lymphoid cell line, 9;22 translocation (Ph[1]), cell line 33; and SK-CML7BN-2 refers to B-cell line 2 with a normal karyotype derived from the same patient. Repeat karyotype analysis was performed to verify the retention of Ph[1] just prior to analysis for *abl* protein and RNA. Cells were maintained in RPMI 1640 medium with 20% fetal bovine serum. We have not observed any consistent pattern of *in vitro* growth rate that correlates to the stage of disease at the time of transformation with Epstein–Barr virus. Cells (1.5 × 10^7) were washed twice with Dulbecco's modified Eagle's medium lacking phosphate and

---

supplemented with 5% dialyzed fetal bovine serum. Cells were then resuspended in 2 ml of the minimal medium. Labeling was started with the addition of [^{32}P]orthophosphate (1 mCi/ml; ICN; 1 Ci = 37 GBq) and continued at 37°C for 3–4 hr.

Immunoprecipitation and Immunoblotting. Immunoprecipitations were carried out as described (10). Cells (1.5 × 10^7) were washed with phosphate-buffered saline and extracted with 3–5 ml of phosphate lysis buffer (1% Triton X-100/0.1 NaDodSO$_4$/0.5% deoxycholate/10 mM Na$_2$HPO$_4$, pH 7.5/ 100 mM NaCl) with 5 mM EDTA and 5 mM phenylmethylsulfonyl fluoride. Extracts were clarified by centrifugation and precipitated with normal or rabbit anti-abl sera (anti-pEX-2 or anti-pEX-5) (17). The precipitated proteins were electrophoresed in a NaDodSO$_4$/8% polyacrylamide gel. ^{32}P-labeled proteins were detected by autoradiography. Alternatively, *abl* proteins were detected by immunoblotting. Extracts from unlabeled cells were clarified, and proteins were concentrated by immunoprecipitation with rabbit antisera against *abl*-encoded proteins [anti-pEX-2 and anti-pEX-5 combined (17)] and then fractionated in 8% acrylamide gels. The proteins were transferred from the gel to nitrocellulose filters, using protease-facilitated transfer (18). The *abl*-encoded proteins were detected using murine monoclonal antibodies as a probe and peroxidase-conjugated goat anti-mouse second stage antibody (Bio-Rad) for development. Rabbit antisera and mouse monoclonal antibodies to *abl* proteins were prepared using bacterially expressed regions of the v-*abl* protein as immunogens (17, 19). Anti-pEX-2 antibodies react with the internal tyrosine kinase domain and anti-pEX-5 antibodies react with the carboxyl-terminal segment of the *abl* proteins.

RNA Analysis. RNA was extracted from 10^8 cells by the NaDodSO$_4$/urea/phenol method (20). Polyadenylylated RNA was purified by oligo(dT) affinity chromatography. Samples were electrophoresed in a 1% agarose/formaldehyde gel and transferred to nitrocellulose. *abl* RNA species were detected by hybridization with a nick-translated v-*abl* fragment probe (21).

DNA Analysis. DNA was prepared from 5 × 10^7 cells of each cell line and processed for Southern blots with a v-*abl* probe as described (21).

RESULTS

Variable Levels of P210^{c-abl} Are Detected in Ph^1-Positive Cell Lines. Ph^1-positive and Ph^1-negative, Epstein–Barr virus-transformed B-lymphocyte cell lines derived from the same patient were examined for P210^{c-abl} synthesis by immunoprecipitation of [^{32}P]orthophosphate-labeled cell extracts with anti-abl sera (Fig. 1). The normal c-*abl* protein P145^{c-abl} was detected at a similar level in multiple Ph^1-positive and Ph^1-negative cell lines. P210^{c-abl} was only detected in the Ph^1-positive cell lines because the *bcr-abl* chimeric gene which encodes P210^{c-abl} resides on the Ph^1 (4, 5, 11, 13). The level of P210^{c-abl} was about 4- to 5-fold higher than the level of P145^{c-abl} in the SK-CML7Bt-33 cell line (Fig. 1A, +). The Ph^1-positive erythroid-progenitor cell line K562 (C) showed a level of P210^{c-abl} about 10-fold higher than P145^{c-abl}. However, the level of P210^{c-abl} was about one-fifth that of P145^{c-abl} in the Ph^1-positive SK-CML16Bt-1 cell line (Fig. 1B, +). Comparison of different autoradiographic exposures roughly indicated that the level of P210^{c-abl} varies over a 20-fold range between these Ph^1-positive B-cell lines. Analysis of four additional Ph^1-positive B-cell lines demonstrated that the level of P210^{c-abl} fell into two general classes; some cell lines had a level of P210^{c-abl} similar to SK-CML7Bt-33 and others had the low level similar to SK-CML16Bt-1 (Table 1). This differs from previous studies with Ph^1-positive myeloid cell lines and patient samples derived from acute-
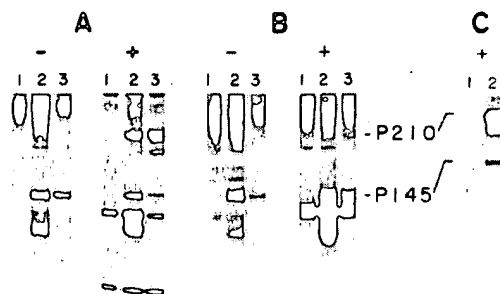

FIG. 1. Detection of variable levels of P210^{c-abl} in Ph^1-positive B-cell lines. Production of P145^{c-abl} and P210^{c-abl} in Epstein–Barr virus-transformed B-cell lines derived from a blast-crisis (A) and a chronic-phase (B) CML patient was examined by metabolic labeling with [^{32}P]orthophosphate and immunoprecipitation. Ph^1-negative (−) and Ph^1-positive (+) cell lines derived from each patient were analyzed. The Ph^1-negative cell line in A, − is SK-CML7BN-2 and in B, − is SK-CML16BN-1. The Ph^1-positive cell line in A, + is SK-CML7Bt-33 and in B, + is SK-CML16Bt-1. The K562 cell line, a Ph^1-positive erythroid progenitor cell line spontaneously derived from a blast-crisis patient (33), is represented in C. Cells (1.5 × 10^7) were metabolically labeled with 2 mCi of [^{32}P]orthophosphate for 3–4 hr and then were extracted and clarified by centrifugation. Samples were immunoprecipitated with control normal serum (lanes 1), anti-pEX-2 (lanes 2), or anti-pEX-5 (lanes 3) and analyzed by NaDodSO$_4$/8% PAGE followed by autoradiography with an intensifying screen (3 days for A and C, 10 days for B).

phase CML patients, in which P210^{c-abl} was detected at a 10-fold higher level than P145^{c-abl} (refs. 10 and 11; Table 1). There was no large difference in level of chimeric mRNA and P210^{c-abl} expressed in four myeloid/erythroid-lineage Ph^1-positive cell lines (K562, EM2, EM3, CML22, and BV173; refs. 9 and 11), despite a 4- to 5-fold amplification of *abl*-related sequences in the K562 cell line.

Detection of different levels of P210^{c-abl} in Fig. 1 could be due to decreased phosphorylation of P210^{c-abl}, a lower level of P210^{c-abl} synthesis, or altered stability of the protein. To help distinguish among these possibilities, the steady-state level of P210^{c-abl} in the cell lines was assayed by immunoblotting. The results show that SK-CML7Bt-33 (Fig. 2A, +) had a higher level of P210^{c-abl} than P145, similar to the results with metabolic labeling (Fig. 1). We did not detect P210^{c-abl} by immunoblotting with 2 × 10^7 cells of line SK-CML8Bt-3 (Fig. 2B, +). Reconstruction experiments using dilutions of cell extracts showed that we could detect about 5–10% the level of P210^{c-abl} expressed in the K562 cell line (data not shown). We infer that the steady-state level of P210^{c-abl} in SK-CML8Bt-3 is lower than the level in SK-CML7Bt-33 by a factor of at least 10. The level of P210^{c-abl} detected in these assays correlated with the amount of P210^{c-abl} tyrosine kinase activity that could be detected *in vitro* (data not shown).

Different Levels of P210^{c-abl} Are Reflected in the Amount of Stable *bcr-abl* mRNA. To identify the basis for detection of variable levels of P210^{c-abl}, we examined the production of the *abl* RNA. RNA blot hybridization analysis using a v-*abl* probe (Fig. 3) showed that the normal 6- and 7-kb c-*abl* mRNAs were present at a similar level in Ph^1-positive and -negative cell lines derived from different patients. However, the 8-kb mRNA that encodes P210^{c-abl} was detected at a 10-fold higher level in SK-CML7Bt-33 (Fig. 3A, +) than in SK-CML16Bt-1 (B, +), which correlated with the relative level of P210^{c-abl} detected in each cell line. Analysis of additional cell lines demonstrated that the level of 8-kb RNA directly correlated with the level of P210^{c-abl} (Table 1). The variation in level of 8-kb RNA detected in these cell lines was not due to loss or gain of Ph^1, because cytogenetic analysis confirmed the presence of Ph^1 in these cell lines (ref. 16 and

Medical Sciences: Konopka *et al.*

Proc. Natl. Acad. Sci. USA 83 (1986) 4051

Table 1. Relative levels of *bcr-abl* expression in Epstein–Barr virus-immortalized B-cell lines and myeloid CML lines

Cell line*	CML phase[†]	Ph[1][‡]	P210[§]	8-kb mRNA[¶]
SK-CML7BN-2	BC	−	−	−
SK-CML8BN-10	Chronic	−	−	−
SK-CML8BN-12	Chronic	−	−	−
SK-CML16BN-1	Chronic	−	−	−
SK-CML35BN-1	Chronic	−	−	−
SK-CML7B5-33	BC	+	+++	+++
SK-CML21Bt-1	Acc	+	+++	+++
SK-CML21Bt-6	Acc	+	+++	+++
SK-CML8Bt-3	Chronic	+	+	±
SK-CML16Bt-1	Chronic	+	+	+
SK-CML35Bt-2	Chronic	+	+	+
K562	BC	+	+++++	++++
BV173	BC	+	+++++	++++
EM2	BC	+	+++++	++++

*Cell lines derived from CML patients by transformation with Epstein–Barr virus as described (16). Names of cell lines indicate patient number and Ph[1] status: SK-CML7Bt indicates a cell line derived from patient 7 that carries the 9;22 Ph[1] translocation; N indicates a normal karyotype. Myeloid-erythroid cell lines (K562, EM2, and BV173) are described in previous publications (9, 11, 22, 33).

[†]Status of patient at the time cell line was derived. BC, blast crisis; Acc, accelerated phase.

[‡]Presence (+) or absence (−) of Ph[1] as demonstrated by karyotypic or Southern blot analysis.

[§]P210[c-abl] detected as described in legend to Fig. 1. B-cell lines derived from blast-crisis and accelerated-phase patients had levels of P210 3- to 5-fold higher (+++) than levels of P145. Chronic-phase-derived cell lines had P210 levels lower than or just equivalent (+) to the level of P145. Myeloid and erythroid lines had levels of P210 5- to 10-fold higher than P145 (+++++).

[¶]Eight-kilobase *bcr-abl* mRNA detected as described in legend to Fig. 2. Symbols: ±, borderline detectable; +++++, level of 8-kb mRNA 5- to 10-fold higher than that of the 6- and 7-kb c-*abl* mRNA species; +++, level of 8-kb mRNA 3- to 5-fold higher than that of the 6- and 7-kb species; +, a level approximately equivalent to that of the 6- and 7-kb messages.

data not shown). There was no difference in the copy number of *abl*-related sequences as judged by Southern blot analysis (Fig. 4). Only the K562 cell line control showed an amplification of *abl* sequences, as previously reported (22, 23). These combined data suggest that differential *bcr-abl* mRNA expression from a single gene template is responsible for the variable levels of P210[c-abl] detected. This could be mediated

FIG. 3. Comparison of *abl* RNA levels in Ph[1]-positive and -negative B-cell lines. The levels of the normal 6- and 7-kb c-*abl* RNAs and the 8-kb *bcr-abl* RNA were analyzed by blot hybridization using a v-*abl* probe. RNA was extracted from Ph[1]-negative lines SK-CML7BN-2 (*A*,−) and SK-CML16BN-1 (*B*,−), from Ph[1]-positive lines SK-CML6Bt-33 (*A*,+) and SK-CML16Bt-3 (*B*,+), and from line K562 (*C*,+) by the NaDodSO[4]/urea/phenol method (20). Polyadenylylated RNA was purified by oligo(dT) affinity chromatography, and 15 μg of each sample was electrophoresed in a 1% agarose/formaldehyde gel and then transferred to nitrocellulose. The blotted RNAs were hybridized with a nick-translated v-*abl* fragment probe (21) and then autoradiographed for 4 days.

by factors influencing the transcription rate of the *bcr-abl* gene or the stability of the mRNA.

DISCUSSION

Several lines of evidence suggest that formation of Ph[1] is not the primary event that affects the stem cell in CML. Patients have been identified that present with the clinical picture of CML but only later develop Ph[1] (1). This observation, coupled with studies of *G6PD* (glucose-6-phosphate dehydrogenase)-heterozygous females with CML that demonstrate stem-cell clonality by isozyme analysis among cell
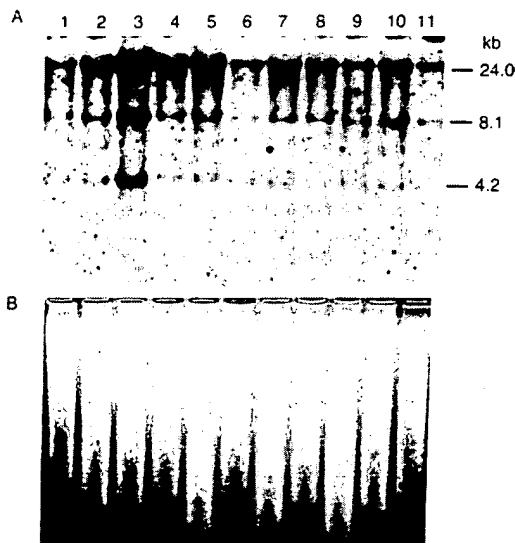

FIG. 4. Southern blot analysis of *abl* sequences in Ph[1]-positive and -negative B-cell lines. High molecular weight DNA (15 μg) was digested with restriction endonuclease *Bam*HI, separated in a 0.8% agarose gel, and then transferred to nitrocellulose. The blotted DNA fragments were hybridized with a nick-translated, 2.4-kb *Bgl* II v-*abl* fragment (1.5 × 10⁸ cpm/μg; ref. 21) and exposed for 4 days. (*A*) Autoradiogram of *abl*-specific fragments in cell lines HL-60 (lane 1), EM2 (lane 2), K562 (lane 3), SK-CML7Bt-33 (lane 4), SK-CML8Bt-3 (lane 5), SK-CML16Bt-1 (lane 6), SK-CML21Bt-6 (lane 7), SK-CML35Bt-2 (lane 8), SK-CML7BN-2 (lane 9), SK-CML8BN-2 (lane 10), and SK-CML35BN-1 (lane 11). (*B*) Ethidium bromide staining of agarose gel prior to transfer to nitrocellulose, showing the level of variation in amount of DNA loaded per lane.

FIG. 2. Analysis of steady-state *abl* protein levels by immunoblotting. Cell extracts prepared from 2 × 10⁷ cells of lines SK-CML7BN-2 (*A*,−), SK-CML7Bt-33 (*A*,+), SK-CML8BN-10 (*B*,−), and SK-CML8Bt-3 (*B*,+) were concentrated by immunoprecipitation with anti-pEX-2 plus anti-pEX-5. Samples were then electrophoresed in a NaDodSO[4]/8% polyacrylamide gel and transferred to nitrocellulose, using protease-facilitated transfer (18). *abl* proteins were detected using a mixture of two monoclonal antibodies directed against the pEX-2 and pEX-5 *abl*-protein fragments produced in bacteria (19) as a probe and a peroxidase-conjugated goat anti-mouse second-stage antibody (Bio-Rad) for development.

populations that lack the Ph[1] marker, supports a secondary or complementary role for Ph[1] in the progression of the disease (24, 25). This chromosome marker is found in chronic, accelerated, and blast-crisis phases of the disease. It is likely that Ph[1] confers some growth advantage, since cells with the marker chromosome eventually predominate the marrow and peripheral blood even in chronic phase. During the phase of blast crisis, many patients develop additional chromosome abnormalities, including duplication of Ph[1], a variety of trisomies, and complex translocations (26). This is suggestive evidence for Ph[1] being a necessary but not sufficient genetic change for the full evolution of the disease.

The realization that one molecular result of Ph[1] is the generation of a chimeric *bcr-abl* protein with functional characteristics and structure analogous to the *gag-abl* transforming protein of the Abelson murine leukemia virus strengthens the argument for an important role of Ph[1] in the pathogenesis of CML. Although the Abelson virus is generally considered a rapidly transforming retrovirus, its effects can range from overcoming growth factor requirements, to cellular lethality, to induction of highly oncogenic tumors in a number of hematopoietic cell lineages (27, 28). Even in the transformation of murine cell targets, there are several lines of evidence that suggest that the growth-promoting activity of the v-*abl* gene product is complemented by further cellular changes in the production of the malignant-cell phenotype (29–31).

The regulation of *bcr-abl* gene expression is complex because the 5' end of the gene is derived from the non-*abl* sequences, *bcr*, normally found on chromosome 22 (6). The level of stable message for the normal *bcr* gene and the normal *abl* gene are both much lower than the level of the *bcr-abl* message and protein from cell lines and clinical specimens derived from myeloid blast-crisis patients (5, 6, 11). Therefore, the high level of *bcr-abl* expression cannot simply be attributed to the regulatory sequences associated with *bcr*. Possibly, creation of the chimeric gene disrupts the normal regulatory sequences and results in a higher level of expression. Variation in *bcr-abl* expression may result from secondary changes in the structure of the chimeric gene or function of *trans*-acting factors that occur during evolution of the disease. Our analysis of P210^{c-abl} and the 8-kb mRNA in Epstein–Barr virus-transformed Ph[1]-positive B-cell lines demonstrates that stable message and protein levels from the *bcr-abl* gene can vary over a wide range. This variation does not result from a change in the number of *bcr-abl* templates secondary to gene amplification but more likely from changes in either transcription rate or mRNA stability. We suspect this range of *bcr-abl* expression is not limited to lymphoid cells. Analysis of peripheral blood leukocytes derived from an unusual CML patient who has been in chronic phase with myeloid predominance for 16 years showed a level of P210^{c-abl} one-fifth that of P145^{c-abl}, as detected by metabolic labeling with [^{32}P]orthophosphate and immunoprecipitation (S.C., O.N.W., and P. Greenberg, unpublished observations). Lower levels of expression of the chimeric mRNA have been demonstrated in clinical samples from chronic-phase CML patients compared to acute-phase CML patients (9). Others have reported chronic-phase patients with variable but, in some cases, relatively high levels of the *bcr-abl* mRNA (32). The sampling variation and the heterogenous mixture of cell types in clinical samples complicate such analyses. Further work is needed to evaluate whether there is a defined change in P210^{c-abl} expression during the progression of CML. It is interesting to note that among the limited sample of Ph[1]-positive B-cell lines we have examined (Table 1), we have seen higher levels of P210^{c-abl} in those derived from patients at more advanced stages of the disease.

It will be important to search for cell-type-specific mechanisms that might regulate expression of *bcr-abl* from Ph[1].

1. Champlin, R. E. & Golde, D. W. (1985) *Blood* 65, 1039–1047.
2. Rowley, J. D. (1973) *Nature (London)* 243, 290–291.
3. Heisterkamp, N., Stephenson, J. R., Groffen, J., Hansen, P. F., de Klein, A., Bartram, C. R. & Grosveld, G. (1983) *Nature (London)* 306, 239–242.
4. Bartram, C. R., de Klein, A., Hagemeijer, A., van Agthoven, T., van Kessel, A. G., Bootsma, D., Grosveld, G., Ferguson-Smith, M. A., Davies, T., Stone, M., Heisterkamp, N., Stephenson, J. R. & Groffen, J. (1983) *Nature (London)* 306, 277–280.
5. Shtivelman, E., Lifshitz, B., Gale, R. P. & Canaani, D. (1985) *Nature (London)* 315, 550–554.
6. Heisterkamp, N., Stam, K. & Groffen, J. (1985) *Nature (London)* 315, 758–761.
7. Groffen, J., Stephenson, J. R., Heisterkamp, N., de Klein, A., Bartram, C. R. & Grosveld, G. (1984) *Cell* 36, 93–99.
8. Gale, R. P. & Canaani, E. (1984) *Proc. Natl. Acad. Sci. USA* 81, 5648–5652.
9. Collins, S., Kubonishi, I., Miyoshi, I. & Groudine, M. T. (1984) *Science* 225, 72–74.
10. Konopka, J. B., Watanabe, S. M. & Witte, O. N. (1984) *Cell* 7, 1035–1042.
11. Konopka, J. B., Watanabe, S. M., Singer, J., Collins, S. & Witte, O. N. (1985) *Proc. Natl. Acad. Sci. USA* 82, 1810–1814.
12. Kloetzer, W., Kurzrock, R., Smith, L., Talpaz, M., Spiller, M., Gutterman, J. & Arlinghaus, R. (1985) *Virology* 140, 230–238.
13. Kozbor, D., Giallongo, A., Sierzega, M. E., Konopka, J. B., Witte, O. N., Showe, L. C. & Croce, C. M. (1985) *Nature (London)*, in press.
14. Davis, R. L., Konopka, J. B. & Witte, O. N. (1985) *Mol. Cell Biol.* 5, 204–213.
15. Konopka, J. B. & Witte, O. N. (1985) *Mol. Cell. Biol.* 5, 3116–3123.
16. Nitta, M., Kato, Y., Strife, A., Wachter, M., Fried, J., Perez, A., Jhanwar, S., Duigou, R., Chaganti, R. S. K. & Clarkson, B. (1985) *Blood* 66, 1053–1061.
17. Konopka, J. B., Davis, J. L., Watanabe, S. M., Ponticelli, A. S., Schiff-Maker, L., Rosenberg, N. & Witte, O. N. (1984) *Virology* 51, 223–232.
18. Gibson, W. (1981) *Anal. Biochem.* 118, 1–3.
19. Schiff-Maker, L., Konopka, J. B., Clark, S., Witte, O. N. & Rosenberg, N. (1986) *J. Virol.* 57, 1182–1186.
20. Schwartz, R. C., Sonenshein, G. E., Bothwell, A. & Gefter, M. L. (1981) *J. Immunol.* 126, 2104–2108.
21. Goff, S. P., Gilboa, E., Witte, O. N. & Baltimore, D. (1980) *Cell* 22, 777–785.
22. Collins, S. J. & Groudine, M. T. (1983) *Proc. Natl. Acad. Sci. USA* 80, 4813–4817.
23. Selden, J. R., Emanuel, B. S., Wang, E., Cannizzaro, L., Palumbo, A., Erikson, J., Nowell, P. C., Rovera, G. & Croce, C. M. (1983) *Proc. Natl. Acad. Sci. USA* 80, 7289–7292.
24. Fialkow, P. J., Martin, P. J., Najfeld, V., Penfold, G. K., Jacobson, R. J. & Hansen, J. A. (1981) *Blood* 58, 158–163.
25. Martin, P. J., Najfeld, V. & Fialkow, P. J. (1982) *Can. Gen. Cytogenet.* 6, 359–368.
26. Rowley, J. D. (1980) *Annu. Rev. Genet.* 14, 17–40.
27. Whitlock, C. A. & Witte, O. N. (1984) *Adv. Immunol.* 37, 74–98.
28. Pierce, J. H., Di Fiore, P. P., Aaronson, S. A., Potter, M., Pumphrey, J., Scott, A. & Ihle, J. N. (1985) *Cell* 41, 685–693.
29. Whitlock, C. A., Ziegler, S. & Witte, O. N. (1983) *Mol. Cell. Biol.* 3, 596–604.
30. Wolf, D., Harris, N. & Rotter, V. (1984) *Cell* 38, 119–126.
31. Klein, G. & Klein, E. (1985) *Nature (London)* 315, 190–195.
32. Stam, K., Jr., Heisterkamp, N., Grosveld, G., de Klein, A., Verma, R., Colemen, M., Dosik, H. & Groffen, J. (1985) *N. Engl. J. Med.* 313, 1429–1433.
33. Lozzio, C. B. & Lozzio, B. B. (1975) *Blood* 45, 321–334.

WISP genes are members of the connective tissue growth factor family that are up-regulated in Wnt-1-transformed cells and aberrantly expressed in human colon tumors

DIANE PENNICA*†, TODD A. SWANSON*, JAMES W. WELSH*, MARGARET A. ROY‡, DAVID A. LAWRENCE*, JAMES LEE‡, JENNIFER BRUSH‡, LISA A. TANEYHILL§, BETHANNE DEUEL‡, MICHAEL LEW¶, COLIN WATANABE‖, ROBERT L. COHEN*, MONA F. MELHEM**, GENE G. FINLEY**, PHIL QUIRKE††, AUDREY D. GODDARD‡, KENNETH J. HILLAN¶, AUSTIN L. GURNEY‡, DAVID BOTSTEIN‡,‡‡, AND ARNOLD J. LEVINE§

Departments of *Molecular Oncology, ‡Molecular Biology, ‖Scientific Computing, and ¶Pathology, Genentech Inc., 1 DNA Way, South San Francisco, CA 94080; **University of Pittsburgh School of Medicine, Veterans Administration Medical Center, Pittsburgh, PA 15240; ††University of Leeds, Leeds, LS29JT United Kingdom; ‡‡Department of Genetics, Stanford University, Palo Alto, CA 94305; and §Department of Molecular Biology, Princeton University, Princeton, NJ 08544

ABSTRACT   Wnt family members are critical to many developmental processes, and components of the Wnt signaling pathway have been linked to tumorigenesis in familial and sporadic colon carcinomas. Here we report the identification of two genes, WISP-1 and WISP-2, that are up-regulated in the mouse mammary epithelial cell line C57MG transformed by Wnt-1, but not by Wnt-4. Together with a third related gene, WISP-3, these proteins define a subfamily of the connective tissue growth factor family. Two distinct systems demonstrated WISP induction to be associated with the expression of Wnt-1. These included (i) C57MG cells infected with a Wnt-1 retroviral vector or expressing Wnt-1 under the control of a tetracyline repressible promoter, and (ii) Wnt-1 transgenic mice. The WISP-1 gene was localized to human chromosome 8q24.1–8q24.3. WISP-1 genomic DNA was amplified in colon cancer cell lines and in human colon tumors and its RNA overexpressed (2- to >30-fold) in 84% of the tumors examined compared with patient-matched normal mucosa. WISP-3 mapped to chromosome 6q22–6q23 and also was overexpressed (4- to >40-fold) in 63% of the colon tumors analyzed. In contrast, WISP-2 mapped to human chromosome 20q12–20q13 and its DNA was amplified, but RNA expression was reduced (2- to >30-fold) in 79% of the tumors. These results suggest that the WISP genes may be downstream of Wnt-1 signaling and that aberrant levels of WISP expression in colon cancer may play a role in colon tumorigenesis.

Wnt-1 is a member of an expanding family of cysteine-rich, glycosylated signaling proteins that mediate diverse developmental processes such as the control of cell proliferation, adhesion, cell polarity, and the establishment of cell fates (1, 2). Wnt-1 originally was identified as an oncogene activated by the insertion of mouse mammary tumor virus in virus-induced mammary adenocarcinomas (3, 4). Although Wnt-1 is not expressed in the normal mammary gland, expression of Wnt-1 in transgenic mice causes mammary tumors (5).

In mammalian cells, Wnt family members initiate signaling by binding to the seven-transmembrane spanning Frizzled receptors and recruiting the cytoplasmic protein Dishevelled (Dsh) to the cell membrane (1, 2, 6). Dsh then inhibits the kinase activity of the normally constitutively active glycogen synthase kinase-3β (GSK-3β) resulting in an increase in β-catenin levels. Stabilized β-catenin interacts with the transcription factor TCF/Lef1, forming a complex that appears in the nucleus and binds TCF/Lef1 target DNA elements to activate transcription (7, 8). Other experiments suggest that the adenomatous polyposis coli (APC) tumor suppressor gene also plays an important role in Wnt signaling by regulating β-catenin levels (9). APC is phosphorylated by GSK-3β, binds to β-catenin, and facilitates its degradation. Mutations in either APC or β-catenin have been associated with colon carcinomas and melanomas, suggesting these mutations contribute to the development of these types of cancer, implicating the Wnt pathway in tumorigenesis (1).

Although much has been learned about the Wnt signaling pathway over the past several years, only a few of the transcriptionally activated downstream components activated by Wnt have been characterized. Those that have been described cannot account for all of the diverse functions attributed to Wnt signaling. Among the candidate Wnt target genes are those encoding the nodal-related 3 gene, Xnr3, a member of the transforming growth factor (TGF)-β superfamily, and the homeobox genes, engrailed, goosecoid, twin (Xtwn), and siamois (2). A recent report also identifies c-myc as a target gene of the Wnt signaling pathway (10).

To identify additional downstream genes in the Wnt signaling pathway that are relevant to the transformed cell phenotype, we used a PCR-based cDNA subtraction strategy, suppression subtractive hybridization (SSH) (11), using RNA isolated from C57MG mouse mammary epithelial cells and C57MG cells stably transformed by a Wnt-1 retrovirus. Overexpression of Wnt-1 in this cell line is sufficient to induce a partially transformed phenotype, characterized by elongated and refractile cells that lose contact inhibition and form a multilayered array (12, 13). We reasoned that genes differentially expressed between these two cell lines might contribute to the transformed phenotype.

In this paper, we describe the cloning and characterization of two genes up-regulated in Wnt-1 transformed cells, WISP-1 and WISP-2, and a third related gene, WISP-3. The WISP genes are members of the CCN family of growth factors, which includes connective tissue growth factor (CTGF), Cyr61, and nov, a family not previously linked to Wnt signaling.

MATERIALS AND METHODS

SSH. SSH was performed by using the PCR-Select cDNA Subtraction Kit (CLONTECH). Tester double-stranded

cDNA was synthesized from 2 μg of poly(A)⁺ RNA isolated from the C57MG/Wnt-1 cell line and driver cDNA from 2 μg of poly(A)⁺ RNA from the parent C57MG cells. The subtracted cDNA library was subcloned into a pGEM-T vector for further analysis.

cDNA Library Screening. Clones encoding full-length mouse *WISP-1* were isolated by screening a λgt10 mouse embryo cDNA library (CLONTECH) with a 70-bp probe from the original partial clone 568 sequence corresponding to amino acids 128–169. Clones encoding full-length human *WISP-1* were isolated by screening λgt10 lung and fetal kidney cDNA libraries with the same probe at low stringency. Clones encoding full-length mouse and human *WISP-2* were isolated by screening a C57MG/Wnt-1 or human fetal lung cDNA library with a probe corresponding to nucleotides 1463–1512. Full-length cDNAs encoding *WISP-3* were cloned from human bone marrow and fetal kidney libraries.

Expression of Human *WISP* RNA. PCR amplification of first-strand cDNA was performed with human Multiple Tissue cDNA panels (CLONTECH) and 300 μM of each dNTP at 94°C for 1 sec, 62°C for 30 sec, 72°C for 1 min, for 22–32 cycles. *WISP* and glyceraldehyde-3-phosphate dehydrogenase primer sequences are available on request.

In Situ **Hybridization.** ³³P-labeled sense and antisense riboprobes were transcribed from an 897-bp PCR product corresponding to nucleotides 601–1440 of mouse *WISP-1* or a 294-bp PCR product corresponding to nucleotides 82–375 of mouse *WISP-2*. All tissues were processed as described (40).

Radiation Hybrid Mapping. Genomic DNA from each hybrid in the Stanford G3 and Genebridge4 Radiation Hybrid Panels (Research Genetics, Huntsville, AL) and human and hamster control DNAs were PCR-amplified, and the results were submitted to the Stanford or Massachusetts Institute of Technology web servers.

Cell Lines, Tumors, and Mucosa Specimens. Tissue specimens were obtained from the Department of Pathology (University of Pittsburgh) for patients undergoing colon resection and from the University of Leeds, United Kingdom. Genomic DNA was isolated (Qiagen) from the pooled blood of 10 normal human donors, surgical specimens, and the following ATCC human cell lines: SW480, COLO 320DM, HT-29, WiDr, and SW403 (colon adenocarcinomas), SW620 (lymph node metastasis, colon adenocarcinoma), HCT 116 (colon carcinoma), SK-CO-1 (colon adenocarcinoma, ascites), and HM7 (a variant of ATCC colon adenocarcinoma cell line LS 174T). DNA concentration was determined by using Hoechst dye 33258 intercalation fluorimetry. Total RNA was prepared by homogenization in 7 M GuSCN followed by centrifugation over CsCl cushions or prepared by using RNAzol.

Gene Amplification and RNA Expression Analysis. Relative gene amplification and RNA expression of *WISP*s and c-*myc* in the cell lines, colorectal tumors, and normal mucosa were determined by quantitative PCR. Gene-specific primers and fluorogenic probes (sequences available on request) were designed and used to amplify and quantitate the genes. The relative gene copy number was derived by using the formula 2^(ΔCt) where ΔCt represents the difference in amplification cycles required to detect the *WISP* genes in peripheral blood lymphocyte DNA compared with colon tumor DNA or colon tumor RNA compared with normal mucosal RNA. The ∂-method was used for calculation of the SE of the gene copy number or RNA expression level. The *WISP*-specific signal was normalized to that of the glyceraldehyde-3-phosphate dehydrogenase housekeeping gene. All TaqMan assay reagents were obtained from Perkin–Elmer Applied Biosystems.

RESULTS

Isolation of *WISP-1* and *WISP-2* by SSH. To identify Wnt-1-inducible genes, we used the technique of SSH using the

mouse mammary epithelial cell line C57MG and C57MG cells that stably express Wnt-1 (11). Candidate differentially expressed cDNAs (1,384 total) were sequenced. Thirty-nine percent of the sequences matched known genes or homologues, 32% matched expressed sequence tags, and 29% had no match. To confirm that the transcript was differentially expressed, semiquantitative reverse transcription–PCR and Northern analysis were performed by using mRNA from the C57MG and C57MG/Wnt-1 cells.

Two of the cDNAs, *WISP-1* and *WISP-2*, were differentially expressed, being induced in the C57MG/Wnt-1 cell line, but not in the parent C57MG cells or C57MG cells overexpressing Wnt-4 (Fig. 1 *A* and *B*). Wnt-4, unlike Wnt-1, does not induce the morphological transformation of C57MG cells and has no effect on β-catenin levels (13, 14). Expression of *WISP-1* was up-regulated approximately 3-fold in the C57MG/Wnt-1 cell line and *WISP-2* by approximately 5-fold by both Northern analysis and reverse transcription–PCR.

An independent, but similar, system was used to examine *WISP* expression after Wnt-1 induction. C57MG cells expressing the *Wnt-1* gene under the control of a tetracycline-repressible promoter produce low amounts of Wnt-1 in the repressed state but show a strong induction of *Wnt-1* mRNA and protein within 24 hr after tetracycline removal (8). The levels of Wnt-1 and *WISP* RNA isolated from these cells at various times after tetracycline removal were assessed by quantitative PCR. Strong induction of Wnt-1 mRNA was seen as early as 10 hr after tetracycline removal. Induction of *WISP* mRNA (2- to 6-fold) was seen at 48 and 72 hr (data not shown). These data support our previous observations that show that *WISP* induction is correlated with Wnt-1 expression. Because the induction is slow, occurring after approximately 48 hr, the induction of *WISP*s may be an indirect response to Wnt-1 signaling.

cDNA clones of human *WISP-1* were isolated and the sequence compared with mouse *WISP-1*. The cDNA sequences of mouse and human *WISP-1* were 1,766 and 2,830 bp in length, respectively, and encode proteins of 367 aa, with predicted relative molecular masses of ≈40,000 (Mᵣ 40 K). Both have hydrophobic N-terminal signal sequences, 38 conserved cysteine residues, and four potential N-linked glycosylation sites and are 84% identical (Fig. 2*A*).

Full-length cDNA clones of mouse and human *WISP-2* were 1,734 and 1,293 bp in length, respectively, and encode proteins of 251 and 250 aa, respectively, with predicted relative molecular masses of ≈27,000 (Mᵣ 27 K) (Fig. 2*B*). Mouse and human *WISP-2* are 73% identical. Human *WISP-2* has no potential N-linked glycosylation sites, and mouse *WISP-2* has one at
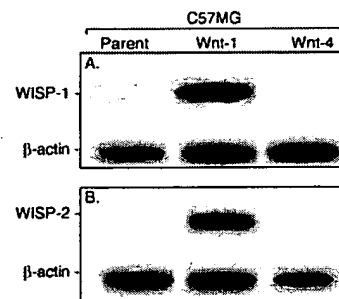

Fig. 1. *WISP-1* and *WISP-2* are induced by Wnt-1, but not Wnt-4, expression in C57MG cells. Northern analysis of *WISP-1* (*A*) and *WISP-2* (*B*) expression in C57MG, C57MG/Wnt-1, and C57MG/Wnt-4 cells. Poly(A)⁺ RNA (2 μg) was subjected to Northern blot analysis and hybridized with a 70-bp mouse *WISP-1*-specific probe (amino acids 278–300) or a 190-bp *WISP-2*-specific probe (nucleotides 1438–1627) in the 3′ untranslated region. Blots were rehybridized with human β-actin probe.
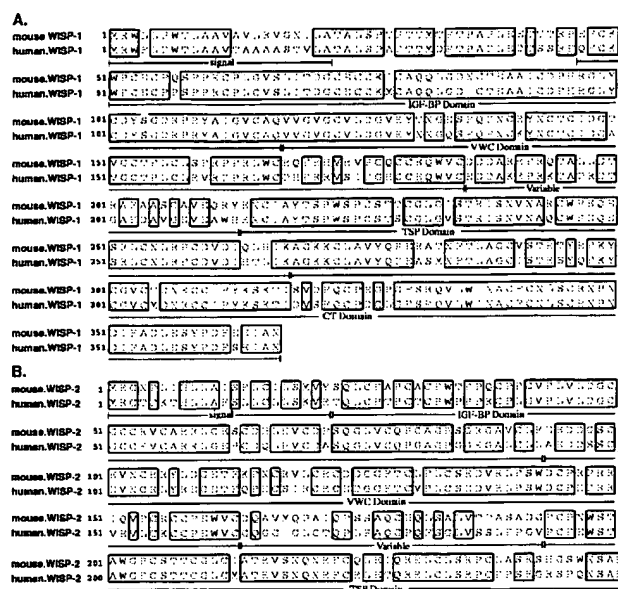
Cell Biology, Medical Sciences: Pennica *et al.*

Proc. Natl. Acad. Sci. USA 95 (1998)   14719

A.

B.

FIG. 2. Encoded amino acid sequence alignment of mouse and human *WISP-1* (*A*) and mouse and human *WISP-2* (*B*). The potential signal sequence, insulin-like growth factor-binding protein (IGF-BP), VWC, thrombospondin (TSP), and C-terminal (CT) domains are underlined.

position 197. *WISP-2* has 28 cysteine residues that are conserved among the 38 cysteines found in *WISP-1*.

Identification of *WISP-3*. To search for related proteins, we screened expressed sequence tag (EST) databases with the WISP-1 protein sequence and identified several ESTs as potentially related sequences. We identified a homologous protein that we have called WISP-3. A full-length human *WISP-3* cDNA of 1,371 bp was isolated corresponding to those ESTs that encode a 354-aa protein with a predicted molecular mass of 39,293. WISP-3 has two potential N-linked glycosylation sites and 36 cysteine residues. An alignment of the three human WISP proteins shows that WISP-1 and WISP-3 are the most similar (42% identity), whereas WISP-2 has 37% identity with WISP-1 and 32% identity with WISP-3 (Fig. 3*A*).

WISPs Are Homologous to the CTGF Family of Proteins. Human *WISP-1*, *WISP-2*, and *WISP-3* are novel sequences; however, mouse *WISP-1* is the same as the recently identified *Elm1* gene. *Elm1* is expressed in low, but not high, metastatic mouse melanoma cells, and suppresses the *in vivo* growth and metastatic potential of K-1735 mouse melanoma cells (15). Human and mouse *WISP-2* are homologous to the recently described rat gene, *rCop-1* (16). Significant homology (36–44%) was seen to the CCN family of growth factors. This family includes three members, CTGF, Cyr61, and the protooncogene *nov*. CTGF is a chemotactic and mitogenic factor for fibroblasts that is implicated in wound healing and fibrotic disorders and is induced by TGF-β (17). Cyr61 is an extracellular matrix signaling molecule that promotes cell adhesion, proliferation, migration, angiogenesis, and tumor growth (18, 19). *nov* (nephroblastoma overexpressed) is an immediate early gene associated with quiescence and found altered in Wilms tumors (20). The proteins of the CCN family share functional, but not sequence, similarity to Wnt-1. All are secreted, cysteine-rich heparin binding glycoproteins that associate with the cell surface and extracellular matrix.

WISP proteins exhibit the modular architecture of the CCN family, characterized by four conserved cysteine-rich domains (Fig. 3*B*) (21). The N-terminal domain, which includes the first 12 cysteine residues, contains a consensus sequence (GCGC-CXXC) conserved in most insulin-like growth factor (IGF)-
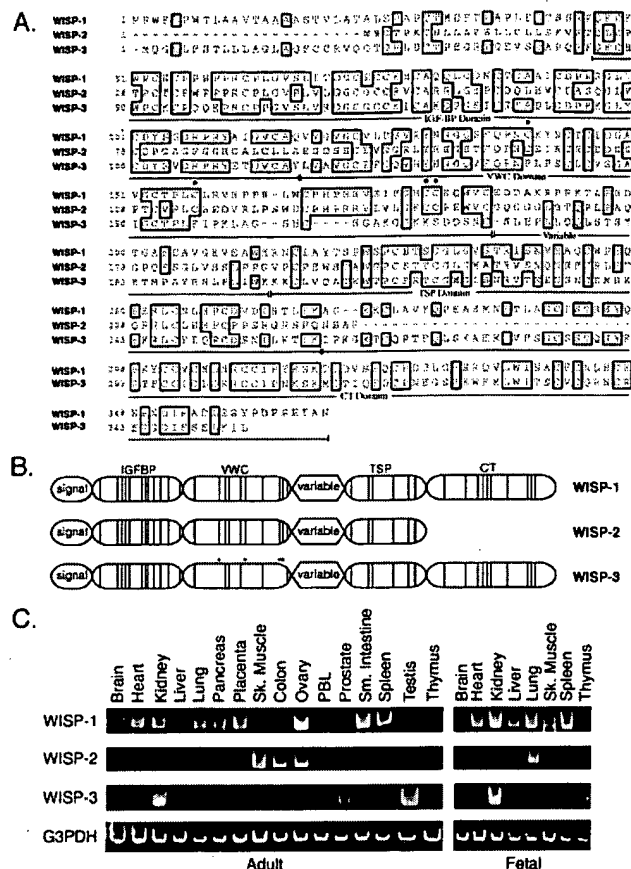
A.

B.

C.

FIG. 3. (*A*) Encoded amino acid sequence alignment of human WISPs. The cysteine residues of WISP-1 and WISP-2 that are not present in WISP-3 are indicated with a dot. (*B*) Schematic representation of the WISP proteins showing the domain structure and cysteine residues (vertical lines). The four cysteine residues in the VWC domain that are absent in WISP-3 are indicated with a dot. (*C*) Expression of *WISP* mRNA in human tissues. PCR was performed on human multiple-tissue cDNA panels (CLONTECH) from the indicated adult and fetal tissues.

binding proteins (BP). This sequence is conserved in WISP-2 and WISP-3, whereas WISP-1 has a glutamine in the third position instead of a glycine. CTGF recently has been shown to specifically bind IGF (22) and a truncated *nov* protein lacking the IGF-BP domain is oncogenic (23). The von Willebrand factor type C module (VWC), also found in certain collagens and mucins, covers the next 10 cysteine residues, and is thought to participate in protein complex formation and oligomerization (24). The VWC domain of WISP-3 differs from all CCN family members described previously, in that it contains only six of the 10 cysteine residues (Fig. 3 *A* and *B*). A short variable region follows the VWC domain. The third module, the thrombospondin (TSP) domain, is involved in binding to sulfated glycoconjugates and contains six cysteine residues and a conserved WSxCSxxCG motif first identified in thrombospondin (25). The C-terminal (CT) module containing the remaining 10 cysteines is thought to be involved in dimerization and receptor binding (26). The CT domain is present in all CCN family members described to date but is absent in WISP-2 (Fig. 3 *A* and *B*). The existence of a putative signal sequence and the absence of a transmembrane domain suggest that WISPs are secreted proteins, an observation supported by an analysis of their expression and secretion from mammalian cell and baculovirus cultures (data not shown).

Expression of *WISP* mRNA in Human Tissues. Tissue-specific expression of human *WISP*s was characterized by PCR

analysis on adult and fetal multiple tissue cDNA panels. *WISP-1* expression was seen in the adult heart, kidney, lung, pancreas, placenta, ovary, small intestine, and spleen (Fig. 3*C*). Little or no expression was detected in the brain, liver, skeletal muscle, colon, peripheral blood leukocytes, prostate, testis, or thymus. *WISP-2* had a more restricted tissue expression and was detected in adult skeletal muscle, colon, ovary, and fetal lung. Predominant expression of *WISP-3* was seen in adult kidney and testis and fetal kidney. Lower levels of *WISP-3* expression were detected in placenta, ovary, prostate, and small intestine.

In Situ **Localization of *WISP-1* and *WISP-2*.** Expression of *WISP-1* and *WISP-2* was assessed by *in situ* hybridization in mammary tumors from Wnt-1 transgenic mice. Strong expression of *WISP-1* was observed in stromal fibroblasts lying within the fibrovascular tumor stroma (Fig. 4 *A–D*). However, low-level *WISP-1* expression also was observed focally within tumor cells (data not shown). No expression was observed in normal breast. Like *WISP-1*, *WISP-2* expression also was seen in the tumor stroma in breast tumors from Wnt-1 transgenic animals (Fig. 4 *E–H*). However, *WISP-2* expression in the stroma was in spindle-shaped cells adjacent to capillary vessels, whereas

the predominant cell type expressing *WISP-1* was the stromal fibroblasts.

Chromosome Localization of the *WISP* Genes. The chromosomal location of the human *WISP* genes was determined by radiation hybrid mapping panels. *WISP-1* is approximately 3.48 cR from the meiotic marker AFM259xc5 [logarithm of odds (lod) score 16.31] on chromosome 8q24.1 to 8q24.3, in the same region as the human locus of the *novH* family member (27) and roughly 4 Mbs distal to c-*myc* (28). Preliminary fine mapping indicates that *WISP-1* is located near D8S1712 STS. *WISP-2* is linked to the marker SHGC-33922 (lod = 1,000) on chromosome 20q12–20q13.1. Human *WISP-3* mapped to chromosome 6q22–6q23 and is linked to the marker AFM211ze5 (lod = 1,000). *WISP-3* is approximately 18 Mbs proximal to CTGF and 23 Mbs proximal to the human cellular oncogene *MYB* (27, 29).

Amplification and Aberrant Expression of *WISPs* in Human Colon Tumors. Amplification of protooncogenes is seen in many human tumors and has etiological and prognostic significance. For example, in a variety of tumor types, c-*myc* amplification has been associated with malignant progression and poor prognosis (30). Because *WISP-1* resides in the same general chromosomal location (8q24) as c-*myc*, we asked whether it was a target of gene amplification, and, if so, whether this amplification was independent of the c-*myc* locus. Genomic DNA from human colon cancer cell lines was assessed by quantitative PCR and Southern blot analysis. (Fig. 5 *A* and *B*). Both methods detected similar degrees of *WISP-1* amplification. Most cell lines showed significant (2- to 4-fold) amplification, with the HT-29 and WiDr cell lines demonstrating an 8-fold increase. Significantly, the pattern of amplification observed did not correlate with that observed for c-*myc*, indicating that the c-*myc* gene is not part of the amplicon that involves the *WISP-1* locus.

We next examined whether the *WISP* genes were amplified in a panel of 25 primary human colon adenocarcinomas. The relative *WISP* gene copy number in each colon tumor DNA was compared with pooled normal DNA from 10 donors by quantitative PCR (Fig. 6). The copy number of *WISP-1* and *WISP-2* was significantly greater than one, approximately 2-fold for *WISP-1* in about 60% of the tumors and 2- to 4-fold for *WISP-2* in 92% of the tumors ($P < 0.001$ for each). The copy number for *WISP-3* was indistinguishable from one ($P = 0.166$). In addition, the copy number of *WISP-2* was significantly higher than that of *WISP-1* ($P < 0.001$).

The levels of *WISP* transcripts in RNA isolated from 19 adenocarcinomas and their matched normal mucosa were
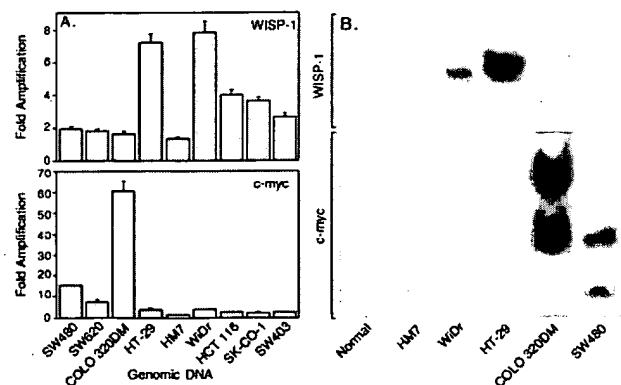

FIG. 4. (*A*, *C*, *E*, and *G*) Representative hematoxylin/eosin-stained images from breast tumors in Wnt-1 transgenic mice. The corresponding dark-field images showing *WISP-1* expression are shown in *B* and *D*. The tumor is a moderately well-differentiated adenocarcinoma showing evidence of adenoid cystic change. At low power (*A* and *B*), expression of *WISP-1* is seen in the delicate branching fibrovascular tumor stroma (arrowhead). At higher magnification, expression is seen in the stromal(s) fibroblasts (*C* and *D*), and tumor cells are negative. Focal expression of *WISP-1*, however, was observed in tumor cells in some areas. Images of *WISP-2* expression are shown in *E–H*. At low power (*E* and *F*), expression of WISP-2 is seen in cells lying within the fibrovascular tumor stroma. At higher magnification, these cells appeared to be adjacent to capillary vessels whereas tumor cells are negative (*G* and *H*).

FIG. 5. Amplification of *WISP-1* genomic DNA in colon cancer cell lines. (*A*) Amplification in cell line DNA was determined by quantitative PCR. (*B*) Southern blots containing genomic DNA (10 µg) digested with *Eco*RI (*WISP-1*) or *Xba*I (c-*myc*) were hybridized with a 100-bp human *WISP-1* probe (amino acids 186–219) or a human c-*myc* probe (located at bp 1901–2000). The *WISP* and *myc* genes are detected in normal human genomic DNA after a longer film exposure.

Cell Biology, Medical Sciences: Pennica *et al.*
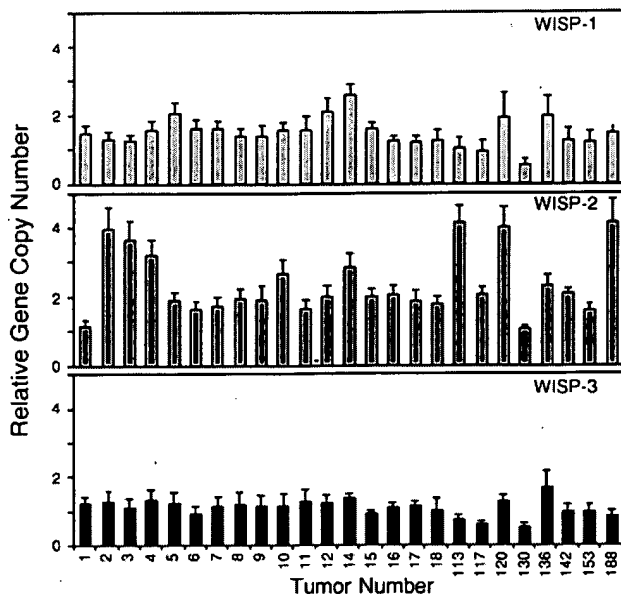
Proc. Natl. Acad. Sci. USA 95 (1998)   14721

FIG. 6. Genomic amplification of *WISP* genes in human colon tumors. The relative gene copy number of the *WISP* genes in 25 adenocarcinomas was assayed by quantitative PCR, by comparing DNA from primary human tumors with pooled DNA from 10 healthy donors. The data are means ± SEM from one experiment done in triplicate. The experiment was repeated at least three times.

assessed by quantitative PCR (Fig. 7). The level of *WISP-1* RNA present in tumor tissue varied but was significantly increased (2- to >25-fold) in 84% (16/19) of the human colon tumors examined compared with normal adjacent mucosa. Four of 19 tumors showed greater than 10-fold overexpression. In contrast, in 79% (15/19) of the tumors examined, *WISP-2* RNA expression was significantly lower in the tumor than the mucosa. Similar to *WISP-1*, *WISP-3* RNA was overexpressed in 63% (12/19) of the colon tumors compared with the normal

FIG. 7. *WISP* RNA expression in primary human colon tumors relative to expression in normal mucosa from the same patient. Expression of *WISP* mRNA in 19 adenocarcinomas was assayed by quantitative PCR. The Dukes stage of the tumor is listed under the sample number. The data are means ± SEM from one experiment done in triplicate. The experiment was repeated at least twice.

mucosa. The amount of overexpression of *WISP-3* ranged from 4- to >40-fold.

DISCUSSION

One approach to understanding the molecular basis of cancer is to identify differences in gene expression between cancer cells and normal cells. Strategies based on assumptions that steady-state mRNA levels will differ between normal and malignant cells have been used to clone differentially expressed genes (31). We have used a PCR-based selection strategy, SSH, to identify genes selectively expressed in C57MG mouse mammary epithelial cells transformed by Wnt-1.

Three of the genes isolated, *WISP-1*, *WISP-2*, and *WISP-3*, are members of the CCN family of growth factors, which includes CTGF, Cyr61, and *nov*, a family not previously linked to Wnt signaling.

Two independent experimental systems demonstrated that *WISP* induction was associated with the expression of Wnt-1. The first was C57MG cells infected with a Wnt-1 retroviral vector or C57MG cells expressing Wnt-1 under the control of a tetracyline-repressible promoter, and the second was in Wnt-1 transgenic mice, where breast tissue expresses Wnt-1, whereas normal breast tissue does not. No *WISP* RNA expression was detected in mammary tumors induced by polyoma virus middle T antigen (data not shown). These data suggest a link between Wnt-1 and *WISP*s in that in these two situations, *WISP* induction was correlated with Wnt-1 expression.

It is not clear whether the *WISP*s are directly or indirectly induced by the downstream components of the Wnt-1 signaling pathway (i.e., β-catenin-TCF-1/Lef1). The increased levels of *WISP* RNA were measured in Wnt-1-transformed cells, hours or days after Wnt-1 transformation. Thus, *WISP* expression could result from Wnt-1 signaling directly through β-catenin transcription factor regulation or alternatively through Wnt-1 signaling turning on a transcription factor, which in turn regulates *WISP*s.

The *WISP*s define an additional subfamily of the CCN family of growth factors. One striking difference observed in the protein sequence of WISP-2 is the absence of a CT domain, which is present in CTGF, Cyr61, *nov*, WISP-1, and WISP-3. This domain is thought to be involved in receptor binding and dimerization. Growth factors, such as TGF-β, platelet-derived growth factor, and nerve growth factor, which contain a cystine knot motif exist as dimers (32). It is tempting to speculate that WISP-1 and WISP-3 may exist as dimers, whereas WISP-2 exists as a monomer. If the CT domain is also important for receptor binding, WISP-2 may bind its receptor through a different region of the molecule than the other CCN family members. No specific receptors have been identified for CTGF or *nov*. A recent report has shown that integrin $\alpha_v\beta_3$ serves as an adhesion receptor for Cyr61 (33).

The strong expression of *WISP-1* and *WISP-2* in cells lying within the fibrovascular tumor stroma in breast tumors from Wnt-1 transgenic animals is consistent with previous observations that transcripts for the related CTGF gene are primarily expressed in the fibrous stroma of mammary tumors (34). Epithelial cells are thought to control the proliferation of connective tissue stroma in mammary tumors by a cascade of growth factor signals similar to that controlling connective tissue formation during wound repair. It has been proposed that mammary tumor cells or inflammatory cells at the tumor interstitial interface secrete TGF-$\beta1$, which is the stimulus for stromal proliferation (34). TGF-$\beta1$ is secreted by a large percentage of malignant breast tumors and may be one of the growth factors that stimulates the production of CTGF and WISPs in the stroma.

It was of interest that *WISP-1* and *WISP-2* expression was observed in the stromal cells that surrounded the tumor cells

(epithelial cells) in the Wnt-1 transgenic mouse sections of breast tissue. This finding suggests that paracrine signaling could occur in which the stromal cells could supply WISP-1 and WISP-2 to regulate tumor cell growth on the WISP extracellular matrix. Stromal cell-derived factors in the extracellular matrix have been postulated to play a role in tumor cell migration and proliferation (35). The localization of *WISP-1* and *WISP-2* in the stromal cells of breast tumors supports this paracrine model.

An analysis of *WISP-1* gene amplification and expression in human colon tumors showed a correlation between DNA amplification and overexpression, whereas overexpression of *WISP-3* RNA was seen in the absence of DNA amplification. In contrast, *WISP-2* DNA was amplified in the colon tumors, but its mRNA expression was significantly reduced in the majority of tumors compared with the expression in normal colonic mucosa from the same patient. The gene for human *WISP-2* was localized to chromosome 20q12–20q13, at a region frequently amplified and associated with poor prognosis in node negative breast cancer and many colon cancers, suggesting the existence of one or more oncogenes at this locus (36–38). Because the center of the 20q13 amplicon has not yet been identified, it is possible that the apparent amplification observed for *WISP-2* may be caused by another gene in this amplicon.

A recent manuscript on *rCop-1*, the rat orthologue of *WISP-2*, describes the loss of expression of this gene after cell transformation, suggesting it may be a negative regulator of growth in cell lines (16). Although the mechanism by which *WISP-2* RNA expression is down-regulated during malignant transformation is unknown, the reduced expression of *WISP-2* in colon tumors and cell lines suggests that it may function as a tumor suppressor. These results show that the *WISP* genes are aberrantly expressed in colon cancer and suggest that their altered expression may confer selective growth advantage to the tumor.

Members of the Wnt signaling pathway have been implicated in the pathogenesis of colon cancer, breast cancer, and melanoma, including the tumor suppressor gene adenomatous polyposis coli and β-catenin (39). Mutations in specific regions of either gene can cause the stabilization and accumulation of cytoplasmic β-catenin, which presumably contributes to human carcinogenesis through the activation of target genes such as the *WISP*s. Although the mechanism by which Wnt-1 transforms cells and induces tumorigenesis is unknown, the identification of *WISP*s as genes that may be regulated downstream of Wnt-1 in C57MG cells suggests they could be important mediators of Wnt-1 transformation. The amplification and altered expression patterns of the *WISP*s in human colon tumors may indicate an important role for these genes in tumor development.

1. Cadigan, K. M. & Nusse, R. (1997) *Genes Dev.* 11, 3286–3305.
2. Dale, T. C. (1998) *Biochem. J.* 329, 209–223.
3. Nusse, R. & Varmus, H. E. (1982) *Cell* 31, 99–109.
4. van Ooyen, A. & Nusse, R. (1984) *Cell* 39, 233–240.
5. Tsukamoto, A. S., Grosschedl, R., Guzman, R. C., Parslow, T. & Varmus, H. E. (1988) *Cell* 55, 619–625.
6. Brown, J. D. & Moon, R. T. (1998) *Curr. Opin. Cell. Biol.* 10, 182–187.
7. Molenaar, M., van de Wetering, M., Oosterwegel, M., Peterson-Maduro, J., Godsave, S., Korinek, V., Roose, J., Destree, O. & Clevers, H. (1996) *Cell* 86, 391–399.
8. Korinek, V., Barker, N., Willert, K., Molenaar, M., Roose, J., Wagenaar, G., Markman, M., Lamers, W., Destree, O. & Clevers, H. (1998) *Mol. Cell. Biol.* 18, 1248–1256.
9. Munemitsu, S., Albert, I., Souza, B., Rubinfeld, B. & Polakis, P. (1995) *Proc. Natl. Acad. Sci. USA* 92, 3046–3050.
10. He, T. C., Sparks, A. B., Rago, C., Hermeking, H., Zawel, L., da Costa, L. T., Morin, P. J., Vogelstein, B. & Kinzler, K. W. (1998) *Science* 281, 1509–1512.
11. Diatchenko, L., Lau, Y. F., Campbell, A. P., Chenchik, A., Moqadam, F., Huang, B., Lukyanov, S., Lukyanov, K., Gurskaya, N., Sverdlov, E. D. & Siebert, P. D. (1996) *Proc. Natl. Acad. Sci. USA* 93, 6025–6030.
12. Brown, A. M., Wildin, R. S., Prendergast, T. J. & Varmus, H. E. (1986) *Cell* 46, 1001–1009.
13. Wong, G. T., Gavin, B. J. & McMahon, A. P. (1994) *Mol. Cell. Biol.* 14, 6278–6286.
14. Shimizu, H., Julius, M. A., Giarre, M., Zheng, Z., Brown, A. M. & Kitajewski, J. (1997) *Cell Growth Differ.* 8, 1349–1358.
15. Hashimoto, Y., Shindo-Okada, N., Tani, M., Nagamachi, Y., Takeuchi, K., Shiroishi, T., Toma, H. & Yokota, J. (1998) *J. Exp. Med.* 187, 289–296.
16. Zhang, R., Averboukh, L., Zhu, W., Zhang, H., Jo, H., Dempsey, P. J., Coffey, R. J., Pardee, A. B. & Liang, P. (1998) *Mol. Cell. Biol.* 18, 6131–6141.
17. Grotendorst, G. R. (1997) *Cytokine Growth Factor Rev.* 8, 171–179.
18. Kireeva, M. L., Mo, F. E., Yang, G. P. & Lau, L. F. (1996) *Mol. Cell. Biol.* 16, 1326–1334.
19. Babic, A. M., Kireeva, M. L., Kolesnikova, T. V. & Lau, L. F. (1998) *Proc. Natl. Acad. Sci. USA* 95, 6355–6360.
20. Martinerie, C., Huff, V., Joubert, I., Badzioch, M., Saunders, G., Strong, L. & Perbal, B. (1994) *Oncogene* 9, 2729–2732.
21. Bork, P. (1993) *FEBS Lett.* 327, 125–130.
22. Kim, H. S., Nagalla, S. R., Oh, Y., Wilson, E., Roberts, C. T., Jr. & Rosenfeld, R. G. (1997) *Proc. Natl. Acad. Sci. USA* 94, 12981–12986.
23. Joliot, V., Martinerie, C., Dambrine, G., Plassiart, G., Brisac, M., Crochet, J. & Perbal, B. (1992) *Mol. Cell. Biol.* 12, 10–21.
24. Mancuso, D. J., Tuley, E. A., Westfield, L. A., Worrall, N. K., Shelton-Inloes, B. B., Sorace, J. M., Alevy, Y. G. & Sadler, J. E. (1989) *J. Biol. Chem.* 264, 19514–19527.
25. Holt, G. D., Pangburn, M. K. & Ginsburg, V. (1990) *J. Biol. Chem.* 265, 2852–2855.
26. Voorberg, J., Fontijn, R., Calafat, J., Janssen, H., van Mourik, J. A. & Pannekoek, H. (1991) *J. Cell. Biol.* 113, 195–205.
27. Martinerie, C., Viegas-Pequignot, E., Guenard, I., Dutrillaux, B., Nguyen, V. C., Bernheim, A. & Perbal, B. (1992) *Oncogene* 7, 2529–2534.
28. Takahashi, E., Hori, T., O'Connell, P., Leppert, M. & White, R. (1991) *Cytogenet. Cell. Genet.* 57, 109–111.
29. Meese, E., Meltzer, P. S., Witkowski, C. M. & Trent, J. M. (1989) *Genes Chromosomes Cancer* 1, 88–94.
30. Garte, S. J. (1993) *Crit. Rev. Oncog.* 4, 435–449.
31. Zhang, L., Zhou, W., Velculescu, V. E., Kern, S. E., Hruban, R. H., Hamilton, S. R., Vogelstein, B. & Kinzler, K. W. (1997) *Science* 276, 1268–1272.
32. Sun, P. D. & Davies, D. R. (1995) *Annu. Rev. Biophys. Biomol. Struct.* 24, 269–291.
33. Kireeva, M. L., Lam, S. C. T. & Lau, L. F. (1998) *J. Biol. Chem.* 273, 3090–3096.
34. Frazier, K. S. & Grotendorst, G. R. (1997) *Int. J. Biochem. Cell. Biol.* 29, 153–161.
35. Wernert, N. (1997) *Virchows Arch.* 430, 433–443.
36. Tanner, M. M., Tirkkonen, M., Kallioniemi, A., Collins, C., Stokke, T., Karhu, R., Kowbel, D., Shadravan, F., Hintz, M., Kuo, W. L., *et al.* (1994) *Cancer Res.* 54, 4257–4260.
37. Brinkmann, U., Gallo, M., Polymeropoulos, M. H. & Pastan, I. (1996) *Genome Res.* 6, 187–194.
38. Bischoff, J. R., Anderson, L., Zhu, Y., Mossie, K., Ng, L., Souza, B., Schryver, B., Flanagan, P., Clairvoyant, F., Ginther, C., *et al.* (1998) *EMBO J.* 17, 3052–3065.
39. Morin, P. J., Sparks, A. B., Korinek, V., Barker, N., Clevers, H., Vogelstein, B. & Kinzler, K. W. (1997) *Science* 275, 1787–1790.
40. Lu, L. H. & Gillett, N. (1994) *Cell Vision* 1, 169–176.

Preferential Channeling of Energy Fuels Toward Fat Rather Than Muscle During High Free Fatty Acid Availability in Rats

Roberto Fabris,[1] Enzo Nisoli,[2] Anna Maria Lombardi,[1] Cristina Tonello,[2] Roberto Serra,[1] Marnie Granzotto,[1] Isabelle Cusin,[3] Françoise Rohner-Jeanrenaud,[3] Giovanni Federspil,[1] Michele O. Carruba,[2] and Roberto Vettor[1]

The preferential channeling of different fuels to fat and changes in the transcription profile of adipose tissue and skeletal muscle are poorly understood processes involved in the pathogenesis of obesity and insulin resistance. Carbohydrate and lipid metabolism may play relevant roles in this context. Freely moving lean Zucker rats received 3- and 24-h infusions of Intralipid (Pharmacia and Upjohn, Milan, Italy) plus heparin, or saline plus heparin, to evaluate how an increase in free fatty acids (nonesterified fatty acid [NEFA]) modulates fat tissue and skeletal muscle gene expression and thus influences fuel partitioning. Glucose uptake was determined in various tissues at the end of the infusion period by means of the 2-deoxy-[1-^{3}H]-D-glucose technique after a euglycemic-hyperinsulinemic clamp: high NEFA levels markedly decreased insulin-mediated glucose uptake in red fiber–type muscles but enhanced glucose utilization in visceral fat. Using reverse transcriptase–polymerase chain reaction and Northern blotting analyses, the mRNA expression of fatty acid translocase (FAT)/CD36, GLUT4, tumor necrosis factor (TNF)-α, peroxisome proliferator–activated receptor (PPAR)-γ, leptin, uncoupling protein (UCP)-2, and UCP-3 was investigated in different fat depots and skeletal muscles before and after the study infusions. GLUT4 mRNA levels significantly decreased (by ~25%) in red fiber–type muscle (soleus) and increased (by ~45%) in visceral adipose tissue. Furthermore, there were marked increases in FAT/CD36, TNF-α, PPAR-γ, leptin, UCP2, and UCP3 mRNA levels in the visceral fat and muscle of the treated animals in comparison with those measured in the saline-treated animals. These data suggest that the in vivo gene expression of FAT/CD36, GLUT4, TNF-α, PPAR-γ, leptin, UCP2, and UCP3 in visceral fat and red fiber-type muscle are differently regulated by circulating lipids and that selective insulin resistance seems to favor, at least in part, a prevention of fat accumulation in tissues not primarily destined for fat storage, thus contributing to increased adiposity and the development of a prediabetic syndrome. *Diabetes* 50:601–608, 2001

I n obesity, excessive energy storage as fat is mainly due to an imbalance between energy intake and expenditure, and the preferential channeling of excess calories as fat rather than protein or glycogen may play an important role in the development and maintenance of the disease. Carbohydrates and lipids share common metabolic pathways, which may be important in the regulation of energy metabolism and fuel partitioning. Insulin stimulates glucose oxidation in skeletal muscle and adipose tissue, but increased blood levels of other macronutrients may interfere with glucose oxidation: for example, although basal glucose utilization remains unaffected by lipid infusion, insulin-mediated glucose utilization decreases, as measured by means of the euglycemic-hyperinsulinemic clamp technique (1). Furthermore, positron emission tomography scanning using fluoro-2-deoxyglucose as a tracer shows that this inhibition mainly takes place in skeletal muscle (2). Free fatty acid (nonesterified fatty acid [NEFA])-induced insulin resistance saves scarce glucose for central nervous system requirements, but this becomes counterproductive in obesity because it inhibits glucose utilization when there is no need to save it. Glucose and NEFA might thus be channeled toward tissues (such as adipose tissue in which insulin sensitivity is maintained or even improved) and contribute to triglyceride synthesis, although the cellular and molecular mechanisms responsible for these processes (particularly for defective muscle glucose uptake) are still under debate. It has been suggested that tumor necrosis factor (TNF)-α may play a relevant role because it is overexpressed in the adipose tissue of obese insulin-resistant rodents and humans, and TNF-α antibodies counteract insulin resistance in the fat and muscle of genetically obese Zucker rats (3).

In addition to substrate competition, which is a very complex metabolic phenomenon involving much more molecular and cellular events than those firstly hypothesized by Randle et al. (4) and others (5–7), other processes and factors are known to regulate fuel partitioning and fat

deposition, including the hormonal milieu (i.e., insulin levels) and the expression of genes whose products play active roles in tissue energy homeostasis, such as leptin and uncoupling protein (UCP)-2 and UCP3 (8,9). Recent evidence suggests that once inside the cells, the fatty acids derived from the uptake of the NEFA released by the hydrolysis of circulating triglyceride-rich lipoproteins or from circulating fatty acids bound to serum albumin (10) act as signaling molecules. They bind to and activate the peroxisome proliferator–activated receptor (PPAR) protein family, a new class of nuclear receptors that can link fatty acids by means of a program of gene expression (11). PPAR-γ modulates the expression of genes involved in adipogenesis, lipid storage, and metabolism, such as fatty acid translocase (FAT)/CD36 (12). Furthermore, it has been hypothesized that cross-talk may exist between insulin action and PPAR-γ functions in mature adipocytes because the thiazolidinediones, a new class of antidiabetic drugs that improve in vivo insulin sensitivity in humans (13), have been found to bind and activate PPAR-γ (14). PPAR-γ is also expressed at lower levels in skeletal muscle (15), but its role in this tissue is not yet fully understood.

We have recently suggested that circulating NEFAs in healthy human subjects directly favor the accumulation and metabolism of fatty acids in adipose depots by modulating the expression of some of these specific adipose genes (16). However, that study did not provide any information concerning the effect(s) of circulating NEFAs on muscle metabolism and gene expression. The aim of the present study was therefore to investigate fuel partitioning during exposure to high plasma NEFA levels similar to those induced by high-fat diets. In particular, we compared the expression of different genes involved in the peripheral control mechanisms of energy balance in white fat and skeletal muscle and their relationships with overall and tissue glucose metabolism.

RESEARCH DESIGN AND METHODS

Surgical procedure and infusion protocol. Adult male lean (Fa/?) Zucker rats (Charles River, Lecco, Italy) of 200 g body weight were housed at 24°C with a 0700–1900 light cycle and had free access to water and food pellets. All of the animals were studied in the morning after 6 h of fasting. The study protocol was approved by the institutional review board of the University of Padova.

Surgical procedure was as previously described (17). At the end of anesthesia, the animals were placed in individual cages with a single slot for the catheters, which were kept under continuous tension. The patency of the arterial catheter was maintained by means of a slow infusion of saline solution.

In a first series of experiments, four groups of six animals each were studied. Twelve hours after surgery, an infusion of 20% triglyceride emulsion (Intralipid; Pharmacia and Upjohn, Milan, Italy) plus heparin (20 U/ml) was started and continued at a rate of 0.7 ml/h for either 3 or 24 h in the two experimental groups, whereas the two control groups received saline solution plus heparin at the same infusion rate. Blood samples were collected before and after 3 and 24 h of infusion to determine blood glucose, plasma insulin, NEFA, and leptin concentrations. The rats were then submitted to a euglycemic-hyperinsulinemic clamp to evaluate overall and tissue glucose utilization (see below).

In a second series of experiments, four other groups of six animals each were infused following the same protocol as that described above. After a 3- or 24-h infusion period, the rats were killed, and tissues were removed for quantification of gene expression. FAT/CD36, GLUT4, TNF-α, PPAR-γ, leptin, UCP2, and UCP3 mRNA levels were assessed in various muscles and visceral fat by means of Northern blotting or reverse transcriptase–polymerase chain reaction (RT-PCR) analysis (see below).

Tissue glucose utilization index. The glucose utilization index was assessed at the end of a euglycemic-hyperinsulinemic clamp. A primed contin-

uous infusion of human insulin (Actrapid HM; Novo Nordisk, Copenhagen) (dissolved in 0.9% saline solution) was administered at a rate of 3 mU/min for 120 min. Arterial blood was sampled at 5-min intervals throughout the clamp to determine plasma glucose concentrations. Starting 1 min after the beginning of the insulin infusion, glucose (20% wt/vol solution) was infused at a rate that was adjusted to maintain plasma glucose at preinfusion levels, as previously described (18).

Glucose utilization in vivo within the individual tissues was studied according to a previously described method (19,20). Briefly, a flash injection of 30 μCi of the nonmetabolizable glucose analog 2-deoxy-[1-³H]-D-glucose ([³H]-2DG) (Amersham Pharmacia, Arlington Heights, IL) was administered in 30 μl 0.9% NaCl solution through the femoral vein, and arterial blood samples were obtained at different times after the bolus administration. Upon completion of blood sampling, the rats were killed, and their adipose tissue and skeletal muscles were quickly removed, collected in liquid nitrogen, and kept frozen at −80°C for subsequent analysis. The glucose utilization index was derived from the amount of 2 deoxy-[1-H]-glucose-6-phosphate ([³H]-DGP) measured in the various tissues as previously described (19), thus using the accumulation of [³H]-DGP as an index of the glucose metabolic rate.

Northern blot and RT-PCR analysis. Total mRNA was isolated from adipose and muscle tissues using the RNAzol method (TM Cinna Scientific, Friendwood, TX), and Northern blots and hybridization were performed as previously described (21) using the cDNA probe of the rat GLUT4, UCP2, UCP3, and leptin genes. Quantitation was performed by scanning densitometry by Image Master VDS (Pharmacia-Biotechnology).

RT-PCR analyses were performed as described (16). *Taq* DNA polymerase (Promega) in 25 μl standard buffer (10 mmol/l Tris-HCl, pH 9, 50 mmol/l KCl, 0.1% Triton X-100, 2.5 mmol/l MgCl₂, and 200 μmol/l dNTPs) and 40 pmol of each specific sense and antisense oligonucleotide primer were used. The primer sequences chosen using the Gene-Works program (IntelliGenetics) were as follows: for FAT/CD36: 5'-AAG AGA GAT GAG GAA CCA GAG C-3', 5'-AGT GAA GGT TCG AAG ATG GC-3'; for TNF-α: 5'-ATG AGG ACT GAA AGC ATG ATC CGG GAC GTG G-3' and 5'-CAA TGA TCC CAA AGT AGA CCT GCC CAG ACT C-3'; for PPAR-γ: 5'-AAC TGC GGG GAA ACT TGG GAG ATT CTC C-3' and 5'-AAT AAT AAG GTG GAG ATG CGA GCT CC-3'; and for leptin: 5'-CAC CAA AAC CCT CAT CAA GCA-3' and 5'-AGC CTG CTC AGG GCC ACC ACC-3'. The primers for β-actin were added at the tenth cycle of each PCR amplification to avoid a plateau situation. All of the genes were amplified using 30 cycles at 94°C for 30 s, 60°C for 30 s, and 72°C for 30 s, followed by a 5-min final extension at 72°C. After amplification, 10 μl of the reaction mixture were separated by electrophoresis (1.2% agarose gel in Tris-acetate-EDTA buffer), visualized using ethidium bromide staining and a QuickImage-D system (Camberra Packard, Milan, Italy), and densitometrically analyzed using Phoretix 1D version 3.0. The number of cycles for the semiquantitative RT-PCR assay and the conditions of the reaction temperature were estimated to be optimal for a linear relationship between the amount of input template and the amounts of PCR product generated over a significant concentration range: 20–100 ng from total RNA. In particular, the linearity of the RT-PCR amplifications for all of the tested genes was measured at 15, 30, and 40 cycles (data not shown). The RT-PCR analyses were performed three times on the same sample from each of the six animals. The intra-assay coefficient of variation was <5%.

Plasma assays. Plasma glucose was measured by means of the glucose oxidase method (Glucose Analyzer; Beckman Instruments) and insulin by means of radioimmunoassay using rat standards (Techno Genetics, Milan, Italy; Linco Research, St. Charles, MO). NEFAs and leptin were determined using commercial kits (Boehringer Mannheim, KK, Tokyo) (recombinant rat leptin; Linco Research).

Statistical analysis. The results are presented as mean values ± SE. Statistical significance was assessed by means of analysis of variance. All of the analyses were made using the Statview statistical package. The level of significance was set at $P < 0.05$.

RESULTS

Metabolic parameters. Intralipid plus heparin infusion significantly increased plasma NEFA and insulin levels in comparison with the saline plus heparin–treated rats, but no significant differences in blood glucose were observed (Table 1). Intralipid treatment was also followed by a significant increase in serum leptin levels, which was evident after only 3 h of infusion (Table 1). No significant differences in food intake and body weight were noted between the two groups of animals (data not shown).

TABLE 1
Metabolic parameters measured during Intralipid plus heparin infusion or saline plus heparin infusion in normal-weight male Zucker rats

	Baseline	3 h	24 h
Free fatty acid (μmol/l)			
Saline	833.9 ± 69.5	694.2 ± 180.5	852.0 ± 54.0
Intralipid	811.2 ± 56.9	1817.4 ± 241.0*†	1861.7 ± 183.1*†
Glucose (mmol/l)			
Saline	5.7 ± 0.7	5.3 ± 0.6	5.7 ± 0.3
Intralipid	5.3 ± 0.2	6.0 ± 0.4	5.7 ± 0.2
Insulin (mU/l)			
Saline	30.1 ± 3.2	33.8 ± 9.5	23.5 ± 3.8
Intralipid	35.1 ± 5.2	74.4 ± 13.5*†	65.9 ± 15.0*†
Leptin (ng/ml)			
Saline	1.66 ± 0.16	1.47 ± 0.16*	0.84 ± 0.14*
Intralipid	1.92 ± 0.17	2.41 ± 0.30*†	2.37 ± 0.28*†

Data are means ± SE. *$P < 0.05$ vs. baseline; †$P < 0.05$ vs. saline plus heparin infusion.

Glucose infusion rate and tissue glucose utilization index during a euglycemic-hyperinsulinemic clamp. The glucose infusion rate was significantly lower in the Intralipid-infused rats than in the saline-treated rats after both 3 h of treatment (38.14 ± 1.74 vs. 18.38 ± 1.26 mg · kg^{-1} · min^{-1}; $P < 0.0002$) and 24 h of treatment (38.14 ± 1.74 vs. 17.89 ± 1.44 mg · kg^{-1} · min^{-1}; $P < 0.0002$). Figure 1 shows that the glucose utilization index was significantly reduced in the same animals in all of the oxidative muscles considered (the red portion of the quadriceps and gastrocnemius, and the soleus) after both 3 (Table 2) and 24 h (Fig. 1) of treatment. Increased NEFA availability was followed by an enhanced glucose uptake in visceral adipose tissue after 3 (Table 2) and 24 h (Fig. 1), but no difference was observed in white fiber–type muscles (white portion of quadriceps and gastrocnemius) or in the subcutaneous fat depot at either time point (Table 2 and Fig. 1). On the basis of these results, the following experiments were performed only in visceral fat and red fiber–type muscle (soleus).

Effects of Intralipid plus heparin infusion on gene expression in visceral fat and red fiber–type skeletal muscle. Postinfusion RT-PCR analysis using specific primers of the RNA isolated from visceral fat, and red fiber–type muscle showed a marked increase in FAT/CD36 mRNA in comparison with the levels in the saline-treated animals after both 3 and 24 h in the soleus but only after 24 h in visceral fat (Fig. 2).

Figure 3A shows that the enhancement of glucose uptake observed after Intralipid plus heparin infusion was paralleled by increased GLUT4 expression in visceral fat after 24 h. GLUT4 mRNA levels were significantly decreased in the soleus muscle after both 3 and 24 h of Intralipid infusion (Fig. 4A).

Because it has been widely reported that TNF-α can affect adipose tissue and muscle metabolism at various levels and it has been demonstrated that TNF-α modulates GLUT4 expression (22), we measured TNF-α's mRNA levels by RT-PCR after Intralipid plus heparin infusion. Figures 3B and 4B show that the levels of TNF-α mRNA were markedly higher in fat and soleus after both 3 and 24 h in comparison with those measured in the saline plus heparin–treated animals.

In addition, because the expression of PPAR-γ protein

appears to be modulated by calorie intake of fat (23), we investigated whether increased levels of plasma fatty acids could affect PPAR-γ mRNA levels and found that these were high after both 3 and 24 h in red fiber–type muscle (Fig. 4C), but only after 3 h in visceral fat (Fig. 3C).
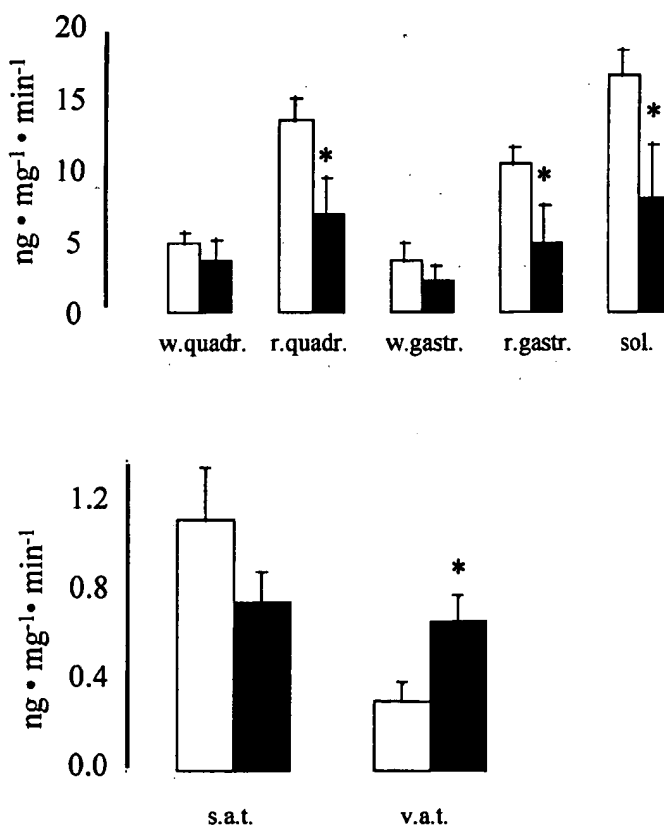
Moreover, the Intralipid infusion markedly increased

FIG. 1. Glucose utilization index measured in various skeletal muscles and adipose tissue depots after 24-h Intralipid plus heparin (■) or saline plus heparin (□) infusion in rats at the end of a euglycemic-hyperinsulinemic clamp (see RESEARCH DESIGN AND METHODS). Each bar represents the mean ± SE of six experiments for each group. r. gastr., red gastrocnemius; r. quadr., red quadriceps; s.a.t., subcutaneous adipose tissue; sol., soleus; v.a.t., visceral adipose tissue; w. gastr., white gastrocnemius; w. quadr., white quadriceps. *$P < 0.01$ vs. saline plus heparin infusion.

TABLE 2
Tissue glucose utilization indexes assessed at the end of a euglycemic-hyperinsulinemic clamp after 3 h of Intralipid plus heparin infusion or saline plus heparin infusion in normal-weight male Zucker rats

	Subcutaneous adipose tissue	Visceral adipose tissue	White quadriceps	Red quadriceps	White gastrocnemius	Red gastrocnemius	Soleus
Control	1.13 ± 0.23	0.32 ± 0.07	4.86 ± 0.65	13.46 ± 1.53	3.64 ± 1.16	10.36 ± 1.17	16.55 ± 1.70
Intralipid	0.93 ± 0.07	0.90 ± 0.17*	4.23 ± 0.50	8.60 ± 1.55*	3.83 ± 0.59	9.10 ± 1.33	10.13 ± 0.32†

The glucose utilization index was derived from the amount of [^{3}H]-2DGP measured in the various tissues as previously described (19), thus using the accumulation of [^{3}H]-2DGP as an index of the glucose metabolic rate. *$P < 0.05$ vs. saline plus heparin infusion; †$P < 0.01$ vs. saline plus heparin infusion.

the levels of leptin mRNA in fat after both 3 (not shown) and 24 h (Fig. 5A). Leptin gene expression in muscle was detected by RT-PCR only after 24 h of Intralipid infusion but was undetectable at baseline and after 3 h (Fig. 5B). Interestingly, mean plasma leptin levels were increased by the first 3-h Intralipid plus heparin in comparison with baseline (Table 1). These results are in line with the reported observation that high-fat feeding leads to increased leptin gene expression in rat adipose tissue and muscle (23).

Because adipose UCP2 has been found to be upregulated by a high-fat diet (24), we investigated whether increased plasma fatty acid levels affect the expression of UCP2 and UCP3 in the visceral adipose tissue and skeletal muscle of normal-weight rats. Figure 5C shows that the mRNA levels of UCP2 were increased 24 h after Intralipid plus heparin infusion in both fat and muscle with respect to those of saline-treated rats. Figure 5D shows that the mRNA levels of UCP3 were increased 24 h after Intralipid plus heparin infusion in muscle, but not in visceral fat, with respect to those of saline-treated rats. Both UCP2 and UCP3 mRNA levels were unchanged after 3-h Intralipid plus heparin infusion (data not shown).

DISCUSSION

The experimental approach used in this study mimics in a short time the increased circulating NEFA levels observed with a high-fat diet. As shown by the reduced glucose
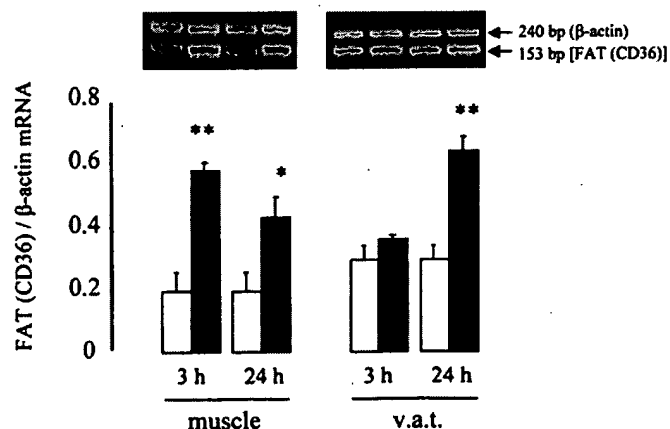

FIG. 2. FAT/CD36 expression after 3 or 24 h of treatment with saline plus heparin (□) or Intralipid plus heparin (■) infusion in the red fiber-type muscle (muscle) and visceral fat (v.a.t.) of normal-weight rats. Top panels: representative agarose gels showing RT-PCR analysis of FAT/CD36 and β-actin mRNA content in fat and muscle samples of one animal. Bottom panels: densitometric analysis of the ratios of FAT/CD36/β-actin mRNA abundance normalized to arbitrary units. Bars represent the mean ± SE of six animals (*P < 0.05, **P < 0.01 vs. saline plus heparin infusion). The FAT/CD36 mRNA levels did not change after saline infusion.

infusion rate during a euglycemic-hyperinsulinemic clamp (which was probably due to increased lipid use by red fiber–type muscles), insulin resistance develops as a result of the greater NEFA availability driven by Intralipid plus heparin infusion. Early enhancement of the gene expression of FAT/CD36 (which is suggested to be involved in NEFA uptake [25]) was evident in rat muscle after 3 h of infusion, and red fiber–type muscle insulin-dependent glucose uptake measured by [^{3}H]-2DG technique decreased in accordance with the competitive action of NEFA on glucose metabolism (4–7).

A number of molecular mechanisms may be involved. First, GLUT4 mRNA levels were reduced in the red fiber–type muscles of the rats infused with Intralipid plus heparin after both 3 and 24 h, and TNF-α gene expression (which is extremely low even if measured by RT-PCR under baseline conditions) was markedly enhanced. This finding is relevant because, although high TNF-α expression has been demonstrated in the adipose tissue of insulin-resistant obese rodents (26) and humans (27), the fact that circulating TNF-α levels in insulin-resistant obese subjects were not detected in all studies (28) raised doubts as to whether adipose-released TNF-α really affects muscle metabolism. Our finding that high levels of circulating NEFAs can directly increase TNF-α mRNA levels in red fiber–type muscle suggests that the putatively increased TNF-α protein may act in a paracrine way in muscle tissues. Because an inverse linear relationship between the maximum glucose disposal rate and muscle TNF-α has been reported (29), this may constitute a critical point in the development of insulin resistance. It has been shown that TNF-α impairs insulin receptor signaling (30,31) and that TNF-α knockout mice have more GLUT4 protein expressed in muscle tissue (32). Our findings suggest that greater NEFA availability may shift red fiber–type muscle metabolism to preferential use of lipids rather than carbohydrates as fuel substrates. This may be at least partially due to the induction of TNF-α and the inhibition of GLUT4 gene expression.

There is a simultaneous increase in the insulin sensitivity of visceral but not subcutaneous fat. The Intralipid infusion significantly increased GLUT4 gene expression in visceral adipose tissue, thus suggesting that energy fuels may be preferentially partitioned to fat rather than muscle. It is interesting to note that both GLUT4 and TNF-α increased in visceral adipose tissue but not in red fiber–type muscles. GLUT4 favors glucose utilization, whereas TNF-α counteracts excessive fat storage by means of various mechanisms (e.g., by stimulating lipolysis [33] and decreasing the activity of adipose tissue lipoprotein lipase [34]). A similar pattern of events has been observed in the
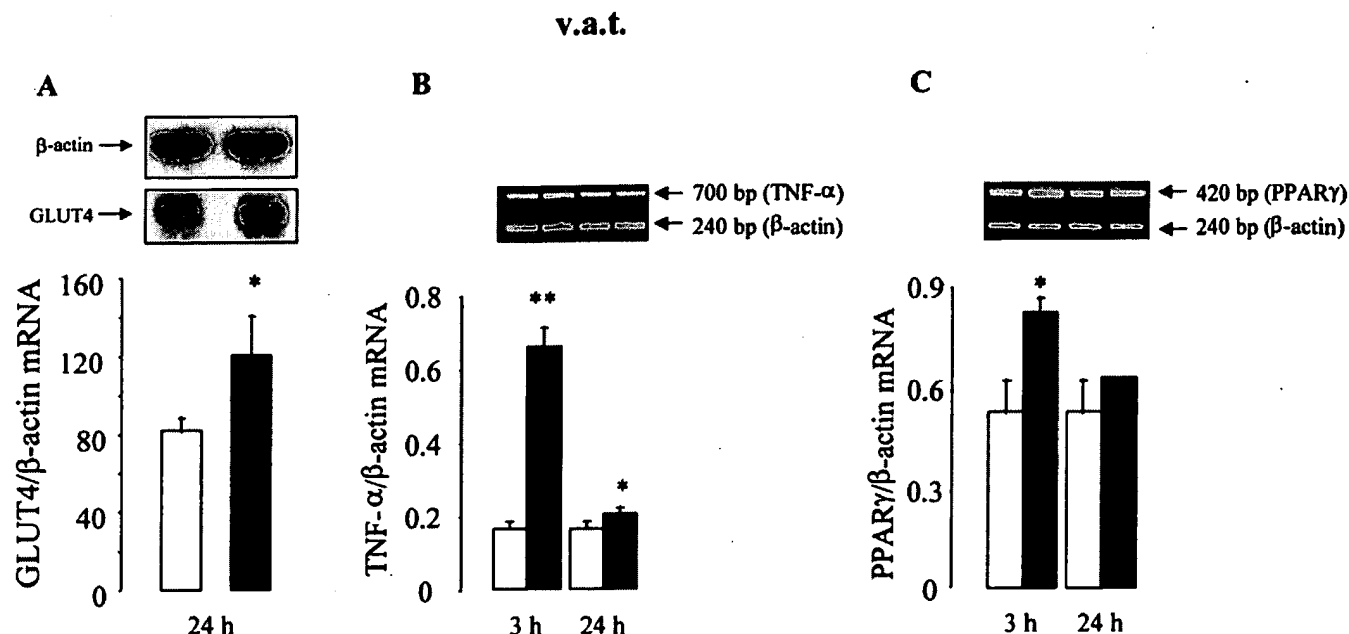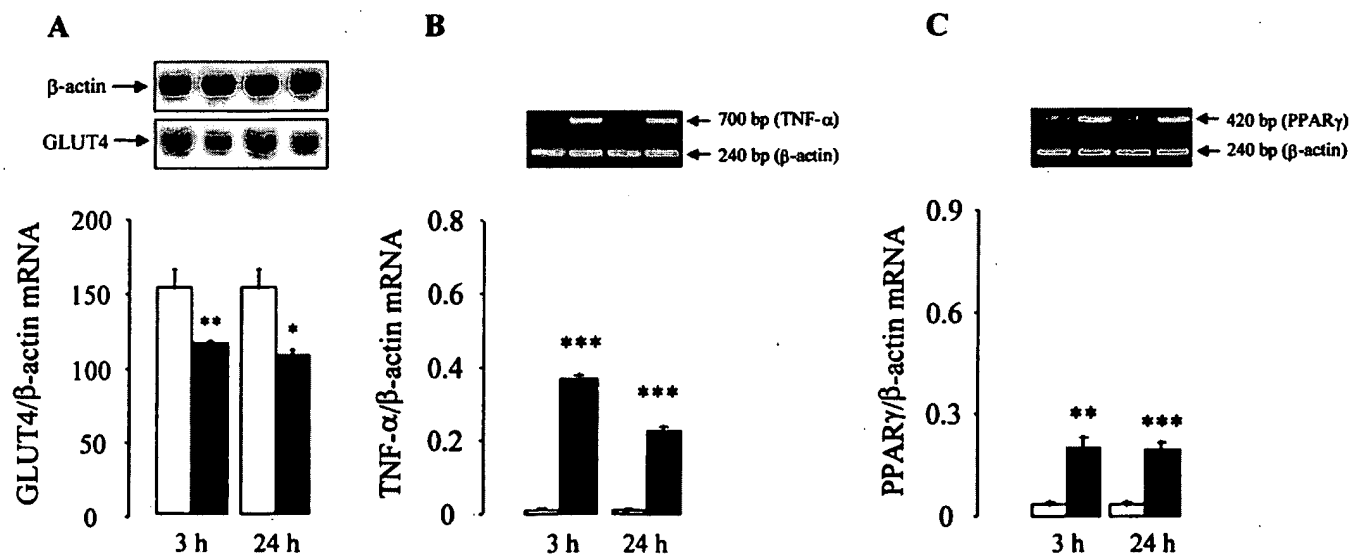
v.a.t.

FIG. 3. GLUT4, TNF-α, and PPARγ mRNA levels after 3 or 24 h of treatment with saline plus heparin (□) or Intralipid plus heparin (■) infusion in the visceral fat (v.a.t.) of normal weight rats. Top panels: representative autoradiograms showing Northern blotting analysis of GLUT4 and β-actin mRNA (A) and representative agarose gels showing RT-PCR analysis of TNF-α (B), PPAR-γ (C), and β-actin (B and C) mRNA content in fat samples of one animal. Bottom panels: densitometric analysis of the ratios of GLUT4/β-actin, TNF-α/β-actin, and PPAR-γ/β-actin mRNA abundance normalized to arbitrary units. Bars represent the mean ± SE of six animals (*P < 0.05 and **P < 0.01 vs. saline plus heparin infusion). The GLUT4, TNF-α, and PPAR-γ mRNA levels did not change after saline plus heparin infusion.

dynamic phase of several animal models of obesity in which fat accumulation is accompanied by increased glucose uptake and GLUT4 gene expression in adipose tissue, and insulin resistance develops at the muscle level (17).

The increased expression of PPAR-γ and leptin in both muscle and adipose tissue after Intralipid infusion may be a means of counterbalancing the development of insulin resistance. After Intralipid infusion, all of the studied tissues showed a higher expression of the PPAR-γ gene, a major adipogenic transcription factor that is poorly expressed in preadipocytes but turned on during adipogenesis (35) and that regulates the expression of most adi-

muscle

FIG. 4. GLUT4, TNF-α, and PPAR-γ mRNA levels after 3 or 24 h of treatment with saline plus heparin (□) or Intralipid plus heparin (■) infusion in the red fiber–type muscle (soleus) of normal-weight rats. Top panels: representative autoradiograms showing Northern blot analysis of GLUT4 and β-actin mRNA (A) and representative agarose gels showing RT-PCR analysis of TNF-α (B), PPAR-γ (C), and β-actin (B and C) mRNA content in muscle samples of one animal. Bottom panels: densitometric analysis of the ratios of GLUT4/β-actin, TNF-α/β-actin, and PPAR-γ/β-actin mRNA abundance normalized to arbitrary units. Bars represent the mean ± SE of six animals (*P < 0.05, **P < 0.001, ***P < 0.0001 vs. saline plus heparin infusion). The GLUT4, TNF-α, and PPAR-γ mRNA levels did not change after saline plus heparin infusion.
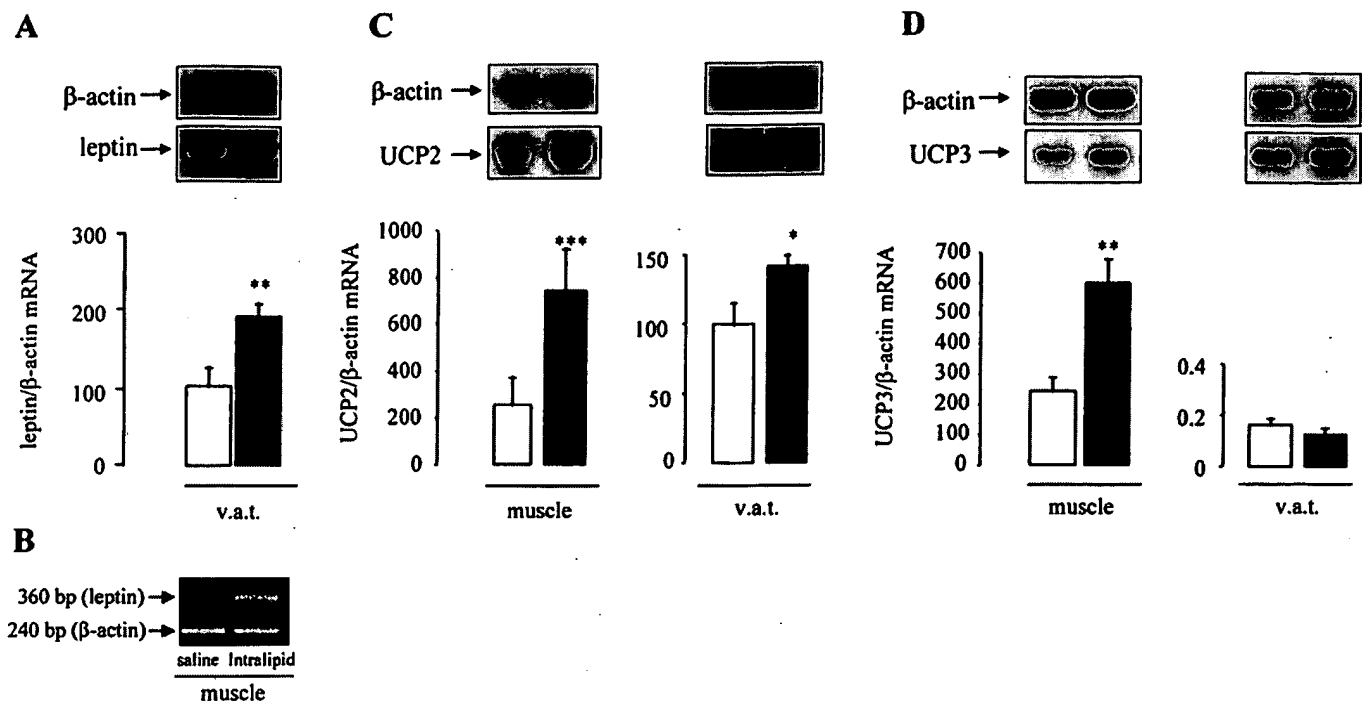
FIG. 5. Leptin, UCP2, and UCP3 expression after 24 h of treatment with saline plus heparin (□) or Intralipid plus heparin (■) infusion in the visceral fat (v.a.t.) and red fiber-type muscle (muscle) of normal-weight rats. Top panels: representative autoradiograms showing Northern blot analysis of leptin (A), UCP2 (C), UCP3 (D), and β-actin mRNA content in fat and muscle (except for leptin) samples of one animal. Bottom panels: densitometric analysis of the ratios of leptin/β-actin, UCP2/β-actin, and UCP3/β-actin mRNA abundance normalized to arbitrary units. B: Representative agarose gel showing RT-PCR analysis of leptin and β-actin mRNA content in muscle samples of one animal. Densitometric analysis of the ratios of leptin/β-actin mRNA abundance is not reported because in saline plus heparin–treated animals, muscle leptin is undetectable. Bars represent the mean ± SE of six animals (*P < 0.05, **P < 0.01, ***P < 0.0001 vs. saline infusion). The leptin, UCP2, and UCP3 mRNA levels did not change after saline plus heparin infusion.

pocyte genes (35). Three different groups have recently demonstrated that PPAR-γ is required for adipogenesis in vivo (36–38), and Barroso et al. (39) have recently reported that two loss-of-function PPAR-γ mutations are associated with severe insulin resistance and type 2 diabetes in humans. Although such mutations are rare, the implication that PPAR-γ is required for normal insulin sensitivity at least in some individuals is an important advance.

It can also be speculated that the high level of PPAR-γ expression observed by us may confer some protection against the development of the skeletal muscle insulin resistance associated with increased circulating NEFA levels. This is consistent with the fact that thiazolidinediones (TZDs) may improve insulin action in skeletal muscle by upregulating the expression of PPAR-γ (40). Furthermore, Kubota et al. (37) demonstrated that, although apparently normal on a regular diet, mice that are heterozygous for PPAR-γ deficiency are partially resistant to high-fat diet–induced obesity and markedly resistant to the insulin resistance that normally accompanies such obesity. Both PPAR-γ overactivity due to TZD stimulation and PPAR-γ underactivity due to haploinsufficiency may protect against NEFA-induced insulin resistance. Lowell (41) suggested that PPAR-γ can be seen as a "thrifty gene" that promotes fat storage to survive starvation when food is scarce and produces excessive fat storage leading to disease when food is plentiful. The mechanism by means of which the TZD-mediated stimulation of PPAR-γ improves insulin resistance has not been definitively established (42), but it is probably related to the transcription

factor's ability to increase the number of small adipocytes by stimulating adipogenesis and to decrease the number of large adipocytes, which are known to produce excess amounts of TNF-α and free fatty acids. Although not affecting adipogenesis, PPAR-γ haploinsufficiency limits further adipocyte hypertrophy, possibly by increasing leptin expression. Kubota et al. (37) have reported that leptin mRNA and circulating protein levels are elevated in high fat-fed PPAR-γ^{+/−} mice, possibly because of a decrease in the PPAR-γ–mediated inhibition of leptin gene expression.

Under our experimental conditions, high levels of circulating NEFAs induced leptin expression in both fat and muscle and increased plasma leptin levels. We did not measure body composition (in particular body fat content), but it seems unlikely that the rapid induction of leptin gene expression observed after Intralipid infusion was a consequence of an increase in fat mass. Although the effects of leptin on satiety are mainly due to its activation of hypothalamic receptors (43), there is also substantial evidence that leptin has important peripheral effects (44,45), including the stimulation of lipolysis with lipid oxidation in white fat pads ex vivo (46) and decreasing in vivo tissue triglyceride stores (47,48). It can therefore be hypothesized that, under our experimental conditions, leptin has an autocrine/paracrine function, i.e., it limits excess fat storage in adipose tissue. Furthermore, leptin mRNA, which is generally undetectable in the skeletal muscle of nonobese rodents (5,49), increased 24 h after an increase in plasma NEFA levels. In skeletal muscle, leptin may be important in the regulation of intermediate metab-

olism (particularly lipid oxidation and storage) (1,45,48), energy expenditure (50), and insulin signaling (51,52). Interestingly, it has been reported that, regardless of its effect on food intake, leptin leads to a marked improvement in insulin sensitivity and glucose disposal in a mouse model of lipodistrophy (53). Leptin expression in the fat and muscle of subjects with high circulating NEFA levels could therefore be involved in counterbalancing excessive fat accumulation and the development of insulin resistance.

Finally, our data demonstrate that Intralipid infusion increased UCP2 and UCP3 mRNA in both adipose tissue and muscle. These findings are in line with the enhanced UCP2 gene expression in both tissues observed in obese subjects (54,55), whose circulating NEFA levels are commonly high. It has been reported that PPAR-γ agonists induce UCP2 gene expression in adipocytes (56), and TNF-α administration increases UCP2 and UCP3 mRNA levels in rat skeletal muscle (57). This molecular event may be ultimately aimed at dissipating energy excess, but UCP2 and UCP3 may also be involved in fatty acid metabolism in the case of a large supply of nutrients (55,58).

In conclusion, our findings suggest that NEFAs are involved in the partitioning of calories to fat by modulating the expression of various genes: FAT/CD36, which enhances fatty acid flux into adipocytes and muscle cells; GLUT4, which is differently affected in skeletal muscle and adipose tissue, thus favoring the preferential use of glucose for triglyceride synthesis; TNF-α, which probably plays a crucial role in the development of insulin resistance in skeletal muscle; PPAR-γ, which promotes cell differentiation and fat storage and also modulates peripheral insulin sensitivity; and leptin and UCPs, which control energy intake and dissipation. Although it is difficult with our experimental approach to attribute the effects seen on the mRNA levels only to elevated plasma NEFAs because also insulin, leptin, and triglyceride levels are increased, nevertheless, it seems possible to speculate that the above mechanisms during a high-fat diet may unbalance energy homeostasis and channel the fuels toward adipose tissue, thus leading to obesity.

REFERENCES

1. Ferrannini E, Barret EJ, Bevilacqua S, DeFronzo RA: Effect of fatty acids on glucose production and utilization in man. *J Clin Invest* 72:1737–1747, 1983
2. Nuutila P, Koivisto VA, Knuuti J, Ruotsalainen U, Teräs M, Haaparanta M, Bergman J, Solin O, Voipio-Pulkki LM, Wegelius U, Yki-Jarvinen H: Glucose-free fatty acid cycle operates in human heart and skeletal muscle in vivo. *J Clin Invest* 89:1767–1774, 1992
3. Hotamisligil GS, Spiegelman BM: Tumor necrosis factor α: a key component of the obesity-diabetes link. *Diabetes* 43:1271–1278, 1994
4. Randle PJ, Garland PB, Hales CN, Newsholme EA: The glucose fatty acid cycle: its role in insulin sensitivity and the metabolic disturbances of diabetes mellitus. *Lancet* i:785–789, 1963
5. Wang J, Liu R, Hawkins M, Barzilai N, Rossetti L: A nutrient sensing pathway regulates leptin gene expression in muscle and fat. *Nature* 393:684–688, 1998
6. Ruderman NB, Saha AS, Vavvas D, Witters LA: Malonyl-CoA, fuel sensing and insulin resistance. *Am J Physiol* 276:E1–E18, 1999
7. Bavenholm PN, Pigon J, Saha AK, Ruderman NB, Efendic S: Fatty acid oxidation and the regulation of malonyl-CoA in human muscle. *Diabetes* 49:1078–1083, 2000
8. Boss O, Samec S, Paoloni-Giacobino A, Rossier C, Dulloo A, Seydoux J, Muzzin P, Giacobino J-P: Uncoupling protein-3: a new member of the mitochondrial carrier family with tissue-specific expression. *FEBS Lett* 408:39–42, 1997
9. Fleury C, Neverova M, Collins S, Raimbault S, Champigny O, Levi-Meyrueis C, Bouillaud F, Seldin MF, Surwit RS, Ricquier D, Warden CH: Uncoupling protein-2: a novel gene linked to obesity and hyperinsulinemia. *Nat Genet* 15:269–272, 1997
10. Björntorp P, Smith U: The effect of fat cell size on subcutaneous adipose tissue metabolism. *Matrix Biol* 2:37–42, 1976
11. Tontonoz P, Graves R, Budavari A, Erdjiument-Bromage H, Lui M, Hu E, Temps P, Spiegelman B: Adipocyte-specific transcription factor ARF 6 is a heterodimeric complex of two nuclear hormone receptors, and RXR. *Nucleic Acids Res* 22:5628–5634, 1994
12. Tontonoz P, Nagy L, Alvarez JGA, Thomszy VA, Evans RM: PPARγ promotes monocyte/macrophage differentiation and uptake of oxidised LDL. *Cell* 93:241–252, 1998
13. Saltiel AR, Olefsky JM: Thiazolidinediones in the treatment of insulin resistance and type II diabetes. *Diabetes* 45:1661–1669, 1996
14. Lehmann JM, Moore LB, Smith-Oliver TA, Wilkinson WO, Willson TM, Kliewer SA: An antidiabetic thiazolidinedione is a high affinity ligand for peroxisome proliferator-activated receptor γ. *J Biol Chem* 270:12953–12956, 1995
15. Vidal-Puig AJ, Considine RJ, Jimenez-Liñan M, Werman A, Pories WJ, Caro JF, Flier JS: Peroxisome proliferator-activated receptor gene expression in human tissues. *J Clin Invest* 99:2416–2422, 1997
16. Nisoli E, Carruba MO, Tonello C, Macor C, Federspil G, Vettor R: Induction of fatty acid translocase/CD 36, peroxisome proliferator-activated receptor-γ2, leptin, uncoupling proteins 2 and 3, and tumor necrosis factor-α gene expression in human subcutaneous fat by lipid infusion. *Diabetes* 49:319–324, 2000
17. Vettor R, Zarjevski N, Cusin I, Rohner-Jeanrenaud F, Jeanrenaud B: Induction and reversibility of an obesity syndrome by intracerebroventricular neuropeptide Y administration to normal rats. *Diabetologia* 37:1202–1208, 1994
18. DeFronzo RA, Tobine JD, Andres R: Glucose clamp technique: a method for quantifying insulin secretion and resistance. *Am J Physiol* 237:E214–E223, 1979
19. Ferré P, Burnol AF, Leturque A, Terrettaz J, Penicaud L, Jeanrenaud B, Girard J: Glucose utilization in vivo and insulin-sensitivity of rat brown adipose tissue in various physiological and pathological conditions. *Biochem J* 233:249–252, 1985
20. James DE, Jenkins AB, Kraegen W: Heterogeneity of insulin action in individual muscles in vivo: euglycemic clamp studies in rats. *Am J Physiol* 248:E567–E574, 1985
21. Postic C, Leturque A, Rencurel F, Printz RL, Forest C, Granner DK, Girard J: The effects of hyperinsulinemia and hyperglycemia on GLUT4 and hexokinase II mRNA and protein in rat skeletal muscle and adipose tissue. *Diabetes* 42:922–929, 1993
22. Stephens JM, Lee J, Pilch PF: Tumor necrosis factor-alpha induced insulin resistance in 3T3-L1 adipocytes is accompanied by a loss of insulin receptor-mediated signal transduction. *J Biol Chem* 272:971–976, 1997
23. Rousseau V, Becker DJ, Ongemba LN, Rahier J, Henquin JC, Brichard S: Developmental and nutritional changes of ob and PPAR gamma 2 gene expression in rat white adipose tissue. *Biochem J* 321:451–456, 1997
24. Matsuda J, Hosoda K, Itoh H, Son C, Doi K, Tanaka T, Fukunaga Y, Inoue G, Nishimura H, Yoshimasa Y, Yamori Y, Nakao K: Cloning of rat uncoupling protein-3 and uncoupling protein-2 cDNAs: their gene expression in rats fed high-fat diet. *FEBS Lett* 418:200–204, 1997
25. Abumrad NA, Harmon CM, Ibrahimi A: Membrane transport of long-chain

fatty acids: evidence for a facilitated process. *J Lipid Res* 39:2309–2318, 1998

26. Hotamisligil G, Shargill NS, Spiegelman BM: Adipose expression of tumor necrosis factor-α: direct role in obesity-linked insulin resistance. *Science* 259:87–91, 1993

27. Hotamisligil GS, Arner P, Caro JF, Atkinson RL, Spiegelman BM: Increased adipose tissue expression of tumor necrosis factor-α in human obesity and insulin resistance. *J Clin Invest* 95:2409–2415, 1995

28. Socher SH, Martinez D, Craig JB, Kuhn JG, Oliff A: Tumor necrosis factor not detectable in patients with clinical cancer cachexia. *J Natl Cancer Inst* 80:595–598, 1988

29. Saghizadeh M, Ong JM, Garvey WT, Henry RR, Kern PA: The expression of TNFα by human muscle: relationship to insulin resistance. *J Clin Invest* 97:1111–1116, 1996

30. Liu LS, Spelleken M, Rohrig K, Hauner H, Eckel J: Tumor necrosis factor-alpha acutely inhibits insulin signaling in human adipocytes: implication of the p80 tumor necrosis factor receptor. *Diabetes* 47:515–522, 1998

31. Peraldi P, Xu M, Spiegelman BM: Thiazolidionediones block tumor necrosis factor-alpha-induced inhibition of insulin signaling. *J Clin Invest* 100:1863–1869, 1997

32. Uysal KT, Wiesbrock SM, Marino MW, Hotamisligil GS: Protection from obesity-induced insulin resistance in mice lacking TNF-alpha function. *Nature* 389:610–614, 1997

33. Green A, Dobias SB, Walters DJ, Brasier AR: Tumor necrosis factor increases the rate of lipolysis in primary cultures of adipocytes without altering levels of hormone-sensitive lipase. *Endocrinology* 134:2581–2588, 1994

34. Kawakami M, Cerami A: Studies of endotoxin-induced decrease in lipoprotein lipase activity. *J Exp Med* 154:631–639, 1981

35. Tontonoz P, Hu E, Spiegelman BM: Stimulation of adipogenesis in fibroblasts by PPARγ2, a lipid activated transcription factor. *Cell* 79:1147–1156, 1994

36. Barak Y, Nelson MC, Ong ES, Jones YZ, Ruiz-Lozano P, Chien KR, Koder A, Evans RM: PPAR gamma is required for placental, cardiac, and adipose tissue development. *Mol Cell* 4:585–595, 1999

37. Kubota N, Terauchi Y, Miki H, Tamemoto H, Yamauchi T, Komeda K, Satoh S, Nakano R, Ishii C, Sugiyama T, Eto K, Tsubamoto Y, Okuno A, Murakami K, Sekihara H, Hasegawa G, Naito M, Toyoshima Y, Tanaka S, Shiota K, Kitamura T, Fujita T, Ezaki O, Aizawa S, Nagai R, Tobe K, Kimura S, Kadowaki T: PPAR gamma mediates high-fat diet-induced adipocyte hypertrophy and insulin resistance. *Mol Cell* 4:597–609, 1999

38. Rosen ED, Sarraf P, Troy AE, Bradwin G, Moore K, Milstone DS, Spiegelman BM, Mortensen RM: PPAR gamma is required for the differentiation of adipose tissue in vivo and in vitro. *Mol Cell* 4:611–617, 1999

39. Barroso I, Gurnell M, Crowley VEF, Agostini M, Schwabe JW, Soos MA, Masien GL, Williams TDM, Lewis H, Schafer AJ, Chatterjee VKK, O'Rahilly S: Dominant negative mutations in human PPARgamma associated with severe insulin resistance, diabetes mellitus and hypertension. *Nature* 402:880–883, 1999

40. Park KS, Ciaraldi TP, Lindgren K, Abrams-Carter L, Mudaliar S, Nikoulina SE, Tufari SR, Veerkamp JH, Vidal-Puig A, Henry RR: Troglitazone effects on gene expression in human skeletal muscle of type II diabetes involve up-regulation of peroxisome proliferator-activated receptor-gamma. *J Clin Endocrinol Metab* 83:2830–2835, 1998

41. Lowell BB: PPARgamma: an essential regulator of adipogenesis and modulator of fat cell function. *Cell* 99:239–242, 1999

42. Spiegelman BM: PPAR-gamma: adipogenic regulator and thiazolidinedione receptor. *Diabetes* 47:507–514, 1998

43. Flier JS: Leptin expression and action: new experimental paradigm. *Proc Natl Acad Sci U S A* 94:4242–4245, 1997

44. Bai Y, Zhang S, Kim K-S, Lee J-K, Kim K-H: Leptin inhibits acetyl-CoA carboxylase in 3T3 pre-adipocytes. *J Biol Chem* 271:13939–13942, 1996

45. Muoio DM, Dohn GL, Fiedorek FT, Tapscott EB, Coleman RA: Leptin directly alters lipid partitioning in skeletal muscle. *Diabetes* 46:1360–1363, 1997

46. Fruhbeck G, Aguado M, Martinez JA: In vitro lipolytic effect of leptin on mouse adipocytes: evidence for a possible autocrine/paracrine role of leptin. *Biochem Biophys Res Commun* 240:590–594, 1997

47. Chen G, Koyama K, Yuan X, Lee Y, Zhou YT, O'Doherty R, Newgard CB, Unger RH: Disappearance of body fat in normal rats induced by adenovirus-mediated leptin gene therapy. *Proc Natl Acad Sci U S A* 93:14795–14799, 1996

48. Shimabukuro M, Koyama K, Chen G, Wang MY, Trieu F, Lee Y, Newgard CB, Unger RH: Direct antidiabetic effect of leptin through triglyceride depletion of tissues. *Proc Natl Acad Sci U S A* 94:4637–4641, 1997

49. Zhang Y, Proenca R, Maffei M, Barone M, Leopold L, Friedman JM: Positional cloning of the mouse obese gene and its human homologue. *Nature* 372:425–432, 1994

50. Gong D-W, He Y, Karas M, Reitman M: Uncoupling protein-3 is a mediator of thermogenesis regulated by thyroid hormone, β3-adrenergic agonists, and leptin. *J Biol Chem* 272:24129–24132, 1997

51. Kellerer M, Koch M, Metzinger E, Mushack J, Capp E, Haring HU: Leptin activates PI-3 kinase in C2C12 myotubes via janus-kinase-2 (JAK-2) and insulin receptor substrate-2 (IRS-2) dependent pathways. *Diabetologia* 40:1358–1362, 1997

52. Kim Y-B, Uotani S, Flier JS, Kahn BB: In vivo administration of leptin rapidly activates phosphoinositide-3-kinase in insulin sensitive tissues (Abstract). *Diabetes* 47:A317, 1998

53. Shimomura I, Hammer RE, Ikemoto S, Brown MS, Goldstein JL: Leptin reverses insulin resistance and diabetes mellitus in mice with congenital lipodystrophy. *Nature* 401:73–76, 1999

54. Millet L, Vidal H, Andreelli F, Larrouy D, Riou J-P, Ricquier D, Laville M, Langin D: Increased uncoupling protein-2 and -3 mRNA expression during fasting in obese and lean humans. *J Clin Invest* 100:2665–2670, 1997

55. Simoneau J-A, Kelley DE, Neverova M, Warden CH: Overexpression of muscle uncoupling protein 2 content in human obesity associates with reduced skeletal muscle lipid utilization. *FASEB J* 12:1739–1745, 1998

56. Aubert J, Champigny O, Saint-Marc P, Negrel R, Collins S, Ricquier D, Ailhaud G: Up-regulation of UCP-2 gene expression by PPAR agonists in preadipose and adipose cells. *Biochem Biophys Res Commun* 238:606–611, 1997

57. Busquets S, Sanchis D, Alvarez B, Ricquier D, Lopez-Soriano FJ, Argilés JM: In the rat, tumor necrosis factor α administration results in an increase in both UCP2 and UCP3 mRNAs in skeletal muscle: a possible mechanism for cytokine-induced thermogenesis? *FEBS Lett* 440:348–350, 1998

58. Samec S, Seydoux J, Dulloo AG: Role of UCP homologues in skeletal muscles and brown adipose tissue: mediators of thermogenesis or regulators of lipids as fuel substrate? *FASEB J* 12:715–724, 1998

Overnight Lowering of Free Fatty Acids With Acipimox Improves Insulin Resistance and Glucose Tolerance in Obese Diabetic and Nondiabetic Subjects

Ana T.M.G. Santomauro, Guenther Boden, Maria E.R. Silva, Dalva M. Rocha, Rosa F. Santos, Mileni J.M. Ursich, Paula G. Strassmann, and Bernardo L. Wajchenberg

Obesity is commonly associated with elevated plasma free fatty acid (FFA) levels, as well as with insulin resistance and hyperinsulinemia, two important cardiovascular risk factors. What causes insulin resistance and hyperinsulinemia in obesity remains uncertain. Here, we have tested the hypothesis that FFAs are the link between obesity and insulin resistance/hyperinsulinemia and that, therefore, lowering of chronically elevated plasma FFA levels would improve insulin resistance/hyperinsulinemia and glucose tolerance in obese nondiabetic and diabetic subjects. Acipimox (250 mg), a long-acting antilipolytic drug, or placebo was given overnight (at 7:00 P.M., 1:00 A.M., 7:00 A.M.) to 9 lean control subjects, 13 obese nondiabetic subjects, 10 obese subjects with impaired glucose tolerance, and 11 patients with type 2 diabetes. Euglycemic-hyperinsulinemic clamps and oral glucose tolerance tests (75 g) were performed on separate mornings after overnight Acipimox or placebo treatment. In the three obese study groups, Acipimox lowered fasting levels of plasma FFAs (by 60–70%) and plasma insulin (by ~50%). Insulin-stimulated glucose uptake during euglycemic-hyperinsulinemic clamping was more than twofold higher after Acipimox than after placebo. Areas under the glucose and insulin curves during oral glucose tolerance testing were both ~30% lower after Acipimox administration than after placebo. We conclude that lowering of elevated plasma FFA levels can reduce insulin resistance/hyperinsulinemia and improve oral glucose tolerance in lean and obese nondiabetic subjects and in obese patients with type 2 diabetes. *Diabetes* 48:1836–1841, 1999

Obesity is commonly associated with insulin resistance and hyperinsulinemia (1,2), two important cardiovascular risk factors (3). The fact that insulin resistance and hyperinsulinemia increase with weight gain and decrease with weight loss (4–6) suggests that the two have a cause-and-effect relationship. It has recently been suggested that free fatty acids (FFAs) are the link between obesity and insulin resistance/hyperinsulinemia (7), based on evidence showing that plasma FFA levels are commonly elevated in obesity (8,9) and that acute elevations of plasma FFA levels produce insulin resistance in healthy and diabetic subjects (10–15). This alone does not prove, however, that the chronically elevated plasma FFAs are responsible for the insulin resistance in obese subjects. Causal links among insulin resistance, hyperinsulinemia, and FFAs might be more convincingly established by the demonstration that lowering of plasma FFAs also lowers insulin resistance and hyperinsulinemia. So far, this has not been shown. Fulcher et al. (16) have failed to see a beneficial effect on insulin resistance of overnight lowering of plasma FFAs in patients with type 2 diabetes. We were similarly unable to demonstrate a statistically significant reduction in insulin resistance after acutely lowering plasma FFAs for 6 h in four healthy volunteers (11). It appears likely, however, that these failures were caused by problems related to the experimental designs (low clamp insulin infusion rates in the Fulcher study, insufficient number of experiments in our study). It was, therefore, the first objective of the present study to test the hypothesis that overnight lowering of plasma FFA concentrations with Acipimox, a long-acting antilipolytic drug, would reduce insulin resistance in obese subjects with varying degrees of insulin resistance.

FFAs not only produce insulin resistance (10–15), but also stimulate insulin secretion (7). Hence, an improvement in insulin resistance produced by lowering of plasma FFAs may not necessarily result in an improvement in glucose tolerance, which depends primarily on the amount of insulin released in response to a glucose challenge and on target tissue sensitivity to the released insulin. To our knowledge, there are presently no published data relating FFA-induced changes in insulin resistance to glucose tolerance. A second objective of this study was, therefore, to evaluate the relationship between FFA-induced changes in insulin resistance and secretion and oral glucose tolerance in the same obese subjects.

TABLE 1
Clinical characteristics of the study subjects

Group	Sex (F/M)	Age (years)	Race (n) White	Race (n) Black	Race (n) Mulatto	Weight (kg)	Body surface area (m²)	BMI (kg/m²)
Lean nondiabetic	7/2	39.1 ± 2.3	5	2	2	59.9 ± 2.2	1.61 ± 0.4	22.9 ± 0.26
Obese nondiabetic	10/3	39.4 ± 1.3	7	3	3	83.8 ± 2.6*	1.82 ± 0.03*	34.1 ± 0.8*
Obese IGT	8/2	43.5 ± 1.6	6	2	2	81.6 ± 4.0*	1.83 ± 0.06*	32.3 ± 1.1*
Obese diabetic	9/2	43.6 ± 1.4	6	2	3	80.5 ± 3.9*	1.79 ± 0.05*	32.4 ± 1.0*

Data are means ± SE or n. *P < 0.01 vs. lean nondiabetic control subjects.

RESEARCH DESIGN AND METHODS

Subjects. We have studied 9 healthy nonobese control subjects without a family history of diabetes, hypertension, dyslipidemia, or other known endocrine or metabolic disease and 34 obese subjects divided into three groups according to the degree of their glucose tolerance. Their clinical characteristics are shown in Table 1. There were no significant differences between the four groups with respect to age, sex, or race. Body weight and body surface area were significantly greater in the obese subjects than in the lean control subjects (P < 0.01). The obese nondiabetic subjects with impaired glucose tolerance (IGT) and the patients with recently diagnosed type 2 diabetes had similar weights, body surface areas, and BMIs.

Patients with clinically significant micro- or macrovascular complications and patients taking lipid-lowering agents or insulin were excluded. None of the volunteers had taken any drugs for at least 3 weeks before the study, and weight had been stable in all subjects for at least 3 months before the study. All subjects consumed a diet containing at least 200 g of carbohydrate for 3 days before the study began. No subject participated in strenuous physical activity. This study was approved by the Ethical Committee of The Hospital das Clinicas, and all subjects gave written informed consent before participation.

Study protocol. All study subjects ate a standard supper at ~7:00 P.M. Acipimox, a potent long-acting antilipolytic nicotinic acid (NA) analog (17), or a placebo was administered in doses of 250 mg at 7:00 P.M. the night before and at 1:00 and 7:00 A.M. on the day of study. The sequence of placebo and Acipimox administration was randomized. At 7:00 A.M. on the day of study, an intravenous cannula was inserted into an antecubital vein, which was kept open with a slow saline drip, and the arm was heated to 50°C in a Plexiglas box to arterialize the blood. A second cannula was inserted into a contralateral antecubital vein for infusion of insulin and glucose. After an equilibration period of 30 min, basal samples were collected for determination of plasma glucose, insulin, and FFA concentrations. Then, euglycemic-hyperinsulinemic clamps were performed by infusing insulin (Novolin R; Novo-Nordisk, Bagsvaerd, Denmark) for 180 min at a rate of 7 pmol · kg⁻¹ · min⁻¹. Euglycemia (~5 mmol/l) was maintained with a variable-rate infusion of 50% glucose. Blood glucose levels were determined at 10-min intervals, and glucose infusion rates (GIRs) were adjusted as needed. Urinary glucose excretion was measured during the clamps and used to correct calculation of peripheral glucose uptake.

On a different day, oral glucose tolerance tests were started at ~7:00 A.M.; 75 g of glucose was administered as a 25% glucose solution over 15 min, and blood samples were drawn at –45, –30, 0, 30, 60, 90, 120, and 180 min for measurement of plasma glucose, insulin, and FFA concentrations.

Analytical methods. Carbohydrate and fat oxidation rates were determined by indirect calorimetry with a computerized flow-through canopy gas analyzer system (Deltatrac Metabolic Monitor; Datex, Helsinki, Finland). Rates of protein oxidation were calculated from urinary nitrogen (N) excretion. Rates of protein oxidation were used to determine the nonprotein respiratory quotient (npRQ) using the tables of Lusk, which are based on an npRQ of 0.707 for 100% fat oxi-

dation and 1.00 for 100% carbohydrate oxidation. It was assumed that for each gram of N excreted in the urine, 6.02 liters of O_2 were consumed and 4.75 liters of CO_2 were produced.

Plasma and urine glucose concentrations were determined with the glucose oxidase method. Plasma FFAs were measured by the method of Chromy et al. (18) as modified by Demacker et al. (19). FFA measurements were corrected for background absorbance in hyperlipemic sera. Plasma insulin was determined by radioimmunoassay with a double antibody, using a modification of the method of Desbuquois and Aurbach (20). The anti-insulin serum cross-reacted completely with proinsulin.

Statistical analysis. All data are presented as means ± SE. Statistical comparisons between placebo and Acipimox experiments were performed using paired Student's t test, and a one-way analysis of variance was used for comparison of different groups of subjects. The incremental areas (above baseline) for glucose and insulin during the glucose tolerance tests were calculated using the trapezoidal rule. Correlations between variables were performed using least-squares regression analysis.

RESULTS

Basal plasma FFA, insulin, and glucose levels. Basal data from all subjects undergoing oral glucose tolerance testing and hyperinsulinemic clamping were pooled and analyzed together.

After placebo treatment, basal (after an overnight fast) plasma FFA levels were significantly lower in the lean nondiabetic control subjects (329 ± 28 μmol/l) than in the three obese groups (560 ± 52, 566 ± 83, and 584 ± 39 μmol/l, respectively). After Acipimox administration, basal plasma FFA levels were 60.4 ± 3.0, 57.9 ± 4.1, 56.5 ± 6.8, and 70.4 ± 3.4% lower than after placebo in lean control, obese nondiabetic, obese IGT, and obese diabetic subjects, respectively (Table 2).

After placebo, basal insulin levels were significantly higher in obese IGT and diabetic subjects than in lean nondiabetic control subjects. After Acipimox administration, insulin levels were ~50% lower than after placebo in all four groups (Table 2).

After placebo, basal plasma glucose concentrations were moderately elevated in diabetic patients (6.8 ± 0.4 vs. 4.98 ± 0.1 mmol/l, P < 0.01). After Acipimox, basal plasma glucose was lower than that after placebo in all groups (P < 0.01). This

TABLE 2
Effect of placebo and Acipimox treatment on basal plasma glucose, insulin, and FFAs

	Lean nondiabetic subjects Placebo	Lean nondiabetic subjects Acipimox	Obese nondiabetic subjects Placebo	Obese nondiabetic subjects Acipimox	Obese IGT subjects Placebo	Obese IGT subjects Acipimox	Obese diabetic subjects Placebo	Obese diabetic subjects Acipimox
Glucose (mmol/l)	4.98 ± 0.09	4.63 ± 0.09*	5.03 ± 0.07	4.70 ± 0.09*	5.85 ± 0.24	5.09 ± 0.20*	6.83 ± 0.44†	5.78 ± 0.23*
Insulin (pmol/l)	82 ± 10	38 ± 6*	96 ± 8	49 ± 7*	114 ± 11‡	60 ± 11*	149 ± 20†	78 ± 10*
FFAs (μmol/l)	329 ± 28	128 ± 13*	560 ± 52†	221 ± 21*	566 ± 83‡	242 ± 55*	584 ± 39†	170 ± 21*

Data are means ± SE. *P < 0.01 for placebo vs. Acipimox; †P < 0.01, ‡P < 0.05 compared with lean control subjects.

TABLE 3
Effect of placebo and Acipimox on basal carbohydrate and fat oxidation rates

Group	Carbohydrate oxidation ($\mu mol \cdot m^{-2} \cdot min^{-1}$)		Fat oxidation ($\mu mol \cdot m^{-2} \cdot min^{-1}$)	
	Placebo	Acipimox	Placebo	Acipimox
Lean nondiabetic	373 ± 22.2	568 ± 26*	41 ± 2	22 ± 3*
Obese nondiabetic	410 ± 36	531 ± 31*	35 ± 3	26 ± 3
Obese IGT	386 ± 36	494 ± 26*	34 ± 3	23 ± 3*
Obese diabetic	424 ± 42	565 ± 64*	36 ± 5	26 ± 4*

Data are means ± SE. *$P < 0.01$ for placebo vs. Acipimox.

decrease, although statistically significant, was small in the two nondiabetic groups (~0.4 mmol/l or ~7%), but larger in the diabetic subjects (~1.1 mmol/l or ~15%) (Table 2).

Basal carbohydrate and fat oxidation. After placebo, rates of carbohydrate oxidation and fat oxidation were similar in all four groups (Table 3). After Acipimox, fat oxidation was ~50% lower and carbohydrate oxidation ~50% higher than after placebo in the lean nondiabetic control subjects. In the three obese groups, fat oxidation was between 26–28% lower and carbohydrate oxidation was between 29–34% higher after Acipimox than after placebo.

Euglycemic-hyperinsulinemic clamps. Plasma glucose concentrations were clamped at 5.0–5.6 mmol/l, and plasma insulin levels were increased to and maintained at 660–720 pmol/l in all studies (Fig. 1).

After placebo, GIRs, reflecting insulin-stimulated glucose uptake (ISGU), were 50% lower in obese than in lean nondiabetic subjects (1.3 ± 0.06 vs. 2.6 ± 0.1 mmol · m^{-2} · min^{-1}, $P <$ 0.001) and ~70% lower in obese subjects with IGT or diabetes

compared with lean nondiabetic control subjects (0.7 ± 0.1 or 0.8 ± 0.1 vs. 2.6 ± 0.1 mmol · m^{-2} · min^{-1}, $P <$ 0.001) (Fig. 2).

After Acipimox administration, GIRs were higher than those after placebo treatment in lean control subjects (+23 ± 4%, $P <$ 0.001) and obese nondiabetic (+131 ± 13%, $P <$ 0.0001), IGT (+111 ± 21%, $P <$ 0.001) and diabetic (+103 ± 27%, $P <$ 0.001) subjects.

There was a linear relationship between changes in GIR (GIR at 180 min – GIR at 0 min) and basal plasma FFAs, such that a decrease in FFAs by 100 μmol/l was associated with an increase in GIR of 0.31 mmol · m^{-2} · min^{-1} in nondiabetic (lean and obese) subjects and of 0.12 mmol · m^{-2} · min^{-1} in obese subjects with IGT or type 2 diabetes (Fig. 3). In the current study, no glucose tracers were used, and, thus, true rates of glucose uptake could not be determined. At the insulin levels attained during hyperinsulinemic clamp (600–700 pmol/l), endogenous glucose production was probably not completely suppressed, and, therefore, true rates of glucose uptake could have been 10–20% higher than the measured GIR.

Oral glucose tolerance. Acipimox treatment lowered plasma glucose and insulin levels in all four groups (Fig. 4).

Areas under the glucose curves (glucose AUC) decreased by a mean of 25, 29, 26, and 21%, respectively, while insulin AUC decreased by a mean of 42, 19, 41, and 26%, respectively, in lean control, obese nondiabetic, IGT, and diabetic subjects (Table 4).
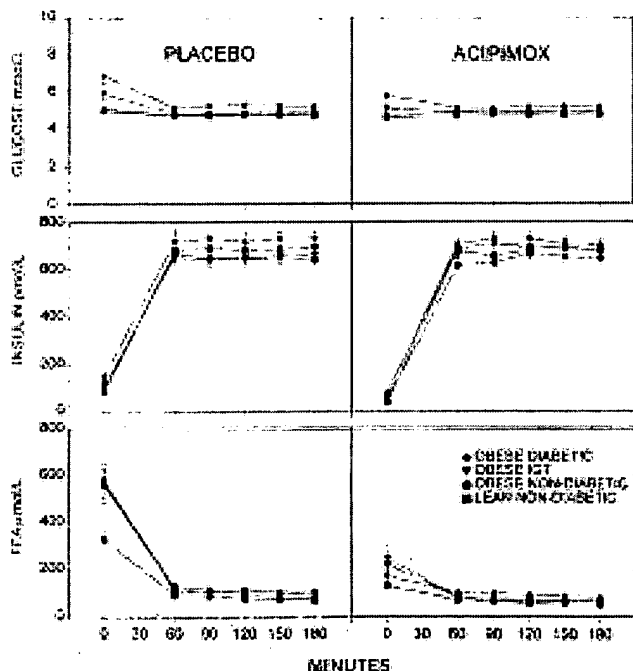

FIG. 1. Plasma glucose, insulin, and FFA levels before and during euglycemic-hyperinsulinemic clamping in lean and obese nondiabetic subjects and in subjects with IGT and type 2 diabetes after overnight treatment with placebo (*left*) or Acipimox (*right*).
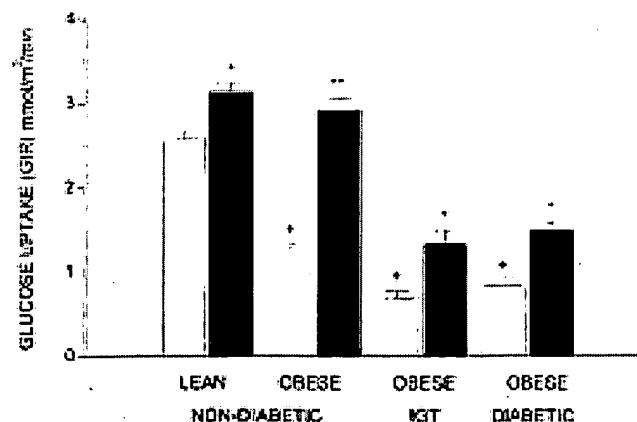

FIG. 2. Rates of glucose infusion needed to maintain euglycemia during hyperinsulinemic clamping (GIR) in lean and obese nondiabetic subjects and in subjects with IGT and type 2 diabetes after overnight treatment with placebo (□) or Acipimox (■). Statistical analysis: *$P <$ 0.001, **$P <$ 0.0001 for placebo vs. Acipimox treatment; +$P <$ 0.001 compared with lean nondiabetic control subjects.
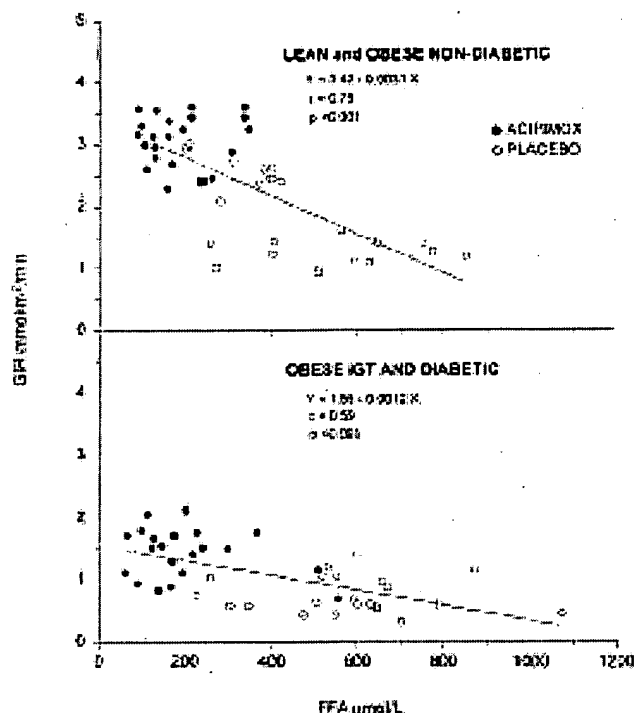
FIG. 3. Correlation between basal FFA levels after overnight treatment with placebo or Acipimox and GIR needed to maintain euglycemia after 150 and 180 min of euglycemic-hyperinsulinemic clamping in lean and obese nondiabetic subjects and in subjects with IGT and type 2 diabetes.

FIG. 4. Plasma glucose (*left*) and insulin (*right*) levels during oral glucose tolerance testing (75 g of glucose) after overnight treatment with placebo or Acipimox.

In the IGT group, mean fasting and 2-h glucose concentrations decreased from 5.7 ± 0.2 and 8.8 ± 0.3 mmol/l, respectively, after placebo to 5.5 ± 0.2 and 7.4 ± 0.3 mmol/l, respectively, after Acipimox ($P < 0.01$). After placebo treatment, 3 of the 10 patients had fasting plasma glucose concentrations 6.1–7.0 mmol/l (110–126 mg/dl), and 8 had 2-h plasma glucose concentrations 7.8–11.1 mmol/l (140–200 mg/dl). After Acipimox administration, only one patient had fasting plasma glucose concentrations 6.1–7.0 mmol/l and only two had 2-h glucose concentrations 7.8–11.1 mmol/l. Thus, according to the new American Diabetes Association guidelines (21) Acipimox improved glucose tolerance from impaired to normal in 8 of 10 subjects.

In the diabetic group, mean fasting and 2-h glucose concentrations decreased from 6.9 ± 0.5 and 13.7 ± 0.7 mmol/l, respectively, after placebo to 5.8 ± 0.4 and 10.3 ± 1.0 mmol/l, respectively, after Acipimox ($P < 0.01$). After placebo treatment, 3 of the 11 patients had fasting plasma glucose concentrations >7.0 mmol/l and 10 of 11 had 2-h glucose concentrations >11.1 mmol/l. After Acipimox administration, all 11 patients had fasting plasma glucose <7.0 mmol/l, and only 4 had 2-h glucose concentrations >11.1 mmol/l. Thus, Acipimox improved glucose tolerance from diabetic to impaired in 7 of 11 subjects.

DISCUSSION

Acipimox, FFAs, and insulin resistance. It was the main objective of this study to examine whether overnight lowering of plasma FFA levels with the potent long-acting NA analogue Acipimox could improve insulin resistance in obese subjects exhibiting a wide spectrum of insulin sensitivities rang-
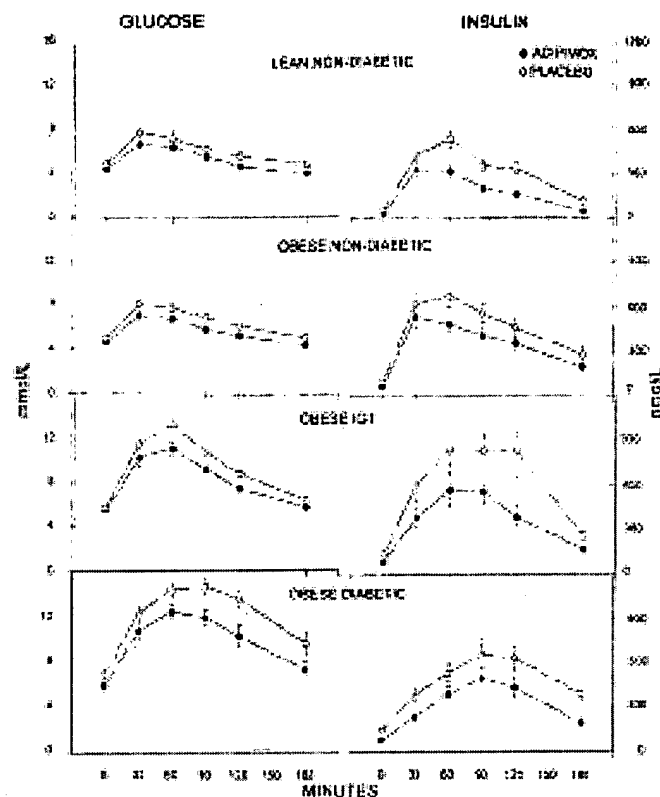
ing from normal to diabetic. Plasma FFA levels were lowered effectively, as evidenced by the fact that at 7:00 A.M. on the day of study, i.e., 6 h after the last dose of Acipimox, and at a time when FFA breakthroughs were most likely to occur (17), plasma FFA concentrations were lower (by an average of ~60%) than after placebo treatment in every one of the 43 study subjects. The decrease in FFAs was associated with an increase in ISGU in all subjects (Fig. 2). The increase was relatively small (23 ± 4%) in the lean nondiabetic control subjects, in whom Acipimox produced only a modest decrease in plasma FFAs (from 329 ± 28 to 128 ± 13 μmol/l). In contrast, in the three obese groups, Acipimox lowered plasma FFA levels from ~600 to between 170 and 240 μmol/l and increased ISGU more than twofold. Lowering of basal plasma FFAs from an elevated to a normal concentration (instead of lowering it to a very low concentration, as was done here) would presumably have had a lesser effect on ISGU. The 131% increase in ISGU was sufficient to normalize insulin sensitivity in the obese nondiabetic subjects. This suggested that elevated plasma FFA levels had been responsible for most of their insulin resistance. On the other hand, in obese subjects with IGT or diabetes, doubling of ISGU was not sufficient to normalize their insulin sensitivity, which remained ~50% below that of the lean nondiabetic control subjects. This suggested that elevated FFA levels were responsible for much, but not all, of the insulin resistance in type 2 diabetes, confirming previous findings from our laboratory (13). The relationship between basal plasma FFAs and GIR (at the end of the clamps) appeared to be linear for nondiabetic and diabetic subjects (Fig. 3). ISGU was zero (i.e., insulin resistance was maximal)

TABLE 4
Effects of placebo and Acipimox on glucose and insulin during oral glucose tolerance tests

| Group | Glucose ΔAUC (mmol · l⁻¹ · min⁻¹) | | | Insulin ΔAUC (mmol · l⁻¹ · min⁻¹) | | |
	Placebo	Acipimox	P	Placebo	Acipimox	P
Lean nondiabetic	214 ± 46	157 ± 26	0.12	48.8 ± 4.3	28.7 ± 3.9	<0.001
Obese nondiabetic	275 ± 30	192 ± 24	<0.02	69.3 ± 10.2	54.0 ± 7.0	<0.03
Obese IGT	701 ± 28	512 ± 31	<0.002	87.5 ± 15.0	52.3 ± 9.1	<0.001
Obese diabetic	1,017 ± 83	785 ± 86	<0.01	62.4 ± 7.7	44.5 ± 7.4	<0.01

Data are means ± SE of ΔAUC (total – basal AUC).

at a plasma FFA level of ~1,100 or ~1,300 µmol/l, respectively, and a decrease in plasma FFAs of 100 µmol/l resulted in a 9.1 or 7.7% reduction in insulin resistance, respectively, in nondiabetic subjects and in subjects with IGT or type 2 diabetes.

The failure of Fulcher et al. (16) to observe significant improvement in ISGU after overnight Acipimox administration in type 2 diabetic patients may have been, at least in part, due to their use of low clamp insulin infusion rates (0.25 mU · kg⁻¹ · min⁻¹). This produced only small increments in ISGU and was likely to obscure an effect of FFAs on ISGU. Despite these methodological problems, however, their data (12) showed that ISGU increased from 99.6 ± 11 to 124 ± 18 mg · m⁻² · min⁻¹ after Acipimox, whereas there was no change after placebo (from 117.3 ± 9.1 to 117 ± 16 mg · m⁻² · min⁻¹). Thus, there was at least a trend toward improved insulin sensitivity with Acipimox, even though these differences may not have been statistically significant.

It has been well established that acute elevations of plasma FFAs produce insulin resistance (10–15). In the present study, we have shown the opposite, namely, that lowering of plasma FFAs improved insulin resistance. It was assumed that Acipimox exerted its effect on insulin resistance via lowering of plasma FFAs and not by direct, i.e., not FFA-related, action. This assumption is supported by the close correlation between plasma FFAs and ISGU (Fig. 3), by the observation of Vaag et al. (22) that Acipimox had no direct effect on basal glucose disposal, and by the report of Saloranta et al. (23) that Acipimox had no direct effect on hepatic glucose production. Confirming many previous reports, we found that lowering of plasma FFA concentrations was associated with a decrease in fat oxidation and an increase in carbohydrate oxidation (7). It should be pointed out, however, that decreasing carbohydrate oxidation is not the mechanism by which FFAs inhibit ISGU. FFAs cause insulin resistance through inhibition of insulin-stimulated glucose transport and/or phosphorylation, as well as by inhibition of glycogen synthesis, processes that require 3–6 h to develop (10,11). FFA-induced inhibition of carbohydrate oxidation, on the other hand, develops almost instantaneously but does not interfere with ISGU for several hours (10). The molecular/biochemical events leading to FFA-induced insulin resistance remain unknown. It has recently been proposed that FFA activation of the hexosamine pathway may play a role in the pathogenesis of insulin resistance (24). This work, however, was performed with rats and needs to be confirmed in human subjects.

FFAs and oral glucose tolerance. Glucose tolerance is a complex process in which the amount of insulin secreted in response to the rising plasma glucose levels and peripheral and hepatic insulin sensitivity play major roles. In the current study, lowering of plasma FFAs with Acipimox reduced insulin levels (insulin AUC) and glucose levels (glucose AUC) both by ~30% during the oral glucose tolerance tests. This indicated that the Acipimox-mediated improvement in insulin sensitivity (~100% during the clamps) was greater than the Acipimox-induced decrease in plasma insulin levels. As a result, 8 of 10 obese subjects with IGT improved to normal glucose tolerance after Acipimox treatment, whereas 7 of 11 obese subjects with type 2 diabetes improved to IGT.

Fasting plasma insulin and glucose. Fasting plasma insulin levels were ~50% lower after Acipimox administration than after placebo in all four study groups. We have recently reported a slightly smaller decrease (~30%) in basal plasma insulin after plasma FFA levels were acutely decreased with NA (25). Taken together, the data suggest that plasma FFAs can support up to almost one-half of basal insulin levels.

Fasting plasma glucose also decreased slightly but significantly in all four groups after Acipimox administration, from ~7% in lean and obese nondiabetic subjects to ~15% in obese patients with IGT or mild type 2 diabetes. Fulcher et al. (16), using the same protocol, also found a ~15% decrease in fasting plasma glucose in eight obese patients with mild type 2 diabetes. Similarly, Worm et al. (26) reported a decrease in blood glucose after 3 days of treatment with Acipimox. Others, however, found no effect of Acipimox on blood glucose (22,27–29). These discrepant results are not surprising. Fasting plasma glucose concentrations are primarily determined by the rate of endogenous glucose production (30). A fall in plasma FFAs can be expected to result in a decrease in the rate of gluconeogenesis. This decrease, however, is more or less compensated for by an increase in the rate of glycogenolysis (31), via a process known as hepatic autoregulation (32). Hence, whether Acipimox will lower blood sugar or not probably depends to a large extent on the hepatic glycogen content. If liver glycogen is low, during fasting, for instance, glycogenolysis will be unable to balance the decrease in gluconeogenesis, and the blood sugar will fall (31,32).

Summary and clinical relevance. NA is an excellent lipid-lowering agent (33). Its use in diabetic patients, however, is not recommended because NA frequently causes deterioration of glucose tolerance (34). This is probably due to the short half-life of NA, which produces frequent breakthrough FFA rebounding (17). Acipimox, like NA, lowers lipids effectively, but unlike NA, it is longer acting and therefore much less prone to produce FFA rebounding (17). In fact, none of the 43 subjects in this study had a demonstrable FFA rebound within 6 h after the last Acipimox dose. Lowering of overnight plasma FFA levels with Acipimox markedly improved insulin resistance, oral glucose tolerance, and basal insulin levels in

obese subjects, regardless of the degree of their preexisting insulin resistance. These findings add to a growing body of evidence showing that elevated plasma FFA levels are an important link between obesity and insulin resistance (25,35). Nevertheless, more and longer studies are needed to demonstrate that long-term inhibition of lipolysis is feasible and effective in the treatment of type 2 diabetes, a disease that is characterized by insulin resistance, dyslipidemia, and a two- to fivefold increase in cardiovascular mortality.

ACKNOWLEDGMENTS

REFERENCES

1. Rabinowitz D, Zierler KL: Forearm metabolism in obesity and its response to intra-arterial insulin: characterization of insulin resistance and evidence for adaptive hyperinsulinism. *J Clin Invest* 12:2173–2181, 1962
2. Ferrannini E, Natali A, Bell P, Cavallo-Perin P, Lalic N, Mingrone G, on behalf of the European Group for the Study of Insulin Resistance (EGIR): Insulin resistance and hypersecretion in obesity. *J Clin Invest* 100:1166–1173, 1997
3. Zavaroni I, Bonora E, Pagliara M, Dall'Aglio E, Luchetti L, Buonanno G, Bonati PA, Bergonzani M, Gnudi L, Passeri M, Reaven G: Risk factors for coronary artery disease in healthy persons with hyperinsulinemia and normal glucose tolerance. *N Engl J Med* 320:702–706, 1989
4. Sims EAH, Danforth E Jr, Horton ES, Bray GA, Glennon JA, Salans LB: Endocrine and metabolic effects of experimental obesity in man. *Rec Prog Horm Res* 29:457–496, 1973
5. Goto Y, Nakayama Y, Yagi T: Influence of the World War II food shortage on the incidence of diabetes mellitus in Japan. *Diabetes* 7:133–135, 1958
6. Schliack V: Mangelernahrung und Diabetes Morbiditat (in German). *Z Klin Med* 151:382–396, 1954
7. Boden G: Role of fatty acids in the pathogenesis of insulin resistance and NIDDM. *Diabetes* 46:3–10, 1997
8. Gorden ES: Non-esterified fatty acids in blood of obese and lean subjects. *Am J Clin Nutr* 8:740–747, 1960
9. Reaven GM, Hollenbeck C, Jeng C-Y, Wu MS, Chen Y-D: Mean plasma glucose, free fatty acid, lactate and insulin for 24 h in patients with NIDDM. *Diabetes* 37:1020–1024, 1988
10. Boden G, Jadali F, White J, Liang Y, Mozzoli M, Coleman E, Smith C: Effects of fat on insulin-stimulated carbohydrate metabolism in normal men. *J Clin Invest* 88:960–966, 1991
11. Boden G, Chen X, Ruiz J, White JV, Rossetti L: Mechanisms of fatty acid-induced inhibition of glucose uptake. *J Clin Invest* 93:2438–2446, 1994
12. Roden M, Price TB, Perseghin G, Petersen KF, Rothman DL, Cline GW, Shulman GI: Mechanism of free fatty acid-induced insulin resistance in humans. *J Clin Invest* 97:2859–2865, 1996
13. Boden G, Chen X: Effects of fat on glucose uptake and utilization in patients with non-insulin-dependent diabetes. *J Clin Invest* 96:1261–1268, 1995
14. Kelley DE, Mintun MA, Watkins SC, Simoneau JA, Jadali F, Frederickson A, Beattie J, Theriault R: The effect of non-insulin-dependent diabetes mellitus and obesity on glucose transport and phosphorylation in skeletal muscle. *J Clin Invest* 97:2705–2713, 1996
15. Bonadonna RC, Zycg K, Boni C, Ferrannini E, DeFronzo RA: Time dependence of the interaction between lipid and glucose in humans. *Am J Physiol* 257:E49–E56, 1989
16. Fulcher GR, Walker M, Catalano C, Agius L, Alberti KGMM: Metabolic effects of suppression of nonesterified fatty acid levels with Acipimox in obese NIDDM subjects. *Diabetes* 41:1400–1408, 1992
17. Fuccella LM, Goldaniga G, Lovislo P, Maggi E, Musatti L, Mandelli V, Sirtori CR: Inhibition of lipolysis by nicotinic acid and by acipimox. *Clin Pharmacol Ther* 28:790–795, 1980
18. Chromy V, Gergel J, Voznincek J, Krombholzová L, Musil J: Assay of serum free fatty acids by extraction-photometric procedure. *Clin Chim Acta* 80:327–332, 1977
19. Demacker PNM, Hijmans AGM, Jansen AP: Enzymic and chemical-extraction determinations of free fatty acids in serum compared. *Clin Chem* 28:1765–1768, 1982
20. Desbuquois B, Aurbach GD: Use of polyethylene glycol to separate free from antibody-bound peptide hormones in radioimmunoassay. *J Clin Endocrinol* 33:732–738, 1971
21. The Expert Committee on the Diagnosis and Classification of Diabetes Mellitus: Report of the Expert Committee on the Diagnosis and Classification of Diabetes Mellitus. *Diabetes Care* 29:1183–1197, 1997
22. Vaag A, Skott P, Damsbo P, Gall MA, Richter EA, Beck-Nielsen H: Effect of the antilipolytic nicotinic acid analogue acipimox on whole-body and skeletal muscle glucose metabolism in patients with non-insulin dependent diabetes mellitus. *J Clin Invest* 88:1282–1290, 1991
23. Saloranta C, Franssila-Kallunki A, Ekstrand A, Taskinen M-R, Groop L: Modulation of hepatic glucose production by non-esterified fatty acids in type 2 (non-insulin-dependent) diabetes mellitus. *Diabetologia* 34:409–415, 1991
24. Hawkins M, Angelov I, Liu R, Barzilai N, Rossetti L: The tissue concentration of UDP-N-acetylglucosamine modulates the stimulatory effect of insulin on skeletal muscle glucose uptake. *J Biol Chem* 272:4889–4895, 1997
25. Boden G, Chen X, Iqbal N: Acute lowering of plasma fatty acids lowers basal insulin secretion in diabetic and nondiabetic subjects. *Diabetes* 47:1609–1612, 1998
26. Worm D, Henriksen J, Vaag A, Thye-Ronn P, Melander A, Beck-Nielsen H: Pronounced blood glucose-lowering effect of the antilipolytic drug acipimox in non-insulin-dependent diabetes mellitus patients during a 3-day intensified treatment period. *J Clin Endocrinol Metab* 78:717–721, 1994
27. Johnston P, Hollenbeck C, Sheu W, Chen Y-DI, Reaven G: Acute changes in plasma non-esterified fatty acid concentration do not change hepatic glucose production in people with type 2 diabetes. *Diabet Med* 7:871–875, 1990
28. Fulcher G, Farrer M, Thow JC, Johnson AB, Davis SJ, Miller M, Orskov H, Alberti KGMM: The glucose-fatty acid cycle in non-insulin dependent diabetes mellitus: the acute effects of inhibition of lipolysis overnight with acipimox. *Diab Nutr Metab* 4:285–293, 1990
29. Berrish T, Elliot C, Cooper B: The role of plasma non-esterified fatty acids during exercise in type 2 diabetes mellitus. *Diabet Med* 10:152–158, 1993
30. DeFronzo RA, Jacot E, Jequier E, Maeder E, Wahren J, Felber JP: The effect of insulin on the disposal of intravenous glucose: results from indirect calorimetry and hepatic and femoral venous catheterization. *Diabetes* 30:1000–1007, 1981
31. Chen X, Iqbal N, Boden G: Effect of FFA on gluconeogenesis and glycogenolysis in normal subjects. *J Clin Invest* 103:365–372, 1999
32. Clore JN, Glickman PS, Nestler JE, Blackard WG: In vivo evidence for hepatic autoregulation during FFA-stimulated gluconeogenesis in normal humans. *Am J Physiol* 24:E425–E429, 1991
33. Carlson LA, Oro L: The effect of nicotinic acid on the plasma free fatty acids: demonstration of a metabolic type of sympathicolysis. *Acta Med Scand* 172:641–645, 1962
34. Garg A, Grundy SM: Nicotinic acid as therapy for dyslipidemia in non-insulin-dependent diabetes mellitus. *JAMA* 246:723–726, 1990
35. Boden G: Free fatty acids, insulin resistance and type 2 diabetes mellitus. *Proc Assoc Am Physicians* 3:241–248, 1999

Identification of a Functional Peroxisome Proliferator-responsive Element in the Murine Fatty Acid Transport Protein Gene*

Brigitte I. Frohnert, To Y. Hui‡, and David A. Bernlohr§

From the Department of Biochemistry, Molecular Biology and Biophysics, University of Minnesota, St. Paul, Minnesota 55108

Fatty acid transport protein (FATP), a plasma membrane protein implicated in controlling adipocyte transmembrane fatty acid flux, is up-regulated as a consequence of adipocyte differentiation and down-regulated by insulin. Based upon the sequence of the FATP gene upstream region (Hui, T. Y., Frohnert, B. I., Smith, A. J., Schaffer, J. A., and Bernlohr, D. A. (1998) *J. Biol. Chem.* 273, 27420–27429) a putative peroxisome proliferator-activated receptor response element (PPRE) is present from −458 to −474. To determine whether the FATP PPRE was functional, and responded to lipid activators, transient transfection of FATP-luciferase reporter constructs into CV-1 and 3T3-L1 cells was carried out. In CV-1 cells, FATP-luciferase activity was up-regulated 4- and 5.5-fold, respectively, by PPARα and PPARγ in the presence of their respective activators in a PPRE-dependent mechanism. PPARδ, however, was unable to mediate transcriptional activation under any condition. In 3T3-L1 cells, the PPRE conferred a small but significant increase in expression in preadipocytes, as well as a more robust up-regulation of FATP expression in adipocytes. Furthermore, the PPRE conferred the ability for luciferase expression to be up-regulated by activators of both PPARγ and retinoid X receptor α (RXRα) in a synergistic manner. PPARα and PPARδ activators did not up-regulate FATP expression in 3T3-L1 adipocytes, however, suggesting that these two subtypes do not play a significant role in differentiation-dependent activation in fat cells. Electromobility shift assays showed that all three PPAR subtypes were able to bind specifically to the PPRE as heterodimers with RXRα. Nuclear extracts from 3T3-L1 adipocytes also showed a specific gel-shift complex with the FATP PPRE. To correlate the expression of FATP to its physiological function, treatment of 3T3-L1 adipocytes with PPARγ and RXRα activators resulted in an increased uptake of oleate. Moreover, linoleic acid, a physiological ligand, up-regulated FATP expression 2-fold in a PPRE-dependent manner. These results demonstrate that the FATP gene possesses a functional PPRE and is up-regulated by activators of PPARα and PPARγ, thereby linking the activity of the protein to the expression of its gene. Moreover, these results have implications for the mechanism by which certain PPARγ activators such as the antidiabetic thiazolidinedione drugs affect adipose lipid metabolism.

‡ Present address: Dept. of Biology, San Diego State University, San Diego, CA 92182.

§ To whom correspondence should be addressed: Dept. of Biochemistry, Molecular Biology and Biophysics, University of Minnesota, St. Paul, MN 55108. Tel.: 612-624-2712; Fax: 612-625-5780; E-mail: david-b@biosci.cbs.umn.edu.

Obesity, defined as an excessive accumulation of body fat, has become an increasingly common health concern in industrialized societies. Excessive adiposity has been linked to the pathogenesis of many diseases, including type 2 diabetes mellitus, coronary artery disease, and hypertension. The increased awareness of the detrimental effects of obesity contributes to the search for a greater understanding of the molecular mechanisms controlling the accumulation of adipose tissue and its metabolism.

A central issue in the function of fat tissue is the method by which adipocytes take up and release fatty acids. This process has been the source of considerable debate (1–3). Because free fatty acids are hydrophobic, they freely crossed membranes by passive diffusion. However, studies in adipocytes, hepatocytes, jejunal enterocytes, skeletal muscle, and heart myocytes support a saturable, protein-mediated mechanism for fatty acid transport (4–8). Thus far, five putative mammalian fatty acid transporters have been identified: fatty acid-binding protein (plasma membrane) (9), 56-kDa renal fatty acid-binding protein (10), caveolin (11), fatty acid translocase (12), and fatty acid transport protein (FATP)[1] (13). FATP is an integral plasma membrane protein with four to six predicted membrane-spanning regions with the highest levels found in skeletal muscle, heart, and fat with lower levels in brain, kidney, lung, and liver. Although FATP mRNA is present at low levels in 3T3-L1 preadipocytes, it is up-regulated 5–7-fold as a consequence of adipose conversion (13, 14). This increase is consistent with the increase in oleic acid uptake shown during preadipocyte differentiation (15).

The differentiation of adipose precursor cells into adipocytes has been shown to be mediated by three groups of transcription factors: peroxisome proliferator-activated receptor γ (PPARγ 1 and 2) the CCAATT enhancer-binding proteins (C/EBP), and the sterol-response element binding proteins (SREBP or ADD1) (16). The importance of PPARs for the development and maintenance of the adipocyte phenotype can be more directly shown by the existence of peroxisome proliferator response elements (PPREs) in the promoters of several genes whose protein products are critical for lipid metabolism and the development of the adipocyte phenotype such as lipoprotein lipase, phosphoenolpyruvate carboxykinase, acyl-CoA synthetase, malic enzyme, and adipocyte lipid-binding protein (ALBP or aP2) (16–21).

PPARs constitute a subfamily of the steroid hormone receptor superfamily. PPARα is predominantly expressed in liver, heart, kidney, and adipose tissue, whereas PPARδ (also known as NUC1 or FAAR) shows a similar expression, with the ex-

[1] The abbreviations used are: FATP, fatty acid transport protein; DMEM, Dulbecco's modified Eagle's medium; FBS, fetal bovine serum; PPRE, peroxisome proliferator response element; PPAR, peroxisome proliferator-activated receptor; Me₂SO, dimethyl sulfoxide; BSA, bovine serum albumin; RXR, retinoid X receptor.

ception of low levels in liver (22–25). Two isoforms of mouse PPARγ have been cloned, γ1 (22, 24, 26) and γ2 (19), which are transcribed from the same gene and alternatively spliced (27, 28). PPARγ1 is expressed in liver, heart, and kidney, similar to PPARα, whereas PPARγ2 is primarily expressed in adipose tissue (29). The two PPARγ isoforms do not appear to differ significantly in ligand binding affinities, ability to bind DNA response elements, or ability to activate transcription. The critical difference identified, thus far, is the distribution of expression.

FATP expression has been shown to be up-regulated in mouse liver by PPARα activators and in white adipose tissues by activators of PPARγ (30, 31). This evidence, together with the differentiation-dependent regulation of FATP in 3T3-L1 adipocytes, led us to investigate the upstream region of the recently cloned FATP gene (32) for a possible PPRE and to examine the role of the various PPAR subtypes in FATP expression. In this report we detail the regulation of the FATP gene, the identification of a functional PPRE, and its up-regulation by PPARα and PPARγ agonists.

EXPERIMENTAL PROCEDURES

Materials—Troglitazone and Delta Selective C were gifts from Alan Saltiel (Parke-Davis) and David E. Moller (Merck). WY14643 was purchased from Cayman Chemical. Linoleic acid and 9-*cis*-retinoic acid were purchased from Biomol. Expression plasmids prPPARα, pSG5-FAAR (PPARδ), pBS-PPARγ2, and pRS-hRXRα were provided by Drs. Donald Jump, Paul A. Grimaldi, Bruce M. Spiegelman, David J. Mangelsdorf, and Ronald M. Evans, respectively.

Plasmid Constructs—Polymerase chain reaction was used to introduce *Nhe*I sites into the upstream sequence of FATP. Reporter constructs pNH11 (−971/+84), pNH13 (−556/+84), and pNH15 (−160/+84) were constructed by ligating varying lengths of FATP upstream sequence into the *Nhe*I and *Hind*III sites of the pGL3-Basic luciferase expression vector (Promega). Construct pNH13ΔP was generated by single-stranded mutagenesis of construct pNH13 using the Muta-Gene *in vitro* mutagenesis kit (Bio-Rad, Hercules, CA) and the oligonucleotide: 5′-CTGGAACATCTCCTGAGTACTTCCTCCTCTCCC-3′. Sequence fidelity and the introduced mutation were verified by sequencing. The PPARγ2 expression construct, pAH215, was made by cutting pBS-PPARγ2 with *Kpn*I and *Xba*I and ligating into pCDNA3.1 (Promega). The expression construct for RXRα, pAH232, was subcloned from pRS-hRXRα into the *Eco*RI site of pCDNA3.1.

Cell Culture and Transfection—CV-1 cells were cultured in DMEM with 10% fetal bovine serum (FBS) until the day prior to transfection experiments, when the cells were plated in phenol red-free DMEM and 10% charcoal-treated FBS. CV-1 cells were transiently transfected using the calcium-phosphate method as described previously (33, 34). Briefly, each well of a 12-well culture plate was transfected with 1 μg of firefly (*Photinus pyralis*) luciferase reporter construct with or without 0.5 μg of expression plasmid for mouse PPARγ2, rat PPARα, or mouse PPARδ. 20 ng of pRL-SV40 (Promega), a vector containing a sea pansy (*Renilla reniformis*) luciferase gene driven by an SV40 promoter, was cotransfected into each well as a transfection control. After approximately 20 h, the calcium phosphate/DNA precipitate was removed by washing three times with phosphate-buffered saline. Cells were then refed and treated for 48 h with either the appropriate PPAR activator or its vehicle, dimethyl sulfoxide (Me₂SO).

3T3-L1 preadipocytes were grown to confluence and induced to differentiate to adipocytes as described previously(35). Briefly, preadipocytes were cultured in DMEM and 10% calf serum. Two days after reaching confluence, cells were differentiated by treatment with 174 nm insulin, 0.5 mm methylisobutylxanthine, and 0.25 μm dexamethasone in DMEM containing 10% FBS. Cells were treated for an additional 2 days with insulin and maintained in DMEM with 10% FBS until they are fully mature adipocytes at day 8.

Transient transfection of 3T3-L1 preadipocytes was performed by calcium phosphate precipitation as described above. Each well was transfected with 1 μg of firefly luciferase reporter construct and 10 ng of pRL-SV40 control vector. In the first set of transfections, cells were maintained in DMEM containing 10% calf serum until transfection mixture was washed off of cells. Cells were then treated with either linoleic acid or ethanol for 24 h in serum-free DMEM. For the second set of preadipocyte transfections, cells were maintained in DMEM with

```
-600 ATGAGGGGTC AAGAGCCCTA AACCTAAGCC TAAGAGCTTA AACTTAGCAC
-550 TCTATAAACT AGGAGAAGGG GGGGCGGGCG CGAAGAAAGA GGAAGGGAGT
-500 AGAGGGCACG AGCTGGGGAG AGGAGGAAGT GGGGCAAAGG GCACAGGAGA
-450 TGTTCCAGGA ACATCGAAAC AGGAGGAGGC AGTGAGCAAG TAGGAGGGCA
-400 GGCAGCAGGG CTGAATCCCA GCTGGGGGGG ACGGCTGCAG CATTCAGTGT
-350 CTTTACCTGT AAAACTGGGG TAGAGGGGGA GAGGGCTGGT CTAGAGGGTT
-300 CTTGTTGACC CCTGGCTGGC TGGGCCGAGA TCTTCATCAC CACCACCACC
-250 CCCATCCCAA CCACCTCTCT GAGACCAATG GCAGCTTCGG GTGGGGGTGG
-200 GGCCGCACTT GCCCAACCTT GGCCTTCGAC TGGCGCTGGA AACAGGCCCT
-150 GGCTGGCTTC TTCCCAAGGA GAACTGTGGG AAGGTCGGCC AAGCGGGACA
-100 GAAAACAAAC TAATCCCCAG GGTGGGCAGG GGGGCGTGGG AGGGTGGTTG
-50  GGAGGGAGGG ACAGGGTAGA GGCACTCAGG GGCGCTGTGA GAAACCCCCA
+1   GGACTCTTCA
```

FIG. 1. **Upstream sequence of the FATP gene.** The putative PPRE is *double underlined.*

10% calf serum for the duration of the experiments. After washing transfection mixture from cells, they were treated with either a PPAR activator or its vehicle (Me₂SO) for 48 h.

3T3-L1 adipocytes grown in 12-well culture plates were transiently transfected as described previously (32) with 500 ng of firefly luciferase construct and 20 ng of pRL-SV40 control vector per well. Briefly, DNA in DMEM was complexed with LipofectAMINE (Life Technologies, Inc.) at the ratio of 1:8 (w/v) for 45 min before addition to the cells. After 4 h, an equal volume of 20% fetal bovine serum in DMEM was added. The transfection mixture was removed after 20 h. The cells were then refed with DMEM containing 10% FBS and treated with either PPAR activator or vehicle for 48 h.

All transiently transfected cells were washed two times with phosphate-buffered saline, lysed, and luciferase activities were determined using the Dual Luciferase Reporter Assay System (Promega) according to the manufacturer's protocol. Firefly luciferase activities were normalized to sea pansy luciferase activities to adjust for transfection efficiency. Activities were also normalized to the promoterless reporter construct, pGL3-Basic.

In Vitro Transcription/Translation—cDNAs for rPPARα, mPPARγ2, mPPARδ, and hRXRα were transcribed and translated *in vitro* from the plasmids prPPARα, pAH215, pSG5-FAAR, and pAH232, respectively. The TNT Coupled Reticulocyte Lysate System (Promega) was used according to the manufacturer's instructions. The following expression plasmids were used prPPARα, pSG5-FAAR (PPARδ), pAH215, and pAH232. Translation products were verified by SDS-polyacrylamide gel electrophoresis.

Gel Electromobility Shift Assays—Nuclear extracts were prepared from day 9 3T3-L1 adipocytes essentially as described previously (36). To study the binding of nuclear hormone receptors to the putative PPRE, a double-stranded oligonucleotide, PPREwt, spanning nucleotides −482 to −453 of the FATP upstream sequence was ³²P-labeled with polynucleotide kinase (Promega). A 15-μl reaction containing and 0.5 ng of PPRE probe and 9 μg of nuclear extract or 0.5–1 μl of *in vitro* translation reaction was incubated for 20 min at 25 °C and 15 min at 4 °C in a buffer containing 20 mM HEPES (pH 8), 60 mM KCl, 1 mM dithiothreitol, 10% glycerol, and 2 μg poly(dI-dC). The DNA-protein complexes were resolved from the free probe by electrophoresis at 4 °C on a 4% polyacrylamide gel in 0.5 × TBE buffer (1 × TBE = 9 mM Tris, 90 mM boric acid, 20 mM EDTA) (pH 8). Double-stranded oligonucleotides composed of the following sequences were used for competition analysis: PPREwt, 5′-GATCTAGAGGAGGAAGTGGGGCAAAGGGCA-CAGGA-3′; PPREmut, 5′-GATCTAGAGGAGGAAGTGGGGCtAtcGGC-ACAGGA-3. PPRE sequence is underlined. Mutated bases are shown in lowercase letters.

Fatty Acid Uptake—3T3-L1 adipocytes between days 7 and 9 were treated for 4 days with either 20 μM troglitazone and 1 μM 9-*cis*-retinoic acid or their carrier, Me₂SO. The adipocytes were then assayed for uptake of oleate essentially as described previously (37). Briefly, cells were first preincubated for 2–4 h in serum-free DMEM and then for 10–30 min at 25 °C in Krebs-Ringer phosphate solution with 2 mM glucose. Oleate uptake was measured at 25 °C by incubating cells in a 100 μM, 1:1 oleate:BSA mixture, which contained trace [³H]oleate (approximately 12,000 dpm/nmol). At various time points, uptake was terminated by aspirating the oleate:BSA mixture from

TABLE I

Comparison of identified PPRE sequences

Consensus sequence derived from listed PPREs. Uppercase letters denote most conserved base(s); lowercase letters indicate a less conserved base alternative. HMG, hydroxymethylglutaryl; PEPCK, phosphoenolpyruvate carboxykinase.

| Gene	Species	Element	Sequence	Protein function	Ref.
HMG-CoA synthase	Rat	HMG	AACT GGGCCA A AGGTCT	Liver ketogenesis/sterol synthesis	48
Acyl-CoA synthase	Rat	ACS(CI)	TTTC AGGGCA T CAGTCA	Fatty acid activation	20
Acyl-CoA oxidase	Rat	ACOA	GACC AGGACA A AGGTCA	Peroxisomal β-oxidation	52, 53
		ACOB	AGCA AGGTAG A AGGTCA		
	Human	hACOX	TAGA AGGTCA C TGGTCA	Peroxisomal β-oxidation	47
Bifunctional enzyme	Rat	BIF	ATGT AGGTAA T AGTTCA	Peroxisomal β-oxidation	54
Malic enzyme	Rat	MEp	TTCT GGGTCA A AGTTGA	Fatty acid synthesis	21
Cytochrome P450 A1	Rat	CYP4A1	AACT AGGGTA A AGTTCA	ω-Oxidation	46
Cytochrome P450 A6	Rabbit	CYP4A6(Z)	AACT AGGGCA A AGTTGA	ω-Oxidation	55
PEPCK	Rat	PCK1	CCCA CGGCCA A AGGTCA	Glycerogenesis and gluconeogenesis	17
		PCK2	AACT GGGATA A AGGTCT		
ALBP/aP2	Mouse	ARE6	CTCT GGGTGA A ATGTGC	Fatty acid binding	19
		ARE7	TACT GGATCA G AGTTCA		
L-FABP	Rat	FABP	ATAT AGGCCA T AGGTCA	Fatty acid binding	56
Uncoupling protein 1	Mouse	URE1	AGTG TGGTCA A GGGTGA	Thermogenesis	50
Lipoprotein lipase	Rat	LPL	AAGA GGGGGA A AGGGCA	Triglyceride clearance	18
Apolipoprotein CIII	Human	APOCIIIB	GCGC TGGGCA A AGGTCA	Triglyceride clearance	57
Muscle-type carnitine Palmitoyltransferase	Human	MCPT I	ATGT AGGGAA A AGGTCA	Fatty acid transport	49
Fatty acid transport Protein		FATP	AAGT GGGGCA A AGGGCA	Fatty acid transport	
		Consensus	AACT AGGTCA A AGGTCA Tg g G		
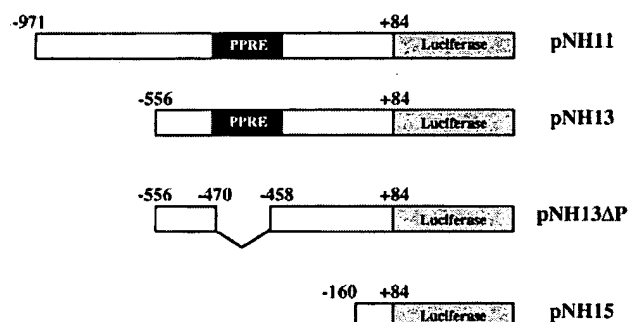
FIG. 2. **Construct map of the luciferase reporter constructs used in transfection assays.** Constructs contain various portions of FATP upstream sequence, as indicated. The putative PPRE is denoted by a *shaded box.*

the cells and washing three times with ice-cold phosphate-buffered saline containing 0.1% albumin and 200 μM phloretin. Cell lysate was then quantitated for radioactivity using a Beckman 3801 liquid scintillation counter.

RESULTS

The Mouse Fatty Acid Transport Protein Gene Contains a Functional PPRE—Previous studies of FATP regulation in mice indicated that transcription was activated in both liver and white adipose tissue by treatment of mice with activators of PPARα or PPARγ, respectively (30, 31). Furthermore, FATP expression was observed to be up-regulated during adipose differentiation, a process known to be mediated in part by PPARγ (14). The upstream sequence of the recently cloned FATP gene (32) was therefore examined for a possible PPRE. A putative PPRE was identified, which is similar to the consensus sequence proposed by Palmer *et al.* (38) (Fig. 1, Table I).

In order to determine whether the putative PPRE identified in the FATP upstream sequence was able to mediate transcriptional activation, portions of the FATP 5′-flanking sequence were tested for their ability to mediate PPAR-activated transcription of a reporter gene. Four luciferase reporter constructs were made, each containing portions of the FATP 5′-flanking region linked to a promoterless firefly luciferase gene. Two of
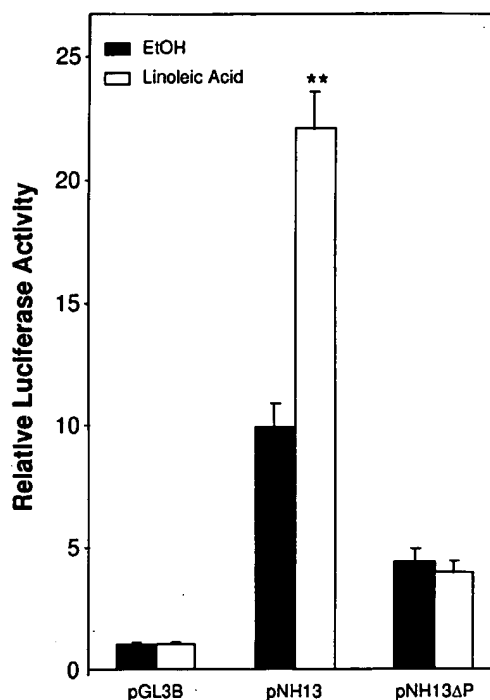

FIG. 3. **Activation of FATP expression in 3T3-L1 preadipocytes by linoleic acid.** 3T3-L1 preadipocytes were transfected with the reporter constructs pNH13 and pNH13ΔP, as well as the control construct, pGL3-Basic. The cells were then treated for 24 h in serum-free medium with either vehicle (EtOH) or 100 μM linoleic acid. *Asterisks* indicate statistical difference from activity of the control-treated construct (** = $p < 0.005$).

these plasmids, pNH11 and pNH13, contained the putative PPRE sequence, while the other two, pNH13ΔP and pNH15 did not (Fig. 2).

In the first set of experiments, two of these constructs, pNH13 and pNH13ΔP, as well as the promoterless pGL3-Basic control construct, were transfected into 3T3-L1 preadipocytes. Following transfection, the cells were maintained for 24 h in serum-free media and treated with 100 μM linoleic acid or its
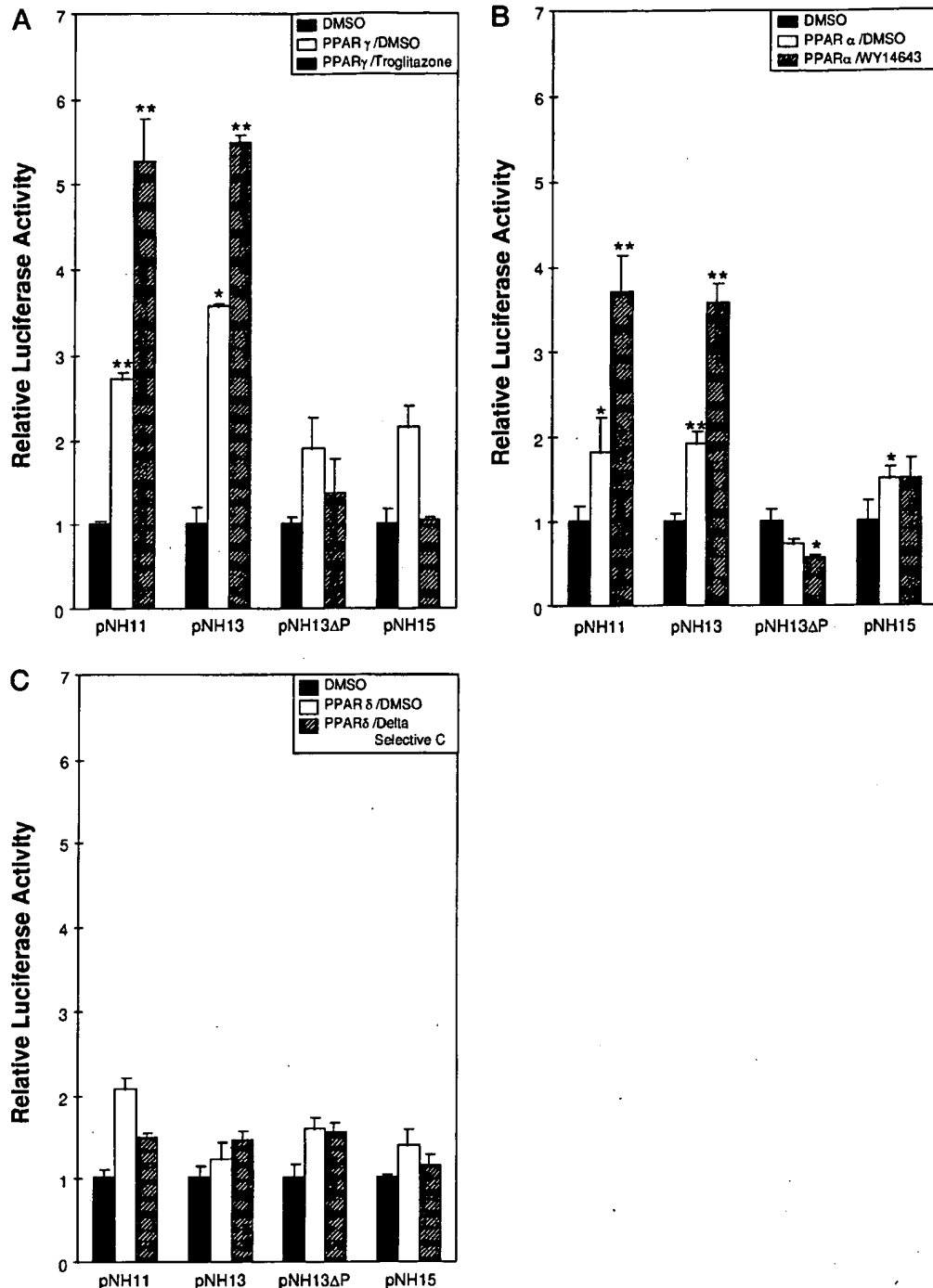
FIG. 4. **The putative PPRE confers selective responsiveness to PPAR-mediated activation.** Reporter constructs were cotransfected with or without an expression vector for PPAR γ (*A*), PPAR α (*B*), or PPAR δ (*C*) and treated for 48 h with activator or vehicle (Me_2SO (*DMSO*)). Activators were 20 μM Troglitazone, 10 μM WY14643, or 40 nM Delta Selective C, respectively. Normalized luciferase activities are shown as mean $\pm$ S.E. (n = 4) and are expressed as -fold induction relative to the activity in the absence of expression vectors and activators. *Asterisks* indicate statistical difference from activity of the reporter construct alone (* = $p < 0.05$, ** = $p < 0.005$).

carrier, ethanol. This experiment was performed in the absence of serum, since serum albumin binds fatty acids, leaving low levels of available fatty acid activator. Linoleic acid treatment activated transcription of the PPRE-containing construct approximately 2-fold over control-treated cells (Fig. 3), but did not affect transcription of the PPRE-deletion construct. Similar results were seen in transfection of 3T3-L1 adipocytes (data not shown). These experiments indicated that the putative PPRE identified in the FATP upstream sequence was indeed functional.

To further characterize the responsiveness of this PPRE to the various PPAR subtypes, all four reporter constructs were transfected into CV-1 cells and assayed for luciferase activity in the presence and absence of various PPARs and their activators. The activators used were troglitazone, a thiazolidinedione (PPARγ activator); WY14643, a fibrate drug (PPARα activator); and the PPARδ activator, Delta Selective C. As shown in Fig. 4*A*, cells transfected with PPARγ and treated with troglitazone demonstrated a 5.5-fold increase in transcription of the PPRE-containing reporter constructs. PPARγ alone was able to activate transcription approximately 3-fold. PPARα was also
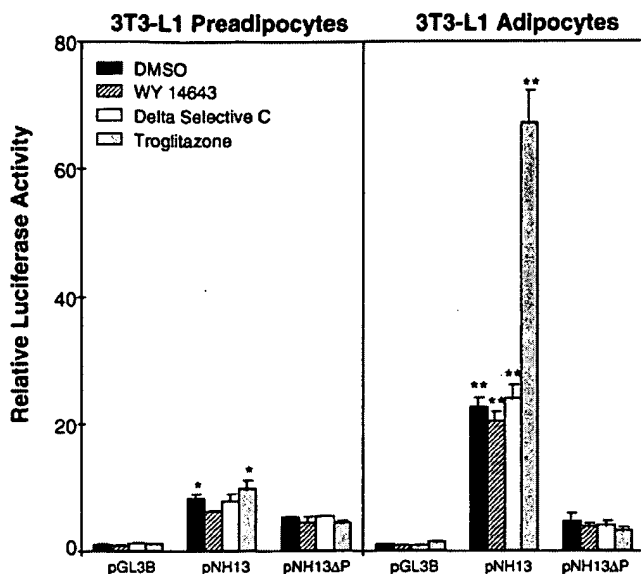
Identification of a PPRE in the FATP Gene

FIG. 5. **Activation of FATP expression by endogenous PPARs in preadipocytes and adipocytes.** 3T3-L1 preadipocytes and adipocytes were transfected with the reporter constructs pNH13 and pNH13ΔP as well as the control construct, pGL3-Basic. The cells were then treated with either vehicle or PPAR activators: 20 μM troglitazone, 10 μM WY14643, or 40 nM Delta Selective C. Luciferase activities were normalized to pGL3-Basic and are shown as mean ± S.E. ($n = 4$). *Asterisks* indicate statistical difference between pNH13 and pNH13ΔP expression (* = $p < 0.05$, ** = $p < 0.005$).

FIG. 6. **Synergistic activation of FATP expression in 3T3-L1 adipocytes by PPAR and RXRα activators.** 3T3-L1 preadipocytes and adipocytes were transfected with the reporter constructs pNH13 and pNH13ΔP as well as the control construct, pGL3-Basic. These cells were then treated with the PPARγ activator, troglitazone (20 μM), and the RXRα activator, 9-cis-retinoic acid (1 μM). Luciferase activities were normalized to pGL3-Basic and are shown as mean ± S.E. ($n = 4$). *Asterisks* indicate statistical difference from control-treated reporter construct (** = $p < 0.005$).

able to activate transcription in the PPRE-containing constructs, albeit to a lesser extent; transcription was increased 4- and 2-fold in the presence and absence of activator, respectively (Fig. 4B). Finally, the PPARδ subtype was unable to positively regulate transcription of any of the reporter constructs, regardless of activator treatment (Fig. 4C). Deletion of the PPRE rendered the promoter unresponsive to any PPAR or agonist combination.

PPRE Involved in Differentiation-dependent Regulation of FATP—In order to determine the role of the FATP PPRE in the process of its gene regulation during the process of adipose differentiation, the luciferase reporter constructs were introduced into both 3T3-L1 preadipocytes as well as mature adipocytes. These experiments relied upon endogenous PPARs to mediate transcriptional activation. Cells were also treated with activators of the various PPAR subtypes to determine whether transcription could be further increased. In preadipocytes, which contain low levels of PPARγ as well as PPARδ, the PPRE containing construct, pNH13, was expressed at about 1.6-fold the level of the PPRE-deletion construct, pNH13ΔP, when both were treated with Me₂SO. Treatment with troglitazone had a small, but not statistically significant, effect on pNH13 expression. In adipocytes, the PPRE-containing construct was expressed at levels 5-fold higher than the PPRE-deletion construct (Fig. 5). Furthermore, troglitazone treatment resulted in a further 3-fold increase in expression. Neither WY14643 nor Delta Selective C caused any significant change in luciferase expression in either preadipocytes or adipocytes.

Synergistic Activation by PPARγ and RXRα Activators—Issemann et al. (39) showed that the RXR ligand, 9-cis-retinoic acid enhances PPAR action. To determine whether RXRα activation affected PPARγ-dependent transactivation, 3T3-L1 adipocytes were treated with either troglitazone, 9-cis-retinoic acid, or both. Retinoic acid did not significantly affect transcription by itself; however, when added to cells in conjunction with troglitazone, it was able to produce an almost 2-fold increase in activity above that produced by tro-
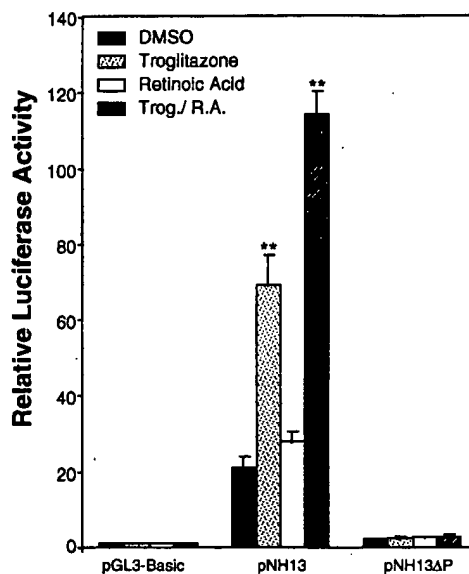
glitazone alone (Fig. 6). This result demonstrates the synergistic activation of the FATP gene in response to activation of both PPARγ and RXRα.

PPARs and RXRα Bind as Heterodimers to the FATP PPRE—In order to determine whether PPARs bind to the PPRE as heterodimers with RXRα, gel mobility shift assays were performed with a double-stranded oligonucleotide containing the FATP PPRE (Fig. 7A). The double-stranded probe, PPREwt, was end-labeled with ³²P and incubated with in vitro translated protein as well as 3T3-L1 nuclear extract. As shown in Fig. 7B, neither PPARs nor RXRα alone could bind to the PPRE; however, all three PPAR subtypes were able to bind as heterodimers with RXRα to the probe. Furthermore, nuclear proteins from 3T3-L1 adipocytes were able to form an in vitro complex with the PPRE (Fig. 7C). In order to test the specificity of the protein-DNA interactions, an excess of unlabeled oligonucleotide (PPREwt) was added to the reactions. The unlabeled oligonucleotide was able to compete for binding of all three PPAR-RXRα-DNA complexes, as well as the nuclear protein-DNA complex. The introduction of 3-base pair substitutions (Fig. 7A) produced an oligonucleotide, PPREmut, which was no longer able to significantly compete for protein binding.

PPARγ and RXRα Activators Cause an Increase in Oleate Uptake—Finally, in order to correlate PPAR-mediated transcriptional activation with putative in vitro protein function, fatty acid uptake was analyzed in 3T3-L1 adipocytes. 3T3-L1 adipocytes were treated for 4 days with either troglitazone and retinoic acid or their carrier Me₂SO. Cells were then incubated with [³H]oleate:BSA mixture (1:1), washed, lysed at various time points, and assayed for radioactivity. As shown in Fig. 8, treatment with the activators of PPARγ and RXRα resulted in a significant increase in oleate uptake. This result is consistent with the up-regulation of FATP transcription by troglitazone and 9-cis-retinoic acid, as shown by the previously described transfection studies, and correlates well with the increase in FATP mRNA expression upon treatment of 3T3-L1 adipocytes
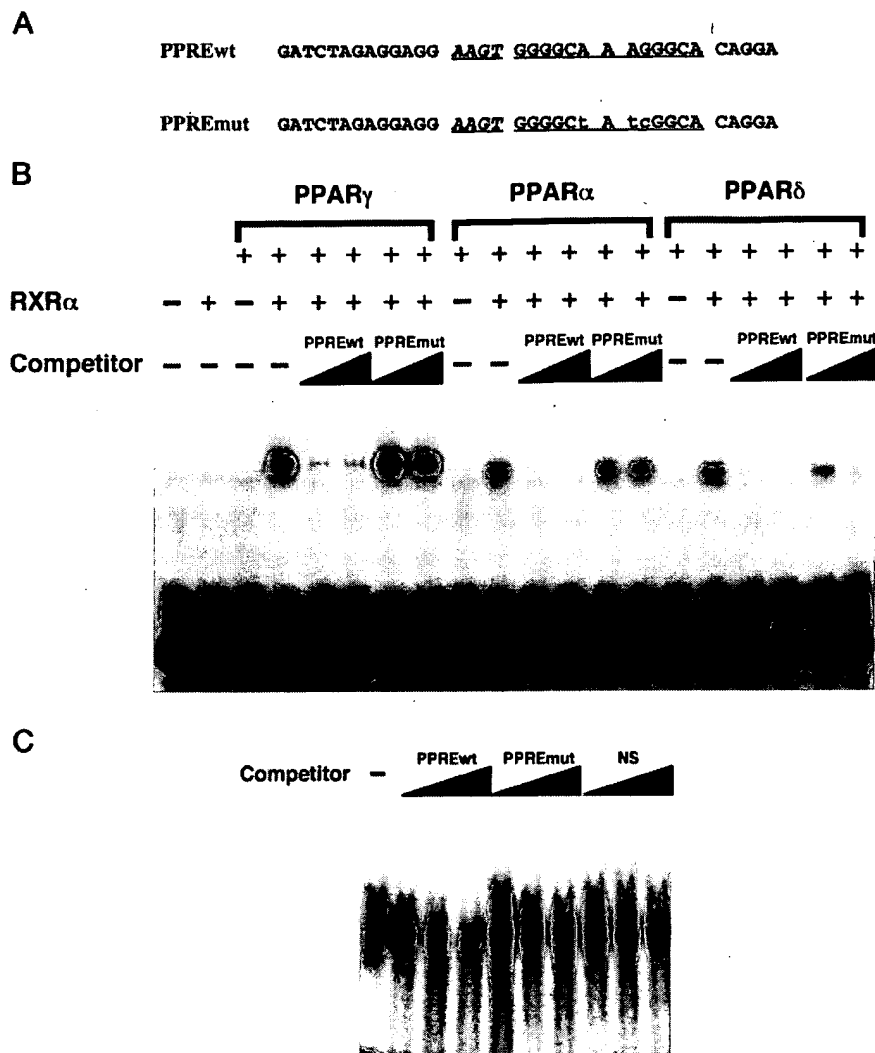
A

PPREwt   GATCTAGAGGAGG AAGT GGGGCA A AGGGCA CAGGA

PPREmut   GATCTAGAGGAGG AAGT GGGGCt A tcGGCA CAGGA

B

FIG. 7. **PPARs and RXRα bind as heterodimers to the FATP PPRE.** *A*, sequences of oligonucleotides used in gel-shift studies. PPRE sequence is *under-lined*; mutated bases are in *lowercase*. *B*, the double-stranded probe, PPREwt, was end-labeled with ^{32}P and incubated with *in vitro* translated PPARs and RXRα. The competitors PPREwt and PPREmut were used in 20- and 100-fold molar excess. Protein-DNA complexes were analyzed by electrophoretic mobility shift assay. *C*, labeled PPREwt probe was incubated with 3T3-L1 adipocyte nuclear extracts with or without competitor. Competitors PPREwt, PPREmut, and NS (a nonspecific competitor oligonucleotide) were added in 20-, 50-, and 200-fold molar excess.

C

with the PPARγ agonist BRL49653, as shown by Martin *et al.* (30).

DISCUSSION

The critical role of PPARs in the regulation of lipid metabolism has become increasingly apparent. Many genes whose products take part in some aspect of fatty acid catabolism, synthesis, or trafficking have been shown to contain functional PPREs (Table I). FATP, which has been argued to play a role fatty acid uptake, is a likely candidate for regulation by this group of nuclear hormone receptors. Indeed, two previous studies have shown that treatment of various cell types with PPAR activators leads to an increase in FATP mRNA levels (30, 31). In this paper we have identified a sequence in the 5' region of the murine FATP gene, which is very similar (16/17) to the consensus sequence for previously identified PPREs (see Table I).

By deletion analysis and mutation of this putative PPRE, we have demonstrated that this PPRE is necessary for the PPAR-mediated up-regulation of FATP expression. Transfection into 3T3-L1 preadipocytes showed that FATP transcription can indeed be activated by the naturally occurring compound, linoleic acid. This fatty acid has been shown previously to be able to activate transcription via both the α and γ PPAR subtypes (40–42). Further transfection experiments into CV-1 cells demonstrated that FATP transcription was activated by both PPARα and PPARγ. Both subtypes activate transcription upon treatment with synthetic activator; however, the receptors are also able to activate transcription in the absence of exogenous activator. This could be explained either by the presence of an endogenous activator, such as a fatty acid or its metabolite, or by a ligand-independent activity of these subtypes (43).

In addition to showing the functionality of the FATP PPRE, our experiments demonstrate a differential activation of gene expression by the various PPAR subtypes. Although both PPARα and PPARγ are able to activate transcription, our studies show that PPARγ mediates a greater response both in the presence and absence of a synthetic activator. PPARδ, in contrast, did not significantly activate transcription, either alone or upon treatment with activator. This difference has been demonstrated previously in other systems (44) and has been hypothesized to reflect the differing roles of the PPAR subtypes in the regulation of fatty acid metabolism. PPARα has been best characterized in the liver, where it up-regulates many genes involved in the catabolism of fatty acids. PPARγ is chiefly active in the adipose tissue, where it contributes to lipid accumulation and the development of the adipose phenotype. In contrast to the other two subtypes, the role of PPARδ in whole-body fatty acid metabolism has not been well defined.

We and others have reported the up-regulation of FATP during adipose conversion (13, 14). We hypothesized that this differentiation-dependent regulation of FATP is mediated by PPARγ and is dependent on the presence of the FATP PPRE. This was investigated in a further series of transfections, which

Identification of a PPRE in the FATP Gene

FIG. 8. **Oleate uptake by 3T3-L1 adipocytes treated with troglitazone and retinoic acid.** 3T3-L1 adipocytes were treated for 4 days with either 20 μM troglitazone and 1 μM 9-*cis*-retinoic acid or their carrier Me$_2$SO (*DMSO*). Cells were then incubated with 1:1 oleate:BSA mixture in Krebs-Ringer phosphate buffer which contained trace [^{3}H]oleate. Cells were washed and lysed at various time points and cell lysate was assayed for radioactivity. *Asterisks* indicate statistical difference between uptake of treated and nontreated cells (* = $p < 0.05$).
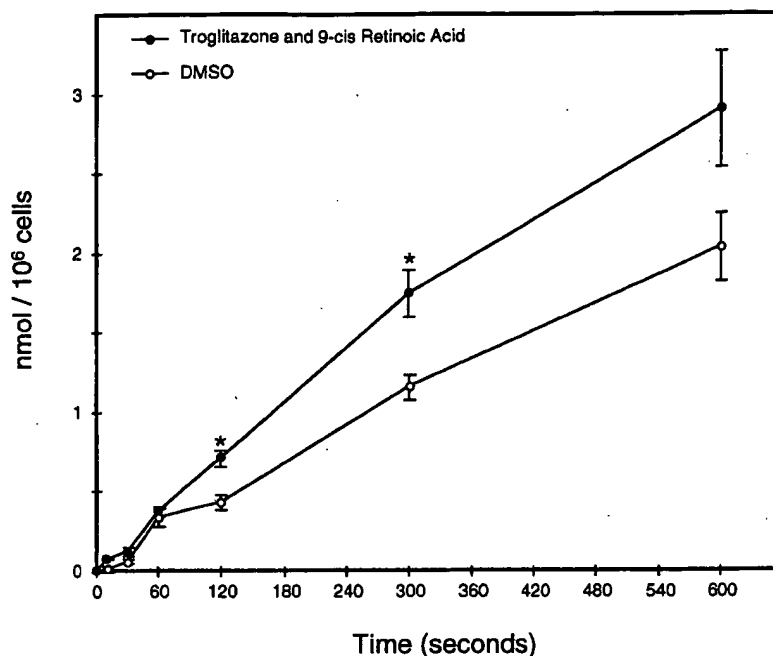
compared transcriptional activity in both 3T3-L1 preadipocytes and adipocytes, in both the presence and absence of synthetic activators. The PPRE conferred a 1.6-fold activation of FATP transcription in preadipocytes. At this point in the differentiation process, PPARγ is present in low levels relative to fully differentiated adipocytes. Exogenous activators of the three PPAR subtypes did not significantly increase transcription above that of untreated cells. In adipocytes, the PPRE conferred a 5-fold increase in FATP expression, and this activation was further stimulated by the PPARγ activator, troglitazone. Neither the activator of PPARα nor PPARδ was able to increase FATP expression over untreated cells. This can be explained by the lack of significant PPARα expression in adipocytes. PPARδ, while present in adipocytes, has been demonstrated in the previously described studies to be unable to activate FATP expression.

Several previous studies have shown a synergistic effect of the RXRα activators, 9-*cis*-retinoic acid on PPAR-activated expression (18, 19, 21, 45–48). This convergence of the PPAR and RXR signaling pathways was also demonstrated in transfection studies of FATP reporter constructs in 3T3-L1 adipocytes. Although the RXRα activator alone was unable to increase expression of FATP in 3T3-L1 adipocytes, it was able to enhance the troglitazone-mediated activation of expression.

The ability of the various PPAR subtypes to bind to the FATP PPRE *in vitro* was examined by electromobility shift assay. As has been shown in other systems, neither the PPARs nor RXRα were able to bind to the PPRE as homodimers (20, 21, 45–50); however, all three PPAR subtypes were able to bind as heterodimers. These protein-DNA complexes were sequence-specific, as shown by competition analysis, and were dependent upon the presence of an intact PPRE. Mutation of 3 base pairs of the PPRE abolished the formation of protein complexes on this element. It is interesting to note that PPARδ, while unable to activate transcription, was able to form a heterodimer complex with the PPRE. This indicates that binding of the receptor heterodimers to an element is not equivalent with transcriptional activity.

In order to correlate FATP regulation by PPARs with its putative function, oleate uptake was measured in cells that were treated with troglitazone and 9-*cis*-retinoic acid. Uptake

was significantly increased in activator-treated cells when compared with control-treated cells. This leads to an interesting model for positive feedback regulation of FATP. Increased FATP expression has been shown to result in increased fatty acid uptake (13). Fatty acids, in turn, are activators of PPARγ and PPARα, which are able to up-regulate the expression of FATP.

We have reported previously the regulation of FATP by insulin via an insulin-responsive element (PLE3) in the upstream region of the FATP gene (-1353 to -1347). The downregulation of FATP by insulin, an anabolic hormone, seems counterintuitive, since fatty acid uptake would be expected to rise in response to insulin stimulation. It is important to note, however, that regulation of FATP at the transcriptional level is unlikely to be the result of the transient postprandial insulin peak, but rather a more chronic hyperinsulinemia, such as in type 2 diabetes mellitus. Furthermore, the majority of type 2 diabetics are obese, a condition associated with a down-regulation of PPARγ expression in adipose tissue (51). The combination of these two factors may contribute to the elevation in serum free fatty acid levels observed in type 2 diabetics. This leads to a possible mechanism for the antidiabetic effects of the drug, troglitazone; by reversing the effects of hyperinsulinemia and obesity on FATP regulation, troglitazone may enable adipose tissue improve fatty acid uptake. Further studies on the function of FATP and its regulation in the diabetic state may lead to insight into both normal and deranged fatty acid metabolism.

REFERENCES

1. Berk, P. D. (1996) *Proc. Soc. Exp. Biol. Med.* **212,** 1–4
2. Zakim, D. (1996) *Proc. Soc. Exp. Biol. Med.* **212,** 5–14
3. Fitscher, B. A., Elsing, C., Riedel, H.-D., Gorski, J., and Stremmel, W. (1996) *Proc. Soc. Exp. Biol. Med.* **212,** 15–23
4. Abumrad, N. A., Perkins, R. C., Park, J. H., and Park, C. R. (1981) *J. Biol. Chem.* **256,** 9183–9191
5. Stremmel, W., and Theilmann, L. (1986) *Biochim. Biophys. Acta* **877,** 191–197
6. Stremmel, W., Lotz, G., Strohmeyer, G., and Berk, P. D. (1985) *J. Clin. Invest.* **75,** 1068–1076
7. Turcotte, L. P., Kiens, B., and Richter, E. A. (1991) *FEBS Lett.* **279,** 327–329

8. Stremmel, W. (1988) *J. Clin. Invest.* **81**, 844–852
9. Stremmel, W., Strohmeyer, G., Borchard, F., Kochwa, S., and Berk, P. D. (1985) *Proc. Natl. Acad. Sci. U. S. A.* **82**, 4–8
10. Fujii, S., Kawaguchi, H., and Yasuda, H. (1987) *J. Biochem. (Tokyo)* **101**, 679–684
11. Trigatti, B. L., Mangroo, D., and Gerber, G. E. (1991) *J. Biol. Chem.* **266**, 22621–22625
12. Abumrad, N. A., El-Maghrabi, M. R., Amri, E.-Z., Lopez, E., and Grimaldi, P. A. (1993) *J. Biol. Chem.* **268**, 17665–17668
13. Schaffer, J. E., and Lodish, H. F. (1994) *Cell* **79**, 427–436
14. Man, M. Z., Hui, T. Y., Schaffer, J. E., Lodish, H. F., and Bernlohr, D. A. (1996) *Mol. Endocrinol.* **10**, 1021–1028
15. Abumrad, N. A., Forest, C. C., Regen, D. M., and Sanders, S. (1991) *Proc. Natl. Acad. Sci. U. S. A.* **88**, 6008–6012
16. Lemberger, T., Desvergne, B., and Wahli, W. (1996) *Annu. Rev. Cell Dev. Biol.* **12**, 335–363
17. Tontonoz, P., Hu, E., Devine, J., Beale, E. G., and Spiegelman, B. M. (1995) *Mol. Cell. Biol.* **15**, 351–357
18. Schoonjans, K., Peinado-Onsurbe, J., Lefebvre, A. M., Heyman, R. A., Briggs, M., Staels, B., and Auwerx, J. (1996) *EMBO J.* **15**, 5336–5348
19. Tontonoz, P., Hu, E., Graves, R. A., Budavari, A. I., and Spiegelman, B. M. (1994) *Genes Dev.* **8**, 1224–1234
20. Schoonjans, K., Watanabe, M., Suzuki, H., Mahfoudi, A., Krey, G., Wahli, W., Grimaldi, P., Staels, B., Yamamoto, T., and Auwerx, J. (1995) *J. Biol. Chem.* **270**, 19269–19276
21. Castelein, H., Gulick, T., Declercq, P. E., Mannaerts, G. P., Moore, D. D., and Baes, M. I. (1994) *J. Biol. Chem.* **269**, 26754–26758
22. Chen, F., Law, S. W., and O'Malley, B. W. (1993) *Biochem. Biophys. Res. Commun.* **196**, 671–677
23. Amri, E. Z., Bonino, F., Ailhaud, G., Abumrad, N. A., and Grimaldi, P. A. (1995) *J. Biol. Chem.* **270**, 2367–2371
24. Kliewer, S. A., Forman, B. M., Blumberg, B., Ong, E. S., Borgmeyer, U., Mangelsdorf, D. J., Umesono, K., and Evans, R. M. (1994) *Proc. Natl. Acad. Sci. U. S. A.* **91**, 7355–7359
25. Jow, L., and Mukherjee, R. (1995) *J. Biol. Chem.* **270**, 3836–3840
26. Zhu, Y., Alvares, K., Huang, Q., Rao, M. S., and Reddy, J. K. (1993) *J. Biol. Chem.* **268**, 26817–26820
27. Tontonoz, P., Hu, E., and Spiegelman, B. M. (1994) *Cell* **79**, 1147–1156
28. Zhu, Y., Qi, C., Korenberg, J. R., Chen, X. N., Noya, D., Rao, M. S., and Reddy, J. K. (1995) *Proc. Natl. Acad. Sci. U. S. A.* **92**, 7921–7925
29. Chawla, A., Schwarz, E. J., Dimaculangan, D. D., and Lazar, M. A. (1994) *Endocrinology* **135**, 798–800
30. Martin, G., Schoonjans, K., Lefebvre, A. M., Staels, B., and Auwerx, J. (1997) *J. Biol. Chem.* **272**, 28210–28217
31. Motojima, K., Passilly, P., Peters, J. M., Gonzalez, F. J., and Latruffe, N. (1998) *J. Biol. Chem.* **273**, 16710–16714
32. Hui, T. Y., Frohnert, B. I., Smith, A. J., Schaffer, J. A., and Bernlohr, D. A. (1998) *J. Biol. Chem.* **273**, 27420–27429
33. Sambrook, J., Fritsch, E. F., and Maniatis, T. (1989) *Molecular Cloning: A Laboratory Manual*, 2nd Ed., pp. 16.32–16.36, Cold Spring Harbor Laboratory, Cold Spring Harbor, NY
34. Chen, C., and Okayama, H. (1988) *BioTechniques* **6**, 632–638
35. Student, A. K., Hsu, R. Y., and Lane, M. D. (1980) *J. Biol. Chem.* **255**, 4745–4750
36. Dignam, J. D., Lebovitz, R. M., and Roeder, R. G. (1983) *Nucleic Acids Res.* **11**, 1475–1489
37. Waggoner, D. W., and Bernlohr, D. A. (1990) *J. Biol. Chem.* **265**, 11417–11420
38. Palmer, C. N., Hsu, M. H., Griffin, H. J., and Johnson, E. F. (1995) *J. Biol. Chem.* **270**, 16114–16121
39. Issemann, I., Prince, R. A., Tugwood, J. D., and Green, S. (1993) *Biochimie (Paris)* **75**, 251–256
40. Krey, G., Braissant, O., L'Horset, F., Kalkhoven, E., Perroud, M., and Parker, M. G. (1997) *Mol. Endocrinol.* **11**, 779–791
41. Kliewer, S. A., Moore, J. T., Wade, L., Staudinger, J. L., Watson, M. A., Jones, S. A., Oliver, B. B., Willson, T. M., Zetterstrom, R. H., Perlmann, T., and Lehmann, J. M. (1998) *Cell* **92**, 73–82
42. Forman, B. M., Chen, J., and Evans, R. M. (1997) *Proc. Natl. Acad. Sci. U. S. A.* **94**, 4312–4317
43. Werman, A., Hollenberg, A., Solanes, G., Bjorbaek, C., Vidal-Puig, A. J., and Flier, J. S. (1997) *J. Biol. Chem.* **272**, 20230–20235
44. Juge-Aubry, C., Pernin, A., Favez, T., Burger, A. G., Wahli, W., Meier, C. A., and Desvergne, B. (1997) *J. Biol. Chem.* **272**, 25252–25259
45. Green, S., and Wahli, W. (1994) *Mol. Cell. Endocrinol.* **100**, 149–153
46. Aldridge, T. C., Tugwood, J. D., and Green, S. (1995) *Biochem. J.* **306**, 473–479
47. Varanasi, U., Chu, R., Huang, Q., Castellon, R., Yeldandi, A. V., and Reddy, J. K. (1996) *J. Biol. Chem.* **271**, 2147–2155
48. Rodriguez, J. C., Gil-Gomez, G., Hegardt, F. G., and Haro, D. (1994) *J. Biol. Chem.* **269**, 18767–18772
49. Mascaro, C., Acosta, E., Ortiz, J. A., Marrero, P. F., Hegardt, F. G., and Haro, D. (1998) *J. Biol. Chem.* **273**, 8560–8563
50. Sears, I. B., MacGinnitie, M. A., Kovacs, L. G., and Graves, R. A. (1996) *Mol. Cell. Biol.* **16**, 3410–3419
51. Montague, C. T., Prins, J. B., Sanders, L., Zhang, J., Sewter, C. P., Digby, J., Byrne, C. D., and O'Rahilly, S. (1998) *Diabetes* **47**, 1384–1391
52. Tugwood, J. D., Issemann, I., Anderson, R. G., Bundell, K. R., McPheat, W. L., and Green, S. (1992) *EMBO J.* **11**, 433–439
53. Osumi, T., Wen, J. K., and Hashimoto, T. (1991) *Biochem. Biophys. Res. Commun.* **175**, 866–871
54. Zhang, B., Marcus, S. L., Sajjadi, F. G., Alvares, K., Reddy, J. K., Subramani, S., and Capone, J. P. (1992) *Proc. Natl. Acad. Sci. U. S. A.* **89**, 7541–7545
55. Muerhoff, A. S., Griffin, K. J., and Johnson, E. F. (1992) *J. Biol. Chem.* **267**, 19051–19053
56. Issemann, I., Prince, R., Tugwood, J., and Green, S. (1992) *Biochem. Soc. Trans.* **20**, 824–827
57. Krey, G., Keller, H., Mahfoudi, A., Medin, J., Ozato, K., Dreyer, C., and Wahli, W. (1993) *J. Steroid Biochem. Mol. Biol.* **47**, 65–73

Coordinate Regulation of the Expression of the Fatty Acid Transport Protein and Acyl-CoA Synthetase Genes by PPARα and PPARγ Activators*

Geneviève Martin, Kristina Schoonjans‡, Anne-Marie Lefebvre, Bart Staels§, and Johan Auwerx¶

From the U.325 INSERM, Département d'Athérosclérose, Institut Pasteur, 59019 Lille, France

Intracellular fatty acid (FA) concentrations are in part determined by a regulated import/export system that is controlled by two key proteins, *i.e.* fatty acid transport protein (FATP) and acyl-CoA synthetase (ACS), which respectively facilitate the transport of FAs across the cell membrane and their esterification to prevent their efflux. The aim of this investigation was to analyze the expression pattern of FATP and ACS and to determine whether their expression was altered by agents that affect FA metabolism through the activation of peroxisome proliferator-activated receptors (PPAR) such as the fibrates and thiazolidinediones. FATP mRNA was ubiquitously expressed, with highest levels being detected in adipose tissue, heart, brain, and testis. Fibrate treatment, which is known to preferentially activate PPARα, induced FATP mRNA levels in rat liver and intestine and induced ACS mRNA levels in liver and kidney. The antidiabetic thiazolidinedione BRL 49653, which is a high-affinity ligand for the adipocyte-specific PPARγ form, caused a small induction of muscle but a robust induction of adipose tissue FATP mRNA levels. BRL 49653 did not affect liver FATP and had a tendency to decrease heart FATP mRNA levels. ACS mRNA levels in general showed a similar pattern after BRL 49653 as FATP except for the muscle where ACS mRNA was induced. This regulation of FATP and ACS expression by PPAR activators was shown to be at the transcriptional level and could also be reproduced *in vitro* in cell culture systems. In the hepatocyte cell lines AML-12 or Fa 32, fenofibric acid, but not BRL 49653, induced FATP and ACS mRNA levels, whereas in the 3T3-L1 preadipocyte cell line, the PPARγ ligand induced FATP and ACS mRNA levels quicker than fenofibric acid. Inducibility of ACS and FATP mRNA by PPARα or γ activators correlated with the tissue-specific distribution of the respective PPARs and was furthermore associated with a concomitant increase in FA uptake. Most interestingly, thiazolidinedione antidiabetic agents seem to favor adipocyte-specific FA uptake relative to muscle, perhaps underlying in part the beneficial effects of these agents on insulin-mediated glucose disposal.

Transmembrane transport of FAs[1] is still poorly understood despite intense investigation. Uncharged molecules and weak acids such as fatty acids can cross membranes rapidly thanks to their lipid solubility. The rate of movement is controlled by mass action and can be enhanced by proteins such as fatty acid-binding protein that act as a cytoplasmic "sink." Recently, however, several studies provided evidence that in addition to these nonfacilitated systems, facilitated transport also contributes to FA transport (1). Several proteins were hypothesized to be acting as FA transporters. Among these, three deserve further attention. First, plasma membrane fatty acid-binding protein, a protein related to the mitochondrial isoform of aspartate aminotransferase, has been suggested to increase FA uptake in cells (2). Since this protein has not yet been cloned, it is difficult to determine its exact role in FA transport processes. The second protein, fatty acid translocase is an 88-kDa membrane protein that has been cloned in mouse and is homologous to the human CD36 cell surface antigen (3). Although CD36 has been shown to bind FAs and might be involved in signal transduction after binding of a specific ligand (long chain fatty acids), it is until now not clear whether it is a transport protein. The only candidate for a long chain FA transporter for which functionality has been directly demonstrated is the fatty acid transport protein (FATP) (4). FATP is a 63-kDa plasma membrane protein with six predicted membrane-spanning domains that has been cloned using a functional expression cloning technique. It increased oleic acid uptake in FATP-transfected 3T3-L1 cells by >3-fold. Interestingly FATP is suggested to act in concert with acyl-CoA synthetase (ACS), an enzyme that prevents efflux of the incorporated fatty acids by their conversion into acyl-CoA derivatives and hence rendering the FA uptake process unidirectional. Furthermore, FATP shows a limited region of homology at the protein level (11 amino acids), with ACS leading to the hypothesis that this common region might reflect a common function, such as a binding site (4). These 11 amino acids residues have also been found to be conserved in the rat and the yeast FATP homologues (5).

Several aspects of intracellular lipid and FA metabolism in cells are subjected to transcriptional control by the peroxisome proliferator-activated receptor (PPAR) family. PPARs are members of the superfamily of nuclear hormone receptors that function as ligand-dependent transcription factors. Three receptor subtypes of PPAR termed α, δ (or β), and γ, have been identified (6–15). These receptors heterodimerize with the retinoid X receptor and alter the transcription of target genes after binding to peroxisome proliferator response elements (PPREs), which consist of a hexameric nucleotide direct repeat of the recognition motif (TGACCT) spaced by 1 nucleotide

[1] The abbreviations used are: FA, fatty acid; FATP, FA transport protein; ACS, acyl-CoA synthetase; PPAR, peroxisome proliferator-activated receptor; BSA, bovine serum albumin; LPL, lipoprotein lipase.
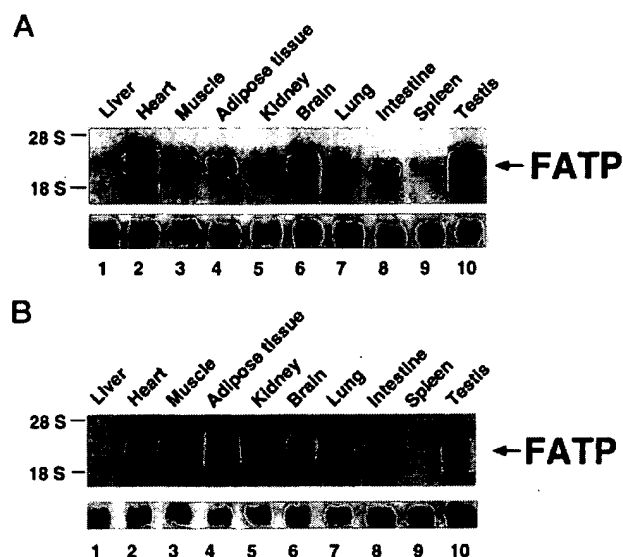
A

B

FIG. 1. Tissue distribution of FATP mRNA expression in mouse (A) and rat (B). Twenty μg of total RNA from the respective tissues was analyzed by Northern blot hybridization for FATP and 36B4 mRNA expression. RNA extraction and analysis was performed as described under "Experimental Procedures."

(DR-1). Several genes with a crucial role in FA metabolism have been shown to contain a peroxisome proliferator response element in their upstream regulatory sequences (reviewed in Refs. 16 and 17). Interestingly, the transcriptional activity of the PPAR subtypes is enhanced by a multitude of chemical compounds including fatty acids, thiazolidinedione antidiabetic agents, prostaglandins, peroxisome proliferators, and fibrate hypolipidemic drugs. In addition to activating PPARs, some of these compounds have been shown to be direct ligands for them. PPARγ directly binds antidiabetic thiazolidinediones (18, 19) and prostaglandin derivatives (18, 20) but not the other activators, whereas PPARα binds leukotriene B4 and the powerful peroxisome proliferator Wy 14643 (21).

In view of the convergence of FA import and PPARs in lipid and energy metabolism, we investigated the effects of two distinct chemical classes of PPAR activators, *i.e.* fibrates (PPARα-specific) and the antidiabetic thiazolidinediones (PPARγ-specific) on tissue-specific *FATP* gene expression. Fibrate treatment induced FATP and ACS expression strongest in liver, whereas BRL 49653, the high affinity ligand for PPARγ, had no effect on liver but induced adipocyte FATP and ACS expression in adipose tissue. The induction of FATP and ACS by PPAR activators was at the level of transcription and was associated with concomitant changes in cellular FA uptake. Interestingly, the stronger effects of BRL 49653 on fatty acid import in adipose tissue relative to the muscle might limit FA uptake and oxidation in the muscle, an effect associated with an improvement in muscle glucose disposal.

EXPERIMENTAL PROCEDURES

Materials—BRL 49653 and fenofibric acid were kind gifts of Dr. De Chaffoy de Courcelles (Janssen Research Foundation, Beerse, Belgium) and Dr. Alan Edgar (Laboratoires Fournier, Daix, France), respectively.

Animal Studies—Animal studies were carried out in compliance with French and European union specifications regarding the use of laboratory animals. Male Wistar rats (90 days old) were treated for 7 days with fenofibrate (Laboratoires Fournier) mixed at the indicated concentrations (by mass) in standard rat chow. The food intake of the rats was recorded every day throughout the treatment period. None of the treatments caused major changes in the amount of food consumed by the animals. Since each rat consumed approximately 20 gm of chow/day, doses of 0.5, 0.05, and 0.005% (by mass mixed in rat chow) correspond to 320, 32, and 3 mg/kg of body weight/day. Adult (95 day) Sprague-
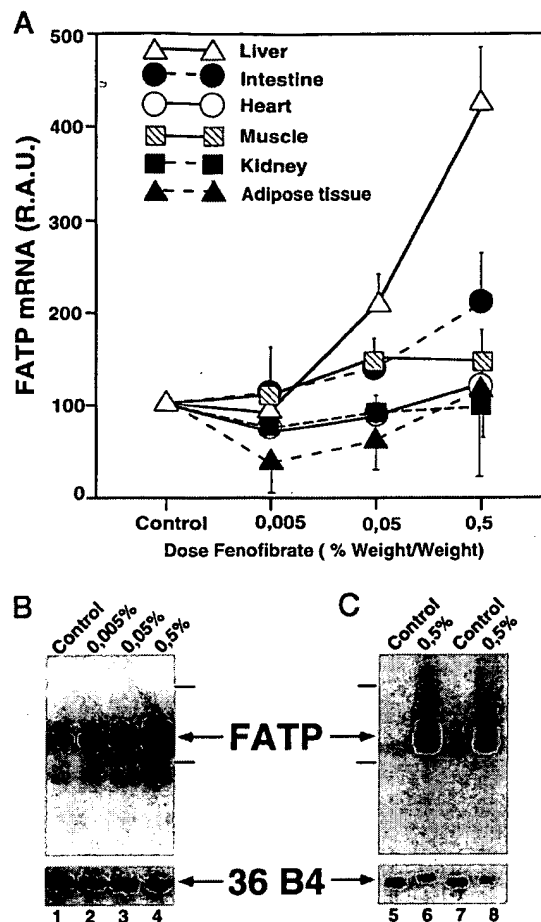
A

B C

FIG. 2. Effect of fenofibrate on FATP mRNA levels. *A*, graph showing the effects fenofibrate mixed with food in the indicated concentrations on FATP mRNA levels. RNA extraction and analysis was performed as described under "Experimental Procedures." *R.A.U.*, relative absorbance units. *B*, effect of increasing amounts of fenofibrate on liver FATP expression in rat. Twenty μg of total liver RNA was analyzed by Northern blot hybridization for FATP and 36B4 mRNA expression as indicated under "Experimental Procedures." *C*, effect of fenofibrate on liver FATP expression in mouse. Twenty μg of total liver RNA tissues was analyzed by Northern blot hybridization for FATP and 36B4 mRNA expression as indicated under "Experimental Procedures."

Dawley rats were group-housed and accustomed to a 12:12 h day:night ratio illumination cycle (light from 8 am to 8 pm). Rats were divided in groups of a minimum of three animals each and were treated for either 7 or 14 days. The first group received BRL 49653 (5 mg/kg/day) by gavage. The second group of animals received 0.5% w/w of fenofibrate (± 0.5 g/kg/day) mixed with their food, whereas the third group of animals served as controls and received 10% carboxymethylcellulose (vehicle for gavage) by gavage. In a separate experiment, adult C57Bl6 male mice were either fed during 14 days with a control chow (n = 3) or the same chow containing 0.5% w/w of fenofibrate. At the end of the treatment period, all animals were weighed and sacrificed by exsanguination under ether anesthesia between 8 and 10 a.m. Epididymal adipose tissue (in rats) and liver (in rats and mice) was removed, weighed, rinsed with 0.9% NaCl, and frozen in liquid nitrogen until RNA preparation.

Cell Culture—The mouse hepatoma and preadipocyte cell lines Fa 32 (rat), ob 1771 (mouse) (22), and 3T3-L1 (mouse; ATCC) were maintained in Dulbecco's modified Eagle's minimal essential medium and supplemented with 10% delipidated and charcoal-treated fetal calf serum, L-glutamine, and antibiotics unless stated otherwise. AML-12 mouse hepatocytes (23) were maintained in Dulbecco's modified Eagle's minimal essential medium/Ham's F-12 supplemented with 10% delipidated and charcoal-treated fetal calf serum, insulin, transferrin, and selenium (Collaborative Research), dexamethasone (0.1 μM), and gentamycin (50 μg/ml). Fenofibric acid and BRL 49653 (both in Me₂SO) were added to the medium at the appropriate concentrations and times
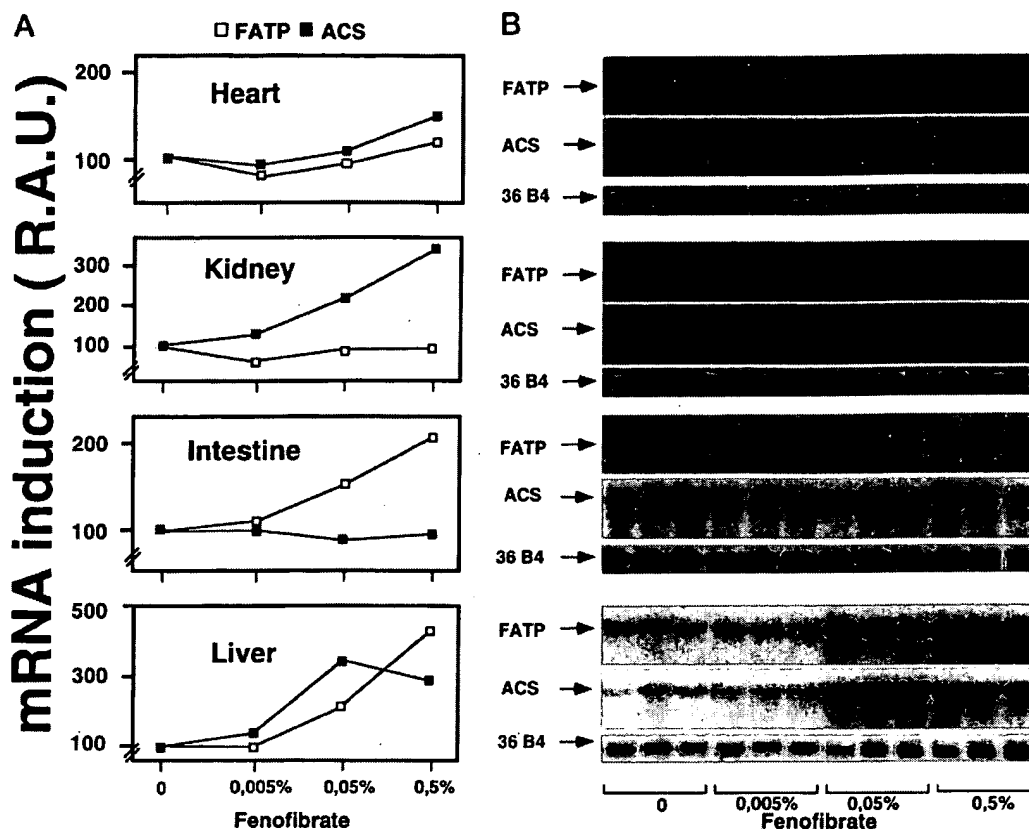

FIG. 3. **FATP and ACS mRNA are in some tissues coinduced by fenofibrate.** *A*, graphs representing the effects of three different concentrations of fenofibrate (0.005, 0.05, and 0.5% (w/w) during 14 days) mixed with food on FATP (*open squares*) or ACS (*filled squares*) mRNA levels. The results represent the mean of three independent samples. *B*, Northern blot showing the regulation of FATP, ACS, and 36B4 mRNA levels by fenofibrate administration. Animal treatment and preparation and analysis of RNA is described under "Experimental Procedures." *R.A.U.*, relative absorbance units.

indicated. Control cells received vehicle only.

3T3-L1 cells were differentiated by a treatment of 2 days with dexamethasone (0.1 μM), isobutylmethylxanthine (0.25 mM), and insulin (0.4 μM); the cells were then maintained for an additional 8 days with insulin until complete differentiation.

Preparation of Albumin-bound Fatty Acids—Radiolabeled [14C]oleate fatty acid was mixed in water at 40 °C, albumin (BSA; fraction V, fatty acid-free, Sigma) was then added from a concentrated stock (20 g/100 ml) to give a final molar ratio of 1/1 by gentle mixing. 2 × Hanks' solution was added to obtain a 1 × final solution. Incubation was carried out at 37 °C for 45 min.

Fatty Acid Uptake Assay—The measurement of uptake of 1-14C-labeled oleate (about 50 mCi/mmol, NEN Life Science Products) was carried out in 24- or 6-well plates with 10^6 cells/ml of medium. Before treatment, the cells were washed with 1 × Hanks' solution. BRL 49653 (100–250 nM) and fenofibric acid (100–250 μM) were added in fresh Dulbecco's modified Eagle's minimal essential medium containing 10% fetal calf serum. After 48 h of treatment, cells were washed with Hanks' solution and incubated for 1 additional h in serum-free, glucose-free medium. Cells were then washed once at 37 °C and twice at 23 °C with 1 × Hanks' solution containing BSA. Hanks' solution without BSA was then added before the assay. A volume corresponding to 1 μCi of [14C]oleate albumin-bound solution was added in each well, and cells were incubated for 1 min at room temperature. The incubation was stopped after 1 min with 3 washes of ice-cold 1 × Hanks' solution without BSA. A complementary experiment has been performed to verify whether aspecific cell surface binding of [14C]oleate could interfere with the assay. For this second assay, the cells were washed under more stringent conditions in 1 × Hanks' solution containing 2% BSA. Cells were then lysed in 400 μl of 0.1% SDS solution. The lysate was counted for 5 min with 4 ml of scintillation solution. The assay was performed on triplicate points.

RNA Analysis—RNA preparation, Northern blot hybridizations, and quantification of total cellular RNA were performed as described previously (24). A mouse FATP cDNA probe was obtained after cloning a reverse transcription-polymerase chain reaction fragment from mouse

adipose tissue RNA using the primers 382 (ATGCGGGCTCCTGGAG-CAGGACAGCC) and 399 (CTGCGTGTCAGGCAGGATGCTCTCAG-GCCC) into pBS-KS. The insert was sequenced and found to be identical to the .reported mouse FATP sequence. The rat ACS probe corresponds to the *Eco*RV restriction fragment of the rat ACS cDNA. The human acidic ribosomal phosphoprotein 36B4 (25) was used as a control probe.

RESULTS

FATP mRNA Is Ubiquitously Expressed—To determine whether FATP expression was ubiquitous or restricted to certain tissues, we hybridized both a mouse (Fig. 1A) and a rat (Fig. 1B) multiple tissue Northern blot with a radiolabeled FATP probe. In both rat and mouse, adipose tissue, heart, brain, and testis showed the highest level of expression. Intestine and muscle show intermediate levels of expression, and low levels are expressed in the liver, kidney, lung, and spleen.

Fenofibrate, a PPARα Activator, Induces FATP mRNA in Vivo—In addition to being building blocks and energy substrates, fatty acids are also important signaling molecules. Besides being activated by peroxisome proliferators and certain thiazolidinediones, the transcriptional activity of PPARs can be activated by fatty acids (reviewed in Refs. 16 and 17). Therefore, we were interested in analyzing whether activation of these PPARs would affect FA uptake in general and FATP expression in particular. To address this issue we first assessed the effect of fibrates, potent PPARα activators, on the expression of the *fatp* gene in rats. Rats were hence treated with different doses of fenofibrate (14 days treatment at the doses 0.005, 0.05, and 0.5% by mass) mixed in food. Next, RNA was isolated from various organs and analyzed by Northern blot hybridization. In liver, FATP mRNA levels increased gradually
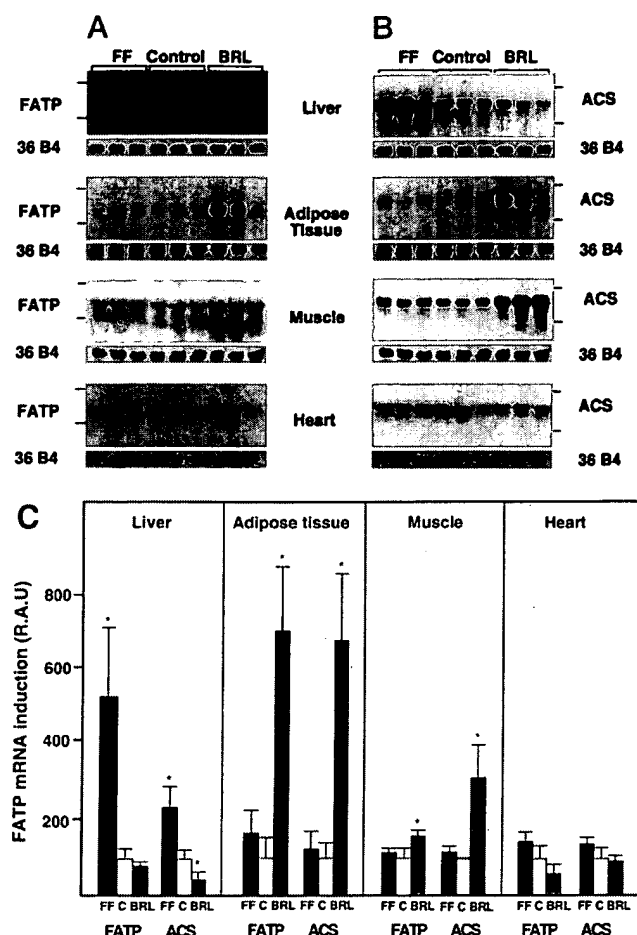
FIG. 4. **Tissue-selective induction of FATP (A) and ACS (B) mRNA in rat liver, adipose tissue, skeletal muscle, and heart by fenofibrate and BRL 49653, respectively.** A, expression of FATP mRNA in liver, epididymal adipose tissue, skeletal muscle, and heart of animals treated with fenofibrate (*FF*, 0.5% (w/w) during 7 days, approximately 0.5 g/kg/day) or BRL 49653 (5 mg/kg/day during 7 days). The blots were stripped and rehybridized with the human acidic ribosomal phosphoprotein 36B4 control cDNA. B, expression of ACS mRNA in liver, epididymal adipose tissue, skeletal muscle, and heart of animals treated with fenofibrate (*FF*, 0.5% (w/w) during 7 days, approximately 0.5 g/kg/day) or BRL 49653 (5 mg/kg/day during 7 days). The blots were stripped and rehybridized with the human acidic ribosomal phosphoprotein 36B4 control cDNA. Animal treatment and preparation and analysis of RNA is described under "Experimental Procedures." C, bar graph summarizing the regulation of ACS and FATP mRNA in liver, epididymal adipose tissue, skeletal muscle, and heart of animals treated with or without BRL 49653. *R.A.U.*, relative absorbance units. Values statistically significant from controls (Mann-Whitney; $p < 0.05$) are indicated by an *asterisk*.

starting from 0.05% fenofibrate and reached a maximal 4.2-fold induction at the highest dose of 0.5% fenofibrate (Fig. 2, *A* and *B*). A representative Northern blot showing the induction of FATP mRNA in the liver is depicted in Fig. 2*B*. Next, the response of FATP mRNA levels to fibrates was studied in intestine, skeletal muscle, heart, and kidney. Only intestinal FATP mRNA expression was slightly induced (2-fold) by the highest dose of fibrate treatment, whereas muscle, kidney, and heart FATP mRNA expression remained unchanged. Also in mice, administration of fenofibrate (0.5%) induced FATP mRNA levels in liver (15-fold) (Fig. 2*C*).

Parallels between the Fibrate Effects on FATP and ACS—Several proteins are hypothesized to enhance fatty acid uptake into cells. In contrast to FATP, which acts as an FA transport protein, ACS prevents the efflux from the imported FAs by converting them into acyl-CoA derivatives, which can subse-

quently be used in both anabolic and catabolic pathways. Therefore, we next analyzed whether there was a parallel between the induction of FATP and ACS after fibrate treatment (Fig. 3). Fenofibrate induced liver and kidney ACS mRNA expression, whereas no change in ACS expression was observed in heart and intestine. Therefore both FATP and ACS mRNA levels seem to be coordinately regulated in liver and heart, since fibrates affect both parameters in a similar fashion. The regulation of ACS and FATP in the kidney and intestine seems to be divergent, since in these tissues only one of the respective mRNAs is regulated by fibrate treatment.

PPARγ Activators Induce FATP mRNA in Adipose Tissue—In addition to the well established effects of peroxisome proliferators such as the different fibrates on PPARα activity, we next tested the effects of the PPARγ-selective ligand BRL 49653 on FATP and ACS expression in various rat tissues after administration of these compounds. Fenofibrate (0.5% (w/w), ±0.5 g/kg/day) induced FATP and ACS mRNA in rat liver (Fig. 4, *A* and *B*), confirming our previous observations (26). By contrast, treatment with fenofibrate did not change FATP and ACS mRNA levels significantly in adipose tissue, skeletal muscle, or heart (Fig. 4, *A* and *B*). Administration of 5 mg/kg/day of BRL 49653 was associated with the expected decrease in serum triglyceride levels (from 167 to 88 mg/dl). Furthermore, this treatment with BRL 49653 resulted in a significant induction of adipose tissue FATP (7-fold) and ACS (7-fold) mRNA levels (Fig. 4). This induction of FATP and ACS mRNA by BRL 49653 was observed in epididymal (Fig. 5) and omental (data not shown) adipose tissue. In perirenal adipose tissue, however, only FATP but not ACS mRNA was induced (Fig. 5). We observed a 1.6- and 3.1-fold induction of respective levels of FATP and ACS mRNA in skeletal muscle after BRL 49653 administration. BRL 49653 did not significantly influence the expression of FATP or ACS in liver, whereas FATP mRNA levels showed a tendency to decrease in the heart after BRL 49653 treatment.

The Induction of FATP and ACS Expression by Fenofibrate Is at the Transcriptional Level—To analyze whether the induction of FATP and ACS mRNAs occurred at the transcriptional level, a nuclear run-on assay was performed on liver nuclei obtained from fenofibrate-treated rats (Fig. 6). In comparison with control liver nuclei, the rate of FATP and ACS transcription was respectively 3- and 3.5-fold higher in nuclei from fenofibrate-treated animals. The transcription rate of acyl-CoA oxidase, a key enzyme in the peroxisomal β oxidation pathway, a positive control for fibrate action, was induced (5-fold), whereas the glyceraldehyde phosphate dehydrogenase gene, a negative control, did not change.

BRL 49653 Induces FATP mRNA Specifically in Preadipocyte Cells, whereas Fibrates Induce FATP mRNA in Cells of Hepatic Origin—To study the cellular mechanism of this induction, we investigated the regulation of the *FATP* gene expression by fibrates and BRL 49653 in hepatocyte (Fig. 7), adipocyte (Fig. 8), and muscle cells cell lines. FATP and ACS mRNA were measured in mouse AML-12 and rat Fa 32 liver-derived cell lines. A strong induction of expression of both FATP and ACS mRNA levels was seen after treatment of these liver-derived lines with fenofibric acid. Fenofibric acid induced both mRNAs optimally within 24 h (Fig. 7*A*) at a dose of 250 μM (Fig. 7*B*). The results of dose response and time course of FATP and ACS induction after treatment with fibrates seem to show an apparent difference between Fa 32 and AML-12 cells. The reason for this apparent difference in induction of FATP and ACS in the two cell lines is most likely caused by the difference in basal levels of FATP, which in Fa 32 cells is barely detectable. In contrast, under basal conditions, AML-12 expresses
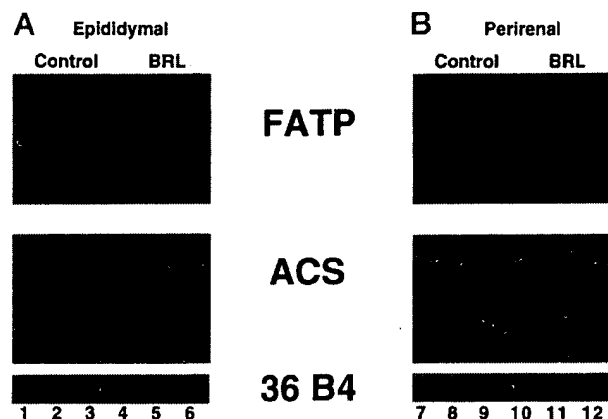
FIG. 5. **BRL 49653 induces FATP and ACS mRNA in different adipose tissue depots.** Expression of ACS and FATP mRNA in epididymal (*A*), and perirenal (*B*) adipose tissue of animals treated with BRL 49653 (5 mg/kg/day during 7 days). The blots were stripped and rehybridized with the human acidic ribosomal phosphoprotein 36B4 control cDNA. Animal treatment and preparation and analysis of RNA is described under "Experimental Procedures."
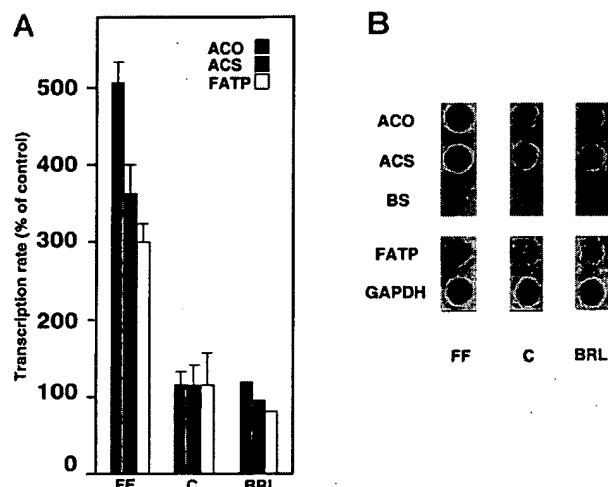

FIG. 6. **The induction of FATP and ACS by fibrates is at the transcriptional level.** Transcription rates were determined for the FATP, ACS, acyl-coA oxidase (*ACO*) and glyceraldehyde-3-phosphate dehydrogenase genes in rat liver nuclei obtained from control, or BRL 49653 (*BRL*)- or fenofibrate-treated rats (*FF*). A pUC-20 template was used as a control (*C*). Densitometric scanning of the results is depicted at the *left panel*. *GAPDH*, glyceraldehyde-3-phosphate dehydrogenase, is used for relative values; *ACO*, acyl-CoA oxidase; *BS*, BlueScript.

FIG. 7. **Regulation of FATP and ACS mRNA expression in the liver-derived cell lines AML-12 hepatocytes (*A*, rat) and Fa 32 (*B*, mouse) by fibrates.** *A*, AML-12 hepatocytes. Time course of FATP and ACS mRNA induction in AML-12 cells treated with fenofibric acid (250 μM). A probe for 36B4 was used as a control. *R.A.U.*, relative absorbance units. *B*, Fa 32 hepatoma cells. Dose reponse of FATP and ACS mRNA induction in Fa 32 hepatoma cells treated for 24 h with the indicated concentrations of fenofibric acid. Cells were grown and mRNA analysis was performed as described under "Experimental Procedures."

lines, no change in L6 ACS and FATP mRNA levels were detected upon treatment with either fenofibrate or BRL 49653 (data not shown).

Induction of FATP or ACS mRNA Levels Results in a Change in FA Uptake into Cells—To verify whether changes in mRNA levels of FATP and ACS were correlated with alterations in fatty acid uptake, we analyzed [^{14}C]oleic acid uptake in Fa 32 and AML-12 hepatic cells, L6 muscle cells, and 3T3-L1 preadipocytes. As shown in Fig. 9, fatty acid uptake of [^{14}C]oleic acid significantly increased after treatment of the liver-derived AML-12 cells with fenofibric acid and after treatment of the differentiated adipocyte-like 3T3-L1 cells with BRL 49653. In Fa 32 cells, fatty acid uptake was also increased (data not shown). The increase, although statistically significant, was however less pronounced than in AML-12 cells. As expected in view of the absence of a major regulation of ACS and FATP mRNA in muscle cells, no effects of either fenofibric acid nor BRL 49653 were observed on FA uptake in L6 muscle cells. The regulation of FA uptake was hence completely consistent with the regulation of respective mRNA levels of FATP and ACS in the various cell models.

DISCUSSION

Both ACS and FATP have been suggested to play a crucial role in the transport of fatty acids into the cell (4). FATP acts as a fatty acid transport protein, whereas ACS prevents efflux of the newly imported fatty acids by their esterification with coenzyme A. Fatty acids are important cellular components that can function both as metabolic substrates or as signaling molecules, by functioning as second messengers and triggering signal transduction pathways or by directly activating transcription factors such as the PPAR family of nuclear receptors. Since FATP and ACS control, in part, the intracellular availability of FAs, important PPAR activators, the aim of the present investigation was to perform detailed analysis of FATP and ACS expression and to establish whether FATP and ACS expression themselves might be subject to control by PPARs.

In the liver, one of the major organs susceptible to peroxisomal proliferation, *FATP* gene transcription is strongly induced upon fibrate treatment. This strong induction is not surprising if one takes the strong induction of peroxisomal β oxidation into account after fibrate treatment. FATP is likely to be responsible in part for the increased FA import necessary to sustain

much higher levels of FATP transcript. This difference between these cells will result in an overestimation of the induction of the FATP in Fa 32 cells, explaining the discordance between relative levels of induction between FATP and ACS in the two cell lines.

To examine FATP and ACS regulation in adipocyte-like cell lines, 3T3-L1 preadipocyte cells were used. First, we analyzed the effects of BRL 49653 on nondifferentiated 3T3-L1 preadipocyte cells. As shown in Fig. 8*A*, a limited effect of BRL 49653 was observed in undifferentiated 3T3-L1 cells. In differentiated 3T3-L1 adipocytes, FATP and ACS mRNA levels were induced 5- and 9-fold after 4 days of treatment with BRL 49653. The ob 1771 preadipocyte cell line (22) was also analyzed (Fig. 8). The addition of BRL 49653 also induced FATP and ACS mRNA levels in this cell line (Fig. 8), whereas fenofibric acid had only a weak effect (data not shown).

Finally the effects of both BRL and fenofibric on L6 muscle cells were analyzed. Unlike in adipocyte or hepatocyte cell
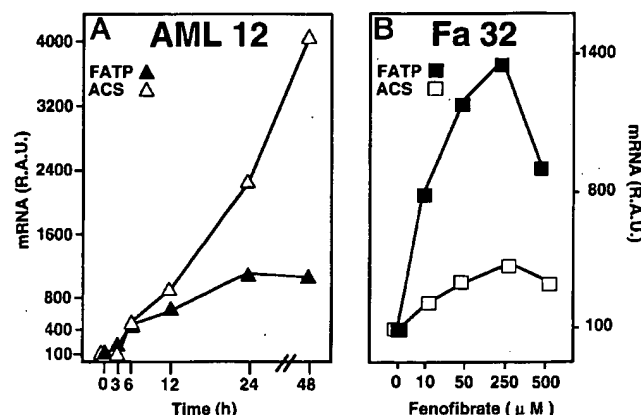
FIG. 8. **Regulation of FATP and ACS mRNA expression in 3T3-L1 preadipocytes (A) and in ob 1771 preadipocytes (B) by thiazolidinediones.** *A*, 3T3-L1 cells. Differentiated or undifferentiated 3T3-L1 cells were treated with BRL 49653 (10 μM) for different time periods. RNA was extracted and analyzed for FATP and ACS expression as described under "Experimental Procedures." A probe for 36B4 was used as a control to normalize the results. *R.A.U.*, relative absorbance units. *B*, ob 1771 cells. Differentiated ob 1771 cells were challenged during 3 days with BRL 49653 (10 μM) and FATP, and ACS mRNA levels were analyzed.
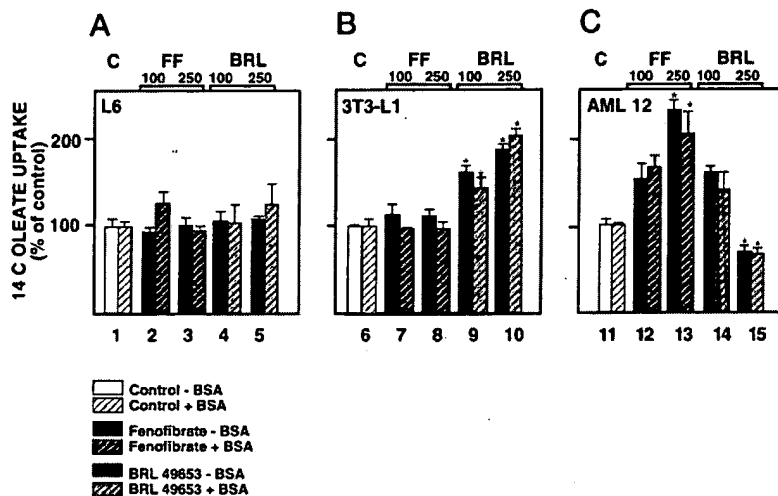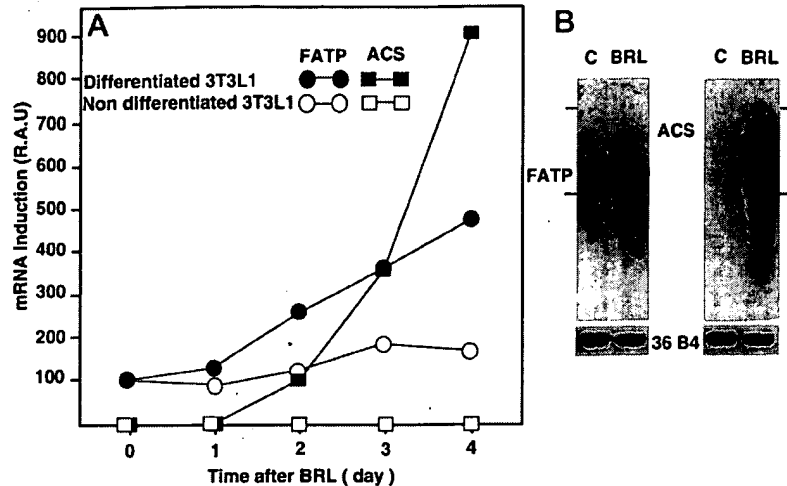

FIG. 9. **Fatty acid uptake is increased in parallel with the changes in FATP and ACS mRNA levels.** [14C]Oleic acid uptake in L6 muscle cells, 3T3-L1 preadipocytes, and AML-12 hepatic cells is shown. Cells were untreated or incubated with either 100 or 250 μM fenofibric acid (*FF*) or 100 or 250 nM BRL 49653 for 24 h. [14C]Oleic acid uptake was then performed as described under "Experimental Procedures." It is indicated whether cells were washed without (−BSA) or with BSA (+BSA).

this increased β oxidation. Furthermore, a striking parallelism exists between the induction by fibrates of a number of genes involved in fatty acid import in the liver. In fact, the mRNAs for lipoprotein lipase (LPL) (27), ACS (this paper and Refs. 27 and 28), and *FATP* genes are all induced after fibrate treatment in the liver. This coinduction of genes seems to prime the cells for more efficient β oxidation. Induced liver LPL expression will increase lipolysis in the vascular bed of the liver, generating more fatty acids, which are then avidly taken up by the cells thanks to the higher levels of FATP expression. Efflux of these imported fatty acids is prevented by induced ACS levels, which in addition, primes them for subsequent metabolism. Therefore it seems that fibrates not only induce β oxidation but also induce genes important for supplying the cells with the extra fatty acids they need to sustain this increase in β oxidation.

In the intestine, FATP was also induced by fibrates, albeit to a lesser extent. The FATP induction in this tissue shows a striking parallel to the induction of CD36 after fibrate treatment in this tissue (29). In contrast to the liver and intestine, heart FATP mRNA levels did not vary substantially under fibrate treatment. The basal levels of FATP expression were, however, very high in heart, which almost exclusively uses fatty acids as energy source. In this tissue, fatty acids are, however, constitutively metabolized to provide energy necessary for the contraction of the heart muscle. Unresponsiveness of FATP expression in the heart to hormonal control could hence be physiologically significant, since the continued function of the heart is far too crucial to allow any form of major

regulation of a transporter vital to its energy supply. This would suggest that in the heart, the FATP promoter is maximally active, resulting in a high level of constitutive FATP gene expression, which would be consistent with the high basal levels of FATP mRNA in this tissue. Similar to the heart, less extreme changes were observed in adipose tissue FATP mRNA after fibrate treatment. The absence of an effect of fibrates on FATP expression in adipose tissue is most likely due to the lower levels of PPARα relative to PPARγ. For kidney and intestine, the regulation of ACS and FATP by fibrates is discordant. This is consistant with the less crucial functions lipids play in kidney and intestinal metabolism. Kidney expressed only low levels of FATP mRNA, and its expression was furthermore refractory to induction by fibrates. Relative to heart and liver, the kidney utilizes relatively little fatty acids, and therefore a coordinate import mechanism is of lesser importance. In intestine, fatty acids are primarily absorbed, but they are less actively metabolized than in heart and liver. Therefore, intestine apparently has an actively regulated transport mechanism, as evidenced by regulation of the expression of both FATP and FAT, another transport protein that is also expressed and highly regulated in this organ (29). Since fatty acids are less actively metabolized and rather resecreted under the form of lipoproteins, there is less need for their conversion to acyl-CoA derivatives and hence less need for coordinated regulation of ACS together with these transport proteins suggested to be implicated in fatty acid transport.

The demonstration of the inducibility of the FATP and ACS

genes by PPARγ ligands such as the thiazolidinedione BRL 49653 has important implications for adipocyte physiology. PPARγ has been shown to promote preadipocyte determination as well as terminal differentiation (13, 30), and its mRNA is itself induced in the earliest steps of adipocyte differentiation before the induction of early marker genes for adipocyte differentiation. Many of these genes induced during adipocyte differentiation encode proteins involved in lipid storage and metabolism. The increase in FATP and ACS expression in differentiated adipocyte-like cells caused by PPARγ ligands will result in an increased delivery of fatty acids to the adipocytes, which possibly sustains a positive regulatory feedback loop involving continued PPARγ activation of the FATP and ACS (28) genes and aimed at promoting and maintaining the mature adipocyte phenotype. In fact, in addition to the thiazolidinediones, certain fatty acid-derived prostaglandin derivatives, whose delivery to the cell is increased by FATP, bind to and/or activate PPARγ (19, 20, 31). This hypothesis is supported by the observation that fatty acids (including arachidonic acid-derived prostaglandins) and fatty acid analogues induce the expression of adipocyte-specific genes and enhance adipocyte conversion (30, 32–35). In addition to being potent PPAR activators (7, 12, 31, 36, 37), fatty acids will provide the necessary building blocks for triglyceride accumulation, ultimately enhancing adipocyte differentiation. The PPAR-mediated activation of FATP and ACS expression in cells of the adipogenic lineage might furthermore in part be responsible for the previously reported capacities of thiazolidinediones to induce adipocyte differentiation and induce the development of obesity (38–46). In this context, it is interesting to note that the PPARγ-mediated effects of BRL 49653 on FATP and ACS expression might act in concert with induced LPL expression and the reduced leptin mRNA and protein levels and the associated increase in caloric intake enhancing energy storage in the adipocytes observed with this compound (47, 48). Interestingly, FATP and ACS are not coordinately regulated in perirenal and epididymal adipose tissue stores. This differential regulation is consistent with the distinct metabolic nature of the different adipose tissue depots (49–51). Further studies are required to determine whether the role of FATP is a consequence of or is causative of the physiologic differences between the adipose tissue depots.

The tissue-selective effects of the various PPAR activators/ligands are highly intriguing and provide insight in their effects on triglyceride metabolism. Fibrate treatment induced FATP and ACS expression strongest in liver, whereas BRL 49653 had no effect on liver, but strongly induced adipocyte FATP and to a lesser extent ACS expression. The effects of fibrates (PPARα activators) on the liver and PPARγ ligands in adipose tissue correlates well with the tissue-specific expression of the respective receptors and suggests that the FATP and ACS genes show a tissue-selective activation similar to the one previously described for the *LPL* gene (27). In this context, we need however to address the discrepancy between ACS and FATP regulation after BRL 49653 administration in skeletal muscle. Muscle tissue expresses very low levels of PPARγ,[2] which is consistent with the absence of an important regulatory effect of PPARγ activators in this tissue as observed for the LPL (27) or FATP (this study) genes. In this context, the induction of ACS expression by BRL 49653 is however difficult to explain. One must however bear in mind that not all of the effects of the thiazolidinediones are mediated via PPARγ activation, and it is has been shown that these agents activate

several other signaling pathways (52–54). Further investigations need to address whether ACS expression, unlike FATP or LPL expression, is subject to such a regulatory circuit.

One remaining question is the relationship between PPARγ, thiazolidinediones, and insulin resistance. It is tempting to speculate that the increase of LPL, ACS, and FATP activity in adipose tissue is related to the antidiabetic effects of the thiazolidinediones. Due to the enhanced triglyceride clearance in adipose tissue, less triglycerides will become available to be hydrolyzed to fatty acids in the vascular bed of the muscle. Furthermore, relative to the strong induction of FATP and ACS in adipose tissue by BRL 49653, very limited inductions of both genes are observed in skeletal and heart muscle, favoring uptake of fatty acids in adipose tissue relative to muscle. In view of the inhibitory effects of fatty acids on insulin-mediated glucose metabolism (55), the decrease in fatty acids delivered to the muscle cells might be responsible for the improvement in insulin sensitivity of this tissue.

In conclusion, FATP and ACS mRNA levels can be regulated in a tissue-specific fashion by PPARα activators and PPARγ ligands. In adipose tissue, the increase in FATP, ACS, and LPL (27) production after treatment with thiazolidinediones will enhance the clearance of plasma triglycerides (27, 56) and provide the (pre)adipocytes with additional fatty acids, which can further stimulate the transactivation capacity of PPAR or which can be stored under form of triglycerides. In the liver, the enhanced production of FATP and ACS after fibrates together with the increase in β oxidation and the reduced production of apoCIII (57), may contribute to the hypolipidemic action of these compounds. This tissue-selective induction of FATP and ACS gene transcription by activators of different PPARs, demonstrates the feasibility of the development of highly specific PPAR subtype-specific agonists and antagonists, which can be used as drugs.

REFERENCES

1. Higgins, C. F. (1994) *Cell* **79**, 393–395
2. Berk, P. D., Wada, H., Horio, J., Potter, B. J., Sorrentino, D., Zhou, S.-L., Isola, L. M., Stump, D., Kiang, C.-L., and Thung, S. (1990) *Proc. Natl. Acad. Sci. U. S. A.* **87**, 3484–3488
3. Abumrad, N. A., el-Maghrabi, M. R., Amri, E.-Z., Lopez, E., and Grimaldi, P. A. (1993) *J. Biol. Chem.* **268**, 17665–17668
4. Schaffer, J. E., and Lodish, H. F. (1994) *Cell* **79**, 427–436
5. Faergeman, N. J., DiRusso, C., Elberger, A., Knudsen, J., and Black, P. N. (1997) *J. Biol. Chem.* **272**, 8531–8538
6. Isseman, I., and Green, S. (1990) *Nature* **347**, 645–650
7. Göttlicher, M., Widmark, E., Li, Q., and Gustafsson, J. A. (1992) *Proc. Natl. Acad. Sci. U. S. A.* **89**, 4653–4657
8. Schmidt, A., Endo, N., Rutledge, S. J., Vogel, R., Shinar, D., and Rodan, G. A. (1992) *Mol. Endocrinol.* **6**, 1634–1641
9. Dreyer, C., Keller, H., Mahfoudi, A., Laudet, V., Krey, G., and Wahli, W. (1993) *Biol. Cell* **77**, 67–77
10. Sher, T., Yi, H. F., McBride, W., and Gonzalez, F. J. (1993) *Biochemistry* **32**, 5598–5604
11. Zhu, Y., Alvares, K., Huang, Q., Rao, M. S., and Reddy, J. K. (1993) *J. Biol. Chem.* **268**, 26817–26820
12. Kliewer, S. A., Forman, B. M., Blumberg, B., Ong, E. S., Borgmeyer, U., Mangelsdorf, D. J., Umesono, K., and Evans, R. M. (1994) *Proc. Natl. Acad. Sci. U. S. A.* **91**, 7355–7359
13. Tontonoz, P., Hu, E., Graves, R. A., Budavari, A. I., and Spiegelman, B. M. (1994) *Genes Dev.* **8**, 1224–1234
14. Amri, E.-Z., Bonino, F., Ailhaud, G., Abumrad, N. A., and Grimaldi, P. A. (1995) *J. Biol. Chem.* **270**, 2367–2371
15. Aperlo, C., Pognonec, P., Saladin, R., Auwerx, J., and Boulukos, K. (1995) *Gene* **162**, 297–302
16. Schoonjans, K., Staels, B., and Auwerx, J. (1996) *J. Lipid Res.* **37**, 907–925
17. Schoonjans, K., Staels, B., and Auwerx, J. (1996) *Biochim. Biophys. Acta* **1302**, 93–109
18. Forman, B. M., Tontonoz, P., Chen, J., Brun, R. P., Spiegelman, B. M., and Evans, R. M. (1995) *Cell* **83**, 803–812
19. Lehmann, J. M., Moore, L. B., Smith-Oliver, T. A., Wilkison, W. O., Willson, T. M., and Kliewer, S. A. (1995) *J. Biol. Chem.* **270**, 12953–12956
20. Kliewer, S. A., Lenhard, J. M., Willson, T. M., Patel, I., Morris, D. C., and

Lehman, J. M. (1995) *Cell* **83**, 813–819

21. Devchand, P. R., Keller, H., Peters, J. M., Vazquez, M., Gonzalez, F. J., and Wahli, W. (1996) *Nature* **384**, 39–43
22. Negrel, R., Grimaldi, P., and Ailhaud, G. (1978) *Proc. Natl. Acad. Sci. U. S. A.* **75**, 6054–6058
23. Wu, J. C., Merlino, G., and Fausto, N. (1994) *Proc. Natl. Acad. Sci. U. S. A.* **91**, 674–678
24. Auwerx, J., Chait, A., and Deeb, S. (1989) *Proc. Natl. Acad. Sci. U. S. A.* **86**, 1133–1137
25. Masiakowski, P., Breathnach, R., Bloch, J., Gannon, F., Krust, A., and Chambon, P. (1982) *Nucleic Acids Res.* **10**, 7895–7903
26. Schoonjans, K., Staels, B., Grimaldi, P., and Auwerx, J. (1993) *Eur. J. Biochem.* **216**, 615–622
27. Schoonjans, K., Peinado-Onsurbe, J., Lefebvre, A. M., Heyman, R., Briggs, M., Cayet, D., Deeb, S., Staels, B., and Auwerx, J. (1996) *EMBO J.* **15**, 5336–5348
28. Schoonjans, K., Watanabe, M., Suzuki, H., Mahfoudi, A., Krey, G., Wahli, W., Grimaldi, P., Staels, B., Yamamoto, T., and Auwerx, J. (1995) *J. Biol. Chem.* **270**, 19269–19276
29. Poirier, H., Degrace, P., Niot, I., Bernard, A., and Besnard, P. (1996) *Eur. J. Biochem.* **238**, 368–373
30. Tontonoz, P., Hu, E., and Spiegelman, B. M. (1994) *Cell* **79**, 1147–1156
31. Yu, K., Bayona, W., Kallen, C. B., Harding, H. P., Ravera, C. P., McMahon, G., Brown, M., and Lazar, M. A. (1995) *J. Biol. Chem.* **270**, 23975–23983
32. Gaillard, D., Negrel, R., Lagarde, M., and Ailhaud, G. (1989) *Biochem. J.* **257**, 389–397
33. Amri, E.-Z., Bertrand, B., Ailhaud, G., and Grimaldi, P. (1991) *J. Lipid Res.* **32**, 1449–1456
34. Distel, R. J., Robinson, G. S., and Spiegelman, B. M. (1992) *J. Biol. Chem.* **267**, 5937–5941
35. Chawla, A., and Lazar, M. A. (1994) *Proc. Natl. Acad. Sci. U. S. A.* **91**, 1786–1790
36. Keller, H., Dreyer, C., Medin, J., Mahfoudi, A., Ozato, K., and Wahli, W. (1993) *Proc. Natl. Acad. Sci. U. S. A.* **90**, 2160–2164
37. Forman, B. M., Umesono, K., Chen, J., and Evans, R. (1995) *Cell* **81**, 541–550
38. Hiragun, A., Sato, M., and Mitsui, H. (1988) *J. Cell. Physiol.* **134**, 124–130
39. Ikeda, H., Taketomi, S., Sugiyama, Y., Shimura, Y., Sohda, T., Meguro, K., and Fujita, T. (1990) *Drug Res.* **40**, 156–162
40. Sparks, R. L., Strauss, E. E., Zygmunt, A. I., and Phelan, T. E. (1991) *J. Cell. Physiol.* **146**, 101–109
41. Kletzien, R. F., Clarke, S. D., and Ulrich, R. G. (1992) *Mol. Pharmacol.* **41**, 393–398
42. Castle, C. K., Colca, J. R., and Melchior, G. W. (1993) *Arterioscler. Thromb.* **13**, 302–309
43. Sandouk, T., Reda, D., and Hofmann, C. (1993) *Am. J. Physiol.* **264**, C1600–C1608
44. Hirshman, M. F., Fagnant, P. M., Horton, E. D., King, P. A., and Horton, E. S. (1995) *Biochem. Biophys. Res. Commun.* **208**, 835–845
45. Teboul, L., Gaillard, D., Staccini, L., Inadera, H., Amri, E. Z., and Grimaldi, P. (1995) *J. Biol. Chem.* **270**, 28183–28187
46. Brun, R. P., Tontonoz, P., Forman, B. M., Ellis, R., Chen, J., Evans, R. M., and Spiegelman, B. M. (1996) *Genes Dev.* **10**, 974–984
47. De Vos, P., Lefebvre, A. M., Miller, S. G., Guerre-Millo, M., Wong, K., Saladin, R., Hamann, L., Staels, B., Briggs, M. R., and Auwerx, J. (1996) *J. Clin. Invest.* **98**, 1004–1009
48. Zhang, B., Berger, J., Zhou, G., Elbrecht, A., Biswas, S., White-Carrington, S., Szalkowski, D., and Moller, D. E. (1996) *J. Biol. Chem.* **271**, 31771–31774
49. Bjorntorp, P. (1996) *Int. J. Obes. Relat. Metab. Disord.* **20**, 291–302
50. Marin, P., Lonn, B., Oden, B., Bengtsson, B. A., and Bjorntorp, P. (1996) *J. Clin. Endocrinol. Metab.* **81**, 1018–1022
51. Shimomura, I., Takahashi, M., Tokunaga, K., Nakamura, T., Yamashita, S., Takemura, K., Yamamoto, T., Funahashi, T., and Matsuzawa, Y. (1996) *Am. J. Physiol.* **270**, E995–1002
52. Buchanan, T. A., Meehan, W. P., Jeng, Y. Y., Yang, D., Chan, T. M., Nadler, J. L., Scott, S., Rude, R. K., and Hsueh, W. A. (1995) *J. Clin. Invest.* **96**, 354–360
53. Maegawa, H., Ide, R., Hasegawa, M., Ugi, S., Egawa, K., Iwanishi, M., Kikkawa, R., Shigeta, Y., and Kashigawa, A. (1995) *J. Biol. Chem.* **270**, 7724–7730
54. Ren, J., Dominguez, L. J., Sowers, J. R., and Davidoff, A. J. (1996) *Diabetes* **45**, 1822–1825
55. Randle, P. J., Garland, P. B., Hales, C. N., and Newsholme, E. A. (1961) *Lancet* **i** 785–789
56. Lefebvre, A.-M., Peinado-Onsurbe, J., Leitersdorf, I., Briggs, M. R., Paterniti, J. R., Fruchart, J.-C., Fievet, C., Auwerx, J., and Staels, B. (1997) *Arterioscler. Thromb. Vasc. Biol.*, in press
57. Staels, B., Vu-Dac, N., Kosykh, V., Saladin, R., Fruchart, J. C., Dallongeville, J., and Auwerx, J. (1995) *J. Clin. Invest.* **95**, 705–712